NOISE MECHANISMS

ADVISORY GROUP FOR AEROSPACE RESEARCH
AND DEVELOPMENT

1974

AGARD-CP-131

AGARD

ADVISORY GROUP FOR AEROSPACE RESEARCH & DEVELOPMENT

7 RUE ANCELLE 92200 NEUILLY SUR SEINE FRANCE

AGARD CONFERENCE PROCEEDINGS No. 131

on

Noise Mechanisms

NORTH ATLANTIC TREATY ORGANIZATION

DISTRIBUTION AND AVAILABILITY ON BACK COVER

AGARD-CP-131

NORTH ATLANTIC TREATY ORGANIZATION

ADVISORY GROUP FOR AEROSPACE RESEARCH AND DEVELOPMENT

(ORGANISATION DU TRAITE DE L'ATLANTIQUE NORD)

AGARD Conference Proceedings No.131

NOISE MECHANISMS

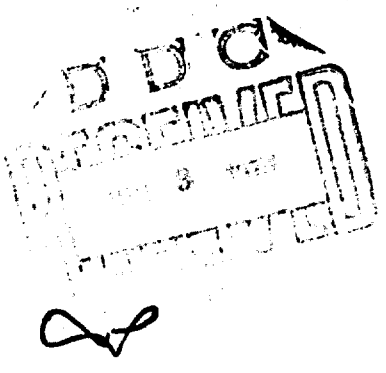

Papers, Technical Evaluation and Discussion of the Fluid Dynamics Panel Specialists' Meeting held in Brussels, Belgium, 19–21 September 1973.

THE MISSION OF AGARD

The mission of AGARD is to bring together the leading personalities of the NATO nations in the fields of science and technology relating to aerospace for the following purposes:

- Exchanging of scientific and technical information;
- Continuously stimulating advances in the aerospace sciences relevant to strengthening the common defence posture;
- Improving the co-operation among member nations in aerospace research and development;
- Providing scientific and technical advice and assistance to the North Atlantic Military Committee in the field of aerospace research and development;
- Rendering scientific and technical assistance, as requested, to other NATO bodies and to member nations in connection with research and development problems in the aerospace field;
- Providing assistance to member nations for the purpose of increasing their scientific and technical potential;
- Recommending effective ways for the member nations to use their research and development capabilities for the common benefit of the NATO community.

The highest authority within AGARD is the National Delegates Board consisting of officially appointed senior representatives from each member nation. The mission of AGARD is carried out through the Panels which are composed of experts appointed by the National Delegates, the Consultant and Exchange Program and the Aerospace Applications Studies Program. The results of AGARD work are reported to the member nations and the NATO Authorities through the AGARD series of publications of which this is one.

Participation in AGARD activities is by invitation only and is normally limited to citizens of the NATO nations.

A large part of the content of this publication has been reproduced
directly from material supplied by AGARD or the authors;
the remainder has been set by Technical Editing and Reproduction Ltd.

Published March 1974

534.836:629.735:621.438:533.6.011.72

Printed by Technical Editing and Reproduction Ltd
Harford House, 7–9 Charlotte St, London, W1P 1HD

FOREWORD

This Specialists' Meeting was held to follow on the meeting on "Aircraft Engine Noise and Sonic Boom", held jointly with the Propulsion and Energetics Panel in May 1969. Emphasis on this occasion was on the fundamental problems of noise generation and attenuation; main aspects considered were noise generation and damping, combustion and jet noise, sonic boom theory and noise due to boundary and shear layer effects. The meeting concluded with a round table discussion.

The Specialists' Meeting was held at the Bibliothèque Royale, Brussels, at the invitation of the Belgian National Delegate to AGARD.

CONTENTS

Technical Evaluation Report

J.E. Ffowcs Williams

University Engineering Laboratory,
Cambridge, England.

Introduction.

The Meeting was convened to study the mechanics of sound generation by turbulent flows. The emphasis was on aeronautical problems arising from the field of aircraft noise control and the decision had been made by the Organising Committee to exclude all aspects of combustion generated noise and noise associated with moving turbomachinery parts. The absorption of sound at internal engine surfaces was also excluded in an attempt to guide the Meeting to concentrate on the fundamental mechanics of sound production.

This report is made under six separate headings which effectively categorise the subject areas into which fell most of the presented papers. They are:-

1. Source Identification.
2. The Influence of Mean Flow Structure on the Generation and Propagation of Sound.
3. Distinctive Large Eddy Structures; Are they Deterministic Events?
4. Excess Noise.
5. The Control of Jet Noise.
6. Problem Areas Likely to Become more Important.

The main technical points arising from the Meeting are outlined and the degree to which they appear to be currently understood is assessed. The paper is in no way intended to be a precis of the proceedings of the Conference and no attempt is made to cover or comment upon contributions of a review nature that were sometimes made to introduce the new material.

There were, in fact, several technical areas on which there was no clear concensus of opinion. Those developing areas are referred to in more detail and some speculation is made on the way they might develop. Also the Meeting brought to light some apparently important technical areas that are only in an embryonic state. This paper is concluded with some recommendations on actions that AGARD might take to foster their development.

2. Source Identification.

The identification and control of the principal noise producing motion in turbulence is the main objective of aerodynamic noise research. In the past, this activity has taken the form of a theoretical modelling of the noise generation process followed by speculative proposals of how the identified noise producing events might be modified by a variation in the mean flow geometry. The experimental checking of those source models is a very recent development, several aspects of which were reported at the Specialist Meeting.

There is no doubt that this activity will have a major role to play in future noise control programmes and it is appropriate now that the early experimental steps have been established to re-examine the basis on which the various source location procedures are built.

Contrary to apparently popular belief there is no uniqueness theorem to guarantee that the 'source' measured by any one of the several existing source location schemes is actually the origin and cause of the observed wave field. In fact, it is known that several different source distributions are capable of generating a common distant radiation field. This follows from a straightforward application of Kirchoff's theorem which states the equivalence of the exterior field generated by a source distribution interior to a closed surface and that generated at the surface by a suitable distribution of monopole and/or dipole sources. Many papers presented at the Specialist Meeting dealt with different aspects of source location but none of them faced up to the difficult issue of interpreting or speculating on the degree of ambiguity that must inevitably be contained in the experimental results. It may be that when it is known for other reasons that the source must be contained in a specific area, for example, within the confines of the jet mixing region, that that added constraint can impart some uniqueness to the source distribution. That seems rather unlikely though because so far as the radiation field is concerned a point multipole expansion is allowed, and the entire distant field can be modelled as originating at any point in the source region, the strengths and orientations of the various multipole moments depending on the exact location of the point at which the source is assumed to exist.

The degree to which this essential ambiguity of source position should be admitted or ignored will no doubt be an important area of further study.

The most straightforward source identification principles are based on exploiting the idea that the propagating sound waves travel without dispersion in the radiation field. They are essentially treated as conforming with ray theory, which they will at high enough frequency. Rays are traced back to the flow to indicate the general area of their origin. These procedures are incapable of distinguishing the location of the source within the characteristic error dimension of one wavelength or so. This error can be reduced by suitable callibration but it cannot be made indefinitely small. Thus these schemes would seem inappropriate for the study of aerodynamic noise sources in the regimes which are well modelled by the acoustic analogy. Those are the cases in which the characteristic dimension of the source is much smaller than the wavelength as it inevitably must be at low enough Mach number.

Where the scales of the source and that of the sound it generates are not so different, a knowledge of the source position, even admitting that the position may be subject to an error of the order of a wavelength, may sometimes be extremely useful information. This is known to be so for supersonic jet noise where the radiated wavelengths are small compared to the length of flow capable of generating sound. In this high frequency regime the optical and acoustical performance of screens and reflectors are identical, and it is a straightforward matter to arrange a system of baffles to indicate the source activity within a visible aperture. The principle adopted is "what is seen can be heard". Applications of this technique to the sources of supersonic jet noise were described at speeds representative of supersonic transport aircraft at maximum power. There the sources convect supersonically throughout the main source region and radiate miniature ballistic shock waves in the general direction of the eddy convection Mach angle. The scale of the radiated waves indicates directly the scale of the eddies that produced them. Consequently, by observing the direction of the radiation field the principal eddy convection speed is established and the peak frequency of the sound indicates the size of the eddies responsible for that sound.

It was reported that tests of this type indicate that the principal eddying motions responsible for jet noise at supersonic transport take-off conditions lie some 10 to 15 diameters downstream of the nozzle in eddies whose scale is about twice that of the local shear layer thickness. They are extremely large eddies and are probably more effectively thought of as deterministic unsteady transient motions, definite enough to admit some deterministic modelling than as the large scale features of some turbulence statistics. The jet scale is big enough to support only 10 of these eddies at any one instant.

A more deliberate investigation using reflector techniques was described by Grosche. He reported experiments performed with the use of a concave mirror, whose surface was part of an ellipsoid of revolution. That part of the sound field with a ray behaviour and originating from the vicinity of a focus will be concentrated on the second focal point at which a microphone is positioned. This microphone-mirror combination constitutes a directional telescope that produces some measure of the source strength in the general vicinity of the second focus.

Grosche described some experimental jet flows which had been surveyed with this ellipsoidal mirror microphone arrangement. No attempt had been made to correct for the frequency distortion of the apparatus but he showed that the straightforward interpretation of the results gave rise to an extremely plausible source distribution. For example, when the shock cell boundaries of an under-expanded supersonic jet flow are placed at the sensitive region there is a significant increase in the measured signal indicating that those boundaries constitute important sources of sound. It was also reported that this procedure had indicated the main source activity in a jet to be concentrated at the points of maximum mean vorticity.

Taken at their face value these results show that the sound sources in a subsonic jet are located within the first 10 diameters of the flow but that the source region extends downstream of 20 diameters in the supersonic case. Particularly strong sources are found near the boundaries of the cells formed by the steady compressive waves present when a supersonic jet emerges from a improperly contoured nozzle.

At low Mach number Grosche showed also that some significant sources appeared to be concentrated at the nozzle boundary. He was able to change the apparent strength of these sources by modifying, with a boundary layer trip upstream of the nozzle exit, the turbulence level in the nozzle flow.

A similar experiment was reported by Laufer in which a microphone is placed at the focus of a parabolic mirror and directed at various parts of an ideally expanded supersonic jet. Laufer said that he hoped to remove most of the frequency distortion brought about by the finite mirror aperture but even without this preliminary, results indicate a very plausible distribution of source activity not dissimilar to that described by Grosche.

Although these ray theory schemes are inherently incapable of resolving source position to within a negligible fraction of a wavelength the steadily mounting circumstantial evidence does indicate that they are extremely useful diagnostic tools.

In the compact source limit, that is the one to which the acoustic analogy pertains, the source location procedures are based on an analytical description of the source terms. Siddon gave the Meeting a comprehensive account of this scheme which is as follows. Suppose that a source distribution Q drives a simple wave field according to

$$\Box^2\phi = Q \qquad 1.$$

this can be written in the retarded integral form

$$\phi(\underline{x},t) = \frac{1}{4\pi c^2}\int_{\infty} [Q](\underline{y},t-r/c)\,\frac{d^3\underline{y}}{r}\;;\; r = |\underline{x}-\underline{y}|, \qquad 2.$$

and the mean square field at large distances can be expressed as an integral over the source field, the integrand being interpreted as the source strength per unit volume,

$$\overline{\phi^2(\underline{x})} = \frac{1}{16\pi^2c^4r^2}\int S(\underline{y})\,d^3\underline{y} \text{ as } r \to \infty\,, \qquad 3.$$

where

$$S(\underline{y}) = \int \overline{Q(\underline{z},t-r'/c)Q(\underline{y},t-r/c)d^3\underline{z}}$$

$$r' = |\underline{z}-\underline{x}|\,, \qquad 4.$$

The function S, though it can formally be thought as the source strength per unit volume, isn't actually any indication of the field that would be generated by unit volume of the source field in isolation. As equation 4 makes clear S is an integral property receiving contributions from all space.

Siddon described a scheme he called 'casuality correlation', whereby equation 2 is multiplied by the field quantity to produce;

$$\overline{\phi^2(\underline{x})} = \frac{1}{4\pi c^2 r}\int \overline{\phi(x,t)[Q](\underline{y},t-r/c)\,d^3\underline{y}} \text{ as } r \to \infty \qquad 5.$$

from which it follows that,

$$\overline{\phi^2(\underline{x})} = \frac{1}{16\pi^2c^4r^2}\int R(\underline{y})\,d^3\underline{y} \qquad 6.$$

where

$$R(\underline{y}) = \overline{4\pi c^2 r\phi(\underline{x},t)[Q](\underline{y},t-r/c)}. \qquad 7.$$

The casuality method equates the function R to the function S both being interpreted as the same source strength per unit volume. R is apparently easily measured according to the prescription given in equation 7, which therefore afford a method of determining the source distribution directly.

This scheme is attractive and ingenious. It has already provided data that is extremely plausible.

Some debate took place regarding the uniqueness of this interpretation and it is worth recording the nature of that debate, since procedures of this kind are likely to feature extensively in future source location experiments.

The function R of equation 6 is equivalent to the function S of equation 3 in the sense that both integrate to the same value. The two functions can therefore differ by any function of zero integral scale, and both could be called the source strength per unit volume. Clearly this definition of the source strength is far from unique and the prescription by which the most meaningful source strength density is determined has yet to be laid down. Perhaps the question is not really significant; it aroused debate because casuality correlations tend to be rather indefinite regarding the number of distinct eddies taking part in the noise production process. No doubt, this is due in part to the indeterminacy of the source field due to the already mentioned essential non-uniqueness of the issue.

It is worth reflecting a little further on other aspects of this problem. The source strength per unit volume S is not necessarily a positive definite function. If the source field were homogeneous then of course it would be positive definite. But that is rather an academic issue since the driven field would then be unbounded and the source location meaningless. S is probably positive when the source field is sufficiently slowly varying, but very little seems to be known about this aspect, which is probably a critical issue, for it does not seem a sensible procedure to regard S as the source strength density in

regions where it is negative. If the source field is sufficiently slowly varying then equation 4 could be written quite formally as

$$S(\underline{y}) = \overline{Q^2(\underline{y})} V_c \qquad 8.$$

where V_c is the correlation volume. This correlation volume tends to be interpreted as the volumetric scale of the sound producing motion. The physical source region when divided by the volume per unit eddy V_c is interpreted as the number N of independent eddies taking part. Siddon reported that experimental estimates of N varied between 10 and a few thousand.

Views were expressed at the meeting that the main noise producing elements of turbulence are likely to be extremely large scale so that a debate resulted as to the reasonableness of the deduction that thousands of independent eddies can be housed in the source region. But actually V_c is not a physical volume but an integral correlation scale. This scale could be small for two reasons. Firstly there is the obvious possibility that the source structure is so fine grained that it really does correspond to minute eddies. But the other possibility is that since the definition of the correlation volume is through an integral, the integral, and hence Vc , could be small even when the eddy size is very large. Most of the activity in the eddy would not then be germain to the source process. For example, equation 1 could be rewritten trivially as

$$\Box^2(\phi - Q) = Q - \Box^2 Q. \qquad 9.$$

Now the field outside the source volume is expressed as the difference between ϕ and Q, though since Q is zero there, the field is identically ϕ. But the source of that field appears to be the right hand side of equation 9, the difference between Q and $\Box^2 Q$ which could very well have a much greater magnitude than Q itself. But the D'Alambertian integrates at retarded time to zero, and this example demonstrates quite clearly the essential non-uniqueness of the source field when viewed from the exterior.

The problem is just as evident when correlation techniques are applied to locate the noise sources on the surface of a rigid aerofoil. This is an area on which confusion had existed in the past. The stresses on the rigid surface are clearly identified as the equivalent sources in the acoustic analogy of the field. But it has been argued that since those stresses do no work they are incapable of communicating energy to the fluid and might well be spurious.

But there is no real doubt that the field can be expressed in terms of surface stresses. A systematic study of the correlation between these surface and field terms was given in a joint paper by Sunyach, Arbey, Robert, Bataille, and Comte-Bellot. They reported correlation between the distant radiation field and pressure measured at various positions around an aerofoil in a low speed flow. They also correlated flow disturbances in the wake shed by the aerofoil at several positions near the trailing edge and identified the trailing edge region as the centre of most active disturbance.

From the trailing edge a pressure field propagat upstream at about the speed of sound, and this pressure is highly correlated with the sound radiated to large distances. The correlation between the surface pressure and the radiation field, when properly treated according to Curle's equation, approaches unity for those pressures measured on the aerofoil surface visible from the observation point. The correlation with pressure fluctuation on the shadow side of the aerofoil rarely exceeds 10^{-1}. Those correlations indicate clearly that the disturbance convects downstream with a speed of the order of the mean flow velocity. Hence the picture emerges that though the disturbances originate at the trailing edge, the important sound producing features are those associated with the pressure pulse travelling upstream, over the aerofoil, at about the speed of sound, generating as it travels a strong surface dipole radiation field. Presumably, the reason for this is that the lifting properties of the aerofoil are determined by trailing edge conditions which, when adjusted, cause the flow about the foil to rearrange itself. That rearrangement occurs just as soon as the flow knows of the trailing edge change. The news propagates from the trailing edge at the speed of sound and the resulting adjustment in surface pressure drives the main radiation field.

In source location experiments with free turbulent flows some approximation to the source strength density is usually made. The favourite these seems to be that since density fluctuations are the essence of sound, a direct measure of density in the source region might well be the most direct method of determining the source strength. Two such methods were described. One by Maussier, Parthasarathy and Cuffel and the other by Dankevala, Grosche and Guest. Both these programmes used optical probing devices from which the variation of density was determined. Both studies lead on to estimates of the source distribution and, again, both the estimates appeared extremely plausible, though again no uniqueness could be claimed.

Several interesting points came to light in the ensuing discussion. The density fluctuation observed by means of an optical beam has contributions from two identifiable terms. Firstly, inertial effects produce pressure changes that drive the density field. This might well be associated with sound. Secondly, the mixing of two streams of different density produces point-wise density variations which are likely to be passive kinetic terms that should be excluded from the computation of source strength.

The possibility that non-equilibrium effects might limit the utility of turbulence measuring schemes based on absorption techniques was brought up by Holbeche. He remarked that it was now known that non-equilibrium effects were important in sonic boom propagation and he would expect that they might well be important in all transient field changes. Since the Meeting had heard that transients were a distinct feature of jet noise at high speed, it might well be that absorption techniques have an essential limitation; they may not be able to respond rapidly enough because of non-equilibrium effects.

Another fundamental point emerged. How in principle could data regarding density perturbations be used to identify the source of sound? As a function of density, the source strength is the D'Alambertian of the density field, that is, the difference between the second time derivative of density and c^2 times the Laplacian of the density perturbation. If this D'Alambertian could be measured directly then the source could be regarded as relatively unambiguous. But in fact only approximations appear possible, and, so far, these approximations do not seem to have been subjected to an error analysis. It was difficult at the meeting to avoid the impression that it was likely to prove extremely difficult to predict the radiated field given only point-wise information regarding the density perturbation in the source region.

From an experimental view point there appears to be advantages in regarding some measure of the pressure fluctuation as the source of sound. Aerodynamic sound is driven by a quadrupole source distribution so that the distant radiation field correlates with the second time derivative of the pressure in the vincinity of the source provided the appropriate acoustic time delay is inserted between the two signals. Experimental papers to exploit this idea were given by Siddon and Meecham and Hurdle. Both reported studies in which pressure had been measured within turbulent flow, subjected to double temporal differentiation, delayed in time and correlated with the far field acoustic pressure. When this correlation is high the near field probe is near a strong source, when it is low it is near a weak source (or, what seems equally possible, far from a strong source!) In this way the source properties of a jet flow were mapped, and in both the reported studies, extremely plausible predictions of the source distributions were made. The main source of subsonic jet noise is around 5 diameters downstream of the nozzle exit.

Relatively small values of the correlation co-efficient are found between the synthesized and measured signal and, as has already been pointed out, this can be interpreted as an indication that the number of distinct eddies taking part in the sound produciton process is very high. There was no uniformity in this aspect of the presented papers. No doubt some of that is due to the non-uniqueness of the source so that a uniform description could not be expected. But also, as Siddon explained, the data is confused by noise generated by the pressure measuring probe. Siddon gave indications that this noise had a very distinct contaminating effect, but, in debate, Siddon did not consider that the probe significantly contaminated the pressure measured in its vicinity. Doubt was expressed that the pressure measured with a probe which disturbed the turbulent shear flow could adequately represent the pressure at that point in the absence of the probe, but experimental view-points were given that this was not a real problem and that the probe distortion effect could be removed by calibration. This was not an unanimous view.

Source location was also the theme of Belleval and Perulli's presentation. They described the study of the infra-red radiation from a hot jet flow. Unsteady infra-red radiation is observed at acoustic frequencies and it is observed that the infra-red variation is correlated with the far field sound. Opinions regarding the significance of this result vary between the two extremes, one believing the correlation to be entirely fortuitous and the other that the source of sound and infra-red are one and the same thing. This issue was not advanced further. At the Meeting Perulli concentrated on the statistics. Infra-red receptor beams are aimed at the flow and the unsteady part of the signal correlated. In this way statistical characteristics of the unsteady infra-red sources are obtained. On the assumption that the time scale, space scales and correlation speeds so measured are also those of the turbulence stress tensor, the statistical data can be used in an estimation of the source strength distribution according to Lighthill's theory. This scheme was described by Perulli. The idea provides potentially valuable information but there is still a very long way to go before an unambiguous interpretation of the data is achieved.

Running through all these papers dealing with the experimental assessment of the source distribution in real sound producing flows is the common thread that the predictions made from the experiments look reasonable. Other distributions might also look reasonable. All the schemes reported do not produced the same result, no doubt due in part to experimental errors and also to basic errors in the approximation schemes. But the biggest room for doubt is the essential ambiguity in the source function. No uniqueness is possible and this is true whether the source is described through theoretical or experimental techniques. Given this state of affairs, developments along these lines are likely to be based on acquiring familiarity with the type of results that can be produced by the application of various plausible diagnostic schemes.

There is no doubt that the experimental application of the method represents an enormous advance on the previous approximate theoretical treatments, and having made that advance it is worth while pausing a little to consider how much gain might be expected from increasingly sophisticated diagnostic aids. Having paused it seems that only experience will tell and that the real meaning of these admittedly not non-unique

descriptions can only be established through continued use. The situation is very similar to that existing when light is reproduced through a hologram image. An observer in the reconstituted field is quite unable to tell whether the field is generated by the original events or by a laser hologram combination. However, experience has taught him that in most cases it is the real event, and one has learnt to rely on that simple interpretation of the source field! But it is not unique! In a similar way the indeterminacy in these acoustic sources might be equally trivial and we will eventually be able to rely on their indicated location of the important sound producing areas. But only experience will tell.

2. The Influence of Mean Flow Structure on the Generation and Propagation of Sound.

The Meeting was reminded of Lighthill's paper at an AGARD meeting 10 years previously where then existing experimental evidence was compared with the predictions of theory. In Lighthill's model the sound increases in proportion to the 8th power of velocity, subject to a modification due to eddy convection through the ambient fluid. That convection increases the efficiency of quadrupole radiation. The only direction imune from convective change is 90 degrees to the jet axis where the 8th power dependence is expected. That experimental data seemed to indicate that though the total power increased in proportion to the 8th power of velocity a 6th power law was more appropriate at 90 degrees, presumably Lighthill thought due to turbulence being relatively less intense at the higher Mach numbers. Lighthill had therefore concluded that the convective effect was there in full, and brought the total power output back up to the measured 8th power proportionality, it being a coincidence that the convective effect exactly compensated for the lethargy of turbulence at high Mach number.

But since then Lush has published in the Journal of Fluid Mechanics an argument that the experiment quoted by Lighthill is not representative of mixing noise, because in experiments he has conducted on a jet emerging smoothly from its nozzle the sound at 90 degrees scales on the 8th power of velocity, exactly as the unmodified Lighthill theory predicts. In the quoted engine experiment nozzle exit conditions were unlikely to be smooth and this is now known to cause a deviation from the 8th power law. That subject will be returned to in Section 4.

Lush went on further to point out that convective effects are not found in experiments made close to the axis of a subsonic jet. Csanady had shown previously that the convective augmentation of the radiation efficiency would be annihilated if the source were surrounded by a flow relative to which it did not move. The acoustic output is determined locally if the source is cushioned by a wavelength or so of moving fluid from its static environment and cannot then be subject to convective amplification. Lush's experimental data confirmed this view, but it remains unknown how much of the difference between the idealized Lighthill model in which sound is assumed to propagate without subsequent interaction with the mean flow or its gradient, and the experimental result is due to the inhibition of convective amplification and how much is due to refraction. Experiments show that the difference between the Lighthill modelling and experiment begin to become obvious at the beginning of the high frequency range where ray theory and simple ideas of refraction apply.

The Meeting was reminded again that acoustic interaction effects with mean flow containing concentrated vorticity are important items of the experimental data. Holbeche described experiments conducted in a 24 foot open jet wind tunnel. There he had investigated sound transmission through a trailing vortex system, the vortices being generated by a delta wing at incidence, and the sound by an electrically driven horn. The results show a major influence of vortex refraction, the sound rays passing through the vortex centre being changed by as much as 10 decibels at reasonable flow speeds. Rays are rotated in the direction of vortex motion the largest change being measured for those rays passing close to the vortex core. Holbeche compared the experimental results with the predictions of ray theory; the comparison is extremely good.

In reply to questions Holbeche said that the singular scattering effects predicted in theoretical analyses that treat the vortex as a compact scatterer have not been found in the experiments though they were deliberately sought. He thought it pertinent however, that any vortex generated with a delta wing has quite a different core structure from that treated in those theories.

Another aspect of the propagation problem was described at the meeting in two separate experimental results where the sound of a noisy jet had been shielded by a nearby small quiet jet through which its noise had to pass to the observation point. Hoch and Hawkins described this effect as measured on models of the Concorde silencer. That consists of buckets which squeeze the jet into a fishtail flow in whose plane the jet is relatively quiet. They described studies of the sound generated when two jets were in close proximity, one silenced by the fishtail process and the other not. It seems that that sound is completely incapable of propagating through the silenced jet. In fact, they came to the conclusion that 'one heard the nearest thing one saw', and in that experiment it was the silenced jet. A Rolls-Royce experiment was described where the noise of a supersonic jet was shielded by up to 10 decibels by an auxiliary small jet at the same pressure ratio passing only 10 per cent of the mass flow of the primary.

The experimental evidence points to major influences of mean flow gradients on any sound propagating through an inhomogeneous flow. When this is the case it is improbable that an adequate description of the jet noise problem can be based on Lighthill's acoustic analogy. Though that analogy is exact it is most unlikely that the stress tensor terms representing the propagation through the various shear layers can ever be known in

sufficient detail for the analogy to prove useful.

Another aspect of the same problem concerns the mechanics by which jet noise is controlled in the, so called, fishtailed jet. It may be that the noise producing eddies are de-energised in the fishtailed flow. In fact, they almost certainly are, and this aspect we shall return to in Section 5, but there are two influences attributable to propagation effects.

The flow structure in these jets appears to be a central fast jet shielded by a relatively slowly moving fan that forms the fishtail. This fan may have two effects; firstly it may effectively isolate the noise producing turbulence on the edge of the central jet, from the environment and so inhibit the convective amplification. In this respect the effect is similar to that noted by Lush for high frequency noise close to the axis of a circular jet; but also the fan provides a flow with different noise propagation characteristics adjacent to the jet and the sound generated in the jet interior may be refracted away from the plane of the fishtail to produce there a zone of relative silence. It does not seem to be known which of these two possibilities is the dominant one; no doubt that will be the subject of future study.

Two theoretical papers bore somewhat on this subject. The first, by Mani, considered the radiation from a point source embedded in a uniform slug flow. The second by Lilley, dealt with developments based on Phillips' equation that accounts implicitly for a spacewise variation of the propagation constants.

Mani's problem is an idealized one, where a point source is located on the axis of a jet contained within a vortex sheet. He has studied the sound radiated into the static environment by the embedded moving source. There was considerable debate as to how well this model problem represents a real jet flow, and no doubt there are always important differences when the frequency is high enough that the acoustic wavelength is comparable with the shear layer thickness. The lower frequency elements should however be modelled adequately provided the shear layer turbulence level is small enough that the sound can be regarded as a small perturbation of an otherwise laminar flow. But this is unlikely to be the case in practice. This point will be returned to below.

What Mani's model problem does, and does in a completely unambiguous way, is to show that mean flow effects can be very considerable indeed and can give rise to consequences that are simply not predictable from the acoustic analogy in which the effects are ignored. Mani quantified the differences as far as the radiated power is concerned. He showed how the effect of convective amplification was negated by 'jet shielding' provided only that the jet is thick enough on a wavelength scale and the mean flow Mach number not negligible. These conclusions are broadly in agreement with Lush's data, but as Lush pointed out at the Meeting, his experimental observation concerned the intensity of sound at separate points, and not the overall power, which was the only parameter considered by Mani.

Mani went on to describe the influence of jet density in the radiation field. He considered the case where the product ρc^2 is conserved across the vortex sheet and therefore as the density is varied so is the speed of sound, and the jet thickness as measured on the wavelength scale. A change in jet density has, therefore, two effects in his model. Firstly, there is a density discontinuity at the shear layer which must have a dynamic effect. Secondly, there is the variation in the wave propertion properties within the jet as the speed of sound is varied, in inverse proportion to the square root of density, and in fact it seemed from the presentation that this latter effect was the more significant. In this model he established the influence of mean flow density on the acoustic power radiated from a point source. On the assumption that this sensitivity of the radiation efficiency to jet density carries over to turbulence produced sound, the strength of the turbulence source of itself being proportional to jet density, Mani found that his model predicted the experimental data obtained at the NGTE and SNECMA extremely well. He makes the important point that the variability of noise with changes in jet density need not be explained entirely in terms of the basic source strength which seems to be the approach taken by most investigators to date. Mani's results show that there may be an equally important effect to do with the radiation impedance and its dependence on density.

Lilley described developments to a theory deliberately aimed at accounting for mean flow inhomogeneities. That is based on the idea that sound can be described theoretically as a small perturbation about a basically laminar flow, and the equation that does that is of course the one used to investigate the stability of that laminar flow. There one considers whether an initial perturbation will grow or die. Questions of stability are bound to feature in this approach to the acoustic propagation problem.

The basic formulation is due to Phillips where he treated the second order terms as known inhomogeneities and studied the way they drive linear perturbations about the steady mean flow, a motion that is directly coupled to the radiating sound field. If the natural motion of the linear field is exponentially growing because of the instability, then clearly it is pointless to assume that the field can remain linear. In the discussion following his paper Professor Lilley said that he intended to take account of the non-linear effects in an approximate manner. However, it was his view that the acoustic radiation problem could still be regarded as an essentially linear one even though non-linear effects would be dominant in controlling the amplitude of the driven response. Some found this notion rather confusing. But again it is demonstrated that by approaching the problem in this slightly different way one uncovers clear fundamental effects

associated with mean flow inhomogeneities which simply couldn't be anticipated by a formal application of the acoustic analogy. Having said that it seems that there is still some way to go before this approach can lead to results that have not been previously derived by some other form of analysis, that is, either from the acoustic analogy or from the other limit, ray theory. In between the problem is complicated, and will probably have to be approached numerically. No numerical results were presented to the meeting.

The philosophy behind this type of modelling was debated at some length. Experimental observations of the jet structure indicate that the flow is very different from a weakly perturbed laminar shear layer. The view that it was most unreasonable to expect sound to propagate through such a very rough jet boundary in a way that even approximated to the transmission of sound through a smooth flow with the profile of the mean jet was expressed forcibly. On the other hand it was reported that stability analyses that modelled the large eddies as evolving weak instability waves driven from a laminar flow with the mean velocity profile have much in common with the measured shear layer turbulence. The convection speed, characteristic scale and even the growth rate of the eddies as they propagate downstream are predicted to high accuracy. This may or may not be a coincidence. Professor Michalke described how in a computation of this kind he had worked out streak lines which bore a remarkable similarity to various visualizations of experimental jet flows. Crighton, Krishnamurthy and Michalke described how they had independently calculated the growth of instability waves on a diverging shear layer and Crighton said that he had continued the analysis to a point where the interaction with the nozzle boundary and the subsequent radiation of sound could be described analytically. They collectively seemed to have no doubt that it was relevant to describe the large noise producing eddies as being the instability products of the primary flow, the stability of which was determined by the mean velocity profile.

Another view was expressed also and seemed to find equal support. That was, that the eddying motions are so intense that they quickly deform the velocity field on which they grow their amplitude being determined by an essentially non-linear process. In fact, an individual eddy grows on a jet whose structure during the eddy evolution time is completely different from that of any nominally steady flow. In fact some felt that the opposite view to stability might be taken. It is not the mean flow that supports instabilities that are observed as the large scale eddies, but it is the large scale eddies, which are the characteristic debris of the initially thin shear layer that determine the mean flow structure. That mean flow is established as the average taken over an ensemble of many individual eddies growing according to the velocity field at their time of existence.

In one view, the mean profile determines the eddies, in the other the eddies determine the mean velocity profile. That debate is likely to continue for a long time and shows every promise of providing fertile ground for progress towards a real understanding of the sound producing elements of turbulence.

3. <u>Distinctive Large Eddy Structures; Are They Deterministic Events</u>?

The Meeting witnessed new developments in the current trend away from the statistical description of turbulence and sound towards a more definite modelling of distinct elementary motions thought to create sound effectively. This is very much the development that Powell foresaw in the meeting organised ten years previously. The attractiveness of the view is easily appreciated, because many of the motions can be visualised effectively and several experiments described at the meeting dealt with particularly graceful eddying forms. The technical relevance of especially powerful isolated sources is obvious since the highest intensity peaks in any noise signal occur infrequently and must be generated by an extremely effective transient force motion. The paper by Naumann and Hermann describing the sound produced by the interaction of a shock wave with a concentrated vortex was a superb example of how beautiful the experimental visualisation of the process can be, and how much deeper it is possible to delve into the detailed physics of the problem once the source process is identifiable in a distinct enough manner that it can be regarded as deterministic. All elements of turbulent flow can be regarded as deterministic when one concentrates on a sufficiently localised sample of that flow; but the innovation seems to be that there are particularly relevant samples to be selected that give rise to extremely powerful sound sources. We can look forward to conditional sampling experiments in which the most effective source motions are extracted from the bulk of the turbulent motions and studied in very much greater depth and detail than has been possible to date. The evidence for this view is as follows.

Measurement of the distant noise field from the Olympus 593 turbo jet that powers Concorde were described. At the highest jet velocities the signal is subjectively categorised as a crackling sound but there appears to be no distinguishable difference in the spectral content of the noise of a crackling and non-crackling jet. The probability distribution of a crackling jet is highly skewed and towards infrequently occurring large compressive pressure transients. The skewness factor in the distant noise field of the Olympus increases from 0.02 to 0.6 as the engine condition is increased from idle to maximum thrust. The effect of skewness is clearly seen in the pressure time history of the radiated field. The short duration high intensity positive pressure spikes distinguish the crackling noise from other turbulent signals. There seems no doubt that these spikes originate in the mixing jet flow and not in some idiosyncrasy of that particular engine. The Meeting was told of similar investigations conducted by Laufer and Kaplan where identical spike formations had been observed experimentally in a smoothly expanded hot model jet flow. Furthermore when the jet was viewed through a focussed acoustic

telescope the tendency for spike formation was at a maximum if the telescope was focussed at a region approximately ten diameters downstream of the nozzle exit. The jet conditions were extremely similar to those of the Olympus at high speed. In the model situation there was no possibility of a cellular standing wave system because the jet was ideally expanded. It was reported that Rolls-Royce experiments with a three inch model jet at the same velocity but not ideally expanded also displayed the spiky crackling characteristics at high speeds. Because of the clear subjective significance of the spikes their possible origin was debated at some length at the meeting. It seems unlikely that they can result from non-linear propagation of a signal that initially starts its journey with an unskewed probability distribution because it is extremely difficult to identify any process by which non-linear effects bring about this skewness.

On the other hand Obermeier described to the Meeting a modelling of the behaviour of sonic booms near a caustic. This modelling led Obermeier to study the behaviour of the Tricomi equation through which he was able to show that on passing through a caustic an 'N' wave acquired momentarily a distinct spikiness in the positive pressure part of the signal with a rounded expansive trough. It was said that spikes were present in the near vicinity of the jet and that the probability distribution of the signal with crackle did not seem to evolve during propagation over a distince from 5 diameters away from the jet to 150 diameters. That indicated the spikes result from a distinctive source activity rather than from some characteristic large amplitude. But the possibility that the signal continually forms new caustics cannot yet be ruled out. It was reported however, that if the jet were exhausted through a notched nozzle that produced a characteristic fishtail, then in the plane of the fishtail the spikes were absent and also the sound there was at a very much reduced level.

If the spikes are generated by a particularly efficient transient source they are probably more easily modelled when they are regarded as deterministic events. Legendre emphasised that it was a matter of common experience that violent events are extremely noisy. In fact the essence of an efficient sound source is that the characteristic time scale of the motion is small enough compared to its scale that the ratio of the two, which forms a characteristic velocity of the motion, is supersonic. Then the eddy is non-compact and falls in the opposite extreme of that treated by the acoustic analogy. Far from the sound being a small perturbation caused by flow, the wave field is then of the same order of magnitude as the basic source motion. An impulsively arrested boundary motion caused all the local energy to be radiated as sound. G. I. Taylor has worked out how all the virtual energy around a slowly moving sphere is shed off as sound if the sphere is impulsively arrested. That is the most effective aerodynamic sound source yet modelled, and it is also the sound source most completely modelled, for there the motion is described in analytical detail. There seems no doubt therefore, that identifiable large eddying motions that either grow rapidly enough, or accelerate sufficiently abruptly, can form extremely useful models of jet noise sources, and the Meeting was presented with several facinating descriptions of such motions.

Poldervaart showed the Meeting the latest of his facinating films produced in conjunction with Wijnands and Bronkhorst. Poldervaart described his study as an aerodynamic game. The experiment consists of an external sound source that generates a sequence of pulses incident upon a supersonic jet. As the pulse interacts with the jet nozzle edge a distinct vortex is formed on the shear layer which travels downstream growing rapidly and generating a clearly visible intense secondary wave. The motion is visualised by a stroboscopic action and by control of the relative phase between jet excitation and visualisation, the motion can be slowed down indefinitely. This scheme offers the potential for studying the minute details of this extremely powerful noise producing eddy. The experimental technique holds enormous potential for the really detailed study of strong aerodynamic noise sources.

Fuchs described correlation measurements that indicate extremely large scale eddying motions in the early part of a mixing jet and he showed that the axially symetric motions were the most effective sound producers in his experiment. It seems that the vortex layers across a jet are highly correlated in those acoustically efficient turbulent elements.

Kuchemann described to the Meeting theoretical studies he has been conducting with colleagues on the rolling up of the thin initial vortex sheet into rapidly growing spiral vortices. To him the most powerful turbulent elements of the jet mixing layer appear as strong individual vortices generating noise as they grow. Linear instability theory is hardly relevant to this process, for the shear layer which is assumed nominally plane in these calculations is quickly convoluted as it is wrapped into the growing vortex spiral. Kuchemann reminded the Meeting of Prandtl's early studies of this process and how developments along this line were showing promise of an effective modelling of the strongest shear layer motions. Laufer and Kaplan's studies concentrated also on the discrete vortex motions but emphasised the interaction between an array of vortices rather than the single growing element. Laufer described experiments in which a shear layer was observed to degenerate into a street of concentrated vortices, which propigate downstream in an initially regular array. As the vortex system travels small deviations in their propagation characteristics cause some vortices to approach one another. Laufer described an extremely interesting process in which vortices amalgamated in a process of pairing that took place abruptly. Such vortex pairing would no doubt cause extremely efficient sound production. Laufer said that the experiments they had conducted with a two dimensional mixing layer indicate that the vortex pairing process is the essential element of turbulent shear layer thickening. When the motion is viewed correctly it can be seen to comprise a relatively distinct array of eddies which continually pair as they

travel downstream into a system of larger and less numerous eddying motions. This view of the turbulent mixing process holds the promise of a much more rational understanding of the sound producing motion than is ever likely to be possible in the conventional statistical description of shear layer turbulence.

An experiment in a similar vein was described by Emmerling. He had studied with Meier and Dinkelacker the pressure perturbation on a plane surface supporting a turbulent boundary layer. They had developed an extremely novel method of measuring the surface pressures in which a test section of the surface was constructed with an array of compliant optically reflecting segments whose deviations under the unsteady pressure could be measured by optical means. Emmerling described in immense detail the behaviour of certain violent transient motions in the boundary layer as they grew and travelled downstream. He reported a very high correlation between the large scale structure across the turbulent boundary layer and the occurrence of distinct pressure eddies at the wall. With this experimental scheme in which distinct motions are measured rather than the statistics of the motion a powerful verification of a dynamic model has been obtained. The experiments are consistent with the view that the large scale motions of the boundary layer induce a changing boundary layer profile which erupts in a locally unstable region to generate extremely active bursts of turbulent energy.

From these presentations, all concentrating on identifiable features embedded in a nominally chaotic flow, one can see that the subject is in a very exciting transitory state in which the statistics of the flow is gradually being de-emphasised. By concentrating on identifiable events in the turbulence there seems to be a promise that important items of the motion will be understood in far greater depth. With that there is every possibility that the understanding will lead to eventual control of the large eddies and the dominant radiated noise.

4. Excess Noise

The Lighthill theory of sound generation by turbulence is an asymptotic theory valid for sufficiently low Mach number. The most outstanding prediction is that the sound intensity will scale on the 8th power of jet velocity. Yet experiment seems to indicate that there is an inevitable departure from the 8th power law as the jet velocity is reduced. In most practical situations the departure occurs at a relatively high speed, at jet exit velocities of 1000 feet per second. But from the clean nozzle flow exhausting from a smooth reservoir of high pressure air the 8th power law can be maintained down to jet speeds of the order of 300 feet per second. The reason that the 8th power law is not maintained to very low speeds is thought to be that there is in addition to the Lighthillian mixing noise other sources of sound which become the dominant sources once the jet speed is reduced sufficiently that the jet mixing noise is smaller than the sound of these other additional sources. The term excess noise has been coined to deal with these other sounds, and since the definition is intended to cover all other sources there can be no unique explanation as to the origin of the excess noise.

One source of sound additional to the mixing noise is that generated when turbulent eddies scatter the wave energy of shock waves that form in improperly expanded supersonic jets. Often the energy so shed is sufficiently powerful that on interacting with the jet nozzle it provokes an eddy in the jet shear layer to travel downstream to scatter the shock energy once more a characteristic time later. That regenerates a sound wave and this process leads to a discreet frequency sound known as screech. The screech cycle is easily controlled and is probably not of great technological significance.

Until recently it was only the frequency of the screech cycle that had been properly predictable from any theoretical modelling. But the meeting heard Harper-Bourne and Fisher describe a quantative modelling of the sound generated by turbulence interacting with an array of shocks in a supersonic jet. They described a model in which a turbulent eddy travels downstream at about the mean shear layer velocity maintaining coherence and surviving the interaction with several successive shocks. In this way the sound generated when the eddy interacts with shocks forms a phased array of acoustic emitters, and this leads to a distinct and predictable directionality of the radiated sound, a directionality wholly attributable to the geometry and phasing of the array. The Harper-Bourne Fisher model takes no account of any possible directionality to the sound radiated by any one shock during vortex excitation. Fisher and Harper-Bourne find experimentally that the strength of the radiated wave is in direct proportion to the pressure difference across the mean shock waves of the jet. They have produced a model in which the strength of the shock associated noise is predicted from the Mach number of the jet and the directionality is determined by the velocity and spacing of the mean shock waves. They showed experimental evidence that the model so produced is in extremely close agreement with the shock associated noise measured on cold model jets and on full scale supersonic aeroengines. This work therefore represents a significant improvement over the previous position where only the qualitative nature of the shock induced noise had been modelled successfully.

A second source of noise additional to that usually described in the Lighthill model concerns the non-isentropic terms in the turbulence stress tensor. These were described by Lilley and by Lush and Fisher. On first sight it seems that these terms describe a source of sound in the unsteady mixing between two streams of different density that increases in proportion to the fourth power of jet velocity. Lush and Fisher showed how a two part model of jet noise, one such source increasing with the fourth power of jet velocity and the other the Lighthillian type increasing with the eighth power of velocity, could be made to fit the experimental data over a wide range of jet speeds. Furthermore the different sensitivity of these two sources to the mean jet density

accounted for the observed tendency for jet noise to increase with the reducing density at low jet velocities but to increase with increasing density at high jet speeds. Lush and Fisher went on to show that this interpretation though consistent with the experimental model was actually no more than an empirical fit because a more careful analysis of the non-isentropic term actually showed that this source generates sound which scales in proportion to the sixth power of velocity and not four.

Some debate arose on this point Professor Lilley not agreeing that the fourth power term vanished on careful analysis, though there seemed little doubt in Lush's mind. The meeting was not presented therefore with a convincing account of the reasons why the temperature effects on jet noise were those experimentally measured though the paper by Lush and Fisher provided an excellent empirical fit to that data. It was not clear that the source of the fourth power of velocity term was properly attributed to the non-isentropic mixing, and bearing in mind that the meeting had already heard Mani's paper in which the temperature dependence had been accounted for, not as a source term but as an effect arising from the variable propagation of sound within the jet, it seems that this subject is far from closed.

Most of the studies conducted under the general heading of excess noise have concentrated on sound generated either within the engine or jet pipe system or by the interaction of turbulence with the nozzle plane. This subject was described by Crighton. It was interesting that though this is an area on which much of the recent jet noise research had been concentrated, and which is clearly the one most relevant to the noise of modern engines with their low specific thrust, Crighton's was the only paper on this topic.

Crighton emphasised that all practical flows would have a certain level of turbulence at the nozzle exit plane. This turbulence would induce an unsteady thrust and to a lesser extent an unsteady mass flow, acoustically equivalent to a dipole and a weak monopole respectively. The sound induced by nozzle based turbulence would therefore scale on the sixth power of velocity at low enough speed and must as the Mach number is reduced overwhelm jet mixing noise. Crighton went on to show that even if the nozzle flow was generated from an absolutely smooth upstream reservoir, the turbulence in the downstream jet mixing layer would inevitably induce unsteady pressure perturbations at the nozzle causing unsteady nozzle exit flow. The nozzle based sound is therefore an inevitable part of jet noise however smooth the upstream conditions. This nozzle based source has a characteristic directionality, the weak monopole exactly cancelled the sound of the dipole in the downstream direction and augments it in the upstream direction. Nozzle based sources have therefore a characteristic tendency to radiate to high angles and into the forward arc. Crighton went on to show how these sources, being attached to the aircraft, are subject to Doppler effects associated with the aircraft motion. These Doppler effects increase the frequency in the forward direction and increase the intensity of the nozzle based sound by the inverse fourth power of the Doppler factor. Crighton reported that these effects were consistent with recent experimental data, and that the directionality of the nozzle based sources is quite the opposite from that due to internally generated sound which tends to radiate preferentially into the rearward arc.

Crighton also described a method of parametric amplification of internal noise. The mechanism here is that sound incident from upstream (or possibly from the outside of a jet pipe) can trigger at the nozzle exit plane a jet shear layer wave which grows exponentially during its initial travel downstream. This growing wave acts back and is scattered by the sharp lip of the nozzle to generate sound very effectively indeed. In fact Crighton said that it was possible to show that this mechanism was capable of accounting for the 34dB amplification effect measured experimentally by Crow, who had shown that the sound of an upstream source could be increased by that factor by jet flow.

In their description of recent studies into Concorde noise reduction Hoch and Hawkins gave a comprehensive listing of experiments relating to excess noise and the effect of forward speed. They showed that even at Concorde engine speeds excess, low velocity index, noise sources were dominant at the lower power settings. Furthermore they were even more dominant in flight where relative velocity reductions de-emphasised the jet mixing noise. They showed also how this sound radiates predominantly at high angles to the jet and how it can be brought under some measure of control by either absorbing internal sound within the engine jet pipe or by the removal of jet pipe turbulence with the use of jet pipe flow straighteners. The Concorde programme has supported many studies into the effect of forward flight on noise and Hoch and Hawkins showed that whereas Lighthillian jet mixing noise is reduced by forward flight, the sound in the forward directions is actually increased. The evidence they gave was consistent with Crighton's model predicting that the sound generated by nozzle based sources was subject to an amplification in proportion to the fourth power of the aircraft Doppler factor.

From the presentations one gathered the impression that virtually all jets, model and engines, are subject to additional noise sources which are proving more difficult to attenuate than the conventional mixing sources which are alleviated by relative velocity effects. No doubt this excess noise area is at the beginning of a growth phase since future jet noise reductions are dependent on some control of the non-mixing noise sources. The theoretical models made no claim to being a comprehensive account of all sources in the excess noise category, but many of the characteristics of a practically important excess noise source did seem to correspond to those predicted by Crighton. On the other hand that agreement may be coincidental since the theoretical ideas all exploit a simplification in the theory dependent on the assumption that the Mach number is low. The Mach number in the jet noise experiments quoted was of the order of unity where the

detailed theoretical modelling could hardly be relevant. Even if the theoretically modelled source is the one most dominant in the practical situation there is still a long way to go before the model is described effectively at the range of parameters characteristic of the actual experimental situation.

5. The Control of Jet Noise

In a joint paper Hoch and Hawkins described the search for jet noise suppression devices that has been sponsored by the Concorde programme and it was interesting to observe how small a part of the problem was occupied by conventional jet noise of the type that has been tackled in the past by multi-tubed and multi-spoked nozzles of one type or another. Certainly the programme had its ad hoc search for nightmare nozzles, but in the main Hoch and Hawkins described a rational process by which efforts are made to identify the principal noise sources which are then tackled one by one.

The most outstanding feature is the directional suppression properties of notched nozzles of the type used on the latest version of the Concorde with the type 28 nozzle system. Static noise reductions of more than 10dB are reported with a thrust loss less than 5 per cent at maximum take-off power, and the fundamental cause of this reduction is still a matter of debate. The notched nozzle flow appears to be a central jet with a subsidiary lateral fishtailed flow emerging from the notches. It seems that this composite flow is not as unstable as the circular jet to lateral disturbances so that the large scale powerful lateral jet motions thought to generate the principal noise of the unsuppressed jet are inhibited. And it may be that the effect of the lateral flow is to shield the noise produced in the central jet core from propagating into the lateral directions. And possibly the sound is simply refracted away from those directions or perhaps the eddy convection effects, so important at these jet speeds, are modified because the eddy is moving less quickly relative to the local environment provided by the auxiliary lateral flow. But whatever the explanation it seems clear that the principal noise generated by a very high speed jet is subject to at least directional control and other previously less important noise problems become dominant issues.

The meeting heard how auxiliary fishtailed jets could be placed adjacent to a noisy high speed jet to shield its noise. Evidently this procedure is not yet optimised but the tests done to date indicate that a distant observer hears only the noise of those parts of the jet with an uninterrupted ambient flow propagation path. 10 decibels of shielding was reported from relatively small jets adjacent to large noisy ones. But again it is not clear whether the auxiliary adjacent jet modifies the sound at source or merely its propagation characteristics.

Only one other item bore directly on the control of jet mixing noise and that was a report from Professor Young that swirl could have a beneficial effect on jet mixing noise though evidence on this point was still extremely sparse.

Most of the remaining discussion on jet noise control dealt with previously unexpected effects that may not concern the jet mixing noise at all. The noise of jet mixing is reduced in flight because the relative motion between the jet and its environment which is the cause of the sound, is then less intense. But Hoch and Hawkins reported extensive results indicating that in most directions the sound is actually increased by flight for a given jet velocity, though the peak noise is reduced. Theoretical explanations of this effect are emerging slowly and most of them hinge on attributing to the acoustic source the convection velocity of the aircraft rather than that of the jet mixing eddies travelling downstream. It seems possible that even in the Concorde situation the noise emitted to most directions is actually not jet noise at all but excess noise generated either within the engine or by unsteady nozzle flow. Jet pipe sound absorbent linings are successful in alleviating much of this noise and some benefit results from straightening the jet pipe flow by means of a honeycomb structure within the jet pipe.

The thread running continuously through the presentation made by Hawkins was that the more detail one discovered by studying in real depth the practical problem the less it seemed to conform with classical models of jet noise. Engineers are at quite a loss in trying to understand the causes and cures. They are also extremely wary of extrapolation from cold to hot models or from models to full scale engines or from static measurements to flight. There is obviously a great deal of fundamental work to be done to provide a firm understanding on which practical advances can be based.

6. Problem Areas likely to become more important

The interaction of flow with sound is an area of increasing interest. The meeting had heard how noise was apparently incapable of being generated by one jet close to a smaller jet or alternatively was incapable of propagating through that quiet jet. It had also heard how the convective amplification effect was inhibited by an extensive mean flow surrounding a turbulent eddy. Theoretical developments indicate a profound change in the character of the sound radiated by a source when that source is adjacent to a strong vorticity concentration.

Since internal noise, and its control by absorbing the waves while they remain within the engine structure is a subject of extreme practical significance, the acoustic behaviour of compliant boundary surface treatments and the influence of mean flow on their sound absorbing characteristics is important. Work on this is still in an early phase only one experiment being reported at the meeting. Kooperhaas described a study he had

conducted with Ronneberger in which they had measured the influence of mean flow on the impedence of a perforated plate. Much of the behaviour could be explained in terms of the resistance offered by the porous plate to flow across it, but there was some indication that non-linear behaviour had to be taken into account, and experiments on that are evidently just beginning.

The possible development of short take-off and landing aircraft calls for lift augmenting devices that might involve the jet being directed at a system of flaps. The interaction of the jet with those flaps is known to be a powerful acoustic source whose control is still in its infancy. The basic noise generated by the flow about the aeroplane as opposed to the engine generated noise is also emerging as an important item on large aircraft in high-drag landing configurations. This is another item that is only now beginning to attract the attention of noise control workers.

The shielding afforded by an airframe structure has yet to be exploited properly. The meeting heard of projects where the engines are located above the wings to shield their noise from the ground. It seems to be an open issue as to how effective such shields can be and there is a real possibility that additional sources will be created by the interaction of jet turbulence with the trailing edge of the shielding wing. It may be necessary to place engines very close to the upper surface of the wing to optimise such shielding effects, in which case problems arise regarding the possible generation of noise in the compressor operating on highly distorted boundary layer inlet flow. Also large unsteady structural loads can be expected on the surfaces beneath the jet mixing region.

The meeting was told that the space shuttle being constructed in the American space programme had new and important sources of noise associated with its novel flight regime.

The emphasis now being placed on discreet eddying motions and the drift away from the statistical approach shows promise for the future. The importance of the noise generated by distinct powerful but isolated events points the need to a conditional sampling approach to experimental jet noise research. The meeting saw the results of several extremely effective flow visualisation techniques and no doubt these will also have an important bearing for the future.

On the theoretical side there is a possibility that non-linear propagation effects must be admitted and studied and their relevance to practical noise problems determined. The current tendency to ignore their effect may be misleading.

Most of the debate on aerodynamic noise concerns the fundamental mechanisms by which sound is created; it rarely ventures into what is technologically the most important area the control of jet noise. There is good reason for this of course because silencers are traditionally studied in commercial companies researching to develop a product. It may well be that the long term progress would be enhanced if research laboratories joined in the search and studied the changes in the flow and in the sound that results from various silencing schemes in very much more depth than has been past practice, and AGARD might have a role to play in encouraging such work.

It became clear at the meeting that there are two new problems of outstanding practical importance. The first is the entire issue of excess noise and its control. The second is the effect of flight on the various sources of sound and the apparent inability to predict the level of noise an aircraft will make given only its noise under static conditions at ground level. The reasons for this should be established as a matter of urgency, and ways of simulating flight effectively either in a wind tunnel possibly similar to that described by De Metz, or in a flying test bed or with a moving engine platform must be found. So far it is far from clear what kind of facility would be most effective but it is becoming obvious that such a facility would be expensive and might well require multi-national support. AGARD could play an important role in defining and encouraging the provision of an effective flight noise simulation facility.

The meeting provided a forum for the exchange of information among specialist workers in the field, but time restrictions had forced many interesting items to be omitted. The field is developing rapidly and AGARD might consider that these specialist meetings should take place more frequently than has been past practice.

Recommendations

It is currently impossible to predict with confidence the noise that will be emitted by an aircraft in flight given only its noise at ground level under static conditions. The noise of all future aircraft will have to be guaranteed to meet definite certification levels so the task of devising a reliable flight noise prediction method is of paramount importance. AGARD might consider the setting up of a working panel to define and recommend ways of providing the means by which this indeterminacy can be removed. It may be that tests have to be conducted under controlled conditions on a moving jet noise platform or a major acoustic wind tunnel may be necessary or a versatile noise flying test bed. Such a facility may require multi-national support of a kind that AGARD might well provide.

The aerodynamic noise field is one that is currently evolving extremely rapidly and many changes occur between the specialist meetings that AGARD organise on the subject. It would be useful therefore to hold the specialist meetings more frequently, possibly annually.

AGARD might stimulate the exchange of information regarding noise suppression techniques which have in the past been developed within commercial institutions where they are not subject to the depth of study required for their detailed understanding. But their development is costly. AGARD might provide the initiative for an aircraft noise reduction programme which could be conducted in sufficient depth that the detailed changes being made by the various silencing schemes were properly understood and documented. A positive effort is needed to inject deep scientific enquiry into practical traditionally ad hoc suppression studies.

OPENING ADDRESS

by

M. R.Legendre
The Chairman of the Programme Committee

Although not myself a specialist in acoustics, I have a strong interest in the subject and I was pleased to accept the Fluid Dynamics Panel's request to organize this Specialists' Meeting; I knew I could rely on the assistance of those who are experts in the field.

Sir James Lighthill is unable to attend our meeting because of other commitments, but his name will be mentioned many times during this conference. We are very happy to have Professor Ffowcs Williams with us; although not a member of the Fluid Dynamics Panel he has given us a very great deal of assistance in preparing the meeting, for which I thank him very much.

I hope this meeting will reach, and perhaps go beyond, the level of the successful one at Saint Louis on Aircraft Engine Noise and Sonic Boom, in 1969. Indeed our purpose is not to repeat the Saint Louis discussion but to extend our understanding beyond that achieved there. It will be a difficult task; noise is closely linked with turbulence, and after 50 years of study we still cannot claim complete understanding of that subject.

After Professor Ffowcs Williams' introductory paper, which will deal with basic mechanisms, you will hear several papers on jet noise. These will show that there has been more marked progress in the field of experimental methods and results than in developing Lighthill's theory. I do not say this in a critical way; we need more knowledge of the existing situation before we can formulate rational theories. I hope the discussion will deal with the correlation between Lighthill's quadrupole theory and the relative displacement of vortex rows moving at different velocities. There are only a few papers on sonic boom, but they contribute well on the subject. The relationship between boundary layers and noise is a difficult subject; we hope more work in this field will result from the papers presented.

We had hoped for papers at our meeting from four other AGARD panels, but in the event we have two only, the Aerospace Medical Panel and the Structures and Materials Panel. We thank those panels very much for their contributions to our meeting.

I thank the Programme Committee for their efforts; now it is for you who are present here to make this conference a success.

IMPULSIVE SOURCES OF AERODYNAMIC SOUND.

by

John E. Ffowcs Williams

University Engineering Department,
Cambridge.

The rapid acceleration of large bodies causes the local motion to shed its kinetic energy into the radiation field. For example, a body steadily moving in potential flow sheds all its 'virtual' energy into sound if it is brought to rest impulsively. Such rapidly accelerated large scale motions therefore represent an extremely efficient source of aerodynamic sound. Motions of this type are discussed with a view to explaining the origin of occasional particularly violent pressure transients that are observed in the noise field of high velocity jets.

Steady flows generate the sound of an organ or flute without the action of surface vibration in a musical but mechanically inefficient manner. The driving flow, with velocity U, develops instabilities that yield an unsteady velocity of magnitude αU say with a characteristic frequency U/l set by the mouthpiece length scale l which is matched to a pipe resonance frequency. The unsteady pressures in the flow, of order, $\rho\alpha U^2$ drive a resonant air motion in the pipe to a sufficiently high amplitude that the driving pressure can be balanced by the radiation pressure at the pipe opening which is small on the acoustic length scale. The oscillating volume flow into and out of the pipe constitutes a compact monopole that forces a radiating pressure field $\rho\alpha U^2 l/r$ associated with which is a resonator response velocity αU. The driven motion within the organ pipe is therefore of the same order as that at the mouthpiece and must have an essential back reaction on the flow even though the energy radiated as sound is extremely small, of order $\alpha^2 M$ times the mechanical energy in the driving flow, M being the Mach number U/c. Therefore, though it is true that the acoustic pressures can be related to the driving flow of which they form a mere by-product, that flow is itself dependant on resonator characteristics. Then the specification of the sound field as a function of the flow parameters, complete as it is, fails to be particularly helpful for the essential problem of determining the source velocity has been avoided by citing it as a parameter. The organ pipe problem will not be fully 'understood' till the intricacies of unsteady flow in a coupled resonator and mouthpiece are worked out in detail, and this is still a very long way off.

In forming the subject of aerodynamic sound Lighthill (1951) deliberately avoided situations in which the unsteady flow might be considered sensitive to the field it drives. He concentrated on problems where sound is generated by flow in the absence of resonators, or sounding boards, and considered only those cases, where energy lost to sound is an insignificant fraction of the energy flux in the flow. But the velocity field driven by the aerodynamic quadrupoles of his accoustic analogy do not actually remain small in comparison with the driving turbulance, for near a quadrupole of strength density ρu^2, the pressure is $\rho u^2(l/r)^3$ and this is associated with a driven velocity field of order u, on the assumption that the source length and time scales are l and l/u respectively. A particular quadrupole in the analogy appears therefore to be highly affected by its induced near field, and it is clear that the acoustic analogy in which the quadrupole strength is considered determined independently if its field can offer no basis for investigating the details of sound evolution in the near field of that eddy. Again, as in the case of the organ pipe, though the analogy provides a complete specification of the sound field in terms of source flow parameters, it leaves a very great deal unsaid. Most of the recent developments in the theory of aerodynamic sound have been in the improved modelling of particular source flows and in the detailed computation of the field in the vicinity of especially strong source centres such as turbulence driven resonant bubbles (Crighton and Ffowcs Williams, 1968) sharp edged surfaces of large scattering cross section (Crighton 1972). These developments follow Lighthill's work inasmuch as the source region is always assumed to be in some sense compact on the acoustic scale and the ratio of flow velocity to the acoustic speed is taken as a small expansion parameter. The energy radiated as sound is in these cases a negligible fraction of that in the flow. Then one can be assured that the source motion is properly determined independently of the sound field and can in sufficiently simple models be evaluated explicitly (Cannell and Ffowcs Williams, 1975).

The low Mach number analogy has to be stretched to its limit to describe most noise problems of aeronautical interest where the relevant Mach numbers are rarely small. They are not at all small in the most important cases, where supersonic jet flows and machinery parts lay down shock waves which are by no means negligible by products of an independently determined source flow. The purpose of this paper is to gather together some thoughts on how this high speed problem might be modelled more effectively and to speculate on the origin of some peculiar characteristics found in the noise field of supersonic jets. In fact the opposite viewpoint to that of the acoustic analogy will be taken, where the source motion is considered much larger than the acoustic length scale, the relevant Mach number is high and the sound field, far from being a negligible by-product of a slow hydrodynamic motion itself constitutes the flow.

Sound is generated by unsteady flow, so that the relevant measure of time scale is that on which the flow changes $u/(\partial u/\partial t)$, u and $\partial u/\partial t$ being written for the characteristic magnitudes of particle velocity and its rate of change. If sound can cross the source motion in a small fraction of this time, then all points are effectively heard instantaneously and the source field is said to be compact. That is the limit treated by the usual acoustic analogy for aerodynamic sound generation. But if the flow changes in a time very much smaller than that required for sound to cross it, then different elements are heard independently and the source is said to be non-compact. The non-compact case corresponds therefore to extremely rapid rates of change in flow velocity the limiting case being that of an impulsive acceleration. We will review some aspects of impulsive motion and then examine their possible relevance to aerodynamic sound.

Consider first some low Mach number impulsive motions in which the velocity u changes discontinuously in a propagating wave across which the pressure rise is $\rho_0 u$, $(u=\int u\,dt)$. Any impulsively started boundary motion will cause such a wave field. For example G.I. Taylor (1942) showed that if a spherical body of density equal to that of the surrounding fluid were subject to an impulse, then one third of the energy imparted by that impulse would radiate as sound. Impulsively driven motions evidently induce sound fields in which the energy is comparable to that of the main flow. It is this feature that makes them extremely interesting within the aerodynamic noise content, their relevance being more obvious possibly from Longhorn's (1952) analysis. From that it is apparent that the energy shed into sound by an impulsively retarded motion is exactly the kinetic energy of the (non-radiating) flow previous to the deceleration. That is a 100% conversion efficiency of the energy of local fluid motion into a radiating sound. This sound production process falls within the category of aerodynamic noise. This view is by no means original though I am not aware of its previous publication. It has certainly been taken by Professor Lyon and colleagues at M.I.T. and W.R. Sears at Cornell. No energy is supplied by surface stresses. The abruptly halted boundary causes the previous local flow to be gradually rearranged and evolve into a sound field. Levine (1972) in a problem of diffraction radiation by steady sources passing rigid obstacles was able to show that all the energy in that part of the steady field disturbed by the obstacle was radiated as sound. Again there is a one to one correspondence between energy radiated in a transient event and that normally stored locally in the near field of a steadily moving source. It is as of the near field which at low Mach number is virtually uninfluenced by compressibility is poised to escape as sound if provoked sufficiently abruptly. Though all these problems involve linear low Mach number motion, it is my view that they give a strong clue to the energetics of all non-compact sources and that the high Mach number aerodynamic sound problems might well be approached quite differently from the low Mach number flows for which the acoustic analogy is helpful. Instead of assuming the source flow known and solving for the small acoustic by-product, one might regard the sound as the vehicle by which most of the energy of unsteady flow is lost provided only that the flow adjusts sufficiently abruptly. Since these motions are the most efficient sources of sound one could then concentrate on the modelling of specific transients in the flow. This point will be returned to later, but first we treat some specific low Mach number cases which help to point the way for the far more difficult high speed jet problem.

The principles involved in motions about abruptly halted boundary surfaces are very simple. Prior to the impulse there is a flow about the body and that flow of course implies a local distribution of kinetic energy. If now the boundary is stopped impulsively, then immediately following the impulse, the flow remains unaltered since information regarding the boundary motion has not yet propagated away from the surface. That information travels at the speed of sound, and the local motion will adjust to the new boundary conditions just as soon as sound has travelled over the flow to convey the news, and it is during this time that the flow is rearranged into a propagating field that transports all the energy to infinity. Viscous effects are negligible, because in the time sound has travelled at speed c over the flow scale l to effect the metamorphosis viscous diffusion has only affected that flow within a distance $\sqrt{\nu l/c}$ of the boundary which is only (the usually negligible fraction) $MR^{-\frac{1}{2}}$ of the complete flow, M and R being the Mach and Reynolds number respectively. The impulse initially affects only the layer to which sound has penetrated, and so long as this is very thin in comparison with the body curvature, the motion induced there is essentially that of a one dimensional wave in which the normal surface velocity jumps to zero from its pre-impulse value u say. This jump is accomplished by an initial pressure discontinuity $\rho_0 u$ which propagates away from the boundary its amplitude decaying in a manner determined by the ratio of distance travelled to the initial radius of curvature. For example the transmutation of the flow about a door slamming shut at a speed of 1/ft/sec. is accomplished by a pressure pulse of about 10^{-3} atmosphere, which is of the same magnitude as the overpressure in a sonicboom. This is the minimum sound field that an abruptly arrested door motion can make and is additional to the sound caused by any vibration that is energised from the kinetic energy of the door itself. The deceleration must be impulsive for this reasoning to apply. In practice this means that the door must be arrested in a time interval smaller than that taken for sound to travel through the disturbed flow, which extends around the body for about a foot or so. The door travels 10^{-3} ft in that time, so an impulsive deceleration is one accomplished within a distance of the order of 10^{-2} inches, a condition only marginally met with most domestic doors. More gradual deceleration processes are capable of absorbing at least some of the energy of the fluid motion so that the event will in general be very much quieter - which is an obviously appreciated everyday observation.

A second commonplace example of an impulsive source is provided by the sudden tensioning of an initially buckled cloth or paper. If in straightening, a length Δ

is taken up by the end motion at a separation velocity V say, then transverse motions over a distance of order Δ must be accomplished also at velocity V within the time Δ/V. These cease abruptly on the sudden tensioning of the material. More probably though the tensioning will generate a membrane capable of supporting transverse oscillations with a characteristic period T say. The flow will be arrested in a time of the order of that period during which sound can travel cT. Only when this dimension is small in comparison to the typical scale l of disturbed motion can this problem be considered impulsive in the sense treated here. The limit implies that the membrane wave speed is very much higher than the speed of sound in the surrounding fluid. The membrane can be arrested only when membrane waves have travelled its length to convey the information regarding the abrupt tensioning. These waves travel at speed l_{cm} say, the length of the membrane l in the period of natural motion $l/_{cm}=T$. Only when this is small compared to the time taken for sound to cross the disturbed area, i.e. $l/_{cm} \ll l/_{c}$, can the acoustic problem be considered truly impulsive, and this we see corresponds directly to the condition that the source region contains a natural velocity faster than the speed of sound. The equivalence of supersonic source phase velocities and impulsive conditions is thereby illustrated. The cracking of a whip is a similar case, where the effective sound radiation can be regarded as a result of either an impulsive tensioning of the whip or a consequence of the wave velocity in the whip reaching supersonic speeds. The two views are equivalent and it is this equivalence that makes the study of impulsive sound generation relevant to the understanding of noise sources associated with supersonic aerodynamic flows. Particle velocities need not be large in these high phase speed or effectively impulsive cases. In fact they must be small if the sonic problem is not to become one of unsteady strong shock waves. But even with abruptly decelerated low perturbation velocities, the acoustic field is very powerful. An acoustic pressure of order $\rho_0 cV$ is induced by the sudden tensioning of a membrane when its ends move apart with speed V as the kinetic energy of the induced flow prior to deceleration is converted into sound. Extremely high acoustic pressure transients are thus formed. The particle velocity in the induced wave is initially of the same order as V. Normal sound waves involve very low velocity levels. A velocity of 1 ft/sec corresponds to a sound of about 150 dB, so that it is easy to appreciate that extremely high levels of sound can be generated aerodynamically by the impulsive deceleration of bodies moving at modest speed. Very often the kinetic energy of the body is also dissipated as sound, passing initially into a mechanical vibration that is acoustically damped. That mechanical part is of course additional to energy provided by the fluid from its initial motion provided only that the velocity change is sufficiently abrupt.

The analogy between impulsively started flows and supersonic motion past thin bodies is of course a familiar one in aerodynamics. In fact the essential linearization involved there can be described as one of treating the perturbation as a weak impulse. Any particular fluid particle of a uniform stream at speed U is caused on 'impact' with the body to acquire a transverse velocity u, say, and to move parallel to the body surface inclined at an angle $\theta \approx u/U$ to the main stream direction. If the change is sufficiently abrupt, and it is provided the flow velocity is much greater than that of sound which cannot then propagate to warn the approaching fluid of imminent change, that change is effected by an impulse. The perturbation velocity $u \approx U\theta$ is consequently part of a wave field in which the pressure rises $\rho_0 cu$ or $\rho_0 cU\theta$, a familiar feature of linearised supersonic flow in which the pressure is determined by the inclination of the flow surface to the main stream direction. There too it is common experience that the energy transported away from the source by the wave field is of the same order as that available in the disturbed flow.

Two elements of a reasonably tractable modelling of an order one efficiency aerodynamic sound production process are therefore

1) weak disturbances around sources in supersonic convective motion and
2) weak disturbances of an abruptly accelerating motion.

Both these situations can be examined by linearised analysis and it is easily shown that they are quite different to those of compact aerodynamic sources in several important aspects, some of which are discussed below. Of course if the perturbations about the mean flow are strong, that is the unsteady velocities rise to near sonic, or even supersonic levels, then the turbulence is more aptly modelled as a random collection of shock waves. It is then pointless to attempt a study of how much sound that turbulence can generate. Rather one should enquire as to how the turbulence was generated by the co-alescence of strong shock waves, such as might result in a siren driven by extremely high pressure air which is split into a periodic assemblage of shocks by the shuttering action of the siren disc. That problem is obviously one in which the bulk of the energy is stored in a propagating wave field that eventually escapes from the region as sound.

Some jets, particularly high powered jets radiate an irregular rough noise often referred to as 'crackle'. There seems to be no observable distinction between the noise spectrum of a crackling jet and others, and the precise conditions necessary for the ingression of crackle are not at all well documented. Whether or not model jets crackle is still a matter of debate amongst research workers as is the entire question of how the phenomenon can be quantified and its cause isolated. There is certainly a common belief that crackle is an attribute of supersonic jets, and some believe it to be the hallmark of a reheated jet flow, but these beliefs seem to have no convincing foundation other than in the fact that supersonic reheated jets often do crackle. The phenomenon is distinctive subjectively and some feel it a particularly annoying feature of jet noise. It is therefore important and very likely to feature in future subjective measures of sound. My personal impression is that crackling is due to particularly

violent pressure transients that occur irregularly a few times per second. Indeed a careful study of the pressure variation at points where crackle is evident has indicated extremely large transients which may well be the cause of crackle. But it is by no means clear from where these transients originate. They have also been observed in the field of a model jet, though there the impression of crackle is not nearly as distinct.

The experimental observations seem to be as follows. The distribution of pressure in these crackling noises is such that there is a very much higher probability of large compressive pulses than there is of rarefaction. The narrow spiked compressive peaks occur a few times per second at full scale and contain a wide spectral distribution. They in fact display the properties of a non-linearly steepend wave. On the other hand the negative going pressure fluctuations are much weaker and of continuous wave form. The spikes are narrow enough that they seem not to contribute significantly to the energy of the sound, but that aspect is still a little confused since the transients are large enough to cause significant non linearities in the response of normally operated acoustic recording apparatus and may well have been imperfectly reproduced in the subsequent analysis. These experimental observations are therefore unconfirmed in detail but there can be no doubt that the positive spiky transients exist in some degree, and it is interesting to speculate regarding their origin. For this the acoustic analogy is not really helpful, nor indeed are any of the schemes that lead back to a pinpointing of the source in some turbulence motions only the statistics of which one could reasonably expect specified. These large transients must originate in a particularly effective discrete event, and for the reasons already outlined, that event is likely to be one in which the flow displays a distinct supersonic phase speed or adjusts to a new condition particularly abruptly. The latter is the more appealing since that would not only account for the high amplitude of the spikes, it would also fit in with the relatively short duration of the observed pressure peaks. But how can such transients occur and why are they inevitable compressive? Some characteristic non linearity is evident.

Non linear propagation could not distort the distribution about the mean, since the convective steepening is equally effective for both positive and negative pressure perturbations. The peaks are certainly big enough to suffer distortion during passage to traditional sound measuring stations but that is in this context a side issue, since it cannot begin to explain their origin. Neither can their predominantly compressive structure be explained by a weak transient source motion, which are all just as likely to generate expansive pulses as they are compressive waves. Their origin is more likely to lie in strongly non linear motion where convective steepening at the source flow concentrates shocks into intense propagating waves while associated unsteady expansions tend to disperse. There are several possibilities for such violent but infrequent transients.

The mixing flow is a chaotic bundle of vorticity which is continually becoming more convoluted as the turbulence cascades to smaller scale. The velocity field strains this turbulence deforming the vortex lines and occasionally the strain will be such as to straighten an initially buckled line. Further strain in the direction of the vorticity must spin up the vortex, and demand work from the straining motion on which it therefore exerts a tension. The abrupt tensioning of such a vortex line might well provide an impulsive source of sound.

Non linear limits on an instability wave might also act sufficiently rapidly that the change is impulsive and thereby an extremely efficient source of radiation. The mean jet flow is certainly unstable to small disturbances which grow presumably until their amplitude is big enough that the waves break into harmonics or are simply arrested. Both limiting processes might act once the particle displacement is a sizable fraction of either the jet diameter or of the instability wavelength. One might expect therefore instability waves to be fed gradually from the mean flow and to shed energy as their amplitude is arrested, the efficiency of that radiation process depending entirely on the time scale over which the change occurs. The mechanics of the deceleration might well be in fact that the surrounding potential flow builds up a compressive wave sufficiently strong to stop the growth. That view is suggested from observations of a shallow water layer jet generating surface waves in a close andogy with the aerodynamic sound problem (Prowse Williams and Hawkings, 1967; Webster, 1970; Prowse Williams, 1970). The main jet flow is sometimes observed to buckle and in doing so sheds powerful surface waves that radiate away from the flow. G.I. Taylor has pointed to the analogy of low Reynolds number jet flow stability criteria with those of the Euler strut to buckling loads. The main body of the turbulent jet might be regarded as low Reynolds number in the sense that turbulent diffusion transports momentum laterally as effectively as would a high viscous stress, and the mean flow might well display the same stability properties as the low Reynoldsnumber laminar jet. Indeed the shallow water jet buckles to generate waves very effectively, and the same is probably true of the turbulent air jet - though it will be some time yet before experimental techniques can confirm or disprove that hypothesis.

Crow and Champagne (1970) describe the coalescence of waves into an abruptly formed 'vortex puff' in another process that would inevitably lead to effective sound generation. Again if this occurs on a time scale smaller than that required for sound to cross the disturbed flow, the sound induced is best regarded as a direct propagation of the abruptly generated pressure into sound.

All of these motions are probably too complex for quantitative analytic modelling but they seem to me to be plausible enough that they form the basis for locating the

source of especially violent and significant waves, and should therefore be at least the subject of debate. It seems certain that quantitative modelling of unsteady flows will remain intractible for some time yet to all but the technologically trivial sources. If real jet flows are to be discussed at all that discussion will be confined as in the foregoing to speculative but plausible qualitative argument. But the idea that clues can be obtained by considering abrupt changes as the essential ingredient for sound production in the opposite extreme to that well modelled by the acoustic analogy for compact sources seems helpful.

Formally of course the acoustic analogy can be extended into the non-compact regime but the task of specifying the source properties can rarely be divorced from that of solving for the entire field. The interaction of the sound with mean flow gradients has to be considered and useful steps continue to be made though the modelling there is often too complex to give clear trends. The work of Phillips (1960) developed by Lilley (1964) and Pao show the emergence of ray theory in the asymptotically non-compact case. Again there the energy in the wave is to be determined locally and calls for a detailed modelling of the flow at the source, a problem that seems inextricably tied to that of compressible turbulence, (Crow, 1966). However the tendency for waves to radiate in the Mach wave direction, for their scale to be dictated by eddy length scales at high speed rather than by eddy frequencies, and for the wave strength to increase in proportion to the eddy lifetime are all predictable (Ffowcs Williams, 1963) and seem in general accord with experiment.

The analogy has also been extended to include surface effects at high speed (Ffowcs Williams and Hawkings, 1969) and to treat shock wave sources in a definite way (Farassat, 1973). But this work has yet to be applied directly to the important practical problem of noise generation by supersonic fans for example - though it is undoubtedly relevant to that problem. The obvious predictions of that theory indicate an important change in the physical source process at high speed. For example, it is the unsteady blade loads that generate the whine of low Mach number turbomachinery - but they can be shown to be utterly irrelevant at high Mach number, where surface pressure radiates away from the source in a manner independent of the instantaneous integral of that pressure which determines the blade loading. It is only when this and similar points have been properly appreciated that real progress can be made towards the minimization of supersonic rotor noise at source. This is an area deserving of detailed and careful analysis.

References

Cannell, P. and Ffowcs Williams, J.E. (1972), 'Radiation from line vortex filaments exhausting from a two-dimensional semi-infinitive duct'. J. Fluid Mech. 58 - 65.

Crighton, D.G. and Ffowcs Williams, J.E. (1968), 'Sound generation by turbulent two-phase flow'. J. Fluid Mech. 36, 585.

Crighton, D.G. (1971), 'Radiation from vortex filament motion near a half plane' J. Fluid Mech., 51, 357.

Crow, S.C. and Champagne, F.H. (1970), 'Orderly structure in jet turbulence'. J. Fluid Mech., 48, 547.

Crow, S.C. (1966), 'Aerodynamic sound emission as a singular perturbation problem'. U. Cal, Lawrence, Radiation Lab. UCRL - 70189.

Farrasat, F. (1973), 'The sound from rigid bodies in arbitrary motion'. Cornell University Ph.D. Thesis.

Ffowcs Williams, J.E. (1963), 'The noise from turbulence convected at high speed'. Phil. Trans. Roy. Soc. A, 255, 469.

Ffowcs Williams, J.E. and Hawkings, D.L. (1967), 'Shallow water wave generation by unsteady flow'. J. Fluid Mech. 31, 779.

Ffowcs Williams, J.E. and Hawkings, D.L. (1969) 'Sound generation by turbulence and surfaces in arbitrary motion'. Phil. Trans. Roy. Soc. A. 1151, Vol. 264.

Ffowcs Williams, J.E. (1970), 'Aeronautical acoustics as a problem in applied mathematics'. Inaugural Lecture, Imperial College.

Levine, M. (1972), 'Diffractions radiation'. Chp. 4 in Papers on Novel Aerodynamic noise source mechanisms at low jet speeds. A.R.C. C.P. No. 1195.

Lighthill, M.J. (1952), 'On sound generated aerodynamically (1) General Theory'. Proc. Roy. Soc. A. 211, 564.

Lilley, G.M. (1964), 'A review of pressure fluctuations in turbulent boundary layers at subsonic and supersonic speeds'. Archivum Mechaniki Stosowanej 2, 16.

Longhorn, A.L. (1952), 'The unsteady subsonic motion of a sphere in a compressible inviscid fluid'. Quart. Journ. Mech. and App. Maths., Vol. V, pt. 1.

Phillips, O.M. (1960), 'On the generation of sound by supersonic turbulent shear layers'. J. Fluid. Mech. 1, 1 - 28.

Taylor, G.I. (1942), 'The motion of a body in water when subjected to a sudden impulse'. Page 300, Vol. III, The scientific papers of G.I. Taylor, C.U.P.

Webster, R.B. (1970), 'Jet noise simulation on shallow water'. J. Fluid Mech. 40, 2.

APPENDIX TO PAPER 1

Oral Script of the Introductory Review Lecture

IMPULSIVE SOURCES OF AERODYNAMIC SOUND

by

J.E. Ffowcs Williams
University Engineering Laboratory,
Cambridge, England.

It was just over ten years ago that AGARD organised in this city a Specialist Meeting on the Mechanism of Noise Generation in turbulent flow. It was then ten years since Lighthill's pioneering papers had given the subject a sound theoretical footing. The highlight of that Meeting was Lighthill's presentation of the jet noise lecture he had given to the American Institute of Aeronautics and Astronautics as the 1963 Wright Brothers Lecture. There he described how his general theory had been extended to high supersonic speeds and how it had been compared in detail with experimental measurements of jet noise. That comparison seemed very satisfactory.

In 1954, Lighthill had assumed, without conclusive experimental evidence, that sound producing turbulent eddies in a jet flow would be convected downstream, and that eddy convection would have a pronounced effect on the noise characteristics. It would tend to amplify the sound radiated downstream and attenuate, though to a lesser extent, the upstream sound (Figure 1). Figure 13 of Lighthill's lecture compared the predicted directionality resulting from eddy convection with that measured on model air jets. There was no doubt that eddy convection was a real effect and papers by Wills, Bradshaw, Ferris and Johnson, Kolpin and Mollo-Christensen, all presented at the Specialist Meeting, provided extremely comprehensive documentation of the variation of eddy convection speed with jet conditions and position in the flow.

Eddy convection increases the acoustic output of turbulence above the basic 8th power law. Lighthill in his figure 15,(Figure 2) showed that experiments indicated close agreement with the 8th power law, an agreement that he argued was due to two competing effects. The amplification caused by eddy convection compensated exactly for the tendency for turbulence to become relatively less intense with increasing jet Mach number. In fact, Lighthill said, without the convective amplification the basic dependence of jet noise on velocity is closer to the 6th power than the 8th. Where convective amplification is absent, at 90 degrees to the jet axis, the measured velocity dependence in the experimental data then available, was closer to six than eight.

Lighthill concluded his lecture on the note that the theory required very little modification to account for most of the experimentally measured features of jet noise. Noise was caused by turbulence and measurements in the sound producing regions of the subsonic jet indicated that the position was that depicted in his figure 6 (Figure 3). Eddies that are thin in comparison with the size of the shear layer, seemed sound to be generated at a constant rate per unit length of the early jet mixing region. In the fully developed jet the acoustic output per unit length of jet scales on the inverse 6th power of distance from the nozzle axis.

Lighthill's lecture was the only one devoted to radiated jet noise at that Specialist Meeting held here ten years ago. There seemed to be a consensus that Lighthill's theory had provided the last word on jet noise and it was now up to the turbulence workers to

measure and understand and change! the turbulence stress tensor identified as the source sound. Since very little is, or probably ever will be, known about turbulence that was rather a depressing point of view, indicating that a general reduction in exhaust speeds was the only reasonable method of jet noise reduction.

Two voices put a slightly different view. Professor Mollo-Christensen regarded the attempts to make the noise fields different from axisymmetric as a promising avenue for further work. In view of what you will hear of the development of the Concorde silencer this remark seems somewhat prophetic, as do some of Alan Powell's statements on that occasion. He was advocating then that the basic elements of sound generation might well be modelled effectively by considering extremely simple unsteady flows, such as those produced by the mutual interaction of concentrated vortices. He also made the point that flow instability was at the root of aerodynamic noise sources. He said that the mean flow instability is the cause of flow breakdown into noise producing turbulence and also, that unstable flow is capable of amplifying any sound with which it interacts.

Much of the development in the last ten years has been along those lines. And a great deal has happened in that ten years, not the least of which is the evolution of the von Karman Institute out of the training centre for experimental aerodynamics!

On the aircraft noise front the biggest change has been brought about by the engineering feasibility of large by-pass ratio engines which exhaust far less kinetic energy per lb of thrust than their pure jet counterparts. This led to a natural de-emphasis of jet noise and a significant improvement in operating economics!

But in the last ten years aircraft noise has become a very much more important issue and is now one of the dominant design features for new aircraft types. Certification rules have been introduced to control their noise and there is every indication that technology will allow a realistic tightening of those regulations and might even lead eventually to the elimination of the aircraft noise nuisance.

The study of jet noise went into a decline about ten years ago as the emphasis moved onto the new noise sources in the high powered turbo-machinery of the large fan-jet engine. That machinery is contained within a cowling, so that there is opportunity to absorb the sound before it escapes to the surrounding atmosphere. The development of surface coating materials, with good sound absorption properties when mounted in an engine environment, has been one of the major recent advances. This step alone is capable of reducing the turbo-machinery noise of an aircraft by between 10 and 20 decibels, sufficient in fact to reveal the previously hidden jet noise. Even with these new fan jet engines, further silencing is dependent on control of jet noise, this time from jets with a relatively low jet velocity.

In the last ten years also there has been an enormous investment in the long range transport fleet. The increasing pressure to alleviate the noise nuisance has led to a search for means of suppressing the noise of the first generation low by-pass ratio jets, and this again has led to a re-emphasis of jet noise, still a major feature of those engines at take-off power. The need here is to devise some silencer that can be added retrospectively to existing aircraft. By controlling their noise, the benefits of the quiet new-technology engines might be felt before the older aircraft are eventually phased out of service.

But the biggest spurt by far to the jet noise control field has come with the advent of the supersonic transport aircraft: that needs a high exhaust velocity, high specific thrust engine. The kinetic energy abandoned in the exhaust flow of a typical supersonic transport during take-off is as much as that lost if a large ocean liner were to fall 100 ft!

A great deal has happened too on the fundamental side and the picture as we now understand it is quite radically different from that depicted by Lighthill ten years ago. In addition to those sources well modelled by the 1963 status of his theory there are new, then unexpected, features which we now see as being crucial. Also it now seems that some of the data used by Lighthill as a basis for checking the theory was misleading, particularly regarding the sound measured at 90 degrees to the jet axis. Modern experiments are performed with cleaner aerodynamic flows and better equipment than they were ten years ago and there seems now to be no doubt that the noise at 90° to the axis of a jet emerging from a steady reservoir scales on the 8th power of velocity, in precise agreement with the basic form of the Lighthill theory (figure 4). It seems therefore that those aspects of the turbulence responsible for the generation of noise do not lose their relative strength with increasing jet Mach number. The reason why the radiated acoustic energy scales so closely on the 8th power of velocity, dispite the amplifying effect of convective eddy motion, is conclusively shown by Lush to be due to a basic breakdown of that convective amplification at high frequencies close to the jet axis. The simple predictions of the convective quadrupole theory are not found there. The frequency of the eddying motion and of the sound it generates, should increase in proportion to jet velocity. Also, because of eddy motion the sound heard ahead is further increased in frequency by the Doppler effect which is at its greatest in the direction close to the jet axis. But a close examination of the experimental data led Lush (figure 5) to point out that this was quite contrary to experience, though at 90° to the axis the spectrum showed the predicted Strouhal dependence on velocity (figure 6). Lush concluded that the sound radiated at 90° was of pure Lighthillian origin but that other effects neglected in the simple modelling must be dominant at high frequencies close to the jet axis. In fact Lush found himself agreeing with Csanady's point of view that convective amplification becomes irrelevant for those sources sufficiently embedded in a flow relative to which they do not convect. Whenever a moving source is shielded by a wave-length or so of moving fluid, its radiation is determined in the local environment relative to which it is static and is quite different from that radiated by a moving eddy in a static environment.

Convective quadrupole theory predicts that the sound radiated close to the jet axis should tend, with increasing jet speed, to increasingly high frequency when measured relative to that at 90° which is immune from the Doppler effect. Lush showed that this prediction is the exact opposite of the trend he measured experimentally (figure 7). Part of the reason for this is that there are at least two identifiable sources of jet noise one of which radiates at higher frequency to high angles. Both these sources will no doubt be subject to refraction and this process has been quantified by Ribner. But for effective refraction the sources must be embedded within the basic jet flow and the sound must propagate across the shear layer. It is difficult to satisfactorily reconcile the conflicting requirements on source location for both convective amplification and refraction to occur simultaneously. For one the source must be deep inside the layer so that the sound propagates out across the gradient, and for the other, the source must be in direct contact with the ambient medium so that the field is effectively that generated by a source travelling through a uniform static environment.

It was about ten years ago that a second important source of jet noise was first recognised. Practical jet pipe flows are turbulent and that turbulence must induce an unsteady mass flow through the nozzle and an unsteady thrust. For low frequency sound, that is sound with wavelength long in comparison with the nozzle diameter, the equivalent monopoles and dipoles associated with these effects are more efficient than the jet quadrupoles and one would expect them to dominate the radiation field. Since the ratio of source scale to wavelength increases with decreasing Mach number these nozzle based sources must be dominant at low jet velocities. This idea was studied

experimentally by Gordon. I reproduce here (figure 8) his experimental curve, published in 1964, showing how the basic jet noise is supplemented by a dipole, and eventually a monopole, which takes over at sufficiently high jet pipe turbulence levels. It seems now that the sixth power velocity dependence of the noise at 90^{o}, quoted by Lighthill in the Wright Brothers Lecture, was generated by such an additional noise source. It was not until sufficiently smooth jet exhaust flows were studied that the basic jet mixing noise was observed in the relatively quieter regions of the jet noise field.

This noise, additional to the jet mixing noise, tends now to be called the excess noise and is the area on which much of the recent jet noise research has been concentrated. This is because it is the principal noise of the modern low specific thrust engine and becuase it is also a dominant feature of the high specific thrust engine at some important operational conditions. Jet mixing noise is highly attenuated by a flight reduction in relative jet velocity. Also jet mixing sources do seem to be amenable to novel suppression methods, and even the static noise field of some high velocity jets appear to be dominated by sources other than jet mixing.

The term excess noise of course covers a multitude of sources, in fact anything additional to that thought to be associated with jet mixing. Unsteady combustion processes and random turbulence within an engine are potential sources of sound. They should be amenable to absorption, and jet pipe sound attenuating liners are becoming standard items of noise control. The turbulence interacting with the nozzle to cause unsteady variation of mass flow and momentum is not so easily controlled. Neither are the mechanics of sound production easily understood. In the practically important regimes the Mach number, the parameter assumed small in the theoretical modelling, is barely small enough to make the modelling relevant.

But even when the model is relevant the problem is not straightforward. I have mentioned how turbulence can cause an unsteady variation of mass flow. But in fact the mass flow will only vary if the fluid inside the jet is sufficiently compliant to allow the internal volumetric change necessary to satisfy the unsteady outlet condition. When this problem is worked out in detail, it is seen that the monopole is essentially weak and the theoretical indications are that it radiates a sound proportional to the sixth power of velocity and not the fourth that is associated with unconstrained aerodynamic monopoles.

But a lower velocity dependence than six is certainly a feature of the experimental data, and this has led to a substantial theoretical search for more efficient sound generating mechanisms associated with the interaction of flow with surfaces of the type that might model a jet exhaust structure. This now is an entirely new development from Lighthill's free quadrupole model, but it rests firmly on Lighthill's theory. The work is aimed at understanding how the radiation of quadrupoles is influenced by the proximity of boundary surfaces. It has become clear that the interaction of turbulence with the sharp edge of a rigid screen accounts for a very substantial additional sound source. Crighton and Leppington have shown that this process does not depend on the detailed edge geometry but rather on the existence of a large screen. Leppington has also shown that this source survives the presence of a second screen, thus modelling the exhaust from a two-dimensional duct. But it is not found near the opening of a parallel circular pipe. There the edge scattering mechanism accounts for the production of sound which scales on the sixth power of jet velocity. In fact that sound is equivalent to an unsteady nozzle based dipole, supplemented by an essentially weaker monopole, representing the reluctantly driven unsteady mass flux from the system.

As part of this theoretical study Levine produced a theory of diffraction radiation in which he described the sound radiated by a steady monopole, dipole or quadrupole moving uniformly with subsonic speed passed a scattering edge. In the absence of a

scatterer the steady non-pulsatile source generates no radiated field. Levine showed that all the potential energy stored in that part of the field subjected to the influence of the edge was in fact transformed by the scattering process into a radiating wave. There seems no doubt therefore that turbulence near sharp-edged scattering surfaces represents a potentially efficient source of sound production.

Now all the problems I have described so far ignore any interaction of sound with the mean flow and its gradient. Such interaction has also been subject to substantial recent theoretical activity. That work is not based on the Lighthill model but rather it seeks to describe with analytical precision the detailed structure of particularly simple perturbations of a modal jet flow. That flow is of course unstable, and if perturbed, disturbances will grow on the jet and generate noise. Its amplitude is uncontained on linear theory. Such instability waves can provide explicitly defined unsteady flow who's interaction with simple scattering surfaces is amenable to analysis. Crighton has studied the problem of sound generation by an unsteady shear layer shed from a semi-infinite screen that initially separates the two flows; also from a semi-infinite duct modelling a jet pipe. This time the radiated sound is influenced by conditions at the sharp edge and Crighton has shown how the scattering efficiency is increased by the imposition of a Kutta condition at the nozzle boundary. The velocity dependence of the sound field is as low as three in some cases. In that work Crighton has argued that even if the emerging nozzle flow were to start off smoothly, the instabilities in the jet would eventually act back on the nozzle and drive in it an unsteady exhaust flow. The radiated sound so produced is described by the unsteady mass and momentum flux induced at the nozzle by the shear layer disturbances.

Looking back on the 1963 Meeting it is remarkable how close this development parallels the thoughts then expressed by Alan Powell. Instabilities are shown to be important as is the insight to be gained by examining in detail those unsteady flows sufficiently simple to admit analytic description. At that Meeting Powell had suggested that the sound radiated by a pair of spinning vortices was one such tractable flow and he outlined a calculation indicating how their sound scaled on the eighth power of velocity. Four years later, Müller and Obermeier analysed this problem by the method of matched asymptotic expansion. That scheme offers an alternative analytical approach to the Lighthill formalism. They found that that sound did not scale on the eighth power of velocity but on the seventh and this seventh power was shown later, by the Lighthill method, to be a general law describing two dimensional aerodynamic sound. It has been shown since, that the one dimensional radiation generated by turbulence scales on the sixth power of velocity. This would be the field radiated in, for example, a long pipe by contained turbulence at sufficiently low Mach number. But the two dimensional problem has more relevance in that it also describes the generation of surface waves on a shallow layer of water excited by unsteady flow. This makes possible the simulation of aerodynamic noise sources in an easily visualized water-table analogue.

The advent of Concorde and the research commissioned by the Anglo-French team has thrown new emphasis on jets with extremely high exhaust velocities. The exhaust speed of the Concorde jet at take-off exceeds by a large factor those jets that have been extensively studied in University Laboratories. Such speeds are only obtainable with hot jets not readily available in the traditional centres of jet noise research. University workers were therefore encouraged to co-operate with the industrial teams in a search for a new jet noise suppression concept. This study has led to some departure of our current modelling of high speed jet sources from those described by Lighthill in the Wright Brothers' Lecture. The jet speed is sufficiently high that the mixing layer eddies convect downstream faster than the speed of sound in the ambient medium for at least 15 diameters of the flow. The sound radiated by such eddies tends to collect in the form of ballistic shocks that radiate away from the jet,

principally in the direction of the eddy Mach angle. The scale of the sound wave is exactly the same as the scale of the eddy that produced it, so that it is possible, by observing the directionality and frequency content of the distant sound field, to infer the convection speed and scale of the dominant sound producing eddies. This work was reported in the Journal of Fluid Mechanics in 1970. It has been found that the main noise sources of the unsuppressed circular high speed jet lie some ten to fifteen diameters downstream of the nozzle, in eddying motion whose scale is about twice that of the local shear layer thickness. Evidently noise is not generated by the main energy containing eddies but by the more deterministic large eddy structure that may well be far more amenable to control. That interpretation is quite different from the one made by Lighthill (figure 3) based on low speed measurements of jet turbulence, and in fact leads to the de-emphasis of the importance of the bulk of turbulence as a source of noise. It also leads one to speculate as to the possible origin of the very large scale eddying motion. Many now believe them to be the early instability products of the mean flow, which eventually break up to form the chaotic turbulence. This view leads one to suppose that their characteristics might well be similar to those of the principal jet instability mode, the jet being regarded as a low Reynold's number laminar flow. The mean velocity distribution is certainly very like that in a low Reynolds number laminar flow, the role of the turbulence being to diffuse momentum in a manner effectively equivalent to a high molecular viscosity. We continue the analogy further and seek now the origin of the large scale sound producing eddies in the instability of the equivalent low Reynolds number laminar flow. G.I. Taylor has shown that such instability has much in common with the instability of the Euler strut. He has drawn the analogy between the compressive buckling of a strut and the buckling of a low Reynolds number jet column. G.I. pointed out that it is easy to experiment with this flow; one does it every time honey is allowed to drop off a spoon onto a slice of toast! The column oscillates on impact with the toast. Those oscillations are the instabilities of the primary jet.

We can look to the shallow water analogue for a simulation of this effect and I show you here (figure 9) a photograph taken of shallow water waves being generated by a jet containing large scale instabilities of the type that might well model the high speed jet noise problem.

This linking of the important sources with the large scale eddies that may well be driven directly from the instability of the primary flow suggests that the source strength would be changed along with a modification of the mean flow stability characteristics. Crighton has shown how an elliptically cross-sectioned jet contained within a vortex sheet has quite different instability characteristics from the round jet. As the aspect ratio of the ellipse is increased, transverse waves are inhibited and the jet takes on some of the characteristics of the two-dimensional jet that is prone to a flapping oscillation. We shall hear from Koch and Hawkins how fishtailed jets have remarkable jet noise attenuation properties in the plane of the fishtail, but some are liable to make much more noise in the transverse plane. This idea is not inconsistent with the view that it is a modification of the large eddy structure, consequent upon a change of jet stability, that is the cause of this change.

Other effects may also be important in those 'fishtail' flows. Maybe the sound generated by turbulence is unable to propagate in the plane of the fishtail and is refracted out of it. Or it may be that the important noise sources are contained in the jet interior and that the extensive fishtail flow shields them from the environment so inhibiting the convective amplification. But whatever the explanation the sound in the previously most important jet noise direction is controlled, and controlled by factor in excess of 10 decibels placing the emphasis for further noise control on a suppression of the sound radiated to high angles. As we have already seen, that sound sometimes differs considerably from what we think is jet mixing noise, and may well fall in the excess noise category in the most important practical applications.

There seems no doubt that these suppression devices that rely on some asymmetry of the flow provide a significant advance in the control of high speed jet noise, (figure 10) and it is interesting to look back to the comments made by Mollo-Christensen at the Meeting ten years ago, when he anticipated that such effects might well be present and exploitable.

We shall hear also from Koch and Hawkins how the noise of one jet can be effectively shielded by a much quieter jet, and this is probably an important principle that has yet to be exploited in a practical design. A Rolls Royce experiment, in which a small triangular jet exhausting a thin lamina containing less than ten per cent of the mass flow, produced an attenuation of the order of 10 decibels in the shielded direction. I show here (figure 11) the field of a conical nozzle at a pressure ratio of 3, with and without the auxiliary jet, and it will be seen that there is a very useful attenuation effect waiting to be exploited.

There can be no doubt from experiments such as these, that the interaction of either the source, or the sound, (or both) with mean flow is an essential consideration which must be mastered before the jet noise problem is adequately understood. The recognition of this led Phillips in 1960 to reformulate the aerodynamic noise problem and model it, not as Lighthill has done by an equivalent set of waves propagating in an ideal acoustic medium, but as a driven system of waves natural to the motion of the mean flow. In this way, by specifically taking account of the variable wave propagation characteristics Phillips' approach contains a potential advantage over the Lighthill model, an advantage that should become more and more obvious as the frequency of sound increases, as it inevitably must at high enough Mach number. We heard Professor Lilley describe at the 1964 Specialist Meeting an application of this theory to the pressure fluctuations under a turbulent boundary layer. This form of analysis has been the subject of extensive recent investigation by Lilley and by Pao. It is obvious that the approach is more complex and more difficult to understand, and, because of that, general consequences of the model are hard to elicite from the theory. But these are early days and I look forward with interest to hearing of Professor Lilley's recent research later in this meeting. Initially at any rate, that theory must be tested on the flows with the simplest velocity distribution, such as the parallel plane shear layer or the parallel circular jet. One would hope though, that the essence of the changes brought about by the incorporation of mean flow effects can be distilled in a sufficiently compact way, that their implications for flows of novel cross-sectional shape can be stated in a way that can lead to distinct design principles. It is certain that those principles would have to be applied to jets of odd geometry, for it is already established that the circular jet is far too noisy to be of general technological interest!

That brings me now to the advertised programme. That concerns the aerodynamics of impulsive sound sources. I include them here because I believe they form an important constituent of high speed jet noise. I show you here (figure 12) the time history of the pressure radiated into the distant field by the Olympus 593 engine operating at high power. You will see that the signal has a distinctive bias towards high amplitude positive short duration peaks. These peaks are the dominant feature of this sound signal and I think that they are now narrow enough to be transients. Furthermore, and this is the important point, they seem to have a sufficiently distinctive shape that they might be modelled by some definite deterministic feature of the source flow, and need not be categorised as random products of turbulence. I think it is the isolation of events such as these, in the experimental procedure known as conditional sampling, that has lead to the very significant recent advances in our understanding of turbulence. Important elements of turbulent flow have a relatively deterministic structure once they are properly viewed! but when everything is viewed simultaneously the signal is confusing and can only be treated statistically. By concentrating on the largest

distinct event one stands a reasonable chance of understanding its origin. Because the 'spikes' are big they are clearly an important item of the jet noise field - possibly the most important item.

Now these spikes arise only at high power conditions, or, more specifically, at high jet velocities. They are found in model jets, and Laufer and Schlinker have observed them on a model jet produced by an extremely smooth electrically heated nozzle flow. They make a further important observation: that is, that the tendency for the signal to be dominanted by spikes is accentuated if the signal is obtained by means of a reflecting telescope focussed at about 10 diameters downstream of the nozzle. This indicates quite clearly that the spikes have their origin in the mixing jet flow and not in some spurious unsteady engine exhaust condition.

I now show you a sequence of noise data taken on the Olympus 593 engine at Rolls Royce as the engine power is progressively increased. (figures 13 to 19). At low power the signal is quite evenly distributed about the positive and negative side. The power spectral density of the signal is shown on the figure as is the probability density. The skewness factor, you will see, is at a low value. As the power is progressively increased a tendency for positive spikes seems to evolve. There is no distinctive change to be seen in the power spectral density but the probability analysis shows an increasing tendency to a skew form. In fact, through the sequence of figures the skewness factor increases monotonically. The dependence of the skewness factor on the jet velocity is shown in figure 20.

The spike formation has a subjective significance too. I would like you now to listen to recordings of the sound depicted on the preceding sequence of diagrams.

As the power is increased and the spikes become evident, the tone becomes harsher, not dissimilar to the sound produced by the tearing of paper, (figure 21) and I think it may well be a contributor to the annoyance of the sound.

The question I now want to address myself to is what type of source mechanism could be responsible for the production or formation of these spikes? I will take the view that they are produced by definite transient events in the jet flow. I do not think they could arise from non-linear propagation effects. This is because non-linear propagation tends to distort the phase of the signal and alter its wave form in a basically symmetrical manner. One can't be certain of this, of course, because the problem of non-linear noise propagation, even though it is described in a definite way by Burger's equation, is still too complicated to work out in detail. But the qualitative trends are probably similar to those known to exist for harmonic waves which evolve into a perfectly regular N wave system symmetric about the positive and negative side. Also non-linear propagation effects tend to distort the phase of the waves, the large amplitude elements travelling faster than the low, and this would inevitably lead to a loss of correlation between the sound heard close to the jet and that heard far away. In fact, when these spikes are heard the correlation between near and far field is remarkably high, as is shown in the next figure, (figure 22) where a correlation coefficient of 50% is measured between the sound five diameters away from the jet axis and 10 diameters downstream of the nozzle and the far field sound measured more than 50 diameters away from the jet. That correlation exhibits a peculiar quality in that it oscillates with a relatively high correlation at separations very much greater than the characteristic period of the signal. This is extremely suggestive of the loss of low frequency information, though of course, if the sound were generated by a conventional quadrupole, there could be no energy at the lowest frequencies. This point is emphasized by a comparison with a synthetic signal, generated by a random sequence of Gaussian pulses, from which the lowest frequency elements have been deliberately removed. The auto correlation of that synthetic signal is shown here, (figure 23). The characteristic undulation at large

time delay is very suggestive of the data measured on the real engine.

We have a clue then that it is not productive to try to explain the origin of these spikes through any quadrupole source model. They are probably generated by far more efficient methods of sound production. Of course, the aerodynamic sources are quadrupole and this is only reconciled with the foregoing view when it is admitted that the quadrupole strength may well depend on details of the radiation field. In other words there may be a significant back-reaction of the field on the flow whenever particularly efficient generating processes are involved. This effect is wholly additional to the way aerodynamic noise theory is conventionally applied.

Sound is generated by unsteady flow, so that the relevant measure of time scale is that on which the flow changes, that is the ratio of the particle velocity to its acceleration. If sound can cross the source in a small fraction of this time, then all points are effectively heard instantaneously and the source field is said to be compact. That is the limit treated by the usual acoustic analogy for aerodynamic sound generation. But if the flow changes in a time very much smaller than that required for sound to cross it, then different elements are heard independently and the source is said to be non-compact. The non-compact case corresponds therefore to extremely rapid rates of change in flow velocity the limiting case being that of an impulsive acceleration. Such cases form extremely efficient sources of aerodynamic sound.

Consider, for example, the sound generated by flows about impulsively arrested bodies. The principles involved are very simple. Prior to the impulse there is a flow about the body and that flow of course implies a local distribution of kinetic energy. If now the boundary is stopped impulsively, then immediately following the impulse, the flow remains unaltered since information regarding the boundary motion has not yet propagated away from the surface. That information travels at the speed of sound, and the local motion will adjust to the new boundary conditions just as soon as sound has travelled over the flow to convey the news, and it is during that time that the flow is rearranged into a propagating field that transports all the energy to infinity. Viscous effects are negligible, because in the time sound has travelled at speed c over the flow scale l to effect the metamorphosis viscous diffusion has only affected that flow within a distance $\sqrt{\nu l/c}$ of the boundary which is only (the usually negligible fraction) $M^{\frac{1}{2}}R^{-\frac{1}{2}}$ of the complete flow, M and R being the Mach and Reynolds number respectively. The impulse initially affects only the layer to which sound has penetrated, and so long as this is very thin in comparison with the body curvature, the motion induced there is essentially that of a one dimensional wave in which the normal surface velocity jumps to zero from its pre-impulse value u say. This jump is accomplished by an initial pressure discontinuity ρcu which propagates away from the boundary, its amplitude decaying in a manner determined by the ratio of distance travelled to the initial radius of curvature. For example the transmutation of the flow about a door slamming shut at a speed of 1/ft/sec. is accomplished by a pressure pulse of about 10^{-3} atmosphere, which is of the same magnitude as the overpressure in a sonic boom.

Large transients must originate in particularly effective discrete events, and for the reasons already outlined, those events are likely to be cases in which the flow displays a distinct supersonic phase speed or adjusts to a new condition particularly abruptly. This would not only account for the high amplitude of the spikes, it would also fit in with the relatively short duration of the observed pressure peaks. But how can such transients occur and why are they inevitably compressive? Their origin is likely to lie in strongly non-linear motion where convective steepening at the source concentrates waves into intense propagating shocks while associated unsteady expansions tend to disperse. There are several possibilities for such violent but infrequent transients.

Mixing flow is a chaotic bundle of vorticity which is continually becoming more convoluted as the turbulence cascades to smaller scale. The velocity field strains this turbulence deforming the vortex lines and occasionally the strain will be such as to straighten an initially buckled line. Further strain in the direction of the vorticity must spin up the vortex, and demand work from the straining motion on which it therefore exerts a tension. The abrupt tensioning of such a vortex line might well provide an impulsive source of sound, - analogous possibly to the sudden tensioning of a string, or sheet of paper.

Non linear limits on an instability wave might also act sufficiently rapidly that the change is effectively impulsive. The mean jet flow is certainly unstable to small disturbances which grow presumably until their amplitude is big enough that the waves break into harmonics, or are simply arrested. Both limiting processes might act once the particle displacement is a sizable fraction of either the jet diameter or of the instability wavelength. One might expect therefore instability waves to be fed gradually from the mean flow but to shed their energy abruptly as their amplitude is arrested, the efficiency of that radiation process depending entirely on the time scale over which the change occurs. The mechanics of the deceleration might well be in fact that the surrounding potential flow builds up a compressive wave sufficiently strong to stop the growth.

Crow and Champagne (1970) describe the coalescence of waves into an abruptly forced 'vortex puff' in another process that would inevitably lead to effective sound generation. Again if this occurs on a time scale smaller than that required for sound to cross the disturbed flow, the sound induced is best regarded as a direct propagation of the abruptly generated pressure into sound.

The vortex pairing process we shall hear Professor Laufer describe is another abrupt motion that might again support impulsive sources. The non-linearity of the problem there seems capable of inducing sudden changes to the otherwise steady downstream vortex drift.

All of these motions are probably too complex for quantitative analytic modelling but they seem to me to be plausible enough that they form the basis for locating the source of especially violent and significant waves, and should therefore be at least the subject of debate. It seems certain that quantitative modelling of unsteady flows will remain intractible for some time yet for all but the technologically trivial sources. If real jet flows are to be discussed at all that discussion will be confined as in the foregoing to speculative but plausible qualitative argument. For that, the idea that clues can be obtained by considering abrupt changes as the essential ingredient for sound production in the opposite extreme to that well modelled by the acoustic analogy for compact sources might well prove helpful.

Much of the material included here is known to the author through his association with Rolls-Royce (1971) Ltd and his involvement in their high speed jet noise research programme. Some of it is of a preliminary nature. The author acknowledges the enthusiastic support of the Rolls - Royce Directors in allowing publication of this data.

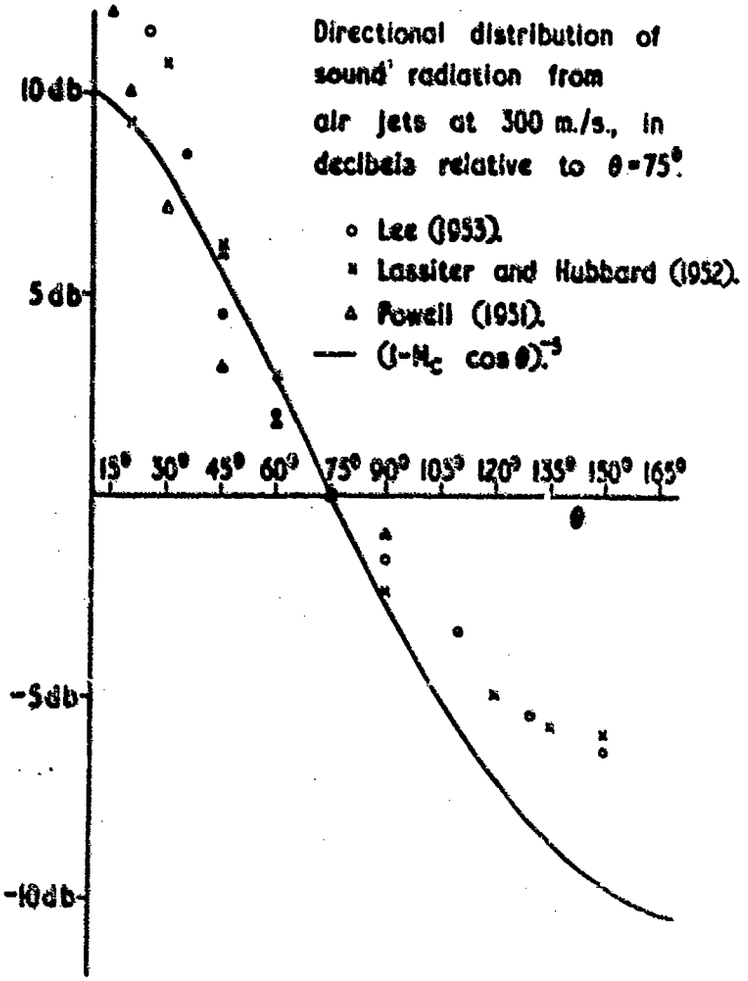

Fig.1 (Fig.13 of Lighthill's paper showing the convective amplification effect)

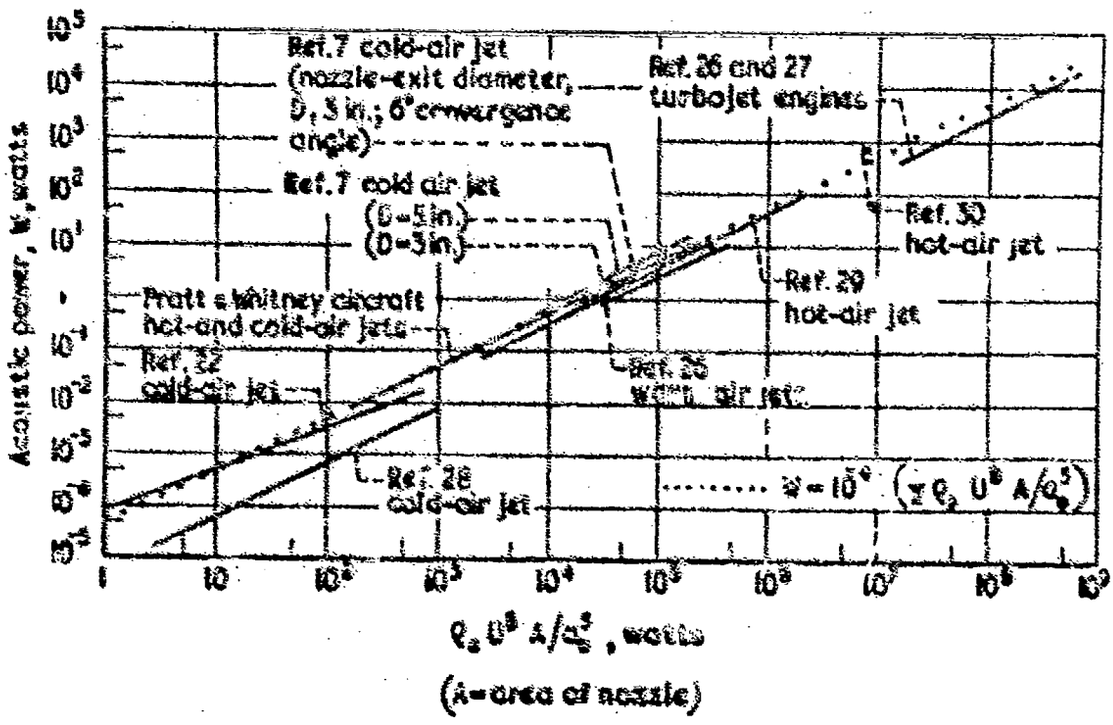

Fig.2 (Fig.15 of Lighthill's paper showing the experimental verification of 8th power law)

Stationary cold jet.

Measurements at Mach number 0·3 and Reynolds number 6×10^5 (Laurence 1956).

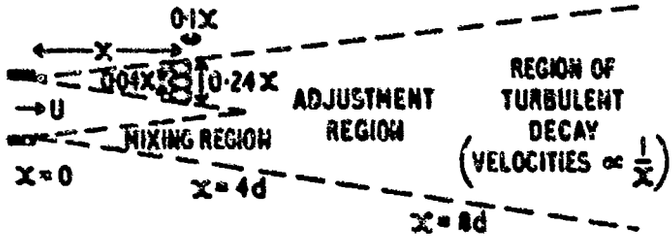

in mixing region { r.m.s. velocity reaches maximum ≃ 0·14U
where mean velocity ≃ 0·5U

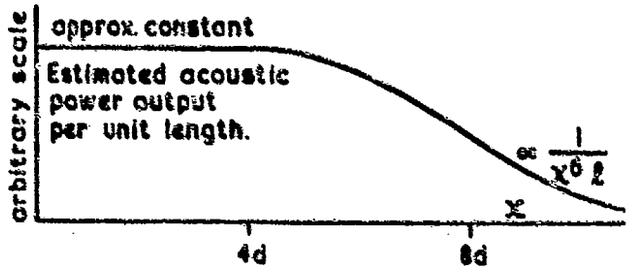

Fig.3 (Fig.6 of Lighthill's paper depicting the characteristics of the sound producing eddies in a jet)

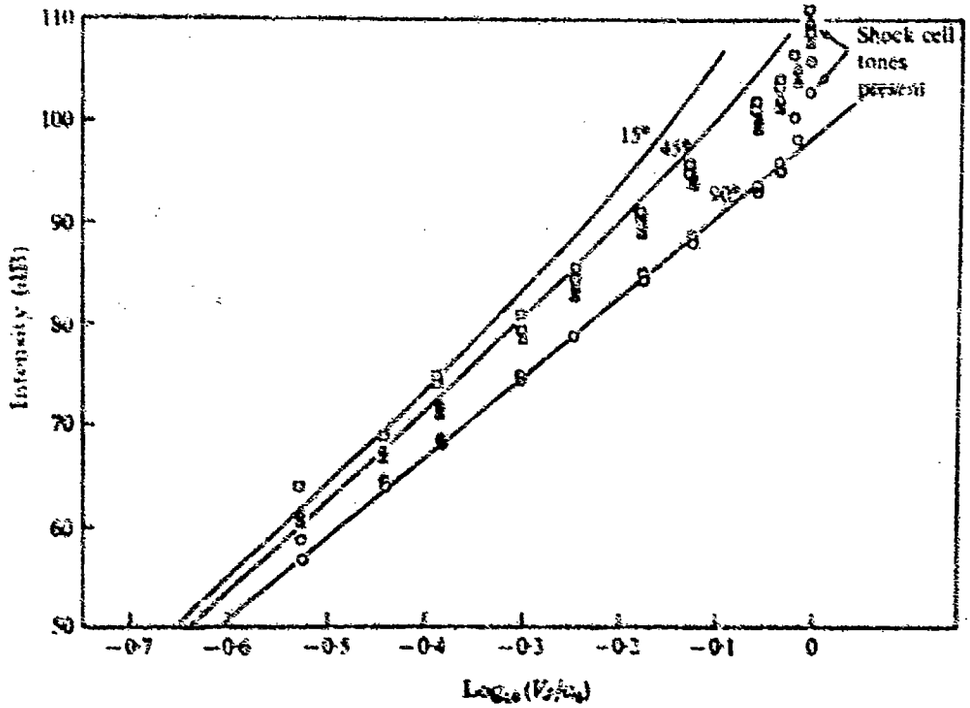

Velocity dependence of intensity compared with theory.
□, 15°; △, 45°; ○, 90°; ——, theory, equation (1).

Fig.4 Lush's experimental data showing the 8th power law at 90°

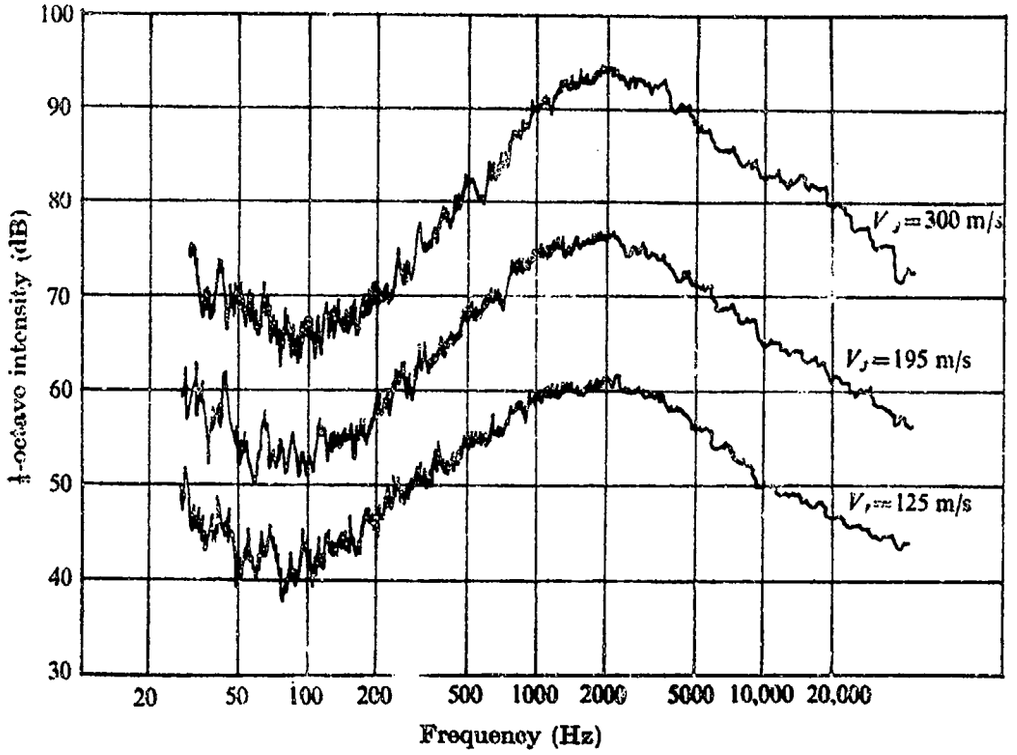

1/3-octave spectra at 15° for various jet velocities.

Fig.5 Lush's data showing the breakdown of the convective amplication effect close to the jet axis

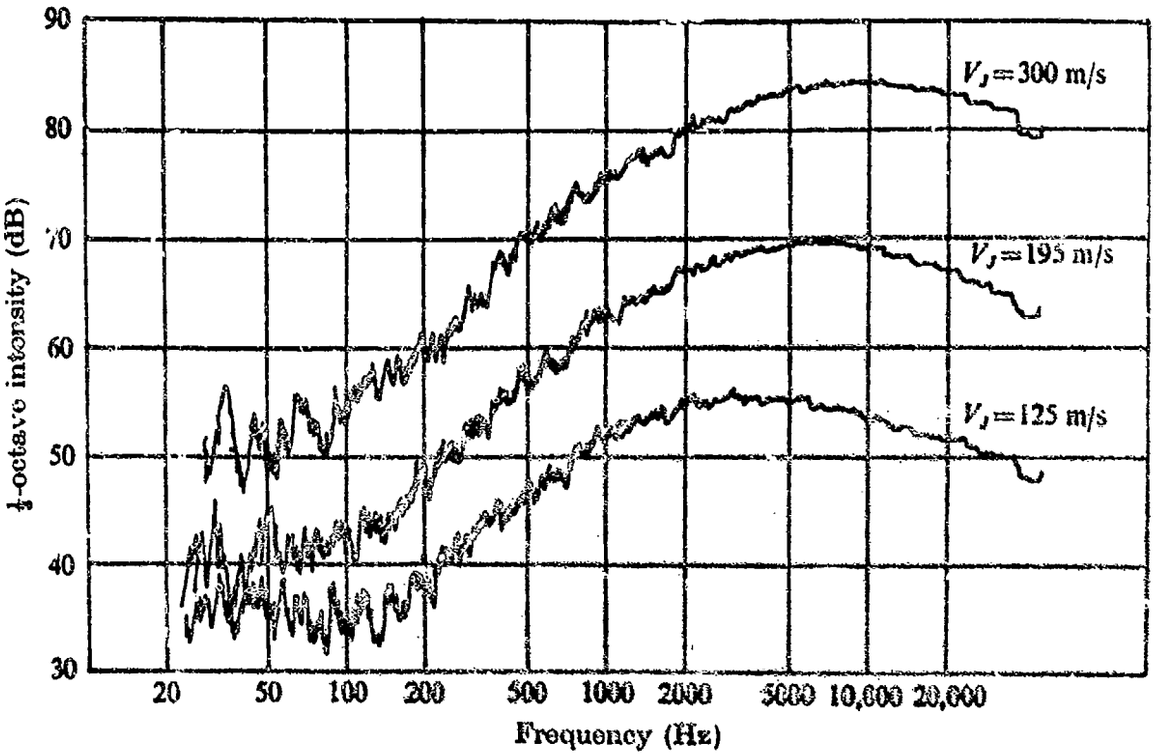

1/3-octave spectra at 90° for various jet velocities.

Fig.6 Lush's data showing the predicted Strouhal number dependance of the sound at 90°

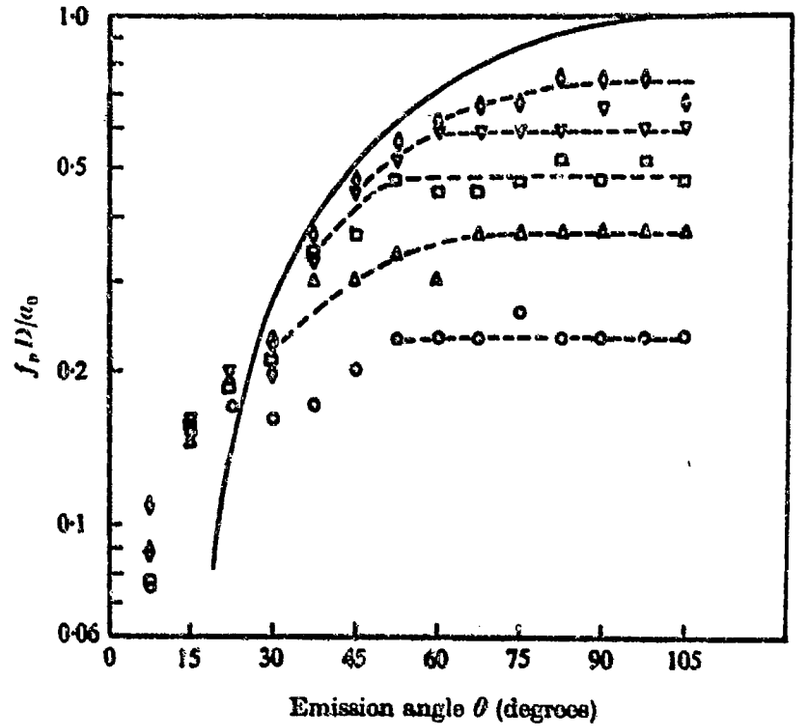

Variation of peak frequency, $f_p D/a_0$, with emission angle compared with theory. V_J/a_0: ○, 0·30; △, 0·41; □, 0·57; ▽, 0·75; ◇, 0·87; ——, theory, equation (16).

Fig.7 Lush's data showing the variation of the frequency with angular position

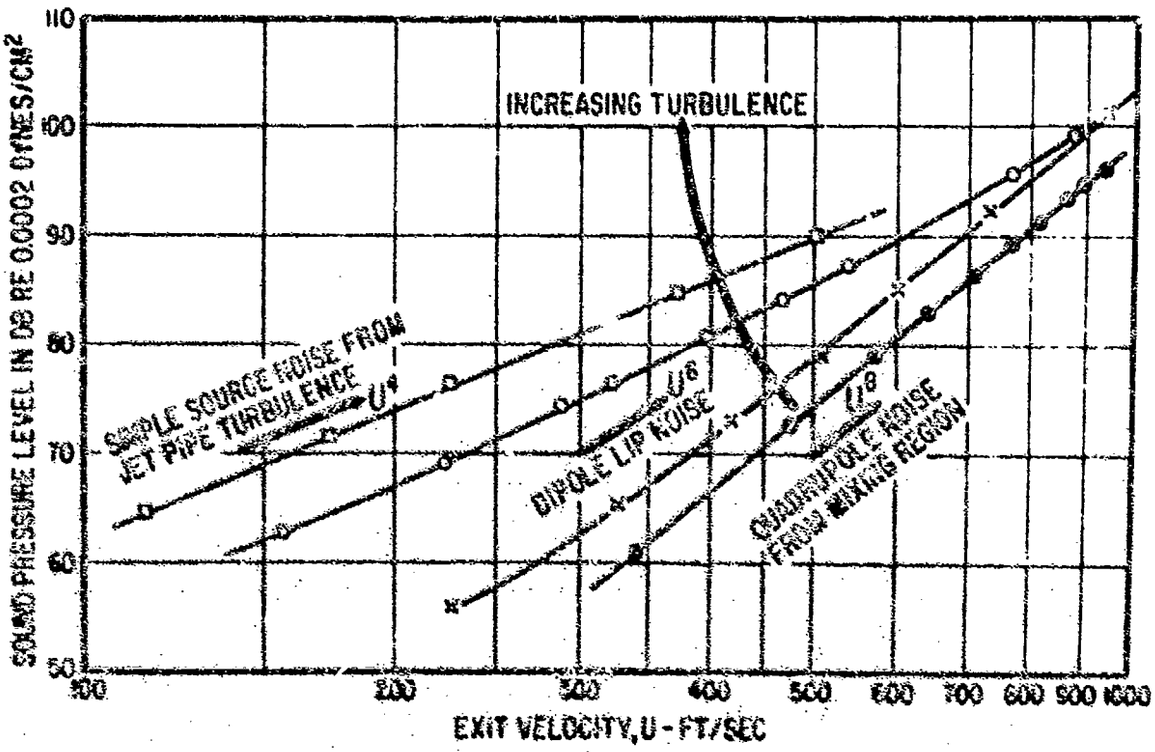

Effect of jet turbulence upon radiated noise.

Fig.8 Experimental data indicating the presence of laterally induced monopole and dipole sources of jet noise. Published by Phowcs Williams and Gordon in 1964.

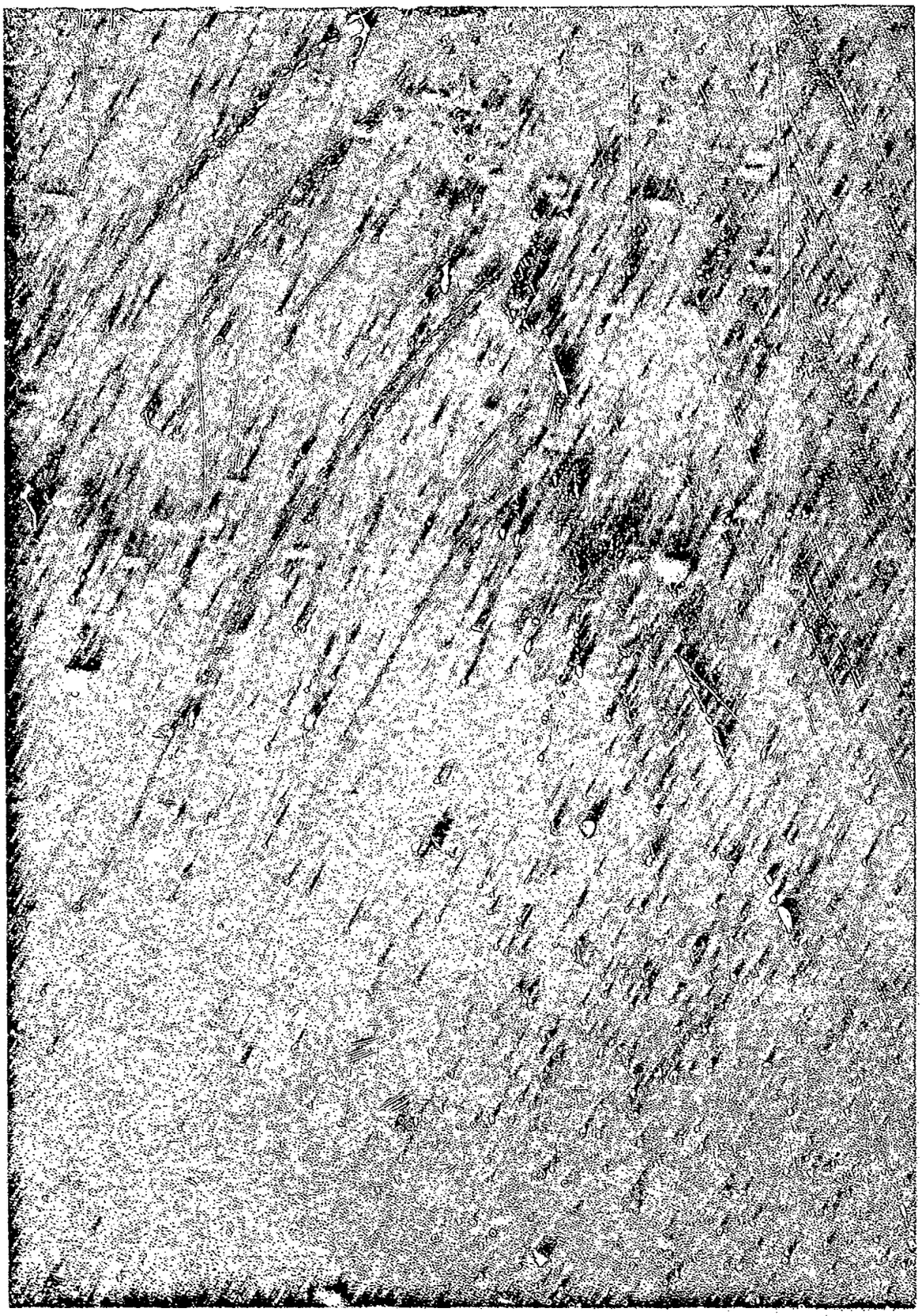

Fig.9 A shallow water simulation of jet noise showing large scale jet instabilities to be the source of particularly strong waves

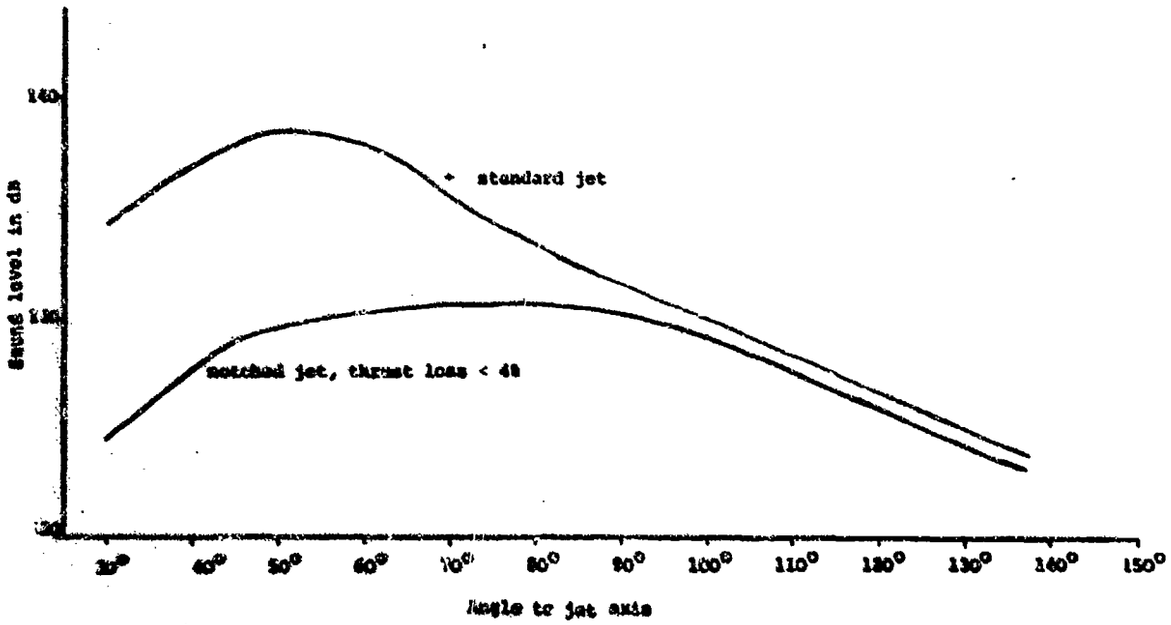

Comparison of the noise produced by a "fish tailed jet" with that of a standard round jet at a pressure ratio of 3.25 and jet temperature 1100°K.

Fig.10 A curve showing a typical suppression of high speed jet noise that is produced by Rolls Royce in a fish tailed jet

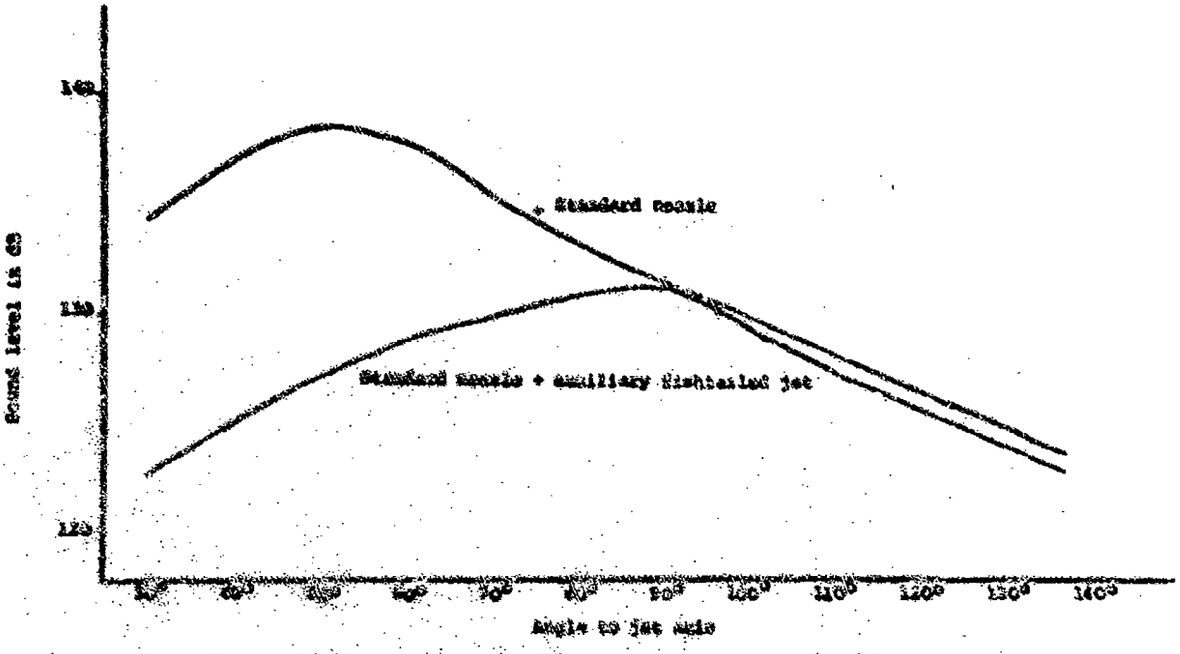

Comparison of the noise produced by a "shielded" jet with that of the bare jet at pressure ratio 3.25 and temperature 1100°K.

Fig.11 Rolls Royce experimental data showing the shielding characteristics of a small fish tailed fan

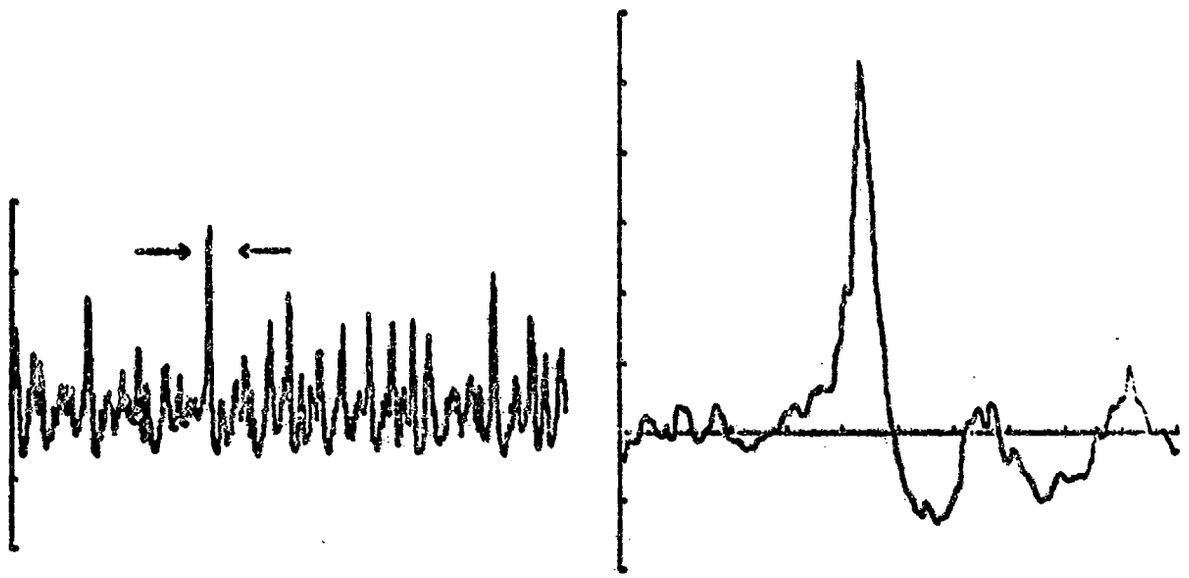

A 100 millisecond sample

A ten millisecond sample

Fig.12 A typical sample of the temporal pressure variation measured in the far noise field of the Olympus engine at high power showing the characteristic bias towards positive short-duration large amplitude pressure transients. The signal is shown on two time scales, the second segment being that indicated between the arrows on the first.

Figures 13 to 19. Rolls Royce data showing Time History of the radiated pressure together with its power spectral density, probability distribution and Skewness factor.

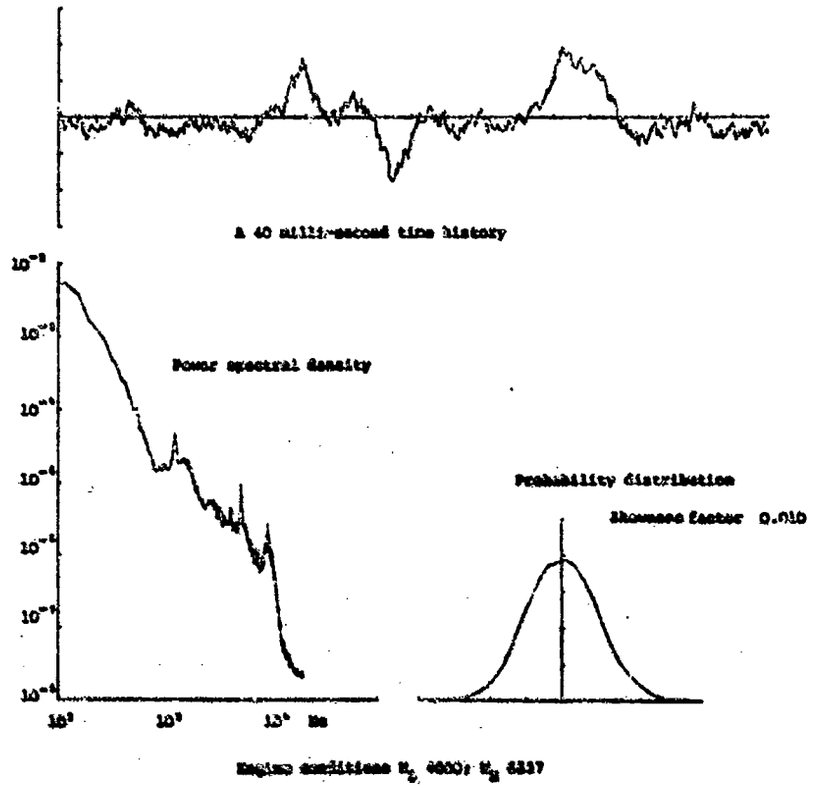

Figure 13

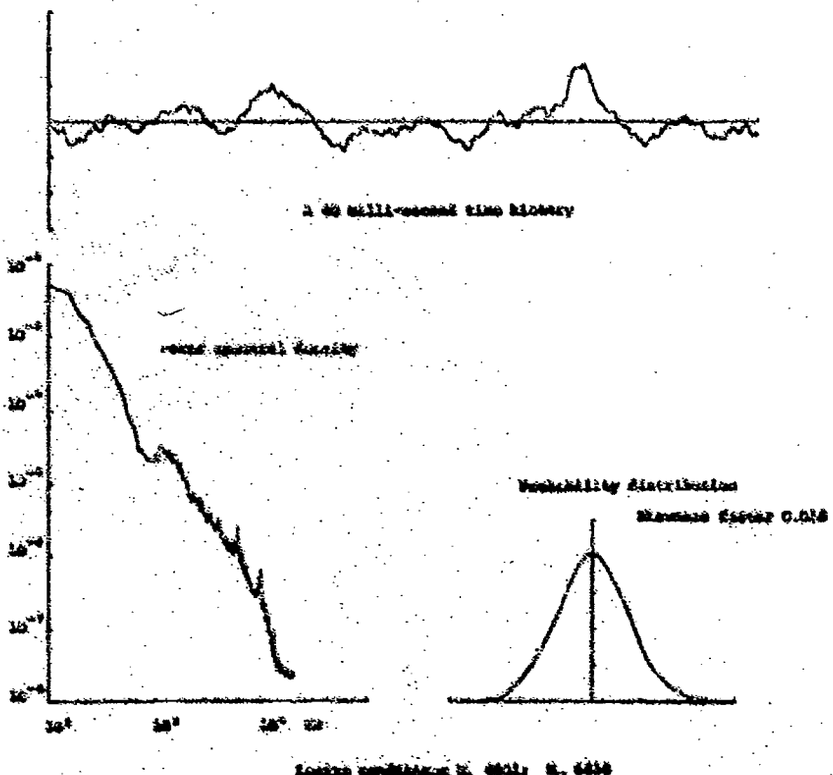

Figure 14

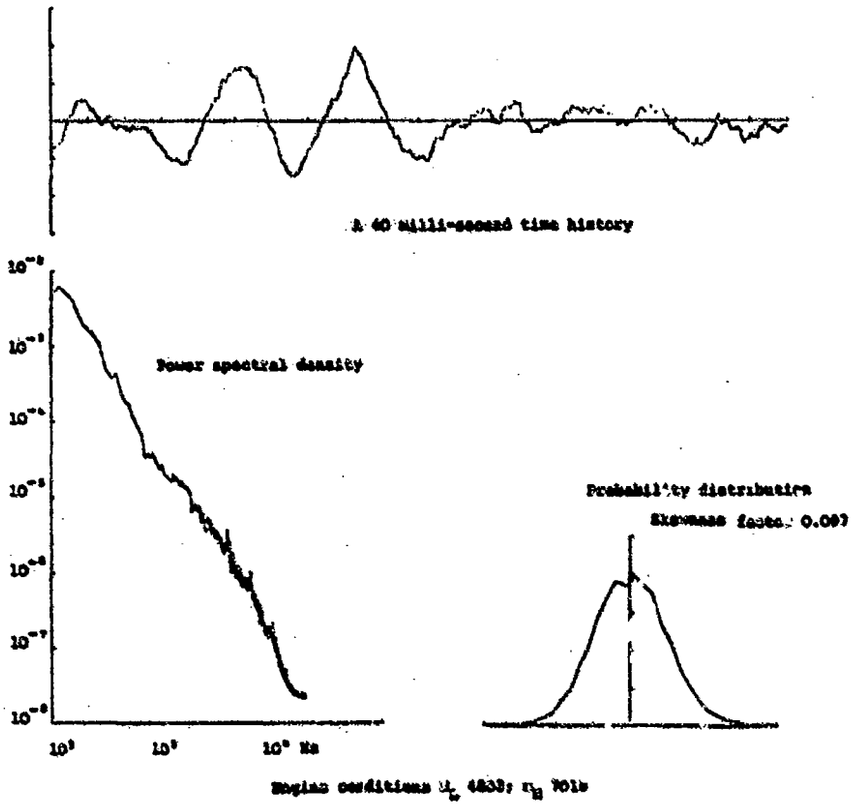

Figure 15

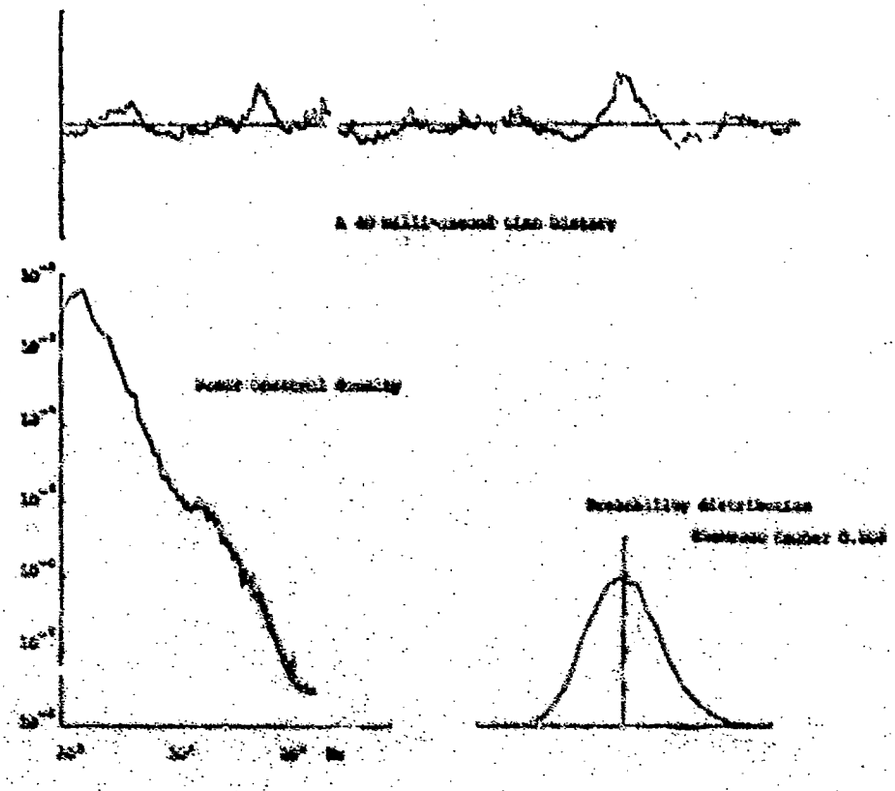

Figure 16

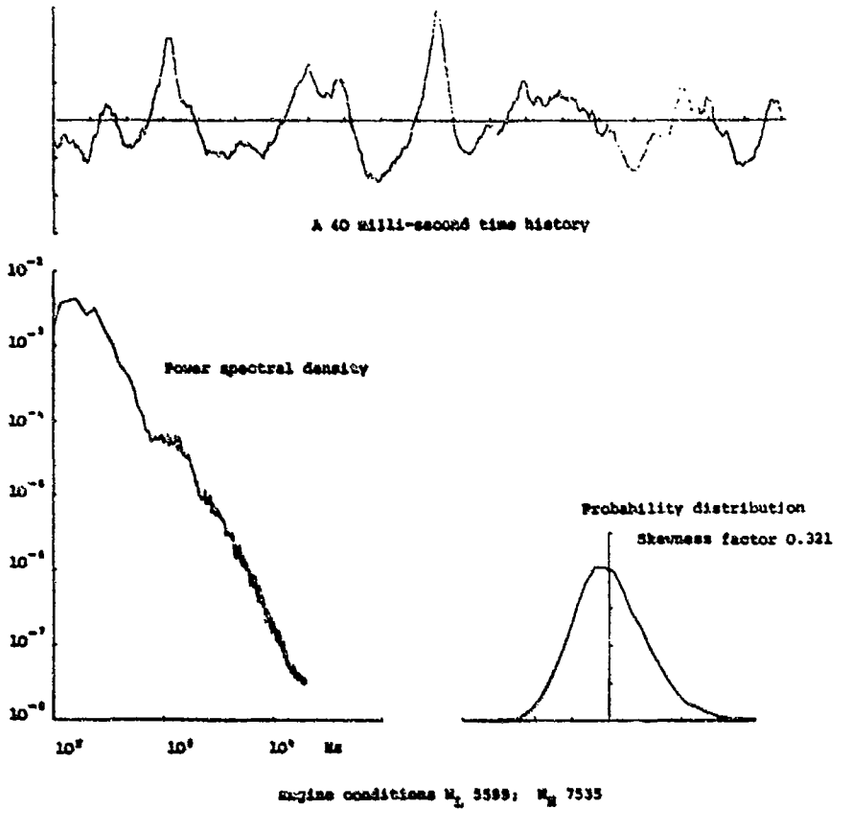

Engine conditions N_1 5599; N_2 7535

Figure 17

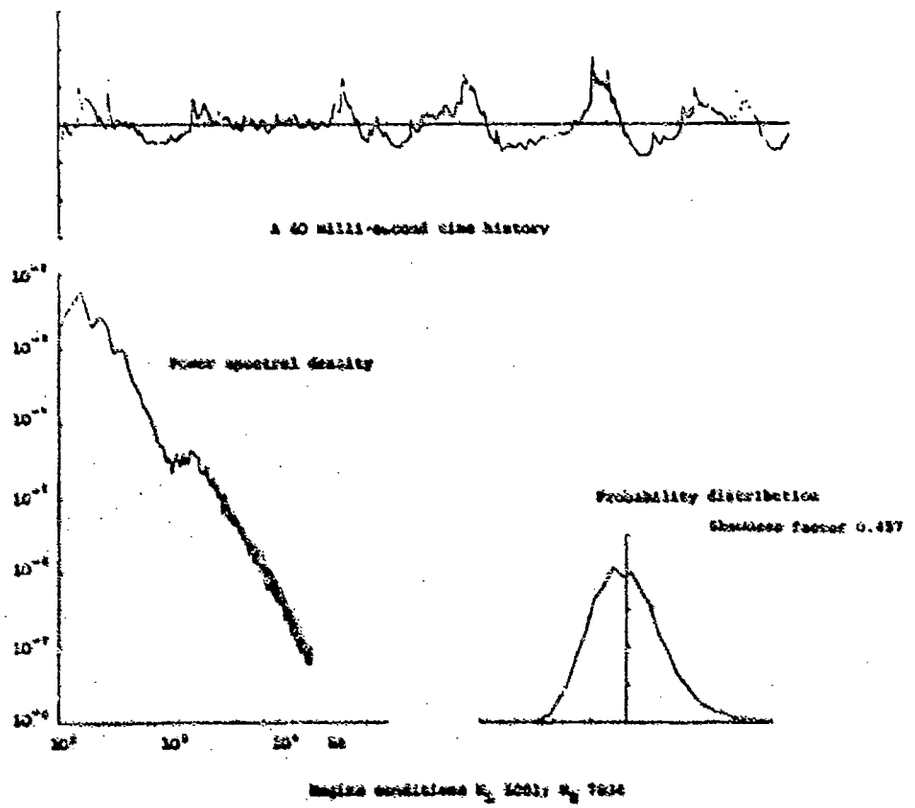

Engine conditions N_1 5081; N_2 7634

Figure 18

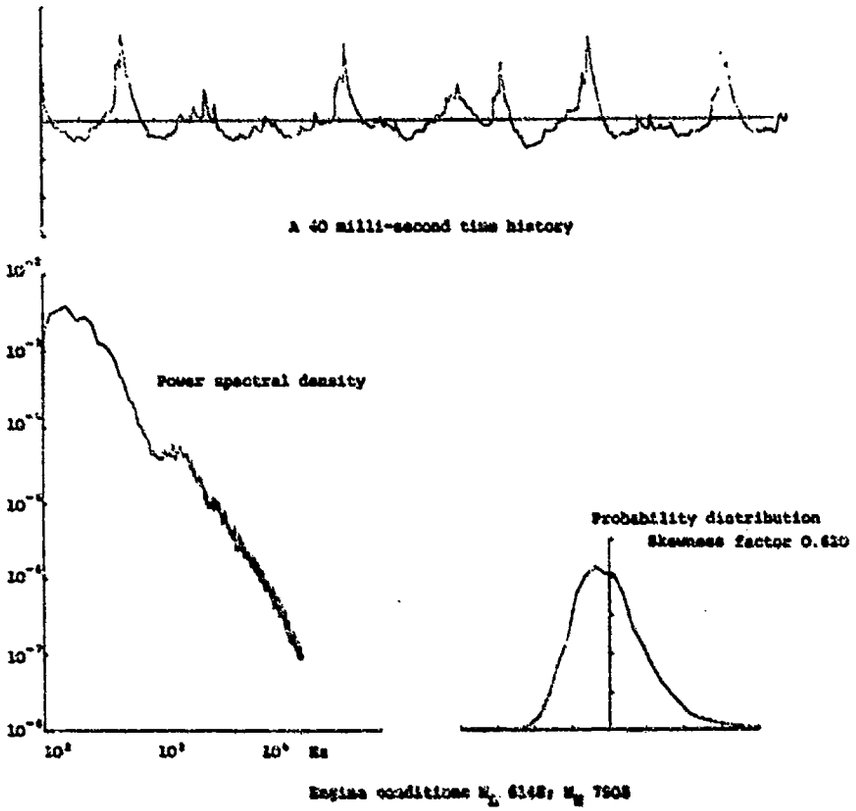

Engine conditions N_L 6148; N_H 7908

Figure 19

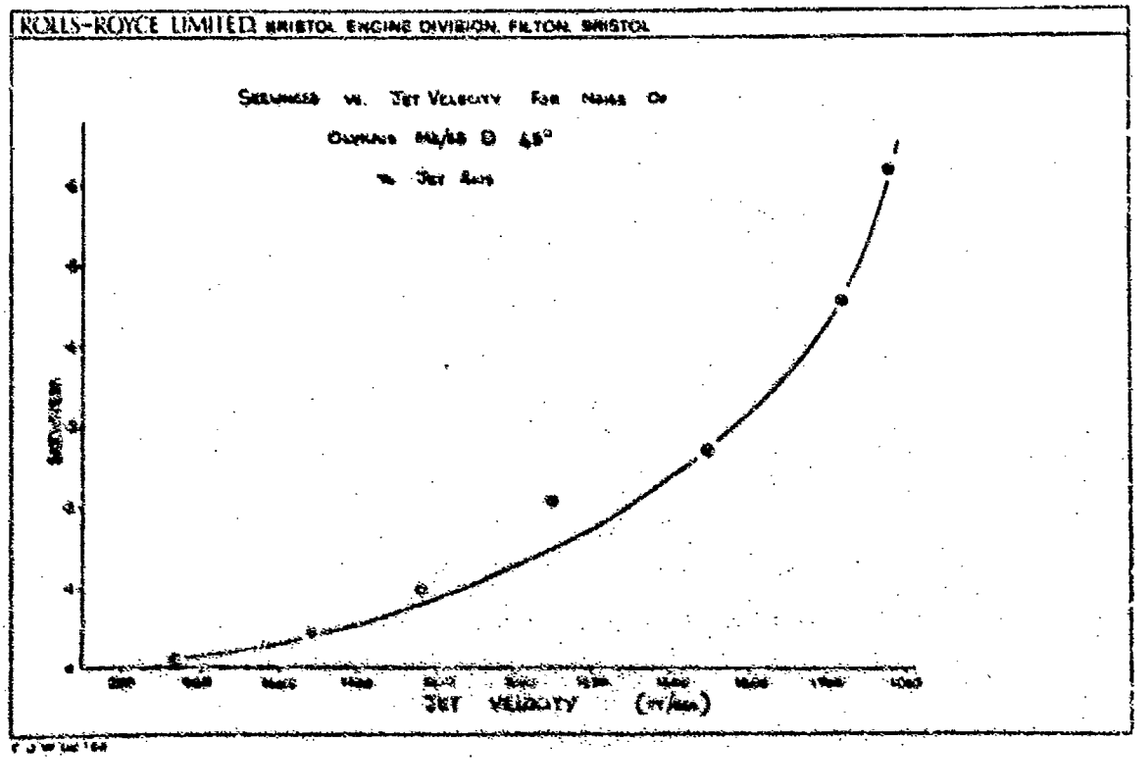

Fig.20 The variation of Skewness factor with jet velocity for the data shown in Figures 13 to 19

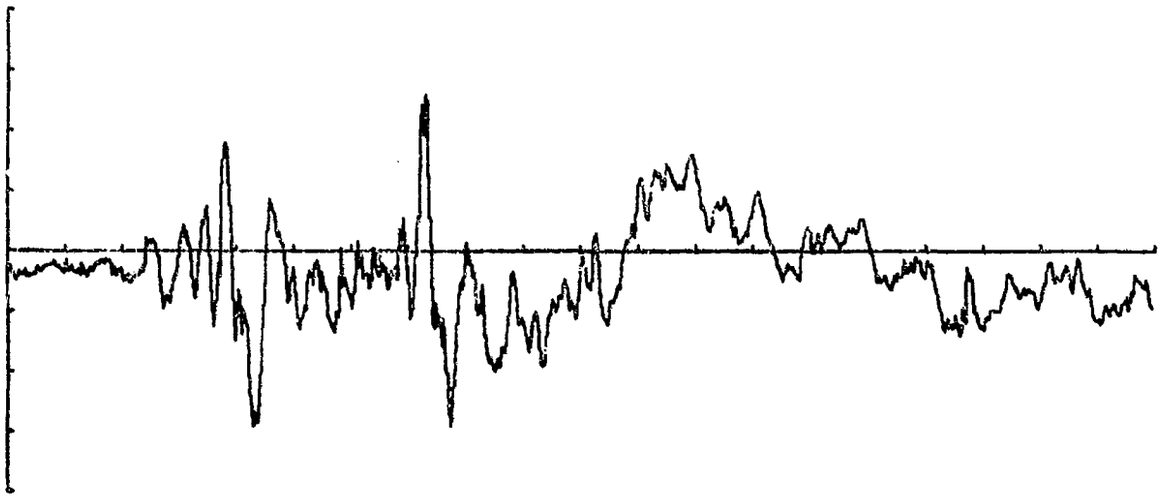

Fig.21 A 20 millisecond sample of the sound pressure radiated by tearing paper

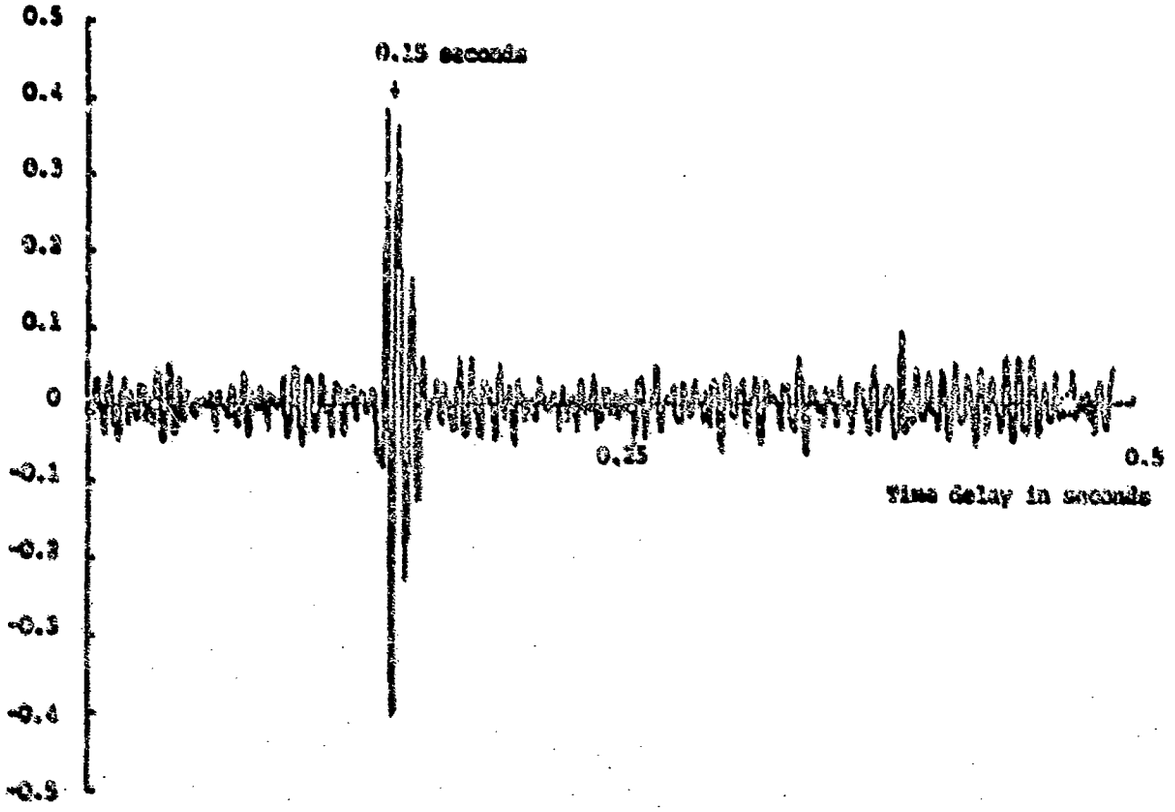

Fig.22 Cross correlation coefficient of the sound radiated by the Olympus 593 engine at high power. The field is measured at two positions one 5 diameters from the axis and 10 diameters downstream of the nozzle and the other is more than 50 diameters away from the jet.

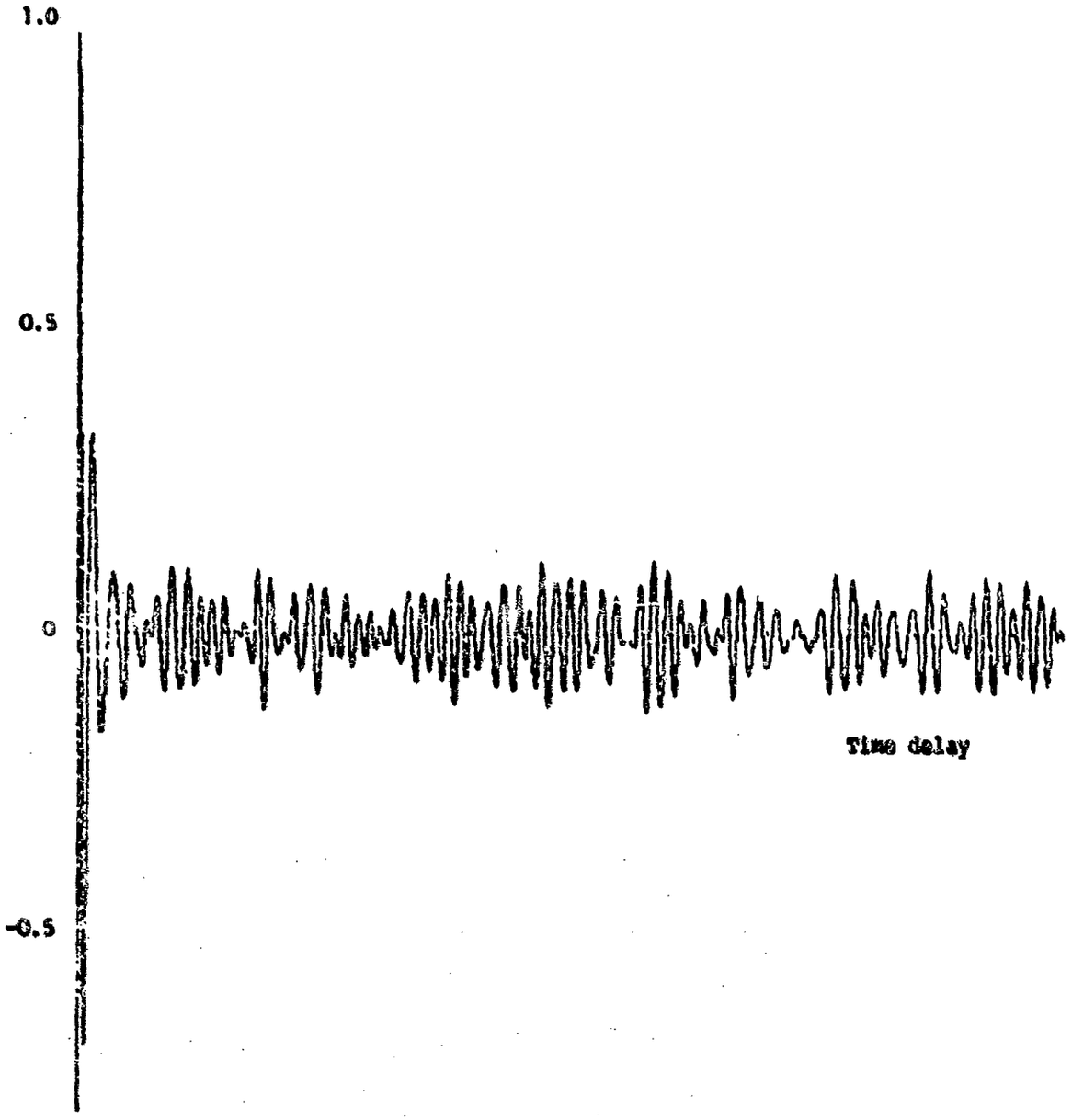

Fig.23 The autocorrelation co-efficient of a signal synthesized from a random sequence of Gaussian pulses from which the lowest frequency elements are excluded.

DISCUSSION

Dr Fuchs: Concerning the debate whether or not model jets do "crackle" and the entire question of how the phenomenon can be quantified and its cause isolated, I would propose a relatively simple approach: Insert a probe microphone in the core of a subsonic jet, say three diameters downstream of the nozzle. When you listen to the pressure signal through earphones you will hear a sound which closely resembles that of jet noise. When one traverses the probe at a constant speed in the lateral direction one may easily distinguish three regions where the statistical character of the signal changes very drastically:

(i) The core region is characterized by a relatively smooth and almost "comfortable" random noise. With increasing distance from the jet axis, however, certain "crackling" events occur at irregular intervals, the intervals being of the order of seconds near the axis. When the probe approaches the mixing region the "crackle" will become more intense and occur at shorter intervals with the still audible random noise remaining almost unaltered.

(ii) In the mixing region the second, irregular noise component has become dominant, and the pressure signal resembles that of a hot-wire signal detected at the same location in the flow. The underlying regular noise pattern is nevertheless detectable by the ear, which seems to easily discriminate between noises of similar spectra but of different statistical character.

(iii) When traversing through the entrainment region, the irregular content gradually decreases again. The impression of "crackle" returns, becomes less frequent, and finally (at approximately two diameters from the axis) dies out leaving the regular jet noise character in the rapidly decaying near-field signal.

The phenomenon described shows that "crackle" may be characteristic for any jet but generally is of minor importance in the radiated far-field. It is very easily isolated by the human ear and may best be studied in a flow region where the "crackling" events occur only occasionally, e.g. right in the middle of the potential core of a model jet.

Prof.Ffowcs Williams: The observations made by Dr Fuchs are very interesting indeed, and I agree that such an experimental approach may well prove effective in studying the basic origin of crackle. If I interpret him correctly, crackle is always a feature of the jet motion but is only coupled effectively to the acoustic field at high jet speeds. If indeed this idea can be verified then it may be much easier to study systematically the basic fluid motions that generate crackle in a jet of low speed where crackle is inaudible in the far field. That would no doubt considerably ease the experimental difficulties of a systematic study.

Dr Obermeier: Prof.Ffowcs Williams discussed among other things the so-called "crackling" noise. Perhaps the following comment may be helpful to develop a quantitative understanding of this phenomenon. If one assumes the existence of pressure distributions in the flow similar to the front or the rear shock of a sonic boom, then it seems reasonable that these shocklike pressure distributions are partly focused and partly scattered by the turbulence within the jet.

In such a case, however, one can expect for the influence of the focussing effect results similar to those given in our Paper No.17 (Ref.1). That means spiked positive pressure fluctuations and rounded negative ones.

To explain the influence of the scattering effects one can refer to our paper[2] where we apply also linear methods to describe the distortion of a N-shaped pressure signature of a sonic boom by turbulence. The basic results of that paper show that this distortion can be explained in a first approximation by the phase scrambling of the single Fourier-components of the total pressure distribution. Again it turns out that the positive pressure fluctuations are spiked and the negative ones are rounded.

1. F.Obermeier — *Sonic Boom Behavior near a Caustic.* AGARD CPP.131, Paper No.17.

2. F.Obermeier, G.Zimmermann — *Das Streuverhalten eines Überschallknalles beim Durchgang durch eine turbulente Schicht.* Max-Planck-Institut für Strömungsforschung, Bericht 114 (1978).

Prof.Ffowcs Williams: As I said in my lecture, I have been unable to think of any finite amplitude propagation effect capable of generating a distinct difference between positive and negative going pressure perturbations and have come to the conclusion that the origin of the crackling spikes must be in the unsteady flow that generates the sound. But Dr Obermeier makes what I think is an extremely valid point, in recognising that if the waves are focussed by some inhomogeneity in the propagation constants a caustic will result and that positive going spikes are a characteristic of acoustic signals near such caustics. That observation seems to throw open the possibility that real life propagation effects are also capable of generating the spikes, so that their origin must remain for the moment an open issue.

EXPERIMENTAL EVALUATION OF FLUCTUATING DENSITY AND RADIATED NOISE FROM A HIGH-TEMPERATURE JET*

by

P. F. Massier,+ S. P. Parthasarathy,# R. F. Cuffel++
Jet Propulsion Laboratory
4800 Oak Grove Drive
Pasadena, California 91103

SUMMARY

An experimental investigation has been conducted to characterize the fluctuating density within a high-temperature (1100°K) subsonic jet and to characterize the noise radiated to the surroundings. Cross correlations obtained by introducing time delay to the signals detected from spatially separated crossed laser beams set up as a Schlieren system were used to determine radial and axial distributions of the convection velocity of the moving noise sources (eddies). In addition, the autocorrelation of the fluctuating density was evaluated in the moving frame of reference of the eddies. Also, the autocorrelation of the radiated noise in the moving reference frame was evaluated from cross correlations by introducing time delay to the signals detected by spatially separated pairs of microphones. The radiated noise results are compared with Lighthill's theory and with the data of Lush. Radial distributions of the mean velocity were obtained from measurements of the stagnation temperature, and stagnation and static pressures with the use of probes.

RÉSUMÉ

Une investigation expérimentale a été conduite afin de caractériser la densité fluctuante au sein d'un jet subsonique à haute température (1100°K) et le bruit irradié tout aux alentours. Des corrélations croisées, obtenues en introduisant un délai de temps dans les signaux détectés à partir de faisceaux laser croisés séparés dans l'espace et disposés selon un système Schlieren, furent utilisées pour déterminer les distributions radiale et axiale de la vitesse de convection des sources mobiles de bruit (tourbillons). L'autocorrélation de la densité fluctuante fut évaluée dans le système mobile de coordonnées des tourbillons. De plus, l'autocorrélation du bruit irradié dans le système mobile de référence fut évaluée à partir des corrélations croisées en introduisant un délai de temps dans les signaux détectés par des paires de microphones séparés dans l'espace. Les résultats du bruit irradié furent comparés avec la théorie de Lighthill et avec les données de Lush. Les distributions radiales de la vitesse moyenne furent obtenues à partir des mesures de température de stagnation et des pressions de stagnation et statiques à l'aide de sondes.

NOTATION

a,b,c	ξ, η and ζ axes of ellipsoid respectively, Eq. (A2-23)	P_t	stagnation pressure
a_o	speed of sound at ambient conditions	p_w	static pressure at the wall
C	cross correlation function		two-point correlation of the density fluctuations = $\overline{\rho_V \rho_H}$
D	diameter of jet at flow separation		
e	voltage signal output of laser detector	C_e	experimental cross correlation function of the laser signals
f	frequency		
g	a function of time, Eq. (A3-2)	r	defined by Eq. (A2-10); also the distance from the center of the nozzle at the exit to a microphone, Eqs. (2) and (3)
G	a fluctuating random scalar function		
I	noise intensity		
ℓ	beam length between edge of jet and knife edge	r	distance from noise source to microphone; also a variable defined by Eq. (A2-15)
L	that portion of the laser beam length which lies within the jet diameter (Fig. A2-1)		
M	Mach number based on speed of sound at ambient temperature	S	sensitivity of the detector
M_j	jet Mach number based on speed of sound at jet temperature	t,t*	time
n	number of sources per unit time which emit sound; also the refractive index	T	time required for sound to travel from the nozzle exit (origin of first sound wave) to a microphone, Eq. (A3-1); also temperature
N_1	number of frequency bands		
N_2	number of nodal points	U	mean jet velocity
p	static pressure	U_c	convection velocity of the eddies

*This work presents the results of one phase of research carried out in the Propulsion Research and Advanced Concepts Section of the Jet Propulsion Laboratory, California Institute of Technology, under Contract NAS7-100, sponsored by the National Aeronautics and Space Administration.

+Group Supervisor #Senior Scientist ++Member Technical Staff

U_0	mean jet velocity at the nozzle exit or downstream of the normal shock wave
x^*	axial distance from flow separation location inside the nozzle
x,y,z	coordinates with the origin at the nozzle exit, see Figs. (A2-1) and (A2-2)
α	ratio of highest frequency at the edge of a band to the lowest frequency of the band, Eq. (A3-3); also a factor in Eqs. (2) and (3)
β	emission angle, the angle between the jet axis and the line joining a microphone with the center of the nozzle at the nozzle exit plane
γ	angular deflection of a laser beam
δ	time increment
ϵ	Gladstone-Dale constant
ζ	coordinate along the z direction with origin on the horizontal laser beam, see Fig. (A2-2)
η	coordinate along the y direction, see Figs. (A2-1) and (A2-2)
θ	angle between the jet axis and a line drawn from a noise source to a microphone
μ	ξ coordinate in moving reference frame, equal to $\xi - U_c\tau$
ξ	coordinate along the x direction, or beam separation distance, see Figs. (A2-1) and (A2-2)
ρ	density
τ	time delay
τ_*	time delay for which the rms density fluctuations decay to one-half the maximum value
φ	autocorrelation functions representing the noise in the various frequency bands, Eq. (A3-3)
Ψ	autocorrelation function in moving frame of reference of the eddies
( )	denotes "function of"
[ ] or $\{\ \}$	denotes "multiplied by"
< >	denotes averages
$\underline{\ }$	denotes a vector quantity when it appears beneath a symbol

SUBSCRIPTS

a	ambient conditions inside the anechoic chamber
c	convection of eddies
d	density
e	emission conditions
H	horizontal beam
i	index
n	noise
q	quadrupole
t	stagnation condition
V	vertical beam
β	at angle β with respect to the jet axis
ζ	along the ζ direction
η	along the η direction
ξ	along the ξ direction
0	initial condition; also nozzle inlet condition
1,2	microphone numbers; also different times or locations; also indexes
78,90	78° and 90° with respect to the jet axis

SUPERSCRIPTS

'	fluctuating quantity (indicated in figures but not in equations)
$\bar{\ }$	average value

1. INTRODUCTION

Perhaps the most significant obstacle to fully understand the noise sources in free jet flows is the formidable task of experimentally characterizing the turbulence that is generated in the shear region. A complete experimental evaluation of the distribution of fluctuating quantities (or noise sources) within jets and the determination of the contribution of each source to the noise radiated at a particular location outside the jet appears at the present time to be almost unobtainable in a practical sense. This is true even with the use of recently developed instrumentation methods coupled with the use of high-speed computers for data analysis purposes. Thus, any investigation of the fluctuating quantities related to the radiated noise requires simplifications in terms of a model that "represents" the real situation.

The experimental investigation to be discussed pertains to one method of characterizing the fluctuating quantities that generate the noise as well as to a method of characterizing the noise that is radiated to the surroundings. In particular, the fluctuating densities in a high-temperature subsonic jet have been characterized by the use of cross correlations that were obtained by introducing time delay to the signals detected from spatially separated crossed laser beams that were projected through the jet. The lasers were set up as a Schlieren system. From the cross correlations of the spatially separated beams the convection velocity of the moving eddies and the fluctuating density autocorrelations were evaluated. Conceptually the eddies consist of statistically random fluctuations in density that can be identified as they move along the flow direction. These eddies are considered to be the noise sources. The density autocorrelation is the envelope of a family of the cross correlation curves. This autocorrelation function is the intensity of the density fluctuations ($\overline{\rho'_1 \rho'_2}$) in the moving frame of reference of the eddies, or also; it is the Fourier transform of the fluctuating density spectrum.

Simplifications introduced into the data analysis procedure include the assumptions of isotropy and homogeneity; however, a method of treating nonisotropic fluctuations is discussed. Then, even though

radial as well as axial distributions of the intensity of the density fluctuations and of the convection velocity were obtained, the characterization is based on a model consisting of point noise sources concentrated along the axis of the jet; consequently, it was assumed that the noise was essentially being radiated from a line antenna.

A distinct advantage in an experimental sense of dealing with the fluctuating density rather than with the fluctuating pressure is that the density and the two-point correlations can be evaluated comparatively easily without disturbing the flow. Such disturbances could occur, for example, with the use of probes, particularly since two probes close to each other would be required in order to obtain two-point correlations.

The radiated noise is compared with the theory of Lighthill (Ref. 1) and with some of the data obtained by Lush (Ref. 2). In addition, it is characterized in terms of the noise cross-correlation coefficient and the autocorrelation function in the moving frame of reference of the eddies. Correlations of the radiated noise were evaluated from the signals obtained with pairs of microphones by introducing time delay.

The experiments were conducted in an anechoic chamber. The jet flow emerged from a convergent-divergent nozzle in which flow separation occurred downstream of the throat because the nozzle was considerably overexpanded. Consequently, a shock structure was established but was contained entirely within the nozzle and the flow was subsonic and shock-free at the nozzle exit as verified by Schlieren and shadowgraph observations. The average stagnation temperature at the nozzle inlet taking into account all tests was about 1100°K (1520°F) and the Mach number at the nozzle exit was about 0.5. Radial distributions of mean values of the velocity, stagnation temperature, stagnation pressure and static pressure were obtained in the jet with the use of probes.

2. CONVERSION OF LIGHTHILL'S THEORY TO THE POINT SOURCES

The theoretical work of Lighthill (Refs. 1 and 3) is based on the concept of quadrupole sources distributed over the volume of the jet. The analysis of the experimental data to be discussed, however, is based on the model of point noise sources concentrated along the axis of the jet. Measurements were made throughout the jet region with the laser beams to obtain radial and axial distributions of the fluctuating density; however, the amount of such mapping is far from adequate for direct use in Lighthill's theory. Nevertheless, it is possible to demonstrate that the Lighthill theory can be converted into a form which for quadrupole sources resembles the autocorrelation function derived directly from the point-source model. The analysis of this conversion is omitted for brevity; however, the procedure followed includes (1) integration of the cross correlation function over a noise source (or eddy), (2) integration over the cross section of the jet, and (3) conversion of the integral along the axis to an integration of the emission time. The emission time is the time interval required for the noise to propagate from a source to a microphone. During this time interval the noise source will have traveled to a new location. The final expression for the correlation function is

$$C(\tau) = \frac{1}{16\pi^2} \int \frac{[2 \sin\theta_1 \cos\theta_1]\,[2 \sin\theta_2 \cos\theta_2]}{r_1[1 - M_c \cos\theta_1]^2\, r_2[1 - M_c \cos\theta_2]^3} R_q \left(x - a_o M_c [0 - t_e],\ t_e;\ t' = 0 + \frac{r_1}{a_o} \frac{r_2}{a_o} \right) dt \quad (1)$$

Equation (1) corresponds to the point-source model, Eq. (A3-1) of Appendix A3. It should be noted that in Eq. (A3-1) the factor $1/16\pi^2$ has been included in the definition of the source strength and as a consequence is contained in the normalized autocorrelation function R_n. The trigonometric terms in the numerator of Eq. (1) result from the definition of the quadrupole as does the quantity $[1 - M_c \cos\theta_2]$ being a cubed term instead of a squared term. R_q in Eq. (1) is the autocorrelation function of a quadrupole in the moving frame of reference of the eddies. Its functional relationship is similar to that of R_n of Eq. (A3-1). The two equations are identical in content.

3. EXPERIMENTAL FACILITY

The experiments were conducted in an anechoic chamber which is described in Ref. 4. During these experiments air from the outside was drawn into the chamber by the small decrease in ambient pressure inside, which was caused by the injector action of the jet. Before entering the chamber the outside air was distributed behind the wedge blocks that lined the room, and then the air entered through small spaces between the wedges as shown in Fig. 1. This minimized the possibility that significant recirculating flow patterns would occur inside the chamber.

Compressed air was supplied on a steady state basis by a compressor plant facility and was heated using a turbojet burner. The burner was located a considerable distance (227 cm) upstream of the nozzle so that good mixing of the flow could occur before it entered the nozzle. The diameter of the duct located between the burner and the nozzle was 30.5 cm. The nozzle throat diameter was 4.1 cm; thus the contraction area ratio was large with low velocities upstream of the nozzle.

The noise produced by the upstream configuration was evaluated from measurements obtained with a 19 mm diameter dynamic microphone probe which was inserted on the centerline inside the large duct at a distance of 70 cm upstream of the nozzle exit plane. The probe had a nose cone and sensed the static pressure fluctuations. These tests were conducted under cold flow (ambient temperature) conditions over a range of stagnation pressures including the pressure at which the hot flow tests were made. The upstream noise inside the duct was predominantly a pure tone at 560 Hz; however, pure tones were not observed outside the jet under hot flow conditions. Hence, the noise generated in the flow upstream of the nozzle was not considered to be a significant contribution to the noise radiated from the jet.

4. INSTRUMENTATION

The noise radiated from the jet was measured with 3 cm and 6 cm dia. B&K microphones. They were placed in the vertical position such that the tips were on a horizontal plane passing through the centerline

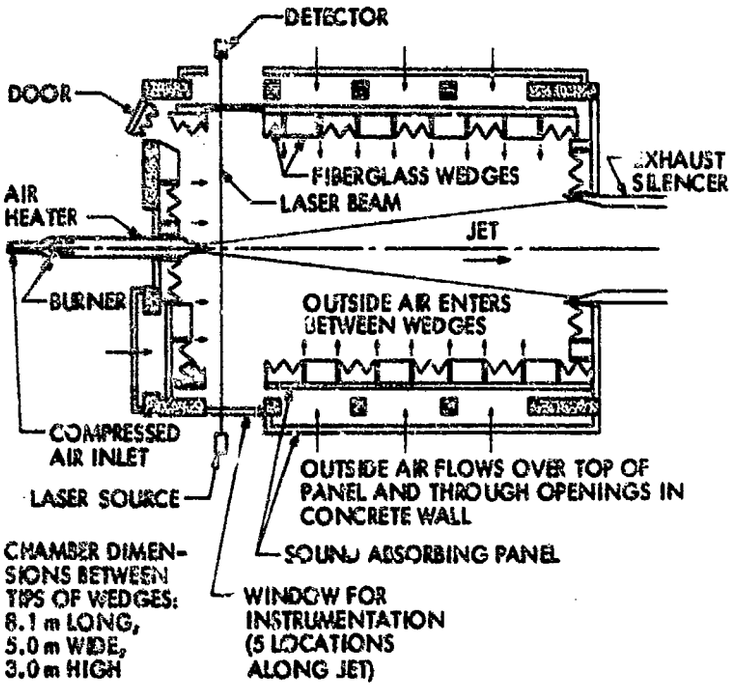

Figure 1. Anechoic Chamber Test Facility

of the jet. Hence, the sound waves grazed over the surfaces of the sensing elements. Eight microphones were located in a 60 cm diameter circle outside the jet stream. A diagram of the arrangement is shown in Fig. 2. The detected noise signals were recorded on magnetic tape and played back through a correlation instrument to obtain cross correlations. The procedure used to analyze the noise signals is discussed in Appendix A3.

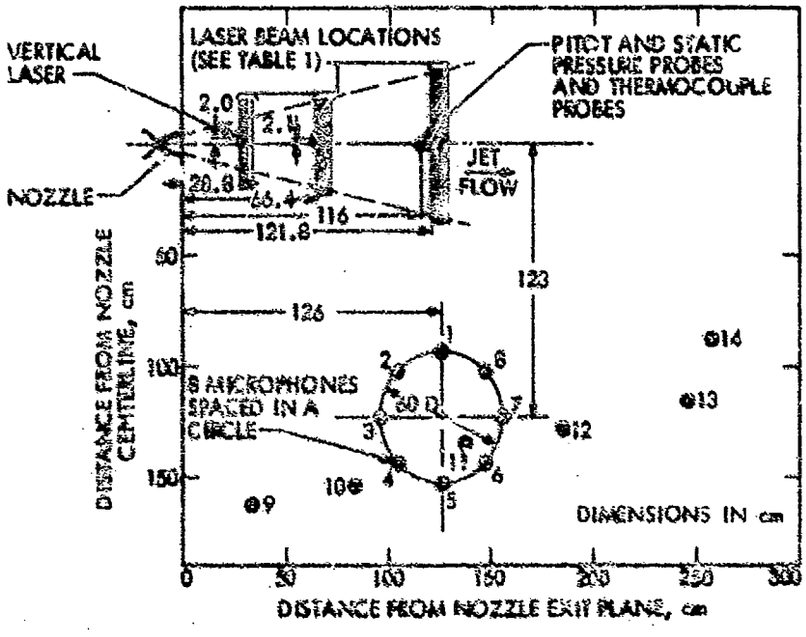

Figure 2. Instrumentation Locations

Crossed laser beams from helium-neon sources were set up as a Schlieren system and projected through the jet as shown in Fig. 2. The beams, about 3 mm in diameter, were deflected by gradients in the refractive index which is related to the density by the Gladstone-Dale constant. Hence, fluctuations in density could be obtained from signals detected by the crossed-beam Schlieren arrangement. One beam was vertical and five additional beams, which were horizontal, were separated spatially across the diameter of the jet. Horizontal separation along the flow direction was obtained by moving the lasers to different locations during an experiment. Thus the jet could be scanned in both directions. The vertical beam could also be moved in either of two directions by adjusting a series of mirrors. Alignment of the knife edges of the Schlieren system and the reasons for the chosen alignment is discussed in Appendix A2.

The detected laser signals were recorded on magnetic tape and then played back through a correlation instrument to obtain the cross correlations in the same manner as the noise signals. The analysis that was used to interpret the laser signals is discussed in Appendix A2 also.

Radial distributions of the mean jet velocity were determined from pitot pressure, static pressure, and from stagnation temperature measurements across the flow. Manometers were used to measure the pressures and shielded thermocouples were used to determine temperatures. Numerous probes mounted in line were used to obtain these pressures and temperatures.

The stagnation pressure at the nozzle inlet was measured with a pitot probe and the stagnation temperature at this location was obtained with a thermocouple probe.

Both Schlieren (in addition to the laser system) and shadowgraph systems were used to observe the flow patterns within the jet.

3. NOZZLE FLOW FIELD

The jet flow discharging from the nozzle exit plane was subsonic; however, for a portion of the distance downstream of the throat within the nozzle the flow was supersonic. Consequently, a discussion of the flow field inside the nozzle is needed to clarify this transition.

At the nozzle inlet the stagnation temperature averaged over numerous tests was 1100°K (1520°F) and the average stagnation pressure was 3.48 bar (50.4 psia). The variation in temperature was not more than ± 15°K and the variation in pressure was not more than ± 0.024 bar. The flow discharged into air at virtually atmospheric conditions inside the anechoic chamber from a convergent-divergent nozzle which was considerably overexpanded. The measured pressure inside the anechoic chamber was only 0.006 bar less than atmospheric pressure. Flow separation occurred inside the nozzle in the divergent section downstream of the throat as indicated by the pressure rise shown below the sketch of the nozzle in Fig. 3. At the

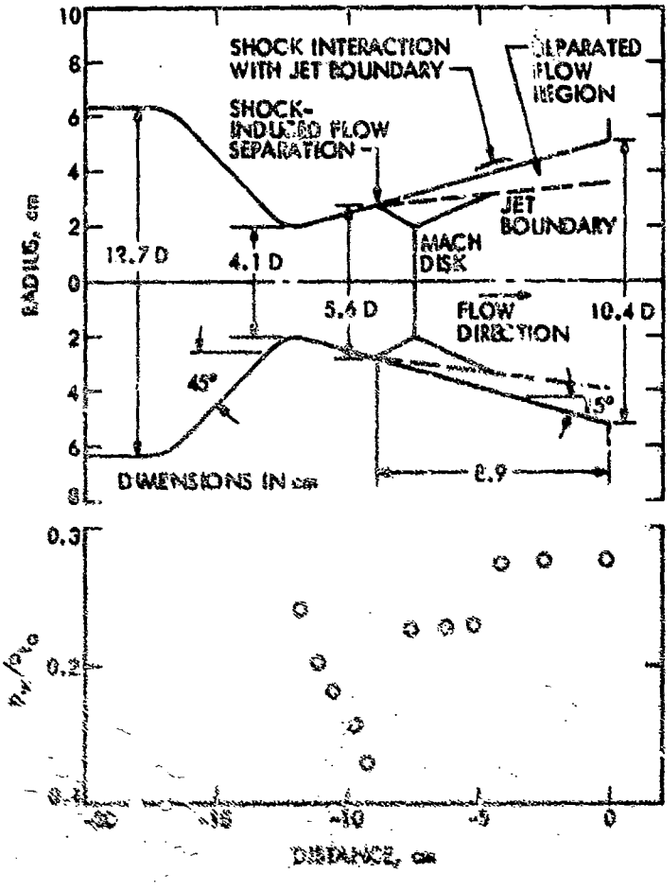

Figure 3. Nozzle Flow Field

Flow separation location (the peak p... near the wall was 3.3 An oblique shock wave associated with the separation was established over the ...l of the nozzle as shown in the figure. This wave projected downstream and intersected with a normal shock (shock disk or Mach disk) which crossed the centerline. The reflected oblique wave which projected ... downstream of this wave intersection was then reflected again from the separated flow region. This second reflection was evidenced from a second rise in the wall static pressure as indicated in Fig. 3. Any noted flow near the wall was cited between the two oblique waves as well as downstream of the second oblique wave. This was concluded from the observed constant wall pressures in these two regions even though the pressure levels differed.

The measurements that were made to locate these waves consisted of (1) wall pressures from which the flow separation and the angles of both of the oblique waves were determined, and (2) pitot probe pressure measurements along the centerline in a cold jet from which the existence and location of a normal shock wave which crossed the axis was established. These waves were probably curved, rather than being straight as shown. Their actual shape are not known because the extent of the measurements was too limited. Additional discussion of these waves and the corresponding flow field may be found in Ref. 5. In addition, the transonic flow field in terms of radial and axial distributions of Mach No. as determined experimentally is given in Ref. 6. The existence of additional weak oblique shock waves (not shown in Fig. 3) which emanated from a location near the tangency between the circular-arc throat and the conical divergent section is discussed in Ref. 7. Flow separation and reattachment that occurred in the vicinity of the curved inlet section when the nozzle inlet was attached to a constant-diameter duct upstream is presented in Ref. 8. Additional flow information together with wall heat transfer measurements which show the boundary layer laminarization effects appear in Ref. 9.

The jet was steady during the experiments discussed here and did not oscillate about the centerline of the nozzle. Such oscillations did occur at lower stagnation pressures when the flow separation point was farther upstream; however, no data was required under those conditions.

The origin of the "free jet", although contained, was actually inside the nozzle downstream of the flow separation point. In the laser beam and in the noise analyses the distances along the flow (x-direction), however, are referenced to the nozzle exit plane. Just downstream of the Mach disk the diameter of the jet was estimated to be about 6 cm and the Mach No. was 0.5. The jet velocity corresponding to this Mach No. is 310 m/sec. The velocity at the nozzle exit plane was probably somewhat lower; however, its value was not determined. For convenience the flow conditions are given in Table 1. All of the shock waves were contained within the nozzle. No such waves were observed in the jet downstream of the exit plane with Schlieren and shadowgraph systems that were used for this purpose.

Table 1

Flow Conditions, and Laser Beam and Microphone Locations

Jet Diameter D, at Flow Separation (Fig. 3) = 5.6 cm

Mach No. at Flow Separation (Fig. 3) = 2.2

Mach No. Downstream of Normal Shock (Fig. 3) = 0.5

Velocity Downstream of Normal Shock (Fig. 3) = 310 m/sec

Average Nozzle inlet stagnation pressure = 3.48 bar (50.4 psia)

Average Nozzle inlet stagnation temperature = 1100°K (1520°R)

Anechoic chamber pressure = 0.98 bar (14.2 psia)

Location of Vertical Laser Beam				Locations of Horizontal Laser Beams				Location of Vertical Laser Beam				Locations of Horizontal Laser Beams			
						Five beams for each value of ξ								Five beams for each value of ξ	
Test No.	x cm	x*/D	y cm	x cm	ξ cm	z cm	Radius cm	Test No.	x cm	x*/D	y cm	x cm	ξ cm	z cm	Radius cm
87	28.8	6.7	2.0	28.8	0	6.5	6.8	103	121.9	23.3	3.9	121.8	0		
88	↓	↓	↓	29.6	1.0	2.5	3.2	104	↓	↓	↓	122.8	1.0	6.6	6.6
89				31.8	3.0	-1.8	2.7	105				123.8	2.0	2.6	2.6
90				34.8	6.0	-5.6	5.9	106				124.8	3.0	-1.7	1.7
						-9.8	10.0	107				125.8	4.0	-5.3	5.3
96	66.4	13.4	2.1	67.2	0.8			108				127.8	6.0	-9.7	9.7
97				68.2	1.8	6.7	7.0	109	↓	↓	↓	129.8	8.0		
98				69.2	2.8	2.7	3.4	Locations of Microphones (Nos. 1 through 8 on 60 cm dia. circle)							
99				66.4	0	-1.6	2.6								
100				71.4	5.0	-5.2	5.6	Test No.	Microphone No. (Fig. 2)		β Deg.	Distance From Nozzle Exit to Microphone, cm			
101				73.4	7.0	-9.6	9.8								
102	↓	↓	↓	76.2	9.8			49	9		78	169			
								41	10		62	175			
								24	11		45	142			
								23	12		35	224			
								20	13		25	271			
								19	14		19	270			

6. JET FLOW FIELD

The radial distribution of the mean value of the jet velocity U, was determined from measurements of the stagnation pressure, the static pressure and the stagnation temperature. This velocity distribution, vertically across the diameter, is shown in Fig. 4 at a distance of 116 cm downstream of the nozzle exit plane. This distance is about 21 jet diameters downstream of the flow separation location in the nozzle with the jet diameter based on the flow separation diameter shown in Fig. 3. It is evident that at this axial location the maximum jet velocity was about 110 m/sec (U_j = 0.27) and that the diameter of the jet had grown to about 60 cm. The region of highest shear (maximum $\partial U/\partial y$) at this axial location occurred over

a radial distance between about 5 and 15 cm. The ratio of the jet mass flux to nozzle mass flux was 13.6.

Also shown in Fig. 4 is the radial distribution of the convection velocity of the eddies U_c, which was determined from laser beam measurements at five positions spaced vertically across the diameter of the jet. The data shows that both the jet velocity and the eddy velocity are reasonably symmetrical about the centerline of the jet. Additional results of the convection velocity are discussed in the next section.

Radial distributions of the stagnation pressure, stagnation temperature and static pressure referenced to ambient conditions are shown in Fig. 5. It should be noted that the static pressure in the flow is below ambient pressure, even this far downstream. If it had been assumed that the static pressure were the same as the ambient pressure, the maximum velocity would have been calculated to be about 7 per cent lower than shown in Fig. 4 and the diameter of the jet would have been about 13 per cent smaller.

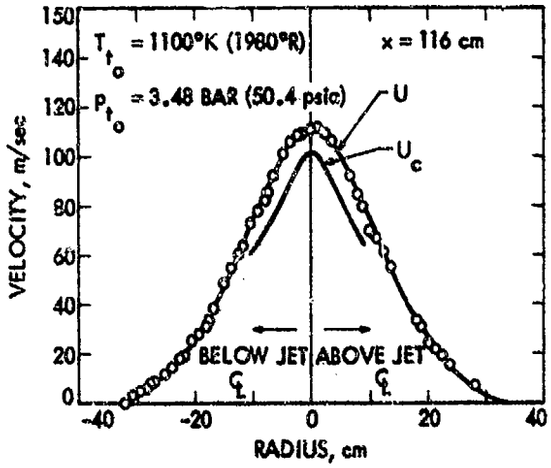

Figure 4. Radial Distributions of Mean Velocity and Convection Velocity

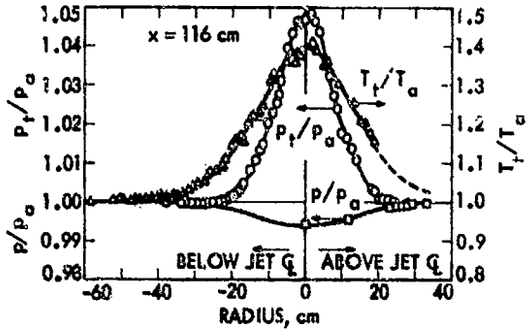

Figure 5. Radial Distributions of Pressure and Temperature

7. CONVECTION VELOCITY

The convection velocity of the eddies U_c, was evaluated at the axial locations where laser beam measurements were made (Fig. 2). It was determined by the separation distance of the laser beams ξ, divided by the appropriate time delay τ, and is based on the loci of the tangent points of the envelope curve for the experimental cross correlations. A comparison of the radial distribution of the convection velocity with the jet velocity is shown in Fig. 4 at a distance of 116 cm from the nozzle exit plane. It is evident that the distributions follow the same trends. At the centerline the ratio of the convection velocity to the jet velocity is 0.9 and near the outer limits of the convection velocity curve shown, the ratio of local convection velocity to local jet velocity is more nearly 0.8. Radial distributions of the convection velocity at the other axial locations are shown in Fig. 6. The distributions are essentially symmetrical about the centerline and the peak values decrease along the flow direction. The crossover of the curves near the outer edges is a result of the spreading of the jet as the distance from the nozzle exit plane increases.

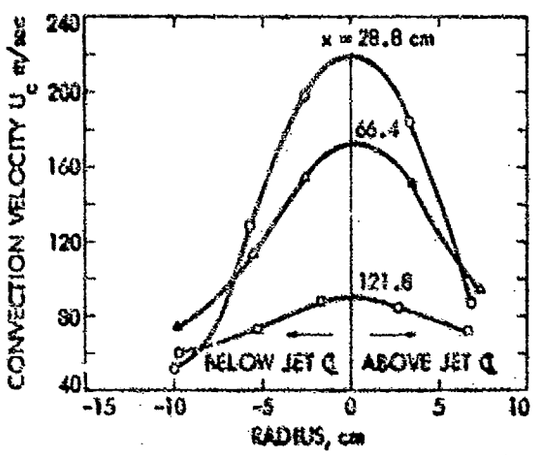

Figure 6. Radial Distributions of Convection Velocity

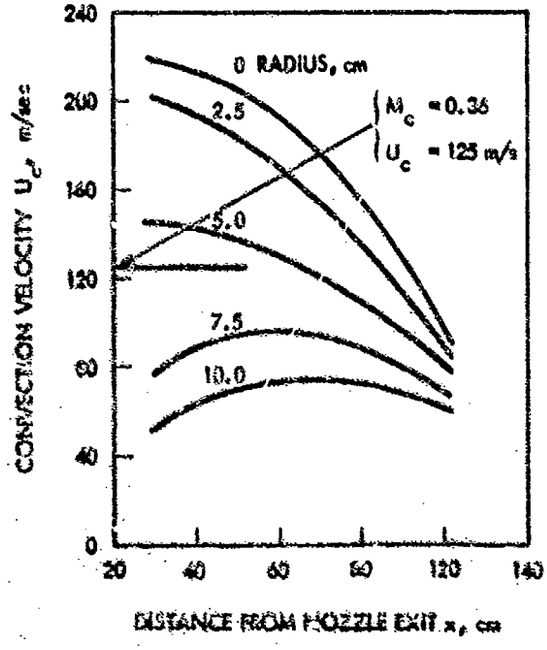

Figure 7. Axial Distributions of Convection Velocity

Distributions along the axial direction at various radii are shown in Fig. 7. At the larger radii the convection velocity would be zero at the nozzle exit (outside the jet). Farther downstream as the jet spread to the particular radius, at which a measurement is being made, the velocity of the eddies would be observed. A maximum value would be expected before the velocity decayed. Such a trend is apparent at radii of 7.5 and 10 cm. Near the centerline there was a continuous decay. A convection velocity of 125 m/sec, which is based on an average throughout the jet, was chosen for evaluation of the noise autocorrelation function in the moving reference frame.

8. EXPERIMENTAL DENSITY FLUCTUATIONS

Typical cross correlations Q_s, of the density fluctuations vs time delay τ, are shown in Fig. 8. At zero separation distance of the vertical and of the horizontal beams ($\xi = 0$) the curve is symmetric about $\tau = 0$. A decay in the intensity, that is, in the peak values of the curves, occurs as the separation distance is increased. The upper envelope of this family of curves is a smooth function as shown. It is the autocorrelation function $2\pi \overline{\rho'_V \rho'_H}^{\tau}$ in the moving frame of reference of the eddies, that is, $2\pi Q_s$ or also; it is the Fourier transform of the fluctuating density spectrum. The locations of the laser beams are shown in the sketch in the upper right-hand corner of Fig. 8. The radius of the measuring station was 10.0 cm. At this axial location of x = 28.8 cm the results obtained at other horizontal beam positions resemble those shown in Fig. 8. The peak correlation values differ, however, as does the steepness of the cross correlation curves, and, of course, the convection velocity.

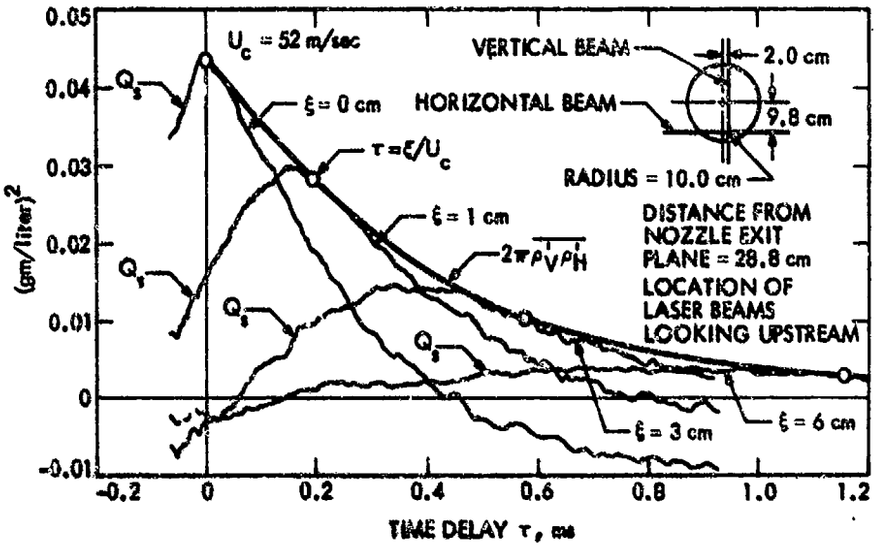

Figure 8. Experimental Correlations of Fluctuating Density vs Time Delay

Distributions across the jet of the rms density fluctuations are shown in Fig. 9 at three axial locations. The position of the vertical beam was about 2 cm off-axis for the two upstream locations as shown in Fig. 2 and given in Table 1, but it was on the axis for the farthest downstream location. At the farthest upstream location (x = 28.8 cm), where the stagnation temperature on the axis of the jet was estimated to be about 1000°K, the ratio of the rms density fluctuation, at a radius of 10 cm, to the mean density at the centerline was 0.21. At the farthest downstream location (x = 121.8 cm), where the stagnation temperature on the jet axis had decreased to about 400°K, the ratio of the rms fluctuating density to the mean density on the jet axis had decayed to 0.008. Minima which occur in the horizontal plane passing through the center of the jet are inferred from the curves. At 28.8 cm the distance from the flow separation location is about 7 jet diameters based on the flow separation diameter. At 66.4 cm this distance is about 13 jet diameters. The larger fluctuations at 13 jet diameters do not contribute as much to the radiated noise as do the fluctuations farther upstream. This is deduced from the results of the noise data discussed in the next section. There, it is evident that the maximum noise intensity occurred at about 4 jet diameters from the flow separation location and that farther downstream there was a continuous decrease in noise intensity. Thus, further clarification is needed before a relationship between the density fluctuations and the radiated noise can be established.

The largest density fluctuations occurred at the larger radial measuring stations of the jet, as shown in Fig. 9, in the region of the highest shear. At the farthest location downstream, about 23 jet diameters, the distribution is essentially uniform even in the region of maximum shear. This farthest downstream position is very near the location at which the radial distribution of the velocity is shown in Fig. 4.

Distributions of the most significant variables related to the fluctuating density are shown in terms of the peak rms fluctuating density (Fig. 9), the convection velocity (Fig. 4), and the time scale of the moving density autocorrelation, which is the time delay at which the rms density fluctuation has a value equal to one-half of its maximum value (Fig. 10). This time scale is nearly constant in the central region across the jet but is larger at the radius of 10 cm, which corresponds to the radius of the Fig. 8 results. In the central region of the jet the time scales are typically about 0.25 milliseconds; whereas, the corresponding time delay scale of the moving noise source is more nearly 0.1 milliseconds as deduced from the noise correlations discussed in the next section. The density fluctuation correlations, however, should not be compared directly with the noise correlations. Instead, as discussed in Appendix A2,

it is the second derivative of the $\overline{\rho_V \rho_H}$ fluctuations with respect to time delay τ, which is related to the density autocorrelation γ_d, and hence to the noise autocorrelation γ_n. Additional experimental data is required before this can be done with sufficient accuracy.

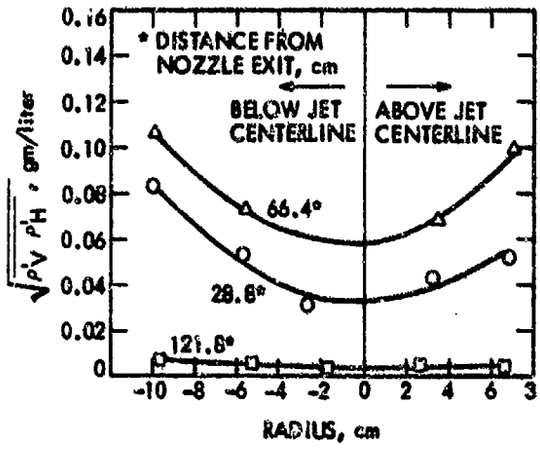

Figure 9. Distributions of rms Density Fluctuations at $\bar{5}$ = 0

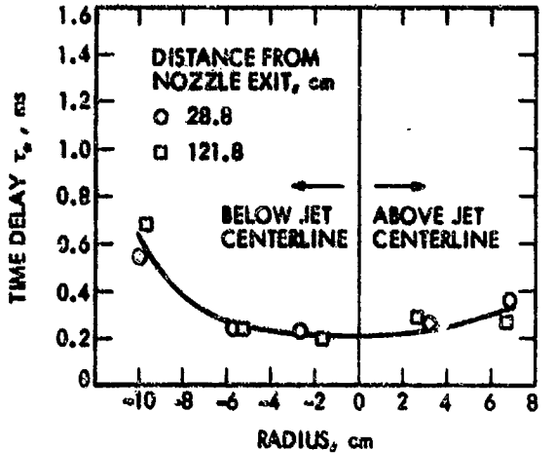

Figure 10. Time Scale Distribution

The decay of the rms value of the density fluctuations vs beam separation along the flow is shown in Fig. 11. These results are given at only three radii at each axial location for clarity but indicate typical trends. The higher rms values at x = 66.4 cm at the larger radii are evident in this figure also. It is apparent that the decay in intensity of the eddies in the high shear region (outer radii) occurs over a comparatively short distance.

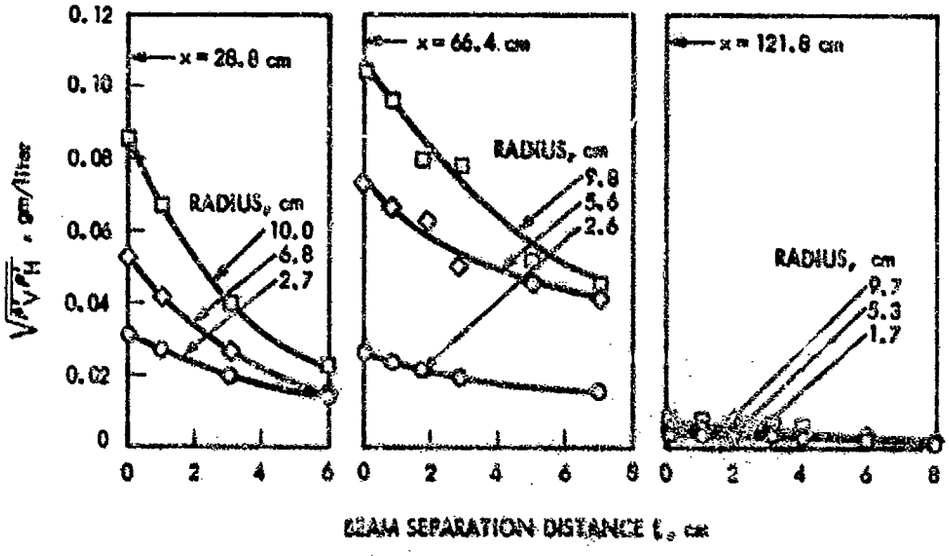

Figure 11. Decay of Density Fluctuations vs Beam Separation

In the experiments the two-point correlation of the density fluctuation Q, was evaluated from the crossed laser beam measurements at several locations. From these values of Q the second time derivative, which is related to the density autocorrelation, was obtained by means of a computer program. An example of the second time derivative is shown in Fig. 12. In this figure the most important result is the maximum value, which occurs at zero time delay. The location at which the curve crosses the horizontal axis is shown also. The significance of the peak value is that it can be introduced into Eq. (A2-22) together with the mean velocity gradient to obtain the fluctuating density auto correlation function γ_d. Then the relationship between the fluctuating density inside the jet and the noise radiated outside can be established by the relationship between γ_d and γ_n. The evaluation of τ_o is discussed in the next section. Determination of the relationship between γ_d and γ_n, however, is beyond the scope of this investigation.

9. RADIATED NOISE

The noise radiated from the jet is presented in two ways, first in terms of a 1/3 octave band analysis compared with Lighthill's theory of convected quadrupoles (Ref. 1) together with a comparison of some of the cold flow data of Lush (Ref. 2), and second is is characterized in terms of the noise cross correlation coefficient as well as the autocorrelation function in the moving reference frame of the eddies.

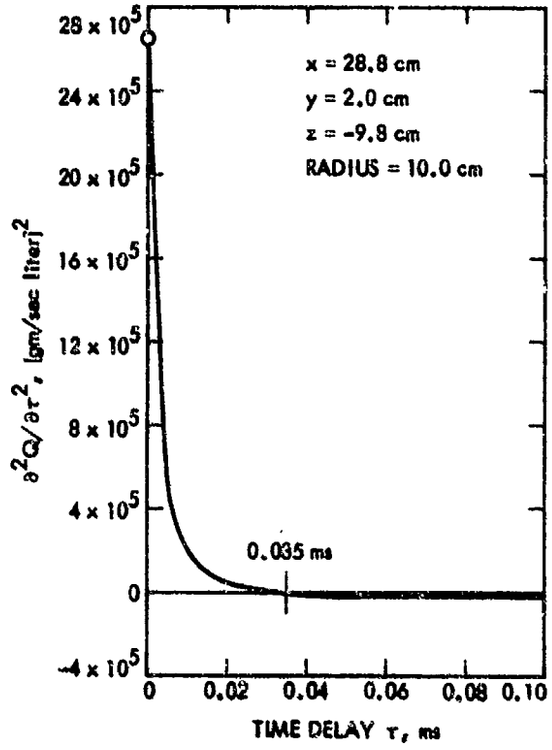

Figure 12. Second Time Derivative of the Density Fluctuation Correlation

In Fig. 13 the differences in sound pressure levels between Lighthill's theory and the experimental values are shown as a function of the non-dimensional frequency parameter fD/a_0, for various values of the emission angle β. The experiments were conducted for only one value of nozzle exit velocity; hence,

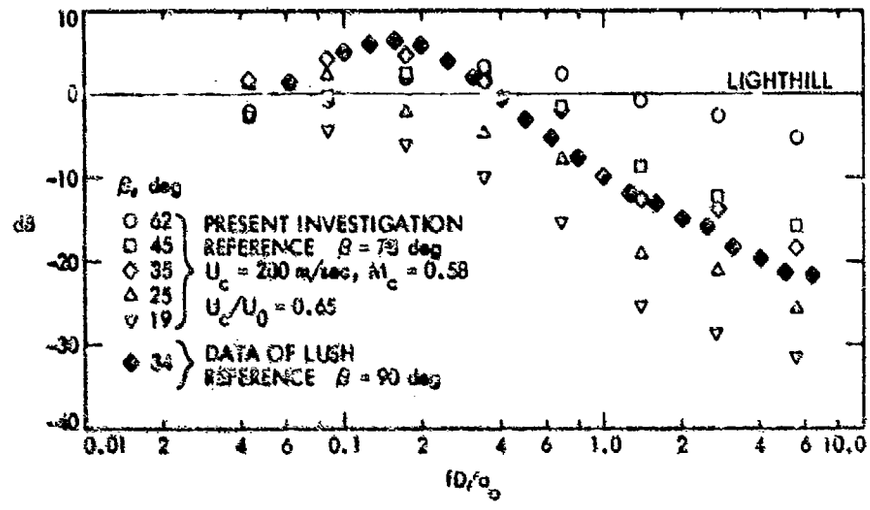

Figure 13. Comparison of Differences in Sound Pressure Levels With Lighthill's Theory

comparisons over a velocity range are not made. The experimental results shown were obtained with microphone Nos. 9 through 14 shown in Fig. 2. The locations of these microphones are given in Table 1. In order to be consistent with the model of convected sources the observed frequency is corrected for a Doppler shift so that the same source frequency is observed for any emission angle. The equation for this relationship in terms of the intensity referenced to an emission angle of 90° is

$$I(f,\beta) = \frac{R_{90}^2}{R_\beta^2} \frac{I\left(f\left\{[1 - M_c \cos\beta]^2 + \alpha^2 M_c^2\right\}^{\frac{1}{2}}, 90^\circ\right)}{\left\{[1 - M_c \cos\beta]^2 + \alpha^2 M_c^2\right\}^{5/2}} \qquad (2)$$

Equation (2) is based on Lighthill's prediction for the far field intensity of the noise generated by a turbulent flow as modified by Ffowcs Williams (Ref. 10) to apply to the noise radiated from a jet. See

also the discussion by Lush (Ref. 2).

Lush showed good agreement between Lighthill's theory and his experimental results for emission angles near 90° over a significant range of the frequency parameter. The data of the present investigation is referenced to an emission angle of 78° which is considered sufficiently near 90° for extrapolation to 90° without much loss in accuracy. Thus for the reference condition of $\theta = 78^\circ$ Eq. (2) becomes

$$I(\theta,\beta) = \frac{R_{78}^2}{R_\beta^2} \frac{I\left(f\left\{\frac{[1 - M_c\cos\beta]^2 + \alpha^2 M_c^2}{[1 - M_c\cos 78]^2 + \alpha^2 M_c^2}\right\}^{\frac{1}{2}}, 78\right)}{\left\{\frac{[1 - M_c\cos\beta]^2 + \alpha^2 M_c^2}{[1 - M_c\cos 78]^2 + \alpha^2 M_c^2}\right\}^{5/2}} \qquad (3)$$

The data of the present experiments shown in Fig. 13 were corrected with the use of Eq. (3). Furthermore, the convection velocity U_c, was chosen to be 200 m/sec. Thus $M_c = 0.58$. This selected value of U_c is based on the distributions shown in Fig. 7. At the nozzle exit (x = 0) the radius of the jet was about 3 cm; hence $U_c \simeq 200$ m/sec and since $U_0 \simeq 310$ m/sec, $U_c/U_0 = 0.65$. This is the same value of U_c/U_0 used by Lush who made use of the results obtained by Davis, Fisher and Barrett (Ref. 11). The quantity α was chosen to be 0.3 as used by Lush.

The results in Fig. 13 indicate that for low angles and high frequencies Lighthill's prediction (the zero dB line) is higher than the experimental data. This probably occurs because of the absence of appropriate accountability in the theory for the effects of refraction of the noise by the flow, and of the convection amplification which results from the source moving with the flow or more slowly than the flow. At low frequencies the experimental results are in reasonably good agreement with the theory especially at the larger angles; however, there is still an effect of the emission angle at the smaller angles. The comparison of the results at $\beta = 35^\circ$ with that of Lush at $\beta = 34^\circ$ is quite good over the entire frequency parameter range despite the significant difference in the stagnation temperatures of the two sets of data. This is the only emission angle common to the data of Lush and to the data of the present investigation.

Characterization of the radiated noise in terms of the autocorrelation function $\alpha\psi_n$, in the moving frame of reference of the eddies is shown as a three-dimensional display in Fig. 14. In this case the convection velocity was chosen to be 125 m/sec ($M_c = 0.36$), instead of 200 m/sec, because the lower value is more nearly a mean value over the extent of the jet as can be seen in Fig. 7. The effect of the convection velocity on the results is largely associated with the relationship between the time t, and the distance x. Since the correlation is determined primarily from geometric considerations, the distance scale in Fig. 14 would not be affected very much by such a difference in velocity but the time scale would. The autocorrelation function $\alpha\psi_n(t, \Delta t)$ reaches a maximum at about 13 cm downstream of the nozzle exit plane and then decays to a small value in about 5 milliseconds or approximately 60 cm from the

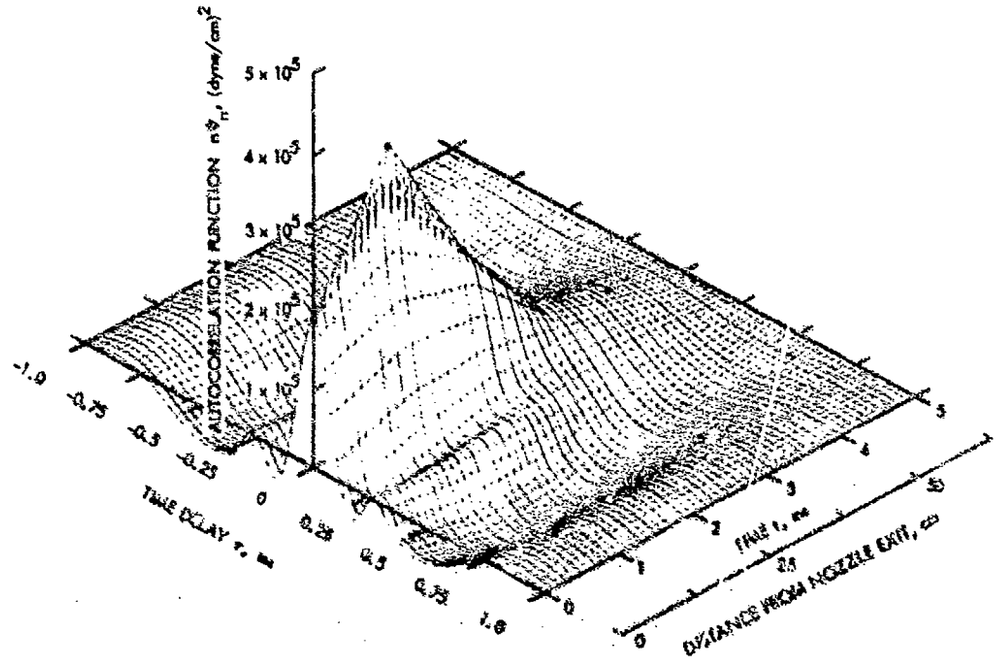

Figure 14. Autocorrelation Function of the Radiated Noise

nozzle. These distances correspond to about 4 and 13 jet diameters respectively from the flow separation location inside the nozzle. The method of evaluating this autocorrelation function is discussed in Appendix A3 and is demonstrated by the use of numerical values in the next paragraph. To acquire the cross correlations from which these results were obtained eight microphones were located in a circle as shown in Fig. 2. The angular region β, covered by the circular array, was between about 35 and 55°. The effects of refraction and convection amplification are, of course, included in the experimental results even

though the moving point-source theory does not take these effects into account.

The following numerical example is a description of the method that was used to compute the autocorrelation function shown in Fig. 14. A constant convection velocity of the eddies was assumed although allowance for a variable velocity could be incorporated into the procedure. Three frequency bands centered at 1, 3, and 9 kHz with $\alpha = 3$ were used to evaluate $\phi_1(\Delta t)$ using Eq. (A3-3) in Appendix A3. Note that this α refers to frequency bands of Eq. (A3-3) and differs from the α of Eqs. (2) and (3). For $\alpha = 3$, the bandwidth is about 1.6 octaves. The time increment δ, which was used to evaluate $g_1(t_2)$ in Eq. (A3-2) was 1.0 ms. Five increments were used which made it necessary to determine g_1 at 6 nodal points.

The experimental correlations $C(\tau)$, were evaluated from the signals of the following pairs of microphones shown in Fig. 2: 1 and 5, 2 and 6, 3 and 7, and 8 and 4. Also, the autocorrelation of microphone No. 1 (1 and 1 with time delay) was used. As an example of the shapes of these curves the experimental cross correlation for Nos. 8 and 4 and the autocorrelation of No. 1 and 1 with time delay are shown in Figs. 15 and 16. A fixed value of τ and a particular orientation of a microphone pair determine a line in the $\Delta t, t_2$ plane. The correlation $C(\tau)$ is a line integral of $n\overline{V}_n$ along this line. To obtain information about $n\overline{V}_n$ in various regions in this plane, different varieties of such paths (and therefore different orientations of microphones) were chosen. Points were then taken from each of these correlation curves

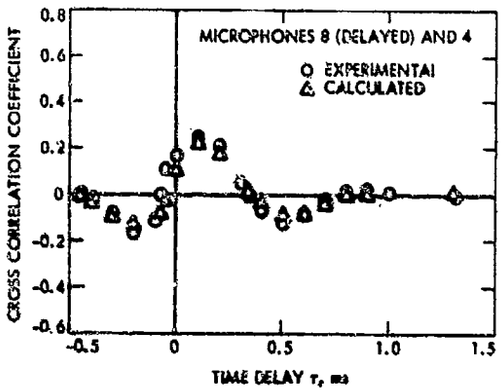

Figure 15. Comparison of Calculated Cross Correlation Coefficients with Experimental Values

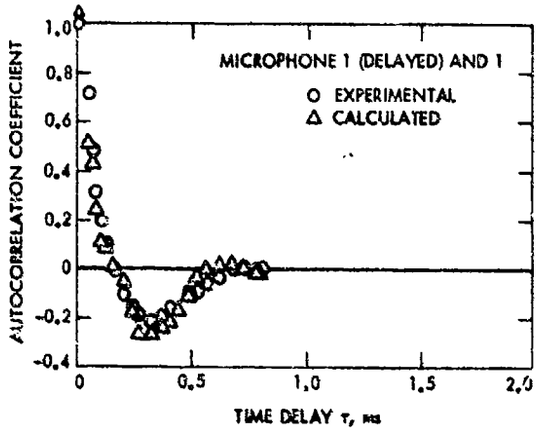

Figure 16. Comparison of Calculated Autocorrelation Coefficient with Experimental Values

at different values of time delay τ, thereby establishing a set of simultaneous equations. In theory, only a total of 18 values was required to evaluate the unknown coefficients since the number of nodal points chosen was 6 and the number of frequency bands was 3. However, a total of about 100 was used for better smoothing since the computation method involved the use of inversion by least squares. The source function in terms of the frequency and time, i.e., $n\overline{V}_n(f_1, t_2)$, obtained by this method for the three bands (Ref. 12) is consistent with observed trends for subsonic jets. For example, the noise sources at higher frequencies occur near the nozzle exit and the lower frequencies extend over a larger distance along the jet.

A check on the inversion by least squares of the computation method using the coarse time step was obtained by inserting the computed coefficients into Eq. (A3-1) and calculating values of $C(\tau)$. These computed values are shown in Figs. 15 and 16 for comparison with the experimental values. It is evident that the agreement is very good and hence, that the inversion gives good results.

10. CONCLUDING REMARKS

In this investigation experiments were conducted on a high-temperature subsonic jet which separated at a supersonic velocity inside the divergent portion of a nozzle. The separated jet flow progressed through a shock structure contained entirely within the nozzle and then became subsonic before it reached the nozzle exit plane.

It was demonstrated from measurements obtained within the jet flow outside the nozzle using spatially separated crossed laser beams set up as a fluctuation system that the noise sources can be characterized by radial and axial distributions of the convection velocity, the magnitude of the density fluctuations, and by correlations of the density fluctuations in the moving frame of reference of the eddies. Likewise, the radiated noise was characterized by correlations of signals detected from pairs of spatially separated microphones outside the jet. Based on this measurement technique of the radiated noise combined with the use of the convection velocity, the autocorrelation function of the noise in the moving reference frame of the eddies was evaluated together with the noise intensity and its spectral distribution. The analyses of the noise sources and of the radiated noise are based on moving point sources in the jet. A feature of these approaches is that they will lead to the determination of a relationship between the noise sources inside the jet and the radiated noise outside the jet based on experimental measurements.

Comparisons of the experimental noise results with Lighthill's theory of convected quadrupoles indicate good agreement at the lower frequencies, especially at the larger emission angles. At low angles and at high frequencies Lighthill's prediction is higher than the data. It is believed that this difference results primarily from neglecting the effects of refraction and of limitations in the accessibility

of convection amplification in the theory. The experimental noise results at one common emission angle agree quite well with the data of Lush even though there was a large difference in the stagnation temperatures of the jets investigated.

11. REFERENCES

1. M. J. Lighthill, "On Sound Generated Aerodynamically," Part I, "General Theory," Proceedings of the Royal Society (London), Series A, Vol. 211, No. 1107, March 20, 1952, pp. 564-587.

2. P. A. Lush, "Measurements of Subsonic Jet Noise and Comparison With Theory," Journal of Fluid Mechanics, Vol. 46, Part 3, April 13, 1971, pp. 477-500.

3. M. J. Lighthill, "On Sound Generated Aerodynamically," Part II, "Turbulence as a Source of Sound," Proceedings of the Royal Society (London), Series A, Vol. 222, No. 1148, February 23, 1954, pp. 1-32.

4. P. F. Massier and S. P. Parthasarathy, "An Anechoic Chamber Facility for Investigating Aerodynamic Noise," Technical Report 32-1564, Jet Propulsion Laboratory, Pasadena, California, September 15, 1972.

5. L. H. Back, P. F. Massier and R. F. Cuffel, "Heat Transfer Measurements in the Shock-Induced Flow Separation Region in a Supersonic Nozzle," AIAA Journal, Vol. 6, No. 5, May 1968, pp. 923-925.

6. R. F. Cuffel, L. H. Back and P. F. Massier, "Transonic Flow Field in a Supersonic Nozzle with Small Throat Radius of Curvature," AIAA Journal, Vol. 7, No. 7, July 1969, pp. 1364-1366.

7. L. H. Back and R. F. Cuffel, "Detection of Oblique Shocks in a Conical Nozzle with Circular-Arc Throats," AIAA Journal, Vol. 4, No. 12, December 1966, pp. 2219-2221.

8. L. H. Back, P. F. Massier and R. F. Cuffel, "Flow and Heat Transfer Measurements in Subsonic Air Flow Through a Contraction Section," International Journal of Heat and Mass Transfer, Vol. 12, No. 1, January 1969, pp. 1-13.

9. L. H. Back, P. F. Massier and R. F. Cuffel, "Flow Phenomena and Convective Heat Transfer in a Conical Supersonic Nozzle," Journal of Spacecraft and Rockets, Vol. 4, No. 8, August 1967, pp. 1040-1047.

10. J. E. Ffowcs Williams, "The Noise From Turbulence Convected at High Speed," Royal Society of London, Philosophical Transactions of the Royal Society (London), Series A, Vol. 255, 1962-1963, pp. 469-503.

11. P. O. A. L. Davies, M. J. Fisher and M. J. Barratt, "The Characteristics of the Turbulence in the Mixing Region of a Round Jet," Journal of Fluid Mechanics, Vol. 15, March 1963, pp. 337-367.

12. S. P. Parthasarathy, "Evaluation of the Noise Autocorrelation Function of Stationary and Moving Noise Sources by a Cross Correlation Method," AIAA Paper No. 73-186, January 10-12, 1973.

13. L. N. Wilson and R. J. Danckevits, "Statistical Properties of Turbulent Density Fluctuations," Journal of Fluid Mechanics, Vol. 43, August 1970, pp. 291-303.

12. ACKNOWLEDGMENTS

The authors greatly appreciate the assistance of Mr. T. H. Slover and Mr. S. J. Kikkert in conducting the experiments, in assembling the test apparatus and in analyzing the data.

A 1 AUTOCORRELATION FUNCTIONS OF A MOVING NOISE SOURCE

Autocorrelation functions for the fluctuating density of a moving noise source can be determined for a jet flow from measurements obtained by the crossed-beam laser-Schlieren method described in Appendix A2. In addition, such functions for the radiated noise can be determined from the cross correlations of the signals detected by a pair of microphones as described in Appendix A3. The moving source autocorrelation functions are important because they can be used to obtain a description of the entire noise field. In the moving reference frame fluctuations occur more slowly; hence, greater accuracy in time derivatives is obtainable. Thus the intensity and spectrum of the fluctuating density within the jet and the intensity and spectrum of the noise, which is related to the radiated sound pressure outside the jet, can be evaluated.

The autocorrelation function in the moving frame of reference of the eddies may be determined as follows: First, let $G(\underline{x},t)$ be a fluctuating random scalar function in the turbulent jet flow. In the present investigation, for example, it would represent the fluctuating density. At every point $\underline{x}$ a convection velocity $\underline{U}_c(\underline{x})$ is defined. If now a hypothetical probe is considered which senses a fluctuating quantity and which follows the motion of the eddies at the convection velocity, the signal observed would be given by $G(\underline{x}_0 + \int_0^t \underline{U}_c\, dt, t)$ where $\underline{x}_0$ is the initial position. Thus the quantity G, is a function of time only because $\underline{x}$ is a function of time taken along the trajectory of the probe.

The autocorrelation function obtained from the signals at different times (different locations) for a probe moving at the velocity $\underline{U}_c$, is given by the ensemble average of G as follows:

$$< \left[G\left(\underline{x}_0 + \int_0^t \underline{U}_c\, dt, t\right)\right] \left[G\left(\underline{x}_0 + \int_0^{t+\tau} \underline{U}_c\, dt, t+\tau\right)\right] >$$

The measurement obtained from the probe at one time after having been delayed by a time interval τ is multiplied by the measurement from the same probe obtained sometime later. If it is assumed that $G(\underline{x},t)$ is locally homogeneous and locally stationary, that is the mean value of G is not changing with time,

$$< G\left(\underline{x}_1,t_1\right) G\left(\underline{x}_2,t_2\right) > = \Psi\left(\underline{x}_1,t_1;\ \underline{x}_2 - \underline{x}_1, t_2 - t_1\right) \qquad \text{(A1-1)}$$

Ψ is a slowly varying function of $\underline{x}$ and t when the flow is approximately homogeneous and approximately stationary. For jets that are strictly stationary there is only a slow change of Ψ with $\underline{x}$ and for this case the right side of Eq. (A1-1) is equal to

$$\Psi\left(\underline{x}_1;\ \underline{x}_2 - \underline{x}_1,\ t_2 - t_1\right) \text{ or } \Psi\left(\underline{x};\ \int_0^{t+\tau} \underline{U}_c\, dt, \tau\right),$$

that is,

$$\Psi\left(\underline{x}_0 + \int_0^t \underline{U}_c\ (t)dt;\ \underline{U}_c\ (t)\tau, \tau\right).$$

This varies slowly with t and rapidly with τ. The coordinate $\underline{x}_0$ refers to the initial point at the nozzle exit. This is the function which is obtained from the laser beam cross correlations described in Appendix A2. There, the method of obtaining the autocorrelation function in the moving frame of reference is developed from the measurements of signals detected by the use of stationary beams. The noise autocorrelation function is converted to the moving reference frame by introducing the value of U_c determined from the laser data.

A 2 LASER SCHLIEREN ANALYSIS

This discussion pertains to the evaluation of the autocorrelation function of the fluctuating density for an observer that moves along the jet flow at the convection velocity of the eddies. The autocorrelation function in this moving frame of reference can be obtained from the detected signals emitted by stationary laser beams. This can be done either if several beams are displaced along the flow direction or else if one of the beams is moved to different positions at which data is obtained. The analytical procedure that will be followed is an extension of that used by Wilson and Damkevala (Ref. 13). A sketch of a typical arrangement is shown in Fig. A 2-1.

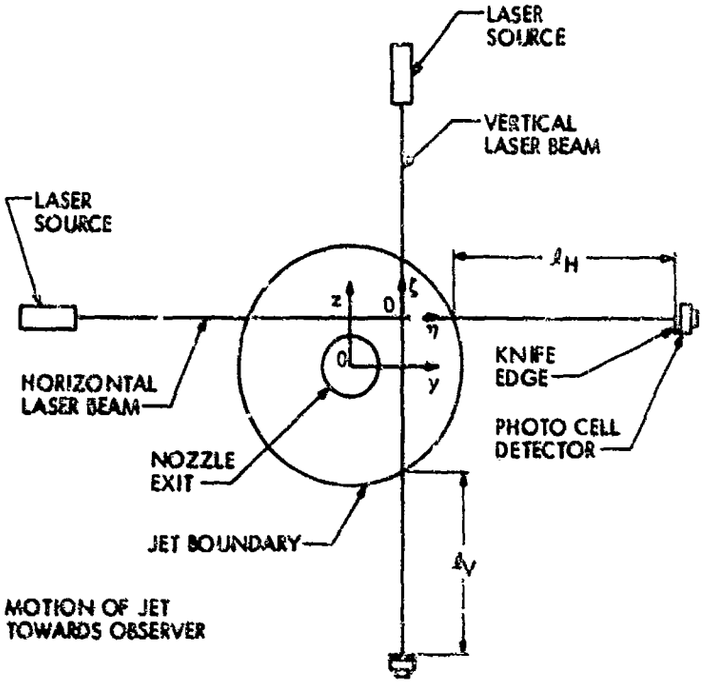

Figure A 2-1. Laser-Schlieren Arrangement

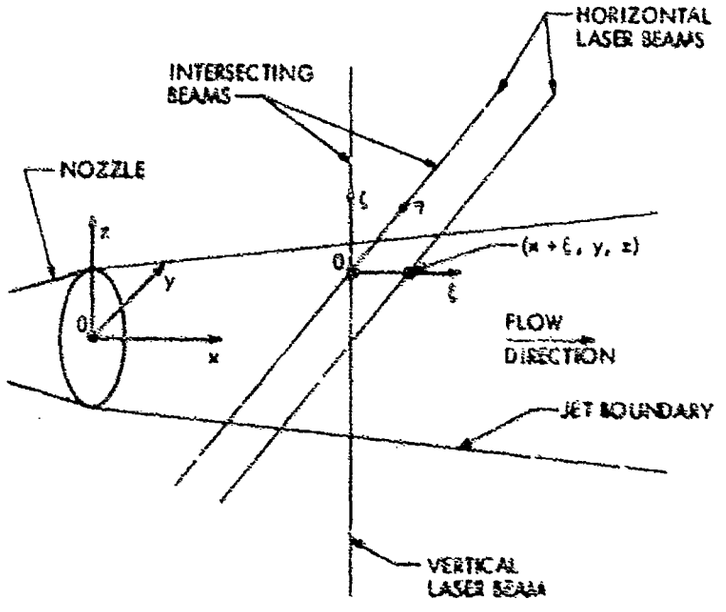

Figure A 2-2. Coordinate Axes x, y, z and ξ, η, ζ

As shown in Fig. A 2-1 the origin of the coordinates x, y and z is on the centerline of the nozzle at the nozzle exit plane. This figure represents a view looking upstream into the jet. Also, the coordinates ξ, η and ζ are in the directions x, y and z respectively but their origin is at the location where the vertical and the horizontal laser beams intersect. If the vertical and the horizontal beams are separated, this origin is located on the vertical beam at the intersection with a horizontal plane passed through

the horizontal beam. Thus, the displacement of a horizontal beam along the flow direction from the vertical beam is taken to be + ξ. The coordinates in three dimensions are shown in Fig. A 2-2.

As the beam passes through the jet it is deflected wherever there is a gradient in the refractive index. It can be shown that if n is the refractive index, the angular deflection γ, of the beam is given by

$$\gamma_H(t) = \int_{L_\eta} \frac{\partial n}{\partial x}\, d\eta \qquad \text{(A2-1)}$$

$$\gamma_V(t) = \int_{L_\zeta} \frac{\partial n}{\partial x}\, d\zeta \qquad \text{(A2-2)}$$

The subscripts H and V refer to the horizontal and to the vertical beams respectively. The dimensions L_η and L_ζ represent those portions of the beam lengths which lie within the jet diameter. Gradients of the refractive index in Eqs. (A2-1) and (A2-2) are taken along the flow direction because it is only the deflections that result from these gradients that will give correlations. If gradients perpendicular to the flow are sensed, Schlieren signals will be obtained; however, their cross correlations would be zero. Thus the knife edges of the Schlieren system must be aligned perpendicular to the flow for both the vertical and the horizontal beams.

The output signals of the Schlieren detectors may be expressed as follows:

$$e_H = S_H \ell_H \gamma_H \qquad \text{(A2-3)}$$

$$e_V = S_V \ell_V \gamma_V \qquad \text{(A2-4)}$$

S is the sensitivity and ℓ the beam length between the edge of the jet and the detector (Fig. A 2-1). The signal from the horizontal beam is delayed by a time interval τ, and thereby a correlation with the other signal is obtained which is the average of the product of the angular deflections as follows:

$$\langle \gamma_H (t - \tau)\, \gamma_V (t) \rangle = \int_{L_\eta} \int_{L_\zeta} \left\langle \left[\frac{\partial n}{\partial x}(t - \tau)\right]_\eta \left[\frac{\partial n}{\partial x}(t)\right]_\zeta \right\rangle d\eta d\zeta \qquad \text{(A2-5)}$$

The relationship between the refractive index and the density is $\partial n/\partial x = \epsilon\, [\partial \rho/\partial x]$ where ϵ is the Gladstone-Dale constant. Then, if Q_ρ is defined as the experimentally determined cross correlation function, its value in terms of the density gradient is established by combining Eqs. (A2-3) and (A2-4) to eliminate γ and n, and by introducing the relation between the refractive index and the density. For convenience, the quantities obtained from measurements are grouped together and equated to those quantities under the integrals that are to be determined. Thus

$$\frac{\langle e_H(t - \tau)\, e_V(t) \rangle}{S_H S_V \ell_H \ell_V \epsilon^2} = Q_\rho(x,y,z,\xi,\tau) = \int_{L_\eta} \int_{L_\zeta} \left\langle \frac{\partial \rho}{\partial x}(x, y + \eta, z, t - \tau)\, \frac{\partial \rho}{\partial x}(x + \xi, y, z + \zeta, t) \right\rangle d\eta d\zeta \qquad \text{(A2-6)}$$

In Eq. (A2-6) by denoting functions of $(y + \eta)$, $(x + \xi)$ and $(z + \zeta)$ it is assumed that in general the laser beams do not pass through the axis of the jet. However, this of course is not a requirement.

A2-1 Stationarity

Note that Q_ρ in Eq. (A2-6) is not a function of the time t, because of the stationarity of a real jet. This is a valid assumption because the time period t, is orders of magnitude larger than the time delay τ, which is measured in milliseconds.

A2-2 Homogeneity

If in addition to local stationarity the fluctuations are considered to be homogeneous over distances for which the correlation in the integrand contributes appreciably to the integral, that is, if there is a weak dependence on x, y and z but a strong dependence on ξ, η and ζ,

$$\left\langle \frac{\partial \rho}{\partial x}(x, y + \eta, z, t - \tau)\, \frac{\partial \rho}{\partial x}(x + \xi, y, z + \zeta, t) \right\rangle = - \frac{\partial^2}{\partial \xi^2} \langle \rho(x,y,z,t)\, \rho(x + \xi, y - \eta, z + \zeta, t + \tau) \rangle$$

$$= - \frac{\partial^2}{\partial \xi^2} Q(x,y,z; \xi, -\eta, \zeta, \tau) \qquad \text{(A2-7)}$$

The defined quantity Q, is the two-point correlation function of the fluctuating density. In a real jet the condition of homogeneity is not strictly satisfied because of the growth in diameter along the flow direction (development of the flow with respect to position). Nevertheless, at beam locations downstream of the nozzle exit plane the influence of changes in ξ, η and ζ on the value of Q is much greater than is the influence of the same changes in x, y and z.

It is permissible to extend the limits of integration to the range of $-\infty$ to $+\infty$ because the correlation in the integrand vanishes for large distances of η and ζ, that is, beyond the boundaries of the eddy, which can be no larger than the jet. Thus, combination of Eqs. (A2-6) and (A2-7) gives

$$Q_\rho(x,y,z,\xi,\tau) = - \int_{-\infty}^{\infty} \int_{-\infty}^{\infty} \frac{\partial^2}{\partial \xi^2} Q(x,y,z; \xi, -\eta, \zeta, \tau)\, d\eta d\zeta \qquad \text{(A2-8)}$$

A2-3 Isotropy

The quantity to be determined in Eq. (A2-8) is the autocorrelation function Q; consequently, this equation must be inverted. In order to simplify this procedure the fluctuations will be considered to be isotropic. The assumption of isotropic fluctuations implies that fixed values of the cross correlation coefficient are spherical surfaces. Furthermore, it implies that as the eddies move downstream they become larger. Actually, however, the peak cross correlations become smaller; hence, the "sizes" (radii) of the spherical surfaces become smaller until they finally diminish. Nevertheless, by assuming isotropy Eq. (A2-8) becomes

$$Q_g(x,y,z;\,\xi,\tau) = -\int_{-\infty}^{\infty}\int_{-\infty}^{\infty}\frac{\partial^2}{\partial\xi^2}\,Q\left(x,y,z;\sqrt{[\xi - U_c\tau]^2+\eta^2,\ \zeta^2},\ \tau\right)d\eta d\zeta \tag{A2-9}$$

Note that in Eq. (A2-9) the quantity $[\xi - U_c\tau]^2$ has been substituted for ξ^2. U_c is the convection velocity of the eddies along ξ (the flow direction); therefore, by this substitution Eq. (A2-9) has been converted into the moving frame of reference of the eddies. The inversion can be accomplished by a change of variables and mathematical manipulation. Thus, define R and μ as follows:

$$R \equiv \sqrt{[\xi - U_c\tau]^2 + \eta^2 + \zeta^2} \tag{A2-10}$$

$$\mu \equiv \xi - U_c\tau \tag{A2-11}$$

Next, consider the influence of x, y and z to be small compared to ξ, η and ζ and combine Eqs. (A2-9) and (A2-10).

$$Q_g(\xi,\tau) = -\int_{-\infty}^{\infty}\int_{-\infty}^{\infty}\frac{\partial^2}{\partial\xi^2}\,Q\ (R,\tau)\ d\eta\ d\xi \tag{A2-12}$$

Then it can be shown that

$$\left[\frac{\partial Q}{\partial\xi}\right]_{\eta,\zeta,\tau} = \frac{\partial Q}{\partial R}\frac{\mu}{R} \tag{A2-13}$$

$$\left[\frac{\partial^2 Q}{\partial\xi^2}\right]_{\eta,\zeta,\tau} = \frac{1}{R}\frac{\partial Q}{\partial R} + \frac{\mu^2}{R}\frac{\partial}{\partial R}\left[\frac{1}{R}\frac{\partial Q}{\partial R}\right] \tag{A2-14}$$

The area integral $\int_{-\infty}^{\infty}\int_{-\infty}^{\infty} d\eta d\zeta$ of Eq. (A2-12) which is the cross sectional area of the jet can be evaluated by the following change of variable:

$$r^2 = \eta^2 + \zeta^2 \tag{A2-15}$$

The integration of r is from 0 to ∞. Thus

$$\int_{-\infty}^{\infty}\int_{-\infty}^{\infty} d\eta d\zeta = 2\pi\int_0^{\infty} r\,dr \tag{A2-16}$$

For integration across the radial plane μ and τ are constant and from Eq. (A2-10) it can be shown that

$$r\,dr = R\,dR \tag{A2-17}$$

The integration of R is from μ to ∞. Therefore Eq. (A2-12) becomes the following after introducing Eqs. (A2-14), (A2-16) and (A2-17):

$$Q_g(\xi,\tau) = -2\pi\int_{\mu}^{\infty}\left\{\frac{1}{R}\frac{\partial Q}{\partial R} + \frac{\mu^2}{R}\frac{\partial}{\partial R}\frac{1}{R}\frac{\partial Q}{\partial R}\right\} R\,dR \tag{A2-18}$$

By integration Eq. (A2-18) becomes

$$Q_g(\xi,\tau) = 2\pi\frac{\partial}{\partial\mu}\left[\mu\ Q\ (\mu,\tau)\right] \tag{A2-19}$$

After a second integration and noting that $\mu = \xi - U_c\tau$, the desired autocorrelation function Q can be made the dependent variable.

$$Q(\mu,\tau) = \frac{1}{2\pi\mu}\int_{\xi=U_c\tau}^{\xi=\mu+U_c\tau} Q_g(\xi,\tau)\ d\xi \tag{A2-20}$$

Then by applying L'Hospital's Rule to Eq. (A2-20)

$$Q(0,\tau_1) = \frac{1}{2\pi}\left[Q_g(U_c\tau,\tau_1)\right] \tag{A2-21}$$

Thus the inversion has been completed for the condition of isotropy. The quantity Q_g is evaluated from measurements made with the laser beams that project through the flow. These measurements are integrations across the eddies. It can be shown, however, that at any fixed value of time delay τ, the point $\mu = 0$ corresponds to the maximum values of the $Q_g(\xi,\tau)$ vs ξ curves. This is accomplished by a Taylor

series expansion and by the requirement of symmetry around $\mu = 0$. It means that the convection velocity U_c, introduced into Q in Eq. (A2-9) can be evaluated experimentally from the $Q_s(\xi,\tau)$ curves. This convection velocity has significance in itself; however, it is also introduced into the relations that characterize the radiated noise.

The quantity which is related to the noise source term in the acoustic equation is the second derivative of $Q(0,\tau_i)$ with respect to time delay τ. The subscript i denotes the values of τ which establish the envelope of the family of cross correlation curves. Thus the noise radiated outside the jet is related to the fluctuating density inside the jet as follows:

$$\Psi_d \propto \left[\frac{\partial U}{\partial y}\right]^2 \left[\frac{\partial^2 Q(0,\tau_i)}{\partial \tau^2}\right] \qquad (A2\text{-}22)$$

The validity of the assumption of isotropy for the fluctuating density is not known by experiment at the present time; consequently, the possibilities of relaxing this assumption by means of other models are in order.

A2-4 Nonisotropic fluctuations

Consider a more realistic concept, that for which the surfaces formed by constant values of the cross correlations are ellipsoidal (rather than spherical) with the major axis a, oriented along the flow in the ξ direction. The other two axes b and c, are not necessarily equal. For this case Eq. (A2-9) may be written as

$$Q_s(x,y,z;\xi,\tau) = -\int_{-\infty}^{\infty}\int_{-\infty}^{\infty} \frac{\partial^2}{\partial \xi^2} Q\left(x,y,z;\sqrt{\frac{[\xi - U_c\tau]^2}{a^2} + \frac{\eta^2}{b^2} + \frac{\zeta^2}{c^2}},\ \tau\right) d\eta d\zeta \qquad (A2\text{-}23)$$

By following the same procedure of inversion as for the isotropic case, Eq. (A2-21) becomes

$$Q(0,\tau_i) = \frac{1}{2\pi}\left[\frac{a^2}{bc}\right]\left[Q_s\left(U_c\tau,\tau_i\right)\right] \qquad (A2\text{-}24)$$

Eq. (A2-24), which applies for ellipsoidal surfaces is the same as the isotropic relation except for the factor $[a^2/bc]$. Hence, it is apparent that this term increases the autocorrelation function because it is likely that the elongation occurs along ξ (or x) in the direction of largest flow expansion of the jet. An experimental evaluation of the factor $[a^2/bc]$ for the fluctuating density has, however, not been accomplished. Therefore, this approach cannot be used in the analysis of the data unless it were merely for comparative purposes with the use of selected values of $[a^2/bc]$. This has not been done, however. When spherical symmetry does not exist, the rotational effect must also be taken into account, however, this effect is not considered here.

A 3 MICROPHONE ANALYSIS

The theory for the evaluation of the autocorrelation function W_n, of the radiated noise as determined from measurements obtained with the use of pairs of microphones is described in detail by Parthasarathy in Ref. 12. There, stationary noise sources are considered first and then the theory is extended to moving sources such as those that occur in subsonic and in supersonic jets. For subsonic jets, as considered in this investigation, the experimentally determined cross correlation function $C(\tau)$, may be expressed as

$$C(\tau) = n \int_{-\infty}^{\infty} \frac{W_n\left(t - \tau - \frac{r_1}{a_o}(t-\tau)\ ,\ t - \frac{r_2}{a_o}(t)\right) dt}{r_1(t-\tau)\left[1 - M_c \cos \theta_1(t-\tau)\right]^2 r_2(t)\left[1 - M_c \cos \theta_2(t)\right]^2} \qquad \text{(A3-1)}$$

The lower limits of integration are:

$$T_2 \quad \text{if} \quad T_2 > T_1 + \tau$$

$$T_1 + \tau \quad \text{if} \quad T_2 < T_1 + \tau$$

In Eq. (A3-1) the autocorrelation function of the noise W_n, contains the constant $1/16\,\pi^2$. The cross correlation function $C(\tau)$, is evaluated from experimental measurements and the unknown variable is the autocorrelation function of the noise W_n, in the moving frame of reference of the eddies. Thus, in order to evaluate W_n Eq. (A3-1) must be inverted. To do this it is convenient to consider W_n as a function of a time difference $\Delta t = t_2 - t_1$ and t_2. By referring to Eq. (A3-1) it will be noted that if t_2 is set equal to $(t - r_2(t)/a_o)$, then Δt is $(r_2(t)/a_o - r_1(t-\tau)/a_o + \tau)$. It is also convenient to represent W_n in the form

$$nW_n(\Delta t, t_2) = \sum_{i=1}^{N_1} g_i(t_2)\, \phi_i(\Delta t) \qquad \text{(A3-2)}$$

Thus, g_i is a function of t_2 only and ϕ_i is a function of Δt only. The quantity $\phi_i(\Delta t)$ is chosen to be the autocorrelation functions representing the noise in the various octave (or wider) bands N_1. These functions are of the type (Ref. 12):

$$\phi_i(\Delta t) = \cos 2\pi f_i \Delta t \, \frac{\sin \frac{\alpha-1}{\alpha+1} 2\pi f_i \Delta t}{\frac{\alpha-1}{\alpha+1} 2\pi f_i \Delta t} \qquad \text{(A3-3)}$$

Thus, Eq. (A3-3) represents an autocorrelation function for each chosen band. The frequency f_i, is at the center of this band and the ratio of the highest frequency at the edge of the band to the lowest frequency is α. For an octave band, $\alpha = 2$.

The other function in Eq. (A3-2), $g_i(t_2)$, is taken to be piece-wise linear with value $g_i(j\delta)$ defined at the nodes $0, \delta, \cdots j\delta \cdots N_2\delta$ along t_2. Therefore, in Eq. (A3-2) there are $N_1 N_2$ unknown coefficients that must be determined to evaluate W_n. These coefficients can be determined from a set of simultaneous equations that result from the use of Eq. (A3-1) if known values of the cross correlations and of the autocorrelations are introduced for $C(\tau)$. Evaluation of the unknown coefficients involves the use of inversion by least squares. Only positive values of the coefficients are selected since the noise is being radiated out of the jet. A numerical example of the procedure is given in Section 9, RADIATED NOISE.

DIRECT MEASUREMENT OF SOUND SOURCES IN AIR JETS USING THE CROSSED BEAM CORRELATION TECHNIQUE

R. J. Damkevala
Cambridge Collaborative
238 Main Street, Cambridge, Massachusetts

F. R. Grosche
DFVLR-AVA Göttingen
Göttingen, W. Germany

S. H. Guest
NASA/George C. Marshall Space Flight Center
Huntsville, Alabama

SUMMARY

Properties of density fluctuations were measured in the turbulent regions of a 2.54 cm air jet, at M = 0.7, 1.0 and 1.94. After calibration tests, it was found that the absorption of infrared radiation at 4.3 microns by the naturally present quantities of carbon-dioxide in air was directly proportional to the air density if a sufficiently wide bandpass (0.08μ)was used. Moreover, regions of the band could be selected that adequately discriminated against temperature variations. The cross-correlation of two such beams intersecting in the jet gave a measure of the local properties at the intersection point.

The paper presents a derivation relating the local density correlation function to the self and shear generated noise in the far field of the jet. The measured correlations are used to predict the axial distribution of source strengths and the spectrum of noise due to a unit volume of turbulence.

LIST OF SYMBOLS

a	velocity of sound
D	jet diameter
I	signal
i	fluctuating component of signal
K	absorption coefficient
k	fluctuating component of absorption coefficient
M	local Mach Number
p	acoustic pressure
p^1	pseudosound pressure
r	radial distance from jet axis
R_E	correlation function in fixed coordinates
R_L	correlation function in moving reference frame
X	position vector of observer location
Y,Z	position vectors inside flow region
$\xi(\xi,\eta,\zeta)$	vector with Y as origin
τ	time delay
θ	angle between flow direction and observer
ρ	fluctuating component of density

1. MEASUREMENT TECHNIQUE

1.1 Optical Crossed Beam Correlation Technique

If a beam of radiation passes through a turbulent fluid which modulates the beam by an absorption process, the transmitted signal $I(t)$ can be expressed in terms of the initial unabsorbed signal I_o and an absorption coefficient $K(t)$ by Beer's Law :

$$I(t) = I_o \, e^{-\int K(t)\, d\eta} \qquad (1\text{-}1)$$

If now we separate the mean and fluctuating parts of the instantaneous signal and the absorption coefficients, it can be shown that:

$$i(t) = \bar{I} \int k(t)\, d\eta \qquad (1\text{-}2)$$

where $\bar{I}$ is the transmitted mean signal level; that is, the mean signal at the photodetector.

The basic crossed beam arrangement using this concept was proposed by Krause and Fisher [1] in 1965. Two beams of radiation, which may be adjusted to a known separation in the flow direction, are passed through the flow field in mutually perpendicular directions. Cross correlation of the fluctuating transmitted signals will yield turbulent properties of the area that is common to both the beam paths. Specifically, if the beams intersect, the time averaged product of the two signals will be finite only in the neighborhood of the intersection point in a region of the dimensions of the turbulent length scales along the two beams. We can therefore write, using the beam geometry shown in Fig. 1:

$$R_E(\xi,\tau) = \frac{< i_1(t)\, i_2(t) >}{\bar{I}_1 \quad \bar{I}_2}$$

$$= \int_{-L_2/2}^{L_2/2} \int_{-L_3/2}^{L_3/2} < k(y_1, y_2+\eta, y_3, t)\; k(y_1+\xi, y_2, y_3+\zeta, t+\tau) > \, d\eta \, d\zeta \qquad (1\text{-}3)$$

L_2, L_3 are the radial scales. We can assume, to a good degree of approximation, that $k(t)$ is reasonably constant within the correlated area. Then, for intersecting beams ($\xi = 0$),

$$R_E(0,0) = < k^2(Y) > L_2 L_3 \qquad (1\text{-}4)$$

Since radial scales are relatively constant across a jet cross section [2], the covariance $R(0,0)$ is thus directly proportional to the intensity of the absorption coefficient fluctuation at the beam intersection point.

As the vertical beam is moved downstream, the correlation function $R_E(\xi,\tau)$ will trace a set of curves similar to those shown in Fig. 2. The envelope of the curves represents the auto-correlation function in a reference frame moving with the fluid at its convection speed. We shall use the symbol $R_L(0,\tau)$ for this autocorrelation function. The rate of fall of $R_L(0,\tau)$ is directly related to the eddy lifetime or decay of turbulence and varies with the region of the jet in which it is measured.

1.2 Relation Between Measured Signals and Thermodynamic Fluctuations

Fluctuations in the absorption coefficient can be related to fluctuations of thermodynamic properties of the gas from the known spectroscopic properties of the radiation employed. Unfortunately none of the constituents of atmospheric air have strong absorption bands in the visible portion of the spectrum. Initial experiments were conducted with ultraviolet radiation beams centered at 1850Å where oxygen has a continuum absorption band [3]. Two problems became apparent. The first was the difficulty of obtaining a strong steady source in this region and the second was that strong scattered signals were obtained from the natural particles in the air jet. The scattered signal varied with the diameter of these particles and also with the concentration of water droplets entrained by the dry jet from the surrounding air.

The fundamental vibration bands of CO_2 in the infrared region around 4.3μ were found to be free from most of these problems. The longer wavelength reduced the amount of scattering from natural tracers, while an electrically heated tungsten-carbide rod (Globar) produced strong steady emission in the infrared. Experiments were conducted in a calibration cell [4], [5] to obtain the exact spectroscopic properties at the pressures, concentrations and temperatures expected in unheated and heated air jets of subsonic and moderately supersonic Mach numbers. It was found that the weak line approximation is valid for low concentrations (< 0.1%) of CO_2 at atmospheric pressure and above. In this case, the absorption is directly proportional to the partial pressure of the CO_2. Figure 3 shows the plots of the derivative of the absorption coefficient, K, with respect to CO_2 concentration, f, versus wavelength with f as a parameter. Using a bandpass setting of .08μ, effects of varying temperature can be minimized in the wings of the band at wavelength settings of 4.2μ and 4.31μ.

All the measurements reported in this paper were made at the 4.31μ setting because of the greater absorption at 4.31μ compared to 4.20μ. The measured signals are proportional to the partial pressure fluctuations of CO_2 and hence to the density fluctuations of the air $\rho(t)$, independent of temperature effects. Therefore, from eqs. (1-3) and (1-4)

$$R_B(Y,\xi,\tau) = \int\int \langle \rho(y_1,y_2+\eta,y_3,t)\ \rho(y_1+\xi,y_2,y_3+\zeta,t+\tau)\rangle\, d\eta\ d\zeta$$

$$= L_2 L_3 \langle \rho(Y,0,t)\ \rho(Y,\xi,t+\tau)\rangle \qquad (1\text{-}5)$$

and $R(0,0) \propto \langle \rho^2(Y)\rangle$ (1-6)

The measured correlation function with intersecting beams will be proportional to the mean square density fluctuations at the intersection point.

2. APPLICATION TO SOUND SOURCE MEASUREMENT

2.1 The Sound Source Integral

We start from Lighthill's formula [6] for the sound radiation field in terms of the quadrupole distribution T_{ij}:

$$\rho(X,t) - \rho_0 = \frac{1}{4\pi a_0^2} \int \frac{(x_i-y_i)\ (x_j-y_j)}{|X-Y|^3} \frac{\partial^2}{\partial t^2} T_{ij}\left(Y, t - \frac{|X-Y|}{a_0}\right) dY \qquad (2\text{-}1)$$

where $T_{ij} = \rho v_i v_j + p_{ij} - a_0^2 \rho\, \delta_{ij}$. (2-2)

The coordinate system for this equation is shown in Fig. 4. At distances x large compared with the dimensions of the jet, equation (2-1) reduces to the form:

$$\rho(X,t) - \rho_0 \approx \frac{x_i x_j}{4\pi a_0^2 x^3} \int \frac{\partial^2}{\partial t^2} T_{ij}\left(Y, t - \frac{|X-Y|}{a_0}\right) dY \qquad (2\text{-}3)$$

Furthermore, in the far field, the pressure fluctuations are dominated by the acoustic radiation field p' so that $\rho - \rho_0$ can be replaced by $1/a_0^2\ p'(X,t)$ [7]. The autocorrelation of the far field pressure fluctuations may be written in a special way to give the relation

$$P(X,t,\tau') = \langle p'(X,t)\ p'(X,t+\tau')\rangle$$

$$= \frac{x_i x_j x_k x_l}{16\pi^2 a_0^4 x^4} \int\int \left\langle \frac{\partial^2 T_{ij}}{\partial t^2}\left(Y, t - \frac{|X-Y|}{a_0}\right) \frac{\partial^2 T_{kl}}{\partial t^2}\right.$$

$$\left.\left(Z, t - \frac{|X-Z|}{a_0} + \tau'\right)\right\rangle dY\ dZ \qquad (2\text{-}4)$$

Here τ' is an arbitrary time delay. The integrand is a time averaged product of the second derivatives of the stress measured at two points Y and Z in the flow. If we consider only statistically steady jets, eq. (2-4) can be written in the alternative form:

$$P(X,\tau') = \frac{x_i x_j x_k x_l}{16\pi^2 a_0^4 x^2} \int\int_{-\infty} \frac{\partial^4}{\partial \tau^4} R_{ijkl}(Y,\xi,\tau)\, d\xi\ dY \qquad (2\text{-}5)$$

where we have substituted

$$\tau_1 = t - \frac{|X-Y|}{a_0}$$

$$\tau_2 = t - \frac{|X-Z|}{a_0}$$

$$\tau = \tau_2 - \tau_1 + \tau' = \frac{\xi\cdot(X-Y)}{a_0|X-Y|} + \tau' \qquad (2\text{-}6)$$

and $R_{ijkl} = \langle T_{ij}(Y,\tau_1)\, T_{kl}(Y,\underline{\xi},\tau_1+\tau) \rangle$ (2-7)

To minimize the effects of convection of space derivatives past the stationary measuring system, we introduce a new frame of reference moving at the convection speed of the covariance R_{ijkl}. The transformation in terms of the convection Mach No. M is made by substituting

$$\underline{\lambda} = \underline{\xi} - a_o M \tau$$

and (2-8)

$$R_L(Y,\underline{\lambda},\tau) = R_{ijkl}(Y,\underline{\xi},\tau)$$

With this transformation, eq. (2-5) becomes [8]

$$P(X,t,\tau) = \frac{x_i x_j x_k x_l}{16\pi^2 a_o^4 x^6 \left[1 - \frac{M\cdot(X-Y)}{|X-Y|}\right]^5} \int\int \frac{\partial^4}{\partial\tau^4} R_L(Y,\underline{\lambda},\tau)\, d\underline{\lambda}\, dY$$

$$= \frac{x_i x_j x_k x_l}{16\pi^2 a_o^4 x^6 (1 - M\cos\theta)^5} \int\int \frac{\partial^4}{\partial\tau^4} R_L(Y,\underline{\lambda},\tau)\, d\underline{\lambda}\, dY \qquad (2-9)$$

where θ is the angle between the vector (X-Y) and the flow direction. For correlation lengths << typical wavelengths of sound, τ can be set equal to zero; i.e. the phase differences within an eddy could be neglected in the moving frame. This would complete the elimination of any apparent convection effects from the integral, the sole effect appearing in the factor $(1 - M\cos\theta)^{-5}$.

The integration with respect to $\underline{\lambda}$ gives the contribution of one "eddy" (which passed through Y at time t) to the far field pressure fluctuations. We shall call this term the sound source integral $S(Y,t)$.

$$S(Y,t) = \int \frac{\partial^4}{\partial\tau^4} R_L(Y,\underline{\lambda},0)\, d\underline{\lambda} \,. \qquad (2-10)$$

2.2 Application to Low Speed Case

In the case of jet turbulence, there will be a large shear gradient in the flow. The far field jet noise can be looked upon as having two distinct components, with separate spectra. One is due to the turbulence alone and is called self-noise. The other arises from cross-coupling of the turbulence with the mean flow shear and is called shear noise.

2.2.1 Self Noise

If there is no appreciable shear in the flow we can obtain R_{ijkl} in terms of the pressure or density covariance using the approach of Ribner [7]. He considers the pressure field as composed of an ambient pressure (which we shall take as zero), a pseudosound field p^0 and a sound field p'. The pseudosound field dominates within and near the turbulence at subsonic speeds constituting what is known as the acoustic near field. Further out it is overridden by the acoustic radiation field p'. The p^0 field is dominated by inertial effects much like the pressure field in an incompressible flow. The acoustic source strength is related to the pseudosound pressure p^0 by the relation from dilatation theory [8]

$$\frac{\partial m}{\partial t} = -\frac{\partial^2 p^0}{\partial t^2} \qquad (2-11)$$

Taking the mean-square value of this,

$$\frac{\partial^4}{\partial\tau^4} R_{ijkl} = \frac{\partial^4}{\partial\tau^4} R_p(Y,\underline{\xi},\tau) \qquad (2-12)$$

where $R_E(Y,\underline{\xi},\tau) = \langle \rho^o(Y,0,t)\ \rho^o(Y,\underline{\xi},t+\tau) \rangle$.

The pseudosound pressure p^o is essentially the local pressure fluctuation in the turbulence at low jet speeds. Thus the source strength can be written in terms of the density covariance as measured by the crossed beam correlation technique after transforming to a moving reference frame: we can write from eq. (2-10)

$$S_{self}(Y,t) = \int \frac{\partial^4}{\partial\tau^4} R_L(Y,\underline{\lambda},0)\ d\underline{\lambda} \tag{2-13}$$

2.2.2 Shear Noise

To bring out the importance of the velocity gradient, Lighthill [9] writes the time derivative of $\rho\ v_i\ v_j$ as space derivatives using the equations of motion

$$\frac{\partial}{\partial t}(\rho\ v_i\ v_j) = p_{ik}\frac{\partial v_j}{\partial y_k} + p_{jk}\frac{\partial v_i}{\partial y_k} - \frac{\partial}{\partial y_k}(\rho\ v_i\ v_j\ v_k + p_{ik}\ v_j + p_{jk}\ v_i)$$

Neglecting the viscous terms in p_{ik} and p_{jk} and the last term which will drop out when integrated over all space,

$$\frac{\partial}{\partial t}(\rho\ v_i\ v_j) = p\left(\frac{\partial v_i}{\partial y_j} + \frac{\partial v_j}{\partial y_i}\right)$$

$$= p^o\ e_{ij} \tag{2-14}$$

The rate-of-strain tensor e_{ij} defines the distortion of a fluid element. In case of strong shear regions like the mixing layers of jets, the mean shear $\bar{e}_{12}$ overrides the fluctuating shear and the dominant quadrupole is $T_{12} \approx \rho v_1 v_2$. The rate of strain in eq. (2-14) can then be replaced by its dominant term dU_1/dy_2, and we obtain the source strength [10]

$$\frac{\partial^2}{\partial t^2} T_{ij} = \frac{\partial^2}{\partial t^2}(\rho\ v_i\ v_j) \approx \left(\frac{dU_1}{dy_2}\right)\frac{\partial p^o}{\partial t} \tag{2-15}$$

and

$$\frac{\partial^4}{\partial\tau^4} R_{ijkl} = a_o^4 \left(\frac{dU_1}{dy_2}\right)^2 \frac{\partial^2}{\partial\tau^2} R_E(Y,\underline{\xi},\tau) \tag{2-16}$$

Equation (2-16) relates the crossed beam covariance $R_E(Y,\underline{\xi},\tau)$ to the source strength. Evaluation of the sound source integral requires correlations in a moving reference frame. Hence, we can write from eq. (2-10) for shear noise:

$$S_{shear}(Y,t) = a_o^4 \left(\frac{dU_1}{dy_2}\right)^2 \int \frac{\partial^2}{\partial\tau^2} R_L(Y,\underline{\lambda},0)\ d\underline{\lambda} \tag{2-17}$$

2.3 Noise Spectrum

Combining eq. (2-6) and (2-8) gives us the relationship between the time scales in the moving and fixed frames of reference

$$\tau = \frac{\underline{\lambda}\cdot(X-Y) + a_o\ \tau'\ |X-Y|}{a_o\ (|X-Y| - M\cdot(X-Y))} \tag{2-18}$$

$$= \frac{\lambda\cos\theta'}{a_o[1 - M\cos\theta]} + \frac{\tau'}{[1 - M\cos\theta]}$$

where θ' is the angle between $\underline{\lambda}$ and $(X-Y)$
and θ is the angle between M and $(X-Y)$

For low speeds the first term on the right hand side will be very small compared to the second, and

$$\tau = \frac{\tau'}{1 - M \cos\theta} \tag{2-19}$$

Hence the frequencies are to be multiplied by a factor $1/(1 - M \cos\theta)$ when obtaining spectrum for noise as perceived by a fixed observer. The energy spectrum is obtained by Fourier transformation of equations (2-13) and (2-17)

$$E_{self}(f_L) = \int \frac{\partial^4}{\partial\tau^4} R_L(\tau') \cos(2\pi f_L \tau')\, d\tau' \tag{2-20}$$

$$E_{shear}(f_L) = a_o^4 \left(\frac{dU}{dy_2}\right)^2 \int \frac{\partial^2}{\partial\tau^2} R_L(\tau') \cos(2\pi f_L \tau')\, d\tau' \tag{2-21}$$

where f_L is the frequency in the moving reference frame and the corresponding frequencies in the fixed frame should be obtained according to

$$f = \frac{f_L}{1 - M \cos\theta} \tag{2-22}$$

2.4 Application to Crossed Beam Technology

The covariances pertinent to the determination of sound source intensities must be measured in, or at least related to, a moving frame of reference given by the transformation

$$\underline{\lambda} = \underline{\xi} - a_o M \tau.$$

With the crossed beam system at 4.3 microns, we measure the two-point density covariance $R_\rho(Y,\underline{\xi},\tau)$ with ξ as a parameter as shown in Fig. 2. The envelope of these curves is $R_L(Y,\lambda=0,\tau)$, each point on the envelope represents the value of the covariance when $\lambda = \xi - U_o\tau = 0$ and hence is an autocorrelation function in a frame moving at the convection speed U_o.

We are interested in evaluating the self and shear noise components of eq. (2-10) given by:

$$S_{self}(Y,t) = \int \frac{\partial^4}{\partial\tau^4} R_L(Y,\underline{\lambda},0)\, d\underline{\lambda} \tag{2-13}$$

$$S_{shear}(Y,t) = a_o^4 \left(\frac{dU_1}{dy_2}\right)^2 \int \frac{\partial^2}{\partial\tau^2} R_L(Y,\underline{\lambda},0)\, d\underline{\lambda} \tag{2-17}$$

Referring to Fig. 2, at $\tau = 0$, $\lambda_1 = \xi_1$ and $R_\rho(Y,\lambda_1,0) = R_\rho(Y,\xi_1,0)$. The curve for λ_1 = constant can then be traced out starting from $\tau = 0$ where $\lambda_1 = \xi_1$, intersecting ξ_2 = constant curve at $\tau_1 = (\bar{U}/U_c^2)(\xi_2 - \xi_1)$, etc.

For shear noise, we can evaluate the second derivatives from the curvature of these $R_\rho(Y,\lambda,\tau)$ traces at $\tau = 0$ as shown in the figure. For self noise, the fourth derivative of the Lagrangian correlations $R_\rho(Y,\lambda,0)$ will be required. Because there are always experimental variations in the heights of the covariances at each value of ξ, derivative measurement is not expected to be very precise.

3. EXPERIMENTAL RESULTS

3.1 Test Set-Up

A 20 mm exit diameter convergent nozzle was used for measurements in subsonic (235 m/sec) and sonic (315 m/sec) velocity jets and a convergent-divergent nozzle having a 22 mm exit diameter was used for measurements at $M = 1.54$ (485 m/sec). Jet velocities were controlled by monitoring the stagnation pressures just upstream of the nozzle. The stagnation temperatures were also recorded. Flow and valve noise were minimized by acoustic treatment in the stagnation chamber.

A photograph of the Crossed Beam Instrument is shown in Fig. 5. The instrument is designed to accomodate almost any radiation source. Two electrically heated tungsten carbide rods are used as infrared sources. Two McPherson Model 218 0.3 meter scanning monochromators were used at the detector end of each beam to filter out all radiation except a .08μ wide band centered at 4.31μ. Indium-antimonide photodetectors (Texas Instruments ISV-1101) were used to measure the transmitted energy. Independent systems were necessitated for each of the two beams to avoid correlating the electrical noise inherent in the source and detectors. The outputs of the photodetectors were amplified and filtered in the frequency range of 150 Hz to 50 KHz.

The optical system employed mirrors to focus the radiation of each source into the flow and then image it onto the monochromator slit. The beams were arranged in such a way that approximately equal lengths of each beam traversed the jet during each measurement. Details of the instrument will be found in Ref. [11].

3.2 Turbulence Measurements

Figure 6 shows measured cross-correlations at various radial locations 2 diameters downstream of the nozzle in the subsonic jet. The stagnation and static temperatures in the jet are noted for each symbol shown in the figure. The temperature variation that existed between measurements did not influence the measured intensities and we can assume the validity of eqs. (1-5) and (1-6). The measured correlation function with intersecting beams is therefore proportional to the intensity of density fluctuations in the flow at the intersection point.

Figure 7 shows the measured intensity profiles for the sonic jet at various axial distances from the nozzle. Although the exit velocity of this jet is sonic, the velocities in the measured regions will be subsonic except for the "laminar" core region. The laminar core extends to about five jet diameters. The intensity profiles at each axial distance in the mixing region peak at a non-dimensional radial distance $(r/D - 0.5)/(y_1/D) = -0.06$. As compared to hot-wire (velocity) measurements, the pressure fluctuations are weighted toward the jet centerline. It is expected that the weighting will be weaker if the jet centerline temperatures are increased, although this has not been checked experimentally. Another feature of the profiles in Fig. 7 is the large turbulence intensities present in the so-called laminar core of the jet. The existence of large pressure fluctuations in the core has been confirmed recently by Lau, Fisher and Fuchs [12] with the help of microphone measurements.

Figure 8 shows relative intensity measurements for the supersonic air jet. The core now extends to approximately ten nozzle diameters.

3.3 Sound Source Distribution

For the unheated subsonic and sonic jets, the low speed formulations of Sec. 2.2 will be applicable. We can obtain R_L from the envelopes of the measured fixed frame space-time correlations as explained in Sec. 2.3. For obtaining the derivatives of R_L we fitted an exponential function by the method of least squares:

$$R_L = e^{B_1|\tau| + B_2|\tau|^2 + B_3|\tau|^3 + \ldots} \tag{3-1}$$

The function R_L is expected to be symmetrical about the $\tau = 0$ axis. This was achieved by taking the modulus of the time lag in the exponent. This method resulted in a better fit to the data near the $\tau = 0$ axis compared to using only even powers of the exponent as suggested by Chu [13]. The least squares routine was used to fit the slopes of the functions rather than the function itself.

Figures 9 and 10 show examples of the type of fit obtained by using five constants in the exponent relation (3-1) for two radial positions in the $M = 0.95$ jet.

Due to insufficient data, we have assumed that the volume integrals with respect to λ in eqs. (2-13) and (2-17) are proportional to the integrand at $\lambda = 0$ and

$$\frac{S_{shear}(Y)}{S_{self}(Y)} = a_0^4 \left(\frac{dy_1}{dy_2}\right)^2 \frac{\frac{\partial^2}{\partial\tau^2} R_L(Y,0,0)}{\frac{\partial^0}{\partial\tau^0} R_L(Y,0,0)} \tag{3-2}$$

We found both the derivatives to be much higher in the mixing region. On the jet centerline and in the core, of course, $dU_1/dy_2 = 0$ and $S_{shear} = 0$. Table I shows the predicted ratios based on our measurements for the subsonic jet:

TABLE I

Jet Mach No. = 0.71

Axial Coordinate y_1/D	Radial Coordinate r/D	S_{shear}/S_{self} (eq. 3-2)
2	.495	1.56
3.5	.36	1.68
3.5	.54	1.40
6.0	.54	-0.52
10.0	.54	0.867

At $y_1/D = 6.0$ the measured R_L did not peak at $\tau = 0$ and consequently the fit with the exponential curve was very poor. The radial coordinates at which the measurements were made did not in general coincide with the regions of peak shear, and hence no estimate of the source strengths could be made for the subsonic jet speed.

We made more detailed surveys in the case of the sonic jet before proceeding with the space-time correlation measurements. The result was a more consistent set of R_L measurements in the peak shear region at each axial location. We were able to compute relative levels of the sound source strengths (again per unit volume) at axial coordinates $y_1/D = 1,2,4,6,8$ and 10. The result is plotted in Fig. 11. Both self and shear noise source strengths show maxima at six diameters from the nozzle.

3.4 The Far Field Noise Spectrum

Figure 12 shows the spectrum, calculated according to eqs. (2-20) and (2-21) for the source coordinates $y_1/D = 10.0$, $r/D = 0.54$. The overall spectrum is obtained by adding the shear and self noise spectra. Table II summarizes the dominant frequencies for various source locations. A field measurement with a microphone at 30 degrees from the jet axis showed that the overall jet noise spectrum has a peak in the 3.15 KHz 1/3 octave band. For the 30-degree angle, and jet Mach No. = 0.71, the frequencies in Table II should be multiplied by 1.76 (assuming convection Mach No. $M = 0.5$). Thus, the peak frequency of overall jet noise agrees well with the dominant frequency of the region between $y_1/D = 4.0$ and 7.0. Dyer [14] has suggested that the peak frequency of the overall noise spectrum is generated by a slice located at 5 diameters from the nozzle.

TABLE II

Jet Mach No. = 0.71

Source Location y_1/D	r/D	Dominant Frequencies f_L Shear Noise	Self Noise	Overall
3.5	0.54			
4.0	.54	1000	2000	
5.0	.54	925	1800	
6.0	.54	1600	2700	2200
7.0	.54	1200	2200	
10.0	0	900	1500	1400

3.5 Comparison with Measurements with the Acoustic Mirror

The distribution of sound source intensities for the same jet was also measured by an elliptical mirror-microphone system. The method is described in detail in [15]. Due to diffraction effects, the spatial resolution and the gain factor of such a mirror microphone system are functions of the acoustic wavelength. The measurements were therefore made in standard octave bands from 2 KHz to 125 KHz. Results for the $M = 1$ jet, corrected for gain factor, are plotted to a linear scale in Fig. 13. The overall noise curve is obtained by adding the sound intensitites for all frequency bands.

The source distribution predicted by the crossed beam correlation method (sum of self and shear noise from Fig. 11) is shown by the dashed line in Fig. 13, normalized with respect to its peak value. The agreement between the two distributions is good in the mixing region. In the fully developed region the crossed beam prediction falls short because it has not been corrected for the increase in jet diameter with axial distance. The location of the pronounced peak in sound source intensity at between six and seven diametrical distances from the nozzle lip corresponds to the transition region of the jet.

4. CONCLUDING REMARKS

The limited data available to us has demonstrated that a technique that measures density fluctuations in the flow can be useful for the prediction of jet noise characteristics. The crossed beam correlation technique has the advantage over a microphone because it does not distrub the flow, is insensitive to temperature changes and measures density fluctuations directly. More exhaustive measurements in air jets of larger diameters should enable researchers to gain insight into the scaling laws of jet noise sources.

ACKNOWLEDGMENTS

The experiments were performed at the Thermal Acoustic Jet Facility of NASA Marshall Space Flight Center and the work supported by the Aero-Astrodynamics Laboratory under contract no. NAS8-27011. The photograph of the Mark II crossed beam instrument was furnished by IIT Research Institute, Chicago, Illinois.

REFERENCES

[1] Krause, F.R. and Fisher, M.J. "Opitcal Integration Over Correlation Areas in Turbulent Flows," 5e Congress International d'Acoustique, Liege, Belgium (1965).

[2] Davis, P.O.A.L., Fisher, M.J. and Barrett, M.J., "The Characteristics of Turbulence in the Mixing Region of A Round Jet," J. Fluid Mech., 15, 337 (1963).

[3] Fisher, M.J., and Jonhnston, K.D., "Turbulence Measurements in Supersonic Shock-Free Jets by the Optical Crossed-Beam Method," NASA TN D-5206, (1970).

[4] Wilson, L.N., "Analysis of Absorption Cell Data," Interim Report J6186 Part I, IIT Research Institute, Chicago, Illinois, (March 1970).

[5] Lysobey, D.J., "Infrared Correlation Spectroscopy with Application to CO_2 Under Atmospheric Conditions," Ph.D. Dissertation, University of Oklahoma, Norman, Oklahoma, (1972).

[6] Lighthill, M.J., "On Sound Generated Aerodynamically, Part I," Proc. of the Royal Society, 211 (1107) pp. 564-587,(March 1952).

[7] Ribner, H.S., "The Generation of Sound by Turbulent Jets," Advances in Appl. Mechanics, Vol. VIII, Academic Press, N.Y. (1964).

[8] Ribner, H.S., "Aerodynamic Sound From Fluid Dilations - a Theory of Sound from Jets and Other Flows," U. of Toronto, Inst. of Aerophysics, UTIA Rep. 86 (1962).

[9] Lighthill, M.J., "On Sound Generated Aerodynamically, Part II," Proc. of the Royal Soc., 222 (1148) pp. 1-32, Feb. 1954.

[10] Wilson, L.N., "Application of Crossed Beam Technology to Direct Measurements of Sound Sources in Turbulent Jets," Final Technical Report Part I, Project J6112, IIT Research Institute, Chicago, Illinois, Feb. 1970.

[11] Dankowski, R.J., "Crossed Beam Instrument Mark II - Operation Manual," Final Technical Report Part II, Project J6112, IIT Research Institute, Chicago, Illinois, April 1970.

[12] Lau, J.C., Fisher, M.J. and Fuchs, H.V., "The Intrinsic Structure of Turbulent Jets," J. of Sound & Vib., Vol. 22, No. 4, (1972).

[13] Chu, W.T., "Turbulence Measurements Relevant to Jet Noise," Univ. of Toronto, Institute of Aerospace Studies, UTIAS Report No. 119, Nov. 1966.

[14] Dyer, I., "Distribution of Sound Sources in a Jet Stream," J. of Acoust. Soc. of Am., Vol. 31, No. 7, (July 1959).

[15] Grosche, F.-R., "Distributions of Sound Source Intensities in Subsonic and Supersonic Jets," Paper presented at the AGARD Specialists' Meeting on Noise Mechanisms, Brussels, Sept. 1973.

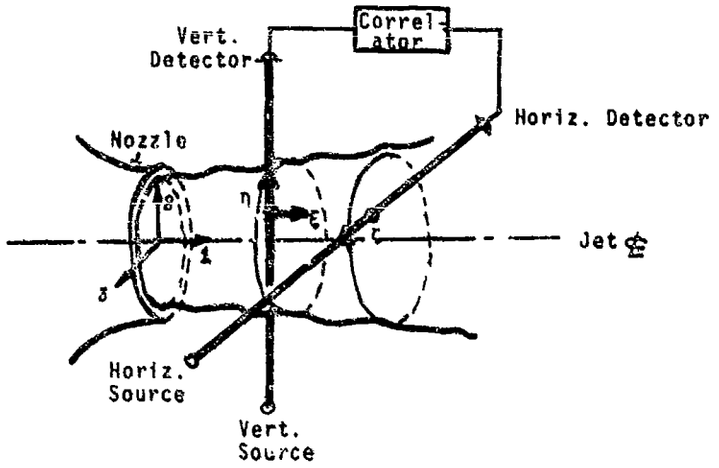

Fig. 1 Crossed beam arrangement in a jet.

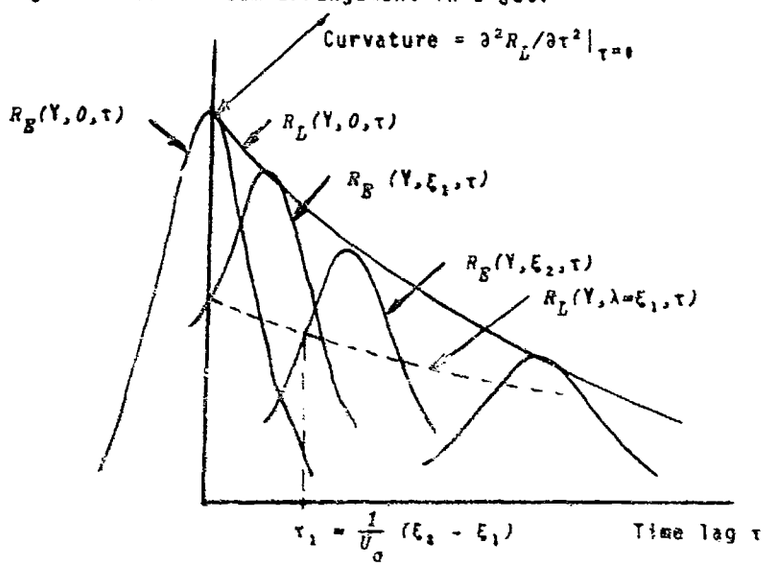

Fig. 2 Space-time correlations R_B and the moving frame auto-correlation functions R_L.

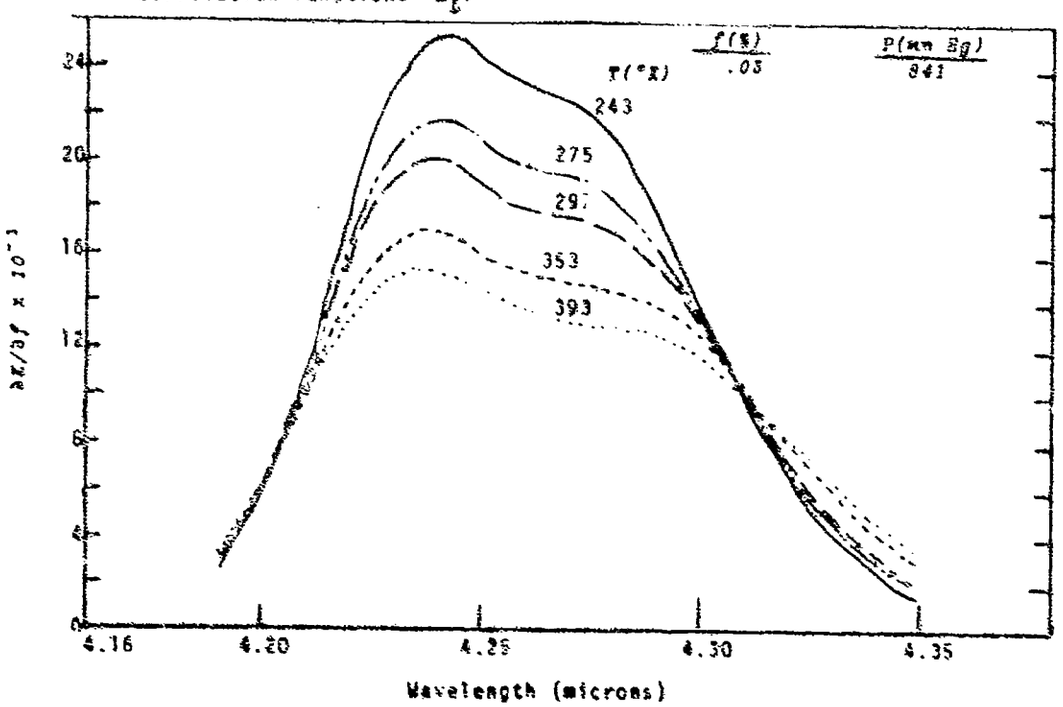

Fig. 3 Derivative of the absorption coefficient with respect to CO_2 concentration, with T as a parameter. From [5].

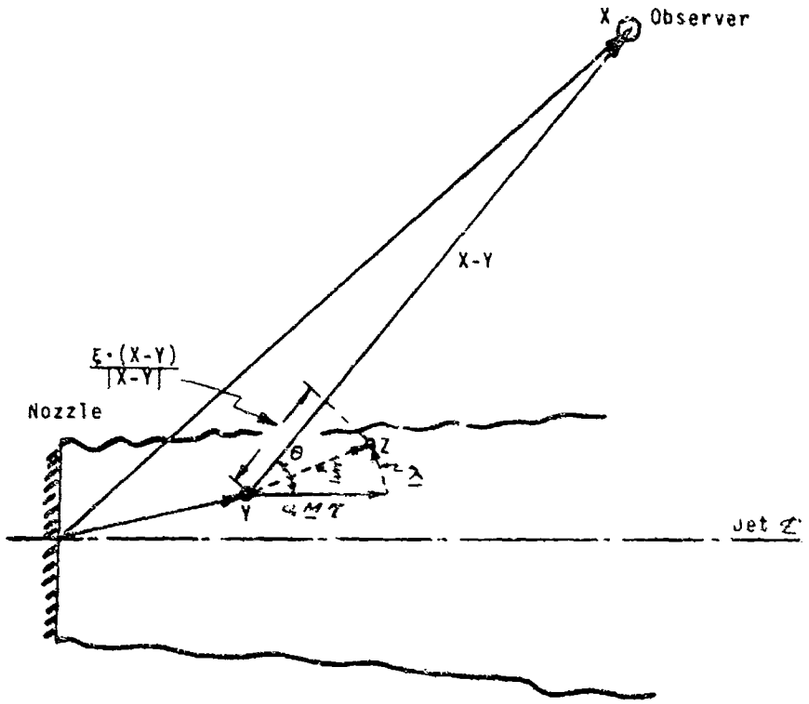

Fig. 4 Coordinate system for jet noise equations.

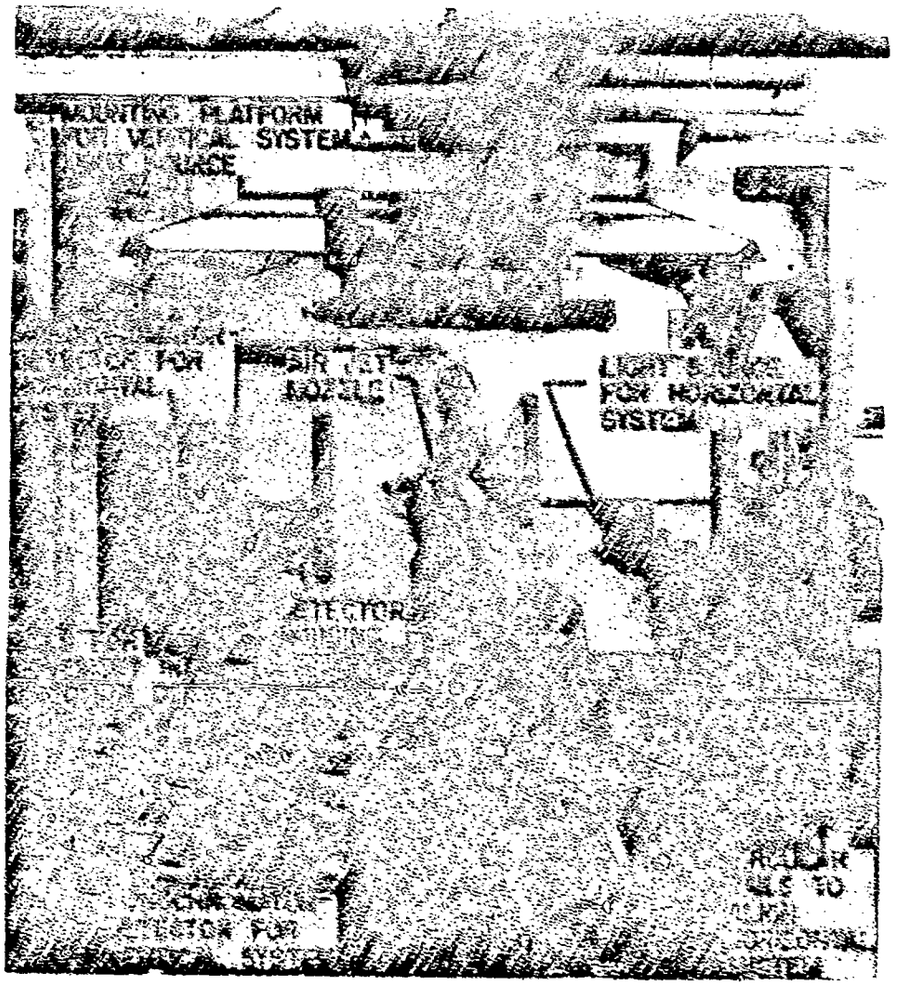

Fig. 5 Photograph of Mark II Crosed Beam Instrument.

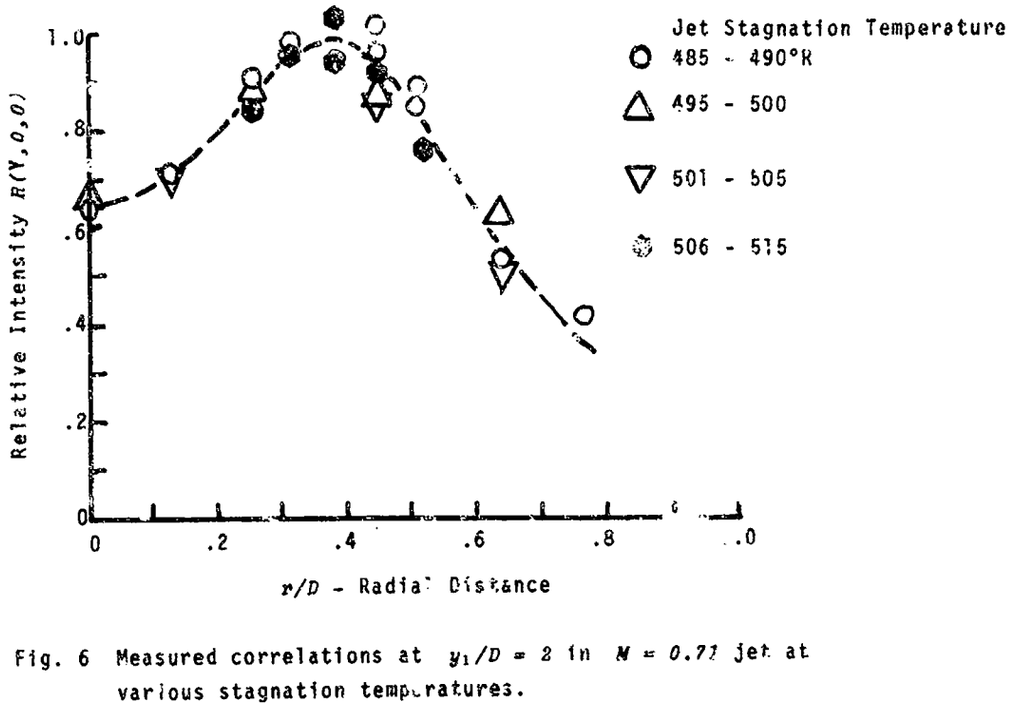

Fig. 6 Measured correlations at $y_1/D = 2$ in $M = 0.71$ jet at various stagnation temperatures.

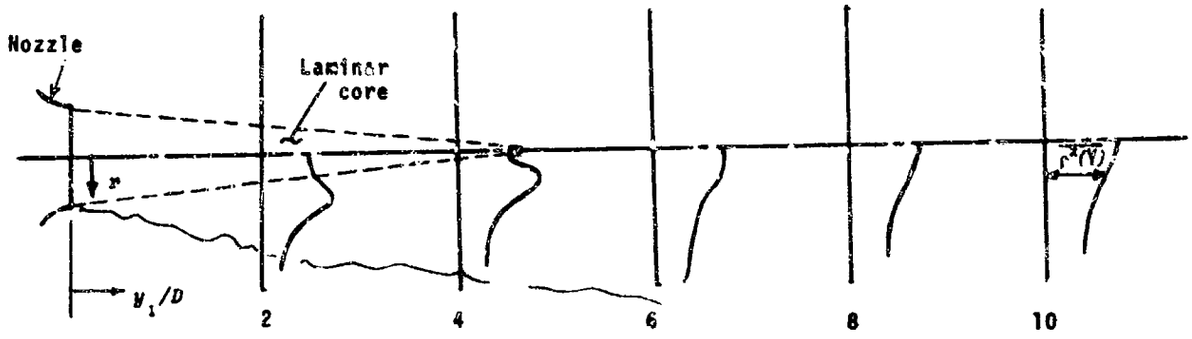

Fig. 7 Relative intensity profiles - jet Mach Number $K = 1$

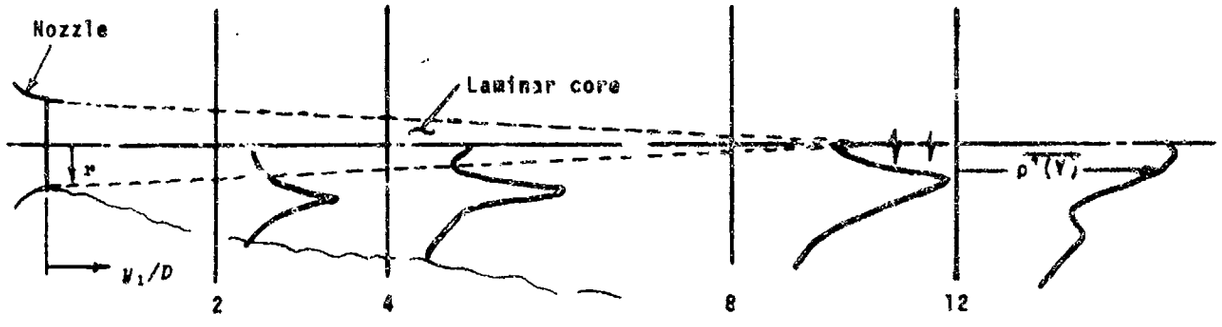

Fig. 8 Relative intensity profiles - supersonic jet at $M = 1.94$

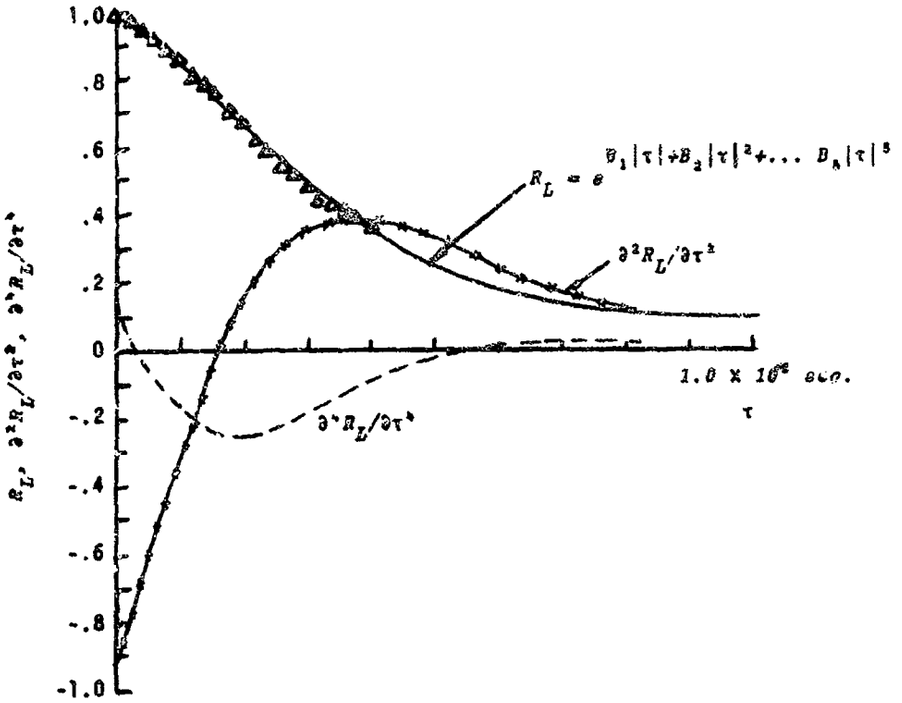

Fig. 9 Moving frame autocorrelation and its derivatives in $M = 0.71$ jet at $y_1/D = 8.0$, $r/D = 0$. Experimental Data is shown by the symbol: Δ.

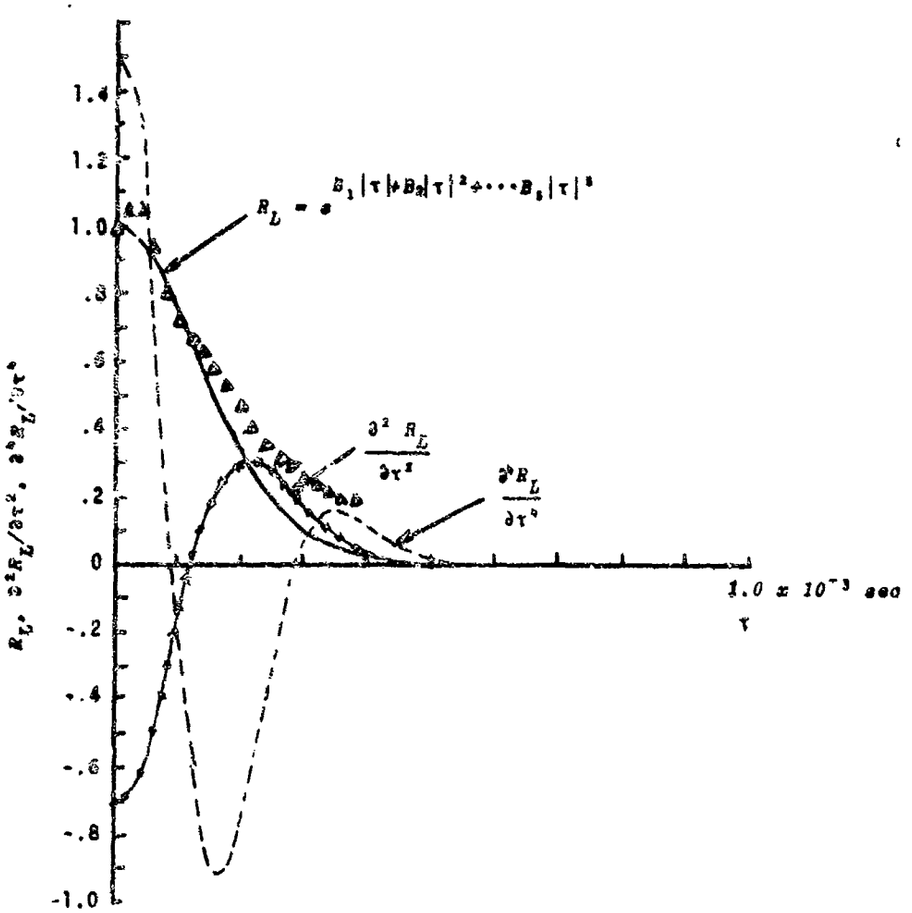

Fig. 10 Moving frame autocorrelation and its time derivatives in $M = 0.71$ jet at $y_1/D = 8.0$, $r/D = 0.64$. Experimental data is shown by the symbol: Δ.

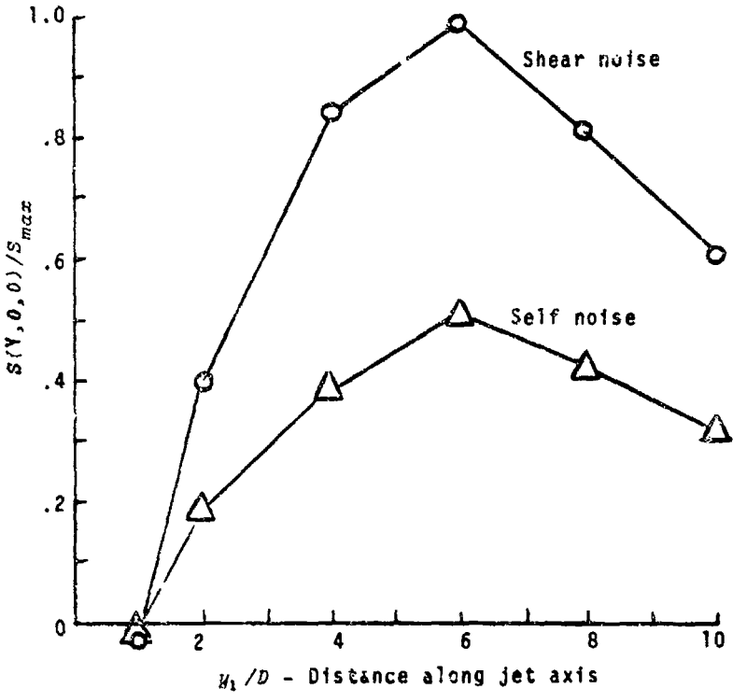

Fig. 11 Distribution of sound source intensity per unit volume in a jet of Mach number $M = 1$.

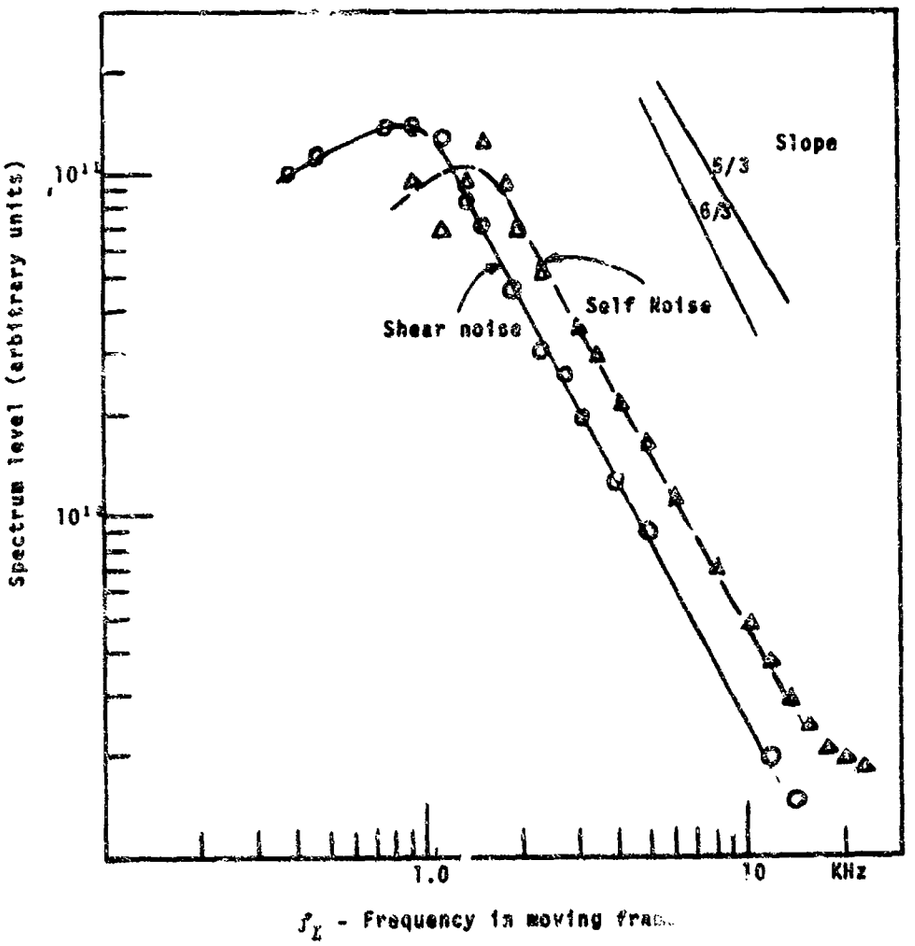

Fig. 12 Self and Shear noise spectra contributed by a unit volume of turbulence at $y_1/D = 10.0$, $r/D = 0.54$.

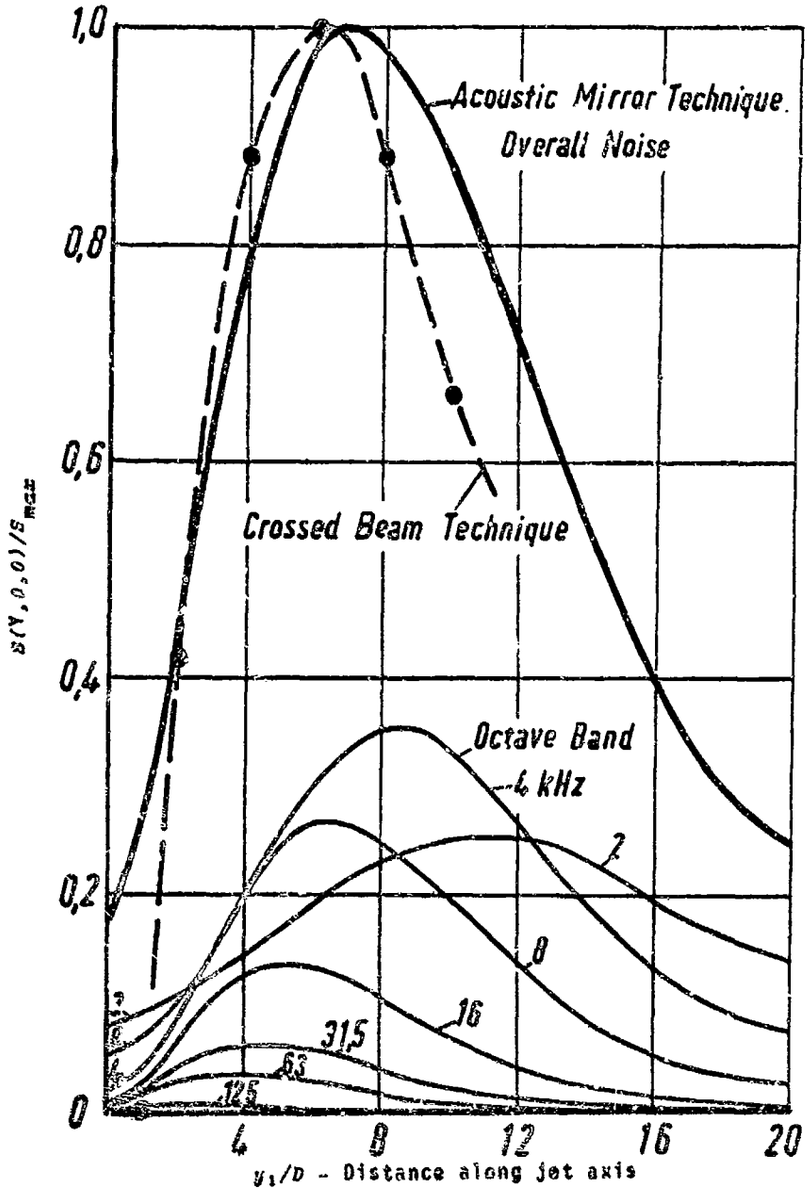

Fig. 13 Distributions of sound source in a jet of Mach number $M = 1$, determined with the Crossed-Beam technique and with the Acoustic-Mirror technique.

DISCUSSION

Dr Fuchs: First, I wonder whether the correlation of intersecting beams in the jet really give a measure of the local mean square density fluctuations at the intersection point,

$$R(0, 0) \propto \overline{\rho^2} .$$

Knowing that the correlation is a measure of how much the absorption processes along one beam path have in common with the absorption processes occurring simultaneously along the whole path of the second light beam, the question really is how are density fluctuations correlated over the whole plane determined by the beams? From correlation measurements in the corresponding turbulent pressure field [J. Sound and Vibration Vol.23 (1972), p.85 Figure 5] one would suggest a considerable contribution of $R(0, 0)$ from fluctuations far outside the beam intersection point. This unwanted contribution makes the interpretation of Figure 6 difficult, especially for $r < 0{,}5$ D.

Second, can the authors work out an experiment with laser beams which could confirm their assumption of small correlation volumes and their prediction of "source strengths and the spectrum of noise due to a unit volume of turbulence"?

Dr Dankevich: If fluctuations far outside the beam intersection point are coherent, their contribution will need to be taken into account. This will not significantly alter the interpretation of the "sound source" equations – they will represent strengths per unit axial distance instead of per unit volume of the jet. Relative intensity profiles like the one shown in Figure 6 will also need reinterpretation. We are now in the process of setting up experiments with lasers as well as focused infrared beams to resolve this question.

DISTRIBUTIONS OF SOUND SOURCE INTENSITIES IN SUBSONIC AND SUPERSONIC JETS

by

F.-R. Grosche*)

Deutsche Forschungs- und Versuchsanstalt
für Luft- und Raumfahrt E. V.
Aerodynamische Versuchsanstalt Göttingen
34 Göttingen, W-Germany

SUMMARY

Clues on the validity of aerodynamic noise theories can be provided by comparison of predicted distributions of sound source intensities in turbulent jets with source distributions determined directly by suitable acoustic measurements.

A method of tracing the sound sources from the sound radiated into the acoustic far field was therefore developed. The sound waves emitted by a small volume of the jet are focussed upon a microphone well outside the flow by means of a large elliptical mirror. The distribution of sound source intensities is investigated by moving the mirror-microphone assembly along and normal to the jet axis.

Results of measurements with subsonic and supersonic jets show interesting details of the noise generation within these jets.

LIST OF SYMBOLS

B	[mm]	width of aperture, see Fig. 6
b	[mm]	distance between center and first minimum of diffraction pattern, see Fig. 6
c	[m/s]	velocity of sound
c_2	[m/s]	velocity of sound at nozzle exit
d	[mm]	nozzle diameter, see Fig. 1
f	[kHz]	sound frequency
f_m	[kHz]	center frequency of an octave band or third octave band
G	[dB]	gain factor of the mirror
I	[Watt/m^2]	sound intensity
I_F	[Watt/m^2]	sound intensity in the free field of a point source of sound, see Fig. 10
I_M	[Watt/m^2]	sound intensity in the maximum of the diffraction pattern of a point source of sound, see Fig. 10
L	[dB]	sound pressure level
L_F	[dB]	sound pressure level in the free field of a point source of sound, see Fig. 10
L_M	[dB]	sound pressure level in the maximum of the diffraction pattern of a point source of sound, see Fig. 10
M		local Mach number
M_2		Mach number at nozzle exit, $M_2 = u_2/c_2$
N	[Watt]	sound power radiated

*) Dr. rer. nat., Institut für Strömungsmechanik, Aerodynamische Versuchsanstalt Göttingen

p_o	[N/m^2]	ambient pressure
p_1	[N/m^2]	settling chamber pressure
Str		Strouhal number, $Str = f_m d/u_2$
T_1	[^{o}K]	settling chamber temperature
u_2	[m/s]	jet velocity at nozzle exit
x, y, z		Cartesian coordinates, x in the direction of the jet axis, see Fig. 1
λ	[m]	acoustical wavelength

1. INTRODUCTION

The following methods are mainly used to investigate the noise emission of turbulent jets, see Fig. 1:

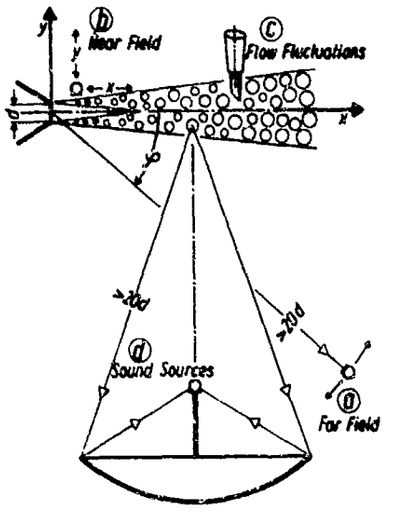

Fig. 1 Methods to investigate the generation of jet noise

a) Acoustical far field measurements. The distance of the microphone from the noise generating part of the jet is larger than 20 nozzle diameters. The frequency spectra and directivity patterns obtained relate to the entire sound producing volume. Measurements of this type, e. g. [1 to 5], can be compared readily with general theoretical predictions like the U^8 law etc. [3, 7], but yield only little information about the structure of the sound source.

b) Acoustical near field measurements. The signals received by the microphone represent not only the radiated sound waves but also the hydrodynamic pressure fluctuations which decrease rapidly with increasing distance from the turbulent flow. This complicates the interpretation of the results, particularly regarding the sound source distribution within the flow. Near field measurements are especially important for determining the loading on structures in the vicinity of jets and other strong sources of aerodynamic sound.

c) Flow measurements. These investigations are concentrated on the sound source itself, no direct information about the radiated sound field is obtained. Mainly hot wire measurements and measurements of the turbulent pressure fluctuations have been published [8 to 16]. Optical remote sensing methods for investigating density fluctuations are described for example in [17 to 32]. In general, the measurements yield the distribution of certain turbulence properties within the flow, from which the spatial distribution of sound source intensity is to be determined by means of the theory of aerodynamic sound generation. Results can only be obtained under certain assumptions, since it is still extremely difficult to provide all the experimental data required for these calculations.

d) Direct acoustical determination of sound source distributions. Indications of the validity of the theories and assumptions applied to method (c) can be provided by comparison of the sound source distributions calculated from flow measurements with source distributions determined directly by suitable acoustic measurements outside the flow. This might be particularly interesting in the case of supersonic and hot jets, considering the various mechanisms of sound generation involved.

The method sketched in Fig. 1 is based on an optical analogy. The sound waves emanating from a small volume of the jet are focussed by a large concave mirror upon a microphone well outside the flow. This technique was first presented in [23 to 26], recent investigations with modified versions are published in [26] and [27]. Other methods to determine the sound source distribution in jets by acoustical measurements are used in [28 to 32].

The objective of the investigations described in this paper was to obtain, by means of the concave mirror technique, detailed information about the distribution of sound source intensities in subsonic and supersonic jets from circular nozzles. Turbulence measurements with an optical method have been conducted at the same test set up by R. J. Dankevala et. al. [33] in order to provide data for a theoretical calculation of the sound source distributions. The results of both investigations are to be compared in detail with each other and with source distributions predicted by other authors, e. g. [34, 35], as soon as the data reduction and analysis of the measurements is completed.

2. CONCAVE MIRROR TECHNIQUE

After successful tests with a preliminary set up using a spherical mirror [23 to 25] an improved system with an elliptical mirror was developed and used for the measurements described in this paper. Fig. 2 illustrates the principle of the system. A large elliptical mirror - a piece of an ellipsoid of revolution - which has two focal points, is positioned in the acoustic far field beside the jet so that one focal point is within the noise generating region of the jet. The sound emitted in the close vicinity of this point is focussed by the mirror upon the other focal point where a small microphone is located. The sound pressure level measured by the microphone is directly related to the sound power radiated to the elliptical mirror by a small volume around the first focal point of the mirror. The microphone is mounted on an arm attached to the mirror. The distribution of sound source intensities within the jet is investigated by moving the mirror-microphone assembly along and normal to the jet axis.

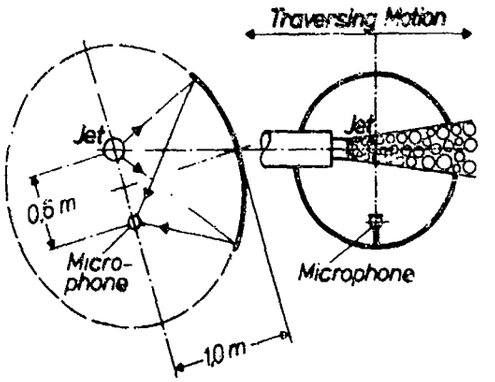

Fig. 2 Acoustic mirror-microphone system with an elliptical mirror, schematic

The essence of this technique is the use of sound waves radiated into the acoustic far field to form an image of the sound sources in a region well outside the jet, and to survey there the sound pressure distribution, which corresponds to the actual sources. Effects of near field pressure fluctuations can be neglected if the distances of both the mirror and the microphone from the jet are large enough. In the case considered here these distances are 1.0 m and 0.6 m (see Fig. 2) compared with a nozzle diameter of 0.02 m. The elliptical contour of the mirror was selected instead of a spherical or parabolic shape because it produces a better image in the vicinity of its focal points.

Fig. 3 shows a photograph of the mirror system. At the left hand side is the settling chamber with a slot nozzle (not used in the experiments described in this paper). The 1/8" B & K*) microphone pointing to the center of the mirror can be recognized in the lower part of the photograph, being mounted on a strutted arm attached to the supporting frame of the mirror, so that its diaphragm is in the lower focus of the elliptical mirror. The diameter of the mirror is approximately 1 m, the distance of the focal points from the center of the mirror is also about 1 m.

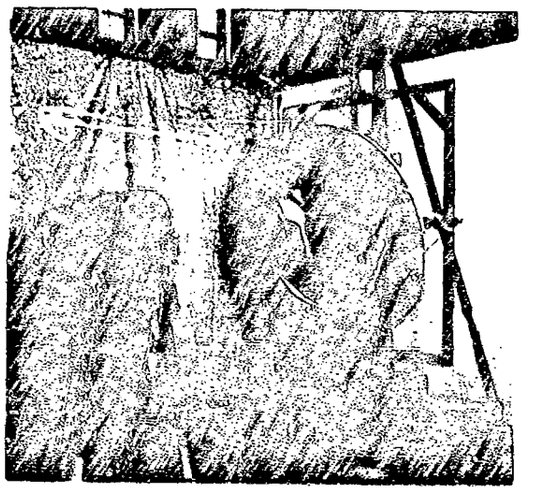

Fig. 3 Acoustic mirror-microphone system at the test rig

The mirror is made of laminated fiberglass. The surface has a metallic coating to render it optically reflecting. This makes it possible to check the adjustment of the system by means of a point source of light.

The traversing unit allows the mirror to move with constant velocity in the directions parallel and normal to the jet axis.

The block diagram Fig. 4 illustrates the measuring system. The signal is fed from the microphone to a B & K amplifier combined with a third octave/octave band pass filter set. The B & K level recorder is started simultanously with the motor of the traverasing unit. Thus the records show immediately the measured sound pressure level versus the location of the focal point within the sound generating flow field. The frequency range of the equipment is approximately 25 Hz to 160 kHz.

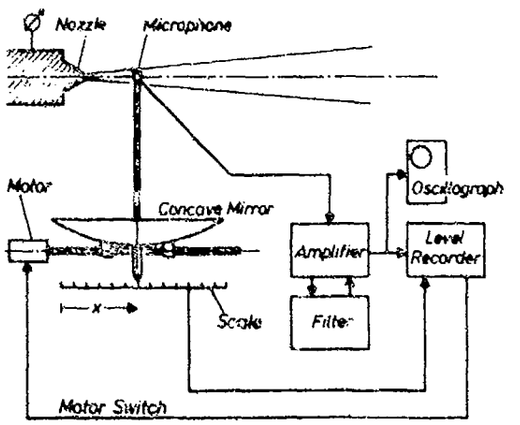

Fig. 4 Block diagram of the mirror set-up

Several points are to be observed when interpreting the measured distributions:

a) Refraction of the sound waves by velocity and density gradients within the jet may slightly shift the measured distributions against the actual source distributions.

*) Brüel & Kjaer

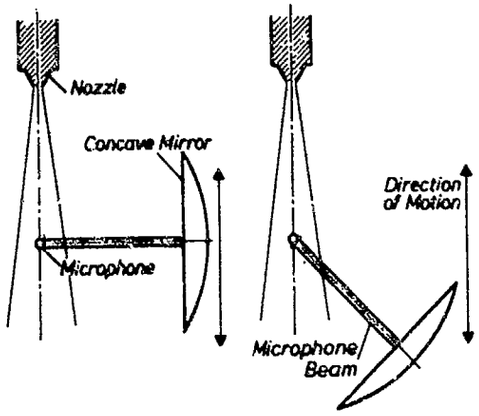

Fig. 5 Different settings of the mirror

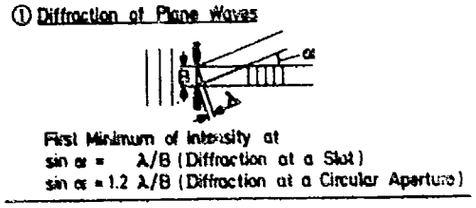

Fig. 6 Diffraction effects

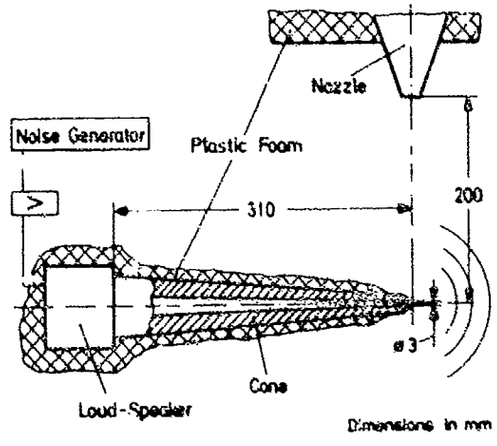

Fig. 7 Point source of sound for calibration of the mirror system

b) The measured distributions are only valid for the part of the total sound power that is collected by the mirror. The results can thus depend upon the orientation of the mirror, if the directional characteristic of the sound field deviates considerably from spherical symmetry. It may be necessary therefore to conduct two or more sets of measurements with different orientations of the mirror (see Fig. 5) and to superimpose the results in a suitable manner.

c) The spatial resolution of the acoustic mirror-microphone system is limited by diffraction of the sound waves at the edge of the mirror. This point is to be discussed more thoroughly: Fig. 6 illustrates the diffraction of plane waves at an aperture of the width B. The angle α indicates the direction of the first minimum of intensity of the diffracted waves with the wavelength λ. In the case of a twodimensional slot, one finds easily the relation $\sin\alpha = \lambda/B$. This equation is modified slightly for a circular aperture to

$$\sin\alpha = 1,2\,\frac{\lambda}{B} \quad , \tag{1}$$

according to textbooks on optics, e. g. [36]. The lower part of Fig. 6 shows diffraction at the edge of a focussing device. The distance b of the first minimum of intensity from the center of the diffraction pattern is obtained under the assumption that Eq. (1) can be applied to this case as an approximation:

$$b = R\cdot\tan\alpha \approx R\cdot\sin\alpha \approx 1,2\,\frac{\lambda}{B}\,R = 0,6\,\frac{\lambda}{\tan\varphi} \quad . \tag{2}$$

Since

$$\tan\varphi \approx 0,5$$

for the elliptical mirror used here, one expects

$$b \approx 1,2\,\lambda \quad . \tag{3}$$

The resolution of the mirror was calibrated by measuring the diffraction patterns of a point source of sound, which is sketched in Fig. 7. Typical diffraction patterns, normalized by the sound pressure level L_M in the maximum of the pattern, are represented in Fig. 8. The loud-speaker of the point source of sound was driven by a random-noise-generator, the microphone signal was filtered in third-octave bands, f_m being the center frequency of the band. The width of the diffraction image of the point source of sound is plotted in Fig. 9 versus the wave length $\lambda = c/f_m$ corresponding to the center frequency f_m.

The distance b varies very nearly as

$$b = 1,3\,\lambda \tag{4}$$

in satisfactory agreement with the estimate Eq. (3). Also given in Fig. 9 is the distance w between the center of the diffraction pattern and the point where the intensity has decreased by 3 dB or 50 %. One finds

$$w \approx 0,6\,\lambda \quad . \tag{5}$$

These values indicate the spatial resolution attainable for different sound frequencies.

The gain of the mirror system is defined by

$$\hat{G} = \frac{L_M}{L_F} \quad , \tag{6}$$

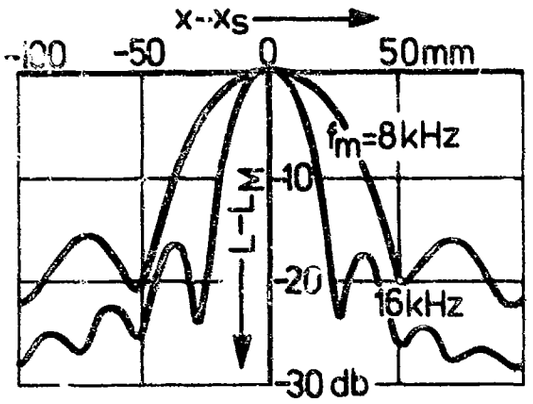

Fig. 8 Normalized diffraction images of a point source of sound at different frequencies

x_S : position of the sound source

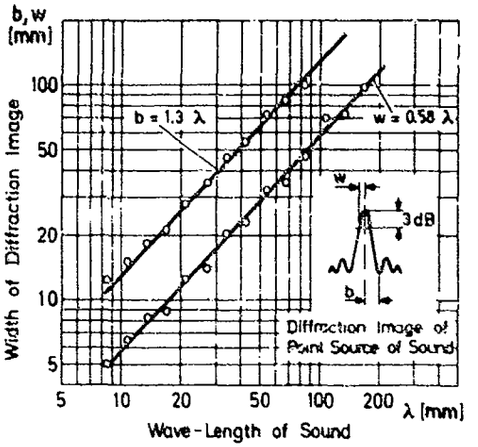

Fig. 9 Width of the diffraction image of a point source of sound as function of the wavelength

with L_M being the sound intensity measured by the mirror-microphone system in the maximum of the diffraction image of the point source of sound, and L_F being the intensity measured by a microphone in the free field at the same distance from the source, see Fig. 10. One expects $\hat{G}$ to vary inversely proportional to the area of the diffraction image which is proportional to λ^2, according to Eq. (4) and (5):

$$\hat{G} \sim \frac{1}{\lambda^2} \sim f_m^2 \quad . \tag{7}$$

This is confirmed by the calibration results plotted in Fig. 10. The gain is given here in dB

$$G = L_M - L_F = 10 \log \frac{L_M}{L_F} = 10 \log \hat{G} \quad . \tag{8}$$

L_M and L_F are the sound pressure levels measured. The 6 dB/octave slope of the measured curve corresponds to Eq. (7). The results of the calibration tests will be used to analyse the measured source distributions by a procedure similar to the one reported in Ref. (28).

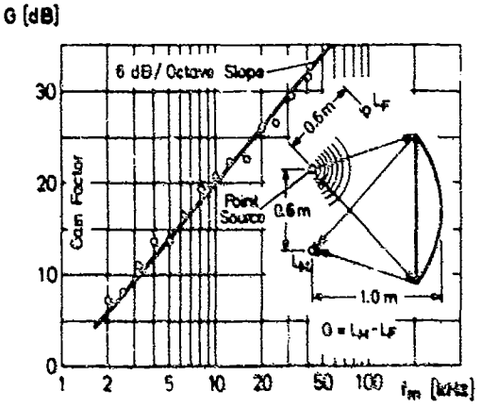

Fig. 10 Gain factor of the elliptical mirror as function of sound frequency

3. MEASUREMENTS OF THE SOUND SOURCE DISTRIBUTION IN SUBSONIC AND SUPERSONIC JETS

The measurements described here are part of a more extensive program to investigate the sound source distributions in jets for different flow conditions which may be related to different sound generating mechanisms. Tests were conducted with cold and heated jets. Optical and acoustical investigation methods were applied to the same flow conditions. This paper is concerned only with the investigation of cold jets by means of the elliptical mirror-microphone system.

3.1 Settling chamber and nozzles

The settling chamber fitted with a convergent nozzle is illustrated by Fig. 11. Several screens and a flow straightener are inserted to reduce the turbulence level. Layers of mineral wool between the screens decrease the internal noise by more than 20 dB. The high flow resistance of these layers helps to prevent separation within the diffusor so that the flow velocity is essentially con-

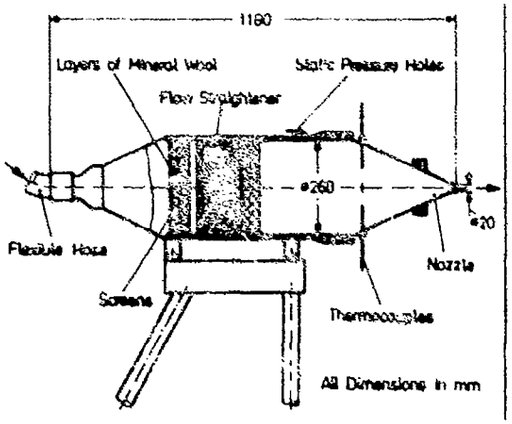

Fig. 11 Settling chamber with nozzle

stant (order of magnitude: 1 m/s) over the entire cross section of the settling chamber. The compressed air is supplied through a flexible hose which isolates the settling chamber from vibrations of the pressure lines. The total temperature T_1 can be determined by four thermocouples mounted in the downstream part of the chamber.

Fig. 12 shows the nozzles used. The convergent-divergent nozzle was designed for fully expanded flow of Mach number $M_2 = 1.9$. The convergent nozzle can be fitted with a turbulence ring.

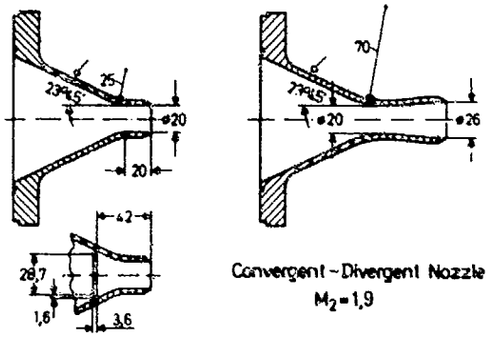

Fig. 12 Convergent and convergent-divergent nozzles

3.2 Test program

Measurements were conducted with the convergent nozzle at Mach numbers $M_2 = 0.7$ and $M_2 = 1.0$, and at supercritical pressure ratios $p_1/p_0 = 2.1$; 3.7; 7.1 which are equivalent to Mach numbers $M = 1.1$; 1.5; 1.9 of a fully expanded flow. During a number of test runs the convergent nozzle was fitted inside with a ring in order to attain a turbulent boundary layer at the nozzle exit, see Fig. 12.

The sound source distribution of the jet from the convergent-divergent nozzle was investigated only at the fully expanded flow condition $M_2 = 1.9$.

The spatial distributions were determined in octave bands with center frequencies $f_m = 2$ kHz up to 125 kHz to provide data for quantitative evaluations. The unfiltered distributions were additionally measured for qualitative comparison between the flow conditions investigated.

4. RESULTS

Some characteristic results are presented in the Figures 13 to 18. Sound pressure levels measured by the acoustic mirror-microphone system are plotted versus the distance x/d between the nozzle exit plane and the focal point in the jet. No corrections for the frequency dependent resolution of the system have been applied to these first graphs which therefore represent the actual sound source distributions only approximately. The mirror was parallel to the jet axis as illustrated in the left part of Fig. 5. Tests with the mirror oriented as in the right part of Fig. 5 gave similar results and will not be further discussed in this paper.

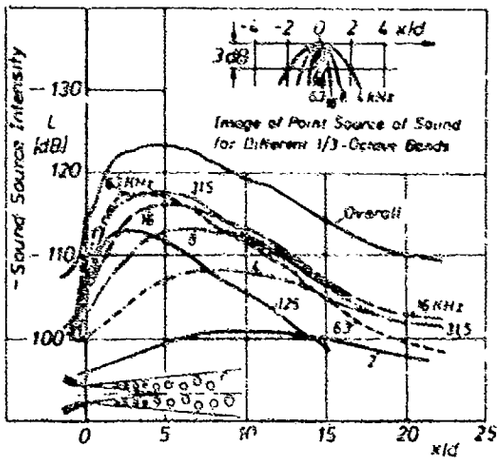

Fig. 13 Distributions of sound source intensity for different octave bands; $M_2 = 1.0$

Fig. 13 shows distributions of the overall noise and of different octave bands for nozzle exit Mach number $M_2 = 1.0$. The turbulence ring was fitted into the nozzle. The maximum of the unfiltered signal (overall noise) occurs about 5 nozzle diameters downstream of the nozzle exit plane, at the end of the mixing zone of the jet. The maxima of the octave bands are shifting towards the nozzle with increasing center frequency of the band. This is in accordance with theoretical arguments. The relation between center frequencies and Strouhal number $Str = f_m \cdot d/u_2$ is given by the following table:

f_m	2	4	8	16	31.5	63	125	[kHz]
Str	0.13	0.26	0.52	1.0	2.0	4.1	8.1	-

Diffraction images of a point source of sound for different frequencies are plotted in the upper right of Fig. 13 at the same scale. The flanks of these images of a point source are considerably steeper than the slopes of the corresponding distributions measured at the jet. This leads to the qualitative conclusion that the limited spatial resolution of the acoustic mirror does not strongly affect the shape of the source distributions measured in the individual frequency bands. A detailed analysis of the corrections necessary to attain absolute values of sound source intensity is under way.

The distribution in the 125 kHz band has a small but distinct maximum at $x/d = 0$, which is reduced to a ripple in the lower frequency bands and in the overall noise distribution. This maximum is probably due to "lip noise" caused by the pressure fluctuations of the turbulent boundary layer inside the nozzle induced by the turbulence ring.

The influence of the jet Mach number upon the sound source distributions is demonstrated by Fig. 14. The distributions of the overall sound intensity are plotted for jets of Mach numbers $M_2 = 0.7$ and 1.0 from the convergent nozzle and for a jet of Mach number $M_2 = 1.9$ from the convergent-divergent nozzle. The dashed lines refer to choked jets from the convergent nozzle with pressure ratios equivalent to Mach numbers 1.1 and 1.9 in fully expanded flow. These measurements were all made with the turbulence ring inserted into the convergent nozzle, but tests without ring showed no significant effect at Mach numbers $M > 1$.

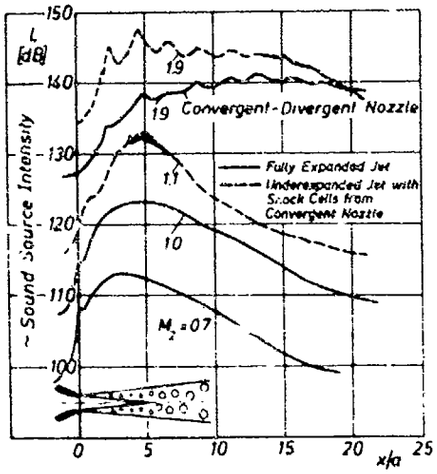

Fig. 14 Distributions of sound source intensity for different Mach numbers (overall noise)

The distributions for Mach numbers $M_2 = 0.7$ and $M_2 = 1.0$ are quite similar to each other, except for the absolute intensity and for a slight shift in the position of the maximum. The supersonic fully expanded jet has a rather flat maximum at approximately $x/d = 14$. According to [31] the mixing zone (and the potential core) of this jet should end at $x/d \approx 9.5$ and the supersonic core should run out at $x/d \approx 19$. The maximum of the sound source distribution is thus between these points; this corresponds well with results of tests published by K. C. Potter and J. H. Jones [3]. Some ripples in the curve indicate noise sources associated with weak shocks in the flow which could be established by shadowgraphs, see Fig. 15.

The distribution of the jet with the same pressure ratio (for $M_2 = 1.9$), but emanating from the convergent nozzle, shows rather strong peaks which could also be identified from shadowgraphs as sound sources due to shock turbulence interaction. A shadowgraph of this jet is reproduced in Fig. 16, the positions of peaks of the measured sound source distribution being indicated by vertical lines. Sound waves radiated from these locations can be recognized in this photograph.

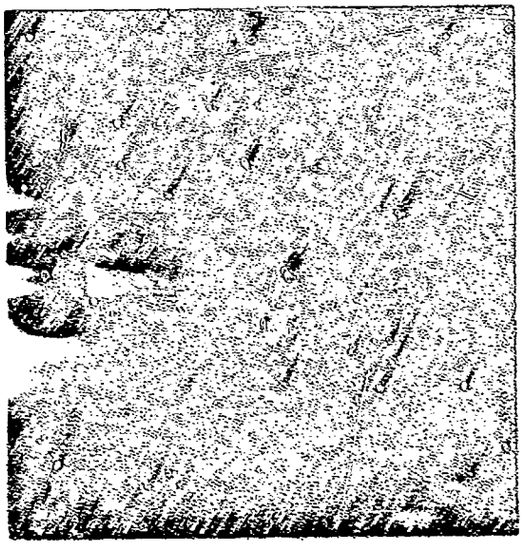

Fig. 15 Shadowgraph of fully expanded jet from convergent-divergent nozzle, $M_2 = 1.9$

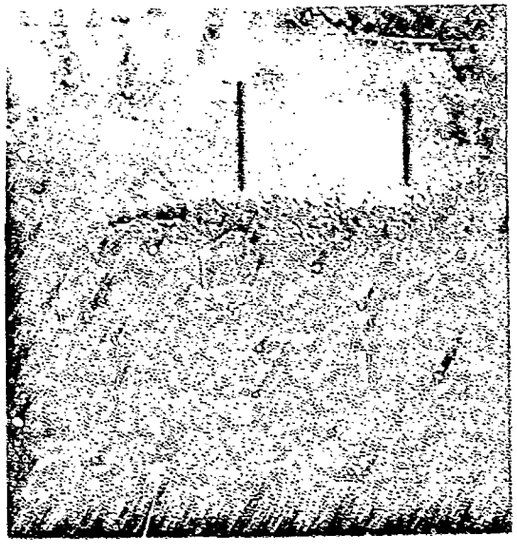

Fig. 16 Shadowgraph of choked jet from convergent nozzle, $M = 1.9$
Vertical lines indicate maxima of sound radiation

A strong fluctuating screech was observed with the choked jet of Mach number $M = 1.1$. The amplitude fluctuations are visible also at the peak of the sound source distribution plotted in Fig. 14. This indicates that the pronounced peak at $x/d \approx 5$ is mainly due to the screech noise radiated.

Fig. 17 demonstrates a very distinct influence of the boundary layer condition inside the nozzle upon the noise generation of subsonic jets (in the given Reynolds number range). Measurements with the clean nozzle, laminar boundary layer, show much higher sound production close to the nozzle than measurements with a turbulent boundary layer inside the nozzle, which was attained by inserting a ring into the nozzle, see Fig. 12. The effect is limited to the region $x/d < 2.5$ and more pronounced with increasing frequency. Although the effect has not yet been investigated very thoroughly, it is believed to be caused by ring vortices or similar disturbances in the laminar-turbulent transition region and its vicinity. Such a structure of the flow field in the region $x/d < 2$ is visible to a certain extent in the shadowgraph Fig. 18.

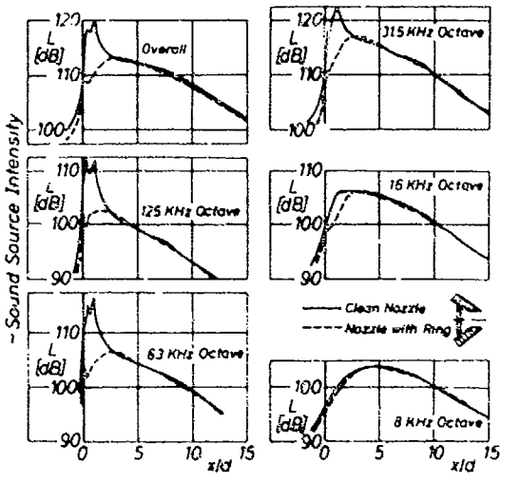

Fig. 17 Distributions of sound source intensity at $M_2 = 0.7$; with and without turbulence ring

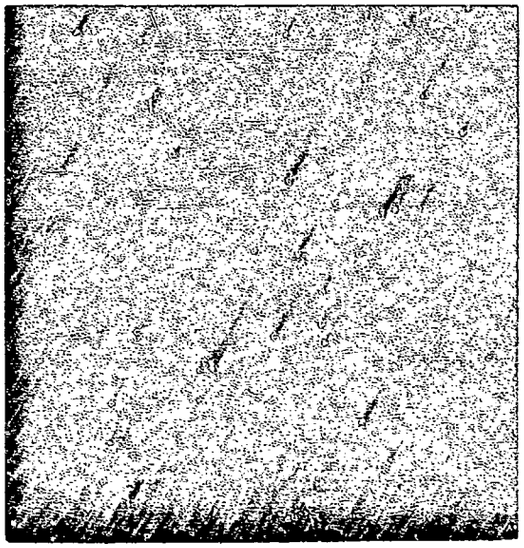

Fig. 18 Shadowgraph of jet from clean convergent nozzle, $M_2 = 0.7$

5. CONCLUSIONS

A new method for determining the sound source distributions in jets from the sound radiated into the acoustic far field was developed and applied to subsonic and supersonic jets from circular nozzles. Interesting details of the noise generation within these flows could be detected already by these measurements, although the results have not yet been corrected for the frequency dependent resolution of the measuring system.

6. REFERENCES

[1] Callaghan, E. E.
Coles, W. D.
Far noise field of air jets and jet engines
NACA Rep. 1329 (1957)

[2] Mollo-Christensen, E.
Kolpin, M. A.
Martuccelli, J. R.
Experiments on the jet flow and jet noise far field spectra and directivity patterns
Massachusetts Insts. Technol. ASRL TR 1007 (1963)

[3] Waterhouse, R. V.
Berendt, R. D.
Reverberation chamber study of the sound power output of subsonic air jets
J. Aero. Sci. 30 (1958), pp. 114-121

[4] Rollin, V. G.
Effect of jet temperature on jet-noise generation
NACA TN 4217 (1958)

[5] Lush, P. A.
Measurements of subsonic jet noise and comparison with theory
J. Fluid Mech. 46 (1971), pp. 477-500

[6] Lighthill, M. J.
Jet noise (Wright Brothers Lecture)
AIAA Journal 1 (1963), pp. 1507-1517

[7] Ribner, H. S.
The generation of sound by turbulent jets
Adv. Appl. Mech. Vol. 8 (1964), pp. 103-182

[8] Laurence, J. C.
Intensity, scale, and spectra of turbulence in mixing region of free subsonic jet
NACA Rep. 1292 (1956)

[9] Davies, P. O. A. L.
Fisher, M. J.
Barrat, M. J.
The characteristics of turbulence in the mixing region of a round jet
J. Fluid Mech., Vol. 15 (1963), pp. 331-361

[10] Bradshaw, P.
Ferris, D. M.
Johnson, R. F.
Turbulence in the noise producing region of a circular jet
J. Fluid Mech., Vol. 19 (1964), pp. 591-624

[11] Chu, Wing T. — Turbulence measurements relevant to jet noise. UTIAS Rep. No. 119 (1966), (Univ. of Toronto)

[12] Jones, J. S. F. — Fluctuating turbulent stresses in the noise producing region of a jet. J. Fluid Mech., Vol. 36 (1969), pp. 529-543

[13] Wooldridge, C. E.; Wooten, D. C. — The structure of jet turbulence producing jet noise. AIAA Paper No. 72-158, AIAA 10th Aerospace Sciences Meeting, San Diego, Calif., Jan. 1972

[14] Fuchs, H. — Space correlations of the fluctuating pressure in subsonic turbulent jets. J. Sound Vibr. 23 (1972), pp. 77-99

[15] Ko, N. W. M.; Davies, P. O. A. L. — The near field within the potential cone of subsonic cold jets. J. Fluid Mech., Vol. 50 (1971), pp. 45-78

[16] Nagamatsu, H. T.; Sheer, J. R.; Bigelow, E. C. — Mean and fluctuating velocity contours and acoustic characteristics of subsonic and supersonic jets. AIAA Paper No. 72-157, AIAA 10th Aerospace Sciences Meeting, San Diego, Calif., Jan. 1972

[17] Krause, F. R.; Fisher, M. J. — Optical integration over correlation areas in turbulent flows. 5e Congres International d'Acoustique, Lüttich, 1965

[18] Fisher, M. J.; Damkevala, R. J. — Fundamental considerations of the Crossed-Beam correlation technique. NASA CR-61352, 1969

[19] Wilson, L. N.; Krause, F. R.; Kadrmas, K. A. — Optical measurements of sound source intensities in jets. Basic Aerodynamic Noise Research Conf., NASA SP-207 (1969), pp. 147-160

[20] Damkevala, R. J.; Kadrmas, K. A. — Turbulence measurements with an infrared Crossed-Beam system near 4.3 microns. AIAA Paper No. 70-235, AIAA 8th Aerospace Sciences Meeting, New York, Jan. 1970

[21] Wilson, L. N.; Damkevala, R. J. — Statistical properties of turbulent density fluctuations. J. Fluid Mech., Vol. 43 (1970), pp. 291-303

[22] Funk, B. H. — Optical probing of supersonic flows with statistical correlation. US Patent 3, 623, 361, Nov. 1971

[23] Grosche, F.-R. — Untersuchungen zur Lärmentwicklung turbulenter Freistrahlen. Teil IV: Zur Verteilung der Schallquellen in turbulenten Strahlen. AVA-Bericht 68 A 20 (1968)

[24] Grosche, F.-R. — Measurements of the noise of air jets from slot nozzles with and without shields. DLR-FB 68-46 (1968), pp. 1-32

[25] Grosche, F.-R. — Zur Schallerzeugung durch einen turbulenten Luftstrahl über einer endlich, ebenen Platte. Mitt. Max-Planck-Inst. Strömungsforsch. u. Aerodyn. Vers. Anst. Nr. 45 (1969), S. 1-129

[26] Chu, W. T.; Laufer, J.; Kao, K. — Noise Source Distribution in Subsonic Jets. Inter-Noise 72 Proceedings, Washington D. C., Oct. 4-6, 1972

[27] Grosche, F.-R. — Untersuchungen zur Schallquellenverteilung turbulenten Gasstrahlen. Vorabdruck 5. Jahrestagung der DGLR Berlin, 4.-6. Oktober 1972, Vortrags-Nr. 72-053

[28] Dyer, I. — Distribution of sound sources in a jet stream. JASA 31, No. 7, July 1959, pp. 1016-1022

[29] Maestrello, L.; McDavid, E. — Acoustic characteristics of a high subsonic jet. AIAA Journal Vol. 9, No. 6, June 1971, pp. 1058-1065

[30] Potter, R. C.
Jones, J. H.
An experiment to locate the acoustic sources in a high speed jet exhaust stream
Wyle Lab. Rep. (1967)

[31] Nagamatsu, H. T.
Sheer, R. E.
Horvay, G.
Supersonic jet noise theory and experiments
Basic Aerodynamic Noise Research Conf.,
NASA SP-207 (1969), pp. 17-51

[32] Bishop, K. A.
Flowcs Williams, J. E.
Smith, W.
On the noise sources of the unsuppressed high-speed jet
J. Fluid Mech. 50 (1971), pp. 21-31

[33] Damkevala, R. J.
Grosche, F.-R.
Guest, S.
Sound source measurement in model air jets using the Crossed-Beam correlation technique
Paper to be presented at the AGARD Specialists' Meeting "Noise Mechanisms", Brussels, Sept. 1973

[34] Pao, S. P.
Lowson, M. V.
Some applications of jet noise theory
AIAA Paper No. 70-233, AIAA 8th Aerospace Sciences Meeting, New York, Jan. 1970

[35] Rotta, J. C.
Berechnung der abgestrahlten Schallenergie turbulenter Strömungen
Vorabdruck 5. Jahrestagung der DGLR Berlin, 4.-6. Oktober 1973, Vortrags-Nr. 72-074

[36] Pohl, R. W.
Optik und Atomphysik
Springer-Verlag Berlin/Heidelberg/New York, 12. Aufl. 1967

Acknowledgements

The development of the acoustic mirror-microphone system was supported by the "Deutsche Forschungsgemeinschaft" (DFG). Most of the measurements were conducted at the Aero-Astrodynamics Laboratory of the NASA Marshall Space Flight Center (MSFC), Huntsville, Alabama, while the author held a Postdoctoral Resident Research Associateship of the National Research Council (NRC). The author expresses his thanks to the DFG, to the NRC and particularly to the staff members of the Aero-Astrodynamics Laboratory and of the DFVLR-AVA Göttingen. Without their help this investigation could not have been accomplished.

CORRELATIONS BETWEEN FAR FIELD ACOUSTIC PRESSURE AND FLOW CHARACTERISTICS FOR A SINGLE AIRFOIL

by M. SUNYACH, H. ARBEY, D. ROBERT, J. BATAILLE
and G. COMTE-BELLOT

Laboratoire de Mécanique des Fluides
Ecole Centrale de Lyon
69130 - ECULLY - FRANCE

SUMMARY

A NACA 6512 $A_{1.0}$ 10 airfoil, whose chord is 8 cm, is placed in a uniform flow ducted into an anechoic chamber with a speed ranging from 20 to 40 m/s.

Its acoustic far field is analyzed in relation with the normal velocity fluctuations in the wake and the pressure fluctuations on the airfoil surface. Cross-correlations measurements show that the aerodynamic pattern close to the trailing edge, on the extrados, controls the noise emission.

RESUME

Un profil NACA 6512 $A_{1.0}$ 10, de corde 8 cm, est placé dans un jet d'air débouchant dans une chambre anéchoïque avec une vitesse de 20 à 40 m/s.

Le champ de pression lointain est analysé en relation avec les composantes normales de la vitesse dans le sillage et avec les fluctuations de pression à la surface du profil. Les résultats expérimentaux obtenus montrent que l'émission sonore est contrôlée par les phénomènes aérodynamiques qui se produisent au bord de fuite, côté extrados.

MAIN NOTATIONS USED

- p : acoustic pressure in the far field
- π : pressure fluctuation on the surface of the airfoil
- v : transverse component of the velocity fluctuation in the wake of the airfoil
- $\tilde{m}$: signal under the tilder is filtered
- $[\ldots]_t$: signal in the bracket at a time delay τ
- $R_{\pi p}(\tau)$: correlation coefficient between π and p, the second signal at a time delay τ, defined as

$$R_{\pi p}(\tau) = \frac{\overline{\pi(t)\, p(t+\tau)}}{\sqrt{\overline{\pi^2}}\,\sqrt{\overline{p^2}}}$$

- e : index referring to the extrados of the airfoil
- i : index referring to the intrados of the airfoil
- τ_0 : acoustic propagation time between the trailing edge of the airfoil and the far field microphone
- C : airfoil chord

1. INTRODUCTION

The aerodynamic noise of a single airfoil was investigated following work by LIGHTHILL (1952, 1954), in which equivalent sources were sought such that placed in an otherwise undisturbed atmosphere they represented the noise generated by the aerodynamic configuration under investigation.

For a fixed obstacle placed in a flow, the acoustic pressure radiated in the far field at point $\vec{x}$ is given, following FFOWCS WILLIAMS (1969), by :

$$p(\vec{x},t) \underset{|\vec{x}|\to\infty}{=} \frac{x_i x_j}{|\vec{x}|^3}\frac{1}{4\pi a_0^2}\int_{\mathcal{V}}\frac{\partial^2}{\partial t^2}T_{ij}\left(\vec{y},t-\frac{|\vec{x}-\vec{y}|}{a_0}\right)d\vec{y}$$

$$+\frac{x_i}{|\vec{x}|^2}\frac{1}{4\pi a_0^2}\int_S n_i\frac{\partial \pi}{\partial t}\left(\vec{y},t-\frac{|\vec{x}-\vec{y}|}{a_0}\right)d\vec{y} \qquad (1)$$

The usual notations and conventional approximations are used :

S : surface of the obstacle

$\vec{n}$: normal to the surface S , towards the exterior

π : pressure on the obstacle

$\mathcal{V}$: volume of the fluid, approximatively the volume of the wake

$$T_{ij} \equiv \rho U_i U_j - (p - a_0^2\rho)\delta_{ij} \approx \rho_0 U_i U_j$$

In order to characterize these different sources, we investigated the correlation between the different sources and the radiated acoustic pressure. Here the method is based on an idea put forward by LEE (1971), which gives an estimation of the noise emitted in the following form :

$$\frac{\overline{p^2}}{\rho_0 c_0} = \frac{\pi}{A a_0^2 |\vec{x}|}\int_{\mathcal{V}} d\vec{y}\int_0^\infty \left\{ \overline{\tilde{v}^2[\tilde{p}]}_{\tau_0-\frac{1}{2f}} + 2\bar{V}\overline{\tilde{v}[\tilde{p}]}_{\tau_0-\frac{1}{2f}} \right\} df$$

$$+\frac{1}{2A\rho_0 a_0^2|\vec{x}|}\int_S d\vec{y}\int_0^\infty \overline{\tilde{\pi}[\tilde{p}]}_{\tau_0-\frac{1}{4f}}\, df \qquad (2)$$

A is the percentage bandwidth of the filter, $\tilde{v}$, $\tilde{v}^2$, $\tilde{\pi}$ and $\tilde{p}$ are the contributions to the signals v, v^2, π and p relative to the frequency f . It will be noted that the filtering effect on the time derivatives introduces modifications to the delay times ($-\frac{1}{2f}$ for a 2 nd derivative and $-\frac{1}{4f}$ for a 1st derivative). The main cross-correlations to be measured are then

$$\overline{\tilde{v}^2(t)\,\tilde{p}(t+\tau)} \qquad \overline{\tilde{v}(t)\,\tilde{p}(t+\tau)} \quad \text{and} \quad \overline{\tilde{\pi}(t)\,\tilde{p}(t+\tau)}$$

However, for the interpretation of the phenomena, other correlations relative to the same signals were considered.

In order to carry out these measurements, pressure transducers were embedded in the surface of the airfoil, hot-wire sensors were placed in the wake of the airfoil, and two microphones were located on either side of the airfoil in the acoustic far field (Fig. 1).

2. EXPERIMENTAL PROCEDURE

Experiments were made in the anechoic chamber of the Ecole Centrale de LYON (BERHAULT & al., 1973) into which is ducted an air jet. The NACA 6512 $A_{1.0}$10 airfoil has a chord of 8 cm. It is placed in the potential core of the jet. Two side-plates extending the rectangular nozzle (30 cm x 15 cm), along its shorter dimension, support the airfoil. The maximum velocity is 38,4 m/s which, for the airfoil, leads to a Reynolds number $Uc/\nu = 2.1 \times 10^5$. The incident turbulent level is reduced to 0.3 %.

The pressure transducers, of the capacitive type, have been specially designed and built in the Laboratory. Their size is small enough to enable several to be simultaneously embedded in the airfoil surface (Fig. 3). Each transducer is connected to a preamplifier Bruel & Kjaer type 2615 through a 15 cm long cable having a capacitance of 100 pF/m. This cable enables the amplifier to be placed at one of the extremities of the airfoil and allows it to be uncoupled mechanically. The overall response of the transducer is shown in Fig. 4 and it is quite close to that of a Bruel & Kjaer 1/8'' microphone. In addition, there is an appreciable reduction in the noise level in the low frequency range.

The X-wires which can be displaced through the wake, are Disa probes type 55A38 (5 μ tungsten wire) ; they are fed by two constant temperature Disa anemometers type 55D01. The transverse velocity component and its instantaneous square are obtained by means of Burr-Brown analog amplifiers (type 3003) and squaring modules (type 4174).

For the far field acoustic measurements, two 1" B & K microphones are located at about 1.60 m from the airfoil, on the normal to its chord, and connected to a B & K preamplifier type 2627.

The electronic equipment used to obtain the spectral and correlation measurements is given schematically in Fig. 2. For the correlation measurements a 29 % bandwith is generally used on the 2107 filter, the frequency ranging from 500 Hz to 5 KHz. In addition to this filtering, all the signals are passed through a A weighted filter to get rid of low frequency spurious signals, part of which only are due to the cut-off frequency (about 100 Hz) of the anechoic chamber.

In the correlation measurements, particularly those concerned with the signals from the pressure transducers embedded in the same side of the airfoil, (intrados or extrados) the slight phase shift, less than 7°, between any two measurement circuits, is taken into account. A phase check is carried out by means of a loudspeaker placed in the far field and emitting towards the two pressure transducers considered.

3. PRESSURE SPECTRA

3.1. Radiated acoustic pressures.

Spectra of the radiated acoustic pressure p_a are given in Fig. 5. The jet contribution which is the background noise in that investigation is also indicated. At increasing velocities the airfoil noise gets less prominent. However, a vortex shedding noise was detectable at the four velocities investigated. The frequencies were approximately 1500, 2500, 3200 and 3600 Hz at 20.2, 29.2, 34.2, and 38.4 m/s respectively. These frequencies can be fitted to the empirical relation

$$f \approx \frac{0.018}{\sqrt{c\nu}}\, U^{4.5}$$

whose form is close to that given by PATTERSON (1972). It corresponds to a Strouhal number of 3.18, if based on the boundary layer thickness (assumed laminar) at the trailing edge.

3.2. Pressure fluctuations at the surface of the airfoil.

Spectra of the pressure fluctuation π_e on the airfoil extrados are given in Fig. 6. In order to compare these spectra with the p_a spectra, the dB scale is again used. Expressed in terms of the external dynamic pressure of the flow, the r.m.s. level is then 2.4×10^{-3} , a very small value in comparison with that encountered for turbulent flows.

A striking result is the resemblance of the π_e and p_a spectra, particularly in the case of the Strouhal frequency and the frequency at which occurs the rapid drop of the spectra.

4. CROSS-CORRELATION MEASUREMENTS

4.1. Cross-correlations $\overline{\tilde{v}^2 \tilde{p}_a}$

Examples of these correlations are given in Fig. 7. In these curves, special attention is paid to the negative extremum because it contributes significantly to the noise if it occurs at a time delay equal to the propagation time τ_e . This is quite clear from (2), noting that $\overline{\tilde{v}^2(t)}_{\tau_e - \frac{x}{a_0}}$ is also equal to $-\overline{\tilde{v}^2(t)}_{\tau_e}$.

However Fig. 7 shows that the time delay at which this extremum occurs depends strongly on the place at which the signal v^2 is taken in the wake. This time delay is close to τ_e only when v^2 is taken near the trailing edge (e.g. point I). It steadily decreases when the signal v^2 is taken further downstream (e.g. point J). The time difference of these extremums is approximatively given by $|x_I - x_J|/U_c$ with $U_c \approx 0.8\, U$ U being the external velocity.

The same behaviour is found for all the frequencies in the observed Strouhal "bump" of the spectra (for example 1.5 KHz $\leq f \leq$ 4 KHz , at U = 38.4 m/s, Fig. 9).

These results tend already to show that the most important contribution to the values integral of expression (2) will come from the neighbourhood of the trailing edge. In that situation, the waves generated close to the trailing edge propagate towards the far field microphone whereas the aerodynamic structures are convected downstream by the flow.

A further comment concerning the correlation $\overline{v^2 p_e}$ is that the optimums are mainly detectable when the signal v is taken near the edge of the wake, Fig. 7, specially on the extrados side. In that region the intermittency coefficient is of the order of 0.20. In the central part of the wake the optimums are probably masked by the interactions of the flow structures related to each side of the wake.

Similar results were obtained in the mixing region of a jet, close to the nozzle (Fig. 8). Findings are here at variance with those of LEE (1971), and LEE & RIBNER (1972) which dealt mainly with sections further downstream. It is considered, however, that omitting the convection effects may lead to assigning too high acoustic contributions to the downstream regions. The influence observed of the nozzle edges and their subsequent regions of discontinuity, may probably be linked to the "excess noise" of low speed jets (CRIGHTON, 1972).

4.2. Cross-correlations $\overline{v p_e}$

A less extensive investigation of these correlations has been made. However the results seem to show that these correlations have a similar behaviour to the $\overline{v^2 p_e}$ correlations.

4.3. Cross-correlations $\overline{\pi_e p_e}$

Curves corresponding to three locations of the pressure transducer are given in Fig. 10 and show that :

(i) - the correlation levels of $\overline{\pi_e p_e}$ are very high (≈ 0.80) whereas those of $\overline{v^2 p_e}$ are at most equal to 0.10.

(ii) - there is a slight drift of the time delay at which occurs a positive extremum, depending on the location of the pressure transducer. It will be shown in section 4-4 that this drift is due to a pressure wave which propagates along the airfoil at sonic velocity.

(iii) - all the positive extremums appear at time delays close to the acoustic propagation time τ_e . The nearer the pressure transducer is to the trailing edge, the closer to τ_e will be the time delay.

(iv) - these findings seem verified for all the frequencies belonging to the Strouhal range of a spectrum.

In consequence, the signal π_e is essentially made up of an acoustic pressure associated with a wave propagating towards the leading edge of the airfoil. To determine the eventual role of π_e as an acoustic source, the value of the correlation $\overline{\pi_e p_e}$ has to be considered at time $\tau_e - 1/4\beta$. The contribution to the surface integral of expression (2) is therefore negligible for points in the vicinity of the trailing edge. This contribution becomes more important as the point of integration $\vec{y}$ moves away from the trailing edge.

4.4. Cross-correlations $\overline{\pi_e \pi_e}$

In order to interpret the drift in the delay time observed in section 4.3, cross correlations have been made between the signals of the pressure transducers embedded in the extrados of the airfoil. A correction was made to allow for any slight phase difference between the transducers, as explained in section 2. Results of Fig. 11 show that a pressure signal travels towards the leading edge, at a speed close to the speed of sound. PATTERSON (1972) seems to have been the first to observe this propagation for a symmetrical airfoil.

It is also interesting to note that this wave keeps propagating when a hydrodynamic perturbation is superposed to the flow and convected downstream by it. For example, Fig. 11 shows the case where a pressure transducer was intentionnally mounted just protruding into the airfoil surface. Measurement of the convection speed U_c of this perturbation leads to $U_c \approx 0.7\,U$, an acceptable value for a turbulent flow. In consequence, it is also possible to conclude that, in the absence of the perturbation, the boundary layer on the extrados of the airfoil is laminar.

4.5. Cross-correlations $\overline{\pi_i \pi_i}$

Similar findings have been obtained for the pressure signals π_i on the intrados of the airfoil. The acoustic part of the pressure seems, however, less important here than on the extrados.

4.6. Cross-correlations $\overline{p_e \pi_i}$, $\overline{p_e \pi_t}$, $\overline{\pi_i \pi_t}$

These various correlations are shown in Fig. 12. They show a phase opposition between π_e and π_t , and the antisymmetrical character of the far field. The low level of the correlations involving π_i is again observed.

4.7. Cross-correlations $\overline{\pi_e v_2}$

For a fixed pressure transducer, Fig. 13, these correlation curves again show the downstream convection of the wake structures.

CONCLUSION

The acoustic field of the airfoil investigated is governed by the aerodynamic phenomena which take place at the trailing edge of the airfoil, especially on the extrados. The field is formed by a strong volume source concentrated in that region and by the interaction of that source with the airfoil surface. This interaction leads to surface sources whose importance seems to become greater further from the trailing edge.

Presently, an attempt is made to evaluate the integrals numerically. Evaluation of the volume integral appears difficult because of the Dirac aspect of the source. The evaluation of the surface integral seems to present less difficulty.

ACKNOWLEDGMENTS

We should like to thank the Electricité de France, Service Machines et Automatismes de Production, for their support.

REFERENCES

- BERNHAULT J.P., SUNYACH M., ARBEY H., et COMTE-BELLOT G. (1973) - Réalisation d'une chambre anéchoïque revêtue de panneaux et destinée à l'étude des bruits d'origine aérodynamique (to appear in Acustica).

- CRIGHTON D.G. (1972) - The excess noise field of subsonic jets. J. Fl. Mech. 56, p. 683-694.

- FFOWCS WILLIAMS J.E. (1969) - Modern methods for flow noise analysis, Dept. of Math. Imperial College London.

- LEE H.K. (1971) - Correlations of noise and flow of a jet. UTIAS Rep. n° 168.

- LEE H.K. and RIBNER H.S. (1972) - Direct correlation of noise and flow of a jet. J. Acoust. Soc. America. 52, p. 1280-1290.

- LIGHTHILL M.J. (1952) - On sound generated aerodynamically, I - General Theory, Proc. Roy. Soc. A 211, p. 564-587.

- LIGHTHILL M.J. (1954) - On sound generated aerodynamically, II - Turbulence as a source of sound, Proc. Roy. Soc. A 222, p. 1-32.

- PATTERSON R.W., VOGT P.G., FINK M.R. (1972) - Vortex noise of isolated airfoils, Paper n° 72 656, AIAA 5 th Fluid and Plasma Dynamic Conference, Boston, Mass. June 26-28.

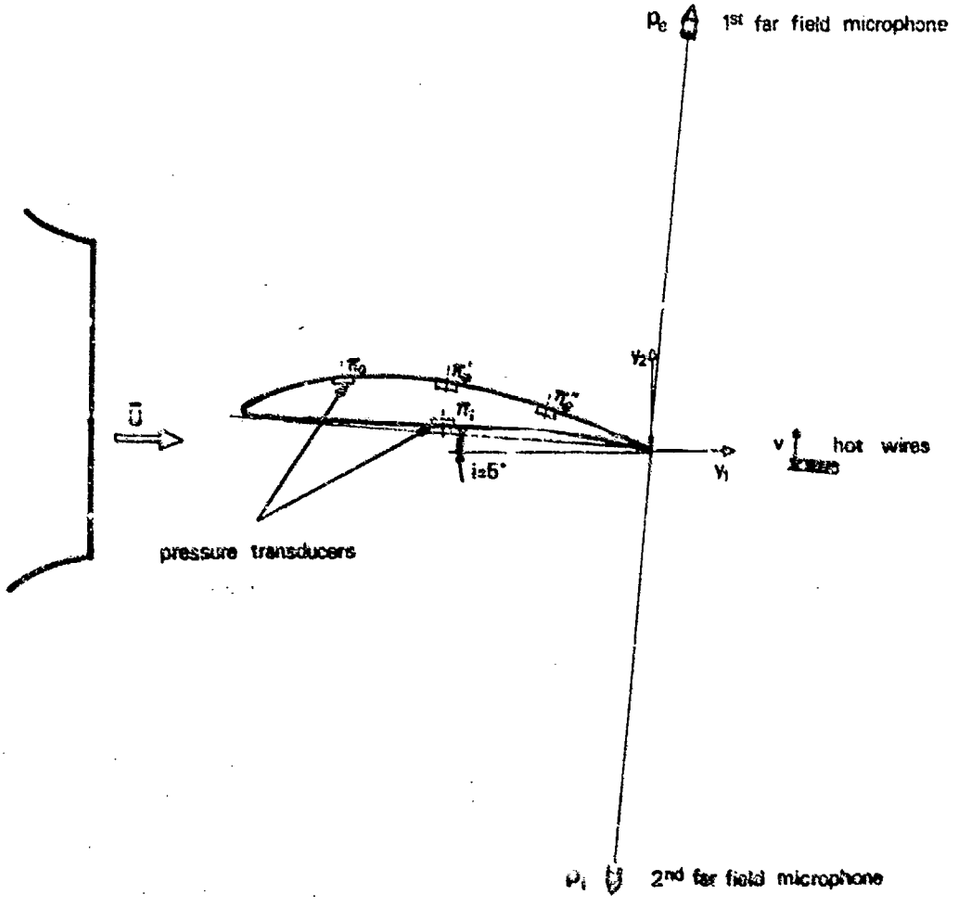

Fig. 1 - Experimental set-up of the airfoil into the flow.

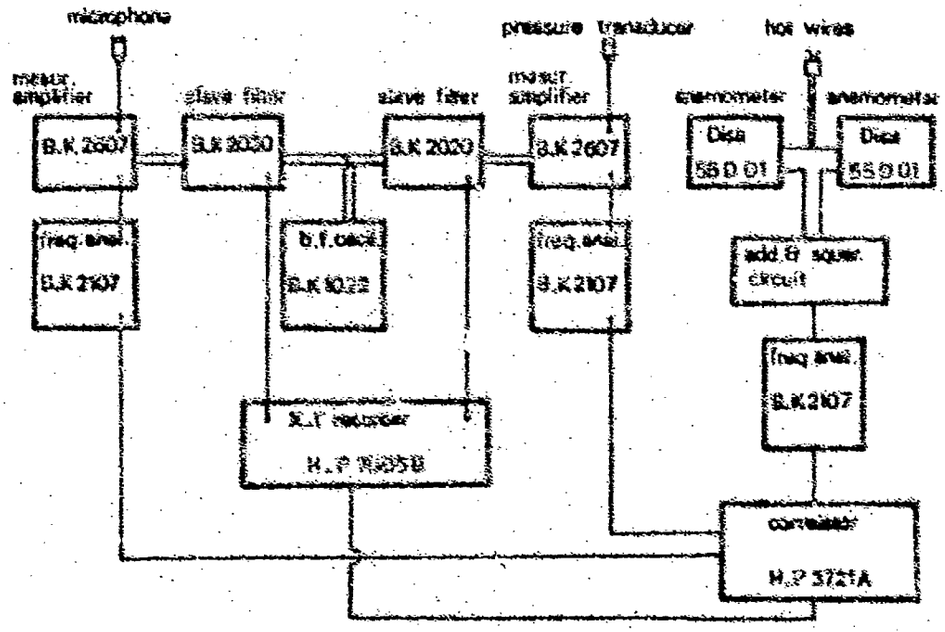

- Fig. 2 - Measuring equipment

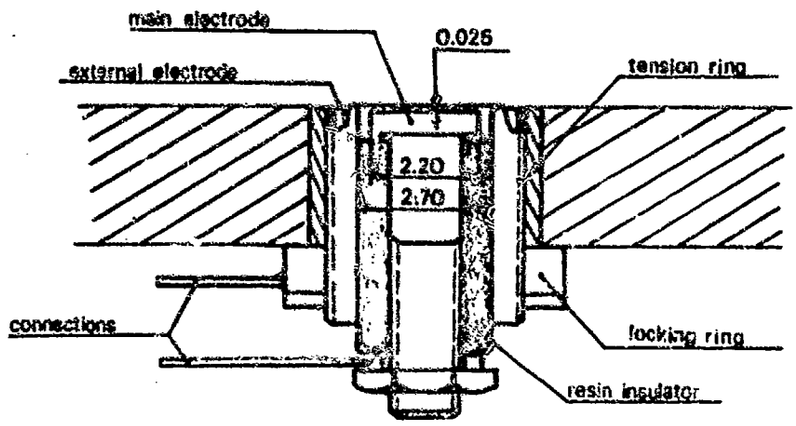

. Fig. 3 - Section of pressure transducer embedded in the airfoil (Scale 10 : 1).

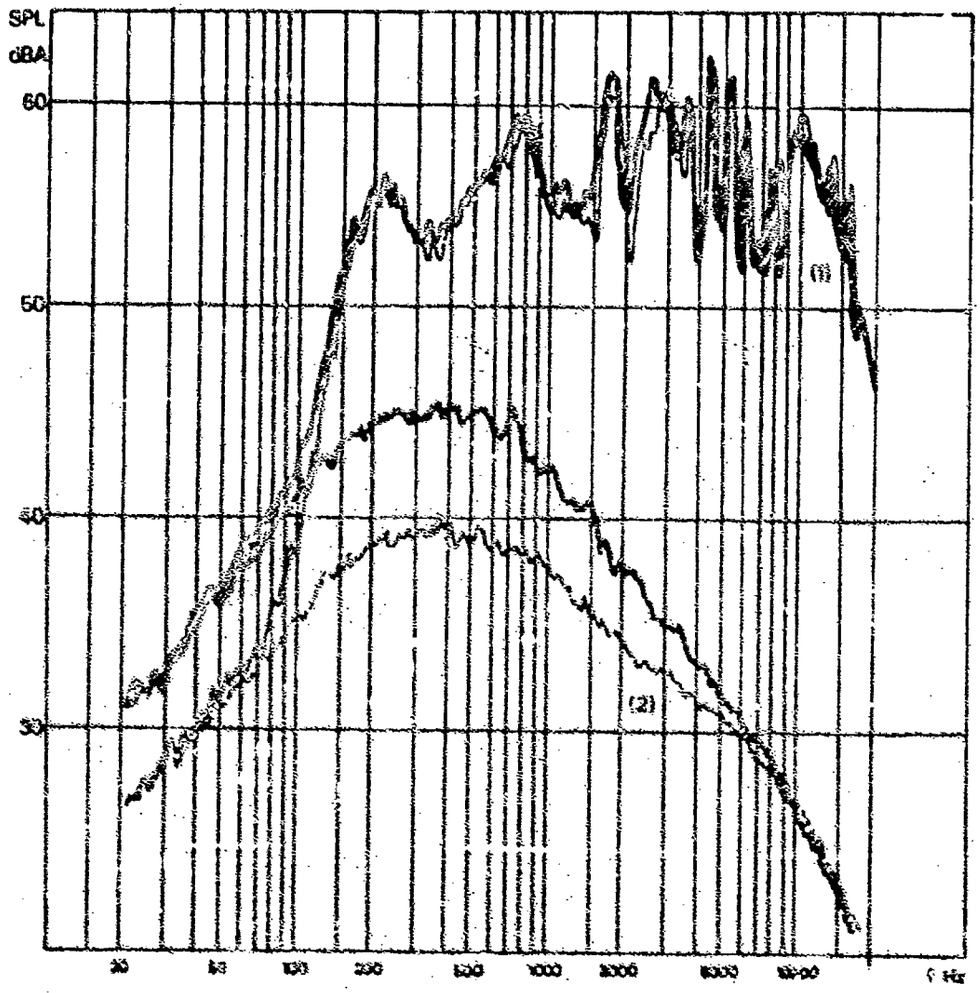

Fig. 4 - Characteristics of the pressure transducer (dark lines) compared with a Brüel & Kjaer 1/8" microphone (light lines) ; (1) Response to a loudspeaker excited by a white noise ; (2) Background noise.

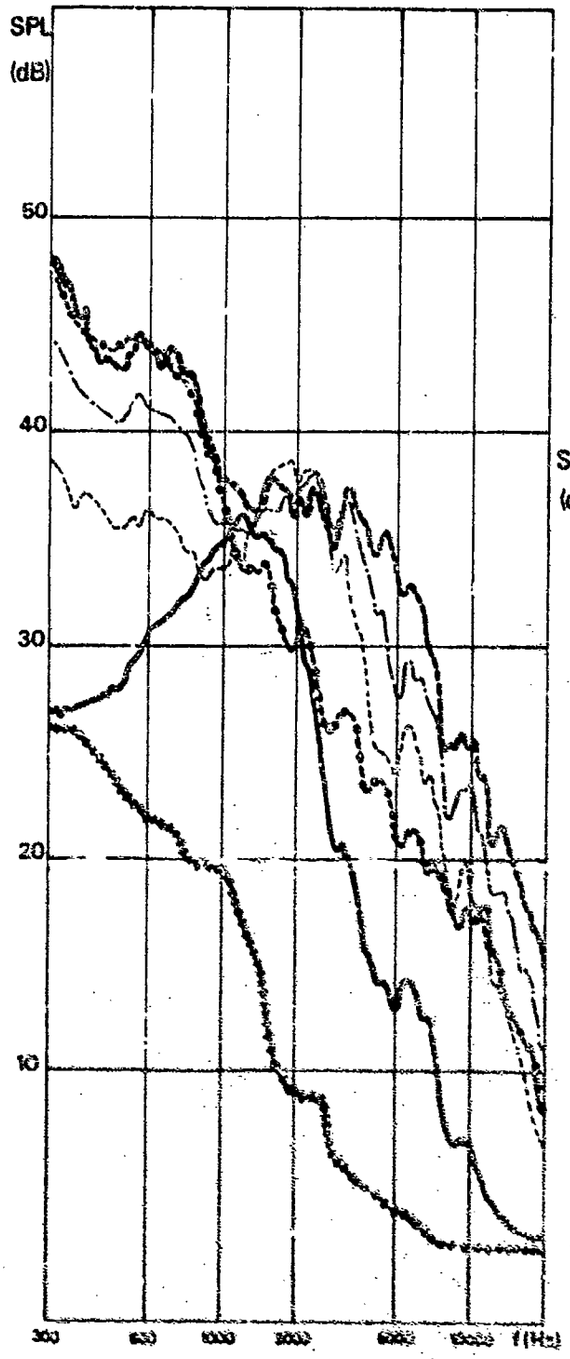

Fig. 5 - Spectra of the far field acoustic pressure p_a :

airfoil	———	20.2 m/s
	- - - - -	29.2 m/s
	— — —	34.2 m/s
	———	38.4 m/s
jet	·····	20.2 m/s
	-·-·-·-	38.4 m/s

Fig. 6 - Spectra of the pressure fluctuation p_s on the extrados of the airfoil

——— 20.2 m/s
- - - - - - - 29.2 m/s
—·—·— 34.2 m/s
——— 38.4 m/s

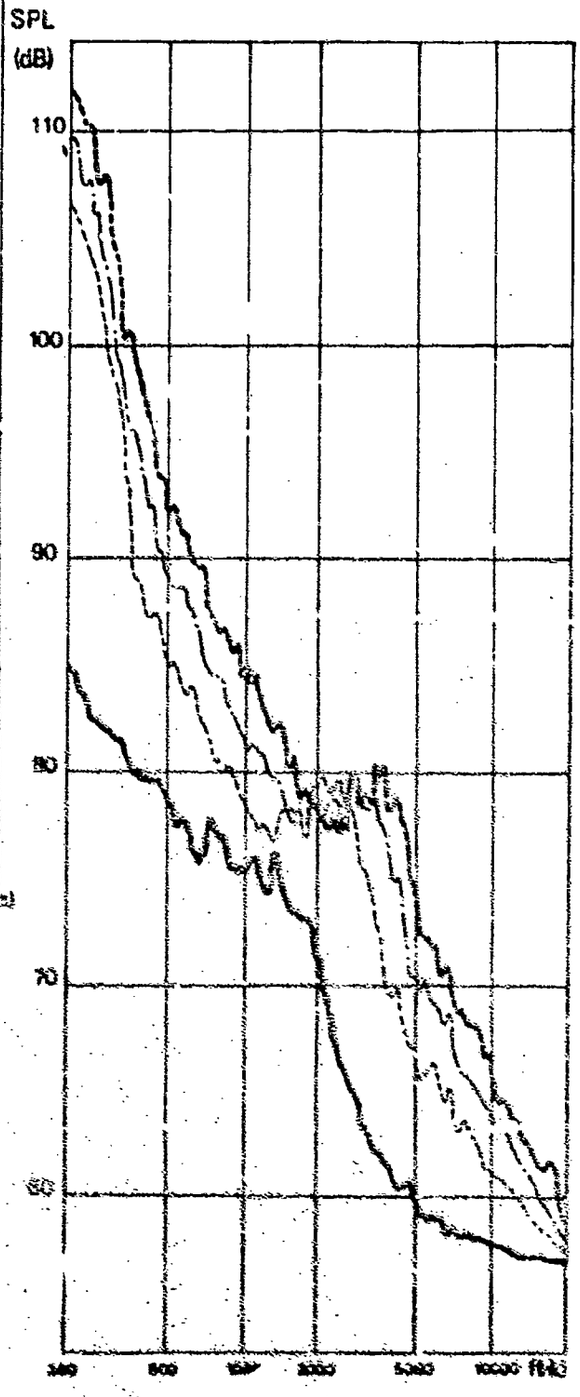

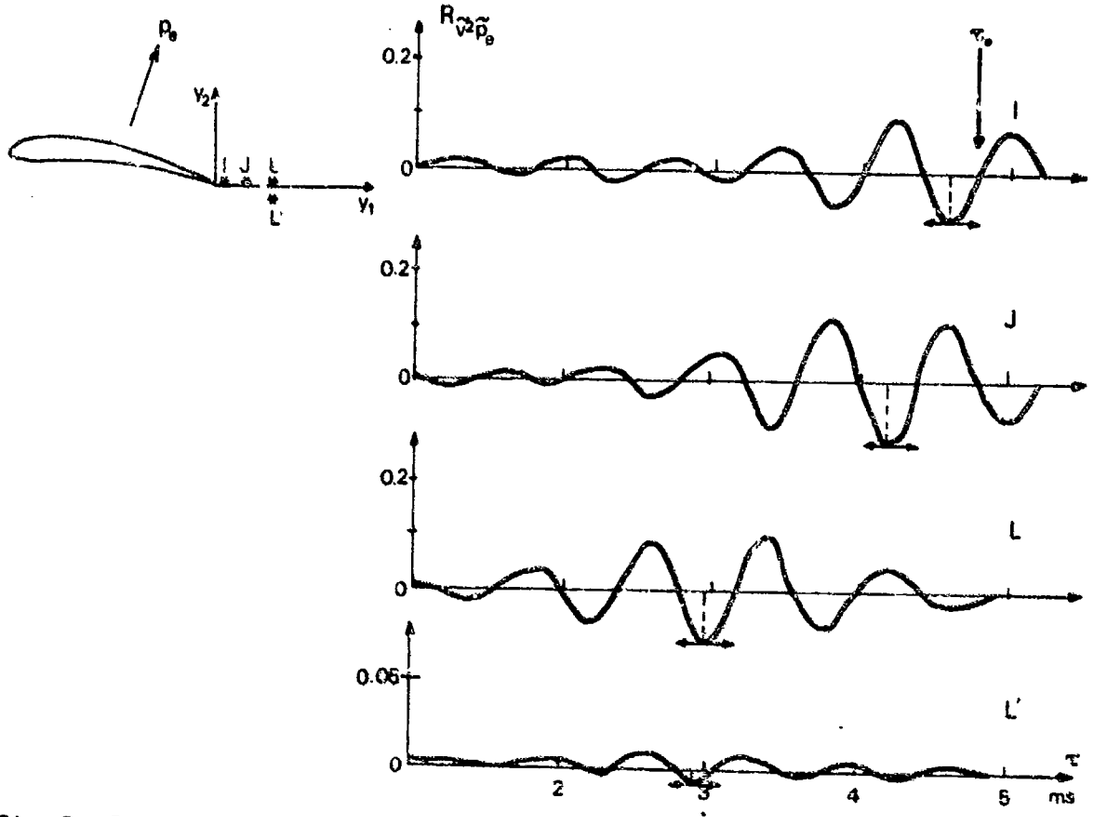

Fig. 7 - Cross-correlations between the far field acoustic pressure p_e (extrados side) and the square v^2 of the transverse velocity component in the wake at points I (0.2 ; 0) - J (1 ; 0) - L (3 ; 0) - L' (3 ; -1) - ($\bar{U}$ = 20,2 m/s ; f = 1500 Hz).

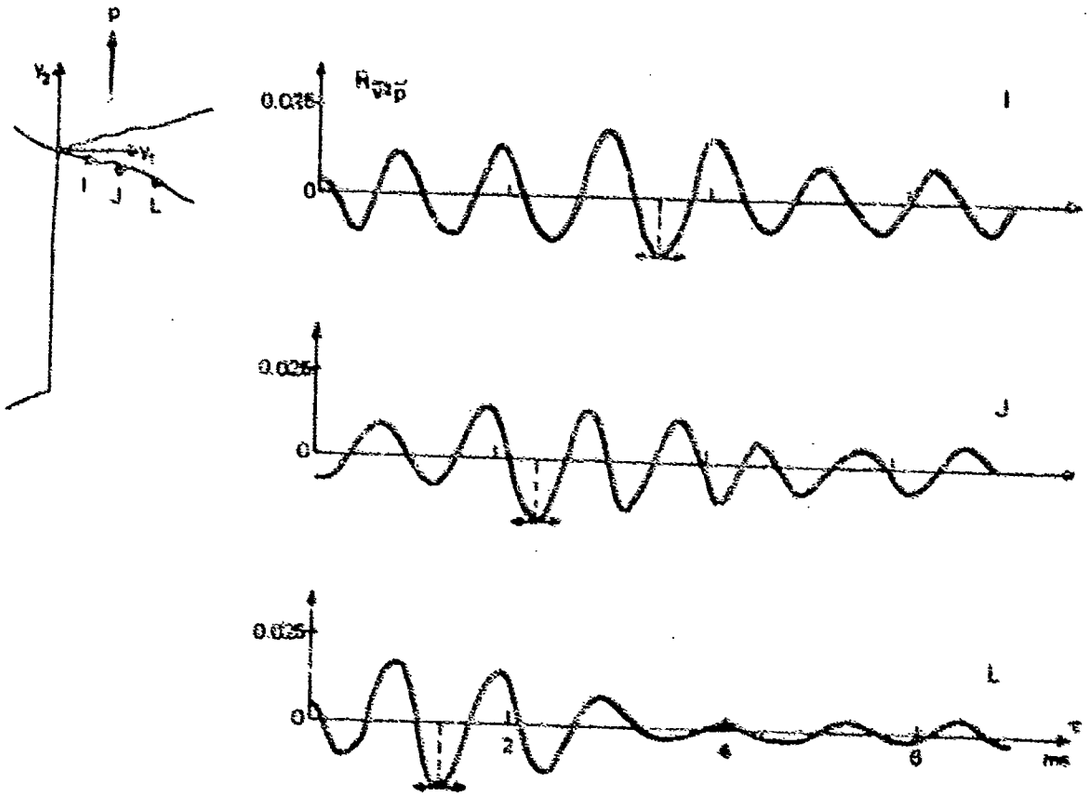

Fig. 8 - Cross-correlations between the far field acoustic pressure p_e and the square v^2 of the transverse velocity component in the mixing region of a jet, at I (2 ; -5.5) - J (4 ; -6) - L (6 ; -6.5) - ($\bar{U}$ = 20,2 m/s ; f = 1500 Hz).

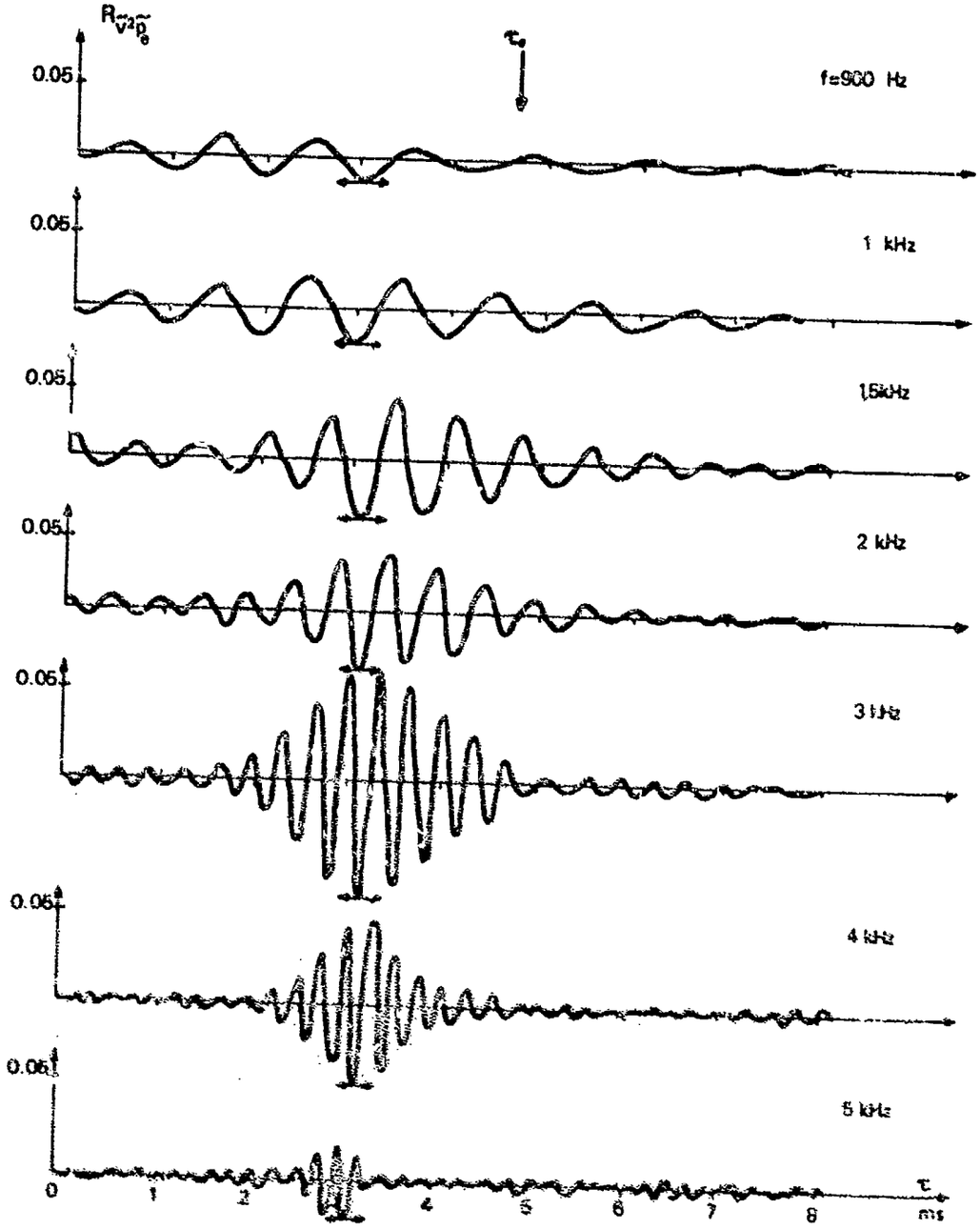

Fig. 9 - Effect of frequency on the cross-correlation $R_{\tilde{v}\tilde{p}_0}$ ($\bar{U}$ = 38,4 m/s).

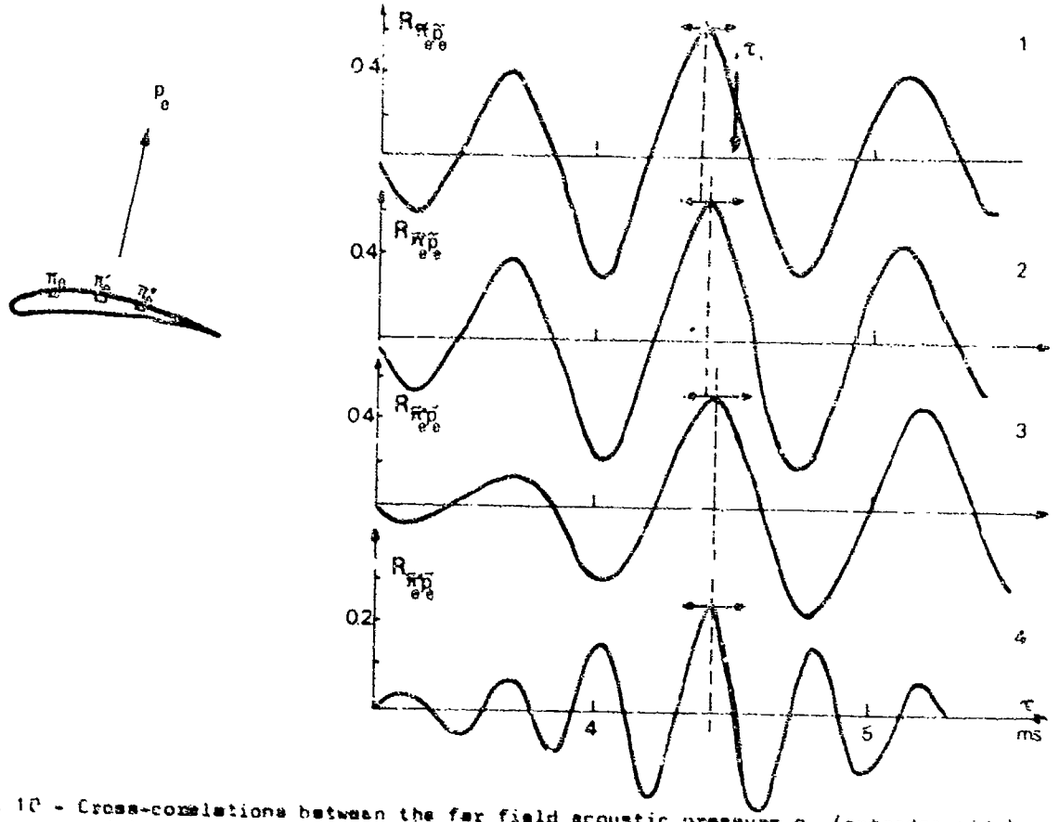

Fig. 10 - Cross-correlations between the far field acoustic pressure p_e (extrados side) and the pressure fluctuation π_e, π'_e and π''_e on the extrados of the airfoil at 25 %, 50 % and 75 % of the chord respectively. $\bar{U}$ = 20,2 m/s ; f = 1500 Hz (curves 1-2-3) and f = 3000 Hz (curve 4).

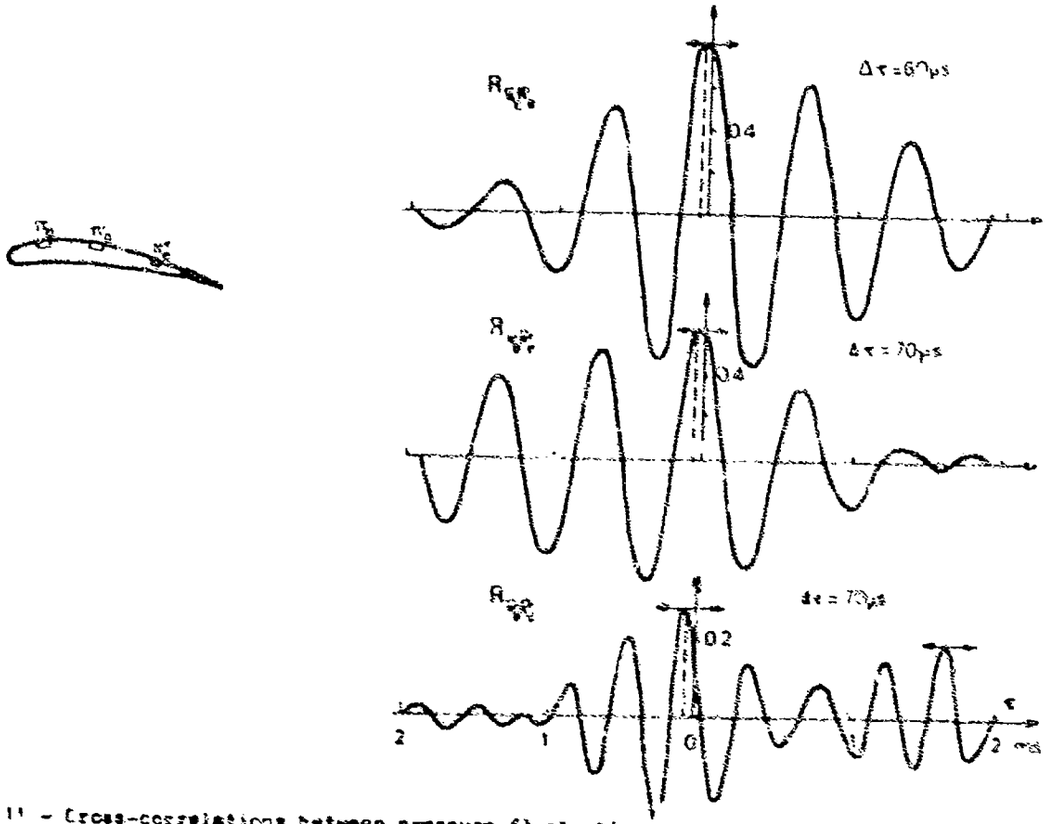

Fig. 11 - Cross-correlations between pressure fluctuation π_e, π'_e, π''_e on the extrados of the airfoil at 25 %, 50 % and 75 % of the chord respectively. In the lower curve the microphone π_e protudes into the flow ($\bar{U}$ = 20,2 m/s ; f = 1500 Hz)

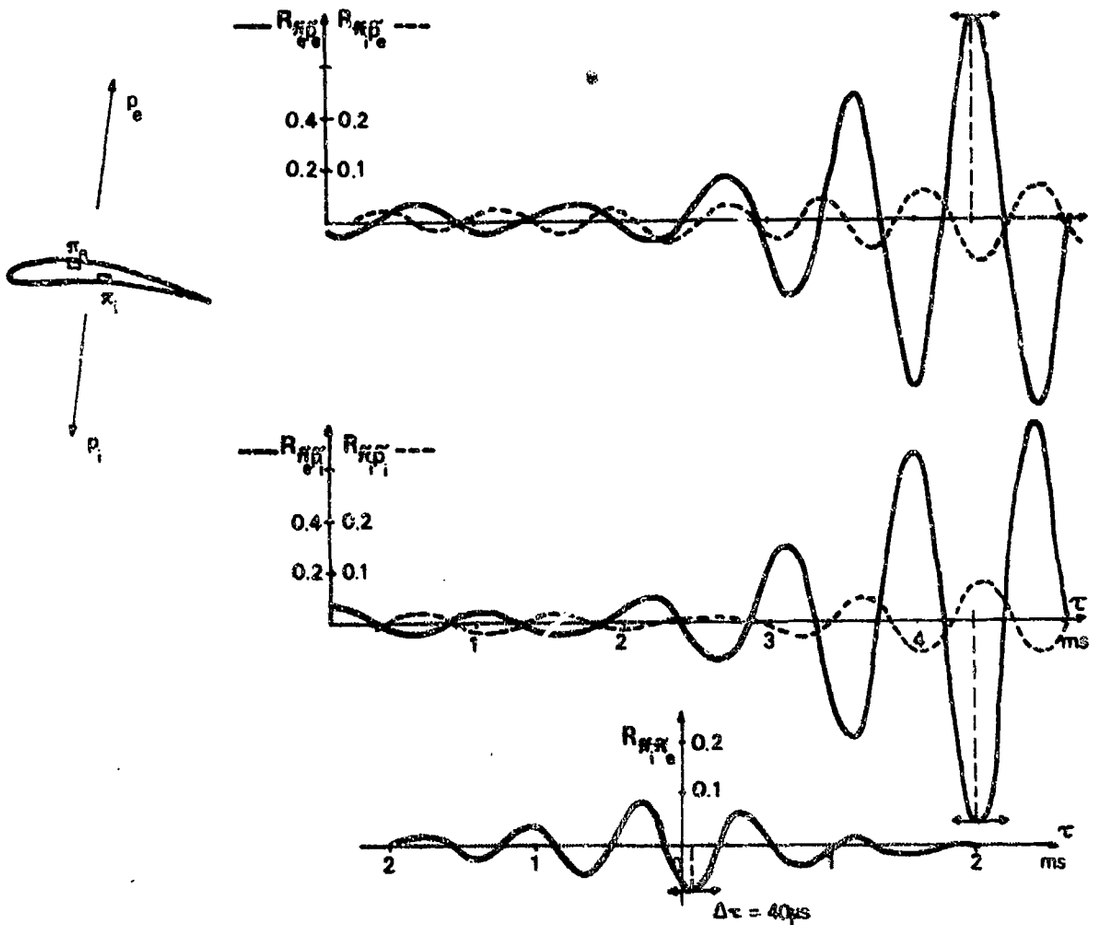

Fig. 12 - Cross-correlations between the far field acoustic pressure and the pressure fluctuation on the airfoil (extrados or intrados) π_e is at 40 % and π_i at 50 % of the chord. ($\bar{U}$ = 20,2 m/s ; f = 1500 Hz).

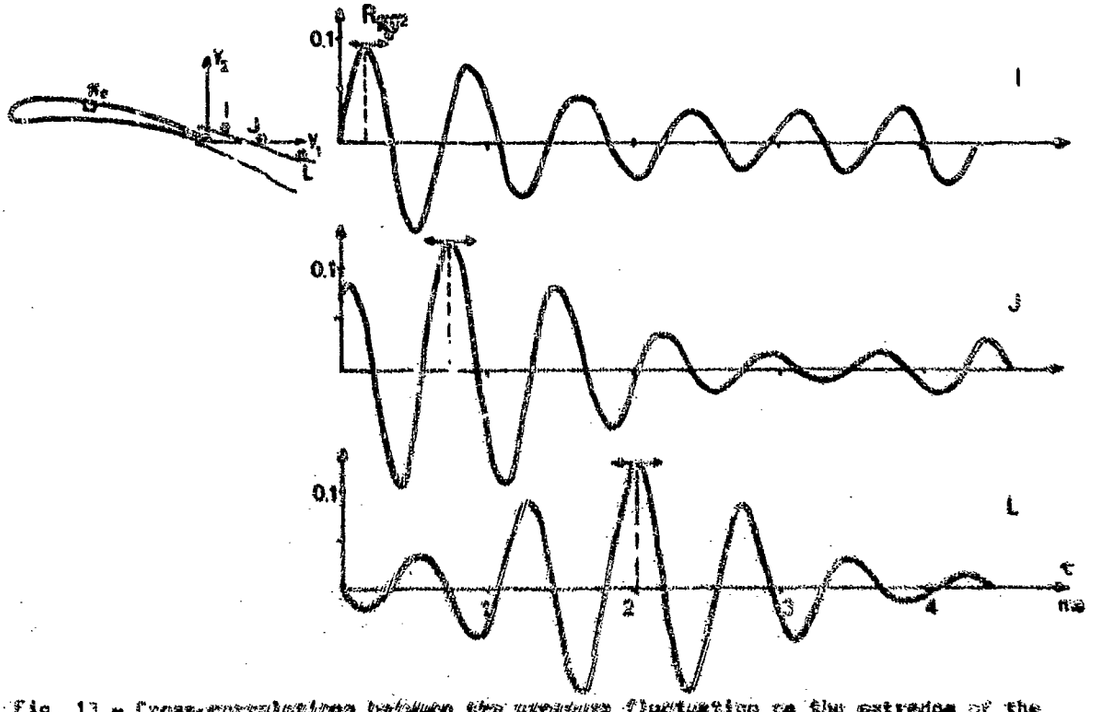

Fig. 13 - Cross-correlations between the pressure fluctuation on the extrados of the airfoil and the square v^2 of the transverse velocity in the wake at points I (0,2 ; 0) - J (1 ; 0) - L (3 ; 0) ; π_e is at 50 % of the chord. ($\bar{U}$ = 20,2 m/s ; f = 1500 Hz).

REPRESENTATION DE LA TURBULENCE D'UN JET CHAUD A PARTIR DE SON EMISSION INFRAROUGE

par Jean-François de Belleval et Mariano Pérulli
(Office National d'Etudes et de Recherches Aérospatiales)
92320 CHATILLON - France

RESUME

La description théorique du rayonnement acoustique d'un jet est, généralement, décrite par des grandeurs caractéristiques de turbulence définies à l'échelle du volume émissif total. Ces grandeurs sont déduites de modèles théoriques ou de mesures utilisant les techniques de corrélation. De ce fait, ces grandeurs sont des grandeurs moyennes dans le temps, c'est-à-dire représentatives de l'ensemble du spectre.

Dans ce travail, après une discussion sur la nature des sources acoustiques qui peuvent exister dans un jet chaud et après un rappel des techniques de faisceaux croisés, on présente sur des exemples une représentation de la turbulence d'un jet chaud à partir de densités spectrales croisées. Il est alors possible de définir en tout point du volume source les grandeurs caractéristiques de turbulence par bandes de fréquence et de connaître ainsi leur dispersion.

- - - - -

REPRESENTATION OF HOT JET TURBULENCE BY MEANS OF ITS INFRARED EMISSION

SUMMARY

The theoretical description of a jet acoustic radiation is usually described by characteristic turbulence data, defined at the scale of the total emissive volume. These data are deduced from theoretical models of from measurements making use of correlation techniques. Hence these data have average values in time, i.e. representing the whole spectrum.

In this paper, after a discussion on the nature of acoustic sources which may exist in a hot jet, and after recalling the crossed beam techniques, is presented, on examples, a representation of a hot jet turbulence by means of crossed spectral densities. It is then possible to define at any point of the source volume the characteristic turbulence data by frequency bands, and thus to know their dispersion.

- - - - -

NOTATIONS :

- $C(\xi,\tau)$: coefficient d'auto-corrélation
- $\vec{y}, \vec{y}', \vec{y}''$: point courant du volume source
- ξ : écart axial des radiateurs
- τ : temps
- V_c : vitesse de convection
- $C_{ab}(\xi,\tau)$: coefficient d'inter-corrélation
- x : axe du jet
- D : diamètre de la tuyère dans le plan de sortie
- x_m : abscisse du maximum du coefficient de corrélation
- $\mathcal{T}$: échelle intégrale de la durée de vie
- $\mathcal{L}_x$: échelle intégrale des longueurs le long de l'axe du jet
- ρ : masse volumique
- t : temps
- $\vec{v}$: vitesse du fluide
- p : pression
- δ_{ij} : tenseur unité
- $\vec{x}$: point d'observation
- τ : temps retardé (temps d'émission)
- $P(x,t)$: auto-corrélation du champ sonore lointain
- $P(x,\omega)$: T.F. de $P(\vec{x},\tau)$
- $I(x,\omega)$: densité spectrale du champ sonore lointain
- $I(x)$: intensité sonore
- θ : angle formé par l'axe du jet et le point d'observation
- c_0 : vitesse du son dans le milieu au repos
- V_j : vitesse locale du jet

1.- INTRODUCTION

L'objet des travaux effectués par l'ONERA [1] en coopération avec la SNECMA [2] sous l'égide des Services Techniques de l'Aéronautique est de définir une procédure de caractérisation des sources de bruit dans un jet chaud. La nécessité d'une telle procédure est apparue dès que certaines limites ont été atteintes en matière de réduction du bruit. En effet, suite aux travaux de LIGHTHILL [3], RIBNER [4] et FFOWCS-WILLIAMS [5], pour des jets froids subsoniques moyens, un accord entre modèles théoriques et mesures sonores dans le champ lointain existe. Ces modèles théoriques permettent de prévoir le champ sonore (directivité et spectre) à l'aide de grandeurs de turbulence définies à l'échelle du volume du jet. Néanmoins, cet accord n'est pleinement réalisé qu'en introduisant sous forme empirique des constantes et en admettant une variation des grandeurs de turbulence suivant des lois déduites des modèles eux-mêmes compte tenu des résultats expérimentaux [6].

De ce fait, le besoin a été ressenti de caractériser les sources de bruit à une échelle spatiale plus fine, par exemple en étudiant la contribution de différentes tranches du jet,

- soit en ne faisant intervenir pour la mesure acoustique que certaines parties du jet (à l'aide de systèmes microphoniques directifs ou bien en n'introduisant dans l'enceinte acoustique qu'une partie du volume source [7]),

soit en adaptant la méthode des sources images en effectuant des corrélations entre microphones placés sur une paroi parfaitement réfléchissante [8].

De plus, pour arriver à une échelle spatiale plus fine, les acousticiens ont développé ou utilisé, pour caractériser la turbulence de jets froids, les fils chauds [9], [10], des capteurs acoustiques [11], la strioscopie laser [12], [13], la mesure de l'absorption infrarouge [14], [15] et, pour les jets chauds, l'émission infrarouge [16], [17]. Par ailleurs, le cas de jets froids est le seul qui ait donné lieu à un début d'exploitation acoustique, par corrélation à partir de mesures au fil chaud et au microphone [10], [11], [18], [19].

2.- DEFINITION DE LA PROCEDURE

Dans le cas de jets chauds de forte ou de faible vitesse, la situation est très complexe sur le plan théorique du fait du mélange d'effets liés soit au gradient de densité, soit à la température qui s'ajoutent et se mêlent à la vitesse. Ces effets ont été constatés expérimentalement [20]. Des tentatives de classification ainsi qu'une analyse théorique détaillée de ces effets, en tant que générateurs de bruit, ont été ou sont actuellement tentés [21], [22].

La méthode de travail proposée par l'ONERA est une méthode globale dont le but essentiel est de pouvoir qualifier l'action de silencieux à structure mécanique ou aérodynamique sur le rayonnement acoustique (directivité et spectre dans le champ lointain). La démarche essentielle qui domine cette méthode consiste à assimiler le volume du jet à un volume rayonnant acoustiquement, caractérisé en tout point par des grandeurs spatio-temporelles.

On admet :

2.1 - que le prélèvement de l'information dans le jet fournit des renseignements locaux sur les sources de bruit ou sur leur émission sonore,

2.2 - que de ce prélèvement on peut déduire l'évolution spatiale des grandeurs de turbulence par traitement hybride du signal,

2.3 - qu'on peut enfin, à partir de ces grandeurs, remonter, par calcul numérique, au rayonnement acoustique dans le champ lointain. Pour cela, on inverse l'équation d'ondes inhomogène dont le second membre décrit la source acoustique. On établit ainsi une correspondance entre le champ sonore lointain et le champ turbulent émissif.

L'ensemble de cette procédure ayant déjà été présenté par ailleurs [1], [2], et [23], nous exposerons dans ce travail des résultats nouveaux relatifs aux points 2.1 et 2.2, après un bref rappel de cette procédure et des précédentes conclusions essentielles.

3.- DESCRIPTION DE LA PROCEDURE

3.1 - Méthode de mesure :

Ayant à explorer des jets essentiellement chauds (de taux de détente 1,2 à 3,4 et de température comprise entre 700 K et 1100 K) créés par combustion de propane (chambre sphérique du Centre d'Essais des Propulseurs, fig. 1) ou de kérosène (laboratoire d'essais de l'ONERA, fig.2), la méthode adoptée, inspirée par GOUTTEBEL [17], consiste à recueillir sur un récepteur muni d'une optique convenable le rayonnement infrarouge d'un petit volume du milieu turbulent étudié. Le montage en est représenté sur la figure 3.

Deux récepteurs [20], dont les axes optiques sont perpendiculaires entre eux et orthogonaux à l'axe du jet, sont utilisés. Chacun de ces récepteurs analyse simultanément l'émission infrarouge en provenance de tous les points du jet situés au voisinage de l'axe optique ; il a cependant été possible de donner à ces radiomètres une certaine sélectivité spatiale le long de cet axe en disposant sur le trajet optique un diaphragme qui joue le rôle de pupille, ce qui confère un poids élevé à l'émission infrarouge du volume situé à la position conjuguée de celle du diaphragme. Si l'on veut améliorer encore la définition spatiale, il est nécessaire d'utiliser deux appareils dont les axes optiques se croisent au point à étudier, et d'employer une méthode

de corrélation.

Cette configuration permet en particulier de définir le coefficient d'autocorrélation $C(\vec{y}, o, \tau)$ de l'émission infrarouge du point considéré. Enfin, si les deux axes sont écartés de la distance ξ, on mesure le coefficient de corrélation croisée $C(\vec{y}, \xi, \tau)$. En traçant les courbes de C en fonction de τ pour différentes valeurs de ξ, on peut faire apparaître les paramètres spatio-temporels de la turbulence.

Ce type de mesures exige la réalisation d'un montage mécanique soigné et insensible aux vibrations, qui permette le déplacement contrôlé et précis de l'axe optique d'au moins un radiomètre pendant le déroulement de l'expérimentation acoustique.

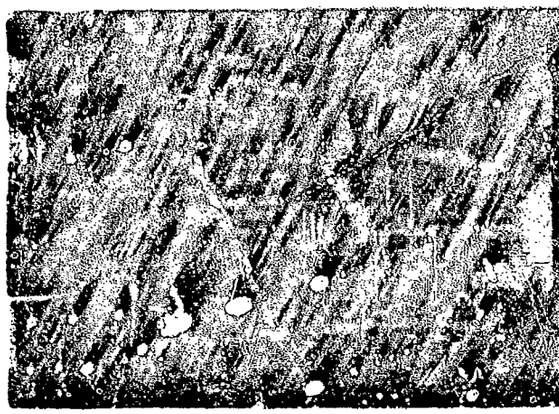

Fig. 1 - Chambre sourde C[illegible]r.

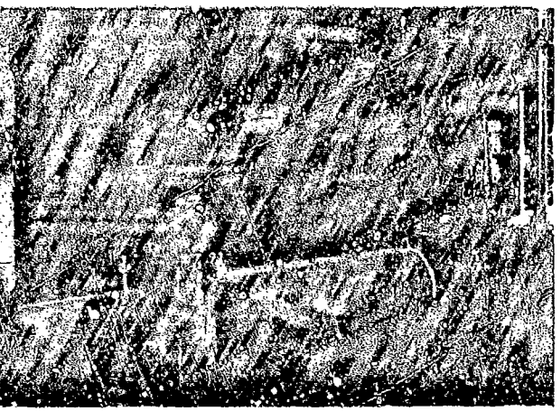

Fig. 2 - Cellule d'essais de l'ONERA.

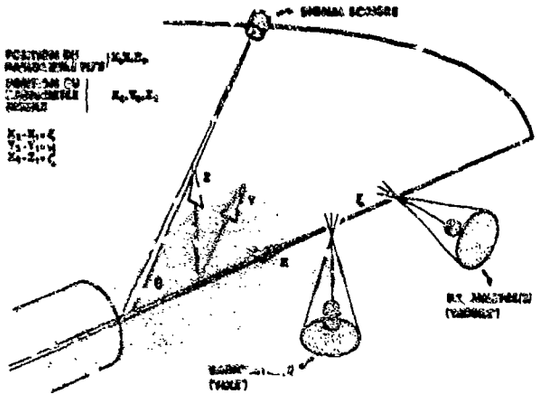

Fig. 3 - Schéma de principe de l'installation.

3.2 - Traitement hybride du signal :

3.2.1 - Intensité de turbulence

Un radiomètre placé à différentes distances du plan de sortie tuyère se déplace suivant une direction transversale. Chacune des deux voies de mesure du radiomètre fournit respectivement la racine carrée de la valeur quadratique moyenne $(\langle \varepsilon^2 \rangle)^{1/2}$ et la valeur moyenne du signal $\langle \varepsilon \rangle$. L'évolution du rapport $(\langle \varepsilon^2 \rangle)^{1/2}/\langle \varepsilon \rangle$ reflète la géométrie de la zone de mélange. Ce rapport, lié à l'intensité de turbulence, est maximum en fin de cône potentiel, ce qui met en évidence l'importance de cette zone pour l'émission sonore.

3.2.2 - Paramètres spatio-temporels

Des coefficients de corrélation $C_{12}(\xi, \tau)$ calculés à partir de mesures, on déduit par calculs élémentaires les grandeurs caractéristiques de la turbulence. Rappelons que l'indice 1 repère le radiomètre 1, l'indice 2 le radiomètre 2 ; ξ est égal à l'écart entre les axes portant les radiomètres 1 et 2 (fig. 3) et τ représente le retard.

Sur la figure 4 est présenté un exemple de coefficient de corrélation $C_{12}(\xi, \tau)$ calculés à partir de mesures effectuées dans une zone B repérée par la position du radiomètre 1, radiomètre de référence ou radiomètre fixe. Une première analyse de ces corrélations [25] montre qu'à l'aide d'une double affinité on peut superposer (fig. 5) les courbes présentées sur la figure 4. Pour un X/D et un 2Y/D donnés, on constate que la partie la plus importante de la courbe se conserve lorsque ξ croît. On définit ainsi une forme représentative de la fonction

de corrélation dans la zone considérée. Cette propriété est encore vraie pour des mesures effectuées à différentes positions X/D et 2Y/D dans le jet.

Signalons également qu'un début d'étude statistique d'une zone du jet semble mettre en cause l'hypothèse de stationnarité du champ turbulent. Des mécanismes à plus grandes échelles paraissent exister. Leurs contributions au rayonnement sonore méritent d'être étudiées.

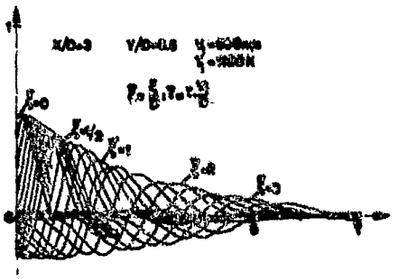

Fig. 4 - Evolution des coefficients de corrélation $C_{12}(\xi,\tau)$ pour différentes distances axiales $\gamma = \xi/D$ séparant les 2 radiomètres.

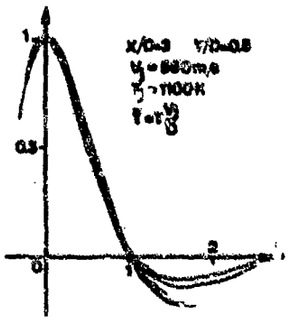

Fig. 5 - Définition d'une forme unique de $C_{12}(\xi,\tau)$ à l'aide d'une double affinité.

Sur la figure 6 est présenté un exemple de profil axial de la vitesse de convection $V_c = \xi_M/\tau_M$ où ξ_M est l'abscisse du maximum de la courbe $C_{22}(\xi,\tau)$. On remarque que cette vitesse passe par un maximum aux alentours de la fin du cône potentiel.

Sur la figure 7 est présenté un exemple de profil axial de l'échelle intégrale de la durée de vie $\bar{\tau} = \int_0^\infty C_{22}(\xi,\tau_M)\,d\xi$ où $C_{22}(\xi,\tau_M)$ est l'ordonnée du maximum de $C_{22}(\xi,\tau)$.

La figure 8 donne un exemple de profil axial de l'échelle intégrale de la longueur de corrélation axiale $\bar{\xi} = \int_0^\infty C_{22}(\xi,0)\,d\xi$ où $C_{22}(\xi,0)$ est l'ordonnée de $C_{22}(\xi,\tau)$ à $\tau = 0$.

Fig. 6 - Profil axial de la vitesse de convection.

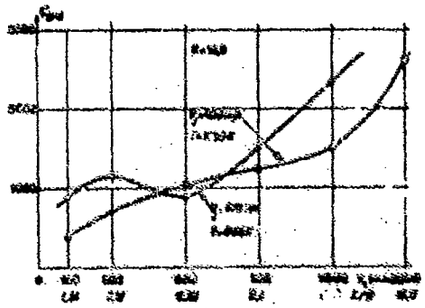

Fig. 7 - Profil axial de l'échelle intégrale de la durée de vie.

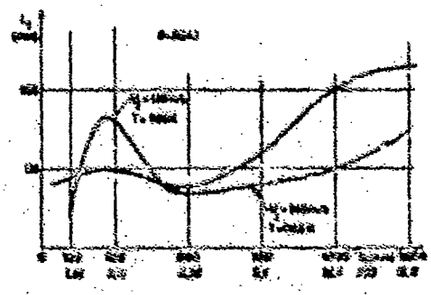

Fig. 8 - Profil axial de l'échelle intégrale de la longueur de corrélation axiale.

3.2.3 - Calcul du champ acoustique

Rappelons seulement les grandes lignes de ce calcul [2] :

de l'équation de propagation des ondes

$$\frac{\partial^2 p}{\partial t^2} - c_0^2 \Delta p = \nabla\nabla : T$$

où ρ est la masse volumique et

$$\vec{\vec{T}} = \rho \vec{v}\vec{v} - \vec{\vec{\sigma}} + (p - c_0^2 \rho)\vec{\vec{\delta}}$$

avec $\vec{v}$: vitesse du fluide, p : pression, c_0 : vitesse du son dans le milieu au repos et $\vec{\vec{\delta}}$ le tenseur unité, on déduit :

$$p(\vec{x},t) = \sum_{i,j} \frac{x_i x_j}{4\pi c_0^2 x^2} \int_{V(\vec{y})} \left[\frac{\partial^2 T_{ij}}{\partial t^2}\right]_{\hat{t}} d\vec{y} \qquad (1)$$

où $p(\vec{x},t)$ est la pression acoustique en $\vec{x}$, à l'instant t et $\hat{t} = t - \frac{|\vec{x}-\vec{y}|}{c_0}$, $\vec{y}$ étant un point courant du volume source.

On peut déduire une description formelle complète du champ sonore à partir des relations :

3.2.3.1 - Auto-corrélation $P(\vec{x},\tau)$ du champ sonore lointain :

$$P(\vec{x},\tau) = \langle p(\vec{x},t)\, p(\vec{x},t+\tau)\rangle$$

$$P(\vec{x},\tau) = \frac{1}{16\pi^2 c_0^4 x^2} \int_{V(\vec{y})} d\vec{y} \int_{V(\vec{y}')} d\vec{y}' \left[\frac{\partial^4}{\partial \tau'^4}\left\{R_{\vec{x}}(\tau',\vec{y},\vec{y}')\right\}\right]_{\tau' = \tau+\tau''} \qquad (2)$$

avec : $\tau'' = \hat{t}'' - \hat{t}'$, $\vec{\eta} = \vec{y}'' - \vec{y}'$, $\vec{y} = \frac{1}{2}(\vec{y}' + \vec{y}'')$

($\vec{y}'$ et $\vec{y}''$ étant deux points courants du volume source)

et, $R_{\vec{x}}(\tau',\vec{y},\vec{\eta}) = \langle \frac{x_i x_j}{x^2} T_{ij}(\vec{y},\hat{t}'') \cdot \frac{x_k x_\ell}{x^2} T_{k\ell}(\vec{y}'',\hat{t}''+\tau')\rangle$

3.2.3.2 - Densité spectrale $I(\vec{x},\omega)$:

$$I(\vec{x},\omega) = \frac{2}{\pi \rho_0 c_0} \int_0^\infty P(\vec{x},\tau) \cos \omega\tau \, d\tau \qquad (3)$$

3.2.3.3 - Intensité sonore $I(\vec{x})$:

$$I(\vec{x}) = \frac{\langle p^2(\vec{x},t)\rangle}{\rho_0 c_0} = \frac{P(\vec{x},\tau)}{\rho_0 c_0} = \frac{\int I(\vec{x},\omega)\, d\omega}{\rho_0 c_0} \qquad (4)$$

3.3 - Conclusions essentielles des premières expériences :

La détermination quantitative de l'émission sonore par les mesures d'émission infrarouge n'étant pas actuellement possible par manque d'une mise à l'échelle des signaux, les premières comparaisons des résultats de calcul avec les mesures acoustiques, pour deux régimes de fonctionnement différents, ne pouvaient être que qualitatives.

Ces premières comparaisons ont montré que :

- le calcul prévoit très correctement le sens des variations des grandeurs acoustiques et, plus spécialement, des paramètres suivants :
- angle d'émission maximale,
- fréquence du maximum de la courbe de densité spectrale, pour l'angle d'émission maximale,
- écart entre le maximum et le minimum de l'intensité sonore.

De plus, l'analyse des corrélations [2] a montré, ainsi que nous l'avons rappelé § 3.2.2, qu'il est possible de donner une forme représentative de la fonction de corrélation du milieu, cette forme présentant des écarts notables avec la forme gaussienne. Ces écarts ne sont pas explicables par les limitations en bande passante de l'instrumentation.

Ces dernières observations nous ont amené à reconsidérer le modèle de turbulence dans le but de mieux représenter les phénomènes.

4.- GRANDEURS CARACTERISTIQUES DE TURBULENCE

4.1 - Vitesse de convection :

4.1.1 - Sur la figure 6 nous avons présenté un exemple de profil axial de vitesse de convection. Cette vitesse est définie par la pente de la droite $\xi = \varphi(\tau_M)$ où τ_M est l'abscisse du maximum de la courbe $C_{\vec{x}} = (\xi, \tau_M)$ (fig. 4).

Des mesures de température et de pression moyennes dans le jet libre, à l'aide de thermocouple et de sonde de Pitot, nous fournissent les profils de vitesse et de température moyennes. On peut alors comparer la vitesse de convection déduite des corrélations à la vitesse locale du jet V_m. Sur la figure 9 on présente un exemple de cette comparaison. On observe en particulier que dans la zone de turbulence développée, ces deux vitesses coïncident (aux erreurs de mesure près).

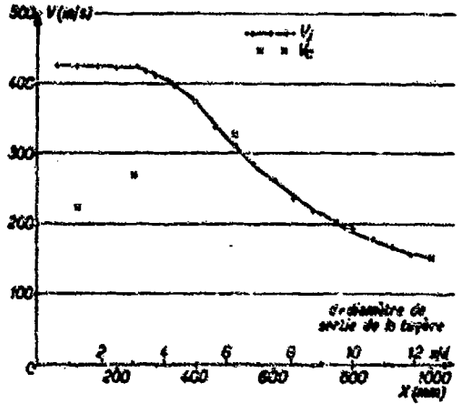

Fig. 9 - Vitesses le long de l'axe du jet.

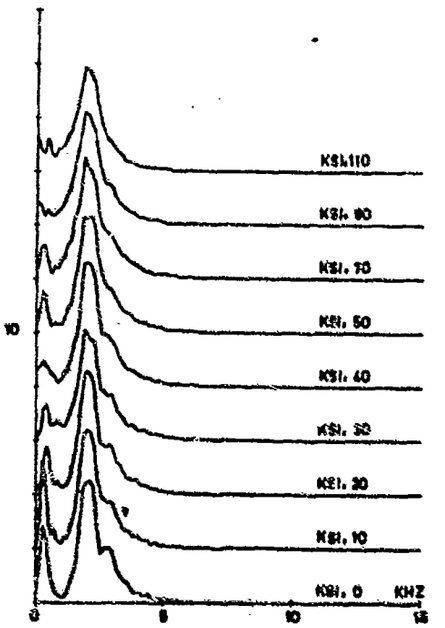

Fig.10 - Corrélation infrarouge-infrarouge.

4.1.2 - Les différents coefficients de corrélation $C_{ss}(\tau, x)$ étant stockés sur bande magnétique numérique, à l'aide d'un programme numérique de transformée de Fourier rapide, on calcule également la transformée de Fourier $C_{ss}(\tau, \omega)$ du coefficient de corrélation. On en déduit la densité spectrale croisée (Fig. 10) et la phase. De la phase, par un calcul élémentaire, on détermine la vitesse de convection pour différentes fréquences. La figure 11a montre un exemple d'évolution de la vitesse de convection en fonction de la fréquence.

Sur la figure 11b, on a porté la courbe $\bar{V} = f(x/\delta)$ déduite des corrélations. De cette dernière courbe on déduit une vitesse de convection représentative de l'ensemble du spectre. On constate que la figure 11a est très semblable à la figure 12 extraite de la référence [27]. Dans ce cas particulier, les auteurs utilisaient des fils chauds dans un jet froid.

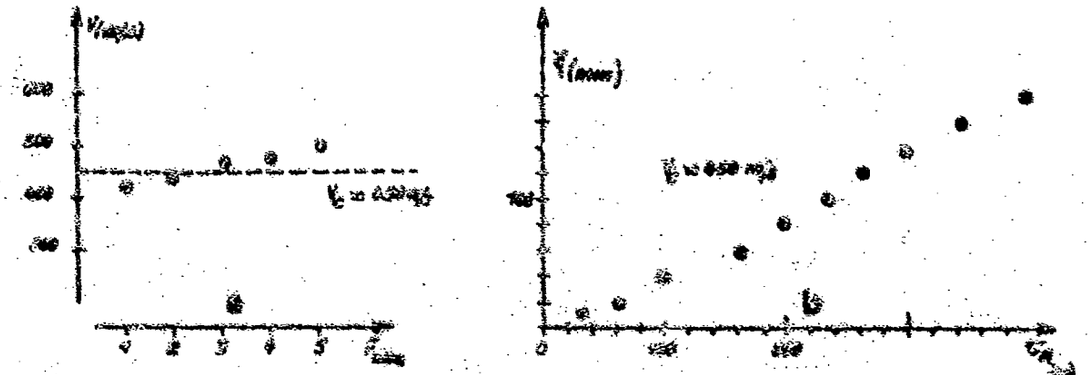

Vitesse par bande de fréquence — Vitesse de convection globale

Fig.11 - Vitesse de convection

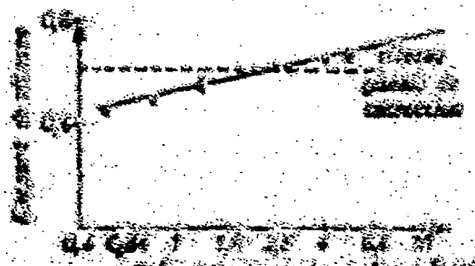

Fig.12 - Variation de la vitesse de convection par bande de fréquence (réf. [27]).

4.2 - Echelle des longueurs :

Des corrélations on déduit (fig. 8) l'échelle intégrale des longueurs représentative de l'ensemble du spectre.

Des densités spectrales croisées, on déduit de même, pour tout point du volume source, une échelle des longueurs pour chaque fréquence du spectre.

Sur la figure 13, on présente le tracé obtenu après calculs de T.F. qui donne directement pour chaque fréquence la variation de l'amplitude de la densité spectrale croisée en fonction de $\frac{y}{\lambda}$ (écart axial des deux radiomètres). On en déduit aisément l'échelle intégrale des longueurs pour la fréquence considérée. On constate que la figure 13 est semblable à la figure 14, également extraite de la référence [27].

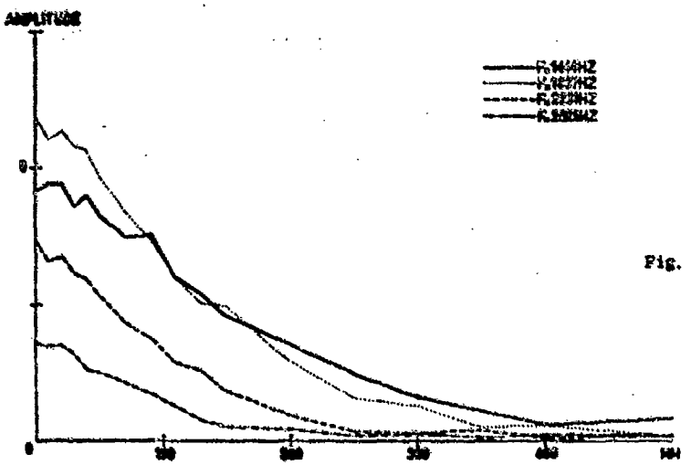

Fig. 13 - Echelle des longueurs.

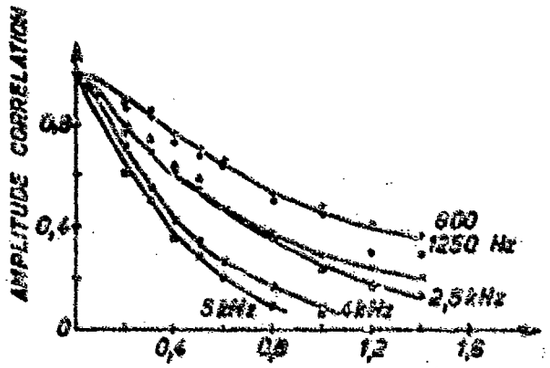

Fig. 14 - Taux de décroissance du maximum de la corrélation pour différentes fréquences (ref. [27]).

4.3 - Conséquences :

Ce mode opératoire présente deux avantages :

4.3.1 - une rapidité et une meilleure précision dans l'obtention de l'information ; en effet, une autre méthode consisterait à effectuer des corrélations de signaux filtrés ; seulement, il faut effectuer un nombre de corrélations égal au nombre de fréquences choisies et, du fait du filtrage, on perd en précision sur la position du maximum du coefficient de corrélation ;

4.3.2 - une meilleure précision dans le calcul acoustique du champ sonore ; en effet, les densités spectrales et les phases (ou vitesse de convection par bandes de fréquence, étant connues, on peut, dans le calcul acoustique (§ 3.2.3), remplacer la fonction $\mathcal{P}(x^0, x)$ par $\mathcal{P}(x^0, \omega)$ (ou $\mathcal{I}(x^0, \omega)$) ; de ce fait sont pris en compte de façon simple, d'une part, le forme du spectre et, d'autre part, la densité d'action de chaque bande de fréquence puisque représentée par l'échelle intégrale des longueurs correspondante et non plus par une échelle intégrale unique pour l'ensemble du spectre.

5.- INTERPRETATION PHYSIQUE DU SIGNAL I.R.

Le signal délivré par les détecteurs, lié à l'émission infrarouge du jet chaud, est une fonction de la concentration et de la température.

Des mesures en laboratoire, actuellement en cours, ont pour but de préciser la loi de variation de ce signal en fonction de ces grandeurs. Néanmoins, à partir de la corrélation infrarouge-son

différentes informations sont déduites et permettent de donner une interprétation physique du signal. Pour cela, des microphones sont placés dans le champ proche, le long d'une ligne parallèle à l'axe du jet et à une distance suffisamment petite pour que chaque microphone rende compte essentiellement du rayonnement acoustique d'une seule tranche du jet.

5.1 - L'analyse spectrale du signal microphonique montre que le maximum du spectre décroît de façon monotone lorsque l'on s'éloigne du plan de sortie tuyère.

5.2 - L'analyse spectrale du signal infrarouge présente le même caractère, avec une pente différente.

5.3 - Des densités spectrales croisées on déduit la contribution du volume source observée par l'infrarouge au rayonnement sonore en fréquence et en directivité. Un exemple typique est présenté :

- lors de mesures effectuées dans un jet libre supersonique issu d'une tuyère à corps central muni d'un silencieux à structure mécanique, la corrélation infrarouge-infrarouge (fig. 15) montre la présence d'une émission spectrale particulière aux alentours de 13 KHz dans un volume limité axialement sur une distance de 140 mm environ (le diamètre de la tuyère étant de 90 mm environ).

Des corrélations infrarouge-microphones placés dans le champ proche (à une distance radiale de 400 mm) on a pu déduire qu'à cette émission spectrale particulière correspond une émission sonore située dans la même bande de fréquence avec un rayonnement maximum à 90° environ.

Ces observations, ayant été effectuées dans l'installation de l'ONERA où des mesures acoustiques dans le champ lointain sont non significatives, ont été confirmées par des mesures acoustiques dans la chambre sourde du CEP$_r$ - GAILLAY à une distance radiale de 6 m (mesures acoustiques dans le champ lointain).

Sur la figure 16 on a porté l'analyse spectrale par tiers d'octave du signal microphonique prélevé dans le champ lointain pour différentes positions angulaires θ (angle formé par l'axe du jet et la direction d'observation).

On remarque que cette émission est effectivement maximum pour $\theta \simeq 90°$. Ainsi on a pu prévoir les conséquences acoustiques de l'existence d'une configuration turbulente située dans un volume bien défini du jet libre. L'analyse de tels résultats par bande de fréquence est actuellement en cours [28] .

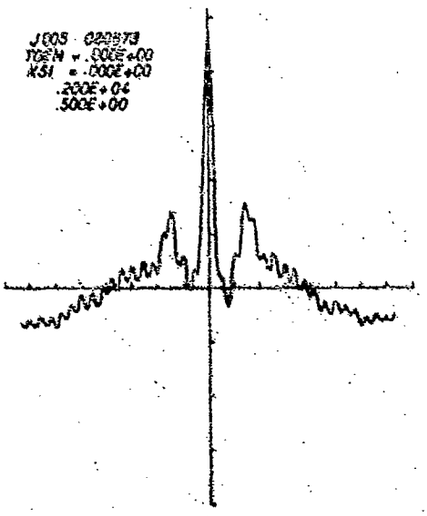

Fig. 15 - Coefficient de corrélation IR-IR.

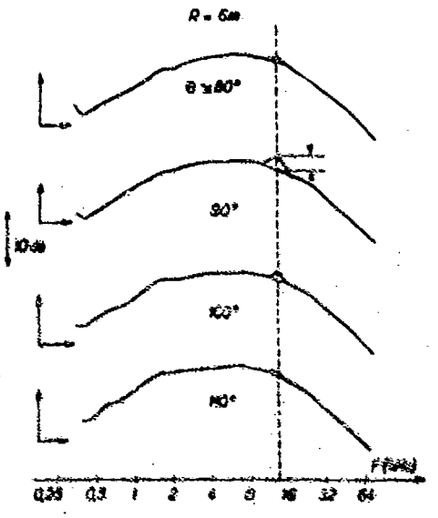

Fig. 16 - Spectre (1/3 d'octave) en fonction de θ.

REFERENCES :

[1] TAILLET J., Description et mise en oeuvre d'une méthode de caractérisation des sources de bruit dans les jets. 8ème Congrès ICAS, Amsterdam, 1972, ICAS paper n° 72-35. L'Astr. et l'Astron. (1973-2). Traduction NASA TT-F 14.851 (1973).

[2] RICHTER G., Etude des sources de bruit de jets chauds; en cours de publication dans la revue ENTROPIE.

[3] LIGHTHILL M.J., Sound Generated Aerodynamically. The Bakerian Lecture, 1961. Proc. Roy. Soc., A, 267, 147 (1962).

[4] KIBNER H.S., The Generation of Sound by Turbulent Jets. In "Advances in Applied Mechanics", vol. 8, (1964), Acad. Press Inc., New-York.

[5] FFOWCS-WILLIAMS J.E., The Noise from Turbulent Convected at High Speed. Phil. Trans. Roy. Soc. Lond., A, 255, 469 (1963).

[6] KOBRYNSKI M., Méthode générale de calcul du champ sonore produit par les jets d'avions à réaction. Note Technique ONERA n° 187 (1971).

[7] POTTER R.C. et JONES J.H., An Experiment to Locate the Acoustic Source in High Speed Jet Exhaust Stream. 74th Meeting of the Acous. Soc. of America, Miami Beach, Florida, Nov. 1967.

[8] MAESTRELLO L., Radiation from and Panel Response to a Supersonic Turbulent Boundary Layer. Boeing Report D1-82-0719, Sept. 1968.

[9] DAVIES P.O.A.L., FISHER M.J. et BARRATT M.J., The Characteristics of the Turbulence in the Mixing Region of a Round Jet. J. Fluid Mech., 15, 337 (1963).

[10] CHU W.T., Turbulence Measurements Relevant to Jet Noise. UTIAS report n° 119, University of Toronto (1966).

[11] SIDDON T.E. et RACKL R., Cross Correlation Analysis of Flow Noise with Fluid Dilatation as Source Fluctuation. Acoust. Soc. America, Fall. Meeting, 82nd Denver, Colo., Oct. 19-22, 1971, paper tt. 12, 18 p.

[12] DAVIES M.R., Quantitative Schlieren Measurements in a Supersonic Turbulent Jet. J. Fluid Mech., 51, 435 (1972).

[13] FISHER M.J. et HARPER-BOURNE M., communication privée.

[14] WILSON L.N., KRAUSE F.R. et KADMAS K.A., Optical Measurements of Sound Source Intensities in Jets. Basic Aerodynamic Noise Research - NASA SP-207, 147 (1969).

[15] FISHER M.J. et KRAUSE F.R., The Crossed Beam Correlation Technique. J. Fluid Mech., 28, 705 (1967).

[16] DRAPER J.S., Infrared Radiometry of Turbulent Flows. AIAA J., 4, 1597 (1966).

[17] SCHETTER K.A., Optical and Acoustical Measurements on Exhaust Plumes. EUROMECH 10, Liblice/Prague (1968).

[18] DYER I., Distribution of Sound Sources in a Jet Stream. J. Acoust. Soc. America, 31, 7 (1959).

[19] LEE M.K., Correlation of Noise and Flow of a Jet. UTIAS report n° 168, University of Toronto (1971).

[20] ROCH R.D., DUPONCHEL J.P., COCCHIO B.J. & REYCE W.D., Etude de l'influence de la masse volumique d'un jet sur son émission acoustique. 1er Symp. Inter. sur les Progrès des Mésures d'Aviation, Marseille, juin 1972.

[21] PAO-TSE CHU et LESLIE KOVASZNAY S.G., Non-linear Interaction in a Viscous Heat Conducting Compressible Gas. J. Fluid Mech. 3, part 5 (1958).

[22] The Lockheed-Georgia Company. The Generation and Radiation of Supersonic Jet Noise. Tech. report AFAPL-TR-72-53, July 1972.

[23] de MICHEVAL J.F., PERULLI M. et CAUFFET C., Computation of the Sound Field of a Jet from Characteristic Turbulence Parameters Measured by Crossed-Beam Techniques. Opto-Electronics, 5 (1973).

[24] CAUFFET C. et CRAMOT L., Radiomètres pour sondage infrarouge des jets libres. Nouvelle Revue d'Optique Appliquée, 3, n° 5, p. 267 (1972).

[25] de MICHEVAL J.F. et PERULLI M., Mesure de la fonction de corrélation caractérisant la turbulence d'un jet chaud libre. C.R. Ac. Sc. Paris, 275 A, (1972), pp 1952-55.

[26] de MICHEVAL J.F., PERULLI M., RICHTER G. et SCHMIDT C., Résultats préliminaires de l'étude de l'émission infrarouge d'un jet chaud. La Recherche Aérospatiale n° 1972-4, pp 37-45.

[27] FISHER M.J. et DAVIES P.O.A.L., Correlation measurements in a Non-frozen Pattern of Turbulence. J. Fluid Mech. 18, (1964), p. 97.

[28] de MICHEVAL J.F., Thèse Université de Paris, à paraître.

DISCUSSION

Dr Dinkelacker: I would like to ask the authors whether they can explain the fact (comp. Figure 9) that the measured convection velocities, V_c, for small distances x from the nozzle are considerably smaller than the corresponding jet velocity, V_j. Is it possible that the correlated parts of the infra red signals in these cases are not generated on the jet axis but by large structures in the turbulent mixing region?

NOISE SOURCE DIAGNOSTICS USING CAUSALITY CORRELATIONS

by

Thomas E. Siddon
Associate Professor
Department of Mechanical Engineering
The University of British Columbia
Vancouver 8, B.C.
Canada

SUMMARY

Due to the complex "mix" of noise mechanisms for current quieter generations of aircraft, it has become more difficult to detect the small changes in overall decibel level which may result from localized design modifications. An increasingly popular diagnostic technique establishes "causative" relationships between individual noise source phenomena and the overall (composite) sound radiation. The method uses real-time cross-correlations between the far field sound pressure and fluctuating physical parameters occurring in, on, and around the noise generating machine. The technique is based on established aeroacoustic theory and has been shown to yield information on acoustic source distributions, their local spectra, and scales of coherence. The present paper reviews the basic causality formalisms and illustrates their use by reference to a number of proven experimental applications. It is shown that by judicious choice of control surfaces the methods can be adapted in unique ways to the elucidation of a number of unresolved noise generation and suppression phenomena. Examples pertaining to jets, suppressor nozzles, rotating fan blades, and flow interaction with leading and trailing edges are included.

PRÉCIS

Le problème d'évaluation de l'effet de modifications géométriques d'éléments d'avions modernes "silencieux" sur le niveau du bruit est d'une complexité considérable. Ceci relève du fait que le changement de la pression sonique résultante soit parfois très faible à cause de l'existence d'un grand nombre des sources discrètes d'émission. Une technique bien utile dans l'analyse de phénomènes de ce genre est celle des relations de causalité entre de sources de bruit et la radiation totale du son dans une direction donée. La corelation de la pression sonore mésurée bien à l'aval de l'appareil avec les variables fluctuantes aux sources près des propulseurs rend possible le calcul de la localization des sources et leurs charactéristiques spectrales, de cohérence, etc. Dans l'article présenté ici on passe en revue la théorie de causalité en ce qui concerne la génération du bruit, suivi d'illustrations prises a'applications practiques au laboratoire. Aussi fait-on démonstration de l'utilité d'un choix approprié de surfaces de contrôle pour l'étude de phénomènes de production et d'élimination de bruit. Les exemples pris de la pratique comportent des jets de vitesse élevée du gas, des embouts supprimateurs, des roues de ventilateurs et les arrêts d'entrée et de sortie de profils aerodynamiques.

1. INTRODUCTION

In the quest for solutions to the aircraft noise problem and, in particular, for a fundamental understanding of noise generation and suppression mechanisms, it will be necessary to resort to a variety of state of the art diagnostic techniques and special probing devices[1]. Traditionally our experimental progress has been based on rather tedious parametric methods involving measurements of overall sound level or local (fluctuating) properties of the source flow. Due to the increasingly complex "mix" of noise mechanisms for current "quieter" propulsion systems it becomes difficult to detect the small changes in overall dB level which may result from localised parametric modifications.

An approach of increasing popularity exploits the "causality" technique of cross-correlation. The quantitative implications of this method were first described by the present author[2,3,4], starting with established aeroacoustic theory. Real time cross-correlations are computed between far field radiated sound and the various source fluctuation variables occurring in, on, and around the noise generating machine. The method has the powerful advantage of being able to discriminate between legitimate source phenomena (those which make a net contribution to the acoustic field) and those intense, sometimes coalescent source fluctuations which make no contribution to the radiation. The correlation functions yield detailed information on acoustic source distributions, their local spectra, and coherence scales, for a wide variety of configurations.[2,3]

The objective of the present paper is to review the basic causality formalisms and to illustrate their use by reference to a number of proven experimental applications. It will subsequently be shown that by judicious choice of control surfaces the methods can be adapted in unique ways to the diagnosis of a number of unresolved noise generation and suppression phenomena. Examples pertaining to jets, suppressor nozzles, fan blades and other sources of surface interaction noise are included.

2. REVIEW OF UNDERLYING THEORY

The basic origins of noise generation in fluid flows can be ascribed to velocity or pressure fluctuations in the source region, either in the volume of "sensible turbulent motion" or at boundary surfaces. The classical Lighthill/Curle solution of the wave equation gives[1]:

$$p(\underline{x}, t) = \int_S \frac{\left[\frac{\partial}{\partial t}\rho u_n\right]}{4\pi r}\, dS(\underline{y}) - \frac{\partial}{\partial x_i}\int_S \frac{[P_i + \rho u_i u_n]}{4\pi r}\, dS(\underline{y}) + \frac{\partial^2}{\partial x_i \partial x_j}\int_V \frac{[T_{ij}]}{4\pi r} \times dV(\underline{y}) \qquad (1)$$

where

$$P_i \equiv -l_j(p\delta_{ij} - \tau_{ij})$$

$$T_{ij} \equiv \rho u_i u_j + (p - c^2\rho')\,\delta_{ij} - \tau_{ij}$$

$[\ ]$ denotes evaluation at retarded time

Thus the radiation from a low speed turbulent flow can be approximated by either of the following equivalent forms*;

$$p(\underline{x}, t) \approx \frac{1}{4\pi x c^2}\int_V \left[\frac{\partial^2(\rho u_y^2)}{\partial t^2}\right]_{t-\frac{r}{c}} dV(\underline{y}) \qquad (2)$$

$$p(\underline{x}, t) \approx \frac{-1}{4\pi x c^2}\int_V \left[\frac{\partial^2 p^{(o)}}{\partial t^2}\right]_{t-\frac{r}{c}} dV(\underline{y}) \qquad (3)$$

Curle introduced the effect of surface/flow interactions by including the surface integral terms in equation (1); such surfaces can be real or may be hypothetical control surfaces selected so as to exclude an uninteresting or excessively complicated region from the field. Whether rigid, or flexible, the radiation from these surfaces will be accounted for by an approximation consistent with (2) and (3):

$$p(\underline{x}, t) \approx \frac{1}{4\pi x c}\int_S \left[\frac{\partial}{\partial t}\left(\rho u_n c + p_s \cos\theta\right)\right]_{t-\frac{r}{c}} dS(\underline{y}) \qquad (4)$$

In equations (2)-(4) the field point at $\underline{x}$ is taken to be far removed from the source region. Turbulent velocity fluctuations u_i and surface normal velocity u_n are assumed small with respect to the ambient speed of sound c. The quasi-incompressible pressure $p^{(o)}$ approaches the total pressure fluctuation in the source volume. Surface stress fluctuation τ is small with respect to surface pressure p_s. The angle θ describes the direction of the field point at $\underline{x}$ with respect to the local surface normal at the source point $\underline{y}$. r is the distance between $\underline{x}$ and $\underline{y}$. (For high speed flows more complicated solutions are needed, to account for the presence of thermal and shear stress fluctuations, together with convective and refractive effects. The existence of such solutions, and their potential importance, are the subject of much current debate).

2.1 Classical approach to source localisation

To date researchers have not been very successful in obtaining detailed information about the spatial distribution and character of elementary sources in noise-generating flows. Traditional attempts have been based on squared and time averaged versions of equations (2) to (4) which yield the radiated acoustic intensity in terms of complex two-point correlations of source fluctuation variables. For example from (2):

$$\frac{\overline{dp^2}}{dV} = \frac{1}{16\pi^2 x^2 c^4}\int_{V'}\left[\frac{\partial^2}{\partial\tau^2}\ \overline{\rho u_x^2 \rho u_x'^2}(\tau, \xi)\right] d^3\xi \qquad (5)$$

ξ is an arbitrary vector separation between two points of detection of the source term ρu_x^2. One of the most successful examples of such an experiment is that of Chu[12] in which the full three dimensional structure of turbulence near a point in a jet exhaust was used to predict the acoustic source radiation from that point. However to duplicate such an experiment for many source points would be formidable because of the enormous number of individual cross-correlation measurements necessary.

2.2 Causality correlation technique

A more direct technique establishes causative relationships between the various source fluctuation parameters and the radiated sound[2,13]. The formalism proceeds as follows. Both sides of the basic radiation equations (1) to (4) are multiplied by sound pressure $p(x,t')$, where $t' = t \pm \tau$, and a time average is taken. Introducing certain properties of stationary random variables, we find the autocorrelation function for volume generated sound from (3) or, equivalently, from (2):

$$\overline{pp'}(\tau) = \frac{-1}{4\pi x c^2}\int_V \left[\frac{\partial^2}{\partial\tau^2}\overline{p^{(o)}p(\tau')}\right]_{\tau + \frac{r}{c}} dV \qquad (6)$$

* The "dilatation" form (3) is usually credited to the combined efforts of Hawkins and Ford, Garcos, and Ribner[14]. Ribner has argued that, unlike (2), equation (3) implicitly accounts for additional radiation due to the presence of rigid surfaces in the source region.

Similarly, equation (4) yields the autocorrelation function for surface interaction noise:

$$\overline{pp'}(\tau) \approx \frac{-1}{4\pi cx} \int_S \left[\frac{\partial}{\partial \tau} \left(\rho \overline{u_n p c} + \overline{p_s p} \cos\theta \right) \right]_{\tau' = \tau + \frac{r}{c}} dS \qquad (7)$$

The causality correlations on the right hand side are functions of τ'; typical correlation functions are shown inset on Figure 1. Such functions may be computed with one of several signal correlators now available on the market.

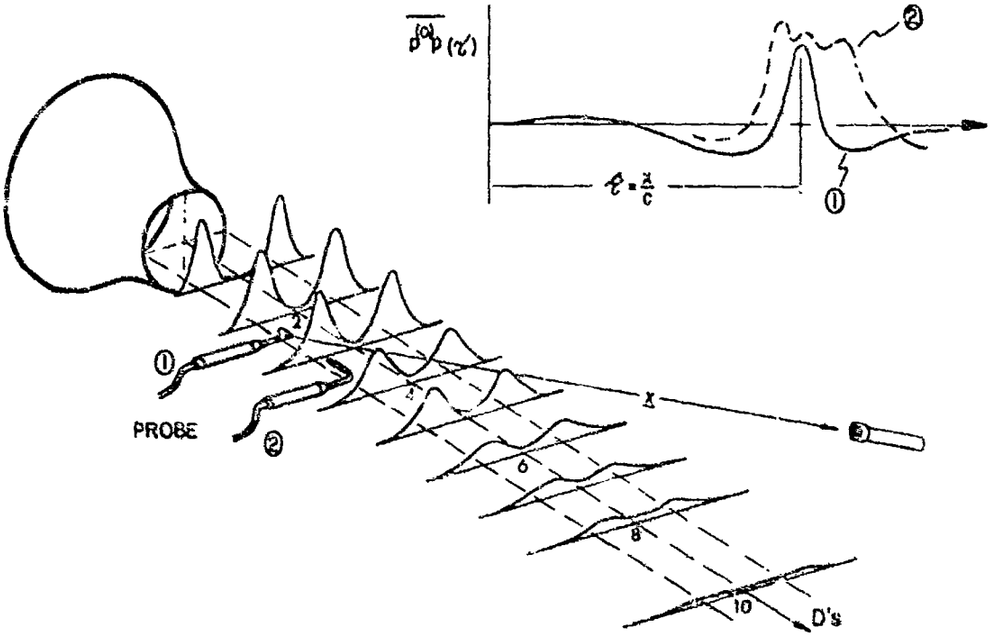

FIGURE 1 NOISE SOURCE DISTRIBUTION IN A ROUND JET BY CAUSALITY CORRELATION. DASHED CURVE SHOWS TYPICAL DIPOLE CONTAMINATION DUE TO SIDE-FORCE FLUCTUATION ON PROBE (2)

The acoustic contributions from each unit of source volume or of surface area are determined explicitly in terms of the causality functions:

$$\frac{d\overline{p^2}}{dV} = \frac{1}{4\pi c^3 x} \left[\frac{\partial^2}{\partial \tau^2} \overline{p^{(2)} p}(\tau') \right]_{\tau' = \frac{r}{c}}$$

$$\frac{d\overline{p^2}}{dV} = \frac{1}{4\pi c^3 x} \left[\frac{\partial^2}{\partial \tau^2} \overline{\rho u_x^2 p}(\tau') \right]_{\tau' = \frac{r}{c}} \qquad \longleftarrow \text{Equivalent forms} \qquad (8)$$

$$\frac{d\overline{p^2}}{dS} = \frac{1}{4\pi cx} \left[\frac{\partial}{\partial \tau} \left(\overline{\rho u_n p c} + \overline{p_s p} \cos\theta \right) \right]_{\tau' = \frac{r}{c}} \qquad (9)$$

Alternative forms of (8) and (9) are possible where the τ - derivatives are replaced by real time derivatives of the source fluctuation quantities. Thus:

$$\frac{\partial}{\partial \tau} \left(\rho \overline{u_n p c} \right) = \rho \overline{u_n \dot{p} c}$$

$$\frac{\partial^2}{\partial \tau^2} \overline{p^{(1)} p}(\tau) = -\overline{\dot{p}^{(1)} p}(\tau) \text{ , etc.} \qquad (10)$$

The two terms on the right hand side of (9) deserve some interpretation. The first describes the radiation per unit area from any pulsating surface which displaces some net volumetric flow into the external medium (monopole contribution). This term is dominant for a small, back-enclosed, omnidirectional loudspeaker. For radiators which are not small compared with a wavelength the Cosθ term in (9) leads to the directional nature of the radiation. Note that some of the directional effect is buried in the correlation function $\overline{p_s p}(\tau)$ as well. This second term will dominate in cases where a stationary or rigidly moving surface experiences momentum fluctuations in response to external flow (dipole contribution). For "non-compact" vibrating surfaces both terms are generally important.

Thus the "surface dipole strength" for a stationary surface or a rigidly rotating fan blade may be deduced by cross-correlating the surface pressure fluctuations p_s with the far field sound. For example the diagnosis of dipole radiation from a flat plate aerofoil of circular planform, with separated flow over one surface, led to a source distribution plot as depicted in Figure 2. (from Ref. 2). Correspondingly, the source strength per unit volume of turbulence can be estimated using either version of (8). A typical result for a low speed turbulent jet, due to Rackl',[11] is depicted in Figure 1.

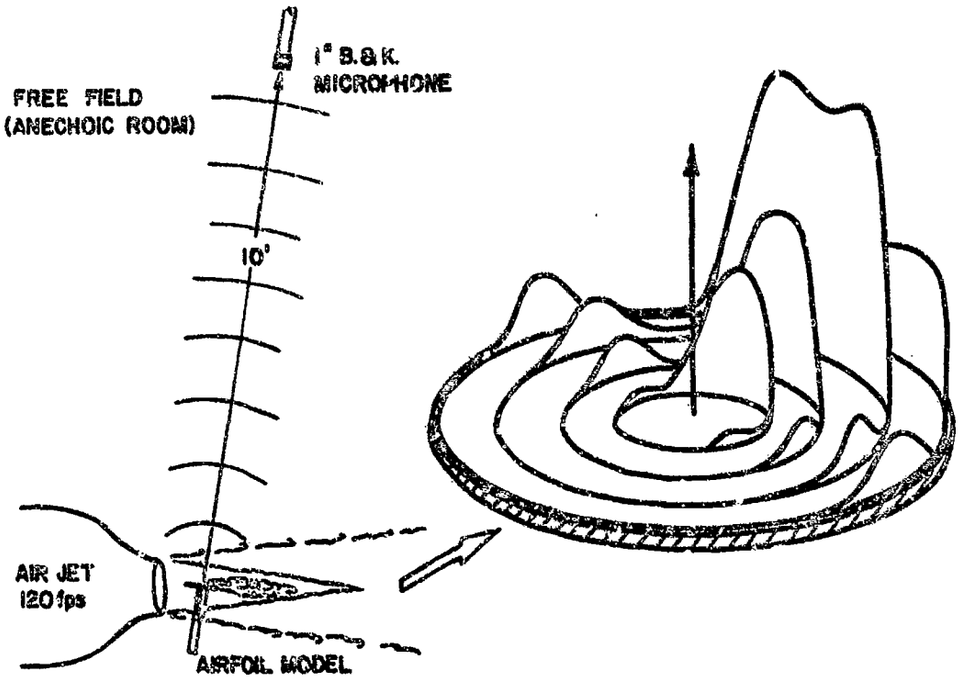

FIGURE 2 SURFACE DIPOLE STRENGTH FOR SEPARATED FLOW OVER DISC SHAPED MODEL (TAKEN FROM REF 2)

2.3 Localised spectra

Fourier transforms of (8) and (9) give the elementary spectra from each unit of surface or volume[2,13]. Thus the contribution to the overall spectral density $\Phi(\omega)$ in a given direction, arising from the dilatation $\rho^{(1)}$ at a point in the flow is:

$$\frac{d\Phi(\omega)}{dV(y)} = \frac{\omega^2}{4\pi c^2 x} \mathcal{F}_c \left[\overline{\rho^{(1)}\rho(\tau)}\right]_{\hat{\tau}} \qquad (11)$$

where $\mathcal{F}_c$ means Fourier cosine transform centered on $\hat{\tau} = r/c$. Such spectra may also be measured directly, by narrow-band filtering the source/field signals before correlation. Hence for a rigid surface (u_n=const) the surface dipole strength of a spectral component would be given by:

$$\left(\frac{d\overline{Q^2}}{dS}\right)_\omega = \frac{\omega}{4\pi c x} \left|\overline{P_s p}\right| \cos\theta \qquad (12)$$

- where $|\overline{P_s p}|$ is the amplitude of the filtered (sinusoidal) correlation function.

2.4 Scales of coherence

The local extent of coherence for the dilatational pressure field is defined by a correlation volume V_c where:

$$\int_{V_\xi} \left[\frac{\partial^2\rho^{(1)}}{\partial t^2}\frac{\partial^2\rho^{(1)'}}{\partial t^2}(\tau,\xi)\right]_{\tau=0} d^3\xi \equiv V_c \cdot \left[\overline{\frac{\partial^2\rho^{(1)}}{\partial t^2}}^2\right] \qquad (13)$$

Here the integrand on the left hand side represents a two-point correlation function for probe separations ξ within the source region. By analogy with equation (6) it follows that the source strength per unit volume for a source point y will be:

$$\frac{d\overline{Q^2}}{dV} = \frac{V_c(y)}{16\pi^2 x^2 c^4}\left[\overline{\frac{\partial^2 p^{(1)}}{\partial t^2}}^2\right] \qquad (14)$$

Equating (14) with (8), and using (10), we get for the correlation volume:

$$V_c(y) = +4\pi x c^2 \frac{\left[\overline{\dot{p}^{(1)}p}\right]_{\hat{\tau}}}{\left[\overline{\dot{p}^{(1)}}^2\right]} \qquad (15)$$

We notice that V_c is directly proportional to the magnitude of the causality correlation $\overline{\dot{p}^{(1)}p}$, evaluated at the appropriate retarded value of $\hat{\tau} = r/c$.

In a similar manner the correlation area for surface monopole strength can be deduced from the first term on the right hand side of (9):

$$S_c(y) = +4\pi x \frac{\left[\overline{\dot{u}_n p}\right]_{\hat{\tau}}}{\left[\overline{\dot{u}_n}^2\right]} \qquad (16)$$

A parallel definition of correlation area for surface dipole distributions is given in Ref. 2.

Thus the causality functions carry information about the local source strength, spectrum, and extent of coherence. The method is not, however, able to resolve the "shape" of coherent regions.

2.5 Arrays of discrete sources

As applied to arrays of discrete, well separated, and uncorrelated sources, the causality approach is not new. For instance, several years ago Goff described a series of source localization experiments wherein each source was characterized by a single near-field reference fluctuation.[16] For such an array our integral distribution expressions (6) and (7) may be reduced to a simple approximate summation, giving the net far field radiation as:

$$\overline{p^2_{net}} = \sum_{m=1}^{M} \left(\frac{d\overline{p^2}}{dS} \cdot S_c \right)_m + \sum_{n=1}^{N} \left(\frac{d\overline{p^2}}{dV} \cdot V_c \right)_n \qquad (17)$$

Here M and N denote the total number of discrete surface-distributed and volume-distributed sources, respectively. The values of $d\overline{p^2}/dS$ and $d\overline{p^2}/dV$ are unique for each of the m^{th} and n^{th} sources.

The contribution to $\overline{p^2}_{net}$ from a single coherent volume source is given by the n^{th} term. Thus:

$$\frac{\left(\frac{d\overline{p^2}}{dV} \cdot V_c \right)_n}{\overline{p^2}_{net}} = \frac{\overline{[\tilde{p}^{(0)}p]^2}_\tau}{\overline{p^2}_{net}\overline{p^{(0)2}}} \equiv C^2_{Max}(\tau) \qquad (18)$$

Here $d\overline{p^2}/dV$ and V_c have been eliminated by substitution of equations (8) and (15). Hence in the special case of discretely separated sources the maximum value of the causality correlation coefficient, squared, yields the fractional contribution to $\overline{p^2}_{net}$ from the source point of $p^{(0)}$ detection. It is not uncommon to further assume all N sources to be of equal strength. Then in the absense of surface radiation the number of sources is estimated from:

$$\boxed{C^2_{Max} \cong \frac{V_c}{V} \approx \frac{1}{N}} \qquad (19)$$

A parallel analysis can be developed for the surface distributed sources.

In conclusion it should be pointed out that a large value of normalised correlation C_{Max} is necessary, but not sufficient, to identify a dominant noise source. One must first of all know that he is indeed measuring a source fluctuation, not merely a near-by acoustic signal. The extent and coherence of continuously distributed source phenomena must be assessed from spatial surveys of the appropriate "causal" relations.

2.6 Illustrative example

It has occasionally been suggested that the causality method is only valid for the case of many spatially uncorrelated sources. There is not such restriction in the analysis of Sections 2.2 - 2.4. In fact where sources posess any degree of counter-coherence (anti-phase components), the causality correlations favor only those residual source phenomena which make a constructive contribution to the radiation in a specific direction. This property may be illustrated with reference to a very simple example.

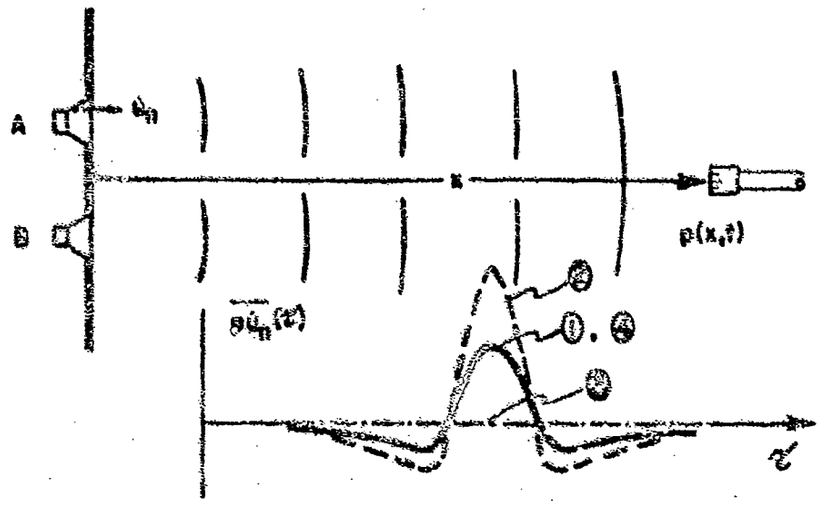

FIGURE 3 SIMPLE ILLUSTRATION OF CAUSALITY FEATURES

We consider two small loudspeakers, each of area S_c, mounted in an infinite baffle. A far field microphone is positioned normal to the baffle and equidistant from the two speakers, as illustrated in Figure 3. On speaker A is fixed a tiny accelerometer, capable of measuring the surface acceleration $\dot{u}_n$. The speakers are driven by low frequency random noise such that the typical wavelengths are large

compared with speaker dimensions. Each speaker cone is assumed to move as a coherent unit. We consider four cases of excitation; the results are summarized in TABLE I, below:

	dp^2/dS	S_c	$\overline{p^2}_{net}$	C_{max}
(1) speaker A only	1	1	1	1
(2) A & B in phase	2	2	4	1
(3) A & B counter phase	0	0	0	0
(4) A & B incoherent	1	1	2	.707

1. First only speaker A is driven. The causality function $\overline{\dot{u}_n p}$ will appear as shown in Figure 1. For this reference situation the quantities dp^2/dS, $\overline{p^2}_{net}$ and C_{max} are arbitrarily given a value = 1. Also the piston area S_p = 1 unit.
2. Now the second speaker is switched on, driven in phase with the first and generating the same surface acceleration $\dot{u}_n$. In this case the far field pressure p is doubled; hence dp^2/dS and S_c are doubled, following equations (9) and (16). It follows that $\overline{p^2}_{net}$ = 4 according to both equation (17) and our common sense. C_{max} remains equal to unity however, since there is only one coherent source, although now twice as large.
3. In this case the second speaker is driven counterphase with the first. Thus, although the source fluctuation level remains unchanged, the far field pressure will be zero due to cancellation. Hence dp^2/dS, S_c and C_{max} are also equal to zero.
4. Now the two speakers are driven with equal rms acceleration $\dot{u}_n$ but from two uncorrelated signal generators. Thus dp^2/dS is unity, as in case 1, because the causality function $\overline{\dot{u}_n p}$ is unaffected by the radiation from B_1. S_c equals the area of a single speaker but since there are now two uncorrelated sources, $\overline{p^2}_{net}$ = 2. The correlation coefficient C_{max} = .707.

3. DETECTION OF SOURCE FLUCTUATIONS

Hot wire and hot film techniques for detecting velocity fluctuations (in the presense of a mean flow) are well established; however difficulties arise when components at arbitrary angles (e.g., u_x) must be measured due to the presense of a steady cooling flow along the hot cylindrical element. A measurement of the pressure $p^{(0)}$ or p_s is conceptually more attractive, in view of the scalar nature of the variable. The difficulties inherent in the accurate measurement of "static" pressure fluctuations in turbulent flow are, on the other hand, well recognized. Earlier work by the present author led to the development of a special error-compensating probe which effected a reduction of turbulence interaction errors to a limited degree, but was rather complicated[17].

3.1 Probe contamination

Recent studies have revealed a more serious difficulty which arises when undertaking causality experiments with a pressure probe of conventional cylindrical geometry (such as probe (2) in Fig. 1)[7,18]. Extraneous radiation due to probe/flow interaction leads to a contamination of the correlation function as shown in Figure 1. To understand, imagine a patch of turbulence convecting past the probe. On interacting with the nose of the probe a localised fluctuating side force is induced, sending a dipole pulse to the field microphone. A short time later the same patch of turbulence interacts with the stem of the probe, sending off another dipole pulse. These dipole pulses are coherent with the basic $p^{(0)}$ fluctuation and therefore make an extraneous contribution to the correlation. Because the contaminants leave the probe earlier and later than the true signal, the result is a tendency for the correlation to be broadened in a peculiar way near the correct value of acoustic travel time, as in Figure 1. Using a shorter nose cone (reducing the distance between nose and pressure port), makes the three contributing effects less distinguishable, so that one is not sure how much dipole contamination is present in the signature.

Thus, causality correlations involving free stream turbulence fluctuations (velocity or pressure) appear to be highly sensitive to the degree of spurious probe interference noise. The situation seems to demand that the probe generated radiation be much weaker than the inherent self-radiation from the adjacent correlation volume V_c. To put the probe contamination effect on a quantitative basis, a parameter called "probe contamination ratio" has been established.[18] PCR is defined as the ratio between the mean-squared acoustic pressure due to dipole-type radiation from the probe surface and the mean-squared acoustic pressure due to genuine quadrupole-type radiation from the adjacent correlation volume of fluid:

$$PCR \equiv \frac{\overline{p^2}_{S_D}}{\overline{p^2}_{V_c}} \tag{20}$$

Subscript S_D denotes an effective dipole radiating area for the probe. Assuming the probe to be small with respect to the correlation volume V_c, and using quasi-steady theory to relate probe force fluctuations to the turbulence induced velocity fluctuations, the PCR is derived in reference 18 for both side force and shear stress fluctuations on a typical probe. For a cylindrical probe aligned with the mean flow, the PCR can be estimated from the relation:

$$PCR \approx \frac{1.4}{(\text{Mach No.})^2} \left(\frac{S_D}{L_c^2}\right)^2 \tag{21}$$

L_c^2 is an equivalent correlation area for the turbulence structure, given nominally by $(U_c)^{4/3}$. The Mach No. parameter shows that for a given ratio S_D/L_c^2, the contamination becomes less severe with increasing mean flow speed. This is because of the U^8 dependency of the dipole contamination compared with the U^6 increase

of the inherent self-radiation. Assuming that a value PCR < 0.1 is desirable in order to avoid overestimation of the correlation functions, it may be shown that when used in a turbulent jet of diameter D, a cylindrical probe of diameter d should meet the following criterion:

$$d < \frac{D}{10}\sqrt{M} \qquad (22)$$

This relation accounts for nose-generated side-force radiation only.[18]

3.2 Foil-type pressure probe

In view of the above finding it became clear that the best possibility for suppressing the extraneous radiation rested in minimizing the surface area of the pressure probe in the direction of the field microphone.[13,18] This consideration led to experiments with a number of foil-shaped or knife-like probes which are designed to be inserted into the source flow such that the plane of the foil is coincident with both the direction of mean flow and the direction of acoustic detection. One such probe, developed by Rackl[18] is labeled (1) in Figure 1. For subsonic use, this probe is made insensitive to velocity fluctuations both normal to, and in the plane of the wedge-shaped foil by locating the pressure sensing ports very near to the trailing edge (two ports register the average of upper and lower surface pressure). Thus this type of probe is capable of giving an almost error-free measurement of $p^{(0)}$ while at the same time minimizing the spurious dipole radiation in the direction of detection.

Current findings suggest however that even a foil-type probe of the configuration shown here does not adequately suppress the contamination due to self generated noise, when used in a small laboratory jet flow (M_a = 0.3, D = 1½ inches). The problem is thought to arise from a drag dipole associated with streamwise force fluctuations on the cylindrical probe stem. Such a contamination source can be significant, except for radiation directions coincident with the axis of the stem. This possibility is being investigated further. In the long run, optical probing devices such as the laser doppler velocimeter may afford the best means of detecting source fluctuations within the volume of the turbulence.

4. APPLICATION TO SUBSONIC JET NOISE

Paradoxically although we claim to know much about the mechanisms of jet mixing noise we are not, to this day, absolutely certain about the basic distribution and spectral character of the elementary sources in subsonic jets. The classical picture, widely accepted and supported by a substantial body of experimental and theoretical evidence, is shown by the left-most sketch in Figure 4.

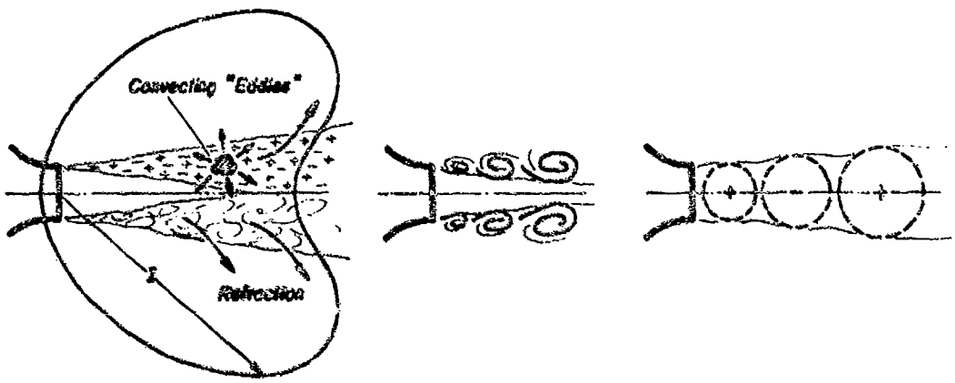

Many Incoherent Sources (Classical) — *Orderly Ring Vortices (Crow & Champagne, Fuchs et al.)* — *Large Cellular Pressure Structure (Mean Sonic – Schlieren & Wake)*

FIGURE 4 POSTULATED MECHANISMS OF JET NOISE

In recent years there have been suggestions that a more coherent flow structure may be responsible for the generation of the noise [19-22]. Two hypothesized mechanisms are shown to the right of the figure. The so-called orderly vortex structure in the center sketch does indeed exist in low Reynolds no. jets, as may be seen by smoke visualization (or Schlieren photography at high Mach no.). At higher Reynolds nos. such a structure probably persists, but gets buried in a broad-band turbulence of much finer scale, just as is the case for a Karman vortex street in a turbulent wake.

4.1 Discussion of causality results

The important question in this author's mind is not whether such a structure develops, but indeed does the structure serve as a significant contributor to the broad band radiated noise? Experiments to be discussed here, based on the causality approach, do not support such a hypothesis, at least for low speed (subsonic) turbulent jets. For example equation (19) suggests that the number of separately coherent (uncorrelated) elemental source volumes in a turbulent flow should be given roughly from a typical value of the normalized causality correlation C_{max}:

$$N = \frac{V}{V_c} = \left(\frac{\overline{p^{(0)2}}}{\overline{p'^{(0)2}}}\right)^{n^2} = \left(\frac{\overline{q^2}^2}{\overline{q^2}_x^2}\right)^{-n} \qquad (23)$$

(Primes denote rms value) Here all fluctuating quantities must be measured in broad band, if at all possible

sources in the jet are to be accounted for in N. Using the above technique with measurements of $\overline{u^2}_x p$, Lee and Ribner[8] obtained estimates suggesting an N of order 2500 for a laboratory jet operating at Mach no.=0.3.

Our independent experiments, utilizing $p'^{(0)}$ as the source fluctuation variable yield an N more than an order of magnitude smaller (about 100 to 150), for a jet of the same Mach No.[9,13] The experimental set-up was illustrated in Figure 1 which also gives the measured source strength distribution, for radiation at 45 degrees to the jet axis. The strongest sources appear to be concentrated in the regions of most energetic turbulence, as the classical models have always predicted. There is no apparent radiation from the core of the jet. Unhappily however, on integrating our distribution of dp^2/dV over the entire jet, following equation 5, the resulting value of p^2_{mat} was found to be almost ten times larger than that obtained from the direct measured sound level at 45 degrees. This leads to the conclusion that the correlations $p'^{(0)}p$, as determined with the foil-type probe are still too large, probably due to radiation resulting from an acoustic drag-dipole acting on the stem of the probe.

On the assumption that the drag force fluctuation can be approximated by the quasi-steady relationship $D(t) = \rho u C_D d_{stem} l_{eff}$, and assuming l_{eff} equals the correlation length L_c for the turbulence, it is possible to estimate a contamination ratio (PCR) equal to about 8, for the drag dipole. This explains the non-closure of our integral check (discussed above), and suggests values of C_{max} more like one eighth of the value 0.08 reported by Rackl in references 9 and 13. Thus the Lee-Ribner estimate of N ~ 2500 is probably close to the truth, for a low speed jet, in view of the much smaller size of the hot wire sensor which was employed by them.

By contrast, in a recent paper by Scharton and White[21] a value N ~ 3 is reported for a near-sonic jet. The corresponding large value of correlation coefficient ($C_{max} = 0.55$) can probably be ascribed to a combination of two factors:

1. The experiment employed a 1/8 inch diameter probe in a 5/8 inch diameter jet. Assuming an effective dipole area $S_p = 2d^2$, equation (21) leads to the prediction that PCR = 7 for the Scharton-White case.
2. The reported value of C_{max} was obtained by octave-band filtering at the jet Strouhal frequency. Thus the estimate of N excludes all possible sources whose characteristic frequencies lie outside the band.

It is apparent that the probe radiation must be weaker than the inherent self-radiation from an adjacent correlation volume V_c. Since the evidence seems to suggest a highly uncorrelated structure for the basic noise generators in subsonic jets, it is insufficient to disregard probe interference noise merely on the basis of little observed change in overall far field level, when the probe is inserted. This is contrary to a suggestion made by Scharton and White[21].

4.2 Comments on coherent structure controversy

In a recent paper concerning "The Wave Mechanics of Boundary-Layer Turbulence and Noise", M.T. Landahl describes the coupling between an "active" mode of small scale motion and a large scale "passive" mode of instability:[25] "The small scale motion originates during the intermittent "bursting" in the wall layer leading to the excitation of large-scale, lightly damped travelling shear waves. It is argued that the passive wave-like mode gives the major contribution to pseudosound, whereas the active bursting mode serves as the predominant source for the radiative noise".

There is an important parallel between Landahl's finding and the current controversy about the role of large scale structure in jet noise. It is well and good to investigate coherent vortex structure from a purely fluid mechanical point of view. However the loudspeaker example of Section 2.6 has shown that certain quasi-periodic phenomena may possess a degree of spatial counter-coherence such that they will be very poor acoustic radiators, even though their inherent pseudo-fluctuation levels are quite large. From the aeroacoustician's point of view the only way of definitively establishing the role of large scale structure is to demonstrate its direct relationship to the far field radiated sound. It is insufficient to draw implications on the basis of normalized cross-correlations between two points in the jet flow, as some have done.

For example, Scharton and White report a high normalized coherence between a point in the potential core of their jet and a second within the shear layer[21]. This does not mean that the source extends into the core of the jet. To the contrary, the much weaker pressure fluctuation levels induced in the irrotational core merely "mimic" the composite pressure field of the adjacent turbulence. Hence they will naturally be well correlated, when normalized by the individual rms values.

Fuchs has reported a similar experiment where two microphones (like A and B in Figure 5) have been displaced progressively around a near-field circumferential path concentric with the jet axis [26]. A large normalized correlation is observed for small angles of circumferential displacement, but C_{max} diminishes rapidly to a value of about 0.1 for 180 degree separation. This observation suggests that of the mean-square near-field pressure energy being detected at either A or B, only about ten percent could be associated with a coherent first-order vortex mode. Even if it were possible for this modest fraction to show up in the far-field sound, it would be of little consequence to the total radiation. Fuchs finds further that the minimum correlation (for 180 degree displacement) can be increased to about 0.4 by narrow-band filtering at a characteristic frequency. However the sound radiation process is not subject to such filtering; it responds to the entire spectral content of $p'^{(0)}$, and depends on its spatial distribution throughout the jet.

Others have argued that if we can somehow destroy the coherent structure, we might simultaneously suppress the small-scale, noise generating turbulence. To the present author this seems like a false optimism. Is it ever possible to mix two fluid streams of substantially different velocity, at high Reynolds number, without generating turbulence?

FIGURE 5 CONFIGURATION FOR TRIPLE CAUSALITY CORRELATION

To help resolve this controversy a new experiment is proposed. As depicted in Figure 5, two probes (hot-wire or pressure) are positioned in the shear layer at r/D = ½ and at symmetrical points with respect to a far field microphone. The following causality correlation is formed:

$$C(\tau) = \frac{\overline{\sqrt{p_A}\sqrt{p_B}\; p}}{\overline{p'_A p'}} \qquad (24)$$

When the tangential separation of A and B is small, C(τ) will attain the same value of C_{max} as if only one source probe were used. The circumferential separation Δθ is then increased symmetrically. If the value of C_{max} remains constant, for Δθ as large as 180 degrees, then we have significant radiation from a first order mode of coherent structure. If C_{max} decreases substantially with Δθ, such a mode is probably insignificant to the radiation. This experiment should be repeated for a wide range of Mach numbers, since it may well occur that circumferential coherent structure becomes increasingly important as transonic conditions are approached.

5. RADIATION FROM RIGID SURFACES

Contrary to the observed non-closure of integration for volume distributed dilatation sources, (occurring for reasons described in the previous section), surface source distributions have been integrated in several circumstances to yield the correct values of p^2_{net}. These experiments utilize correlations between surface pressure p_s and the corresponding sound, in accordance with equations 7 and 9. Closure was reported for various types of flow interaction with a small disc-shaped airfoil inserted into a jet flow[9,13], such as the case depicted in Figure 2. Incident turbulence was found to cause strong leading edge radiation, while in smooth flow at low angle of attack, vortex shedding leads to a source concentration along the trailing edge. Similar experiments by others[16,17] have helped to provide insight into the mechanisms of noise generation at trailing edges and nozzle lips. The emerging picture seems to suggest that alternate vortex shedding, with a fairly narrow band of preferred frequencies, leads to a time-dependent relaxation of the Kutta condition at the trailing edge. The "stagnation streamline" switches cyclically from upper to lower surface inducing a fluctuating dipole concentration near the edge, as depicted in Figure 6:

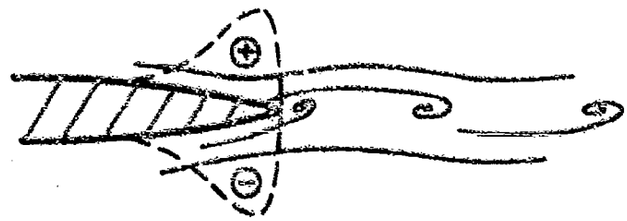

FIGURE 6 MECHANISM OF TRAILING EDGE NOISE

The spectrum of the force fluctuation is broadened by the turbulence in the boundary layers. For frequencies which are sufficiently high the resulting acoustic radiation has a cardiod directivity, with a sharp null in the downstream direction. In the forward direction one partner in the dipole "couple" is shielded from the radiation field; hence an upstream null is not observed. This diffraction phenomenon has been described by Keyden and Chaveau[18]. By replacing the discontinuous impedance afforded by the rigid trailing edge with a short compliant element of more gradually decreasing impedance, the strength of both the force field and of the noise is reduced substantially.

In another experiment we have studied the surface dipole distribution on a large rigid surface placed adjacent to a turbulent jet.[9,13] The reflected sound "imitates" the radiation from an instantaneously identical image jet behind the surface, as depicted in Figure 7. By cross-correlating the surface pressures p_s with the far field sound at various angles, contours of apparent surface source strength are obtained. On integrating these distributions over the surface Koch was able to account for the entire radiation from the image jet, to an acceptable degree of accuracy. These experiments showed the strongest sources to be located between 5 and 6 diameters downstream in a Mach 0.3 jet.

Presently we are extending these techniques to the study of source mechanisms on rotating fan blades[19]. Ultimately our objective is to investigate the broad band sources of blade noise with a view to evaluating the relative roles of turbulent boundary layers, vortex shedding, flow separation, tip interference phenomena and inflow disturbances. The experiments utilize causality correlations between the blade pressure fluctuations at various transducer locations on a low speed, 7 bladed airfoil-type fan, and the overall far-field sound on the axis of rotation. The blade pressure signal is transmitted off the rotating shaft with a miniature telemetry set. Our initial studies have produced highly

periodic correlation functions with dominant spectral content at the blade passage frequency, as depicted on Figure 8. The periodic component was unexpected in view of the theoretical null for rotational noise on the axis of rotation. Examination of the data suggests a harmonic coupling between a one-per-revolution blade pressure periodicity and a seven-time-per revolution discrete tone in the far field sound. The causality technique localises the phenomenon to the outer portion of the rotor disc as illustrated by the span-wise source strength distribution given in Figure 8. Our interpretation of the underlying mechanisms is to be found in Ref. 27.

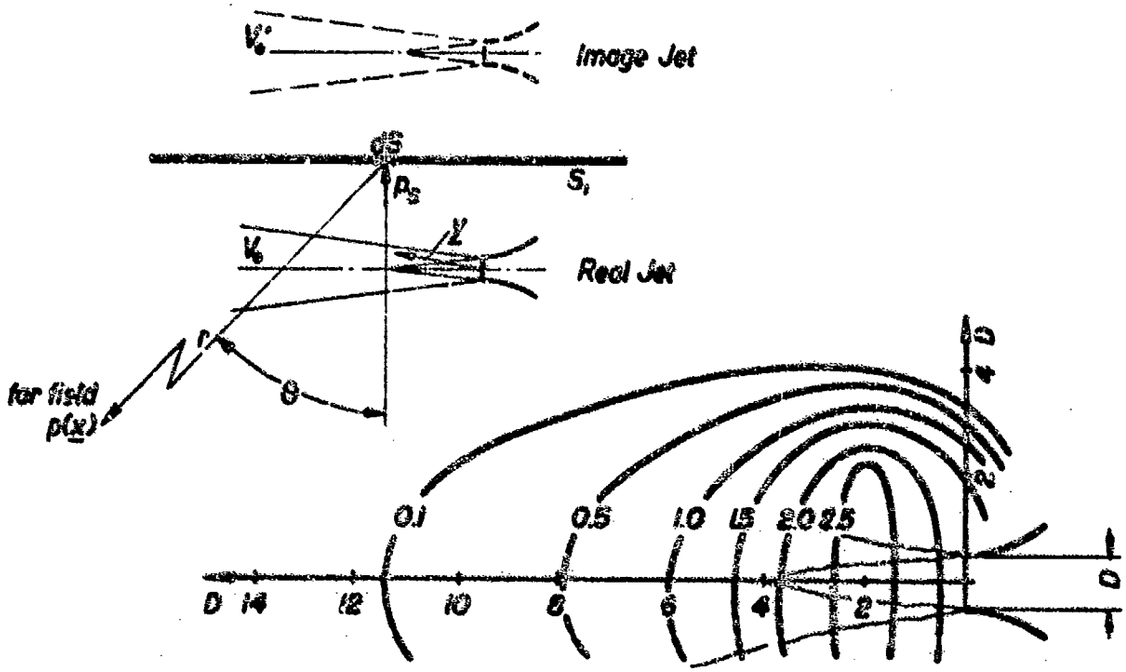

FIGURE 7 SOURCE STRENGTH OF IMAGE JET BY CAUSALITY CORRELATION

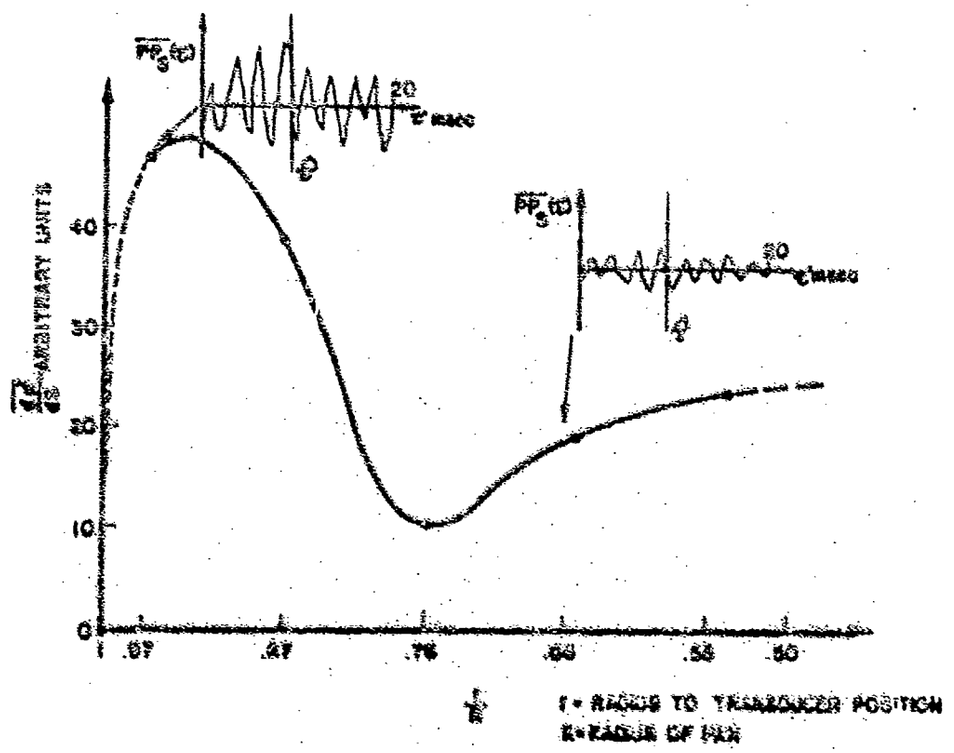

r = RADIUS TO TRANSDUCER POSITION
R = RADIUS OF FAN

FIGURE 8 SPAN WISE DISTRIBUTION OF SOURCE STRENGTH ON ROTATING FAN BLADE

6. APPLICATION TO SUPPRESSOR STUDIES

The causality methods have important advantages in the study of noise reduction features for multi-element suppressor nozzles. For example edge radiation from nozzle lips arises from instabilities in the developing shear layers, in similar manner to the trailing edge mechanism depicted in Figure 6. This edge radiation may contribute to a lower limit on the noise reduction obtainable from given nozzle configurations. In particular, as the basic jet is broken down into smaller and smaller nozzle elements the effective length of trailing edge surfaces increases proportionately; it is conceivable that the edge radiation may rise to the same magnitude as the suppressed jet noise. The acoustic fractions associated with this "lip" noise can be assessed by measuring the appropriate surface dipole distributions, using simple multiple-nozzle rigs as depicted in Figure 9.

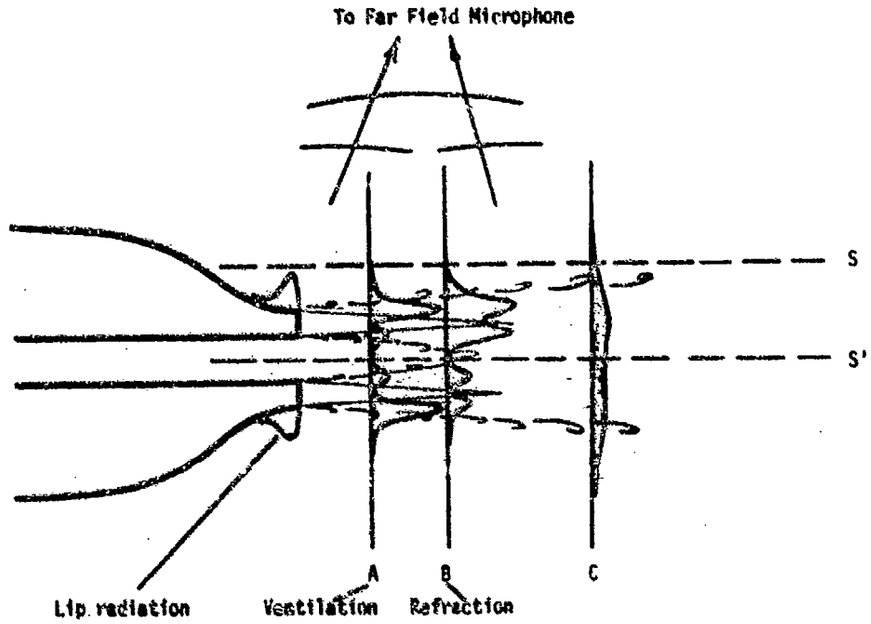

FIGURE 9 BASIC SUPPRESSOR ELEMENT EXPERIMENTS USING PAIRED NOZZLES

If the probe contamination difficulties described in Section 4 can be minimized it will also be possible to investigate the volume-distributed source strength in multi-element nozzles. Thus typical profiles for paired-jet configurations might be measured, as sketched in Figure 9. Curve A depicts a possible result for two closely spaced round nozzles where shear reduction by entrainment plays a dominant role. On the other hand Curve B illustrates a possible outcome for two parallel slot nozzles of high aspect ratio, where shielding by refractive channelling is more significant. By measuring such profiles for several streamwise stations the relative importance of these two contributing effects might be assessed for the entire disturbed flow, including the region of jet interference. Using corresponding profiles for a single isolated jet as base-line, quantitative information on local source suppression will be obtained. As an additional feature, examination of the time domain records will yield information on path length distortions due to refractive effects and may enable the separation of sound which refracts around the near side (shielding) jet from that which transmits directly through.

7. ACOUSTIC FLUX THROUGH NEAR FIELD PLANES

In the formulation of the causality theory, the control surface S may be selected to coincide with solid surfaces bounded within the source region or, by an extension of Huygen's principle, it may be taken as an imaginary surface which completely encloses (or partially cuts through) the source region. In this latter case the surface is to be regarded as an equivalent impervious membrane which vibrates with the same motion as the fluid at corresponding points. Steady (d.c.) flows through the imagined surface are disregarded in this approach. Some typical near field cutting planes are depicted as S and S' in Figure 9.

A survey of accelerations $\ddot{\zeta}_n$ and pressures p_n over the control surface will enable estimates to be made of the acoustic flux per unit area. This is achieved by correlating the appropriate surface variables with an acoustic pressure measured in the far field of the surface, following equation (9). By taking the control surface close to but not cutting into the disturbed flow, information on spatial source distribution will be obtained without actually probing the flow. The jet-image experiment of Section 5 represents one successful application of such a technique (using a rigid surface). The approach is especially attractive for investigations of supersonic jet noise, where in-flow probing becomes a formidable, if not impossible task. In the case of multiple element suppressor nozzles, surfaces such as S and S' in Figure 9 can be selected to yield information on the contours of acoustic flux from both the shielding and shielded jets, with respect to the far field direction.

The footprint of acoustic radiation from a rolling pneumatic tire has similarly been evaluated by defining a plane, imaginary control surface outside of the tire side wall.[3] This experiment clearly localizes the dominant source mechanism to the immediate vicinity of the "contact patch" between tire and road.

8. CONCLUDING COMMENT

Although the diagnostic techniques described herein are far from being perfected, this author believes that the causality method will prove to be of immense value in future studies of noise generation phenomena. The biggest weakness seems to lie in the area of in-flow probing for the source fluctuation quantities. Much current activity centers around the development of non-intrusive (optical) probing devices; while these may ultimately prove to be a more successful substitute, we would be unwise to overlook entirely the possibilities for improvement to our established base of mechanical probing technology.

ACKNOWLEDGEMENT

The author is grateful for the assistance of Dr. R. Rackl and Mr. L.J. Leggat; much of the experimental data is drawn from their graduate research at the University of British Columbia. Thanks are also extended to numerous associates, especially Dr. H.S. Ribner, Dr. N.J. Ganzakein, Mr. C.T. Savell, Dr. W.C. Meecham, Dr. W.T. Chu and Dr. T. Scharton. Each has been a source of inspiration to some aspect of this paper. Financial support has been generously provided by the National Research Council of Canada, under Grant No. A7106 and the Defense Research Board of Canada, under Grant No. 9611-03.

REFERENCES

1. SIDDON, T.E. - Jet Noise Research - Progress and Prognosis (Invited Paper) presented at INTERNOISE 72, Washington D.C., October 4-6, 1972. Published in Conference proceedings, pp. 452-457.
2. SIDDON, T.E. - Surface Dipole Strength by Cross Correlation Method, abstract J. Acoust. Soc. Amer., July 1970, full paper in JASA, Vol. 53, No. 2, pp. 619-633, Feb. 1973.
3. CLARK, P.J.F. and RIBNER, H.S. - Direct Correlation of Fluctuating Lift with Radiated Sound for an Airfoil in Turbulent Flow, J. Acoust. Soc. Amer. 46, pp. 802-805 (1969).
4. RACKL, R. and SIDDON, T.E. - Jet Noise Study Using Image Techniques, Proceedings of 3rd Canadian Congress of Applied Mechanics, Calgary, 1971, pp. 473-474.
5. SIDDON, T.E. - New Correlation Method for Study of Flow Noise, Proceedings of 7th International Congress on Acoustics, Budapest, August 1971, pp. 533-536.
6. LEE, H.K. and RIBNER, H.S. - Direct Correlation of Noise and Flow of a Jet, The Journal of the Acoust. Soc. of America, Vol 52, No. 5 Part 1, November 1972, pp 1280-1290.
7. SIDDON, T.E. and RACKL, R. - Cross Correlation Analysis of Flow Noise with Fluid Dilatations as Source Fluctuation, presented at 82 Meeting of Acoust. Soc. Amer, Denver, Colorado, Oct 1971 Abs. JASA Jan/72.
8. SIDDON, T.E. - Noise Generation Mechanisms for Passenger Car Tires, paper G2-11 presented at 84 meeting of the Acoust. Soc. of Amer., Miami, Florida, November, 1972, abstract in JASA, January 1973.
9. RACKL, R. - Further Studies on Cross-Correlations between Fluid Dilatations and Flow Noise, Paper XX8 presented at 84th Meeting of Acoust. Soc. of Amer., Miami, Florida, November, 1972.
10. HAYDEN, Richard E. - Fundamentals Regarding Reduction of Noise Arising from Jet Interaction with Deployed Lift-Augmenting Flaps, Paper V2 presented at 84 Meeting of Acoust. Soc. Amer, Miami, Nov. 1972.
11. PINKEL, B. and SCHARTON, T.D. - Reduction of Noise Generated by Flow of Fluid over Plate, paper V5 presented at 84th meeting of Acoust. Soc. Amer, Miami, Florida, November, 1972.
12. MEECHAM, W.C., and HOWLE, P.H. - Correlation Investigation of the Noise Generating Region of a Jet Engine by Means of the Simple Source Model, Interagency Symposium on Trans. Noise, Stanford Univ, March 1973.
13. RACKL, R. - Two Causality Correlation Techniques Applied to Jet Noise, Ph.D. Thesis, University of British Columbia, April, 1973.
14. RIBNER, H.S. - Aerodynamic Sound From Fluid Dilatations, Univ. of Toronto, Institute of Aerophysics Rep. No. 86, July 1962. Also AFOSR TN 2436.
15. CHU, W.T. - Turbulence Measurements Relevant to Jet Noise, UTIAS Report 119, 1966.
16. GOFF, K.W. - The Application of Correlation Techniques to Some Acoustic Measurements, The Journal of the Acoust. Soc. of America, Vol. 27, No. 2 March 1955, pp. 236-246.
17. SIDDON, T.E. - Investigation of Pressure Probe Response in Unsteady Flow (Invited Paper), Proc. of NASA Basic Noise Research Conference, Washington, D.C., July 1969, (NASA SP 207).
18. SIDDON, T.E. - Design of Pressure Probes for Hot Supersonic Jets, Bolt, Beranek and Newman, in-house report, July 1971.
19. CROW, S.C. and CHAMPAGNE, F.H. - Orderly Structure in Jet Turbulence, Boeing Sci. Research Labs, Seattle, Wash., DOC D1-82-0591 (1970).
20. FUCHS, H.V. - Space Correlations of the Fluctuating Pressure in Subsonic Turbulent Jets, J. Sound Vib. 23 (1), pp. 77-99, 1972.
21. SCHARTON, T.D. and WHITE, P.H. - Simple Pressure Source Model of Jet Noise, J. Acoust. Soc. Amer. 52 pp. 399-411 (1972).
22. LAUFER, J., KAPLAN, R.E., and CHU, W.T. - Acoustic Modeling of the Jet Noise Abatement Problem, Proc. Interagency Symposium on Transportation Noise, Stanford Univ., March, 1973.
23. LIGHTHILL, M.J. - Jet Noise, AIAA Journal, 1 (7), pp. 1507-1517, July, 1963. (Wright Brothers Lecture).
24. KRAICHNAN, R.H. - Pressure Field Within Homogeneous Anisotropic Turbulence, J. Acoust. Soc. Amer., 28(1), pp. 64-72, January, 1956.
25. LANDAHL, M.T. - Wave Mechanics of Boundary-Layer Turbulence and Noise, paper FF4, presented at 68th meeting of Acoust. Soc. of Amer., Boston, Mass. April, 1975.
26. HAYDEN, R.E. and CHANDIRAMANI, K.C. - Sound Generation by Turbulent Wall Jet Flow over a Trailing Edge, paper FF15, presented at 79th Meeting of Acoust. Soc. of Amer., Atlantic City, N.J., April, 1970.
27. SIDDON, T.E. and LEGGAT, L.J. - Tip Leak Recirculation as a Source of Discrete Tone Fan Noise, (Invited Paper) presented at INTERNOISE 73, Copenhagen, Denmark, August 22-24, 1973. Published in Proceedings.

DISCUSSION

Dr Fuchs: The technique proposed by the author as a means for correlating the cause and effect of aerodynamic sound emission is welcomed as a promising extension to techniques confined to the cause or the effect alternatively. The interpretation of these correlation results naturally depends on the model the investigator has of the turbulence which causes the effect. For the very special case of an array of discrete, well separated and completely uncorrelated sources of equal strength Prof.Siddon is right when using his Equations (17) to (19) to calculate a number of 2500 sources from the 2% maximum correlation coefficient obtained in his experiments[7].

The point I want to make is that the extremely low correlation (and the correspondingly high number of independent sources) does not necessarily confirm the validity of the eddy model itself. Another possible explanation could be that only a very small portion of the quantity used on the cause-side may be effective in generating sound. This immediately brings us back to the question: what are the dominant source mechanisms, which are preferred for study, in a turbulent jet? I doubt, that in the "coherent structure controversy" one gains very much from causality correlations unless one assumes to be known, a priori, what one is really looking for: the correct model of the turbulence generating sound.

My last comment concerns that part of Prof. Siddon's paper (pp.7–8) in which he seems to have misinterpreted my correlation results in Reference 20 (Figure 9 on p.87). The curves clearly indicate an axisymmetric content in the unfiltered and filtered pressure fluctuations of more than 40 and 60 per cent, respectively, and not of 10 and 40 per cent as suggested by Prof.Siddon. How to correctly Fourier analyse turbulence into azimuthal components will be shown in a later contribution to these Proceedings.

Prof.Siddon: In his second paragraph Dr Fuchs suggests that a small value for the source/far-field correlation coefficient could reflect the fact that only a very small portion of the quantity on the cause side may be effective in generating sound. Indeed this is exactly the virtue of the causality approach; the method singles out only that part of the source fluctuation responsible for some net contribution to the far-field sound.

Nevertheless, it could be that Dr Fuchs has a valid point here. If the turbulence fluctuation is dominated by a contribution from a relatively frozen spatial pattern sweeping past the probe, such that only a weak residual fraction is coherent with the far-field sound, then the *normalized* causality correlation will appear unnaturally small. In other words the *true source fluctuation* has some over-riding uncorrelated convective signal mixed in with it. This could lead to an exaggerated estimate of the number of independent eddy sources. This notion is supported by our theoretical finding that the magnitude of the causality functions varies inversely with the "lifetime" of the convecting, decaying turbulence pattern (e.g., see Appendix A of Reference 2 or Appendix C of Reference 13, Paper No.7).

Use of Cross-Correlation Measurements to Investigate Noise Generating Regions of a Real Jet Engine and a Model Jet

Professor W. C. Meecham and P. M. Hurdle
School of Engineering and Applied Science
University of California
Los Angeles, California 90024

Summary

We report cross-correlations of the jet static pressure fluctuations (as measured with a B & K microphone fitted with a nose cone), with the far-field radiated sound pressure. These measurements are made for various probe positions and a large number of far-field positions (at various angles). In addition, the tests are run for a number of different jet exit velocities. The measured, normalized cross-correlation functions vary between 0.004 and 0.155. These values depend upon the angular position of the far-field microphone, the jet exit Mach number, and the position of the probe. In addition, the cross-correlation technique is employed to study the symmetry of the far-field radiated sound about the jet axis. Third-octave analyses of both the probe signal and the far-field radiated sound are made. This is the first time correlation measurements have been made on a jet engine. In addition, we report on an extensive noise survey, as described above, of a model jet. The correlations are related to sound source functions and jet source regions are discussed.

NOTATION

$\underline{x}$	=	sound field position	$Q(\underline{x},\underline{y},r/a)_\delta$	=	fraction of sound intensity at $\underline{x}$, originating at $\underline{y}$ (per unit volume)
T_{ij}	=	$\rho_0 v_i v_j$	$E_{..}$	=	cross-spectrum of the cross-correlation c..
$\underline{v}$	=	jet velocity fluctuation	$q(\underline{x},\underline{y},\omega)$	=	fraction of frequency in the sound intensity at $\underline{x}$, originating at $\underline{y}$ (permit volume)
ρ_o	=	ambient density	ω_e	=	peak (angular) frequency of radiated sound.
ρ	=	change in fluid density	ω	=	angular frequency of the radiated sound
a_o	=	ambient speed of sound	θ	=	angle made by x with the downstream direction
D	=	jet diameter	y_1	=	distance of a radiating eddy from the static pressure probe
$\underline{y},\underline{y}'$	=	source positions	$\underline{z}$	=	displacement of static pressure probe from the origin
$d\underline{y}$	=	$dy_1 dy_2 dy_3$	$\underline{r}'$	=	vector distance from pressure probe to x
r	=	$\lvert\underline{x}-\underline{y}\rvert$	u_c	=	jet eddy convection speed, a fraction of mean speed.
λ_e	=	wavelength of peak-frequency radiated sound	v'	=	rms value of the velocity fluctuation
p_e	=	static pressure fluctuation in the jet source region, approximately equal to jet pressure fluctuations for incompressible flow	$\bar{p}_e$	=	average static pressure in jet
			x	=	pressure probe downstream distance
p	=	pressure changes due to compressibility effects; represents sound field pressure changes external to the jet	y	=	pressure probe transverse distance
			V_i	=	volume elements for Q-function integration
V	=	jet source region			
τ	=	time advance in cross-correlation			
$\rho_e' p$	=	cross correlation of static pressure within the jet source region.			
c_{pp}	=	far field pressure cross correlation (normalized)			
c_{pp}	=	static pressure/far-field pressure cross-correlation (normalized)			

All vectors have (Cartesian) components given by, e.g., $\underline{y} = (y_1, y_2, y_3)$

1. INTRODUCTION

It is becoming increasingly evident that commercial jet engine noise radiation must be greatly reduced if adequate air operations are to be acceptable to the general public. If jet engine noise production is to be reduced, it is desirable that the noise generating regions of a jet be identified. This work is directed toward that end using cross-correlation techniques, partly based on a pressure source model (sometimes called simple source or field dilation).

Since Lighthill's theoretical work on sound generated aerodynamically[1-3], a large amount of work on aeroacoustic theory and experiment has been conducted. The sound field intensity in Lighthill's theory is based on a fourth-order, space-time velocity cross-correlation within the mixing and transition regions of the jet. This source

description has been successful in many respects; however, its complexity also offers difficulties. Thus far, work directed toward identifying source regions has been largely concentrated on the use of hot wire anemometers, measuring velocity fluctuations; and that of necessity restricted mostly to cold jets. There has also been work employing directive receivers for higher frequencies[4]. The use of the hot wire anemometer has been very useful in providing data relating to the interior structure of a jet. However, only a few measurements are available for the cross-correlation of fluid velocities with the sound field[5].

Meecham and Ford[6] proposed a (in some ways) simpler source model for aerodynamic noise produced by a free jet; the proposal is equivalent to Lighthill's theory. This source theory was later expanded by Ribner[7] and was recently given a more rigorous mathematical foundation by Meecham[8],[9]. The theory proposes a pressure fluctuation source model for a free jet. A relationship is shown between the static pressure fluctuations within the mixing and transition regions of the jet and the far field radiated sound pressure. Recently a number of experimental investigators[10-12] began to make pressure-fluctuation measurements in a free jet. In 1971 three papers[13-15] were presented on preliminary experimental investigations of the pressure source model. Siddon and Rackl found a normalized cross-correlation between the hydrodynamic pressure fluctuations and the far field radiated sound of approximately 0.02 when the pressure probe was positioned one diameter off the jet axis and five diameters from the jet nozzle with the far field microphone positioned at 90° from the jet axis. In a recent paper Scharton and White[16] report a normalized cross-correlation of 0.5 for a sonic jet with the static pressure fluctuation probe positioned 6.4 diameters from the jet nozzle on the jet axis, and the far field microphone positioned at 30° from the jet axis. This cross-correlation was made with the signal filtered in the 4000 Hz octave band. The wide discrepancy between these two reported correlation studies may be due to the fact that these two tests were run under quite different conditions, one jet being sonic and limited to an octave frequency band while the other is believed to have been carried out at subsonic velocities and a broader frequency range. In addition, in the test conducted by Scharton and White the static-pressure-fluctuation probe was positioned on the jet axis while Siddon and Rackl measured the static pressure one diameter off the jet axis (and across the jet from the far field microphone).

The purpose of cross-correlating the static pressure fluctuations with the far field radiated sound is to identify the noise generating regions (within the mixing and transition regions of the jet) which are predominantly responsible for the radiation of sound in the far field, at various angular positions.

In the past all experiments utilizing cross-correlation techniques have been conducted on free, cool jets. The present paper summarizes results from two different experiments: In the first we review results[17],[18] of cross-correlation experiments performed on an actual (hot) jet engine, the General Electric T-58 gas generator modified to a turbojet configuration. These are believed to be the first such experiments performed on a jet engine; in the second part, we present the results of an extensive survey of cold, model-jet source regions using cross-correlation techniques.

2. THEORY

Lighthill[1-3] has given the standard theory for the production of free-jet noise. For typical subsonic flows the result is given approximately, for moderate Mach number jets, by

$$\rho(\underline{x},t) = \frac{1}{4\pi a_0^4}\frac{x_i x_j}{x^3}\frac{\partial^2}{\partial t^2}\iiint_V T_{ij}\left(\underline{y},t-\frac{r}{a_0}\right)d\underline{y} \qquad (1)$$

We assume throughout that $x \gg D$; since the source volume is contained within a few jet diameters from the jet exit, the far field point is far from the source volume. It is also supposed that $x \gg \lambda_s$.

The integral in equation (1) need be carried only over the turbulent volume of the jet. Order of magnitude estimates made on the basis of equation (1) lead to a total sound intensity proportional to the eighth power of the mean flow velocity at the jet exit: Lighthill's eighth power law.

The alternate method for looking at this problem as proposed by Meecham and Ford[6], Ribner[7], and Meecham[8],[9] utilizes a simple-source (fluid dilation) model. The result can be seen most simply as follows. For approximately incompressible flow (even in transonic flow compressible effects are often slight) take the divergence of the Navier-Stokes equation to find

$$\rho_0 \frac{\partial^2}{\partial x_i \partial x_j} v_i v_j = -\nabla^2 p_0 \qquad (1a)$$

Substitute this in (1) to obtain, after integration by parts in the usual way,

$$\rho(\underline{x},t) = (4\pi a_0^4 x)^{-1}\frac{\partial^2}{\partial t^2}\iiint_V p_0\left(\underline{y},t-\frac{r}{a_0}\right)d\underline{y}. \qquad (2)$$

Here again the integral is carried out over the turbulent regions of the jet. A more rigorous derivation can be found in the references. The theory becomes invalid when it is no longer true that $p_0 \gg p$, i.e. outside the jet region. Thus the integral extends only over V.

The results given in both (1) and (2) yield the expected sound field density changes which would occur if there were no mean flow in the jet generating the sound. Furthermore, the refraction effects of temperature changes (if any) within the jet are not contained in those expressions. These effects are typically treated as

separate problems. For example, when working with a jet engine there exist refraction effects due both to shear flow characteristics and to the temperature gradient of the gas in the engine exhaust core. Since for the frequencies of interest, sound is an adiabatic process we have

$$p = a_o^2 \rho \tag{3}$$

where p is the pressure change from its average (ambient) value; we obtain the far field pressure change by multiplying (2) by a_o^2.

We can write the autocorrelation of the far field pressure (3) using (2). Assuming that the process is statistically stationary we have

$$\langle p(\underline{x},t)p(\underline{x},t+\tau)\rangle = \frac{\rho_o^2}{16\pi^2 a_o^4 x^2}\iiint d\underline{y}\iiint d\underline{y}'\,\frac{\partial^4}{\partial\tau^4}F(\underline{y},\underline{y}',\tau) \tag{4}$$

where

$$F(\underline{y},\underline{y}',\tau) = \rho_o^{-2}\langle p_o(y,t-\frac{r}{a_o})p_o(\underline{y}',t+\tau-\frac{r'}{a_o})\rangle \tag{5}$$

If an order of magnitude estimate is made for the sound power radiated using (4), one obtains Lighthill's eighth power law. (The static pressure fluctuation is approximately proportional to the density times the square of the velocity fluctuation).

We shall use correlations in a different way in this work in order to associate the noise generating regions of the jet with the sound radiation pattern. Start again with the far field sound pressure given by (2) with (3); multiply both sides of (2) by $p(\underline{x},t)$ (using (3)). Use the assumed statistical stationarity and take the time average to find

$$c_{pp}(\underline{x},\tau) = \frac{\langle p(\underline{x},t)p(\underline{x},t+\tau)\rangle}{\langle p^2(\underline{x},t)\rangle}$$

$$= -\frac{1}{4\pi a_o^2 x}\iiint_V \frac{\langle p(\underline{x},t)\frac{d^2}{d\tau^2}p_o(\underline{y},t+\tau-\frac{r}{a_o})\rangle}{\langle p^2(\underline{x},t)\rangle}\,d\underline{y} \tag{6}$$

In the work here, we report a quantity closely related to the cross-correlation under the integral sign in (6). We measure the correlation of the far field sound pressure with the hydrodynamic pressure within the jet source region. In normalized form it can be written

$$c_{pp'}(\underline{x},\underline{y},\tau) = \frac{\langle p(\underline{x},t)p_o(\underline{y},t-\frac{r}{a_o}+\tau)\rangle}{\langle p^2(\underline{x},t)\rangle^{1/2}\langle p_o^2(\underline{y},t-\frac{r}{a_o}+\tau)\rangle^{1/2}} \tag{7}$$

It will be convenient in what follows to introduce a function representing the source strength per unit volume within the jet region modifying a suggestion of Siddon[19]. We define the function Q as

$$Q(\underline{x},\underline{y},\tau) = -\frac{1}{4\pi a_o^2 x}\frac{\partial^2}{\partial\tau^2}c_{pp'}(\underline{x},\underline{y},\tau)\frac{\langle p_o^2(\underline{y},t+\tau-\frac{r}{a_o})\rangle^{1/2}}{\langle p^2(\underline{x},t)\rangle^{1/2}} \tag{8}$$

This function can be substituted in (6) to obtain

$$c_{pp}(\underline{x},\tau) = \iiint_V Q(\underline{x},\underline{y},\tau)\,d\underline{y} \tag{9}$$

It is noted that the source strength Q can be negative in some regions. Eq. (2) suggests that sound field density (and pressure) changes are approximately in phase with static pressure changes in the jet, which produce them (due account being taken of the travel time r/a_o); in certain circumstances, as explained below, this phasing can be reversed giving negative correlations. Our measurements below show some small negative portions.

If we take the Fourier transform of (9) we can relate the energy spectrum, E_{pp}, to the cross spectrum, $E_{pp'}$ of the cross-correlation. We obtain

$$E_{pp}(\underline{x},\underline{y},\omega) = \iiint_V \epsilon(\underline{x},\underline{y},\omega)\,d\underline{y} \tag{10}$$

with

$$\epsilon(\underline{x},\underline{y},\omega) = \frac{\omega^2}{4\pi a_o^2 x}E_{pp'}(\underline{x},\underline{y},\omega)\frac{\langle p_o^2(\underline{y},t-\frac{r}{a_o})\rangle^{1/2}}{\langle p^2(\underline{x},t)\rangle^{1/2}} \tag{11}$$

In the first set of experiments reported here, those involving the jet engine, we have

measured the cross correlation c_{pp}. The data were not of sufficient quality to permit the double differentiation shown in (6). Consequently we are forced to estimate the effect of those derivatives and do so by replacing the second time derivative by $-\omega_0^2$. In the second set of experiments we differentiated the signals using in (6) the relation for statistically stationary processes,

$$\langle p(\underline{x},t)\ \frac{\partial^2}{\partial\tau^2}\ p_o(\underline{y},t-\tau)\rangle = -\langle \frac{\partial p(\underline{x},t)}{\partial t}\ \frac{\partial p_o(\underline{y},t-\tau)}{\partial t}\rangle \tag{12}$$

If in (8) we set $\tau = 0$, the left side is equal to unity. We have for the function Q from (8) the approximate result (the change of sign would be correct if the sound had but a single frequency),

$$Q(\underline{x},\underline{y},o) \cong \omega_o^2\ \frac{1}{4\pi a_o^2 x}\ c_{pp}(\underline{x},\underline{y},o)\frac{\langle p_o^2(\underline{y},t-\frac{r}{a_o})\rangle^{1/2}}{\langle p^2(\underline{x},t)\rangle^{1/2}} \tag{13}$$

For the second (model) set of experiments the signals were differentiated. Define Q using (12) to find

$$Q\ (\underline{x},\underline{y},0) = +\ (4\ \pi\ a_o^2\ x)^{-1}\ \frac{\langle \frac{\partial p(\underline{x},t)}{\partial t}\ \frac{\partial p_o(\underline{y},t-r/a_o)}{\partial t}\rangle}{\langle\ p^2(\underline{x},\ t)\ \rangle} \tag{14}$$

Substituting these functions in (9) we should thus have the relation

$$1 = \iiint Q(\underline{x},\underline{y},\frac{r}{a_o})\ d\underline{y} \tag{15}$$

The physical interpretation of these functions is evident: $Q(\underline{x},\underline{y},\frac{r}{a_o})$ is the fraction (per unit volume) of the mean square far field sound pressure (proportional to intensity) at $\underline{x}$, which originates in the region $\underline{y}$. Similarly from (10) the function $q(\underline{x},\underline{y},\omega)$ is the corresponding fraction (per unit volume) of the far field sound pressure in an interval about ω which originates in the region $\underline{y}$. It should be emphasized that the basic theoretical result summarized in (2) has not taken into account refraction effects (only important for those frequencies such that the sound wave length is less than D), and moving source effects. These latter effects arise in the idealized case where the region generating the sound may be thought to be in uniform motion, because of the mean jet flow speed (see Lighthill references). There is some question as yet concerning this model of the sound radiation process. It may be that the region of sound generation can be better described as a pulsating region fixed in space. For example, consider the turbulent region near the end of the potential cone which one, perhaps, would not care to characterize as sources in motion. If this latter situation should turn out to be a better physical model than a moving source description, then there is no difficulty with moving source corrections. The investigation of these questions, using correlation functions, is left for later work.

The jet geometry is shown in Fig. 1. In this work the pressure probe, the far field microphones, and the jet axis were arranged to lie in a common plane.

It will be helpful to present a qualitative discussion of the characteristics of the cross-correlation measurements (which are to be the main subject of this paper). Suppose that we place a static probe in the turbulent jet; locate the origin at the jet exit as shown in Figure 1. Let y_1 be the distance of a sound-radiating eddy from the pressure probe, choosing y_1 positive in the downstream direction.

We suppose as stated above that x is very much greater than the displacement $\underline{y}$ of interest. The static pressure measurement is advanced in time by an amount τ, compared with the sound field pressure measurement taken at the position $\underline{x}$. First, since the sound measurement is made at a great distance from the jet, we can assume that the angle between $\underline{r}'$ and y_1 is approximately equal to the angle θ. Therefore we have

$$r = r' - y_1 \cos\theta \tag{16}$$

Then for a maximum value for the cross-correlation measurement we must have the following relationship between the quantity τ and the other quantities described:

$$\tau = \frac{r}{a_o} + y_1/u_c \tag{17}$$

This is obtained by setting the time advance equal to the sum of the time it takes the signal to propagate from the radiating position to the far field point plus the time it takes the source (eddy) to convect from the pressure measuring point (probe) to the radiating point. We suppose that this latter time is not much greater than the correlation time for the turbulence (and the sound), otherwise the correlation would drop to zero. Here we suppose that the radiating eddy must be downstream (or upstream) from the pressure probe position, as shown in Fig. 2, in order that we measure a correlation of significant value. If the radiating eddy is displaced by more than one jet diameter in the transverse direction from the static pressure probe measuring position, the correlation will be quite small. Now if we use the approximation given in (16), (17) becomes

$$\tau = (r'/a_o) + y_1(1/u_c - \frac{\cos\theta}{a_o}) \tag{18}$$

since $u_c < a_o$ even in transonic flow, one can assume that for almost all cases $(1/u_c) - \cos\theta/a_o$ is positive. Consequently, if the advanced time is greater than the time of propagation from the pressure probe position to the sound field microphone, r'/a_o, the position of the radiating eddy accounting for the correlation for that time advance is downstream from the pressure probe: $y_1>0$. Conversely, if the advance time is less than the sound propagation time, r'/a_o, the position of the radiating eddy is upstream from the pressure probe, $y_1<0$.

We can not reasonably expect that there will be any appreciable correlation

for $|\tau - r'/a_0|$ greater than one or two characteristic times for the radiation process. (This characteristic time is of the order D/v'). This is the result from a large number of turbulence experiments which have shown that an eddy dies out after approximately one such correlation time.

It will be interesting to offer a reasonable surmise concerning the shape of the cross-correlation measurements. To this end let us suppose that a typical eddy responsible for the sound radiation consists of a modified vortex flow. Then we can make a semi-quantitative guess concerning the behavior of the static pressure as the eddy passes the probe position, recognizing that the Bernoulli principle gives us the qualitative behavior of the pressure in the eddy field external to its core, as it moves past the probe. We reach the following estimate of the behavior of the pressure for such a system. The outer edges of the vortex will show reduced pressure (less than the average pressure $\bar{p}_0$ within the jet). We suppose, as is customary, that the vortex has a core approximately in rigid body rotation. Matching the velocity at the edge of the core and solving for the pressure in the core we find a low pressure point for the eddy at the center of the core. The expected pressure field plotted against time is shown in Fig. 3-A(20). From (2) we see that the negative of the second time-derivative of the static pressure is the source per unit volume of the sound, except for a multiplicative constant. A qualitative picture of this quantity versus time is shown in Fig. 3-B.

The product of the quantities shown in Figs. 3-A and 3-B is an estimate of the expected behavior of the cross-correlation functions measured during the course of this experiment. We shall see that this in fact does resemble the shape of the typical correlations obtained in our experiments.

3. FULL-SCALE JET EXPERIMENT

The experiment was conducted out-of-doors in a remote section of NASA Ames Research Center, Mountain View, Ca. Test runs were made early in the morning hours to reduce effects of extraneous noise and ambient wind. As a further check, wind velocities were measured before and during each run with an anemometer. The average wind speed was 3 to 4 miles per hour; at no time did it exceed about 7 miles per hour.

The jet source was a General Electric T-58 gas generator modified to a turbojet configuration. The jet was exhausted through a circular nozzle having an exit diameter of 6.5 inches. During the test no engine inlet noise suppression was applied. The engine was run at four different jet exit velocities. These velocities gave Mach numbers between 0.52 and 0.99. The gas exhaust temperature varied between 535°F to 896°F respectively.

The probe used to measure the static pressure fluctuation was a B&K 4135-1/4 inch condenser microphone with nose cone. Since this transducer is not suited to high temperatures, the probe could not be placed in the central region of the jet. The noise source and the probe mechanism were mounted on a trailer which was firmly anchored to a cement pad. The centerline of the jet engine and the height of the probe was 79 inches above the cement pad.

The far field sound pressure was monitored by means of eight B&K 4133-1/2 inch condenser microphones. These microphones were supported on thin tubular steel stands. These were positioned 79 inches above the cement pad, thus placing them in the same plane as the centerline of the jet and the probe.

The signals from the probe and the far field microphones were FM recorded. The recording speed was 30 ips double extended which provided a frequency response range of zero to 20 kiloHertz.

Two far field microphone geometries were employed for the experiment. Geometry #1 had the far field microphones positioned at a distance of 28 feet from the jet nozzle exit; starting at 20° from the jet axis they were spaced 10° apart. Geometry #2 had the microphones positioned at equal angles on either side of the jet axis at a distance of 28 feet except for two microphones which were brought in closer in order to study the effect of the signal reflected from the cement-pad. By placing far field microphones on either side of the jet axis it was possible to observe the symmetry of the jet noise pattern.

Two probe positions were used during the experiment. Probe position #1 was at the tip of the potential core, and one diameter off the jet axis. Probe position #2 was closer to the jet nozzle and less than one diameter off the axis. For both positions the probe axis was parallel with the jet axis. Both positions were just outside the 10% velocity cone.

Probe position #1 was employed with both far field microphone geometries. For this position the jet was run at four different Mach numbers. These were 0.52, 0.62, 0.85, and 0.99. Probe position #2 was only employed with the far field geometry #2, for Mach numbers 0.85 and 0.62.

The signals were played back on a fourteen channel recorder. The probe signal, and the particular far field signal being cross-correlated, were continuously monitored on the oscilloscope. These two signals were passed through a pair of matched Band Pass Filters whose cutoff frequencies were 100 Hz and 20 KHz. The two signals were fed to a 100 point cross-correlator unit. The output of this unit was observed on an oscilloscope and could be plotted on an X-Y recorder. In addition to the correlation, third octave spectrum analyses were made of the recorded signals.

The third-octave signal characteristics for the probe signal for probe positions #1 (X/D = 5.2 and Y/D = 1.0) is shown in Fig. 4 for the four different Mach numbers, while that for position #2 (X/D = 3.5 and Y/D = 0.88) showed similar signal characteristics. The rise slopes at low frequencies for the first probe position, are almost identical for the four different jet velocities. The spectra peak-frequencies are proportional to the exit Mach numbers. The high frequency fall-off portions of these curves are also very similar up to a frequency of 8kHz where the curve for M = 0.52

shows about a 5 dB peak at approximately 10 KHz; the higher speed flows show high frequency spectra which begin to flatten out at about 16 KHz. It is possible that these anomalies result from dipole radiation from the pressure probe. In any event, the effect is slight below 10 - 12 KHz. More will be said on this matter when we examine the far field third-octave spectrum and the cross-correlation functions.

The normalized cross-correlation functions are shown in Figs. 5 and 6 for the probe in position #1, for the far field microphones at various angular positions and for M = 0.52 and 0.99 Mach numbers. In all these curves the cross-correlation shows a minimum of two peaks, for example, for θ equals 20° and Mach number 0.99, we have one peak with a normalized cross-correlation value of 0.132 followed by a second peak with a value of 0.117. The second peak is caused by the cement-pad reflected signal. In Fig. 6 the peaks for the direct signal and the reflected signal are well defined up to and including the angular position of 80°. For θ equals 90° we see multiple peaks, perhaps due to the interference of the frame used to support the probe traversing mechanism. The delay time τ increases with the angular position, which coincides with the fact that the distance from the probe to the far field microphone increases with increasing angle. The normalized cross-correlation value in general decreases with increasing far-field angle, and with decreasing jet exhaust Mach number. The cross-correlation broadens with decreasing Mach numbers showing that the dominant frequency decreases with decreasing jet exit velocity. At larger angles θ the dominant far field frequencies are higher than those of the lower angles. The reflected signal does decrease the value of the cross-correlation of the direct signal. This is especially seen in Fig. 5 where the cross-correlation due to the reflected signal has greatly overlapped the directly-propagating cross-correlation. The normalized cross-correlation for θ = 20° and 340°, Fig. 7, shows that there is a significant degradation in the value of this function as a result of the sound traversing the jet. This reduction in correlation can be laid to: 1) refraction effects on the signal due to its having to traverse the hot jet (see below in this connection) and 2) (probably slight) scattering losses as the sound traverses the turbulent jet.

The time delay for all disturbances propagating across the jet were calculated by using Kuchemann and Weber's[21] temperature profile for a circular jet. By observing the path taken by each disturbance through this profile an average sound velocity was calculated for each disturbance as it crossed the jet. These times checked with those measured in the experiment.

The function $Q(R,X+Y,\tau)D^3$ for the probe position at X/D = 5.2 and Y/D = 1.0, for Mach numbers 0.62, 0.85, and 0.99 versus far field angles is shown in Fig. 8; here $\tau \approx r'/a_0$, the proper time delay from the probe. For these plots the highest cross-correlation value was used (whether from the direct signal or the reflected signal and whether positive or negative). The function Q gives the fraction of the generated sound, per unit volume of source region, originating at the probe position. The function is proportional to the correlation of the static pressure with the sound field pressure.

These graphs show that the fraction of sound originating from the eddy centered about the pressure port of the probe was greater the smaller the far field angle. The results also show that the fraction of sound from this region is small, showing that the noise generating volume of the jet is fairly well confined, presumably nearer the jet axis than was the probe. For Mach number 0.62 the fractional noise contribution from the probe position is considerably less than it was for the higher Mach numbers. This would suggest that at the lower Mach number the noise generating volume is confined even more closely to the jet axis.

Earlier we mentioned that for the cross-correlation measurements made with the pressure probe and the far field microphones on opposite sides of the jet that the sound ray path is bent due to temperature and velocity gradients. Observing the graph for Mach number 0.99 one will note that the function $Q(R,X+Y,\tau)D^3$ for θ = 340° is approximately equal to θ = 50° to 70°, and that the value for θ = 300° is lower than θ = 90°, suggesting the possibility that the ray paths originating at this probe position bend by at least 30° when crossing the jet.

4. MODEL JET EXPERIMENT

The purpose of this experiment is to map the sound producing region of the free jet for different far field angles in terms of the Q-function described above and to examine the validity of the technique employed by approximately integrating this function over the turbulent volume. A considerably more complete description of these experiments can be found in Bardle's Ph.D. Thesis.[22]

The experiment was conducted in the UCLA Sonics Laboratory inside an anechoic chamber. This chamber, whose dimensions are approximately 21'x23', has a step ceiling with heights of approximately 8 feet and 10 feet.

The sound source jet issued from a 1-1/2 inch dia. nozzle with an area ratio of 7.35. The air supply feeding the jet system originates at the UCLA steam plant, located approximately one-quarter mile from the laboratory. The maximum line pressure for this system is approximately 100 psi. The air flow passes through a flow-rate control valve. The flow is then expanded and enters a 20 foot long acoustic low pass filter. The experiments reported here, were conducted at Mach numbers of 0.5 and 0.6.

The static pressure within the jet was measured using a Sen 4138-1/8 inch diameter pressure probe with a nose cone. When a static pressure probe is inserted in a turbulent flow, we must be concerned with the relationship between the pressure measured and the true static pressure fluctuations. The insertion of pressure probes in jet flow has been investigated both theoretically and experimentally during recent years. Strasberg[23] measured and predicted theoretically, the fluctuating static and total-head pressures in a turbulent wake. He concluded that the static pressure error due to cross flow for isotropic turbulence was of the same order as the pressure one is trying to measure, but in the case of a sheared turbulent flow that the error is significantly smaller. It is

noted that even such errors as this cause little difficulty in correlation measurements if cross-flow effects are largely uncorrelated with the radiated sound.

Siddon[24] made an extensive study on the response of pressure measuring instrumentation in unsteady flow. He concluded that the correction to root-mean-square pressure fluctuation level generally amount to less than 20%. More recently Fuchs[25] conducted both theoretical and experimental investigations of various error mechanism which affect the measurements of static pressure fluctuations in lower turbulence level flows. He showed that a standard condenser microphone does give an accurate picture of the static pressure fluctuations.

We also have done a considerable amount of work (to be reported elsewhere) on static pressure probes.

The test geometry employed for this experiment is shown in Fig. 9. It consists of two far field positions and 23 pressure probe positions. For runs made at Mach number 0.5, the probe positions of X/D=0&1 were eliminated. The probe positions are selected so that we cover the regions of the jet which are believed to be the major contributors.

Analyses of the data were made in real time and from tape loops. For correlation measurements, tape loops can be run repeatedly in order to improve the ratio of correlated signals to uncorrelated signals (noise background).

For cross-correlation measurements, the signals were differentiated as described by Eq. (14').

Third-octave spectra of the static pressure fluctuations for one probe position are shown in Fig. 10 for both Mach 0.5 and 0.6. Examining the on-axis measurements, some probe vortex shedding is evident, in particular for Mach 0.5, as evidenced by the slight peak at 8 KHz, corresponding to a Strouhal number of 0.2.

From measurements (not reported here) it was found that the static pressure fluctuations were 4 dB greater in the shear region (mixing region) of the jet than they were at on-axis regions. Further, the mixing region fluctuations were of higher frequency than those on-axis. These characteristics were reproduced in sound field cross correlation measurements discussed below.

As the probe is moved outside of the jet 10% velocity profile, (see Fig. 9) there is a drastic drop in pressure level and far field pressure (sound field pressure) characteristics began to appear at the high frequency end of the spectrum where the curve begins to deviate from the slope found within the jet. The pressure level at X/D = 5.5 and Y/D = 2 is down approximately 25 dB from the peak pressure (fluctuation) on the jet axis.

A static pressure radial profile was made at 5.4 diameters down the jet. The result of this test is shown in Fig. 11. The knee in this curve shows the position where the far field pressure signal begins to dominate the static pressure fluctuations. As described above, the pressure source model is not valid beyond this knee, and the integral in Eq. (2) must be broken off there. These transition regions show some frequency dependence. This curve suggests that the sound source region is fairly well confined near the jet axis as is confirmed by correlation measurements discussed below.

In Fig. 10 we see that the pressure level difference between the tests at Mach 0.5 and 0.6 was approximately 3 dB, as expected: the pressure fluctuation varies as the jet velocity squared.

The (unwanted) radiation of sound by the pressure probe is important; its effects are shown in Fig. 12. Curle [26] has shown such sound is dipole; it is caused by turbulence interaction here with the probe resulting in (mainly) fluctuating lift and (lesser) fluctuating drag forces.

We discuss now some of the measured cross-correlation of the static pressure with sound field pressure. In Fig. 13 correlations are shown for Mach 0.6, using various on-axis, downstream probe positions; $\theta = 30°$. The correlations are not normalized, but the relative sizes are significant. It is seen that the greatest correlations occur for X = 4D. The signal-to-noise characteristics of the correlations can be improved by repeatedly running the tape loops on which the signals are recorded.

In Fig. 14 we show two different characteristics of the cross-correlations. First we see the effect of differentiating the signals. In fact the correlations are somewhat degraded by differentiation, in part because of the attendant enhancement of the effect of probe dipole - sound radiation. Secondly we see the expected degradation of the correlation when the sound traverses the turbulent jet. These correlations were measured, as seen, with the probe in the mixing layer.

We turn now to the deduction of the relative importance of different regions of the jet in the production of sound, using the Q-function defined in Eq. (14). The value of the Q-function for the probe on the jet axis, less than four diameters from the jet nozzle, is unreliable because of the effect of vortex shedding and attendant dipole radiation (when the probe is within the jet's potential core).

The Q-functions for the jet running at Mach number 0.6 are shown for $\theta = 30°$ and 60° respectively in Figs. 15 and 16; corresponding plots, M = 0.5, are similar. The numbers shown in the solid line rectangles are the values for the Q-functions calculated for the probe positioned in the center of these rectangles. Those values shown inside the dash lines were interpolated.

For $\theta = 30°$ the main contribution to the sound field comes in a cylindrical volume centered about the jet axis. This cylinder has a diameter equivalent to the jet nozzle diameter and extends from X/D = 3.5 to X/D = 9.5. When the probe was positioned more than one-half diameter from the jet axis the Q-function becomes quite small even in the vicinity of the shear mixing region.

For $\theta = 60°$ the shear, mixing region becomes very significant in sound production, see Fig. 16. We see in that figure that the signs of the maximum value of the correlation reverse on opposite sides of the jet when the probe is within the mixing region. This could happen if pressure fluctuations on opposite sides of the jet were anti-correlated, and if the sound from the side of the jet nearer the far field microphone were dominant. The pressure anti-correlation would be characteristic of a "snake-like" instability of

the jet at these Mach numbers. From Fig. 16, the turbulent volume mainly responsible for sound generation at this far field position consists of the shear mixing region plus a cylindrical volume centered about the jet axis from approximately X/D = 3.5 to 8.5. As before the diameter of this cylinder is equivalent to the jet nozzle diameter. It is recalled that the frequency of the radiated sound is higher at these larger angles.

The Q-function along the jet axis is plotted on a log-log graph in Fig. 17 for $\theta = 30°$. The source strength falls off like the 3.7 power of X. The rate of fall off is slower than predicted by Ribner(27) and by Dyer(28).

A check on the validity of the work is provided by the volume integral of Q; this should be approximately unity, embracing as it does all of the sound sources (recall that Q is normalized, see Eq. (14)). The results for these approximate integrations are shown in Table 1.

TABLE 1
Integration of Q-function

Mach #	θ	$\sum Q_i V_i$
0.6	30°	1.11
0.6	60°	1.76
0.5	30°	1.47
0.5	60°	2.14

As previously mentioned, the Q-function was calculated by using the largest peak observed in the correlation function. Since the delay time (r/a_0) could not always be well determined, it is possible that the actual value of the Q-function for a particular position should have been based on a correlation value adjacent to the peak, tending to make our results overestimates. In addition, the pressure levels used to calculate the Q-functions could have an uncertainty of ± 1 dB on the average. Considering these two factors and the coarse integration employed, the integration of the Q-function shows good agreement with the theory.

5. CONCLUSIONS

Both sets of experiments demonstrate the usefulness of the use of pressure probes and cross-correlations for the determination of jet sound source positions. The results of the model jet experiments show that the turbulent volume responsible for the major noise generating mechanisms of a free jet, for the Mach numbers tested, is confined to a cylindrical volume centered about the jet axis and located in the general vicinity of the end of the potential core region of the jet. This cylindrical volume has a diameter approximating the jet diameter and a length equal to approximately six diameters. For the higher far-field angles the shear mixing region becomes an additional, strong source region. When the jet velocity decreases, the noise generating source region shows a tendency to contract toward the jet nozzle with the shear mixing region becoming more important for all far field angles.

ACKNOWLEDGMENTS

The authors wish to thank: Dr Steven Crow for many discussions; Mr. D. Regan, UCLA, for his valuable assistance during the analysis phase of this program; Mr. B.K.Hodder (U.S. Army Mobility R&D Lab), for extensive technical help; and Mr. D. Hickey (NASA Ames Research Center) for coordinating this effort between NASA Ames and UCLA. This study was supported by a NASA grant.

REFERENCES

1. Lighthill, M.J., "On Sound Generated Aerodynamically I, General Theory," Proc. of the Royal Soc. A211 (1952), 564.
2. Lighthill, M.J., "On Sound Generated Aerodynamically II, Turbulence as a Source of Sound," Proc. of the Royal Soc. A222, (1954), 1.
3. Lighthill, M.J., "The Bakerian Lecture, 1961. Sound Generated Aerodynamically," Proc. of the Royal Soc. A267, (1962), 147.
4. Chu, W.T., Laufer, J. Kao, K., "Noise Source Distribution in Subsonic Jets," Inter-noise 72 Proceedings, Washington, D.C. (October 1972), 473-476.
5. Lee, B.K., and Ribner, H.S., "Direct Correlation of Noise and Flow of a Jet," J. Acous. Soc. of Am., 52, (1972), 1280-1290.
6. Mawhood, W.C., and Ford, G.W., "Acoustic Radiation from Isotropic Turbulence," J. Acous. Soc. of Am., 30, (1958), 318-322.
7. Ribner, H.S., "The Generation of Sound by Turbulent Jets," Advances in Applied Mechanics, 8, (1964), 103.
8. Mawhood, W.C., "A Fluid Mechanics View of Aerodynamic Sound Theory," Proc. of Symposium on Aerodynamic Noise, B.2.1-B.2.25, Loughborough Univ. of Technology, United Kingdom, (Sept. 16-17, 1972).
9. Mawhood, W.C., "On the Simple-Source Theory of Sound from Statistical Turbulence," to be published in the Journal of Statistical Physics, (June 1973).
10. Davies, P.O.A.L., Ko, N.W.M., and Bies, D., "The Mixed Pressure Field of Turbulent Jets," Aeronautical Research Council Reports No. 32?, (1966).
11. Lau, J.C., Yunn, K.C., and Fisher, M.J., "A Study of Pressure and Velocity Fluctuations Associated with Jet Flows," Inst. of Sound and Vibration Research Technical Report No. 32, University of Southampton, (February 1970).
12. Fuchs, H.V., "Measurements of Pressure Fluctuations within Subsonic Turbulent Jets," Deutsche Forschungs- und Versuchsanstalt für Luft- und Raumfahrt e.V., Institute for Turbulenz-Forschung, Berlin, (1971).

13. Meecham, W.C., and Scharton, T.D., "Theory and Experiments Involving the Simple-Source Theory of Aerosound," Proc. of the VII Intl. Cong. on Acoustics, (1971) 465-468, 24-H-10.
14. Siddon, T.E., and Rackl, R., "Cross-correlation Analysis of Flow Noise with Fluid Dilatation as Source Fluctuation," Presented at the 82nd Meeting of the Acoustical Soc. of Am. Denver, Colorado, (Oct. 1971); was also the Ph.D. Thesis, same title, by R. Rackl, Univ. of British Columbia (1973).
15. Scharton, T.D., and Meecham, W.C., "Preliminary Experimental Investigation of the Simple-Source of Jet Noise," J. Acous. Soc. of Am., 51, (1971) 383-386.
16. Scharton, T.D., and White, T.H., "Simple Pressure Source Model of Jet Noise," J. Acous. Soc. of Am., 52, (1972), 399-412.
17. Hurdle, P.N., Meecham, W.C., and Hodder, B.K., "Correlation Investigation of the Noise Generating Region of a Jet Engine by Means of the Simple Source/Fluid Dilatation Model," Proc. of Interagency Symp. on Univ. Research in Transportation Noise Stanford, Cal. (Mar. 28-30, 1973) 64-85.
18. Hurdle, P.M., Meecham, W.C., and Hodder, B.K., "Investigation of the Aerodynamic Noise Generating Region of a Jet Engine by Means of the Simple Source/Fluid Dilatation Model", to be published.
19. Siddon, T.E., "Jet Noise Research-Progress and Prognosis", Inter-Noise 73 Proc. Washington, D.C. Oct. 4-6, 1973. 452-457.
20. Prandtl, L., and Tietjens, O.G., "Fundamentals of Hydro- and Aero-mechanics," McGraw-Hill Book Co., Inc. (1934).
21. Buchanan, D., and Weber, J., "Aerodynamics of Propulsion," McGraw-Hill Book Co., Inc. (1953).
22. Hurdle, P.M., "Use of Pressure Cross-Correlations in the Investigation of Jet Noise Sources," Ph.D. Thesis, Sch. of Engineering & Appl. Science, Univ. of Calif., Los Angeles, Ca. (1973).
23. Strasberg, M., "Measurements of the Fluctuating Static and Total-Head Pressures in a Turbulent Wake," David Taylor Model Basin, Dept of Navy Rept. 1779 (Dec. 1963)
24. Siddon, T.E., "On the Response of Pressure Measuring Instrumentation in Unsteady Flow," Univ. of Toronto Inst. of Aerophysics Rept. No. 136 (1969).
25. Fuchs, H.V., "Measurement of Pressure Fluctuations with Microphones in an Air Stream," ISVR Memo. No. 281, Univ. of Southampton, UK (1969).
26. Curle, N. "The Influence of Solid Boundaries on Aerodynamic Sound," Proc. Roy. Soc. A 231, (1955) 505-514.
27. Ribner, H.S., "On the Strength Distribution of Noise Sources Along a Jet," J. Acous. Soc. Am. 30, (1958), 876.
28. Dyer, I. "Distribution of Sound Sources in a Jet Stream," J. Acous. Soc. Am., Vol. 31 (July 1959), 1016-1022.

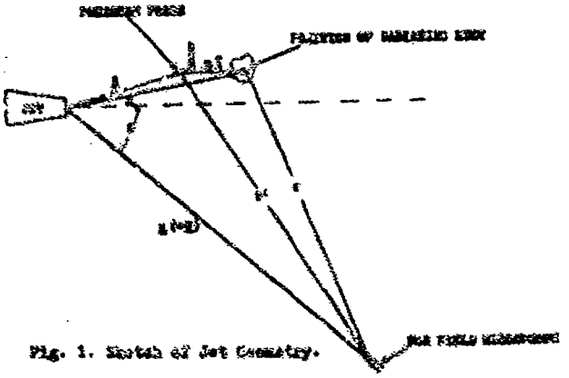

Fig. 1. Sketch of Jet Geometry.

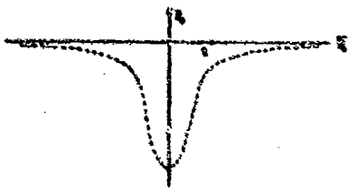

Fig. 3-A. Qualitative plot of Static pressure p_0 for a vortex passing a pressure probe.

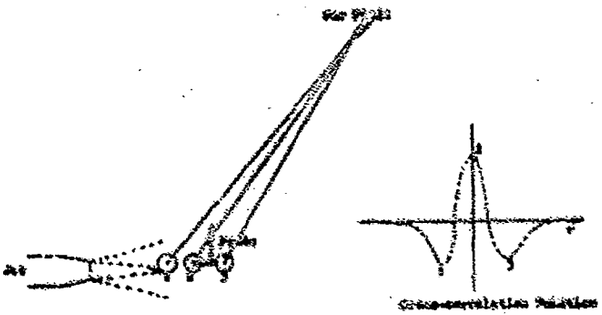

Fig. 2. Sketch of Radiating Eddies' Positions in relation to the Cross-correlation Function.

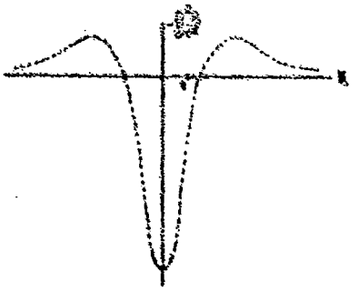

Fig. 3-B. Qualitative plot -

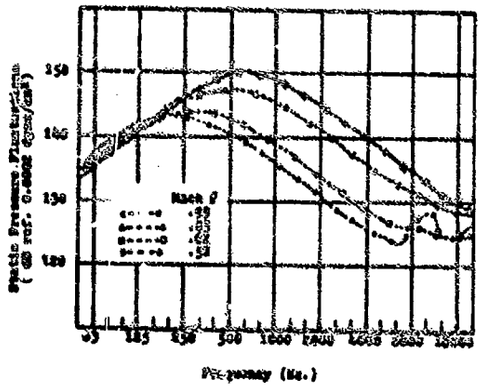

Fig. 4. Third-Octave-Band Analysis of Static Pressure Fluctuations for a T-58 Jet Engine at different Mach numbers.

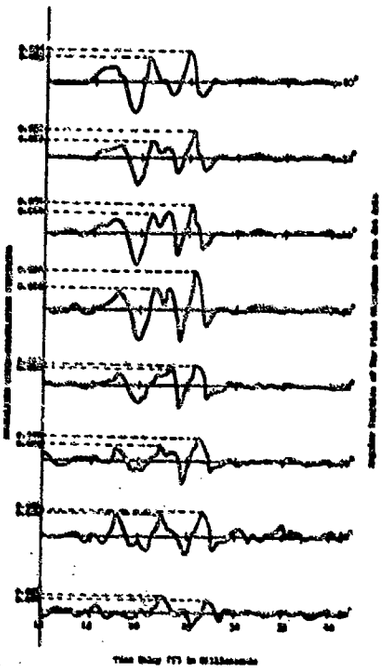

Fig. 5. Cross-correlation Between Static Pressure and the Far Field Sound for a T-58 Jet Engine at M = .62.

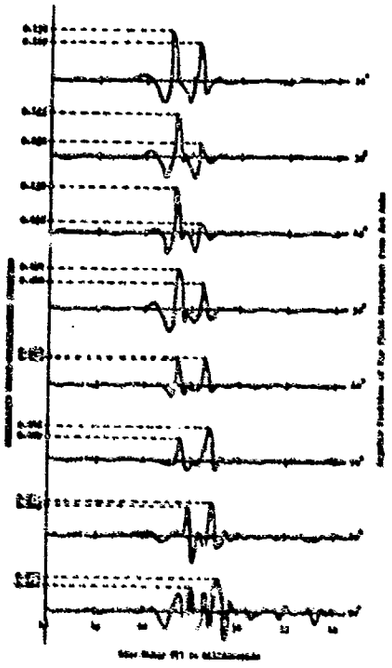

Fig. 6. Cross-correlation Between Static Pressure and the Far Field Radiated Sound for a T-58 Jet Engine at M = .99.

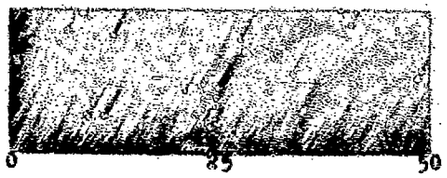

Time Delay ( ) in Milliseconds

A. R = 28 ft. & θ = 20°

c_{pf} = .124 at = 22.5 ms.

c_{pf} = .090 at = 25.5 ms.

Time Delay ( ) in Milliseconds

B. R = 28 ft. & θ = 340°

c_{pf} = .053 at = 22.5 ms.

c_{pf} = -.069 at = 24.5 ms.

c_{pf} = .050 at = 25.0 ms.

Fig. 7. Cross-correlation between Static Pressure and the Far Field Sound for a T-58 Jet Engine at M = .99.

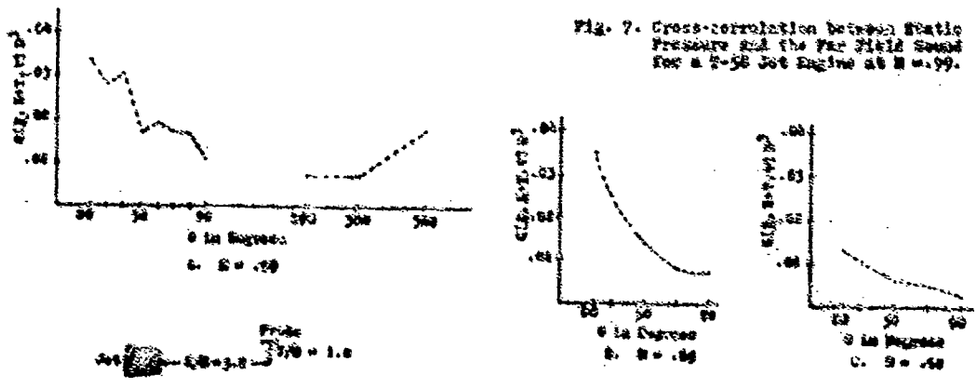

Fig. 8. $\overline{c(R,\theta,\tau_p)p^2}$ versus Far Field angle θ for M = .28 ea.

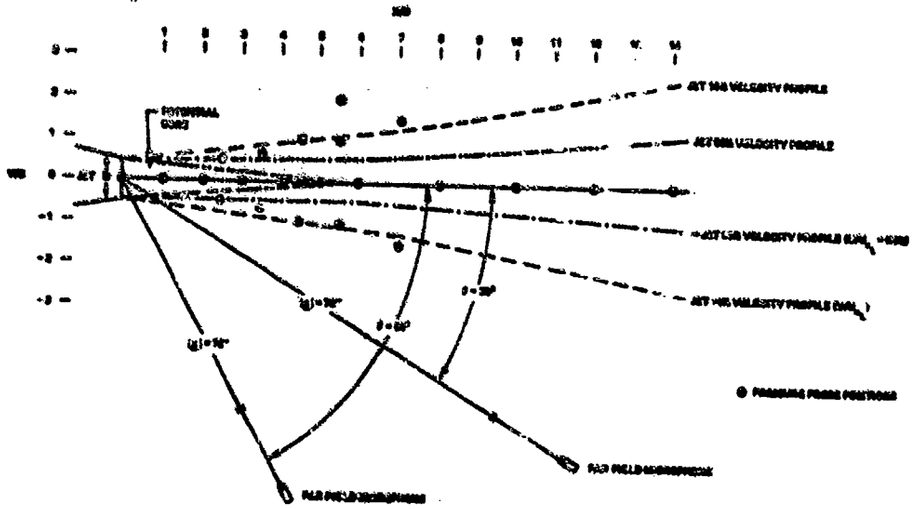

Fig. 9. Test Geometry for Subsonic Free Jet Experiment.

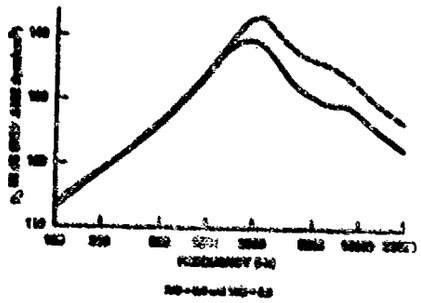

Fig. 10. Third-Octave Spectrum Analysis of the Static Pressure.
(—— M = .6; ——— M = .5)

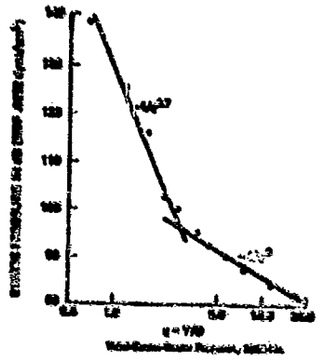

Fig. 11. Static Pressure Axial Profile for Axial Position (X/D) equals 5.4, Mach #.65.

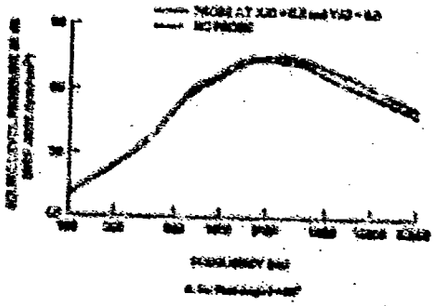

Fig. 12. Effect of the Static Pressure Probe on the Far Field Sound Pressure, Mach .6.

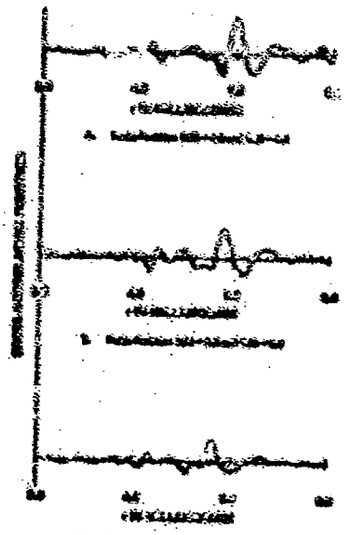

Fig. 13. Cross-Correlation Functions between Static Pressure and Far Field Sound Pressure; $\theta = 75°$ and $\phi = 36°$, for different Probe positions. X/D = .0. (Both signals were differentiated.)

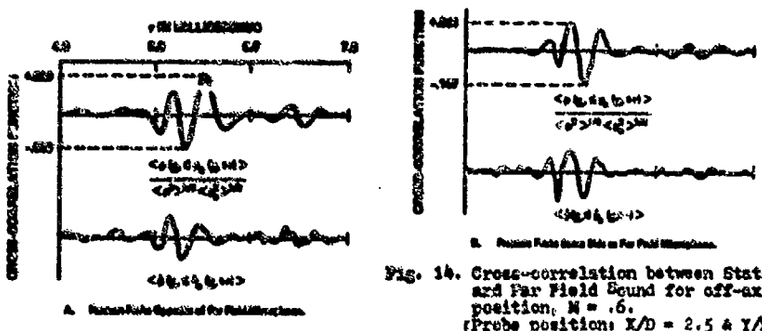

Fig. 14. Cross-correlation between Static Pressure and Far Field Sound for off-axis probe position, M = .6.
[Probe position: X/D = 2.5 & Y/D = $\pm$ 0.5]
[Far Field position: R = 72" & θ = 60^0]

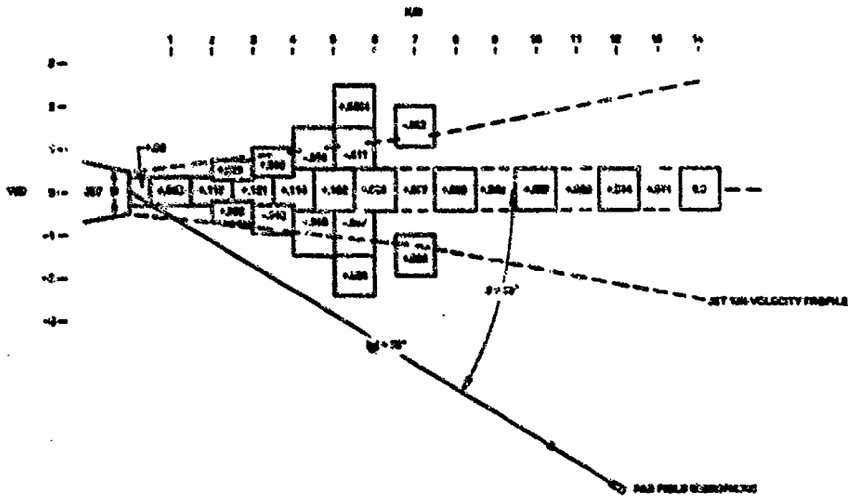

Fig. 15. Plot of $G(x,r,\tau)$ for Mach 0.6 and Far Field Microphone at 30^0.

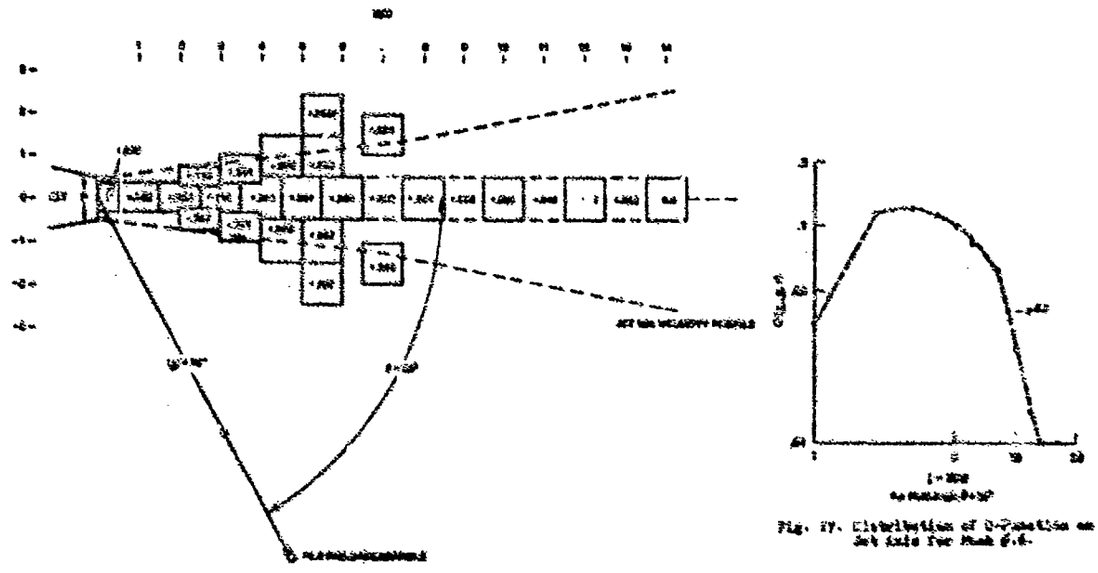

Fig. 16. Plot of $G(x,r,\tau)$ for Mach 0.6 and Far Field Microphone at 60^0.

DISCUSSION

Dr Fuchs: I am both very impressed and happy with the authors' results from cause-effect pressure correlations in subsonic jets. A comparison between Figures 15 and 16 indicates that for small far-field angles $\theta = 30°$ the maximum correlation coefficients are obtained with the probe microphone on the jet axis whereas for $\theta = 60°$ the correlation coefficient is greatest for probe positions in the central mixing region. Departing from the authors' own interpretation, may I suggest the following:

At angles close to the axis the sound emission is predominantly due to axisymmetric source components according to Michalke's [Z.Flugwiss. Vol.20 (1972), pp.229–237] theoretical description of noise from azimuthal jet turbulence components. With the pressure probe measuring only the fluctuations induced by these symmetric components when positioned on the axis of symmetry, the high correlation values there can be understood without assuming that "the sound source region is fairly well confined near the jet axis". In this case the on-axis probe seems to best monitor the cause.

At higher angles from the axis the sound may be due to higher-order azimuthal source components. These, however, can't be traced on the axis. Hence, though Figure 16 shows considerable correlation coefficients on the axis, the optimum values (up to 0.357) are obtained with the probe in the mixing region. It is particularly interesting to note that correlations with probes on opposite sides of the jet have opposite signs, thus indicating a dominant first azimuthal source component or "snake-like" jet instability as pointed out by Meecham and Hurdle.

Concerning the effect of vortex shedding and attendant dipole radiation (when the probe is within the jet's potential core) may I ask whether there are reasons to suspect this of dominating the correlations other than that of the high degree of correlation itself? I, nevertheless, agree that large correlation coefficients are at variance with a model in which thousands of eddies contribute to the far-field noise.

Finally, did the author make sure that the rectangles in Figures 15 and 16 could be taken as something like independent eddy volumes, and how did they consider the fact that Q_i is negative in some regions when performing the summation $\Sigma Q_i V_i$ in Table 1? Also, did the authors find that filtering of the pressure signals may increase the correlation coefficients (a phenomenon which was reported in Reference 16)?

Prof.Meecham: The proposals involving Michalke's discussion of sources seem possible to us. The remarks concerning on and off-axis measurements of the sources are consistent with Michalke's discussion. We do like the physical view which we proposed of course; the idea that the lower frequency, higher-intensity sound (observed at smaller angles to the jet axis) originates in the unstable region at the end of the potential core seems to us appealing. And we also like the physical idea that the higher frequency sound observed at larger angles originates in the mixing layer, as our measurements may seem to suggest. There no doubt are other viewpoints which lead to this physical model.

Concerning the evidence for dipole sound from the probe: we feel that when the probe is within the potential cone, and in particular when the probe is very near the exhaust exit, such dipole sound is important within the radiated sound field. For reasons outlined within the body of the work we feel that such sound is unimportant when the probe is outside the potential core.

From our viewpoint the rectangles referred to need not be centered on independent eddy volumes (see Equation (15) and related remarks). The negative values of Q_i were not of importance in calculating Table 1. We did not do much work with filtered signals, but do believe that such filtering could enhance the correlation coefficients.

SOME EXPERIMENTAL OBSERVATIONS OF THE REFRACTION OF SOUND BY ROTATING FLOW

by

G F Butler, T A Holbeche and P Fethney
Aerodynamics Department, Royal Aircraft Establishment,
Farnborough, Hampshire, England GU14 6TD

SUMMARY

Some experimental and theoretical studies of the interaction of sound with a rotating flow-field in the form of an aerodynamic vortex are described.

The experiments were carried out in the acoustically-treated working-section of the RAE 24-foot diameter open-jet wind tunnel. Vortices were generated by setting a sharp-edged slender wing at incidence in the tunnel airstream and the effect of the vortex flow downstream of the wing trailing-edge on the noise propagating from a small loudspeaker source was investigated over a range of sound frequencies and wind speeds.

Considerable refractive redistribution of the sound energy by the vortex flow occurred, leading to far-field regions of markedly decreased and increased sound intensity. Qualitatively, these effects are consistent with the predictions of ray theory, although the interaction persisted down to frequencies where ray theory might be regarded as inapplicable.

Some possible reasons for the observed differences with theory are briefly discussed.

1 INTRODUCTION

Refraction becomes of considerable importance in the propagation of sound whenever the ray bending, caused by velocity and temperature gradients in the medium is great enough to produce a significant redistribution or redirection of the sound energy. Some familiar practical illustrations of marked sound refraction effects which can occur in the atmosphere may be recalled: the occurrence of sonic booms only within a ground corridor of finite width (about 60 km), the inaudibility of thunderstorms beyond a certain critical distance, the occurrence of zones of silence around intense explosions on the ground, and the noticeable noise reductions which occur near the ground on a hot, sunny day.

Significant ray bending can also occur within rotating flows typified by a vortex or an eddy and in this paper the results of some recent studies at the RAE into this interesting phenomenon are presented. The effects observed may well have some eventual practical application to the reduction of aircraft noise. Vortices are always produced by aircraft in flight and situations can occur, particularly for rear-engined aircraft, where noise from the engines may propagate through a vortex (or vortex system), originating at the wing trailing-edge, before reaching an observer on the ground. The possibility that vortex refraction might be responsible for the somewhat lower than expected levels of sideline noise that have been reported for these aircraft configurations was suggested, in fact, a few years ago.

Sound propagation through rotating flows having concentrated vorticity has been considered theoretically by several authors (1, 2, 3, 4) for situations when the sound wavelength is much smaller than the length scale of the flow so that ray theory can be applied. In Ref (5) a wave equation approach, which avoids the above restriction, was applied to the analogous problem of the scattering of a plane sound wave passing through a single vortex of finite radius. Lindsay (1) examined sound rays travelling through a potential vortex, while for a cylindrically-stratified velocity field, both Cooke (2) and Salant (3) derive a simple differential equation for the path of a sound ray through a vortex.

The geometry and differential equation for the ray-path in polar coordinates are shown in Fig 1. Also shown is a reminder that at any point, the ray vector, which is the direction of energy propagation, is formed from the vector sum of the wave normal ($\underline{n}$) and flow velocity ($\underline{V}$).

Although this differential equation can be solved exactly for ray paths in particular flow fields, we can illustrate the general effects of sound propagation through rotating flow with some results due to Georges (4) who applied a ray-tracing computer program to calculate the paths through a potential vortex with a viscous core. The azimuthal velocity as a function of vortex radius is shown in Fig 2 and ray paths for plane waves travelling through such a vortex are shown in Fig 3 for two values of the maximum velocity V_{max}. (The circle of arrows indicates the radius of maximum velocity.) It can be seen that the outer potential flow apparently has little effect on the ray paths, but that the viscous core refracts the sound rays strongly in the direction of rotation, with greater bending the greater the value of V_{max}. The important implication of this ray bending is that sound energy is redistributed to give a region of intensification where rays converge and one of reduced intensity where the rays diverge. Whilst it is difficult to trace individual sound rays experimentally, changes of sound intensity can be measured, so that the prediction of the redistribution of energy provides a test for the validity of ray theory with a given vortex structure.

2 EXPERIMENTAL STUDIES

Some preliminary experimental investigations of the interaction of sound with the leading-edge vortex produced by a sharp-edged slender delta wing at incidence have been carried out in the acoustically-treated 24-foot low-speed open-jet wind tunnel at RAE Farnborough (6) and were reported earlier (7). The working-section boundary walls of this tunnel, Fig 4, have been lined with sound-absorbing material to render it suitable for acoustic experiments. Tone-burst tests, Figs 5 and 6, have shown that negligible reflections occur above about 1 kHz with a 7½ cm thick layer of polyether foam material on the walls. With the

addition of acoustic wedges (30 cm long) reflections do not become significant down to about 200 Hz. Ref (6) includes a more general discussion of acoustic considerations applying to noise testing in subsonic wind tunnels, as well as some further information on the tunnel acoustic environment.

The reasons for using a delta wing at incidence in this work are principally that a stable, strongly-rotating flow-field is easily produced, whose properties are reasonably well-defined. The regions of increased and decreased sound intensity were clearly detected (7), but a detailed interpretation of the results was made difficult because of acoustic interference effects produced by reflections from the wing surface.

These difficulties arising from the reflected sound field were overcome in the present work by mounting the sound source behind the delta wing, so that the sound travelled through the rotating flow downstream of the trailing edge. However, in this region, although no acoustic interference effects arise, the flow structure starts to become modified by bound vorticity shed from the wing, which gives rise to an additional vortex from the trailing-edge rotating in the opposite sense. This can be seen from Fig 7 where the formation of vortex sheets behind a lifting slender delta wing is illustrated. Near the trailing-edge, however, the leading-edge vortex is the stronger and remains a principal feature of the flow. The refractive effect of the secondary vortex system is relatively small.

The experimental arrangement is shown in Fig 8. The delta wing, which had a 70° leading-edge sweep and 1.53 m chord, was supported from a central pillar, with the loudspeaker source mounted on a support from the model so that sound transmitted through the trailing vortex system would be detected by the travelling microphone. The latter was a '$\frac{1}{2}$-inch' Brüel and Kjaer Type 4133 free-field microphone fitted with a 'nose cone' Type UA 0386. The source and microphone were arranged to be in the same plane perpendicular to the free-stream direction. The loudspeaker (Goodmans miniature horn-type) was excited with a third-octave sample of white noise, and the signal from the microphone was filtered to the same bandwidth to reduce the intrusion of broadband tunnel background noise. The sound pressure level was recorded on a Brüel and Kjaer level recorder Type 2305 which was synchronised with the microphone traverse system. The third-octave sound pressure levels in digital form were also displayed on a General Radio "Real Time" Analyser set up in parallel with the level recorder system.

In the earlier experiments (7), the angle of incidence of the delta wing, the wind speed and the sound frequency were varied to test both the effect of vortex strength and wavelength parameter ka. In the present series it was decided to dispense with the incidence variation and to consider a more extensive range of frequencies. Accordingly, the incidence was set at 15° and by using two loudspeakers (one for frequencies greater than 3 kHz, one for frequencies less than 4 kHz), a total of fourteen third-octave bands from 800 Hz to 16 kHz was covered. The wind speed was varied over the range zero to 36 m/s in steps of 12 m/s, corresponding to a free stream Mach number increment of 0.035, and non-dimensional azimuthal velocities in the vortex (V_{max}/c) of approximately 0.025, 0.05 and 0.075 respectively (8) at the three values of tunnel wind speed used. The microphone was traversed over a distance of about 2.5 m to give an angular range (ϕ) of approximately 40° at the source (Fig 8).

For each frequency and wind speed a traverse was also made with no signal fed to the loudspeaker in order to determine the level of the tunnel background noise in the particular third-octave band of interest. In general, the tunnel noise was much weaker than the signal from the loudspeaker except at the highest wind speed when at frequencies below 2 kHz the tunnel noise was intrusive. The tunnel background noise spectrum at a wind speed of 30 m/s is illustrated in Fig 9.

Measurements were taken with the loudspeakers at two stations downstream of the trailing edge (0.25 m and 0.5 m) in order to look for differences produced by the development of the secondary vortex. A few traverses were also made with the wing at zero incidence (when no leading-edge vortices are produced) to show that the effects observed were associated with the rotating flow and not due to some unexpected feature of the free-stream flow or its interaction with the source. This aspect was investigated thoroughly in the previous tests (7), when it was shown that there was very little change (less than 1 dB) in the sound field with the wing at zero incidence as the wind speed was increased. This conclusion was confirmed by the present investigation.

Time considerations did not allow us to make actual measurements of the flow rotational velocity downstream of the trailing-edge in parallel with the acoustic tests, but a simple flow visualisation technique (a photograph of the track of a small light tethered paper cone) was used to demonstrate the presence of two contra-rotating vortices in the wake and to determine the approximate location of the vortex centres. Fig 10 shows the traces of the cones in the plane of the loudspeaker and microphone traverse and it can be seen from this that whilst the leading-edge (primary) vortex still dominates the flow, the trailing-edge (secondary) vortex is by no means negligible and may have some effect on the sound rays. This possibility will be discussed later in Section 4 where the experimental results and theoretical predictions are compared.

3 THEORETICAL MODEL

In this section, ray theory is used to predict the effect of the leading-edge vortex on the sound intensity distribution. The flow field of a leading-edge vortex consists of an inner viscous core, an outer core formed by a rolled-up vortex sheet and an outer inviscid flow. Measurements made in such a vortex (8), shown in Fig 11, indicate that within the outer core region, the azimuthal velocity, V_θ, shows only small variation with radius and that the diameter of the inner viscous core is less than 10% of the diameter of the outer core. This suggests that a flow model with V_θ = constant (see Fig 12) will be suitable for calculating the ray paths, except for rays which pass very close to the centre of the vortex. For such a velocity field, the ray equation given in Fig 1 may be integrated exactly to yield the following expression for the ray paths:

$$\theta = \pm \left\{ V \alpha \operatorname{sgn} \bar{V} + \frac{2}{(1 - V^2)^{\frac{1}{2}}} \tan^{-1} \left[\frac{e^{\alpha} + \operatorname{sgn} \bar{V} V}{(1 - V^2)^{\frac{1}{2}}} \right] \right\} + K \qquad (1)$$

where $V = V_\theta/c$ is the non-dimensional azimuthal velocity,

c = the velocity of sound,

$\bar{V} = r A - V$

$\alpha = \cosh^{-1} (| \bar{V} |)$,

r, θ are defined in Fig 1,

and A, K are constants for a particular ray.

A is given in terms of the initial slope of the ray by

$$A = \frac{-V}{1 - V^2} \pm \left\{ (1 - V^2) \left[1 + (1 - V^2) \left(\frac{dr}{d\theta} \right)_0^2 \right]^{\frac{1}{2}} \right\}^{-1}$$

and K is determined from the condition that $\theta = 0$, $r = 1$ at the source.

Equation (1) is valid up to the point of closest approach of the ray to the vortex centre. After this point, the path is the mirror image of that before the turning-point.

Ray paths given by equation (1) are shown in Fig 13 for $V = 0.05$ over the region $r < 1$. Regions of ray focusing and divergence are clearly indicated. The corresponding sound intensity distributions at $r = 1$ are shown in Fig 14 for $V = 0.01$, 0.03 and 0.05. The sound intensity is calculated by considering an initially uniform distribution of rays and comparing the number of rays which arrive in a given angular segment with and without the vortex present.

4 COMPARISON OF EXPERIMENTAL RESULTS WITH THEORETICAL MODEL

Some experimental sound-intensity distributions obtained with third-octave bands of white noise centred at 12.5 kHz and 3.15 kHz are shown in Figs 15 and 16 respectively. The source position was 25 cm downstream of the trailing edge, and the measured sound levels for no wind and at each of the three test wind speeds are compared. The horizontal scale gives the angular position of the microphone (ϕ) relative to the line from the source through the estimated primary or secondary vortex centre. The radius of the primary region of rotating flow is approximately 15 cm giving non-dimensional wave numbers, ka, of about 9 and 35 at 3.15 kHz and 12.5 kHz respectively.

The regions of increased and reduced sound intensity can be seen clearly, being particularly marked at the highest test frequency band with a maximum reduction of about 9 dB and a maximum increase of about 6 dB. The effect of the flow becomes more pronounced as wind speed increases (ie greater rotational velocity in the vortex) and less pronounced as the frequency of the sound is decreased (ie when the wavelength of the sound approaches the length scale of the flow-field). Similar trends were observed in the results obtained with the sound source 50 cm downstream of the wing trailing edge.

Qualitatively the agreement between the theoretical (Fig 14) and experimental results (Figs 15 and 16) is quite good insofar as the regions of maximum decrease and increase of intensity move to the left as the azimuthal velocity increases. However, there are some differences in detail and, in order to offer some possible explanations for this, the data of Figs 14 and 15 will be discussed, since the experimental data at the higher frequency is likely to be more relevant to the predictions of ray theory.

First of all, one may consider the possible qualitative effects of the secondary (trailing-edge) vortex on the sound intensity distributions of Fig 15. Based on the theoretical results of Fig 14, one may assume that over the region of reduced sound intensity, the primary (leading-edge) vortex gives the smooth variation shown by the dotted curves in Fig 15b and c. The secondary vortex is weaker than the primary and, as a first approximation, its effect will be similar to that of a (primary) vortex system having a lower azimuthal velocity (such as Fig 15a). Also, since the secondary vortex rotates in the opposite sense, the rays will be bent towards the right and the positions of the regions of amplification and attenuation will be reversed. Qualitatively, this corresponds very well with Fig 15, where the shaded area represents the suggested effect of the secondary vortex. A comparison of Fig 15b and c shows further that while an increase in V is diverting the primary pattern to the left, the suggested secondary effect is diverting its pattern to the right, a result which is consistent with the preceding argument.

Although the theoretical curves of Fig 14 were chosen so that the regions of increased and decreased sound intensity would coincide approximately with the experimental data of Fig 15, the values of V in Fig 14 turn out to be lower than the corresponding values in Fig 15. There are probably two reasons for this. First, the theoretical model does not represent the experimental situation exactly in that the region of constant velocity is estimated to be $r \leq 0.3$ in the experiments compared with $r < 1.0$ for the theoretical calculation. The ray bending which causes the major part of the redistribution of energy is found to take place very close to the centre of the vortex, and the outer part of the flow simply has the effect of diverting this pattern further to the left.

Secondly, the basic assumption of ray theory is that the sound wavelength is extremely small. This implies that with sound of finite wavelength at acoustic frequencies, the interaction with the vortex flow will not be complete and consequently the rays will be refracted less than predicted by ray theory. A comparison

of Figs 15 and 16 shows that at the lower frequency of 3.15 kHz (Fig 16), the redistribution of sound energy is less marked than at 12.5 kHz (Fig 15), although the size of the vortex region (diameter ~ 30 cm) is of course unchanged. Experiments were carried out at frequencies down to 800 Hz, but it was found that below about 2 kHz (wavelength ~15 cm) the vortex was having very little effect, the difference between the intensity patterns at zero and maximum wind speeds being less than 1 dB.

In conclusion, a brief comment is made on the second region of reduced intensity which appears on the extreme left of Fig 15 a and b. This is believed to be an interference effect caused by the convergence of rays of finite wavelength - the intensity calculations leading to Fig 14 did not take the phase of the converging rays into account.

5 REFERENCES

1 R B Lindsay Compressional wave-front propagation through a simple vortex. J. Acoust. Soc. Amer. Vol 20 (1948), pp 89-94.

2 J C Cooke The refraction of sound by a vortex. RAE Technical Report 67175 (1967)

3 R F Salant Acoustic rays in two-dimensional rotating flows. J. Acoust. Soc. Amer. Vol 46 (1969) pp 1155-1157.

4 T H Georges Acoustic ray paths through a model vortex with a viscous core. J. Acoust. Soc. Amer. Vol 51 (1972) pp 206-209.

5 E-A Müller and K R Matschat The scattering of sound by a single vortex and by turbulence. Technical Report of the Max-Planck-Institut für Strömungsforschung. Göttingen (1959).

6 T A Holbeche and J Williams Acoustic considerations for noise experiments at model scale in subsonic wind tunnels. RAE Technical Report 72155 (1972). See also AGARD Report 601 Paper 8 (1973).

7 E G Broadbent, T A Holbeche and G F Butler Interaction of a vortex core with acoustic radiation. RAE Technical Memorandum Aero 1462 (1972) (also paper presented at Euromech 34, Göttingen September 1972).

8 P B Earnshaw An experimental investigation of the structure of a leading-edge vortex. Aeronautical Research Council London. Reports and Memoranda No 3281 (1962).

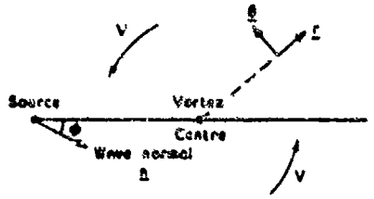

Fig.1a Geometry for refraction by rotating flow

$$\frac{r\,d\theta}{dr} = \frac{1+V(rA-V)}{\pm\left[(rA-V)^2-1\right]^{\frac{1}{2}}}$$

Where $A = V_0 + \frac{1}{\sin\phi}$

V_0 = Flow velocity at the source (non-dimensional)

Fig.1b Differential equation for ray path in cylindrically-stratified flow

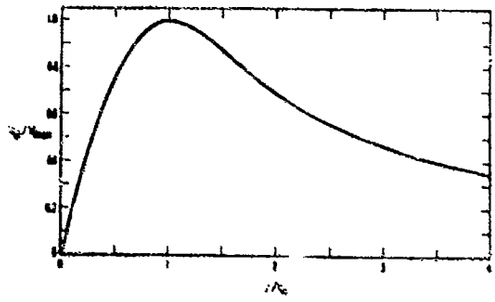

Fig.2 Velocity field of potential vortex with viscous core (after Georges[4])

$V_{max}/C = 1/20$

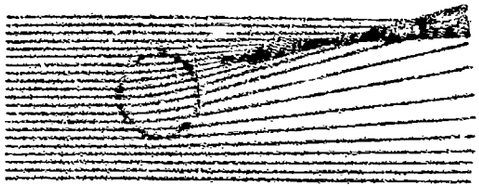

$V_{max}/C = 1/10$

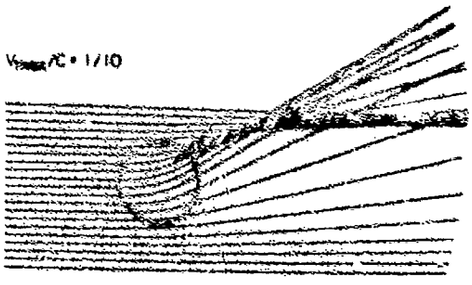

Fig.3 Acoustic ray paths through a viscous vortex (after Georges[4])

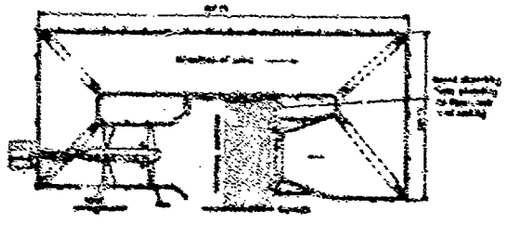

Fig.4 Details of 3.0ft wind tunnel at RAE Farnborough showing partial acoustic treatment

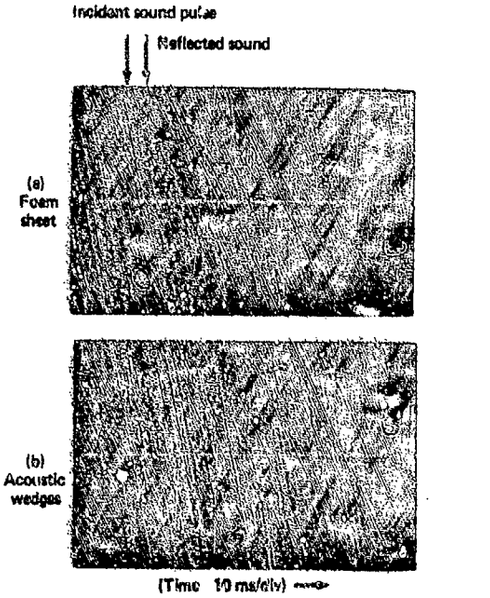

Fig.5 Sound reflection effects with tone bursts in acoustically-treated working section of 24ft wind tunnel

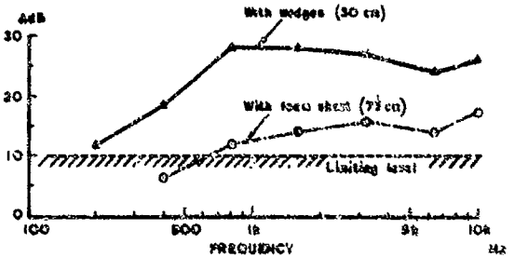

REFLECTION TESTS : 24 ft TUNNEL

Fig.6 Variation of ratio of incident/reflected sound pressure level (Δ) with frequency at measuring position in tunnel working section

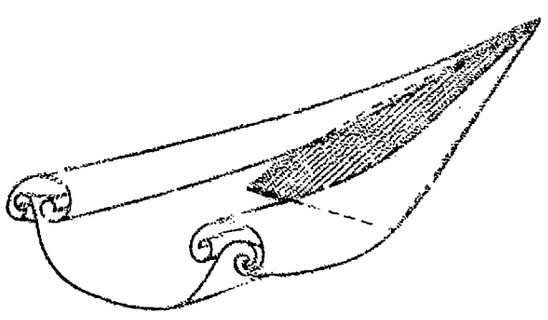

Fig.7 Model of the flow past a lifting aerofoil wing (after P.L. Maltby)

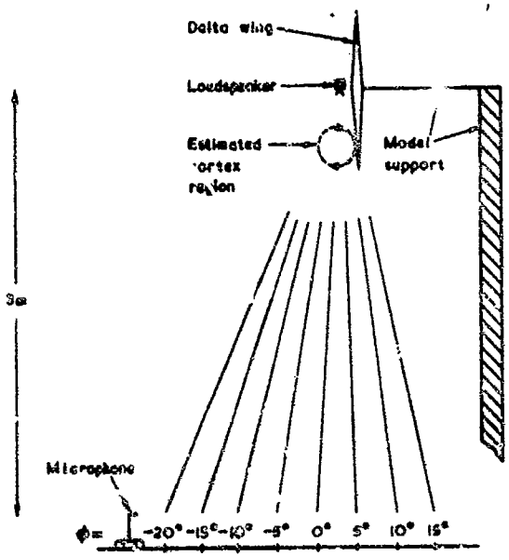

Fig.8a Configuration for vortex refraction experiments

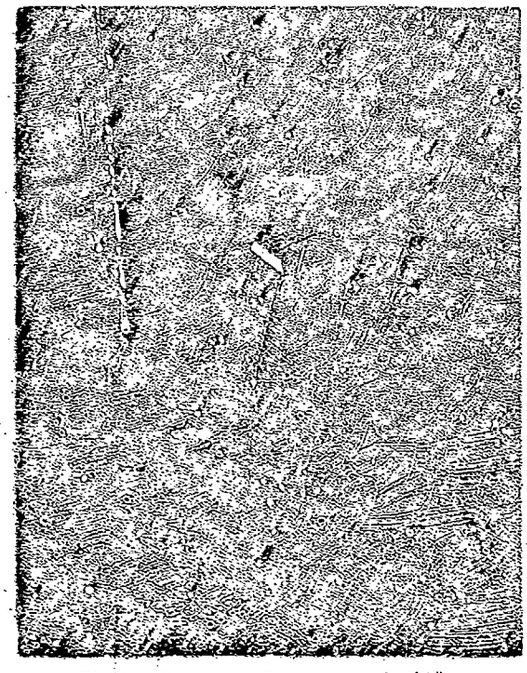

Fig.8b Experimental arrangement in RAE 5ft wind tunnel

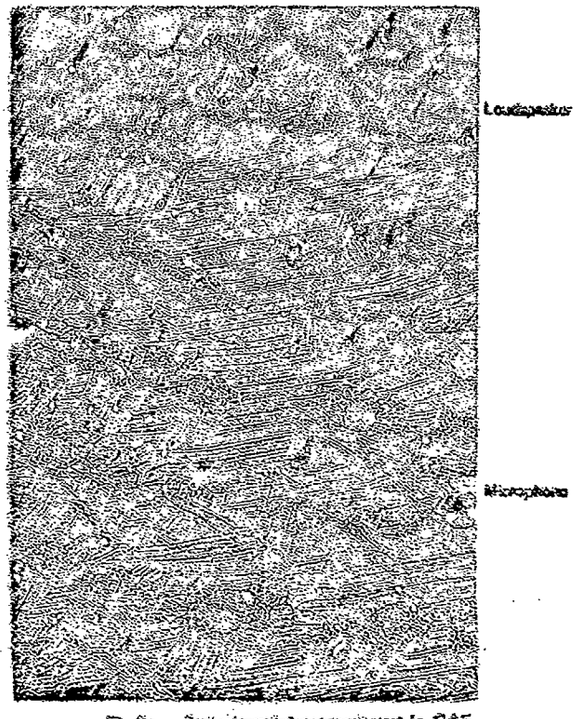

Fig.8c Experimental arrangement in RAE 5ft wind tunnel

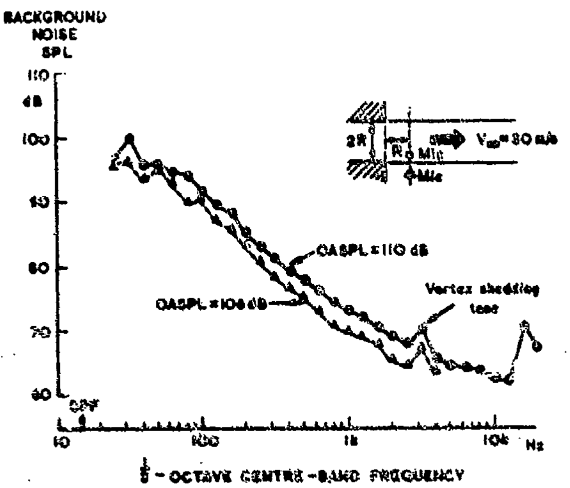

Fig.9 Spectrum of background noise in 24ft tunnel at a wind speed of 30 metres/second (~100 ft/s)

Fig.10 Visualisation of the leading-edge and trailing-edge vortices formed behind the delta wing at incidence

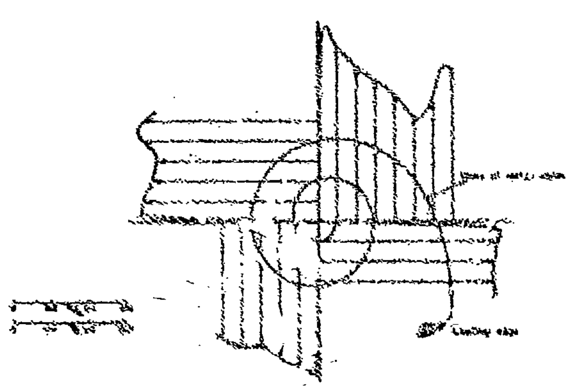

Fig.11 [illegible] of [illegible] velocity with swirls in five quadrants (after Earnshaw[8])

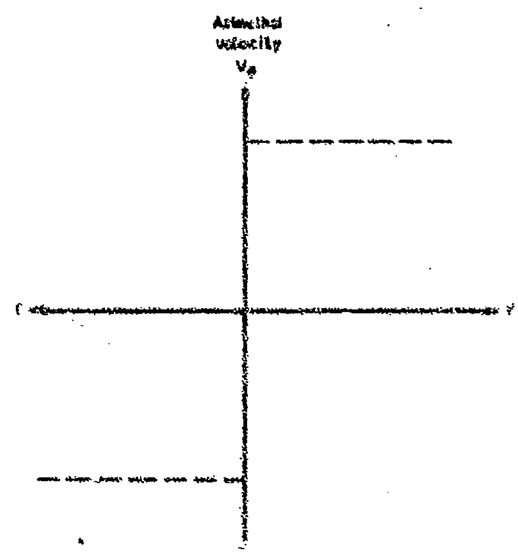

Fig.12 Simplified model of the flow field of a leading-edge vortex

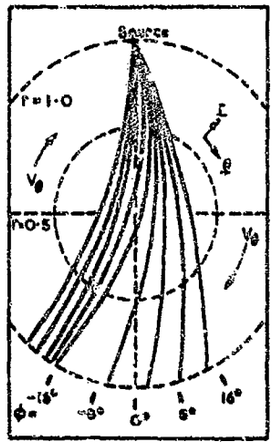

Fig.13 Ray paths through a rotating flow with constant azimuthal velocity

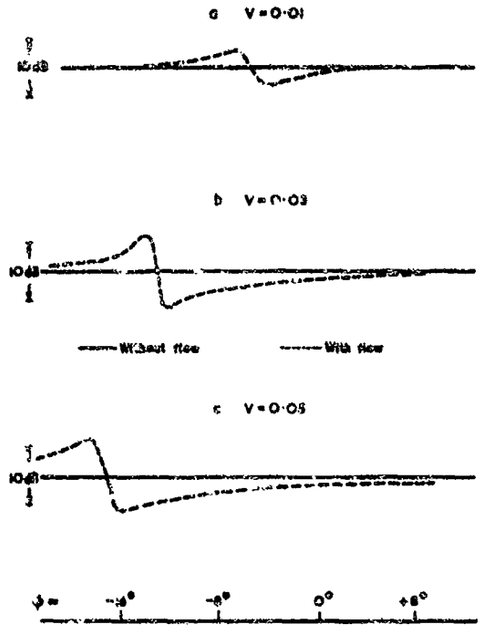

Fig.14a-c Refraction by a vortex with constant azimuthal velocity: theoretical results (ray theory)

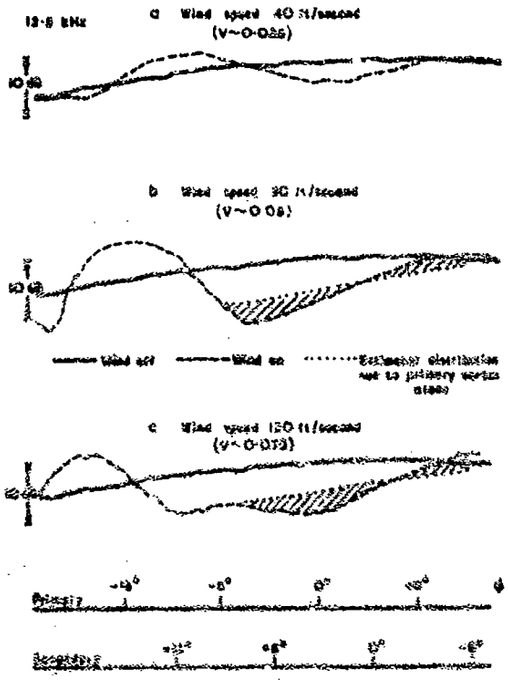

Fig.15a-c Refraction by the vortex system downstream of the trailing edge of the delta wing at incidence: experimental results at 12·5 kHz

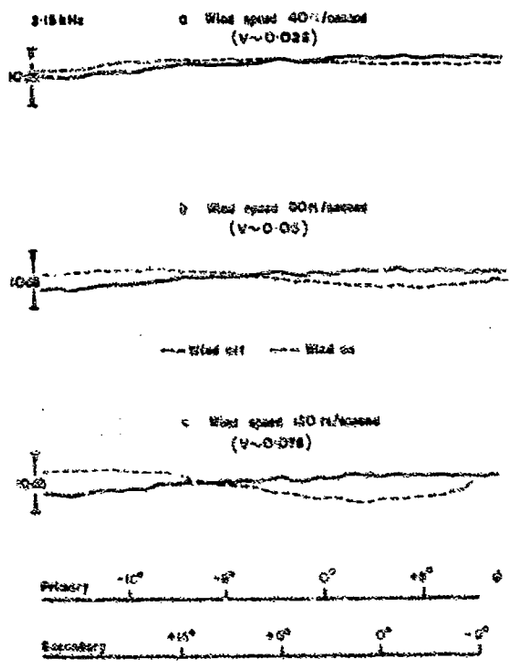

Fig.15a-c Refraction by the vortex system downstream of the trailing edge of the delta wing at incidence: experimental results at 3·15 kHz

DISCUSSION

Dr Dinkelacker: I would like to mention that at the Max-Planck-Institut für Strömungsforschung in Göttingen extensive theoretical and experimental work has been done on scattering of sound by vortices and turbulence. References on this work can be found in a paper by D.W.Schmidt and P.Tilmann in the Journal of the Acoustical Society of America (1970).

THE ISSUE OF CONVECTIVE AMPLIFICATION IN JET NOISE

Ramani Mani
Mechanical Engineering Laboratory
General Electric Research and Development Center
Schenectady, New York 12301

SUMMARY

The present study considers three problems of the sound power and power spectrum produced by moving acoustic sources shrouded by jet flows. The jets are assumed (for simplicity) to be characterized by a slug flow or top hat type mean velocity profiles. The sources are simple harmonic in their own frame of reference and are assumed to convect with the same velocity as the jet. The first problem considers the case of a monopole source convecting along the axis of a round jet. The second problem considers the case of convected line sources in a plane or two-dimensional jet. This is motivated by the need to understand the effect of off-axis lines of convection. The last problem is a variation of the first wherein the jet density and temperature are allowed to differ from those of the ambient. It is motivated by the need to understand the noise from heated jets.

The studies are all motivated by one notion, namely, that Lighthill's original idea of ascribing jet noise to convected sources radiating freely to the ambient needs revision to allow for mean flow "shrouding" effects. The studies explain several experimentally observed features of jet noise such as the failure to exhibit convective amplification (particularly at high frequencies and shallow angles to the exhaust axis) and associated failure of peak frequencies in the power spectrum to shift linearly with jet velocity. Implications for the jet density exponent issue for heated jets are also considered. The study may be regarded as moving source solutions to the Phillips equation for jet noise with a specific velocity profile, namely the top hat profile. The advantage of choice of a simple velocity profile is to obtain solutions valid for arbitrary frequencies.

1. INTRODUCTION

The Lighthill equation for aerodynamic noise for an inviscid gas, in the absence of mass, force or energy sources, may be written as:

$$\frac{\partial^2 \rho}{\partial t^2} - a_0^2 \nabla^2 \rho = \frac{\partial^2}{\partial x_i \partial x_j} (T_{ij}) \qquad (a)$$

where $T_{ij} = \rho u_i u_j + (p - a_0^2 \rho)\delta_{ij}$. A feature of (a) worth noting is that if we write $u_i = u_i' + U \delta_{1i}$ where U is uniform and steady, then we may show rigorously (using the continuity equation) that ρ satisfies:

$$(\frac{\partial}{\partial t} + U \frac{\partial}{\partial x})^2 \rho - a_0^2 \nabla^2 \rho = \frac{\partial^2}{\partial x_i \partial x_j} (T'_{ij}) \qquad (b)$$

where $T'_{ij} = \rho u_i' u_j' + [p - a_0^2 \rho]\delta_{ij}$. The simplicity of the stationary medium wave operator in (a) has been sacrificed in favor of the convected wave operator in (b) but an advantage has been gained in that the velocity dependent part of T'_{ij} is now $\rho u_i' u_j'$. Since the u_i' differ from u_i by the subtraction out of a steady uniform part $U \delta_{1i}$ it becomes plausible that the approximation of $(\rho u_i' u_j')$ by $(\rho_0 u_i' u_j')$ may be valid for such higher Mach numbers than the replacement of $(\rho u_i u_j)$ by $(\rho_0 u_i u_j)$. The jet noise problem is complicated by the fact that U itself varies (particularly in the transverse direction) but the transformation of (a) into (b) does serve to illustrate one of the motivations that has led investigators, most notably O. M. Phillips [1], to describe the aerodynamic sound generation problem in terms of a convected wave equation rather than a stationary medium wave equation. For example, the starting point of [1] is equation (2.8) of [1] wherein a convected wave equation is obtained for $\log(p/p_0)$ with a source term on the right hand side involving only velocity fluctuations.

The difficulty with the convected wave equation of the general type as developed by Phillips [1] is that it is very difficult to obtain general solutions to it. Studies with the Phillips equation as starting point generally employ an asymptotic, high frequency analysis thus rendering the analysis most suitable for high velocity jets. The present study is motivated by the need to develop solutions pertinent to lower frequencies (and hence lower jet velocities). For such lower frequencies, it seems permissible to approximate the true jet velocity profile by a slug flow or top hat type velocity profile jet.

There are two aspects of the presence of a mean flow that do receive explicit

recognition in Lighthill's work [2]. One is the recognition that transverse gradients of the mean flow could couple with gradients of the fluctuating flow to produce "shear noise". The other, more subtle effect of the flow (in view of the largely solenoidal nature of the u_i) is that the noise generation process is best ascribed to moving sources. It may be said that as important as Lighthill's recognition of the quadrupole order of jet noise was his recognition that the sources must be viewed in a convected frame of reference in order to preserve source compactness and in order not to artificially inflate the time rate of change of the turbulence (a frozen, subsonically convected pattern of turbulence radiates no sound). Peculiarly however this very insistence on use of convected sources led to a major difficulty of the theory because the effect of motion on the acoustic output of a source is to enhance its output, an effect described as "convective amplification". This led to a prediction that jet noise power could exhibit a higher than an eighth power dependence on jet exhaust velocity, a result never observed experimentally. Jet noise data show a very good eighth power dependence over a wide velocity range upto jet exit Mach numbers of 2.

Three good explanations have been given for the tenacity of the observed eighth power dependence. First (as proposed by Lighthill himself) it is experimentally observed that turbulence intensity (RMS turbulence level ÷ jet mean velocity) drops off somewhat as jet exit Mach numbers are raised. Second the finite eddy life time correction to Lighthill's moving source solutions of Pfowcs Williams and Ribner [3, 4] tends to reduce the radiative efficiency of the quadrupoles at higher jet velocities (and associated higher frequencies). Finally as pointed out by Ribner [5], Powell [6] and Csanady [7] the fact that the moving quadrupoles are embedded in fast moving fluid (with respect to which they are not moving at all) indicates that only limited convective amplification will occur - in fact at very high frequencies no convective amplification will occur.

Recent experimental evidence suggests that the last explanation is probably the most pertinent one. The reduction of turbulence intensity with increasing jet speed is experimentally found to be too small to effectively counterbalance the theoretically predicted convective amplification. Measurements by Davies, Fisher and Barratt [8] have shown that the finite eddy life time correction of Ribner and Pfowcs Williams cannot be significant for subsonic jet Mach numbers. Most importantly, recent careful jet noise experiments by Lush [9] lend strong support to the third explanation. Lush analyzed jet noise spectra at various angular positions in terms of a source frequency parameter (which corrects out the Doppler shift effect). He found that for off axis locations and for low enough values of the source frequency parameter, the predicted convective amplification does indeed occur. It is at shallow angles to the jet axis and for high values of the source frequency parameter that the convective amplification fails to occur. Such a detailed picture of jet noise can be shown to be fully compatible with the idea that the shrouding of a moving source by fast moving fluid inhibits convective amplification.

Three model problems, all involving the calculation of total power emitted by a monopole source convecting along the axis of a slug flow jet are outlined in this study. The source fluctuates in its own frame of reference at a source frequency ω_0.

2. FIRST MODEL PROBLEM (Figure 1)

Consider the problem of determining the sound field due to a fluctuating monopole point source translating at a uniform subsonic velocity Mc (where M < 1, M being the Mach number and c is the speed of sound). The source translates along the axis of a round jet whose velocity profile we assume to be a slug flow velocity profile. Also, the jet velocity is taken equal to that of the source. The problem is illustrated in Figure 1. The monopole source is assumed to have a time dependence in its own frame of reference of $q_0 \cos(\omega_0 t)$. The mean jet density and temperature are assumed to be the same as that of the ambient.

Analytically, we wish to determine an acoustic velocity potential ϕ which satisfies in region I (outside the jet)

$$\nabla^2\phi - \frac{1}{c^2}\phi_{tt} = 0 \tag{1}$$

and in region II (within the jet)

$$(1 - M^2)\phi_{xx} + \nabla_1^2\phi - \frac{2M}{c}\phi_{xt} - \frac{\phi_{tt}}{c^2} = \frac{q_0}{\rho_0}\cos(\omega_0 t)\delta(x - Mct)\delta(y)\delta(z), \tag{2}$$

where ∇_1^2 stands for the Laplace operator in the y - z plane. At the jet still-air interface, i.e., at r = a, we require (a) continuity of pressure, p, where

$$p = -\rho_0\phi_t, \qquad \text{in region I,} \tag{3}$$

and

$$p = -\rho_0(\phi_t + Mc\phi_x), \quad \text{in region II,} \tag{4}$$

and (b) continuity of radial acoustic particle displacement, say η, where

$$\phi_r = \eta_t, \qquad \text{in region I,} \tag{5}$$

and

$$\phi_r = \eta_t + M c \eta_x, \quad \text{in region II.} \tag{6}$$

An elegant procedure of solution suited to the above problem has been given by Morse and Ingard [10] and we follow closely their method of solution.

Let $\tilde{\phi}$, $\tilde{p}$, etc., denote the Fourier transforms with respect to time of the corresponding physical quantities. Thus

$$\tilde{\phi} = \frac{1}{2\pi} \int_{-\infty}^{\infty} \phi \, e^{j\omega t} \, dt \qquad j = \sqrt{-1} \tag{7}$$

and

$$\phi = \int_{-\infty}^{\infty} \tilde{\phi} \, e^{-j\omega t} \, d\omega.$$

Also, we write $\cos(\omega_0 t) = \frac{1}{2}[\exp(j\omega_0 t) + \exp(-j\omega_0 t)]$. The problem for the transforms is

$$\nabla^2 \tilde{\phi} + k^2 \tilde{\phi} = 0, \qquad \text{in region I,} \tag{1'}$$

$$(1 - M^2)\tilde{\phi}_{xx} + \nabla_2^2 \tilde{\phi} + 2jkM\tilde{\phi}_x + k^2 \tilde{\phi} = \frac{q_0 \delta(y)\delta(z)}{4\pi\rho_0 Mc}$$

$$\times \left[\exp\left(\frac{j(k - k_0)x}{M}\right) + \exp\left(\frac{j(k + k_0)x}{M}\right)\right], \qquad \text{in region II;} \tag{2'}$$

$$\tilde{p} = j\omega\rho_0 \tilde{\phi}, \qquad \text{in region I,} \tag{3'}$$

$$\tilde{p} = -\rho_0(-j\omega\tilde{\phi} + Mc\tilde{\phi}_x), \qquad \text{in region II;} \tag{4'}$$

$$\tilde{\phi}_r = -j\omega\tilde{\eta}, \qquad \text{in region I,} \tag{5'}$$

$$\tilde{\phi}_r = -j\omega\tilde{\eta} + Mc\tilde{\eta}_x, \qquad \text{in region II.} \tag{6'}$$

Let $\tilde{\phi} = \tilde{\phi}^+ + \tilde{\phi}^-$ and similarly for $\tilde{p}$ and $\tilde{\eta}$ where $\tilde{\phi}^+$ corresponds to the solution with the term $\exp(j(k - k_0)x/M)$ in equation (2') and $\tilde{\phi}^-$ to the term involving $\exp(j(k + k_0)x/M)$. Note that $k = \omega/c$, $k_0 = \omega_0/c$, etc.

Consider in detail the problem for $\tilde{\phi}^+$. Intuitively, it is clear that $\tilde{\phi}^+$, $\tilde{p}^+$, $\tilde{\eta}^+$ all have an x-dependence of the type $\exp(j(k - k_0)x/M)$. "Factoring" this dependence out, one is left with the following problem in the y - z plane:

$$\nabla_2^2 \tilde{\phi}^+ + k^{+2}\tilde{\phi}^+ = 0, \qquad \text{in region I;} \tag{8}$$

$$\nabla_2^2 \tilde{\phi}^+ + \kappa^{+2}\tilde{\phi}^+ = \frac{q_0 \delta(y)\delta(z)}{4\pi\rho_0 Mc}, \qquad \text{in region II;} \tag{9}$$

where

$$k^{+2} = \left(\frac{1 - M^2}{M^2}\right)\left[\left(\frac{k_0}{1 - M} - k\right)\left(k - \frac{k_0}{1 + M}\right)\right] \tag{10}$$

and is ≥ 0 only if $k_0^+ \geq k \geq k_0^-$, where $k_0^+ = k_0/1 - M$ and $k_0^- = k_0/1 + M$.

$$\kappa^{+2} = \frac{1}{M^2}\left[(\kappa_0^+ - k)(k - \kappa_0^-)\right], \tag{11}$$

where

$$\kappa_0^+ = k_0(1 + M), \quad \kappa_0^- = k_0(1 - M).$$

Also, let

$$\underline{\kappa}^{+2} = -\kappa^{+2} = \frac{1}{M^2}\,[(k - \kappa_0^+)(k - \kappa_0^-)]. \tag{12}$$

Note that

$$k_0^+ \geq \kappa_0^+ \geq k_0 \geq k_0^- \geq \kappa_0.$$

The fact that $\kappa^{+2} \geq 0$ only if $k_0^+ \geq k \geq k_0^-$ expresses the result that in the far field the moving source yields a frequency spectrum containing frequencies in the range $\omega_0/1 - M \geq \omega \geq \omega_0/1 + M$ which is what we expect from the Doppler shift formula. We restrict our attention to this range of k. The matching conditions for equations (8) and (9) are that, at r = a,

$$\tilde{\phi}^+(r = a^+) = \frac{k_0}{k}\,\tilde{\phi}^+(r = a^-) \qquad \text{(pressure matching conditions)}, \tag{13}$$

$$\tilde{\phi}_r^+(r = a^+) = \frac{k}{k_0}\,\tilde{\phi}_r^+(r = a^-) \qquad \text{(transverse particle displacement matching condition)}. \tag{14}$$

To solve equations (8), (9), (10), and (11) in the range $k_0^- < k < k_0^+$ and with restriction to outgoing waves at infinity, in the range $k_0^- \leq k \leq \kappa_0^+$ we assume, for $\tilde{\phi}^+$ in regions I and II,

$$\text{in I:} \qquad \tilde{\phi}^+ = A_I^+ H_0^{(1)}(k^+r)\exp\frac{j(k - k_0)x}{M}, \tag{15}$$

$$\text{in II.} \qquad \tilde{\phi}^+ = \left[A_{II}^+ J_0(\kappa^+r) - \frac{jq_0H_0^{(1)}(\kappa^+r)}{16\pi\rho_0Mc}\right]\exp\frac{j(k - k_0)x}{M}, \tag{16}$$

and if $\kappa_0^+ \leq k < k_0^+$, in region II,

$$\tilde{\phi}^+ = \left[A_{II}^+ I_0(\underline{\kappa}^+r) - \frac{q_0K_0(\underline{\kappa}^+r)}{8\pi^2\rho_0Mc}\right]\exp\frac{j(k - k_0)x}{M}. \tag{17}$$

(The form for $\tilde{\phi}^+$ in region I is independent of whether $k \geq \kappa_0^+$ or $k \leq \kappa_0^+$.)

Note that the change of sign κ^{+2} depending on whether $k \in [k_0(1 - M), k_0(1 - M)]$ is associated with the fact that if the jet in the present problem were of infinite radius (i.e., the moving fluid occupied all space) the Doppler shifted frequencies would range over $\omega_0(1 - M)$ to $\omega_0(1 + M)$. In other words, as is well known, there is a difference in the Doppler shift frequencies depending on whether the observer moves towards a source or whether the source moves towards the observer. This difference will be seen latter to play a key role in suppressing convective amplification at high frequencies.

Equations (15) and (16) or (15) and (17) may now be readily solved for A_I^+ and A_{II}^+ by using the matching conditions (13) and (14). Since we are interested in far field pressures far outside the jet, we only give the result for A_I^+:

(a) if $k_0^- < k < \kappa_0^+$,

$$A_I^+ = \frac{q_0k\,k_0\kappa^+[Y_0(\kappa^+a)J_1(\kappa^+a) - Y_1(\kappa^+a)J_0(\kappa^+a)]}{16\pi\rho_0Mc[k^2\kappa^+H_0^{(1)}(k^+a)J_1(\kappa^+a) - k^+k_0^2J_0(\kappa^+a)H_1^{(1)}(k^+a)]}\,; \tag{18a}$$

(b) if $\kappa_0^+ < k < k_0^+$,

$$A_I^+ = \frac{-qk\kappa^+k_0[K_0(\underline{\kappa}^+a)I_1(\underline{\kappa}^+a) + I_0(\underline{\kappa}^+a)K_1(\underline{\kappa}^+a)]}{8\pi^2\rho_0V[k^2\underline{\kappa}^+I_1(\underline{\kappa}^+a)H_0^{(1)}(k^+a) + k_0^2k^+I_0(\underline{\kappa}^+a)H_1^{(1)}(k^+a)]}\,. \tag{18b}$$

Equation (18) essentially completes the formal solution to the problem. The far field pressure and the radial acoustic velocity may be computed by using $\tilde{p} = j\omega\rho_0\tilde{\phi}$ and $\tilde{\phi}_r$. In this problem, every point on a cylindrical surface concentric with the jet experiences the same pressure time history. Morse and Ingard [10] have discussed thoroughly the problem of determining the power spectrum and total power radiated by the source and their concluding result is that the power spectral density extends over a frequency range $[\omega_0/(1 + M)] < \omega < [\omega_0/(1 - M)]$ and is given by

$$(16\pi\rho_0Mc\omega)|A_I^+|^2 = I(\omega). \tag{19}$$

The total power is given by

$$P = \int_{\omega_o/(1+M)}^{\omega_o/(1-M)} I(\omega)\,d\omega. \tag{20}$$

Actually Morse and Ingard [10] consider the case of a monopole point source convecting at Mc in free space, for which case

$$A_I^+ = \frac{-jq_o}{16\pi\rho_o Mc}, \tag{21}$$

and hence

$$I(\omega) = \frac{q_o^2\omega}{16\pi\rho Mc}, \qquad \text{for } \frac{\omega_o}{1+M} \le \omega \le \frac{\omega_o}{1-M}, \tag{22}$$

and the total power is

$$P = \frac{q_o^2\omega_o^2}{8\pi\rho_o(1-M^2)^2c}. \tag{23}$$

Thus, in the case of a convected monopole, the convective amplification is as $(1 - M^2)^{-2}$.

If we take the limit as $k_o a \to 0$ of equation (18), we find that A_I^+ tends to (independent of whether $k > \kappa_o^+$ or $k < \kappa_o^+$)

$$A_I^+ \to \frac{-jq_o\omega}{16\pi\rho_o Mc\omega_o}, \tag{24}$$

so that

$$I(\omega) = \frac{q_o^2\omega}{16\pi\rho_o Mc}\left(\frac{\omega}{\omega}\right)^2, \qquad \text{for } \frac{\omega_o}{1+M} \le \omega \le \frac{\omega_o}{1-M}, \tag{25}$$

and

$$P = \frac{q_o^2\omega_o^2(1+M^2)}{8\rho_o c\pi(1-M^2)^4}. \tag{26}$$

In the general case, A_I^+, $I(\omega)$ and P are given by equations (18a), (18b), (19) and (20), and specific results will be discussed in the following.

The total power emitted by such a source nondimensionalized by $[q_o^2\omega_o^2/8\pi\rho_o(1-M^2)^2c]$ and expressed in dB is plotted as a function of $(k_o a)$ and M in Figure 2.

Shown by single points on the extreme right in Figure 2 are points given by $20 \log_{10}(1 - M^2)$, being the correction if there were no convective amplification at all corresponding to Csanady's suggestion [7]. The portions of the curves corresponding to corrections > 0 dB indicate underestimates of convective amplification as estimated from a freely moving source model and conversely.

Clearly, such curves confirm the frequency dependent nature of convective amplification. The curves flatten as we move to the right and if we identify the point on each curve (for the different Mach numbers) at which the correction is within a decibel of the limit as $(k_o a) \to \infty$, one deduces that beyond a source Strouhal number $[(2f_o a)/Mc]$ of 0.5 there would be no significant convective amplification. Figure 15 of Lush's paper [9] indicates lack of convective amplification beyond $[2f_o a/Mc]$ of about 0.5.

Finally, we consider the implications with regard to Strouhal scaling of the results shown in Figure 2. As a starting point, in Figure 3 we show under the curve labelled M = 0.3, one-third octave intensities obtained by Lush [9] in Figure 8 of his paper for a jet Mach number of 0.37 at 90°. This curve is chosen as a base line because at that low Mach number of 0.37 and location (90° to jet axis) we expect little convective amplification effects. The abcissae are shown in Strouhal numbers, St = (2fa/Mc), and the ordinates are only relative decibel levels.

An intensity spectrum at 90° was chosen because, in addition to lack of convective amplification effects, the 90° location also provides a very good and clean measure of the intrinsic strength of the sources (their frequency distribution). This is because that location is largely characterized by "self noise". A basic assumption of the process used in deriving Figure 4 is that the frequency distribution of the "intrinsic source strengths" does follow Strouhal scaling with respect to velocity. This is, of course, excellently borne out by Figure 8 of reference [9] where Lush shows that, at the 90° location, Strouhal scaling with respect to velocity was obtained. The basic argument of what follows is to point out that the radiative efficiency of the sources is frequency

dependent and, being higher for the low frequencies than for the high frequencies, causes peak frequencies of the sound power spectrum to scale with velocity much slower than a first power (as is assumed in conventional Strouhal scaling). The particular low Mach number datum used to establish this result (taken in this case as the 90° intensity spectrum of Lush [9]) is not the main issue of this paper: a different datum would lead to the same qualitative conclusions. Ideally, perhaps, one would have to work out separately the "shear noise" and "self noise" portions of the power spectra.

The spreading of the source frequency due to the Doppler shift makes it a little difficult to apply Figure 2 directly. However, it can be shown that the Doppler spreading will be narrower than conventional moving source results would indicate [11]. Further, if we are interested in the sound power spectrum, it seems reasonable to apply Figure 2 to Figure 3 as follows. For each Strouhal number St and Mach number M, determine a source frequency parameter $k_0 a = St \cdot \pi M$ and then determine the decibel correction from Figure 2. Starting with the curve labelled M = 0.3, such a frequency dependent correction procedure was applied to derive the curve labelled M = 0.5, M = 0.7 and M = 0.9 from the curve labelled M = 0.3. As expected, one observes a shift back of the peak frequency (in terms of the Strouhal numbers) at which the sound power spectrum peaks. The spectra are pretty flat as is typical of jet noise but an attempt was made to estimate the peak Strouhal number as a function of jet Mach number and the results are shown in Figure 4. Undoubtedly by a purely fortuitous coincidence, the curve in Figure 5 is fitted very well by a relation of the type $(St)_p = (0.21)/M$. Since the Strouhal number itself is given by $(f_p D/V)$, Figure 5 suggests that the peak frequency in the sound power spectrum is independent of jet velocity being given (in the case of Figure 5) by $[(0.21)c/D]$. Such a tendency for the peak frequency to be independent of jet velocity has been noticed in several experiments.

The suggestion that emerges therefore is that the tenacious adherence of the total power to an eighth power law as well as the tendency of peak frequency of the power spectrum to be relatively insensitive to jet velocity are both manifestations of the same result indicated by Figure 2, namely the inhibition of convective amplification with increasing frequency and jet velocity.

3. SECOND MODEL PROBLEM (Figure 5)

In this case we study the acoustic output of a line acoustic source convecting at jet velocity in a plane slug flow jet. The problem is two-dimensional and this enables us to allow the line source to convect along a line displaced from the jet centerline by an amount σh. First of all we should note that the convection amplification factor for a freely moving line velocity source is $(1 - M^2)^{-3/2}$. Thus all the convection amplification factors shown in Figure 6 are in decibels with respect to $(1 - M^2)^{-3/2}$.

The convection amplification factor now depends on M, $k_0 h$ and σ. The interest in case of Figure 6 is really in how the results vary with σ in the range of $0 \leq \sigma < 1$. It is seen from Figure 6 that over a range of $(k_0 h)$ extending from 0.01 to 1.0 and Mach numbers ranging from 0.5 to 0.9 the convection amplification factors are relatively insensitive to σ. There is a slight variation (of order 1 dB or so) at the highest value of $(k_0 h)$ but basically we may interpret Figure 6 as indicating that the precise location of the line of source convection is unimportant. The physical explanation for this result appears to be that by and large what determines the convective amplification is the total extent of "shrouding" to which the moving source is exposed. This "total extent" is not different for asymmetric as contrasted to symmetric convection.

This model problem lends confidence to the notion that we may continue to use centerline source convection for the round jet problem at least as far as power estimates are concerned. It is hardly necessary to point out that using noncenterline source convection in the round jet problem would create considerable analytical complications owing to the ensuing lack of axial symmetry.

4. THIRD MODEL PROBLEM (Figure 7)

This model problem is similar to that of Figure 1 with the difference that now the jet density and speed of sound ρ_1 and c_1 are different from that of the ambient ρ_0 and c_0. However, we impose the condition that $\rho_0 c_0^2 = \rho_1 c_1^2$ to ensure that the static pressure inside the jet is the same as that of the ambient (this assumes that the specific heat ratio of the jet fluid is the same as that of the ambient). The mathematical formulation is similar to that for the first problem except that we have to constantly account for the differences in mean density and speed of sound inside and outside the jet. The details are too laborious to outline here and we confine ourselves to a discussion of the results.

As before we compute the nondimensional power $P' = [P \div \rho_0^2 \omega^2 / 8\pi\rho_0 c_0 (1 - M^2)^3]$ where now $M = V_1/c_0$. The principal types of calculations performed with this model are illustrated in Figures 8 - 10. We first fix a value of jet velocity $= V_1/c_0$. (In Figures 8, 9 and 10, three values of $M_0 = 0.5$, 0.7 and 0.9 are shown.) Now also fixing the value of the frequency parameter $(k_0 a)$ we compute the variation of the nondimensional power with (ρ_1/ρ_0) where (ρ_1/ρ_0) is allowed to vary from 0.3 to 1.0. Now this variation of the power with (ρ_1/ρ_0) is next fitted by a relation of type power $\sim (\rho_1/\rho_0)^{n'}$. The n' is determined by fitting the best straight line on a log-log plot of P' versus (ρ_1/ρ_0). The fitting is done by a least squares method.

The purpose of the above exercise is probably clear to the reader. We are trying to address ourselves to the so-called jet density exponent issue for the noise of heated jets. This is the question of how the acoustic power of a jet may be expected to vary with changing jet density at fixed jet velocity. Having derived η' from the calculations of P' as a function of (ρ_1/ρ_0), we note that since q_0 itself varies as ρ_1 (whether one uses the quadrupole or simple source approach to jet noise) the true variation of the power with (ρ_1/ρ_0) will be as $(\rho_1/\rho_0)^{\eta}$ where $\eta = \eta' + 2$.

In Figures 8 - 10, plots of η as a function of $[k_0 a/\pi M_0]$ are shown for $M_0 = 0.5$, 0.7 and 0.9. The Lighthill theory of jet noise [2] considers sources radiating freely into the ambient and hence picks up only the effect on power due to the effect of density on q_0. Thus [2] would predict $\eta = 2$ independent of jet velocity or frequency. The present results are more complicated showing η to be a function of jet velocity and frequency. (Note that $(k_0 a/\pi M_0)$ may be termed a source Strouhal number since it is $[\omega_0(2a)/2\pi V_J]$.)

These results are in fact in rough agreement with what is probably the best published experimental data on this subject, namely the work in [12]. To show this we have shown in Figures 11 and 12 some such comparisons. These figures are taken from [12] with points superposed from present work. In Figure 11, we show the empirically determined exponent η for the total power of a heated jet as a function of $M_0 = V_J/c_0$ by the SNECMA-NGTE study of [12]. To compare these results with those of the present study it is necessary to estimate a source Strouhal number. Based on the jet noise of low Mach number jets (where Doppler shift effects should be negligible) the dominant source Strouhal numbers may be estimated to lie between 0.5 and 0.6. The experimentally determined exponents for source Strouhal numbers of 0.5 and 0.6 are shown for $M_0 = 0.5$, 0.6, 0.7, 0.8, 0.9 and 0.95 are shown in Figure 11 and are seen to bracket the SNECMA-NGTE data quite well except for the case of $M_0 = 0.5$. A feature of the present theory is that it turns out that (taking the limit as $k_0 a \to 0$) at very low velocities, the exponent η is predicted to go to zero (i.e. no influence of jet density on jet noise power at fixed jet exit velocity). Several possible explanations for such discrepancies at the low velocity end suggest themselves. One is that experimentally it is most difficult to determine such exponents at the low velocity end since internal sources due to combustion could influence the jet noise measurement (it can be shown that such an effect will explain experimentally observed indices lesser than that predicted by a calculation procedure which considers only the jet noise). Secondly the present calculations do need extension to other order multipoles.

Figure 12 is simply taken out of [12] and shows that at a given jet exit velocity (subsonic) the effect of heating is to raise the low frequency portion of the power spectrum but to depress the high frequency end. This is in accord with Figures 8 - 10 where as marked, $\eta > 0$ corresponds to portions of the spectrum that will be lowered by heating the jet and vice versa.

In summary, all three model problems have been pursued with the notion that there may be purely acoustical explanations for several features of jet noise such as those of Strouhal scaling and the jet density exponent issue provided that we recognize that the sources do not radiate freely to the ambient but are subject to a shrouding or enveloping effect of their immediate ambient which is the mean jet flow.

This research has been partially supported under contract with the U.S. Air Force.

5. REFERENCES

1. Phillips, O. M., "On the Generation of Sound by Supersonic Turbulent Shear Layers," J. Fluid Mech., 9, pp. 1-28 (1960).

2. Lighthill, M. J., "Jet Noise," American Institute of Aeronautics and Astronautics Journal, 1, pp. 1507-1517 (1963).

3. Ffowcs Williams, J. E., "The Noise from Turbulence Convected at High Speed," Phil. Trans. Roy. Soc., A 255, pp. 469-503 (1963).

4. Ribner, H. S., "Aerodynamic Sound from Fluid Dilatations: A Theory of Sound from Jets and Other Flows," University of Toronto, Institute for Aerospace Studies, Rept. 86 (AFOSR TN 3430), 1962.

5. Ribner, H. S., "Energy Flux from an Acoustic Source Contained in a Moving Fluid Element and Its Relation to Jet Noise," J. Acoust. Soc. Amer., 32 (9), pp. 1159-1160 (1960).

6. Powell, A., "Concerning the Noise of Turbulent Jets," Journal of the Acoustical Society of America, 32, pp. 1609-1612 (1960).

7. Csanady, G. T., "The Effect of Mean Velocity Variations on Jet Noise," Journal of Fluid Mechanics, 26, pp. 183-197 (1966).

8. Davies, P. O. A. L., Fisher, M. J., and Barratt, M. J., "The Characteristics of the Turbulence in the Mixing Region of a Round Jet," J. Fluid Mech., 15, pp. 337-367 (1963).

9. Lush, P. A., "Measurements of Subsonic Jet Noise and Comparison with Theory," Journal of Fluid Mechanics, 46, pp. 477-500 (1971).

10. Morse, P. M. and Ingard, K. U., Theoretical Acoustics. New York: McGraw-Hill. See pages 728-732 (1968).

11. Mani, R., "A Moving Source Problem Relevant to Jet Noise," Journal of Sound and Vibration, 25, pp. 337-347 (1972).

12. Hoch, R. G., et al, "Studies of the Influence of Density on Jet Noise," presented at the First International Symposium on Air Breathing Engines, Marseille, France, June 19-23, 1972.

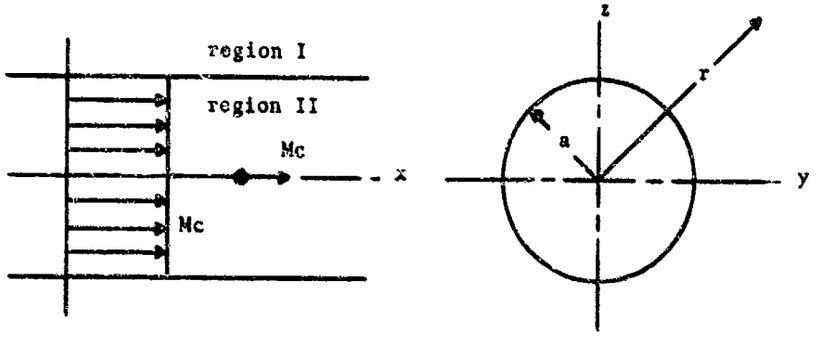

FIGURE 1. First Model Problem.

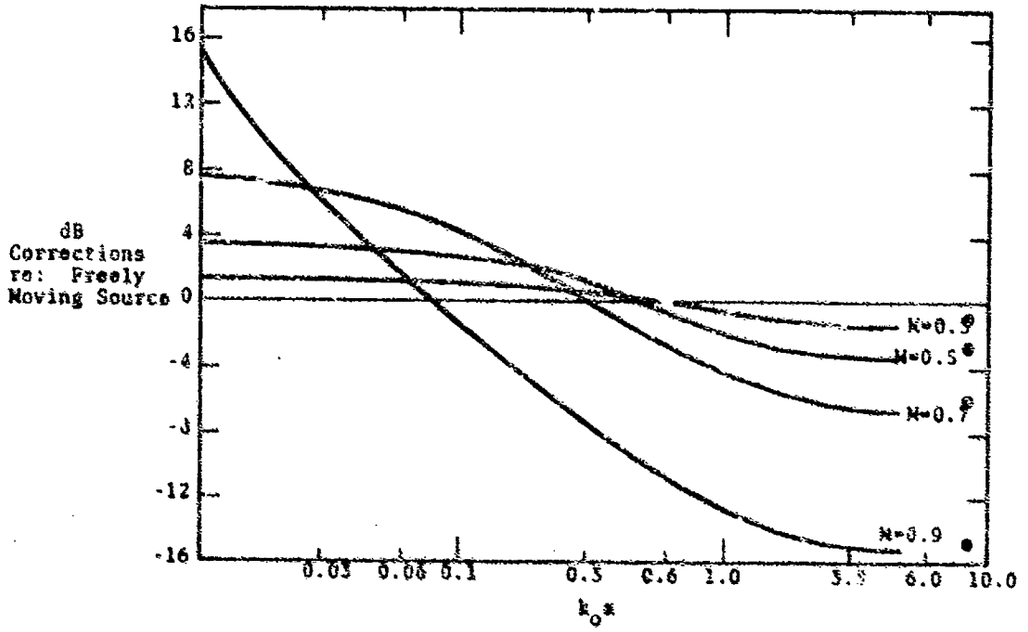

FIGURE 2. Corrective Amplification as Function of M and k_0a.

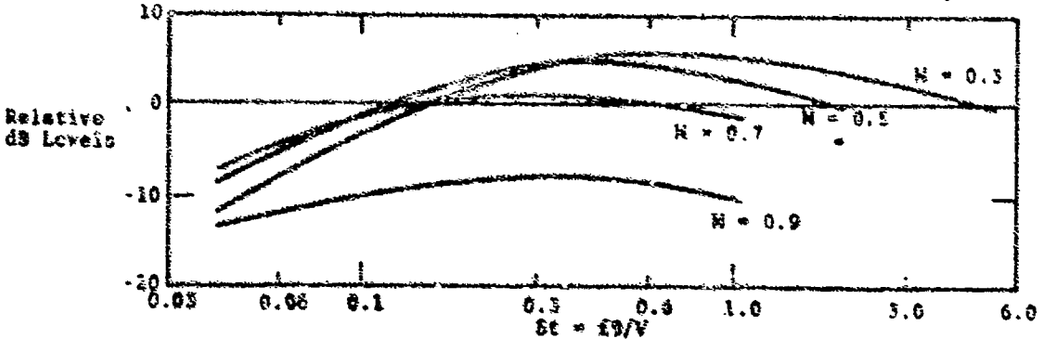

FIGURE 3. Implications for Spectral Scaling.

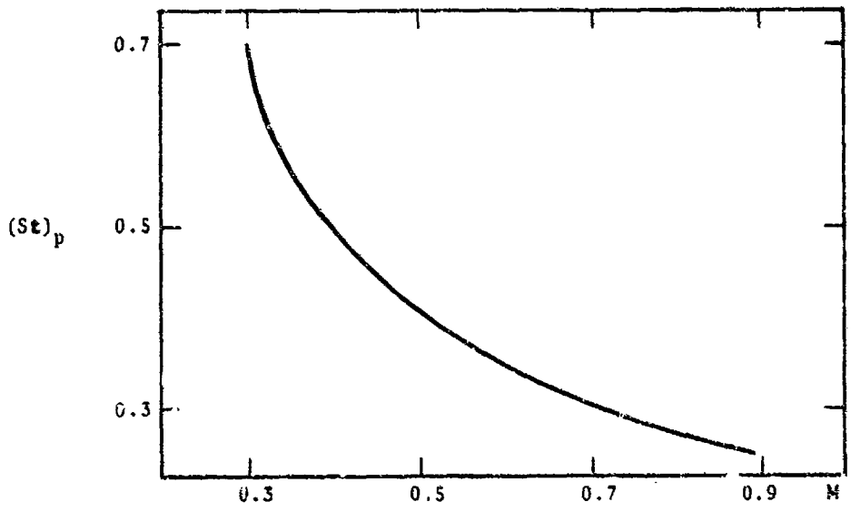

FIGURE 4. Peak Strouhal Number as Function of Jet Mach Number.

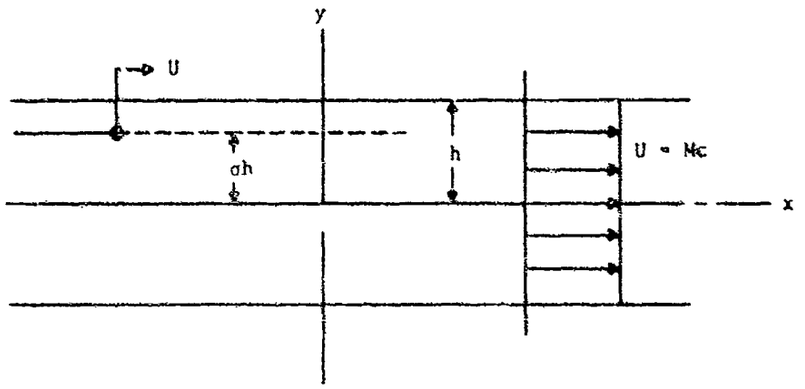

FIGURE 5. Second Model Problem.

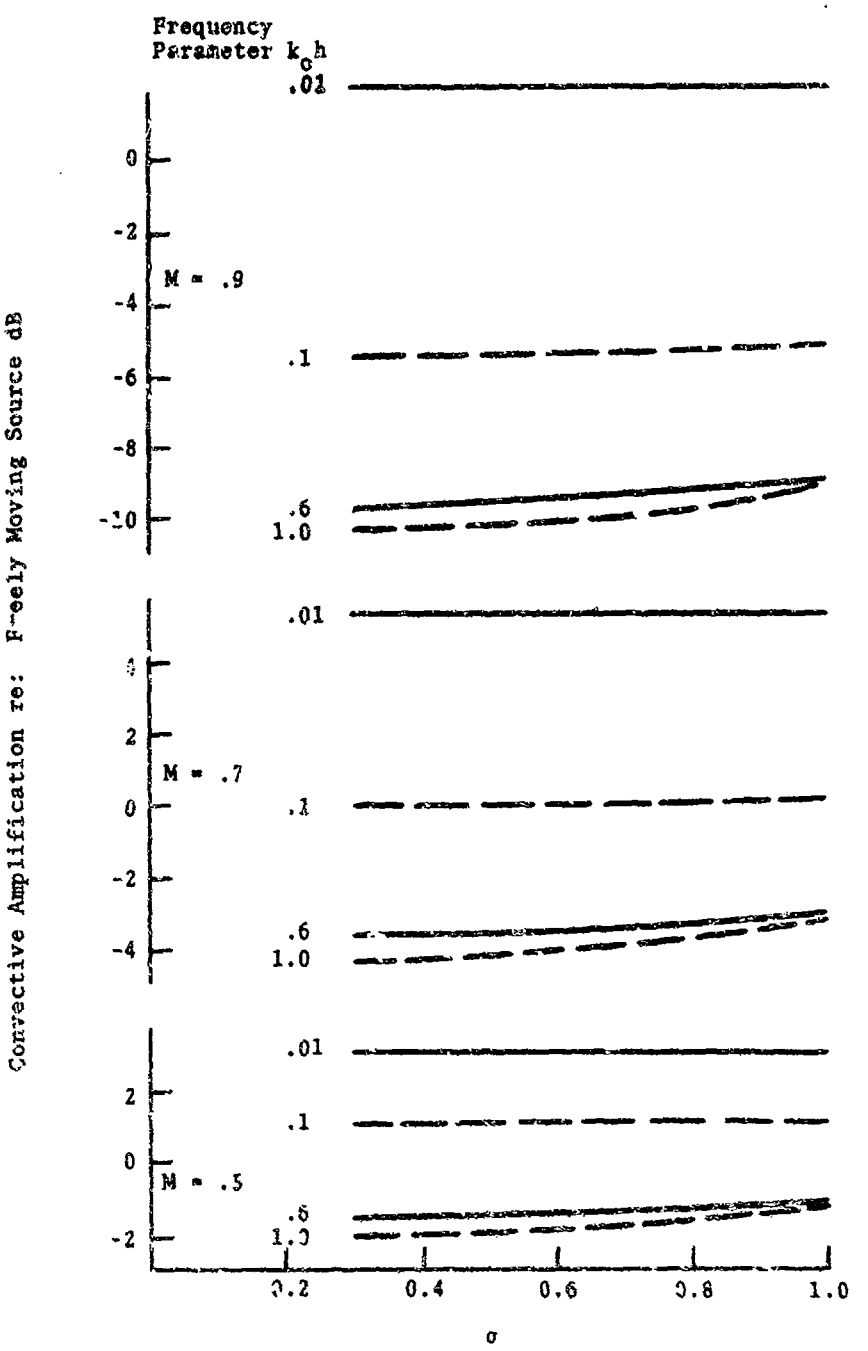

FIGURE 6. Results of Second Model Problem.

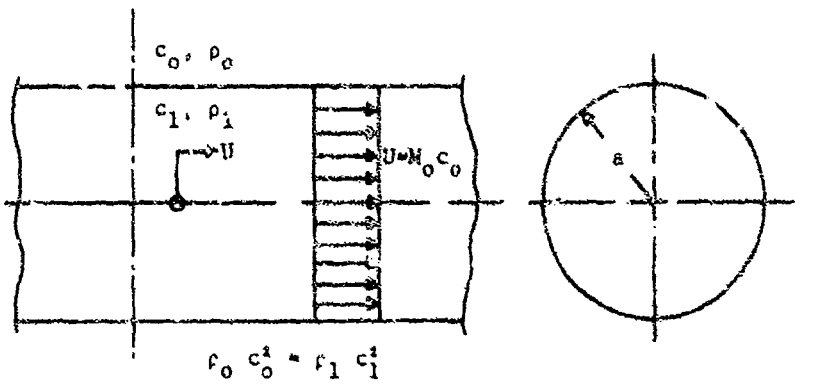

FIGURE 7. Third Model Problem

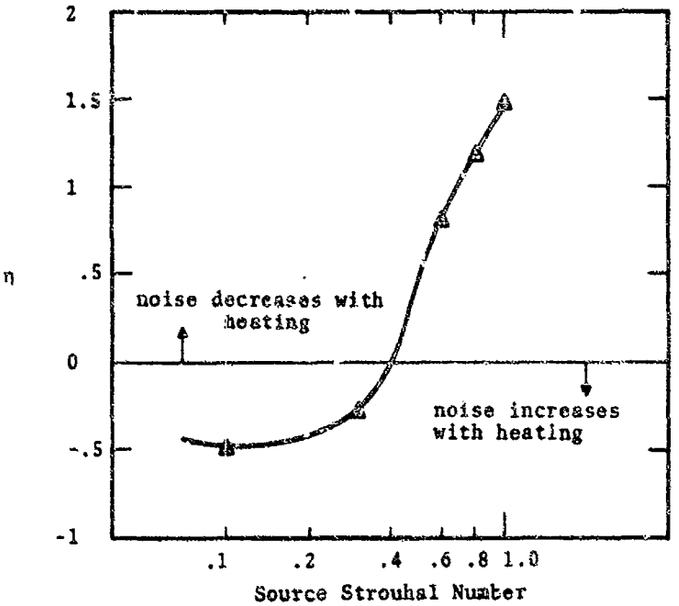

FIGURE 8. η as Function of $(St)_o$ for $M_o = 0.5$.

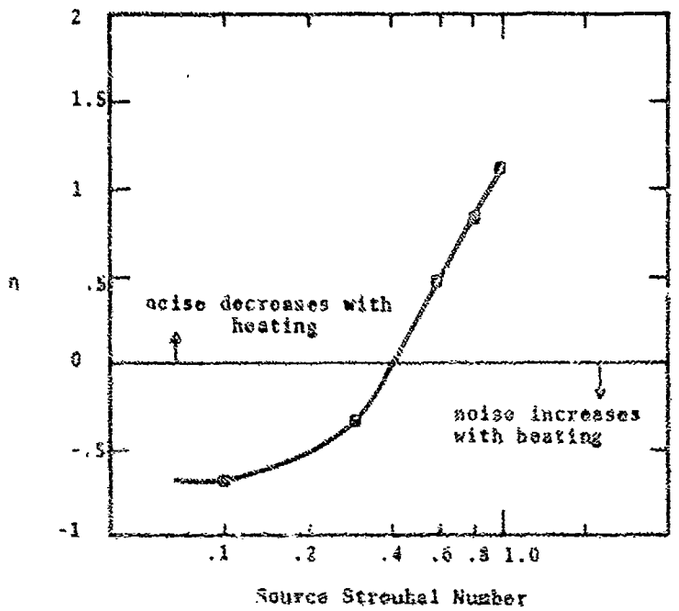

FIGURE 9. η as Function of $(St)_o$ for $M_o = 0.7$.

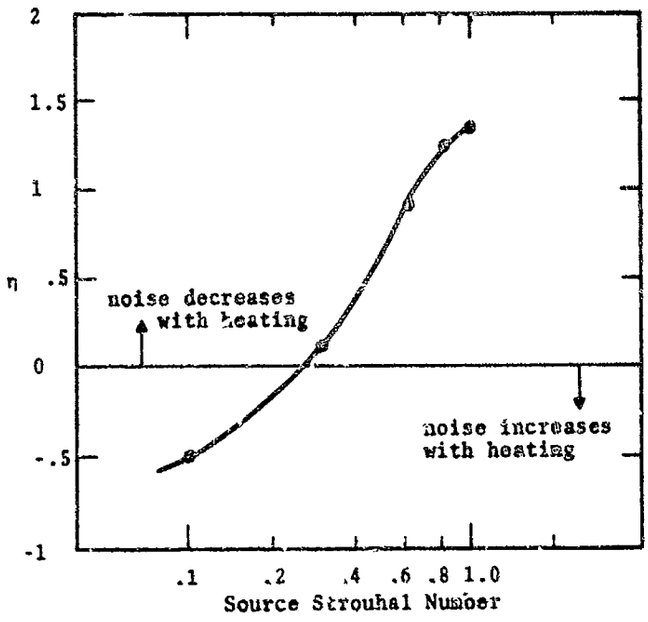

FIGURE 10. η as Function of $(St)_o$ for $M_o = 0.9$.

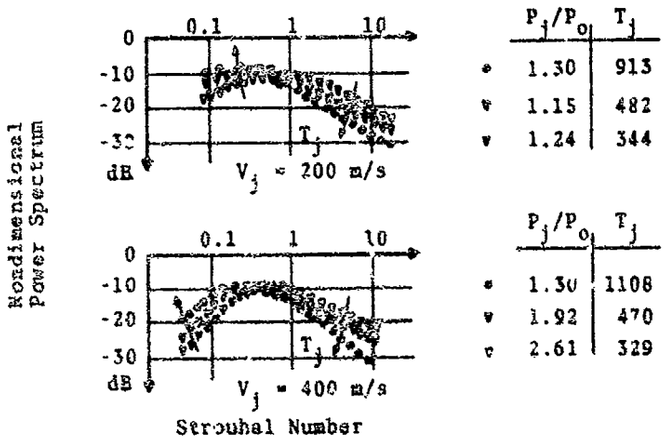

FIGURE 12. Figure 19 of [12].

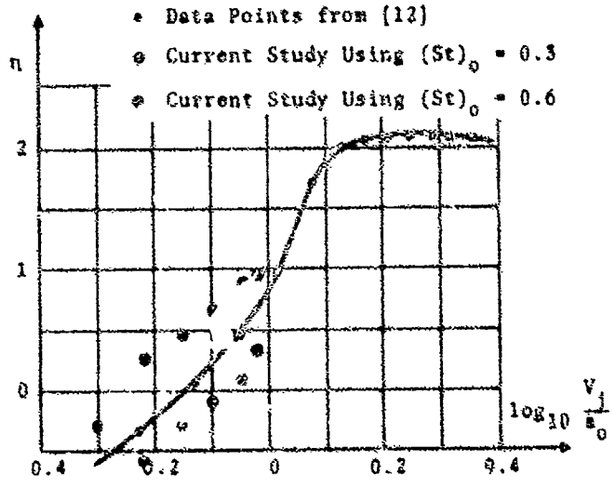

FIGURE 11. Figure 17 of [12].

THE NOISE FROM SHOCK WAVES IN SUPERSONIC JETS

by

M Harper-Bourne, M J Fisher

Institute of Sound and Vibration Research
University of Southampton
Southampton SO9 5NH, England.

SUMMARY

A theoretical model is proposed for the prediction of the characteristics of broadband shock associated noise from jets operated above the critical pressure ratio. The model regards each shock cell end as a source of acoustic radiation with relative phasing set by the time of eddy convection between them. This leads to a prediction for the peak frequency of this noise component as a function of both pressure ratio and angle of observation which is amply confirmed by experimental results.

The model is also extended to the prediction of the spectrum of shock associated noise and these predictions are also compared with experimental data.

It is also shown that the intensity of shock noise is a function only of pressure ratio, and is independent of jet stagnation temperature and hence jet efflux velocity.

1. INTRODUCTION

The shock waves in an incorrectly expanded supersonic jet will interact with the jet turbulence to produce a source of noise in addition to that due to the turbulent mixing. This source has two components, one of which consists of discrete tones harmonically related, often termed screech and the other more broadband but strongly peaked, often termed shock associated noise. The former, which involves an acoustic feedback from the source region to the nozzle, was studied in some detail by Powell [1], but the latter, which is essentially from the same source but without the acoustic feedback is very poorly documented. This more broadband component has been studied extensively at the ISVR in recent years. The study has comprised two separate but complementary facets, namely using an optical method, the crossed beam schlieren technique [2], to probe the nature of flow field near the shocks and also obtaining a comprehensive set of measurements of the sound field.

The majority of the sound measurements were obtained in the Institute's anechoic chamber using a 25 mm dia. convergent nozzle with air at ambient temperature. A specially designed silencer with settling chamber was used to eliminate air supply noise and provide a uniform exit flow.

The influence of shock associated noise on the variation of noise levels with jet efflux velocity is shown in Figure 1. It can be seen that at an angle of observation of $\theta = 30^0$ to the jet axis no significant change in the general dependency observed at sub-critical pressure ratios occurs when the nozzle chokes (i.e., $M_j > 1$). By contrast at $\theta = 90^0$ and 143^0 an extremely rapid increase of noise levels ensues once shock waves appear in the flow field. Furthermore over this range of angles the noise field becomes progressively less directional as the pressure ratio is increased. It is to be emphasised however that the results presented here are for an unheated jet flow. For high stagnation temperature jets these changes are far less dramatic than observed here due, as we shall show below, to the increased contribution of mixing noise. On the other hand it is to be emphasised that the levels presented in Figure 1 are not due to a significant contribution from the discrete tones or screech as a result of the precautions outlined below.

In the early stages of this work some difficulties were experienced as a result of these discrete tones particularly in the optical measurements. It was found, for example, that with a normal nozzle configuration these tones were non-stationary, their amplitude varying, on occasions, by a factor of five while the jet was being operated at ostensibly constant conditions. Subsequently it was found that an acoustic reflector (a metal plate) surrounding the nozzle in the nozzle exit plane eliminated this non-stationarity. However, it also had the unwanted effect of making the screech tones very dominant. They were much reduced, however, and remained stationary when the plate was covered with an appropriate layer of acoustic foam. Addition of a small projection on the nozzle lip was subsequently found sufficient to eliminate the screech. This configuration was employed therefore for the majority of our experimental program except for noise measurements in the upstream arc ($\theta > 90^0$) where the lesser but still effective expedient of covering metal surfaces close to the nozzle exit with acoustic foam was employed. These difficulties do however highlight the very real problems associated with a definitive study of broadband shock associated noise. First it is inevitably accompanied by some degree of mixing noise, while the presence of screech, if it is permitted to persist, can introduce even further uncertainties into the measured trends and dependencies.

2. DEPENDENCE OF OVERALL LEVELS

A more informative manner of presenting the data of Figure 1 for pressure ratios above the critical value is shown in Figure 2. Here the overall sound pressure level at 90^0, appropriately normalised for nozzle diameter and distance of observation, is plotted against the parameter β where

$$\beta = \sqrt{M_j^2 - 1} \qquad (1)$$

and M_j is the fully expanded local jet Mach number, a function of the pressure ratio only. It can be seen that apart from the smaller β values the measured levels are directly proportional to the fourth power of β. Also shown is an estimate for the mixing noise based on an extrapolation of the lower speed data shown in Figure 1. It can be seen that as this 'estimated mixing noise' contribution falls progressively below the measured levels so the β^4 law is more accurately obeyed. This suggests therefore that the broadband shock associated noise itself follows a β^4 law, but that at the lower β values the total noise follows a rather slower dependence due to the presence of mixing noise. Further evidence for this is presented in Figure 3, showing data for the upstream arc, $\theta = 143^0$. Here it is seen that the 'estimated mixing noise' is negligible at all but the lowest pressure ratios and the straight line relationship is obeyed over the entire range of measurement. Comparison of the lines drawn on Figures 2 and 3 indicate furthermore that they differ by only 2 dB, indicating again that the shock associated noise is relatively omnidirectional. Also shown in Figure 3 is the noise from jets at several stagnation temperatures in the region of 1100^0K. It can be seen that at a sufficiently high value of β, ie, pressure ratio, the points coincide with the cold jet line thus indicating that the shock noise is virtually independent of jet temperature.

The β^4 dependence observed above suggests that the amplitude of the 'sources' producing this noise varies as β^2. Consideration of the normal shock relationships, furthermore, shows that this is precisely the dependence of the pressure difference across a normal shock of upstream number M_j. Thus superficially it appears that the source strength associated with the shock associated noise is proportional to the pressure difference across the shock waves. Of course it can be argued that these relationships will not apply directly to this case because the shocks in the jet are not normal but oblique. Some reassurance on this matter was gained from the crossed beam schlieren measurements. The variation of the mean square level of the measured density gradient fluctuations with axial position is shown in Figure 4. It can be seen that the variation is dominated by a series of almost equally spaced peaks, each one occurring at the point where the shock waves terminate in the jet shear layer. Furthermore, measurement of the variation of these peak levels as a function of pressure ratio show that they also follow a β^4 dependence. This suggests that there is a strong connection between the sound intensity and the density fluctuations at the shocks and also that the parameter β^2 is a good representative of the oblique shock strength.

In summary therefore it appears that the overall level of shock associated noise is principally a function of jet pressure ratio and is relatively independent of either angle of observation or jet stagnation temperature. Whether or not it is the dominant noise source for a given pressure ratio however depends on these parameters since they set the mixing noise levels.

3. SPECTRAL CHARACTERISTICS

A model, for the prediction of the spectral characteristics of shock associated noise, has been evolved by extending Powell's original model for the discrete components. In this model the end of each shock cell is taken as a source of acoustic energy and the relative phasing between the sources is set by the convection of turbulent eddies between them. This model is well justified by the schlieren measurements which showed that the peak levels (Figure 4), of the density gradient fluctuations coincided with the shock positions at the end of each cell. The peak levels also varied as β^4 as did the sound field whereas between these peaks the variation of the density gradient fluctuations was found to be a far weaker function of β. Thus it appears that these shock regions are intimately associated with the production of the shock associated noise.

3.1 RELEVANT FLOW FIELD MEASUREMENTS

The model employed therefore consists of an array of sources in line with the nozzle lip and almost equally spaced with separation L. The measured dependence of shock spacing on pressure ratio is shown in Figure 5. This is in nominal agreement with a theoretical derivation due to Pack [3] which yields :

$$L = \text{const}.D.\beta \qquad (2)$$

A good average value of the constant for the array (about eight shockwaves) is 1.1. For a detailed representation the small linear variation noted in Figure 6 is included as follows :

$$L_n = L_1 - (n-1).\Delta L \qquad (3)$$

where $\Delta L/L_1$ is about 6% and the constant in (2) for L_1 is 1.31.

It is assumed that the convection of a turbulent eddy along this line of sources causes each to emit an acoustic signature at the time of arrival of the eddy. The similarity of these signatures and therefore the extent they interfere on combining, depends on how much the eddy distorts (changes identity) during convection.

To quantify this and the convection velocity, a crossed beam schlieren system was used to optically monitor and compare, with the aid of a digital correlator, the time history $F(t)$ of fluctuations occurring at two separate shockwaves, m and n.

Cross correlations obtained this way, for the typical shockwave pairs - 4/4, 4/5 and 4/6 are presented in Figure 7. It is found from the peak value of 4/5, that the fluctuations at shockwaves 4 and 5 are about 60% correlated ($C_1 = 0.6$) whereas for the further apart combination 4/6, the similarity is much reduced ($C_2 = 0.2$). These typical observations therefore suggest that significant interference between the sound from individual sources can occur, particularly for adjacent sources.

Also evident on Figure 7 is that the peak values occur at time delays given by

$$\tau_c = \frac{x_n - x_m}{U_c}, \qquad (4)$$

where U_c is the eddy convection velocity and this is seen to be about $0.7\,U_J$. (The same was also obtained in a subsonic jet.)

The cross correlations were repeated using analogue filters to analyse the signal fluctuations contained in a narrow frequency band $(d\omega)$ centred on frequency ω. In this instance the correlation function tends to oscillate indefinitely and in the limit (as $d\omega \to 0$) we obtain a standard statistical result :

$$\frac{\overline{F_m(t).F_n(t+\tau)}}{d\omega} = S_{mn}(\omega)\cos\left[\omega.\left(\tau - \frac{x_n - x_m}{U_c(\omega)}\right)\right] \qquad (5)$$

This peaks at a time delay which varies only slightly with frequency and therefore $U_c(\omega)$ is nominally equal to the group convection velocity Figure 8. Also shown in Figure 8 is the variation of the filtered correlation coefficient for the adjacent source combination (4/5). This relates to the spectral amplitude (modulus of the cross power spectral density) and is defined as

$$C_i(\omega) = \frac{S_{mn}(\omega)}{S^{\frac{1}{2}}_{mm}(\omega).S^{\frac{1}{2}}_{nn}(\omega)} \qquad (6)$$

where $i = |n-m|$.

It tends to vanish at the high frequencies, Figure 8, but is otherwise nearly constant. A useful empirical rule, representing Gaussian decay, is

$$C_i(\omega) = C_1^{i^2}(\omega) \qquad (7)$$

It is found (reference [4]) that the more sheared a flow is, the more rapidly does the turbulence distort. The effect of increasing the pressure ratio is to move the shockwaves further downstream where the shear is less by virtue of the increased shear layer width. However, the shock spacing also increases and the turbulence must travel further between the adjacent shocks. These two effects tend to cancel with the result that the correlation coefficient is independent of pressure ratio.

3.2 FORMULATION OF THE SOUND FIELD

Having outlined some useful flow statistics the sound field for the postulated source model may now be formulated.

The nth source, located distance x_n from the nozzle, contributes to the acoustic far field pressure an amount :

$$p_n(r_o,t) = \frac{F_n(t-r_n/a_o)}{r_o} \qquad (8)$$

where F is now the (random) source fluctuation evaluated at retarded time. This has a spectral density $G_{nn}(\omega)$, a continuous function of frequency and presumed independent of angle of observation θ.

Summing the contributions from an array of N such sources and squaring and time averaging, yields an expression for the sound intensity :

$$\overline{p^2(r_o,\theta,t)} = \frac{1}{r_o^2}\sum_{m=1}^{N}\sum_{n=1}^{N}\overline{F_m\left(t-\frac{r_m}{a_o}\right).F_n\left(t-\frac{r_n}{a_o}\right)} \qquad (9)$$

The fluctuations of p are statistically stationary and it then follows that :

$$\overline{F_m\left(t-\frac{r_m}{a_o}\right).F_n\left(t-\frac{r_n}{a_o}\right)} = \overline{F_m(t).F_n\left(t+\frac{r_m-r_n}{a_o}\right)} \qquad (10)$$

Now in (8) it is evident that source fluctuations in a given band of frequencies must be responsible for the sound radiated in that same band. Therefore consider again the limiting case of a very narrow bandwidth. The sound intensity (9) per unit bandwidth is $G_p(r_o,\theta,\omega)$. Also, on the basis that eddy convection controls the relative source phasing, the cross correlation (10) above therefore takes the form of (5) which we evaluate at the time delay :

$$\tau = \frac{r_m - r_n}{a_o} = \frac{x_n - x_m}{a_o}\cos\theta \qquad (11)$$

Therefore in this instance (10) is equal to :

$$G_{mn}(\omega).\cos\omega\left(\frac{x_n - x_m}{a_0}.\cos\theta - \frac{x_n - x_m}{U_c}\right)$$

$$= G_{mn}(\omega).\cos\left[\frac{\omega(x_n - x_m)}{U_c}(1 - M_c\cos\theta)\right] \qquad (12)$$

where M_c is the ratio of U_c, to the ambient speed of sound a_0 and $(1-M_c\cos\theta)$ is a Doppler factor incorporating the variation in retarded time and source phasing.

Finally, inserting (12) in (9) a general expression for the spectral density of shock associated noise is obtained, namely :

$$G_p(r_0,\theta,\omega) = \frac{1}{r_0^2}\sum_m\sum_n G_{mn}(\omega)\cos\left[\frac{\omega(x_n - x_m)}{U_c}(1 - M_c\cos\theta)\right] \qquad (13)$$

3.3 BRIEF COMPARISON WITH MEASUREMENT

For a preliminary comparison it is plausible to ignore the somewhat small variations in shock spacing noted previously. (This aspect is reconsidered later.) Therefore using an average value L, (13) becomes :

$$G_p(r_0,\theta,\omega) = \frac{1}{r_0^2}\sum_m\sum_n G_{mn}(\omega)\cos\left[\frac{(n-m)\omega L}{U_c}.(1 - M_c\cos\theta)\right] \qquad (14)$$

Consideration of this summation indicates that it will tend to have a maximum value whenever the argument of cosine term is either zero or equal to an integer multiple of 2π for non-zero values of $(n - m)$. The former condition clearly occurs only at the Mach angle, $\theta = \cos^{-1}(1/M_c)$ when it exists. Experience indicates however that at this angle the mixing noise frequently dominates and we shall not consider the possibility further.

The latter condition suggests that the shock associated noise might exhibit a peak value at a frequency given by

$$f_p = \frac{U_c}{L(1 - M_c\cos\theta)} \qquad (15)$$

and harmonics thereof. Consideration will show that with this combination of convection speed, shock cell spacing and angle of observation, the radiation from all sources interferes constructively at this specified frequency. At other frequencies this constructive interference is less complete and hence lower levels of noise are anticipated.

Confirmation of these ideas is presented in Figure 9 where the spectrum of noise radiated from a shock free convergent-divergent nozzle is compared with that from a convergent nozzle operated at the same pressure ratio. It is clear that the extra noise radiated by the convergent nozzle is contained in a spectral region centred on the frequency given by (15), above.

The variation of this peak frequency with both angle, velocity and shock spacing is found to follow the prediction of (15) closely. The change with angle is shown in Figure 10 for several pressure ratios indicating the apparent Doppler shift.

4. APPLICATION OF MODEL

Using (14) for guidance a means of collapsing the measured spectra was initially sought for scaling purposes. A computational study of the measured spectra was then undertaken to quantify the normalised source parameters required for a general prediction technique.

4.1 INTERPRETATION

The expansion of (14) contains essentially two different types of terms. These correspond respectively to $n = m$ and $n \neq m$. The former terms are the individual source spectral densities, for instance $G_{44}(\omega)$ and their sum represents the group source spectrum, $G_0(r_0,\omega)$.

The latter terms are responsible for the interference, demonstrated previously and their sum can be either positive (constructive interference) or negative (destructive interference), depending on frequency and angle of observation. In the event that the sources were to be completely uncorrelated, these terms would of course be zero and the noise spectrum then simply equal to $G_0(r_0,\omega)$.

The expansion of (14) is therefore expressed in the following form :

$$G_p(r_0,\theta,\omega) = G_0(r_0,\omega) + G_1(r_0,\omega)\cos\left[\frac{\omega L}{U_c}(1-M_c\cos\theta)\right] + G_2(r_0,\omega)\cos\left[\frac{2L}{U_c}(1-M_c\cos\theta)\right] + \text{etc} \qquad (16)$$

where the cosines are harmonically related and correspond respectively to,

$$|m - n| = 0, 1, 2, 3, \ldots (N - 1).$$

and the spectral amplitudes are defined as follows :

$\|m - n\|$		
0	$G_0(r_0,\omega) = \frac{1}{r_0^2}\left[G_{11}(\omega) + G_{22}(\omega) + G_{33}(\omega) + \text{etc}\right]$	(17a)
1	$G_1(r_0,\omega) = \frac{2}{r_0^2}\left[G_{12}(\omega) + G_{23}(\omega) + \text{etc}\right]$	(17b)
2	$G_2(r_0,\omega) = \frac{2}{r_0^2}\left[G_{13}(\omega) + \text{etc}\right]$	(17c)
3	etc	etc

Each component in (17 b, c, etc) can be related to its respective source strengths in (17a) by using a correlation coefficient, similar to that discussed previously, equation (6). However, to compute the shock noise spectrum it is the spectral amplitudes which are required in (16) and these it will be observed, could be produced by any combination of source strengths etc in (17). Therefore without loss of accuracy, it is permissible to introduce an average correlation coefficient, to be determined empirically and relating directly an interference amplitude (17 b, c, ..) to the group source spectral density (17a). When this is done the following expression is obtained from (17) for the interference amplitude in general :

$$G_i(r_0,\omega) = 2.\frac{(N-i)}{N} \cdot C_i(\omega) \cdot G_0(r_0,\omega) \qquad (18)$$

where $i = |m - n| \neq 0$ and $C_i(\omega)$ is a group average correlation coefficient which like (6) cannot exceed a value of one.

It was noted earlier that the correlation coefficient tends to be independent of pressure ratio . Therefore the spectral level in (16), for example the peak value, is essentially controlled by the level of the source spectral density. But consideration of (16) and (18) indicates that the spectral distribution is determined by the following three parameters:

$$G_0(r_0,\omega) \;, \quad C_i(\omega) \quad \text{and} \quad \frac{\omega}{U_c} \cdot \left[1 - M_c\cos\theta\right]$$

Unlike the first two terms, the last one is a function of both frequency $\omega(= 2\pi f)$ and the fundamental peak frequency equation (15). For convenience, it can be expressed as f/f_p. Now when the Doppler factor is allowed to vary, for instance by varying θ, the interference contribution in (16) shifts in frequency, relative to the invariant source spectrum. Therefore the spectrum measured for different θ, are unlikely to be a unique function of f/f_p. This is borne out in practice.

4.2 SPECTRAL COLLAPSE AND SCALING

The overall sound intensity is given by the integral of (16) with respect to frequency, namely

$$\overline{p^2(r_0,\theta,t)} = \int_0^\infty G_p(r_0,\theta,\omega)\, d\omega \qquad (19)$$

From Figures 2 and 3 its dependence (in dB) is given as

$$OASPL = 158.5 + 10\,LOG_{10}\left[\left(\frac{D}{r_0}\right)^2 B^4\right] \quad (dB) \qquad (20)$$

Within the angular region of interest, the interference terms in (16) virtually vanish upon integration in (19). It therefore follows that the overall strength of the sources has the same dependence as the sound intensity, namely

$$\int_0^\infty G_0(r_0,\omega)\, d\omega \propto \left(\frac{D}{r_0}\right)^2 B^4 \qquad (21)$$

It will be noted that because the sound intensity is omnidirectional in this region, the same must also be true of the source spectral density, thereby confirming our original assumption.

Equation (21) can be used to determine the dependence of $G_0(r_0,\omega)$. First, however, it is necessary to postulate a frequency dependence, in order to perform the integration. In common with problems of this nature we postulate that the source spectrum will peak at some constant value of a Strouhal number σ_p and that the spectrum shape is solely a function of σ. (The latter will also be assumed for the correlation coefficient.)

$$\text{and} \quad \sigma = \frac{\omega s}{U} \qquad (22)$$

The length scale x is taken to be proportional to the scale of the turbulent eddies intersecting a shock wave. This will be proportional to the local shear layer width and therefore roughly proportional to shock position from the nozzle

$$\text{ie} \qquad x \propto L \qquad (\alpha\beta D)$$

Initially it seemed logical to associate the velocity U with the convection velocity. This would then yield a typical frequency equal to the rate of intersection. Unfortunately, for a given jet stagnation temperature U_c does not vary much over the pressure range tested. Nevertheless, between the hot and cold data the velocity does change and by a factor of up to two. A comparison of these data, following the methods outlined below, however, showed that the source spectrum remained invariant with increased flow velocity. We do not currently understand the reasons for this observation. Its acceptance as an experimental observation however suggests a scaling for source spectra on the parameter $\omega L/a_0$.

The source spectral density is therefore expressed in the following form :

$$G_0(r_0,\omega) = g(p_J/p_0) \cdot H_0\left(\frac{\omega L}{a_0}\right) \qquad (23)$$

where H_0 is a universal spectrum shape function.

Inserting (23) in (21) the dependence on pressure ratio is established :

$$g(p_J/p_0) \propto \left(\frac{U}{r_0}\right)^2 \cdot \frac{U}{a_0} \cdot \beta^5 \qquad (24)$$

This result is used to normalise the measured sound spectral density. Now when (23) is incorporated in (16) it is found that the normalised spectrum is theoretically a unique function of f/f_p when the quanity $(1 - M_c\cos\theta)/M_c$ is held constant.

Shown in Figure 11 are the spectral levels measured at different pressure ratios for an unheated jet. These have been corrected using (24) and because $(1 - M_c\cos\theta)/M_c$ is nearly constant, they are plotted against f/f_p. A satisfactory degree of collapse is observed except at low frequencies, where for the low pressure ratios mixing noise dominates the levels. Figure 12 shows data for which $(1 - M_c\cos\theta)/M_c$ is comparable to the previous case, but for a stagnation temperature of 1100°K. Again a useful degree of collapse is observed while comparison of the two sets of data also demonstrates the utility of this method for a range of stagnation temperatures.

4.3 PREDICTION OF SPECTRUM

For a general prediction technique the following information is required in (16) as a function of $\sigma = \frac{fL}{a_0}$:

(a) the normalised group source spectral density $H_0(\sigma)$, and

(b) the set of correlation coefficients, $C_i(\sigma)$.

In practice only the first coefficient, $C_1(\sigma)$ need be tabulated if equation (7) is used. As will be shown below, a slight modification involving the unequal shock spacing, is actually needed to (16) before a satisfactory prediction formula is realised. The quantities (a) and (b) are determined through a computational study of the choked jet noise spectra, measured at different angles to the jet axis and for a range of pressure ratios, thereby providing a suitable variation of both $(1 - M_c\cos\theta)$ and β respectively. A measurement survey of sufficient angular detail was only available for the unheated jet and this data alone is used.

The spectral amplitudes are independent of angle θ and therefore the directivity of (16) at constant frequency is due solely to the cosines. This permits (16) to be solved as an even Fourier series with independent variable f/f_p.

With constant frequency the equation predicts for the spectral level, a series of harmonically related peaks of equal level corresponding to constructive interference. These occur at $f/f_p = 1, 2, 3,$ etc. (This is always true providing there are two or more sources present.) However, where f/f_p does extend to values of 2 or more in the measured directivity, only the fundamental peak is well defined. A similar observation can be made of the sound spectrum, Figure 9, where the fundamental is seen to dominate the spectral distribution. Of course, in this case, the harmonics are anticipated having different peak levels due to the frequency dependence of (a) and (b) above. However a drastic loss of coherence (b) at high frequencies is discounted here for the reason that the fundamental is readily discerned at smaller angles (eg $\theta = 60°$) when it then occurs at frequencies comparable to the missing higher harmonic peaks in Figure 9.

These discrepancies apparently stem from the same oversimplification, namely the use of a constant shock spacing L. This was found to reduce by about 6% from one cell to the next, see Figure 6, also equation (3). The effect of incorporating (3) in the generalised result (13) is most easily visualised when $\Delta L/L$ is assumed very small. In this instance the expansion of (13) is in part identical with (16) (for which L was assumed constant) but additional interference terms arise. The first of these $(i = 1)$ is equal to

$$\frac{4\pi}{r_o^2} \cdot \frac{\Delta L}{L_1} \cdot \left[G_{12}(\omega) + 2G_{23}(\omega) + 3G_{34}(\omega) + \text{etc} \cdot \right] \frac{f}{f_{p_1}} \cdot \sin\left[2\pi f/f_{p_1} \right] \qquad (25)$$

It will be seen that these terms are in quadrature with their corresponding cosines in (16). Also they have a frequency weighting. Taken as a whole, their effect is to generally enhance the destructive interference below the fundamental peak and 'fill in' above the peak as is observed in the measurements.

To simplify matters, the spectral amplitudes $G_{mn}(\omega)$ in the sine terms are assumed equal for any given value of $|m - n|$. This can be justified when the relative contribution of the sines to the sound spectrum is not unduly large.

Now incorporating (3) in (13) we obtain, for the sound spectral density,

$$\phi_p(r_o,\theta,\omega) = \frac{1}{r_o^2} \sum_m \sum_n G_{mn}(\omega) \cos\left[\frac{\omega L_1}{U_c} (1 - M_c\cos\theta).(|n - m| - \frac{\Delta L}{L_1} \sum_m^{n-1} K) \right] \qquad (26)$$

Then expanding and re-arranging in the manner of (16), an expression suitable for programming is obtained :

$$G_p(r_o,\theta,\omega) = G_o(r_o,\omega)\left[1 + \sum_{i=1}^{N-1} \frac{2(N-i)}{N} \cdot C_i(\omega) \cdot \sum_{s=0}^{N-(i+1)} \cos\left[\frac{\omega L_1}{U_c} (1 - M_c\cos\theta).(i - \mu_{si}) \right] \right] \qquad (27)$$

where

$$\mu_{si} = \frac{\Delta L}{L_1} \cdot \left(\sum_{K=o}^{i} K + iS \right) \qquad (28)$$

A least squares analysis enabling a 'best fit' of (27) to the measured directivity was established. The data was initially adjusted to remove mixing noise using an extrapolation of subsonic measurements but this affects the low frequencies only and is of uncertain accuracy. Putting $N = 8$, $\frac{\Delta L}{L_1} = 0.66$ and $U_c = 0.7\, U_j$, the directivities for a wide range of frequencies and different pressure L_1 ratios were processed and the resulting source spectral levels normalised using (24). The results are presented plotted against Strouhal number in Figure 13.

A very reasonable collapse for the source spectral estimates is observed in Figure 13(a). The scatter at low frequencies is thought due to inadequate correction for the mixing noise at the lower pressure ratios. The original assumption regarding source frequency, namely that $f_s \alpha \frac{U_c}{L}$, is used here. However, U_c varies little in this data and is approximately equal to a_o. The shock cell spacing L does vary, by a factor of 2.3 and the collapse therefore confirms its importance in controlling source frequency.

The spectrum peaks around a Strouhal number of 0.65 at approximately 160 dB. At the extremities, it changes by roughly 6 dB per octave ($\alpha \pm 2$).

Shown in Figure 13(b) are the computed values of correlation coefficient for adjacent sources ($i = 1$). Considerable scatter is observed but the values lie within the permissible range. The flow measurements, Figure 8(a) were used here to suggest a mean variation (solid line).

The solid lines in Figure 13 are taken to be the universal spectral characteristics for the shock associated noise of a choked jet. Using these along with equation (7) and (27) a prediction programme has been written.

Some confirmation of the validity of the programme and the above analysis is given in Figure 14, where the comparisons with measurement are observed to be generally satisfactory. The largest discrepancies are found in the downstream quadrant ($\theta = 45^\circ$ in Figure 14). Here the source spectrum tends to emerge above the measurements and there is some suggestion that low and mid range frequencies tend not to radiate efficiently at the smaller angles.

More recent predictions (not shown here) but for jets heated to 1160°K, also agree equally well with measurement providing the frequency parameter is defined as fL/a_o i.e., independent of flow velocity.

5. CONCLUSIONS

The shock waves in a choked jet are responsible for a source of broadband sound. The intensity of this 'shock associated noise' is virtually independent of angle of observation and jet velocity but a function only of pressure ratio. In particular, it is proportional to the fourth power of the shock strength (θ). Its noise spectrum is distinct from that of mixing noise, and is characterised by a peak. The frequency of this peak varies with angle in the manner of a Doppler shift and is proportional to jet velocity and inversely proportional to shock spacing.

A simple model for the shock noise sources was successfully developed to represent the sound radiated to the far field. The principal assumption, namely, that each shock cell end may be regarded as a compact source of acoustic radiation, with relative phasing set by the time of eddy convection between them, was amply substantiated. A detailed application of this model to the sound measurements resulted in a number of fundamental conclusions :

The sound can be decomposed into two components (1) a group source contribution equal to the sum

of the individual source intensities and (ii) an interference contribution, arising as a result of the sources being correlated. The two components combine to form an interference ripple in the sound spectrum. Consideration of the relative phase and differences in retarded time for these almost equally spaced sources, explains the variation in peak frequency. Also, slight variations in spacing account for the virtual absence of harmonics of this frequency. A successful decomposition of the measured spectra is achieved and utilised in a prediction programme.

Using the model to compare hot and cold jet data, it is tentatively concluded that the characteristic frequency of sound radiated by individual sources is independent of the eddy velocity! No explanation for this essentially empirical observation is currently available. It is hoped that future work to examine the detailed physical processes associated with the shock/turbulence interaction mechanism, revealed herein, will also incorporate the rationale for this observation.

REFERENCES

1. A POWELL On the mechanism of choked jet noise Proc. Phys. Soc. B. (1953) Vol.66, 1039-1056.

2. M J FISHER and F R KRAUSE The crossed beam correlation technique J. Fluid Mech. (1967) Vol. 28, 705, 717.

3. D C PACK A note on Prandtl's formula for the wave-length of a supersonic gas jet Quart. Journ Mech. and Applied Math (1950) Vol III Pt.2.

4. P O A L DAVIES, M J FISHER and M J BARRATT The characteristics of the turbulence in the mixing region of a round jet J. Fluid Mech. (1963) Vol.15, Pt.3, 337-367.

ACKNOWLEDGEMENTS

The authors are particularly grateful to Dr P A Lush for his invaluable advice and also to D. C L Morfey. We are also indebted to Rolls Royce for making available the hot jet data and for their financial support together with that of the National Gas Turbine Establishment.

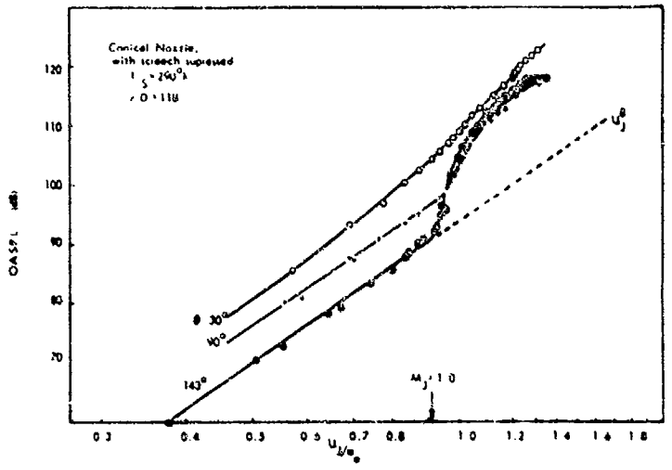

FIG 1 VELOCITY DEPENDENCE OF OVERALL INTENSITY OF JET NOISE AT SEVERAL ANGLES TO THE JET SHOWING SHOCK ASSOCIATED NOISE.

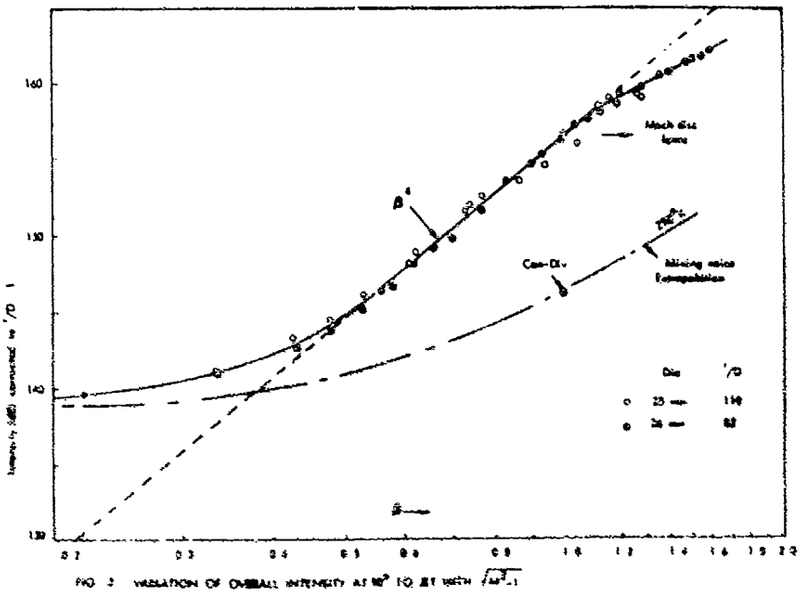

FIG 2 VARIATION OF OVERALL INTENSITY AT 90° TO JET WITH $\sqrt{M_j^2 - 1}$

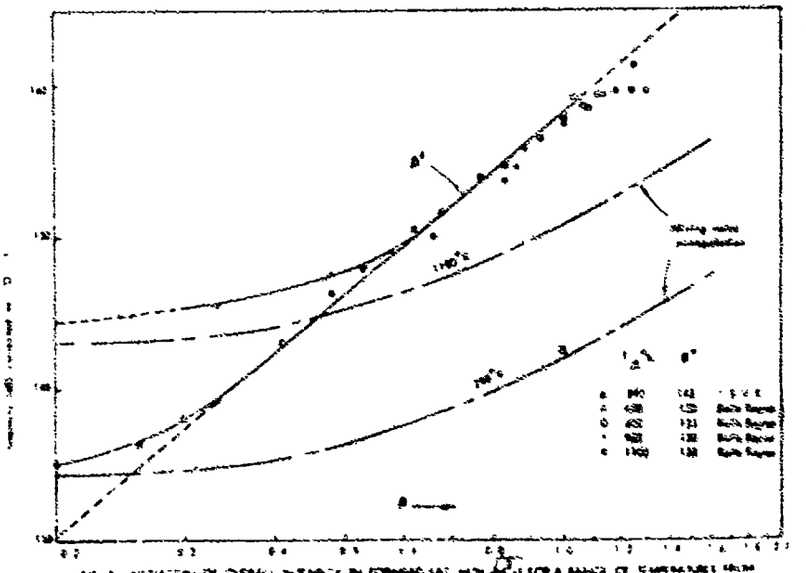

FIG 3 VARIATION OF OVERALL INTENSITY IN FORWARD ARC WITH $\sqrt{M_j^2 - 1}$ FOR A RANGE OF TEMPERATURES FROM COLD TO 1460°K

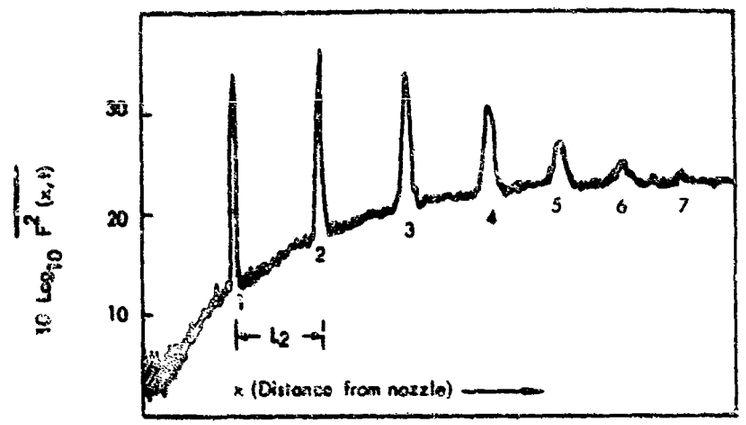

FIG. 4 VARIATION OF SCHLIEREN INTENSITY ALONG THE SHEAR LAYER

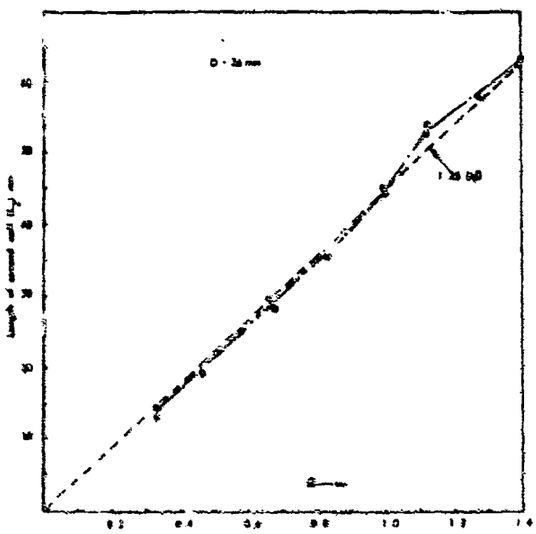

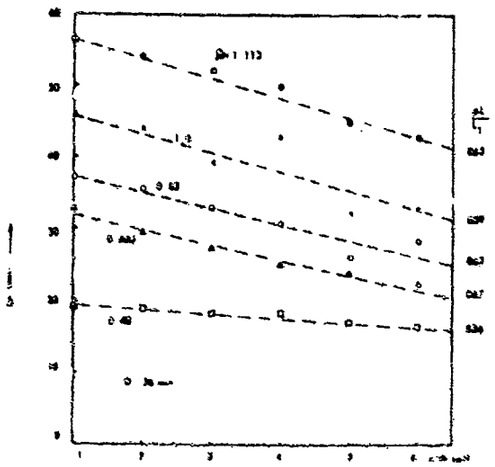

FIGURE 5 VARIATION OF SHOCK SPACING WITH $\sqrt{x/L}$, MEASURED WITH LASER-SCHLIEREN

FIGURE 6 MEASURED VARIATION OF SHOCK SPACING ALONG JET

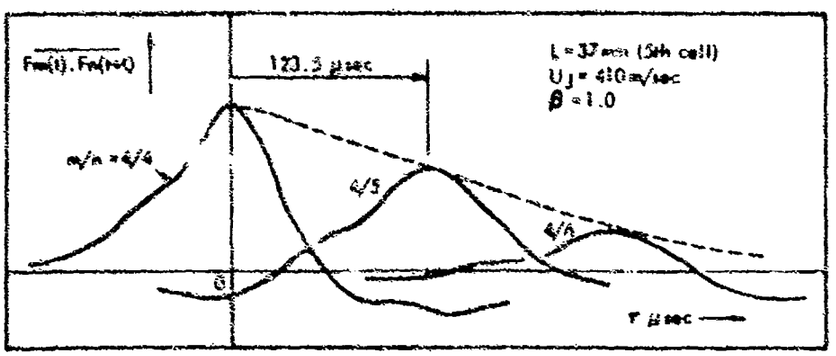

FIG 7 CORRELATION MEASUREMENTS BETWEEN SHOCKWAVES 4,5 AND 6 USING LASER - SCHLIEREN ON 36 mm DIA. JET

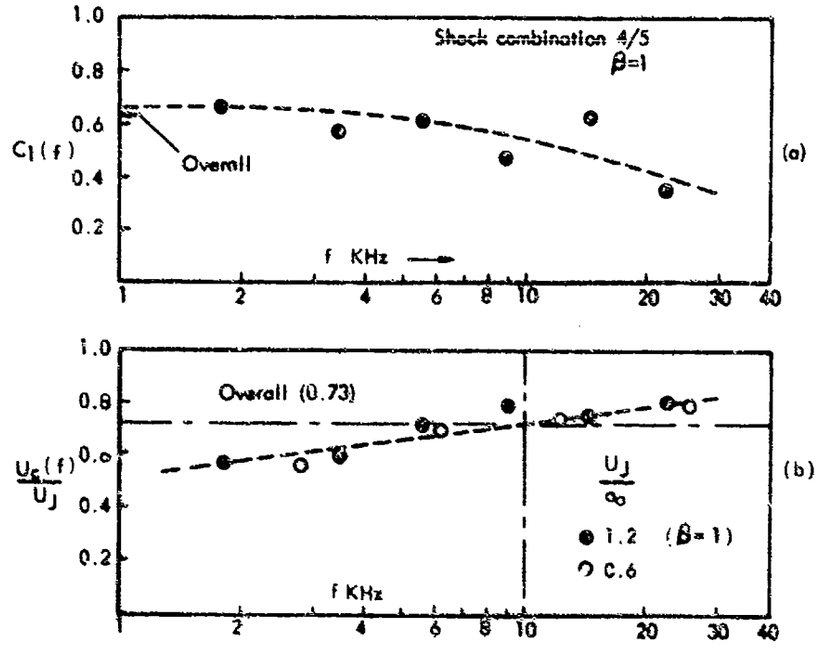

FIG 8 VARIATION WITH FREQUENCY OF (a) THE CORRELATION COEFFICIENT AND (b) PHASE VELOCITY, BETWEEN SHOCKWAVES 4 AND 5 (FREQUENCIES CORRECTED TO 25mm DIA. NOZZLE).

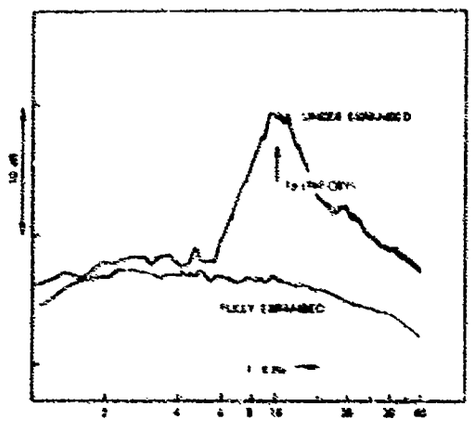

FIG 9 COMPARISON OF SUPERSONIC JET NOISE SPECTRA FOR A FULLY EXPANDED AND UNDER EXPANDED FLOW (θ = 90°, S = 1.4)

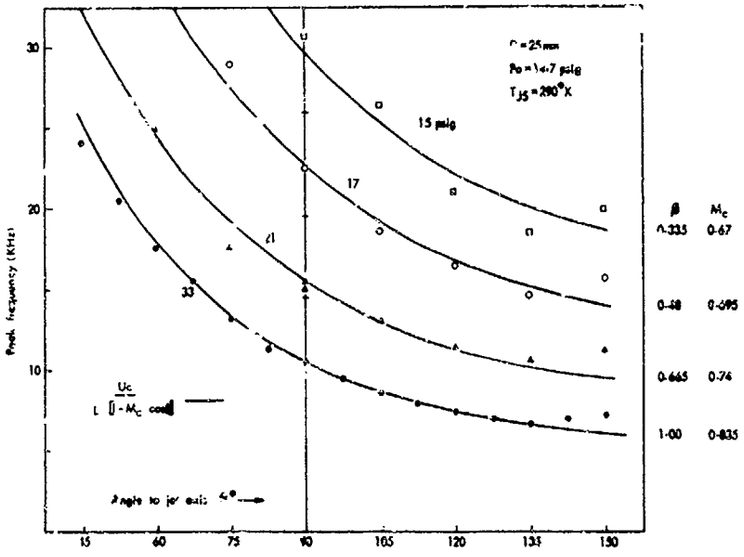

FIG 10 VARIATION OF PEAK FREQUENCY WITH ANGLE TO JET FOR VARIOUS PRESSURES SHOWING DOPPLER SHIFT AND INVERSE DE[illegible]NCE ON SHOCK SPACING

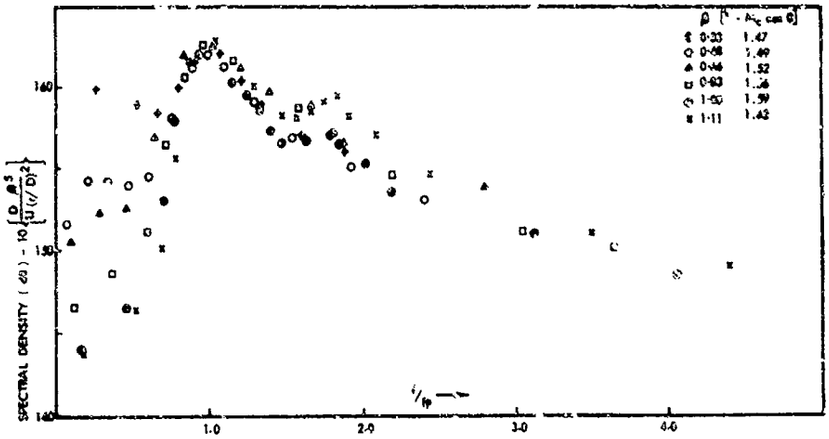

FIG. 11 SPECTRAL COLLAPSE OF DATA AT 135° AND AT VARIOUS PRESSURE RATIOS FOR A COLD JET

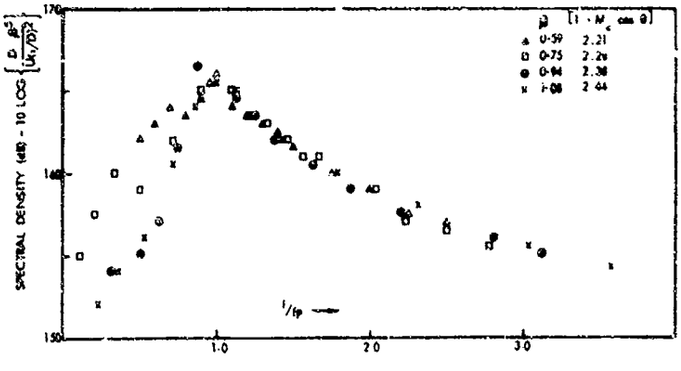

FIG 12 SPECTRAL COLLAPSE OF DATA AT [illegible] AND AT VARIOUS PRESSURE RATIOS FOR A [illegible] AT 1100°K

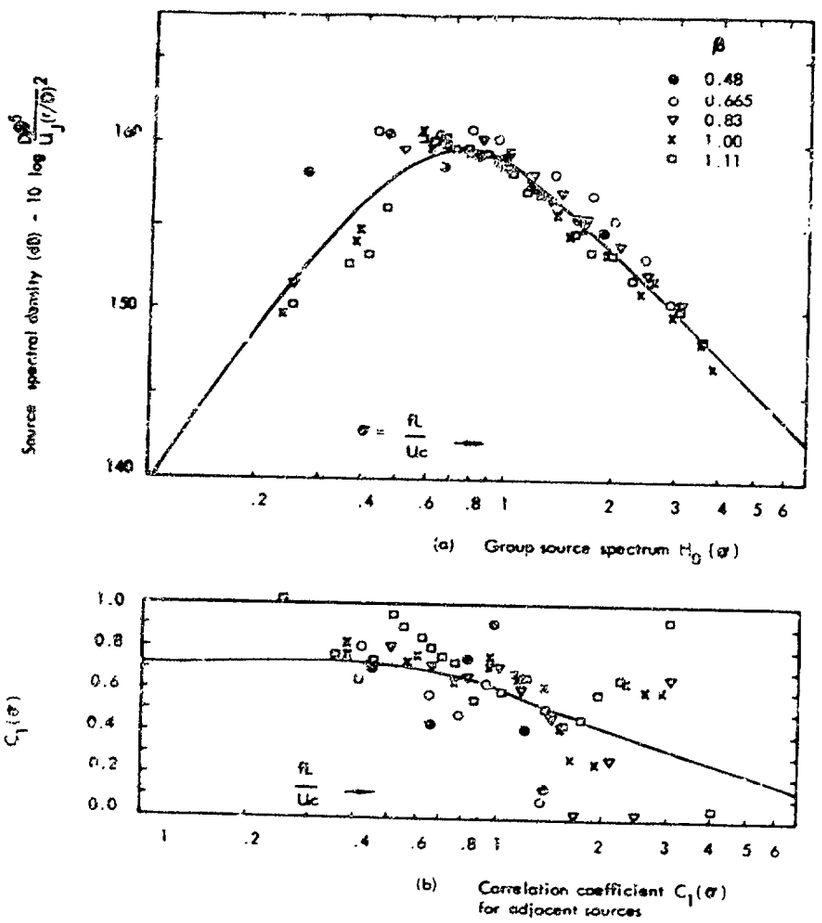

FIG. 13 NORMALISED SOURCE SPECTRAL CHARACTERISTICS OBTAINED FROM COMPUTATIONAL STUDY OF MEASURED SOUND SPECTRA

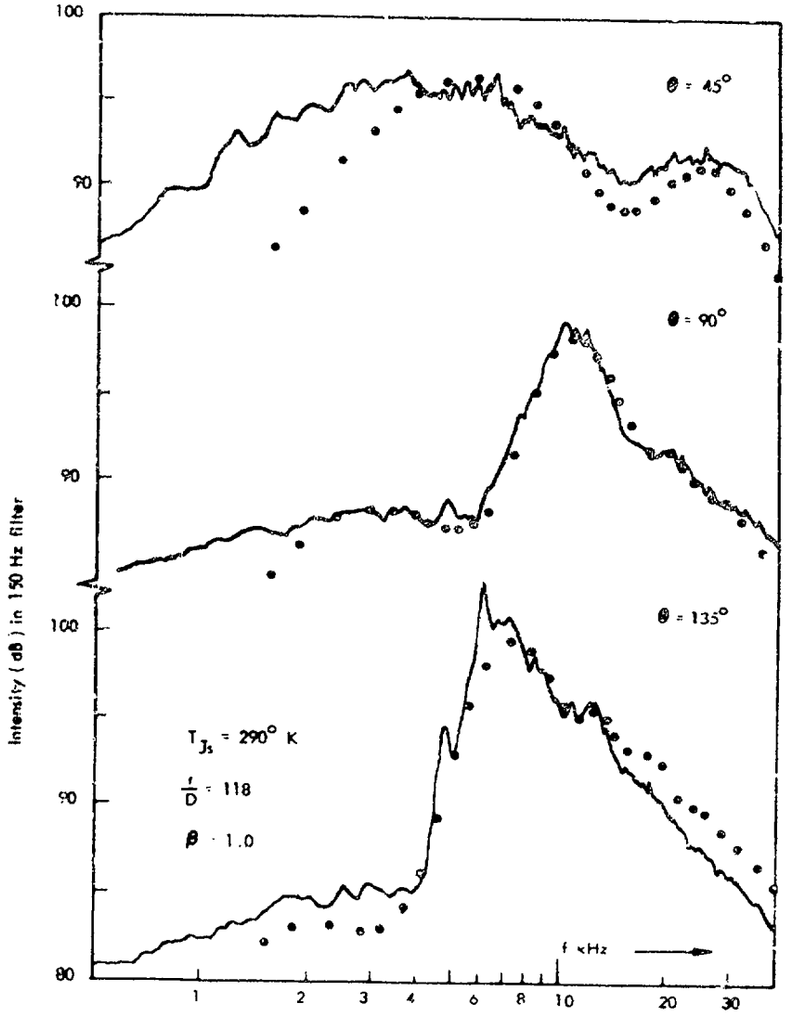

FIG. 14 COMPARISON OF MEASURED (——) AND PREDICTED (o) SOUND SPECTRA.

NOISE FROM HOT JETS

by

P.A. LUSH and M.J. FISHER

INSTITUTE OF SOUND AND VIBRATION RESEARCH

UNIVERSITY OF SOUTHAMPTON

GREAT BRITAIN

SUMMARY

Measurements of the noise from several independent workers of hot sub-sonic jets show that the noise decreases relative to the unheated jet at high jet velocity but increases at low velocity. The decrease at high velocity has previously been explained by the reduction in the jet density for the hot jet and this explanation is confirmed by the present study. The increase in noise at low velocity is attributed to an additional source caused by entropy fluctuations which varies as U^4 compared with U^8 for the usual mixing noise. A simple theoretical model using Lighthill's theory of aerodynamic sound is proposed and this gives very good agreement with the experimental results, but the theoretical model cannot be justified rigorously. However it could provide a satisfactory method for prediction of the noise from hot jets and a basis for the collapse of data.

NOTATION

a	local speed of sound
a_o	ambient speed of sound
A	coefficient of $(U_j/a_o)^8$
B	coefficient of $(U_j/a_o)^4$
C_v	specific heat at constant volume
C_p	specific heat at constant pressure
D	jet diameter
f	frequency
I	sound intensity
k	density parameter
p	pressure
R	distance from source to observer
S	entropy
S_j	entropy in jet
S_o	ambient entropy
t	time
T_{rr}	Lighthill stress tensor
T_j	jet temperature
T_o	ambient temperature
u_i	fluid velocity
u_r	fluid velocity in direction of observer
U, U_j	jet velocity
v	transverse velocity component
x_i	space variable
ρ	density
ρ_j	jet density
ρ_o	ambient density
γ	ratio of spacific heats

1. INTRODUCTION

Until recently it was widely accepted that the effect on the jet noise of increasing the jet temperature at a constant jet velocity would be a reduction in the noise radiated as a result of a reduction in jet density. However measurements of the noise from hot subsonic jets carried out by NGTE (National Gas Turbine Establishment) and also independently by SNECMA (since published jointly in ref. (1)), indicate that while this reduction does occur at high jet velocities, at low velocities the radiation actually increases relative to the unheated jet. At this stage work at ISVR concentrated on finding an explanation for this increase in noise. Previous experimental work on heated jets had generally found a very small effect on the radiation (ref. 2), certainly less than that expected because of density reduction. These results led Ribner (ref. 2) to suggest that the reduction of radiation due to reduction in jet density was to some extent cancelled by an additional source of noise due to fluctuations in entropy. This suggestion was followed up at ISVR by an attempt to separate the extra source from the usual mixing noise using the NGTE data. It was found that the observed velocity dependence of the radiation could be explained by the addition of an extra source with a velocity dependence of U^4. It was further found that the usual mixing noise component, which was assumed to vary as U^8, decreased in strength with increasing temperature in a way very similar to that expected theoretically. Also the U^4 component increased with increasing temperature in a way compatible with a

model based on entropy fluctuations. A similar analysis of some new hot jet noise results from Lockheed Georgia Co. confirmed these findings (ref. 3). The analysis of these two sets of data together with the development of a theoretical model based on entropy fluctuations was published at the British Acoustical Society 1973 Spring Meeting (ref. 4).

However a closer examination of the theoretical arguments showed that this source would actually vary as U^6 and not U^4. Unfortunately it was not possible to reconcile the experimental results with an additional source of velocity dependence U^6. At this stage it was conjectured that the additional noise was generated upstream of the nozzle by the combustion process, although the close agreement between widely differing rigs made this seem unreasonable. NGTE then carried out some experiments using an electrical heater and generally these showed good agreement with the previous tests, indicating that combustion was not involved. Further confirmation was produced by recent ISVR results, for which an electrical heater was also used. In fact these results completely confirmed the presence of an additional temperature dependence source varying as U^4. These recent ISVR results have now been completely analysed and are presented in this paper together with the previously published NGTE results.

One important difference between this work and that published previously by others is that we have concentrated exclusively on the analysis of the radiation at 90° to the jet axis, and not the radiation at the peak angle. The reason for this is that at 90° to the jet, the effects of source convection and refraction of sound are eliminated and the analysis can concentrate on changes in the source strength. At the peak angle of radiation, the effects of convection and refraction are superimposed upon the changes in source strength and since both are likely to be functions of temperature, it would be impossible to separate the two effects.

In view of the very close agreement observed between the ISVR and NGTE results, it is worthwhile outlining the main differences between the two experimental rigs. The NGTE measurements were made in the large anechoic chamber at Pyestock and the jet was heated by burning hydrogen in the plenum chamber upstream of the nozzle. Total temperatures up to about $900^\circ K$ could be achieved. Considerable care was taken to ensure that the noise radiated from valves and the burner were minimised. Free entrainment of the outside air kept the chamber temperature near to the ambient. The ISVR measurements were made in the large anechoic chamber at the University and in contrast to the NGTE measurements the air was heated electrically. The maximum total temperature obtainable in this case was about $500^\circ K$. Again great care was taken to minimise rig noise but no special provisions were made for ventilating the chamber. However it was found that the chamber temperature did not rise above $35^\circ C$. The effect of the change ambient temperature was allowed for by making measurements at a constant ratio of total temperature t the ambient.

2. THEORETICAL CONSIDERATIONS

Ribner's suggestion of noise radiated from entropy fluctuations was investigated using the framework of Lighthill's theory of aerodynamically generated sound. In this theory, a turbulence region generates sound as if it were a distribution of acoustic quadrupoles of strength given by,

$$T_{rr} = \rho u_r^2 + p - a_o^2 \rho \quad , \tag{1}$$

where u_r is the fluid velocity in the direction of the observer. The viscous contribution to this source strength has been omitted as usual. For a cold, i.e. unheated, flow, the term in $p-a_o^2\rho$ will be nearly zero, since the pressure and density fluctuations will be largely isentropic and the sound speed (temperature) will be nearly equal to the ambient value. Thus in a cold flow the main contribution to the sound generation is from the term ρu_r^2 (Reynolds' stresses). However in a heated flow, the term $p-a_o^2\rho$ will not be zero because the pressure and density will no longer be isentropically related. From the thermodynamic relation,

$$\frac{dS}{C_v} = \frac{dp}{p} - \frac{\gamma d\rho}{\rho} \tag{2}$$

it can be seen that the density fluctuation for instance will be composed of an isentropic pressure fluctuation and an entropy fluctuation at constant pressure. The pressure fluctuation contained in $p-a_o^2\rho$ will partially cancel, leaving a contribution from the entropy fluctuation. The fluctuating density is given by

$$\rho' = \frac{p'}{\bar{a}^2} - \frac{\bar{\rho} S'}{C_p} \tag{3}$$

where $\bar{\rho}$ and $\bar{a}$ refer to mean values of density and speed of sound respectively.

Since we are restricting our attention to the radiation at 90° to the jet, the expression for T_{rr} simplifies considerably because the mean velocity $\bar{u}_r$ will be very small so that terms involving it can be neglected. With this simplification and using (3), equation (1) becomes,

$$T'_{90^\circ} = \bar{\rho} v'^2 + \left(1 - \frac{a_o^2}{\bar{a}^2}\right) p' + \frac{\bar{\rho} a_o^2 S'}{C_p} \tag{4}$$

where the mean terms have been dropped since they do not contribute to the rate of change of T_{rr} which is what is required for the far field radiation. Also the triple product of fluctuating quantities has been neglected. The first term is the contribution from the Reynolds' stress and the mean density is taken to be that in the centre of the shear layer. In general this is given by

$$\bar{\rho} = k\rho_j + (1-k)\rho_o \tag{5}$$

where k is a parameter lying between and 1, which represents the position in the shear layer, e.g. $k=\frac{1}{2}$, would correspond to the arithmetic mean. For small variations in jet density, the mean density would also be approximately given by the geometric mean $\sqrt{\rho_j \rho_o}$, but this result becomes inaccurate if the jet density is substantially less than the ambient. The second term is proportional to the temperature difference between the source region and the ambient. In the case of heated jets the

coefficient of p' can never be greater than unity and varies rather slowly with temperature. If it is assumed that p' varies in a similar way to $\rho v'^2$, then the term can be combined with the Reynolds' stress term and the overall density dependence assumed to be ρ. However this term may be important for jets with temperatures or speeds of sound substantially below the ambient value. This point has been discussed in some detail by Lighthill (ref. 5).

However the third term of (4) proportional to fluctuations of entropy does appear to give a source of acoustic energy. Moreover, if it is assumed that the magnitude of the entropy fluctuations is a function of temperature only and independent of velocity, then it can immediately be seen that the acoustic intensity of this source will vary as U^4, since the rate of change of source strength will be proportional to velocity. It is assumed that the entropy fluctuations are simply proportional to the mean entropy difference across the shear layer. In the absence of static pressure gradients, as in a jet flow, the equation of state for a gas may be used to give,

$$S' \sim S_j - S_o = C_p \log_e \frac{T_j}{T_o} \tag{6}$$

If finally it is assumed that the Reynolds' stress term and the entropy term in (4) are independent (i.e. uncorrelated) source terms, the intensity of the total acoustic radiation may be estimated from the sum of the squares of the two terms times the fourth power of a typical frequency. This results in an expression of the form,

$$I = A\left(\frac{U_j}{a_o}\right)^8 + B\left(\frac{U_j}{a_o}\right)^4 \tag{7}$$

where

$$A \propto \left(\frac{\bar{\rho}}{\rho_o}\right)^2 = \left(k\,\frac{\rho_j}{\rho_o} + 1 - k\right)^2 \tag{8}$$

and

$$B \propto \left(\frac{\bar{\rho}}{\rho_o}\right)^2 \left(\frac{S'}{C_p}\right)^2 \propto \left(\frac{\bar{\rho}}{\rho_o}\right)^2 \left(\log \frac{T_j}{T_o}\right)^2 \tag{9}$$

The coefficient B may also be written in terms of ρ_j/ρ_o since $T_j/T_o = \rho_o/\rho_j$. The log term may be expanded to give approximately

$$\frac{\rho_o - \rho_j}{\frac{1}{2}(\rho_o + \rho_j)}$$

and if $\bar{\rho}$ is taken to be the arithmetic mean

$$\tfrac{1}{2}(\rho_o + \rho_j)$$

the coefficient B becomes,

$$B \propto \left(1 - \frac{\rho_j}{\rho_o}\right)^2 \tag{10}$$

The two coefficients A and B will also in general be functions of the Strouhal number fD/U_j and the ratio of the observer distance to the nozzle diameter, R/D. In the following work, the values of the coefficients are always corrected to R/D=1, assuming an inverse square law dependence.

3. ANALYSIS OF RESULTS

The results for the radiation at 90° are analysed assuming that the radiation intensity is given by equation (7), in which the coefficients A and B are assumed to be functions of temperature ratio, T_j/T_o and, in the case of filtered results, functions of Strouhal number, fD/U_j. The method of analysis consists essentially of matching the measured velocity dependence to the theoretical result (7) by suitably adjusting the values of the coefficients A and B. This process is continued by trial and error until a good fit has been obtained. This analysis was carried out first for the overall intensity at all the temperature ratios tested, then it was extended to the radiation in 1/3 octave frequency bands by studying the measured results at a constant Strouhal number, fD/U_j, rather than a fixed frequency. The use of the Strouhal number ensures that the same source is observed whatever the jet velocity and jet diameter. In this way the variation of A and B with both frequency (Strouhal number) and temperature ratio can be determined.

Typical examples of curve fitting for the ISVR results are shown in figures 1 and 2. The first is for the overall intensity and the other for a Strouhal number of 0.1. Note the extremely good fit that can be achieved over the whole velocity range especially for the temperature ratio of 1.7. The same process was also carried out for the NGTE results although the curve fitting was less exact in this case because the velocity range was more limited. (Incidentally the agreement between this method of analysis and the intercept-slope technique used in ref. 5 is very good, but the new method is much quicker). Where they overlap the two sets of data agree very well, especially the cold results.

Since we are mainly interested in the variation of the two coefficients with temperature ratio, these variations are shown in figure 3, for the overall intensity and in figures 4, 5 and 6 for the 1/3 octave intensity at three Strouhal numbers, 0.1, 0.3 and 1.0. It can be seen that the variations for each coefficient are qualitatively the same for the overall and the filtered results. The ISVR results fit very well into the gap in the NGTE results, although the coefficient of U^8 shows a more rapid decrease with temperature. This is particularly noticeable at Strouhal numbers above 1.0 and indeed the decrease is much more rapid than the most rapid variation predicted by the theory. It is thought that this reduction in the high frequencies for the ISVR results alone is due to atmospheric absorption, which has not been corrected for.

Spectra for each coefficient, combining the two sets of results are shown in figures 7 and 8 and these confirm the good agreement between the two sets. Again the reduction in the high frequencies for the coefficient of U^8 in the ISVR results can be seen especially for the temperature ratio of 1.7.

4. DISCUSSION OF RESULTS

The analysis of these results shows that the noise from hot jets may be separated into two components one of which is the usual mixing noise assumed to vary as U^8 and the other a source which appears to vary as U^4. It is found that both of these components vary with total temperature ratio. The coefficient of U^8 generally decreases rather slowly with temperature but the coefficient of U^4 increases rapidly at small temperature ratios and tends to level off at the higher temperature ratios. (figures 3, 4, 5, 6). These effects occur more or less equally over the whole spectrum and the spectrum of the additional source is very similar in shape to the usual mixing noise spectrum. It is possible that the peak frequency is slightly lower for the coefficient of U^4. Because of the good agreement between two independent sets of results and with the confirmation from two other sources, namely Lockheed Georgia Co. and SNECMA, it seems likely that the appearance of an extra source is a real effect and not peculiar to the rig used.

A theoretical model based on the noise generated by entropy fluctuations has been studied and in its simpler interpretation, the theory predicts an extra source of monopole order whose intensity varies as U^4 in agreement with the observed result. The temperature dependence can also be estimated and these results are given by equations (8), (9) and (10). If the variations (8) and (10) are superimposed on the appropriate figures, 3, 4, 5 and 6, it can be seen that there is a tolerable agreement between the measured points and the theory. The value of k in (8) has been taken as 0.5 in this case, to give the best fit over the whole temperature range. However a value near 0.75 would be more suitable for the ISVR results alone. Such agreement would normally indicate that the theoretical model was adequate and could be used with confidence for prediction purposes. However in this case the simple interpretation of the theory appear to be incorrect on a closer examination.

In the derivation of the theory it has been assumed essentially that the entropy of a particle of fluid following the motion is constant, i.e.,

$$\frac{DS}{Dt} = 0, \tag{11}$$

or in other words that the molecular diffusion effects of viscosity and thermal conduction are absent. Thus fluctuations in entropy at a point are caused by the convection of fluid parallel to the entropy gradient. Thus the rate of change of entropy can be partially, at any rate, replaced by a divergence which is known to represent a higher order source, in this case, a dipole. The complete source term can be found by examining the rate of change of $p-a_o^2\rho$ (see equation (1)). Using the thermodynamic relation (2), equation (11) may be written as

$$\frac{Dp}{Dt} = a^2\frac{D\rho}{Dt} \tag{12}$$

With the help of the equation of continuity, this expression may be used to give an equation for $\frac{\partial p}{\partial t}$ which is part of what is required, i.e.

$$\frac{\partial p}{\partial t} = -u_i\frac{\partial p}{\partial x_i} - a^2\rho\frac{\partial u_i}{\partial x_i}$$

$$= -(\gamma-1)\, p\frac{\partial u_i}{\partial x_i} - \frac{\partial}{\partial x_i}(pu_i) \tag{13}$$

Using the continuity equation again to give $\frac{\partial \rho}{\partial t}$, the expression for the rate of change of $p-a_o^2\rho$ is given by

$$\frac{\partial}{\partial t}(p-a_o^2\rho) = -(\gamma-1)\, p\frac{\partial u_i}{\partial x_i} - \frac{\partial}{\partial x_i}(p-a_o^2\rho)u_i\ . \tag{14}$$

In this expression both pressure and density may be referenced to their ambient values p_o and ρ_o. The first term, which involves the fluid dilatation, is a monopole source because the pressure perturbation $p-p_o$ will vary as U^2, and gives a velocity dependence for the far field variation of at least U^5. The second term is a divergence and consequently it represents a dipole source. Since the space derivative will be converted into a time derivative for the far field radiation, there will be an extra two powers of velocity in the velocity dependence yielding U^6 rather than U^4 for the entropy component of $p-a_o^2\rho$. Even if the viscous dissipation and heat conduction terms are included in equation (14), they do not produce a variation of U^4.

However the experimental results quite clearly show a U^4 variation although, if the results are analysed assuming that it is U^6, it is possible to produce a satisfactory fit to the data at temperature ratios below 1.4. For higher temperature ratios however it is not possible and a U^4 result is much

more satisfactory. Thus it does not seem to be possible to reconcile currently accepted theory with the observed result.

There are at least two possible reasons for this discrepancy. Firstly, even though the theory may be correct, it is possible that serious errors have been made in determining scaling laws, because in a heated flow, the dynamics of the turbulence may be substantially changed. For instance it has been assumed that turbulent velocity fluctuation varies as U and the pressure fluctuation as U^2 and this may not be correct in a heated flow. Secondly, the extra sound may not be generated in the jet turbulence at all but be coming from some point upstream of the nozzle, in which case the theoretical treatment would be different. At present neither of these possibilities has been explored thoroughly.

5. CONCLUSIONS

Experimental results show that a heated jet has an extra source of noise which varies as U^4 and increases in strength with the difference in temperature (or density) between the jet core and the ambient. In addition to this effect, the usual mixing noise which varies as U^8 decreases in strength with temperature in the way usually expected i.e. it varies as the square of the mean density between the jet core and the ambient. A simple theoretical model based on the sound generated by entropy fluctuations gives a very plausible explanation of the observed results, but the theory cannot be justified rigorously. However the theory does give a method for the prediction of the noise from hot jets and a basis for the collapse of data.

Acknowledgement.

The authors are grateful to Professor G.M. Lilley and Dr. C.L. Morfey for their assistance with the theoretical work and to Mr. B. Edwards who carried out the experimental work. The authors are also grateful to NGTE, Pyestock, for supplying their original data.

References.

1. Hoch, R.G., Duponchel, J.P., Cocking, B.J. and Bryce, W.D. Studies of the influence of density on jet noise.
J. Sound Vib. Vol 28, 1973, pp 649 - 668.

2. Ribner H.S. The generation of sound by turbulent jets. Advances in Applied Mechanics Vol. 8 1964 Academic Press Inc.

3. Lush P.A. and Burrin R.H. The generation and radiation of supersonic jet noise. Vol. V. An experimental investigation of jet noise variation with velocity and temperature.
Lockheed Georgia Co. Tech. Report AFAPL-TR-72-53 1972

4. Lush P.A., Fisher M.J. and Ahuja K.K. Noise from hot jets. Proceedings of the British Acoustical Society 1973 Vol 2 No. 2.

5. Lighthill M.J. On sound generated aerodynamically. II Turbulence as a source of sound.
Proc. Roy. Soc. A 1954 Vol 222, 1-32.

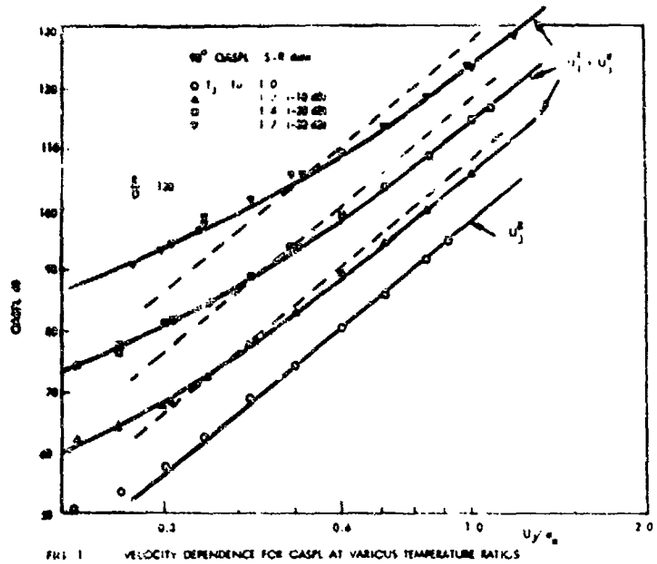

FIG. 1 VELOCITY DEPENDENCE FOR OASPL AT VARIOUS TEMPERATURE RATIOS

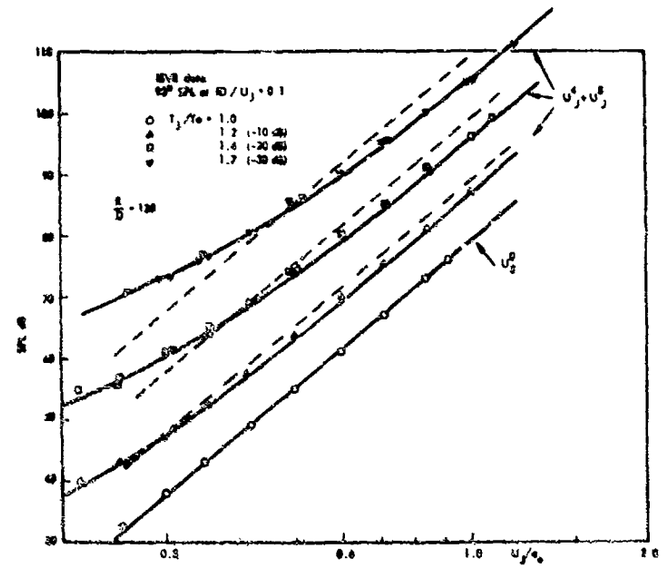

FIG. 2 VELOCITY DEPENDENCE AT CONSTANT STROUHAL NUMBERS FOR VARIOUS TEMPERATURE RATIOS

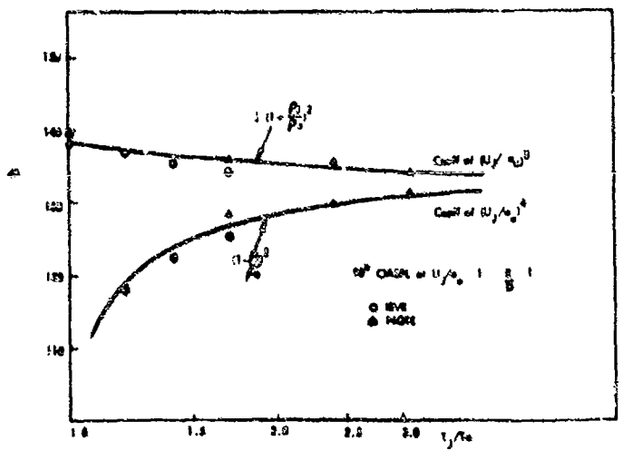

FIG. 3 COEFFICIENTS OF U_j^8 AND U_j^8 FOR OASPL AS A FUNCTION OF TEMPERATURE RATIO

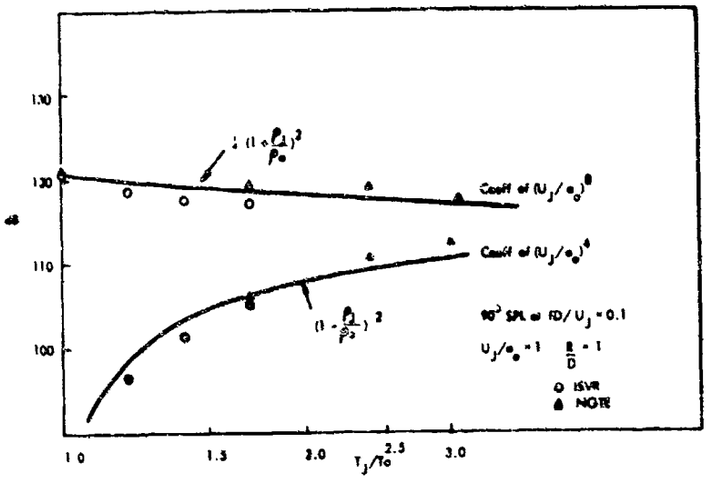

FIG. 4.5.4. COEFFICIENTS OF U_j^4 AND U_j^8 AS A FUNCTION OF TEMPERATURE RATIO FOR VARIOUS STROUHAL NUMBERS.

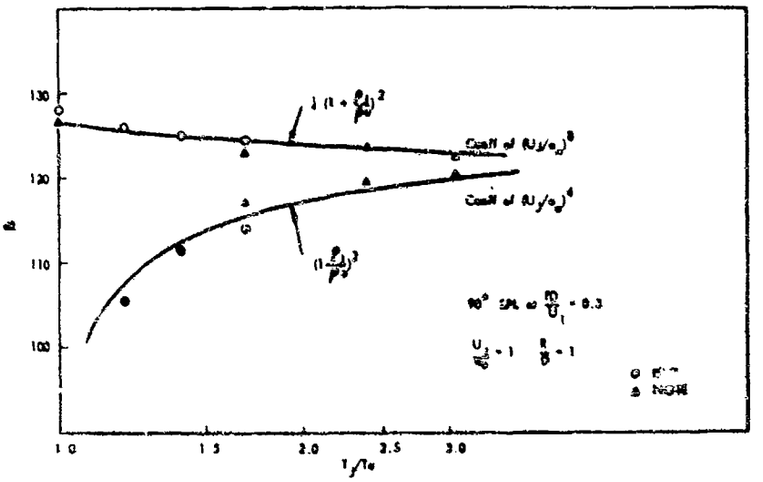

FIG 5

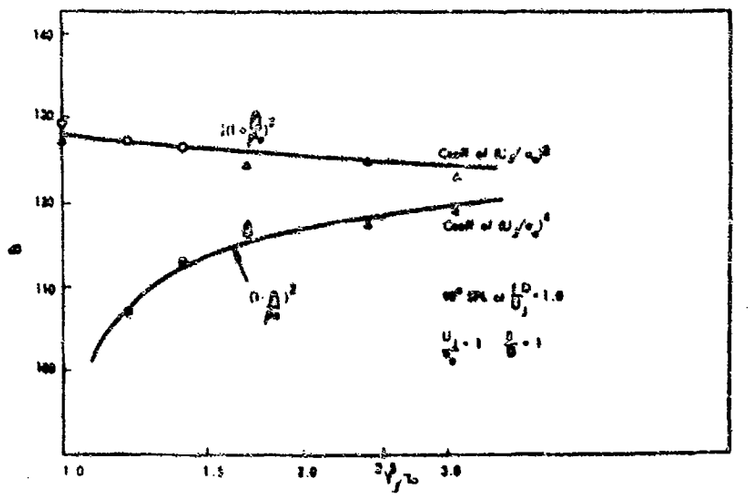

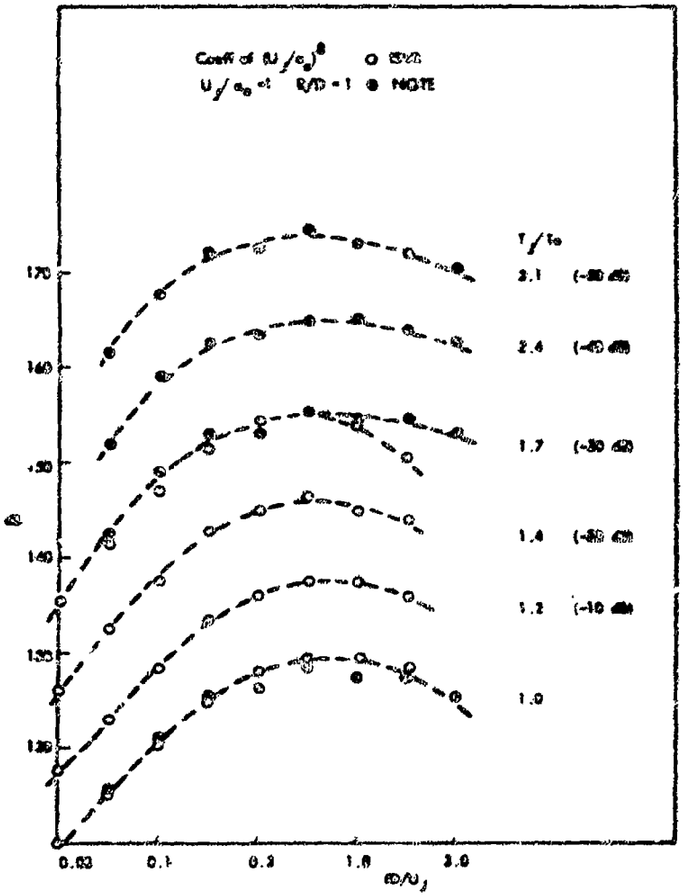

FIG. 7. SPECTRUM FOR COEFFICIENT OF U_j^8 FOR VARIOUS TEMPERATURE RATIOS.

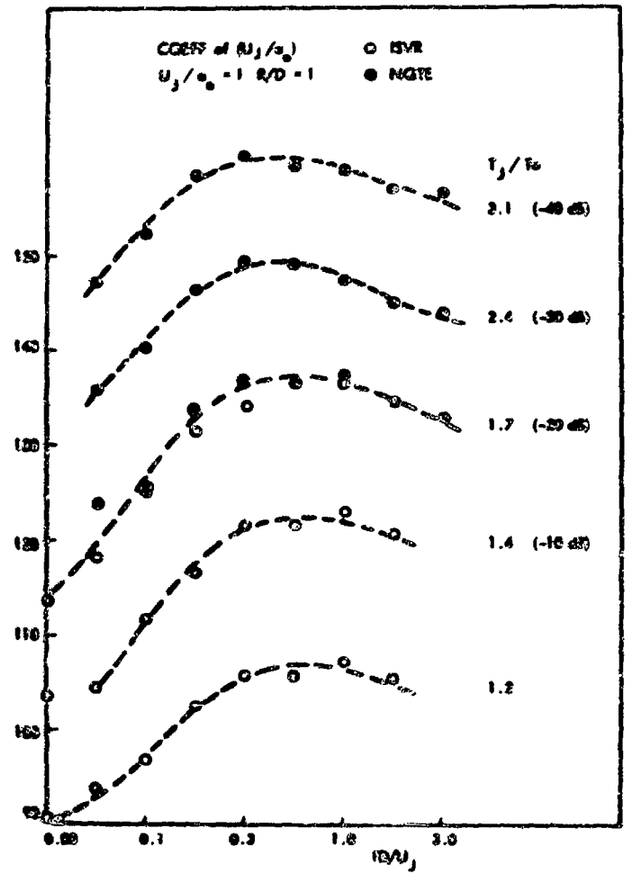

FIG. 8. SPECTRUM OF COEFFICIENT OF U_j^4 FOR VARIOUS TEMPERATURE RATIOS

ON THE NOISE FROM JETS

G. M. Lilley

Department of Aeronautics and Astronautics
University of Southampton, England

SUMMARY

The recent careful experimental results of Lush and others have displayed results for the directivity and spectra of jet noise which are not easily reconciled with the normal dimensional treatments of jet noise based on Lighthill's moving source model involving convective amplification. Although Lighthill's theory is exact, nevertheless it is almost impossible a priori to evaluate the Lighthill source function T_{ij}. In most elementary applications it is usual to approximate T_{ij} by a term proportional to the product of the mean density and the mean square of the velocity and to assume that all possible sources within the jet flow contribute with equal efficiency. For noise generation in the mixing region of a jet, such approximations infer no interaction between the flow and the wave motion leading to the emitted sound. Experiments on the other hand show that changes in mean temperature and mean velocity distributions do modify the intensity and directivity of the radiated sound and hence some further investigation is needed into the generation of noise from shear flows.

A modification of Lighthill's theory is discussed in which pressure disturbances in the jet are treated as an inner flow problem which is matched to the outer flow radiation problem. In this treatment the source function involves quadratic and higher order small disturbance terms. This approach, although more complicated mathematically than the exact theory of Lighthill, has the advantage that it draws attention directly to the role played by the mean velocity and temperature distributions on the generation and propagation of the emitted sound.

The model in its simplest form can be reduced to a vortex sheet model and thus draws attention to the stability characteristics of the vortex sheet. In the more general treatment the stability characteristics of the mixing region are considered and its least stable modes are regarded as dominating the large-scale eddy motion. The linear stability theory is extended to deal with non linearities and, as a result, the amplitude of the large-scale motion is determined. This is compared with the measured large-scale structure of the jet. From this model the main characteristics of the source function are found.

The paper concludes with some results from this new formulation and comparison is made with experiment.

NOTATION

a	speed of sound
A	constant
B	constant
C	constant
d	jet diameter
$b(R)$	source function
h	specific enthalpy
K	constant
l	scale of turbulence
$M = \frac{V}{a_0}$	Mach number based on the external speed of sound
p	pressure
$q(R)$	flow function in the diffraction equation
$\underset{\sim}{Q}$	heat flux vector
$r = \frac{1}{\gamma} \ln p$	
R	radius
S	surface
t	time
T_{ij}	stress tensor (Lighthill)
$\underset{\sim}{v}$	velocity
V	volume and reference velocity
$\underset{\sim}{x}$	distance (position of observer)
$\underset{\sim}{y}$	position of source
γ	ratio of specific heats
Δ	source function
ρ	density
ν_T	eddy kinematic viscosity
Φ	dissipation function
ω	radian frequency

1. INTRODUCTION

Lighthill's theory of aerodynamic noise applied to the problem of the noise generation from the mixing zone of a turbulent jet depends for its success on the knowledge of the properties of the space-time covariance of the stress tensor T_{ij} throughout the mixing region. Currently no theoretical predictions exist for this covariance and few experimental data are available. The illusive character of the T_{ij} covariance is perhaps more readily realised when it is stated it involves, in general, fourth order quantities and includes the effects of refraction and diffraction of the pressure field of the turbulence by the flow itself. The difficulties in the evaluation of the T_{ij} covariance has been the major stumbling block in making detailed inroads into the prediction of noise generation from jets and to a better understanding of the noise characteristics of the generated noise. The problem can be put another way. From what is known of the structure of turbulent jets is it possible to set up a suitable physical model, which when fed into Lighthill's theory can adequately predict the major characteristics of the acoustic radiation? A number of such physical models are described below and each is shown to describe some of the essential characteristics of the radiated noise when the results of the theory are compared with experiment.

2. THE BASIC THEORY

The flow conservation equations for a Newtonian fluid using rectangular Cartesian tensor notations are:-

Continuity $$\frac{\partial \rho}{\partial t} + \frac{\partial \rho v_i}{\partial x_i} = 0 \qquad \ldots\ldots\ldots\ldots 1$$

Momentum $$\frac{\partial \rho v_i}{\partial t} + \frac{\partial \rho v_i v_j}{\partial x_j} + \frac{\partial p}{\partial x_i} = \frac{\partial \tau_{ij}}{\partial x_j} \qquad \ldots\ldots\ldots\ldots 2$$

Energy $$\frac{\partial \rho h}{\partial t} + \frac{\partial \rho v_j h}{\partial x_j} - \frac{\partial p}{\partial t} - v_j \frac{\partial p}{\partial x_j} = \frac{\partial Q_j}{\partial x_j} + \Phi \qquad \ldots\ldots\ldots\ldots 3$$

State (perfect gas) $$p = \frac{\gamma - 1}{\gamma} \rho h \qquad \ldots\ldots\ldots\ldots 4$$

where τ_{ij} is the viscous stress tensor, $\dot{Q}_j$ is the heat flux vector, $\Phi = \tau_{ij} \frac{\partial v_i}{\partial x_j}$ is the dissipation function, h is the specific enthalpy and γ is the ratio of the specific heats. Other symbols have their usual meanings.

In order to perform certain operations on these equations we will also make use of their corresponding forms in vector notation. This is place of 1, 2, 3 we write respectively

$$\frac{D \ln \rho}{Dt} + \nabla . \underline{v} = 0 \qquad \ldots\ldots\ldots\ldots 5$$

$$\frac{D \underline{v}}{Dt} + a^2 \nabla r = \frac{\nabla . \underline{\tau}}{\rho} \qquad \ldots\ldots\ldots\ldots 6$$

$$\frac{\rho D(\frac{p}{\rho^\gamma})}{Dt} - \frac{Dp}{Dt} = \nabla . \dot{Q} + \Phi \qquad \ldots\ldots\ldots\ldots 7$$

where $r = \frac{1}{\gamma} \ln p$, and $a^2 = \frac{\gamma p}{\rho}$ is the square of the local sound speed.

In Lighthill's theory of aerodynamic noise he combines the time derivative of 1 with the divergence of 2 to derive an inhomogeneous wave equation for the density ρ. This equation is written

$$\frac{\partial^2 \rho}{\partial t^2} - a_o^2 \nabla^2 \rho = \frac{\partial^2 T_{ij}}{\partial x_i \partial x_j} \qquad \ldots\ldots\ldots\ldots 8$$

where $T_{ij} = \rho v_i v_j - \tau_{ij} + (p - \rho a_o^2) \delta_{ij}$ is the effective stress tensor for density fluctuations in an aerodynamic flow.

The corresponding equation for the pressure is

$$\frac{\partial^2 p}{\partial t^2} - a_o^2 \nabla^2 p = \frac{a_o^2 \partial^2}{\partial x_i \partial x_j} (\rho v_i v_j - \tau_{ij}) + \frac{\partial^2}{\partial t^2} (p - a_o^2 \rho) \qquad \ldots\ldots\ldots\ldots 9$$

Both forms of Lighthill's equation have been used extensively especially in the approximate form where the forcing function is replaced by $\frac{\partial^2}{\partial x_i \partial x_j} \rho_o v_i v_j$. Some results based on this and related approximations are discussed below.

Lighthill's theory of aerodynamic noise is appealing since it replaces the actual flow by an equivalent flow at rest in which are embedded sources of strength $\frac{\partial^2 T_{ij}}{\partial x_i \partial x_j}$, which can move in this uniform fluid at rest having a constant speed of sound a_o. Thus in the analogy the sources move but not the fluid. Hence when T_{ij} is known throughout the real flow the wave equation 8 can easily be solved and the density fluctuations, and thence the mean sound intensity, can be evaluated in the field outside the flow. But T_{ij} cannot be estimated by any current theory for a turbulent flow and hence at most the sound intensity in the far-field and its directivity can only be found to some order of approximation. The problem is made more complicated when it is realised, as indeed was stressed by Lighthill, that T_{ij} not only includes the fluctuations produced by the turbulent flow but also includes those effects resulting from the interaction between the turbulent flow and the wave motion generated by the flow. Thus unless these latter effects of refraction and diffraction are properly included in evaluating T_{ij} the final results for the far-field intensity will be in error since these phenomena present in the real flow will have been ignored in the analogy. Lighthill was fully aware of these difficulties in the application of his theory but stressed that at least in certain cases of the generation of noise in aerodynamic flows such phenomena would not be of major importance in determining the far-field intensity and the total acoustic power output from such flows. It is clear that any improvement in Lighthill's theory must in some measure allow these phenomena to play a primary rather than a secondary or subsidiary role in the formulation of the dominating equations.

Before we turn to this aspect of our problem let us consider the separate terms in T_{ij}. The first term $\rho v_i v_j$ is the momentum flux per unit volume in the i^{th} direction resulting from fluid crossing a surface perpendicular to the j^{th} direction. The second term $-\tau_{ij}$ is just the viscous stress tensor and so in a turbulent fluid we see that it is augmented by the Reynolds stress $\rho v_i' v_j'$. The third term $(p - \rho a_o^2)$ is normally considered to be of small order in comparison with $\rho v_i v_j$ at least in flows in which the temperature only differs slightly from the ambient medium. Outside the flow, where only sound waves exist, the fluctuations in $(p - \rho a_o^2)$ are identically zero.

Many interpretations have been placed on the term $\nabla^2 (p - \rho a_o^2)$ in the past. What is not usually stated however that in turbulent flow fields disturbances will be predominantly non-isentropic even though isentropic disturbances, in the form of sound waves, will be present also. The general equation for pressure fluctuations within a turbulent flow is from 9

$$\nabla^2 p' = -\frac{\partial^2}{\partial x_i \partial x_j}\left(\rho v_i v_j - \tau_{ij}\right)' + \frac{\partial^2 \rho'}{\partial t^2} \qquad \ldots\ldots\ldots\ldots 10$$

where prime denote fluctuations in time. On the other hand in a weak isentropically disturbed flow

$$\nabla^2 p'_{(i)} = \frac{\partial^2}{\partial t^2} \rho'(i) \qquad \ldots\ldots\ldots\ldots 11$$

where suffix (i) denotes an isentropic fluctuation. Hence on an order of magnitude basis, denoting v_e for the velocity scale of the turbulent fluctuations, V_o the typical mean speed, and ℓ the length scale of the turbulent fluctuations, we find in a turbulent flow in which there is a coexisting sound field,

$$\frac{p'}{\rho_o} = O\left(M_o^2 \left[\frac{p'(r)}{\rho_o} - \frac{v_o^2}{V_o^2}\right]\right) + \gamma \frac{p'(i)}{\rho_o} \qquad \ldots\ldots\ldots\ldots 12$$

where $M_o = V_o/a_o$, and suffix (r) denotes the rotational or non-isentropic part. At sufficiently low Mach numbers the pressure fluctuations within a flow could be dominated by the disturbances due to the sound field. In the absence of sound waves p'/p_o will be of $O(M_o^2)$. The corresponding fluctuations in enthalpy or temperature can be determined by making use of the linearised perturbation of the equation of state

$$\frac{p'}{\rho_o} = \frac{\rho'}{\rho_o} + \frac{h'}{h_o} \qquad \ldots\ldots\ldots\ldots 13$$

It follows that

$$\frac{h'}{h_o} = O\left(\frac{h'(r)}{\rho_o}(1 - M_o^2) + M_o^2 \frac{v_o^2}{V_o^2}\right) + (\gamma-1)\frac{\rho'(i)}{\rho_o} \qquad \ldots\ldots\ldots\ldots 14$$

showing that in low Mach number flows the fluctuations in enthalpy are dominated by the fluctuations in density and not of pressure. Therefore when in such flows sound waves are absent the enthalpy fluctuations are just a function of the non-isentropic part of the density fluctuations which are not necessarily Mach number dependent.

By way of example let us consider the case of the low Mach number flow in a hot turbulent jet. The following approximate results will hold for a turbulent Prandtl number of unity:-

$$-\overline{h'v'} = v_T \frac{d\bar{h}}{dy}$$

$$-\overline{u'v'} = v_T \frac{d\bar{u}}{dy} \qquad \ldots\ldots\ldots\ldots\ldots 15$$

$$\frac{-\overline{h'v'}}{\sqrt{h'^2}\sqrt{v'^2}} = 0.5$$

$$\frac{-\overline{u'v'}}{v'^2} = 0.4$$

It follows that

$$\frac{\sqrt{\overline{h'^2}}}{\bar{h}} = 0.8 \frac{\sqrt{\overline{v'^2}}}{\bar{h}} \frac{d\bar{h}/dy}{d\bar{v}/dy} \qquad \ldots\ldots\ldots\ldots\ldots 16$$

and hence near the centre of the mixing region having an overall difference in enthalpy of $(h_j - h_o)$ and in velocity of $\bar{v}_j$.

$$\frac{\sqrt{\overline{h'^2}}}{\bar{h}} \sim 1.6 \frac{\sqrt{\overline{v'^2}}}{\bar{v}_j} \frac{(h_j - h_o)}{(h_j + h_o)} \qquad \ldots\ldots\ldots\ldots\ldots 17$$

Thus we see that

$$\frac{\sqrt{\overline{h'^2}}}{\bar{h}} = K \frac{\sqrt{\overline{v'^2}}}{\bar{v}} \qquad \ldots\ldots\ldots\ldots\ldots 18$$

where K is a function of h_j/h_o only. When the jet is very hot, with $h_j/h_o \gg 1$, it is seen that the non-dimensional enthalpy fluctuations are nearly double the corresponding velocity fluctuations. We now find in low Mach number flow that

$$(p' - \rho' a_o^2) \sim 0 \left(K \bar{\rho} \frac{\sqrt{\overline{v'^2}}}{\bar{v}} a_o^2\right) \qquad \ldots\ldots\ldots\ldots\ldots 19$$

and is independent of Mach number as $M_o \to 0$. In low Mach number flows we thereby deduce that the third term in T_{ij} dominates over the remaining two terms and has a magnitude independent of Mach number. We can explain this result another way. It is not the pressure fluctuations which dominate in the term $(p' - \rho' a_o^2)$ within a turbulent flow but the non-isentropic density fluctuations, since as $M_o \to 0$

$$(p' - \rho' a_o^2) \to 0 \quad (\rho'_{(T)} a_o^2) \qquad \ldots\ldots\ldots\ldots\ldots 20$$

These results and general conclusions have only been obtained from a crude order of magnitude analysis. They do however guide us into a more complete formulation of the source function in Lighthill's analysis.

If we now return to equation 2 we note that

$$-\nabla^2 p = \frac{\partial^2(\rho v_i v_j - \tau_{ij})}{\partial x_i \partial x_j} - \frac{\partial^2 \rho v_i}{\partial x_j} \qquad \ldots\ldots\ldots\ldots\ldots 21$$

Similarly from 2 and 3

$$\frac{\partial^2 p}{\partial t^2} = -\frac{(\gamma - 1)}{2} \frac{\partial^2}{\partial t^2} \rho v^2 + (\gamma - 1) \frac{\partial}{\partial x_j} (Q_j + v_i \tau_{ij} - \rho v_j h_o) \qquad \ldots\ldots\ldots\ldots\ldots 22$$

where $h_o = h + \frac{1}{2}v^2$ is the specific stagnation enthalpy. This equation demonstrates that the local fluctuations in pressure in a turbulent flow are jointly the result of fluctuations in kinetic energy within a small volume surrounding the local point and the fluctuations in the flux of total energy crossing the surface of the volume. The inhomogeneous equation for the pressure is therefore

$$\nabla^2 p + \left(\frac{\partial^2}{\partial t^2} - a_o^2 \nabla^2\right) p = a_o^2 \frac{\partial^2(\rho v_i v_j - \tau_{ij})}{\partial x_i \partial x_j} - \left(\frac{\gamma - 1}{2}\right) \frac{\partial^2}{\partial t^2} \rho v^2$$

$$+ (\gamma - 1) \frac{\partial^2}{\partial t \partial x_j} (Q_j + v_i \tau_{ij} - v_j (h_o - h_s)) \qquad \ldots\ldots\ldots\ldots\ldots 23$$

and the role of the fluctuations in total energy flux, as a source term in the generation of sound from a turbulent flow when the stagnation enthalpy is many times the static enthalpy, h_o, in the medium at rest outside the flow, is clearly demonstrated.

We have indeed established the identity

$$\frac{\partial}{\partial t}(p - \rho a_o^2) \equiv (\gamma - 1)\frac{\partial}{\partial x_j}(\dot{Q}_j + v_i\tau_{ij} + \rho v_j(h_o - h_s)) - \frac{\gamma - 1}{2}\frac{\partial \rho v^2}{\partial t} \quad \ldots\ldots\ldots 24$$

We note for future use that

$$(\gamma - 1)h_o = a_o^2$$

so an alternative form for 24 is

$$\frac{\partial}{\partial t}\left(\frac{p - \rho a_o^2}{a_o^2}\right) \equiv \frac{\partial}{\partial x_j}\left(\frac{\dot{Q}_j + v_i\tau_{ij} + \rho v_j(h_o - h_s)}{h_o}\right) - (\gamma - 1)\frac{\partial}{\partial t}\left(\frac{\rho v^2}{2a_o^2}\right) \quad \ldots\ldots\ldots 25$$

We have included the viscous and heat conduction terms for completeness in equations 23 to 25. In many practical applications these terms can however justifiably be neglected.

Some explanation of the source term in equation 23 is clearly necessary since it differs appreciably from that given by Lighthill. Firstly whereas in Lighthill's expression for T_{ij} it was deduced that sound is generated by fluctuations in momentum flux we now find that sound is generated through the second source term, in addition directly from the fluctuations in kinetic energy. Finally the fluctuations in total energy flux across surfaces within the flow result in sound generation. These indeed are new and significant results.

The solution of equation 23 taken over a volume V enclosed by a surface S is, following Curle,

$$(p - p_o)(\underline{x},t) = \frac{1}{4\pi}\int_V \left[\frac{\partial^2}{\partial y_i \partial y_j}(\rho v_i v_j - \tau_{ij})\right]\frac{dV}{r} - \frac{(\gamma - 1)}{4\pi a_o^2}\int_V \left[\frac{\partial^2 \rho v^2}{\partial t^2}\right]\frac{dV}{r}$$

$$+ \frac{1}{4\pi}\int_V \left[\frac{\partial^2}{\partial y_j \partial t}\left(\frac{\dot{Q}_j + v_i\tau_{ij} + \rho v_j(h_o - h_s)}{h_o}\right)\right]\frac{dV}{r} + \frac{1}{4\pi}\int_S \left[\frac{1}{r}\frac{\partial p}{\partial n} + \frac{p}{r^2}\frac{\partial r}{\partial n} + \frac{1}{a_o r}\frac{\partial r}{\partial n}\frac{\partial p}{\partial t}\right]\frac{dS}{r} \quad \ldots 26$$

where $[\ ]$ denotes evaluation at the retarded time $t - r/a_o$, and $r = |\underline{x} - \underline{y}|$ is the distance from source to observer n is the outward normal from the volume of fluid to the surface. Following Curle's analysis we find that after application of the divergence theorem twice equation 26 reduces to

$$(p - p_o)(\underline{x},t) = \frac{1}{4\pi}\frac{\partial^2}{\partial x_i \partial x_j}\int_V \left[\rho v_i v_j - \tau_{ij}\right]\frac{dV}{r} - \frac{(\gamma - 1)}{4\pi a_o^2}\int_V \left[\frac{\partial^2 \rho v^2}{\partial t^2}\right]\frac{dV}{r}$$

$$+ \frac{1}{4\pi}\int_V \left[\frac{\partial^2}{\partial y_j \partial t}\left(\frac{\dot{Q}_j + v_i\tau_{ij} + \rho v_j(h_o - h_s)}{h_o}\right)\right]\frac{dV}{r}$$

$$+ \frac{1}{4\pi}\frac{\partial}{\partial x_j}\int_S n_i\left[\rho v_i v_j - \tau_{ij} + p\delta_{ij}\right]\frac{dS}{r} - \frac{1}{4\pi}\int_S n_i\left[\frac{\partial \rho v_i}{\partial t}\right]\frac{dS}{r}$$

where n_i are the direction - cosines of the outward normal to the surface. The corresponding result obtained by Curle, allowing for the fact that we are solving for pressure whereas Curle solved for density is

$$(p - p_o)(\underline{x},t) = \frac{1}{4\pi}\frac{\partial^2}{\partial x_i \partial x_j}\int_V \left[\rho v_i v_j - \tau_{ij}\right]\frac{dV}{r} + \frac{1}{4\pi a_o^2}\int_V \left[\frac{\partial^2}{\partial t^2}(p - a_o^2\rho)\right]\frac{dV}{r}$$

$$- \frac{1}{4\pi}\frac{\partial}{\partial x_j}\int_S n_i\left[\rho v_i v_j - \tau_{ij} + p\delta_{ij}\right]\frac{dS}{r} - \frac{1}{4\pi}\int_S n_i\left[\frac{\partial \rho v_i}{\partial t}\right]\frac{dS}{r} \quad \ldots\ldots\ldots 28$$

The differences between 27 and 28 lie entirely in the use in 27 of the expanded form of

$$\frac{\partial}{\partial t}\,(p - \rho a_o^2) \ .$$

We note other forms of 27 can be derived but for our purposes this appears to be the most convenient one.

In the far-field at many wave-lengths from the flow 27 becomes, for cases where the surface integral is unimportant,

$$(p - p_o)(\underline{x},t) \sim \frac{1}{4\pi a_o^2} \int_V \left[\frac{\partial^2}{\partial t^2}\,(\rho v_i v_j - \tau_{ij} - \frac{(\gamma - 1)}{2}\ v^2)\right]\frac{dV}{r}$$

$$+ \frac{1}{4\pi} \int_V \left[\frac{\partial^2}{\partial y_j \partial t}\left(\frac{\dot{Q}_j + v_i \tau_{ij} + \rho v_j (h_o - h_s)}{h_o}\right)\right]\frac{dV}{r} \qquad \ldots\ldots\ldots\ldots\ 29$$

If we denote a typical frequency in the flow in a frame at rest as $\omega_o = \frac{V_o}{\delta_o}$ then the contribution per unit volume of the first integral in 29 to the total acoustic power output is

$$\frac{\rho^2}{\rho_o^2}\ \frac{v_o^4}{v_o^4}\ \frac{M_o^5}{\delta}\ \rho_o V_o^3 \quad \text{which is the usual result for a volume distribution of quadrupoles.}$$

For the second integral we must first note that strictly the equation of continuity has not been used in the derivation leading to 26, 27 or 29. Thus although it appears to have a magnitude of $O(M_o^6)$ we find that it is also possible for this term to be $O(M_o^4)$. This arises since the non-viscous, non-heat conduction term is

$$\frac{\partial^2}{\partial y_j \partial t}\left(\frac{h_o - h_s}{h_o}\right)\rho v_j = \frac{\partial}{\partial t}\left\{\frac{\rho v_j}{h_o}\ \frac{\partial (h_o - h_s)}{\partial y_j} - \left(\frac{h_o - h_s}{h_o}\right)\frac{\partial \rho}{\partial t}\right\} \qquad \ldots\ldots\ldots\ldots\ 30$$

Thus the contribution to the total acoustic power output per unit volume is

$$\frac{\rho^2}{\rho_o^2}\ \frac{v_o^2}{v_o^2}\ \frac{M_o}{\delta}\left(\frac{h_{oj} - h_o}{h_o}\right)^2 \rho_o V_o^3$$

The second integral in 29 is unimportant in the case of a cold jet but in a hot jet velocity and density fluctuations are amplified by the term $(h_{oj} - h_o)$ where h_{oj} is the mean specific total energy in the case of a hot jet.

The general problem of the evaluation of volume integrals involving div $\rho \underline{v}$ can be illustrated further. From the equation of continuity we have the identity.

$$\int_V \left[\frac{\partial \rho}{\partial t}\right]\frac{dV}{r} = -\int_V \left[\frac{\partial \rho v_i}{\partial y_i}\right]\frac{dV}{r}$$

On application of the divergence theorem and assuming that the surface integral vanishes

$$\int_V \left[\frac{\partial \rho}{\partial t}\right]\frac{dV}{r} = -\int_V \left[\frac{\partial \rho v_x}{a_o \partial x}\right]\frac{dV}{r} \qquad \ldots\ldots\ldots\ldots\ 31$$

, where $v_x = \dfrac{v_i (x_i - y_i)}{r}$ is the component of velocity in the direction from $\underline{y}$ to $\underline{x}$. We note that in the equation of continuity the rotational part of $\underline{w}$ to the divergence is zero so that ρv_x appearing in 31 represents only the irrotational contribution. Thus from 31 we see that

$\rho' = O\left(\rho v_x / a_o\right)$ a result true both for irrotational (or isentropic) and rotational disturbances. Therefore returning back to 30 we see there is a difficulty in placing an order of magnitude to ρv_j appearing on the left hand side. In the form given on the right hand side, in which the equation of continuity has already been employed, no such difficulty exists for ρv_j and $\frac{\partial \rho}{\partial t}$ are their total fluctuating values. In 31, on the other hand v_x refers to the particle velocity (irrotational) and not to the total fluctuating velocity. In particular v_x is not proportional to V_o. Other forms of 30

can be used to justify the results in this section. For instance noting that for any scalar quantity X

$$\frac{\partial}{\partial t}\ \rho X + \frac{\partial}{\partial x_j}\ \rho v_j X = \rho \frac{DX}{Dt} \qquad \ldots\ldots\ldots\ldots\ 32$$

we see that

$$\frac{\partial^2}{\partial y_i \partial t}\ \rho v_j \left(\frac{h_s}{h_o} - 1\right) = \frac{\partial}{\partial t}\left(\rho \frac{D}{Dt}\left(\frac{h_s}{h_o} - 1\right)\right) - \frac{\partial^2}{\partial t^2}\ \rho\left(\frac{h_s}{h_o} - 1\right) \qquad \ldots\ldots\ldots\ 33$$

which leads to the same order of magnitude results quoted above. A further comparison with experiment is made in later section.

So far we have concentrated on an investigation of the terms in T_{ij} involved in Lighthill's theory of aerodynamic noise with a view to seeking their respective orders of magnitude and their variation with the Mach Number of the flow. We now turn to one other aspect of Lighthill's inhomogeneous wave equation for the density within and outside a turbulent flow. In this formulation $T_{ij} = \rho v_i v_j - \tau_{ij} + (p - \rho a_o^2)\,\delta_{ij}$ is only relevant in solving aerodynamic problems when it is independent, or nearly so, of the density fluctuations within the flow. Thus the right and left hand sides of the inhomogeneous wave equation are then regarded as independent. It follows that if terms in T_{ij} exist which are linear in the disturbance density then these cannot be regarded as 'source terms' but must be grouped along with the other linear terms in ρ' on the left hand side of the inhomogeneous wave equation. They represent phenomena such as refraction, convection and diffraction of density fluctuations generated within the flow and influenced by it. If such terms appear on both sides of the equation then a solution of the resulting integral equation can only be solved by iterative methods. We therefore seek a formulation of the equation for, say, the disturbance pressure in which the 'source' term is to a good approximation independent of the disturbance pressure. From the discussion above it appears that the dominant source term, in the generation of noise from turbulent flows, should be that associated with the rotational components of the fluctuating velocity and the non-isentropic part of the density fluctuations. Further when pressure is the dependent variable no terms involving pressure can appear in the source function.

We conclude this section by re-emphasising the problems in the evaluation of volume integrals of the 'source' function when that function is nearly a complete divergence. We find that such a term of monopole type degenerates into a dipole term, i.e. a pole of one order higher in magnitude, and so on. However there can be problems arising in performing this operation as we have seen in equation 31 above thus a monopole term like $\frac{\partial^2 \rho}{\partial t^2}$ cannot be replaced by a dipole term just because $\frac{\partial \rho}{\partial t} = -\frac{\partial \rho v_j}{\partial x_j}$, without considering in some detail as to how this term should be interpreted. In this case we observed that the velocity in the dipole term was not the total velocity in a turbulent flow but only its irrotational component. It would therefore appear to be essential to replace all 'source' terms involving $\frac{\partial}{\partial x_j}(\rho v_j X)$ by their expanded forms and employing the equation of continuity before evaluating its order of magnitude or dependance on velocity say. Thus in the present case the full solution of the inhomogeneous wave equation for the pressure can be written,

$$\begin{aligned}
(p-p_o)(\underline{x},t) = {} & \frac{1}{4\pi} \frac{\partial^2}{\partial x_i \partial x_j} \int_V \left[\rho v_i v_j - \tau_{ij}\right] \frac{dV}{r} \\
& - \frac{(\gamma-1)}{8\pi a_o^2} \int_V \left[\frac{\partial}{\partial t} \rho v^2\right] \frac{dV}{r} \\
& + \frac{1}{4\pi} \int_V \left[\left(\frac{h_s}{h_o} - 1\right) \frac{\partial^2 \rho}{\partial t^2}\right] \frac{dV}{r} - \frac{1}{4\pi} \int_V \left[\frac{\partial \rho v_j}{\partial t}\ \frac{\partial h_s/h_o}{\partial x_j}\right] \frac{dV}{r} \\
& + \frac{1}{4\pi}\ \frac{\partial}{\partial x_j} \int_V \left[\frac{\partial}{\partial t}(\dot{Q}_j + v_i \tau_{ij})\right] \frac{dV}{r} - \frac{1}{4\pi}\ \frac{\partial}{\partial x_j} \int_V \left[\rho v_j \frac{\partial h_s/h_o}{\partial t}\right] \frac{dV}{r} \\
& + \frac{1}{4\pi} \frac{\partial}{\partial x_i} \int_S \ell_j \left[\rho v_i v_j - \tau_{ij}\right] \frac{dS}{r} + \frac{1}{4\pi} \int_S \ell_j \left[\frac{\partial}{\partial t}(\dot{Q}_j + v_i \tau_{ij} - \rho v_j)\right] \frac{dS}{r} \\
& - \frac{1}{4\pi} \int_S \ell_j \left[\rho v_j \frac{\partial h_s/h_o}{\partial t}\right] \frac{dS}{r}
\end{aligned} \qquad \ldots\ldots\ldots\ 34$$

The volume integral terms have already been referred to above and indicate the presence of monopole, dipole and quadrupole distributions in disturbed aerodynamic flow. The surface integral terms are similar to those found by Curle, except for the heat conduction and the viscous stress work terms and the final term in equation 34. Thus we see that noise can be generated by fluctuations in

momentum flux and mass flux across surfaces as well as related fluctuations in the total energy flux. It is of course not implied that all these additional terms, from those noted by Lighthill, lead to an order of magnitude greater than the contribution to the noise intensity from the well-known quadrupole term $\rho v_i v_j$. What is implied that these additional terms, having there origins in the fluctuations in temperature within the aerodynamic flow, cannot be ignored without due note of their order of magnitude. One such case is that of low speed hot jet flows which will be considered later.

3. A GENERALISED WAVE EQUATION

In this section we will derive a convective wave equation which avoids some of the difficulties experienced with the use of the Lighthill source function. We commence with equations 5, 6 and 7. On combining 6 and 7 we find after some rearrangement

$$\frac{\partial \tau}{\partial t} = \frac{\partial}{\partial x_j} \underbrace{\frac{(\dot{Q}_j + v_i \tau_{ij} - \rho v_j h_s)}{\rho h}} - \underbrace{\frac{\partial}{\partial t} \frac{\rho v^2}{2}}_{\rho h} \qquad \ldots\ldots\ldots\ldots\ldots 35$$

a result corresponding to equation 22 and therefore having a similar significance. From the 'mechanical' energy equation found from the scalar product of $\underline{v}$ with 6 we derive the remaining part of $\frac{D\tau}{Dt}$ i.e.

$$v_j \frac{\partial \tau}{\partial x_j} = -\frac{1}{a^2} \frac{D}{Dt} v^2/2 + \frac{v_i}{(\gamma - 1)\rho h} \frac{\partial \tau_{ij}}{\partial x_j} \qquad \ldots\ldots\ldots\ldots\ldots 36$$

so

$$\frac{D^2 \tau}{Dt^2} = \frac{D}{Dt} \frac{1}{\rho h} \frac{\partial}{\partial x_j} (\dot{Q}_j + v_i \tau_{ij} - \rho v_j h_s) - \frac{D}{Dt} \frac{1}{\rho h} \frac{\partial}{\partial t} \frac{\rho v^2}{2}$$
$$+ \frac{D}{Dt} \left(\frac{v_i}{\rho a^2} \frac{\partial \tau_{ij}}{\partial x_j} \right) - \frac{D}{Dt} \left(\frac{1}{a^2} \frac{D}{Dt} \frac{v^2}{2} \right) \qquad \ldots\ldots\ldots\ldots\ldots 37$$

Further from 6

$$\frac{\partial}{\partial x_i} \left(a^2 \frac{\partial \tau}{\partial x_i} \right) = \frac{D^2 \ln \rho}{Dt^2} + \frac{\partial}{\partial x_i} \left(\frac{1}{\rho} \frac{\partial \tau_{ij}}{\partial x_j} \right) - \frac{\partial v_i}{\partial x_j} \frac{\partial v_j}{\partial x_i} \qquad \ldots\ldots\ldots\ldots\ldots 38$$

so that finally we derive Phillips[4] convected wave equation

$$\frac{D^2 \tau}{Dt^2} - \frac{\partial}{\partial x_i} \left(a^2 \frac{\partial \tau}{\partial x_i} \right) = \frac{D}{Dt} \left\{ \frac{1}{\rho h} \frac{\partial}{\partial x_j} (\dot{Q}_j + v_i \tau_{ij}) + \frac{v_i}{\rho a^2} \frac{\partial \tau_{ij}}{\partial x_j} \right\}$$
$$- \frac{\partial}{\partial x_i} \frac{1}{\rho} \frac{\partial \tau_{ij}}{\partial x_j} + \frac{\partial v_i}{\partial x_j} \frac{\partial v_j}{\partial x_i}$$
$$+ \frac{D}{Dt} \left\{ \frac{\gamma - 1}{2} \frac{v^2 v_j}{a^2} \frac{\partial \ln \rho}{\partial x_j} - \frac{v_j}{\rho h} \frac{\partial \rho h_s}{\partial x_j} - \frac{\gamma}{a^2} \frac{\partial}{\partial t} \frac{v^2}{2} - \frac{v_j}{a^2} \frac{\partial}{\partial x_j} \frac{v^2}{2} \right\} \qquad \ldots\ldots\ldots\ldots\ldots 39$$

where the final term can also be written

$$\frac{D}{Dt} \left\{ -\frac{(\gamma - 1)}{a^2} v_j \frac{\partial h_s}{\partial x_j} - v_j \frac{\partial \ln \rho}{\partial x_j} - \frac{(\gamma - 1)}{a^2} \frac{\partial v^2/2}{\partial t} - \frac{1}{a^2} \frac{D}{Dt} \frac{v^2}{2} \right\}$$

Apart from viscous and heat conduction terms we see that the dominant source terms in 38 are

(a) $\frac{\partial v_i}{\partial x_j} \frac{\partial v_j}{\partial x_i} - \frac{D}{Dt} \left\{ \frac{\gamma - 1}{a^2} \frac{\partial v^2/2}{\partial t} + \frac{1}{a^2} \frac{D}{Dt} v^2/2 \right\}$

(b) $-(\gamma - 1) \frac{D}{Dt} \left(\frac{v_j}{a^2} \frac{\partial h_s}{\partial x_j} \right)$

and (c) $-\frac{D}{Dt} \left(v_j \frac{\partial \ln \rho}{\partial x_j} \right)$

These source terms although similar in 22 character to those in Lighthill's equation nevertheless do not involve the variable τ. Apart from the first term they all show a dependence of fluctuations in a frame moving with the field. The first term deserves special attention. In the case of fluctuations in velocity superimposed on a uniform flow this term is quadratic in the perturbation velocity. However, in the case of a shear flow it becomes the product of the mean flow transverse gradient times the gradient of the perturbation velocity field plus quadratic terms. The term linear in the perturbation velocity is however also a function of the pressure fluctuation and hence should not appear as a source term.

A more satisfactory equation for fluctuations in r therefore needs to be found and this has been the subject for detailed investigation by Lilley[5] and co-workers for a number of years. An equation, which is suitable for slowly diverging shear flows, has been obtained and is such that the 'source' function contains no terms linear in the dependent variable r'. The left hand side of the equation includes gradient terms involving the mean velocity and the mean temperature or enthalpy. We assume that such gradients are slowly varying functions of the distance downstream and are dominated by their values in the transverse direction. The equation, which is of third order in r', is

$$\frac{\bar{D}^3}{Dt^3} r' - \frac{\bar{D}}{Dt}(\bar{a}^2 \nabla^2 r') - \frac{\partial \bar{a}^2}{\partial x_2}\frac{\bar{D}}{Dt}\frac{\partial r'}{\partial x_2} + 2\bar{a}^2 \frac{\partial \bar{v}_1}{\partial x_2}\frac{\partial^2 r'}{\partial x_1 \partial x_2} = A(\underline{x}, t) \quad \ldots\ldots\ldots\ldots\ldots 40$$

where $\frac{\bar{D}}{Dt} = \frac{\partial}{\partial t} + \bar{v}_1 \frac{\partial}{\partial x_1}$ and $\bar{v}_1$ and $\bar{a}$ are respectively the mean speed parallel to the jet axis and the mean speed of sound. Both $\bar{v}_1$ and $\bar{a}$ are assumed to be strong functions of the transverse coordinate x_2 but are also weak functions of the axial coordinate x_1. This equation can also be written in terms of axisymmetric coordinates, (r, θ, z). The 'source' function A (x, t) involves products, squares and higher order products of the perturbation quantities and indeed we find it contains two groups of such quantities one of which is multiplied by, and is therefore augmented by, the mean flow gradients. A (x, t) being a non-linear function of the perturbation quantities is a true 'source' function. Our main difficulty is that we have replaced a seemingly simple source function $\partial^2 T_{ij}/\partial x_i \partial x_j$ in Lighthill's theory by one which is more complex and for which the physical significance of the individual terms is far from obvious. Nevertheless, although this might be regarded as a major objection to this form of analysis, the formulation of the inhomogeneous generalised wave equation for the variable r has certain specific advantages over Lighthill's seemingly simple attack on the problem of aerodynamic noise. The notable advantage is that the first order effects of refraction and convection are included in the left hand side of the equation.

The method of solution of equation 40 presents many difficulties and to date no formal analytical solution is available. The main attempts so far have been associated with the development of strip theory methods which aim at finding the contribution to the far-field intensity from a local strip or slice of the turbulent flow allowing for the influence and interaction between the upstream flow and the turbulent flow at the downstream station under consideration. This effect of 'memory' in respect of the disturbances present at a given station appears to be of major importance as seen from the experimental work of Crow[6], Fisher[7] and his coworkers and others. The related approach assumes that the local turbulent structure is in equilibrium and is determined completely by the local time averaged values of velocity and temperature and their distribution. It is further argued that at each station along the jet the fluctuations in velocity are dominant in a certain frequency and hence the spectrum of the radiation noise receives its main contribution in a given frequency band from one section of the jet. (The question of the value of this dominant frequency at each section, and its dependence on the large scale structure of the local flow, is the subject of a separate investigation). Thus with this model, apart from the inclusion of the mean flow effects in the left hand side of the generalised convective wave equation, the evaluation of the far-field intensity is similar to that in Lighthill's theory. In both theories it is assumed that the relevant source function is known so that its space-time covariance can be formulated at least to some acceptable approximation. In this type of model it is found that the results for the intensity, spectrum and directivity are not greatly dependent on the form chosen for this covariance. Rather it is the manner in which the scaling functions of length and time involved with the slowly varying character of the progressing flow to distances downstream that governs the characteristics of the far-field radiation.

One essential difference exists between this model and that based on Lighthill's acoustic analogy. In the latter all sources distributed throughout the turbulent flow radiate equally efficiently. In the model used here this is not so. The characteristic equation for a parallel mixing region at a local strip downstream of the nozzle exit can be written (with R equal to the radius in cylindrical polar coordinates)

$$\frac{d^2\zeta}{dR^2} + q(R)\zeta = h(R) \quad \ldots\ldots\ldots\ldots\ldots 41$$

where ζ is the Fourier coefficient of the fluctuations of r and is a function of the axial and circumferential components of wave-number and frequency. q(R) and h(R) are determined from the known properties of the flow at this station. The far-field intensity and spectrum can be determined from $\zeta\zeta^*$. It is found that Lighthill's result that all sources contribute to the far-field intensity in any given direction does not apply since q(R) possesses transition points and these modify the solution to the inhomogeneous wave-equation to that of the diffraction equation. The result is that in certain directions depending on wave number, frequency and the local Mach number the radiation in a particular direction is severely attenuated as compared with the radiation to other directions. In the high frequency limit the so-called cut-off at small angles is identical with what one would calculate on the basis of the effect of refraction based on ray acoustics. The theory based on the diffraction equation 41 is however valid at all wave numbers and frequencies except in so far as the local parallel shear flow model is a reasonable representation of the true slowly diverging shear flow.

Solutions of equation 41 can be obtained for arbitary source functions and their distribution. The solution around the transition points, the zeroes of q(R), have been found by Phillips, Lilley and more recently by Pao[8] in terms of Airy functions. Such solutions are valid over a wide range of frequency and wave-number. It is possible that a numerical solution now being undertaken will extend the range of current solutions of this equation.

The usefulness of such solutions depends critically on the source function, at least with regard to its spectrum around its band of dominant frequencies. Experiment confirms that these dominant frequencies are closely related to the dominant modes of the shear layer as evaluated according to linear theory and modified by non-linear treatment to include the effects of mode distortion due to vortex stretching and the effects of finite growth towards a finite amplitude. Although the complete relationship between these modes and the large scale structure of the turbulent motion, the effects of the intermittent nature of the turbulent flow and phenomenon such as turbulent bursts, are not yet fully understood, it is clear that a working model is being evolved for the large scale structure of the turbulent shear flow from which the source function can be evaluated. However as emphasised previously it is the changes in the slowly varying structure of the shear layer which appear to dominate the characteristics of the sound radiation. It is because of this that experiments on the effective noise source location in given frequency bands are urgently needed to confirm the elementary calculations which have been performed.

4. COMPARISON WITH EXPERIMENT

In a uniform hot jet issuing from a nozzle into a stationary atmosphere the noise generated in the mixing region can be evaluated from equation 34, which is repeated here for convenience.

$$(p - p_o)\ (\underline{x}, t) \sim \frac{1}{4\pi} \int_V \left[\left[\frac{\partial^2}{\partial t^2} \left(\rho v_x^2 - \frac{\gamma - 1}{2} \rho v^2 \right) \right] \frac{dV}{a_o^2 r} \right.$$

$$+ \frac{1}{4\pi} \int_V \left[\left[\left(\frac{h_s}{h_o} - 1 \right) \frac{\partial^2 \rho}{\partial t^2} \right] \frac{dV}{r} \right.$$

$$- \frac{1}{4\pi} \int_V \left[\frac{\partial \rho v_j}{\partial t} \frac{\partial h_s/h_o}{\partial y_j} \right] \frac{dV}{r} + \frac{1}{4\pi} \int_V \left[\frac{\partial}{\partial t} \left[\rho v_x \frac{\partial h_s/h_o}{\partial t} \right] \right] \frac{dV}{a_o r} \qquad \text{..... 34}$$

We have neglected all viscous and heat conduction terms. The far-field sound intensity per unit volume of mixing region can therefore be written in the following form, on introducing velocity and length scales in the turbulent flow of v_o and ℓ_o respectively, and on the assumption that the various integrals are uncorrelated one to another,

$$i(x) \sim \frac{\rho_o v_e^3}{16\pi^2 x^2 \ell_o} \cdot H_e \frac{\rho_e^2}{\rho_o^2} \frac{v_o^2}{v_e^2} \left[\frac{v_o^2}{v_a^2} \left(\frac{v_e}{a_o} \right)^4 + \frac{v_o^2}{v_e^2} \left(\frac{v_e}{a_o} \right)^2 \right.$$

$$\left. K^2 + \left(\frac{h_{se}}{h_o} - 1 \right)^2 \frac{\ell_o^2}{\delta^2} \right] \qquad \text{..... 42}$$

where suffix 'e' denotes a suitable mean value and δ is the local width of the flow.

On inserting suitable values for the various quantities appearing in equation 42 we see that the far-field noise intensity can be written

$$I(\underline{x}) = A \left(\frac{V_j}{a_o} \right)^8 + B \left(\frac{V_j}{a_o} \right)^6 + C \left(\frac{V_j}{a_o} \right)^4 \qquad \text{..... 43}$$

where $\frac{C}{A} = \text{const.} \left(\frac{h_{sj}}{h_o} - 1 \right)^2$ and $B/A = O(1)$. A more careful analysis could indicate that our constant, which is of order unity, in the expression for $\frac{C}{A}$ should be a weak function of the ratio h_j/h_o. In this section V_j is the jet exit velocity and h_{sj} is the stagnation specific enthalpy at the jet exit with h_j the corresponding value of the specific static enthalpy.

Now in the recent careful experimental studies on hot jets made by Lush[9], Cocking and Jamieson[10], Lush has shown that good agreement exists between the different sets of experimental data over a wide range of values of V_j/a_o and temperature. The experimental results fit the above law at 90° to the jet axis when

$$\frac{C}{A} = \frac{4 (h_{sj} - h_o)^2}{(h_{sj} + h_o)^2} \quad \text{and} \quad B \sim 0$$

which agrees roughly with our prediction. Thus the predicted result that hot turbulent eddies moving into different regions of mean enthalpy produce enhanced density fluctuations in a turbulent flow, leading to increased sound, appears to be verified experimentally.

It can however be queried as to why the term in M_e^6 in equation 42 and the corresponding term in equation 43, do not figure in the experimental results. However although a replot of the experimental data demonstrates clearly the presence of an intermediate range of Mach number where a M_e^6 law holds little is gained over the establishment of the law for the asymptotes of the intensity curve at very low and very high subsonic Mach numbers.

As stated in Section 3 the elementary results obtained from the solution of the convected wave equation indicate the so-called high frequency cut-off at small angles as is found in experiments such as those reported by Lush. Other features of the calculated results, such as the attenuation of certain frequencies in certain angles depending on the Mach number of the flow and the wave-number, have yet to be compared in detail with experiment. At angles other than cut-off some of the results obtained from the solution of this equation will not differ greatly from those of Lighthill's solution. Thus it is of interest to display the detailed results found from Lighthill's theory when a reasonably good approximation to the flow field is incorporated. Many of the features of this calculation have been given before[11] but the more recent calculations have displayed many interesting features such as the slow variation in the peak Strouhal number with jet exit Mach number and the characteristic slopes of the low and high frequency parts of the spectrum. Further results are that roughly half the total radiated noise is generated in the mixing region upstream of the end of the potential core. This result is true for jet exit Mach numbers (V_j/a_o) less than about 2 and where the jet is shock free.

5. CONCLUSIONS

Although many of the overall features of jet noise are well predicted by Lighthill's acoustic analogy theory of aerodynamic noise nevertheless it is found that a serious defect in the theory is that in its applications the interaction between the flow and the disturbances generated by it cannot readily be incorporated. An attempt at including the essential features of this interaction form the main direction for the present work reported in this paper.

However, it is also demonstrated that certain features of the Lighthill theory have not previously been uncovered such as the effect on the radiated noise at low Mach numbers from jets at elevated temperatures. It is shown that as the Mach number is reduced the noise no longer follows a V^8 law, as for a cold flow, but progressively changes to a V^4 law at sufficiently low Mach numbers.

6. REFERENCES

1. M. J. Lighthill — On sound generated aerodynamically I. Proc. Roy. Soc.(A) 211 (1952).
2. M. J. Lighthill — On sound generated aerodynamically II. Proc. Roy. Soc.(A) 222 (1954).
3. N. Curle — The influence of solid boundaries upon aerodynamic noise. Proc. Roy. Soc.(A) 231 (1955).
4. O. M. Phillips — On the generation of sound by supersonic turbulent shear layers. J. Fluid Mech., 9 (1960).
5. G. M. Lilley — (To be published) 1973.
6. S. C. Crow and F. H. Champagne — Orly structure in jet turbulence. J. Fluid Mech., 48 (1971).
7. J. C. Lau, H. V. Fuchs and M. J. Fisher — A study of pressure fluctuations associated with jet flows. University of Southampton, I.S.V.R. Report 28 (1970).
8. S. P. Pao — (unpublished) 1973.
9. M. J. Fisher, P. Lush and N. Harper Bourne — Jet noise. J. S. and V., Vol. 28, no. 3, 1973.
10. B. J. Cocking and J. B. Jamieson — (unpublished) 1972.
11. G. M. Lilley — On the noise from air jets. ARC 20376, 1958.

DISCUSSION

Prof.Michalke:

1. The Equation (24) derived in the paper

$$\frac{\partial}{\partial t}\,(p - a_0^2\rho) \;\equiv\; (\gamma - 1)\,\frac{\partial}{\partial x_j}\,(\dot{Q}_j + v_i\tau_{ij} + \rho v_j(h_0 - h_s)) - \frac{\gamma - 1}{2}\,\frac{\partial}{\partial t}\,(\rho v_i^2)$$

seems to indicate that for an inviscid and non-conducting flow with small changes of enthalpy $h \approx h_0$ the term $\partial/\partial t(p - a_0^2\rho)$ does not vanish. On the other hand, using the equation of state and the thermodynamic relation

$$\frac{\rho}{\rho_0} = \left(\frac{p}{p_0}\right)^{1/\gamma} e^{-(S-S_0)/c_p}$$

where S is the entropy and c_p the heat-capacity coefficient at constant pressure, one can easily derive the equation

$$\frac{\partial}{\partial t}\,(p - a_0^2\rho) \;\equiv\; \left(1 - \frac{h_0}{h}\right)\frac{\partial p}{\partial t} + \frac{a_0^2}{c_p}\,\rho\,\frac{\partial s}{\partial t}\,.$$

This equation shows that for $h \approx h_0$ the term $(\partial/\partial t)/(p - a_0^2\rho)$ is non-zero only if entropy fluctuations would be present. Can you show that in this special case the remaining terms are identical in both equations?

2. Equation (12) implies that the pressure fluctuations p' will be of $O(M_0^2)$ in absence of sound waves. Contrary to this, Fuchs (1972) found in the core of a jet $p' \sim O(\rho_0 \bar{U} u')$ where $\bar{U}$ is the mean speed. Could you please explain how the estimate (12) has been derived and what assumptions have been made?

Prof. Hayes: In reply to the comments by Dr Michalke I agree with him that entropy fluctuations are always present in [illegible] flows and hence are sources of noise even in cold flows. In his second question I have assumed that $u' \sim U$ in the expression given by Fuchs so that p' is $O(M_0^3)$.

MECHANISMS OF EXCESS JET NOISE

D.G. CRIGHTON
Mathematics Department,
Imperial College of Science and Technology,
London S.W.7, England.

SUMMARY.

Excess noise is a term used to describe the deviations of measured noise fields from the predictions of Lighthill's theory of pure jet mixing noise. This paper defines the current state of theoretical understanding of those excess noise fields which are not directly attributable to rotating machinery, or to shock waves in supersonic jets. It is shown that unsteady flow interaction with the jet pipe can generate intense forward arc and sideline noise levels, while abnormally high rear arc levels are suggested to arise from the propagation of genuine sound fields across the exit plane, with associated refraction and diffraction effects. A further process, not yet properly quantified, is related to the instability of a (fully turbulent) jet to certain preferred large scale disturbances, and leads to a mechanism ("parametric amplification") by which internal sound fields may be greatly augmented in either the rear or forward arcs.

1. INTRODUCTION.

Broad-band deviations from the predictions of Lighthill's theory of jet mixing noise are particularly apparent in the sideline direction, and in the forward arc of the aircraft. Rather similar deviations are found in model experiments, in high by-pass ratio turbofans, and in high speed turbojets operating at reduced power settings. They are not necessarily related to machinery noise, or to shock-turbulence interaction in imperfectly expanded supersonic jets. In many cases a critical situation arises in the approach and flyover phases of aircraft operations, in which the forward arc broad-band noise field may be completely dominated by "excess noise". In part this is due to the fact that excess noise sources may be sufficiently powerful to be readily detectable statically (as, for example, in the series of experiments conducted by Gordon on spoiler-generated noise [1]). In part, however, it is also due to the fact that flight effects on mixing noise and on excess noise may be very different, being capable in some cases of significantly amplifying forward arc excess noise, while suppressing mixing noise, with the result that excess noise fields which are undetectable statically may become dominant in flight. Examples of such effects are provided by the NASA/General Electric flyover tests [2] involving a variety of suppressor nozzles, in which virtually every possible combination of increase or decrease in rear or forward arcs is exhibited by different nozzles in flight. Thus, while there is clearly no possibility of any universal excess noise source, or of any universal forward speed effect, it is equally clear that models of possible processes are badly needed, by which correlation, prediction and control techniques could begin to be formulated, at least for some categories of engine.

As far back as 1965, two possible mechanisms of excess noise were clearly recognised, though detailed quantification of the processes is a much more recent matter. This paper offers a brief review of the basic features of the relevant theoretical work, with emphasis on properties which might lend themselves to source identification experiments, and to the development of correlation techniques. The two mechanisms referred to above concern (i) the generation, by obstacles within the tailpipe, of unsteady flow, which then generates sound by interaction with the nozzle as the unsteady flow is convected downstream across the exit plane, and (ii) the generation of noise by unsteady flow around an obstacle within the tailpipe, the noise then propagating as sound down the tailpipe, suffering diffraction by the nozzle and refraction by the mixing layer in its path to the ambient air. (No clear distinction can, of course, be made between (i) and (ii) unless the obstacle concerned is more than a characteristic wavelength upstream of the nozzle; equally, there is no absolute significance in the exit plane as the sound source in (i) - any plane within a wavelength of the exit is equivalent to it.) A third mechanism is concerned with the jet as a "high-gain amplifier" of internal noise (to use Crow's [3] terminology), an issue which is mentioned again below, and then discussed at greater length in §4.

In the next section we look at the results of some simple theoretical models relevant to the interaction of unsteady pressure fields with inhomogeneous surfaces such as the engine tailpipe. Section 3 then reviews current knowledge on the question of sound propagation out of a jet pipe, about which a number of problems remain open. One issue in particular is raised by the fact that the situation of interest concerns the propagation of sound out of the open end of a jet pipe in the presence of flow. In that situation, a sound wave travelling down the tailpipe can trigger off unstable modes on the downstream shear layer, a phenomenon which Crow [3] has shown to occur even in experiments on a high speed fully turbulent shear layer. As well as generating a primary sound field of their own (the field examined by Crow), the unstable modes react back on the nozzle, generating the same sort of interaction sound fields as discussed in §2. This is an aspect of the problem which has escaped the attention of previous investigators. It deserves attention primarily because the interaction sound field generated by unstable shear layer oscillations has a directivity quite different from that of the diffracted sound field which has been the subject of many studies. Accordingly, §4 sets forth current ideas on the triple interaction between an incident sound wave, a jet pipe, and an unstable shear layer.

At no stage is any mathematical detail set out here. The aim throughout is to show how even severely simplified models of the physical processes can lead to simple descriptions of the sound field, and that these descriptions have, at the very least, a great deal in common with the rather curious features of the excess noise fields found in practice.

2. SOUND FROM FLOW-SURFACE INTERACTION

In Lighthill's theory |4| of turbulence-generated noise in an unbounded medium, a complete specification of the flow through given values of the quadrupole stress T_{ij}, composed mainly of the fluctuating Reynolds stresses, is taken for granted; Lighthill's theory then provides the prescription according to which the sound field is to be calculated. Curle's extension |5| of that theory to include surface effects gives an analogous prescription for the sound field - provided a complete specification of surface velocities and stresses is available, in addition to the knowledge of T_{ij} already assumed. Curle's work thus constitutes no more than a formal theory of surface effects; a deductive theory, on the other hand, would assume a knowledge of T_{ij} only, and from this calculate the values of the surface pressures and velocities, and hence the sound field. In this way there would be no possibility of inconsistencies arising, as they often do in formal theories, from mutually conflicting assumptions made simultaneously about T_{ij} and the surface fields. The confusion prevalent some years ago on the question of surface effects provides an adequate warning of the danger in using formal expressions for the sound field. Such expressions have found their use, of course, in particular as applied by Ffowcs Williams & Gordon |6| and Ffowcs Williams |7| to the hypothetical surface at the nozzle exit, to predict the dominance at sufficiently low exhaust speeds of monopole and dipole sources associated with unsteady flow at the nozzle. We shall see shortly how certain versions of those predictions still stand after the application of deductive methods.

A deductive approach to the problem of flow-surface interaction noise is then simply one in which Lighthill's equation - i.e., the wave equation with a known quadrupole (T_{ij}) inhomogeneity - is to be solved subject to appropriate boundary conditions on the surface. As in Lighthill's theory, estimates of the strength and frequency content of T_{ij} are regarded as given independently by incompressible flow arguments, or possibly from measurement. Ideally, of course, one would like to calculate the internal flow and the sound field simultaneously, not merely postulate one and calculate the other; in a very few cases, noted below, it is indeed possible to do this, and the results agree with those predicted from the deductive theories.

The first problem of any importance for our purposes was that solved by Ffowcs Williams & Hall |8|. A semi-infinite rigid plate is immersed in unsteady or turbulent flow characterised by a velocity U and a length scale ℓ. Regarding the flow as acoustically equivalent to a volume distribution of uncorrelated quadrupoles corresponding to turbulent eddies, Ffowcs Williams & Hall show that the scattered field from an eddy of characteristic frequency f distant r_o from the plate edge exceeds the direct field (given by Lighthill's theory) by a factor of $(f\, r_o/a_o)^{-3/2}$, provided the eddy lies within a wavelength of the edge, so that $f\, r_o/a_o \ll 1$. In particular, for the dominant eddies we have $f \sim U/\ell$, $r_o \sim \ell$, and the scattered intensity exceeds the direct intensity by a factor M^{-3}. (Here $M = U/a_o$ is the Mach number, assumed less than unity.) Moreover, the angular distribution of the scattered intensity is essentially as $\sin^2 \frac{1}{2}\theta$ (where $\theta = 0$ is the continuation of the plate), and so has its maximum value on the plate. Generalisations of this problem have been considered |9, 10|; for example, if the plate is compliant and fluid loading effects large, the intensity law $I \sim U^5 \sin^2 \frac{1}{2}\theta$ is modified to $I \sim U^6 \sin^2 \theta$. Although the latter looks very much like the field of a dipole transverse to the plate, there is not necessarily any multipole interpretation of these fields scattered by obstacles with dimension much larger than a wavelength.

These intensity laws are confirmed in detailed examination of a couple of specially simple flows. In one |11|, a line vortex passes round the edge of a plate, and in so doing radiates sound. In the other |12|, a vortex sheet leaves a splitter plate and develops unstable Helmholtz oscillations. Sound is then generated principally by the interaction between the unstable shear layer and the plate - or equivalently, by the unsteady shedding of vorticity at the trailing edge. In both problems, the internal flow and the associated sound field are calculated simultaneously. Errors in the internal flow can have grave consequences for the sound field. For example, small and apparently innocuous approximations to the internal flow can be regarded as equivalent to the application of sources and forces to the fluid, and at low Mach numbers these can produce a dominant, though spurious, sound field, thus making more complicated problems quite unsuited to purely numerical attack.

Regarding the semi-infinite plate in these calculations as some model of the tailpipe nozzle, we see enough differences between the intensity and directivity of the edge - scattered sound and of the jet mixing noise to justify more complicated models. Leppington |13| accordingly considered the interaction between a Lighthill eddy quadrupole and a semi-infinite circular duct, with neglect of mean flow and the associated instabilities of the shear layer. In the low frequency limit ($f\, D/a_o \ll 1$, D the duct diameter), he showed for the axisymmetric mode that $I \sim U^6 (1 - \cos\theta)^2$, while for the first azimuthal mode, the sinuous mode often seen in high-speed jets, that $I \sim U^6 \sin^2\theta$, θ being measured

from the exhaust direction (i.e., the continuation of the duct).

These results are both of potential importance, and deserve the closer examination of them given in |14|. There the unstable shear layer oscillations triggered by unsteady flow were considered, and it was shown that the interaction of such unstable modes with the duct from which the shear layer is shed generates sound fields with the parametric variations $I \sim U^6 (1 - \cos\theta)^2$, $I \sim U^6 \sin^2\theta$ at low frequencies, while $I \sim \tan\frac{1}{2}\theta$ at high frequencies for any order of azimuthal variation. It was also shown that the low frequency results can be interpreted very simply in terms of monopole and dipole sources at the exit plane. The dipole corresponds to the cos θ part for the axisymmetric mode and to the sin θ for the sinuous mode, and the dipole strength is equal to the net unsteady axial thrust fluctuation and to the net cross-stream thrust fluctuation in the two cases, respectively. In the axisymmetric mode, a weak variation in the mass flow accompanies the thrust fluctuation, and in the absence of any field incident from upstream infinity in the pipe, the mass flow monopole and the thrust dipole are coupled so as to produce the (1 - cos θ) factor. (This exclusion of an incident field coming down the pipe toward the exit is supposed to restrict our attention to the results of local unsteadiness near the exit, the case of an incident field being discussed separately in §3.)

The multipole interpretations are very useful in leading to numerical estimates of the sound power in the scattered fields, and in predicting the effect of forward motion. Let the r.m.s. unsteady thrust fluctuation be a fraction ε of the steady thrust, let $S = f D/U$ be the Strouhal number characterising the thrust fluctuation, and let the duct move in the upstream direction, $\theta = \pi$, at Mach number M_a. Suppose also that the unsteady levels relative to the nozzle remain unchanged. Then the details of the calculation show that

$$I \sim \left(\frac{x}{a}\right)^2 \left(\frac{D}{r}\right)^2 \varepsilon^2 S^2 (1 - \cos\theta)^2 \rho U^3 M^3 (1 + M_a \cos\theta)^{-4}, \qquad (2.1)$$

or

$$I \sim \left(\frac{x}{a}\right)^2 \left(\frac{D}{r}\right)^2 \varepsilon^2 S^2 \sin^2\theta \rho U^3 M^3 (1 + M_a \cos\theta)^{-4}, \qquad (2.2)$$

these referring, respectively, to the axisymmetric case (fluctuation in axial thrust) and to the sinuous mode (fluctuation in cross-stream thrust).

The important features of these results are (i) the sixth power intensity law, (ii) the forward or sideline weighting of the directivity factors, (iii) the amplification of these fields in the forward arc under forward motion. As far as the predicted levels goes, one can show that the efficiency of the fields, with ε = 1%, is $10^{-4} M^3$, which is to be compared with values of around $10^{-4} M^5$ for the efficiency of jet mixing noise under typical (i.e., not particularly clean) exit conditions. A 1% net thrust fluctuation may seem excessive, though many agree that such a level might well be exceeded in real engines, and one can show in any case that even under the cleanest possible exit conditions ε must exceed 10^{-3}.

What these calculations have really done is to provide a rigorous justification for much earlier and more primitive, ideas about "nozzle-based" sources (or "lip noise" sources). Those earlier ideas |6,7| simply asserted that thrust fluctuations would act as exit plane dipoles, mass flow fluctuations as monopoles. The detailed calculations show that these ideas are essentially right, provided, in the axisymmetric mode, one recognises that the monopole and dipole are in fact coupled so as to produce the (1 - cos θ) directivity. The Doppler factor $(1 + M_a \cos\theta)^{-4}$ representing forward motion effects has also been seen before (e.g. in |2, Appendix|). The derivation given there, however, does not differentiate between mixing noise sources, which are not carried along with the aircraft, and excess noise sources which are. Thus one might get the impression that the Doppler factor should apply in all cases, even when only pure mixing noise is present. The derivation of the Doppler factor in Eq. (2.1) makes it very clear that the factor only applies to excess noise sources of the monopole or dipole type which are carried along with the aircraft. Moreover, a source should not be further than a typical wavelength from the exit plane if the Doppler factor is to apply. A source hidden deep in the jetpipe would presumably not display that factor, as the power generated by a source could not be affected by effects, such as relative motion, occurring several wavelengths away. It might possibly display a different factor, if its sound field could gain energy from the mean flow in crossing the shear layer, and that is a possibility discussed later, in §4.

We conclude then that excess noise in the forward and sideline directions may be caused by unsteady flow interaction with the tailpipe. If the unsteadiness is highly correlated (ε = 1% or so) the intense fields described by Eq. (2.1 - 2.2) will be generated. If the exit plane fields are not well correlated, all that can usefully be said is that the interaction sound field still has a forward directivity ($I \sim \tan\theta/2$, except very near θ = π, whatever the azimuthal order). It seems from the examples quoted here that high rear arc levels cannot be caused by these mechanisms, though we should mention one case |15| which has been found in which the monopole and dipole exit plane sources do not couple so as to produce the (1 - cos θ) factor. Thus it may be possible for exit plane sources to generate excess noise fields peaking in the rear arc, although the evidence to be presented next suggests that this is not likely to be so.

3. SOUND PROPAGATION OUT OF A DUCT.

In many engines, the rear arc fields display abnormally high broad-band levels around the high angles (90° - 70°) to the exhaust at which turbine and compressor tones are often heard. In many cases these fields are appreciably attenuated by acoustic lining of the tailpipe (as, for example, in Gordon's spoiler noise experiments at model scale |1|). These two properties, coupled with the fact that the fields generally vary relatively slowly with exhaust speed, suggest strongly that the fields arise from the propagation across the exit plane, with associated refraction and diffraction effects, of fields which already exist as sound within the tailpipe. The sound presumably has its origin in unsteady flow over various obstacles within the tailpipe; however, the fact that the sound propagates as such away from the obstacle leads to a very different directivity outside the pipe from that ultimately generated from the creation of a non-propagating unsteady pressure field by the obstacle. And, further, the two mechanisms call for quite different suppression techniques. Acoustic lining may attenuate the rear arc fields under discussion here, but would not be expected to attenuate forward arc fields of the kind examined in §2 (unless, as is possible, the liner reduces the inhomogeneous jump in conditions at the nozzle, making the properties of the tailpipe more like those of the shear layer, with corresponding reduction of interaction noise). On the other hand, screens or grids which might be used as turbulence suppressors, in an attempt to reduce the fields of §2, would not be expected to attenuate the rear arc fields unless the screens had an appreciable acoustic impedance.

We now summarise the essential facts about sound propagation out of a hard-walled duct. Firstly we neglect all effects of flow, and at first we also take a two-dimensional parallel plate representation of the duct. The results for the parallel plates are extremely similar to those for a circular duct (where results for the latter are available at all), while the exact solution for the parallel plates is so much more tractable than that for the circular duct, allowing the important features to be stated simply. Let the duct have width 2R, let k be the wavenumber $2\pi f/a_o$ with f the frequency and a_o the sound speed, and write H for the Helmholtz number kR. In the case of the circular duct we are generally concerned with values of H between, say, 10 and 100, in the broad-band excess noise context.

For a given value of H, there are N + 1 modes which can propagate unattenuated in the duct, N being the integral part of $2H/\pi$, the modes having variation $\cos \frac{n\pi}{2R}(y - R)$ across the duct, with $n = 0,1,2,\ldots, N$. The field incident on the exit plane from any source distribution further than a diameter or so inside the duct can be expressed as a sum of these propagating modes only, non-propagating near-field modes being exponentially cut off over a distance of order R. If H is at all large, however, it may be necessary to retain a large number of modes in the sum, particularly if the source function is not well-matched to the duct geometry. This makes modal description much more appropriate to the tones generated by rotating machinery than to broad-band noise generated by randomly unsteady flow

With these limitations in mind, consider a mode of order n incident on the exit plane from a source well inside the duct. If n is even we write N for the integral part of H/π, while if n is odd N will denote the integral part of $H/\pi + \frac{1}{2}$. Then the radiation pattern consists of a set of N lobes, of which N - 1 lie entirely in the rear arc, $0 < \theta < \pi/2$, while the Nth starts in the rear arc and contains all the forward arc field. (Our terminology corresponds to regarding the duct as a tailpipe rather than an intake, so that $\theta = 0$ would be the exhaust direction if there were flow.) The amplitude along successive lobes decreases steadily as θ increases from 0 to $\pi/2$; further, the amplitude along rays in the final lobe decreases steadily from its peak, attained at an angle less than or equal to $\pi/2$, as θ increases into the forward arc. These features are exhibited in Figure 1, which is a logarithmic polar intensity plot for a mode with n = 2 at a Helmholtz number H = 20, corresponding to, say, a frequency of 2KHz in an engine of 3 ft. diameter. This value of n is chosen since it gives rather large forward arc levels compared with those for n = 0, 1 or 3. Even so, it is clear that the intensity at, say, 120° is 10 dB below that at 60°, and some 28 dB below the peak. A large number of such plots, covering a wide range of frequencies and a variety of source excitations, is given in |16|.

Details of the amplitude and phase can only be found from the full Wiener-Hopf solution to this diffraction problem (see, e.g., |17| for references). This solution lends itself to rapid computation, even though its analytical form is not especially simple. The exact solution to the corresponding problem for the circular duct is considerably more complicated, both computationally and analytically. It is therefore worthwhile drawing attention to the merits of a well-known approximate procedure which yields essentially the right features in very simple terms. In the approximation, the field at the exit plane is taken as that generated by the incident wave alone, with neglect of both the reflected waves and the nonpropagating near-field around the duct lip, and the duct is then regarded as fitted with an infinite rigid flange in the exit plane. Thus, the velocity is then prescribed over the whole of the exit plane, and the radiated field can be readily calculated throughout the rear arc, $0 \leq \theta < \pi/2$. Both the approximations seem plausible at high frequencies for angles well below $\pi/2$, but the procedure does not constitute a rational approximation in any known sense. Despite this, and although it cannot predict anything in the forward arc and might be expected to be poor everywhere except at high frequencies, and poor at all frequencies near the sideline, the approximate procedure does have the following remarkably useful properties:- (i) the directions along which the field vanishes - i.e., the directions which define the lobe structure - are predicted exactly by the approximate method, when applied to the parallel plate duct, for all modes and frequencies;- (ii) it leads to very simple expressions for the radiated field, from which qualitative features

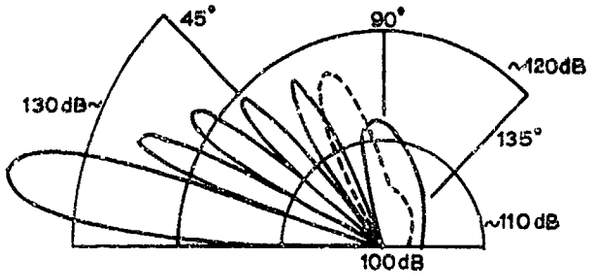

Fig. 1 Far-field directivity pattern. Parallel plate duct. Helmholtz number H=20. Mode number n=2. Dotted line is final lobe for the case n=1, H=20. Taken from [18]

can be easily discerned (for example, the qualitative effects of change of the field incident from inside the duct can be seen very quickly, such changes arising perhaps from change in the properties of the duct walls): - (iii) it does not seem to involve a large absolute error, whatever the frequency parameter H. Candel [18] has examined the error incurred in the parallel plate duct for values of H between 4 and 20. He shows that the maximum error in the radiated intensity never exceeds 7 dB, and that over most of the rear arc the field is correctly predicted to within 1 - 2 dB by the approximate method. It can also be shown that the approximate method gives exactly correct results in the low frequency regime kR << 1, where the field shape is essentially isotropic. (This is rather surprising, since the idea that the duct can be baffled without real change in the rear arc field is clearly inappropriate when kR << 1, while the condition kR << 1 is precisely the condition which ensures that strong reflected waves and near-field components will exist in the duct in addition to the incident field.) The limit kR << 1 does not represent a case of any importance here (it would involve frequencies lower than 100 Hz in real engines), but it emphasises the usefulness of the approximate method at all frequencies.

As examples of the very compact expressions produced by the approximate method, we quote the well-known formulae for the directivity pattern of the far-field intensity produced when a plane wave is incident inside the duct, viz

$$I \propto \left(\frac{\sin (H \sin \theta)}{\sin \theta}\right)^2 \qquad \text{(parallel plate duct)}, \qquad (3.1)$$

$$I \propto \left(\frac{J_1 (H \sin \theta)}{\sin \theta}\right)^2 \qquad \text{(circular duct)}. \qquad (3.2)$$

These are, of course, just the expressions for the directivity of a rigid "piston" oscillating with prescribed velocity and surrounded by a rigid baffle.

It is unfortunate that no approximation has yet been devised to predict the forward arc fields in a similar fashion. However, the general importance of the forward arc can easily be sketched in using the remarks already made. The sideline field can be found approximately, and we know from studies of the parallel plate duct that the field decreases steadily from the sideline into the forward arc. In the frequency regime of interest here (10 < H < 100 say) we conclude at once that the forward arc fields are very much smaller than the fields at angles up to around 70° in the rear arc.

The effect of flow upon the features described above is not known, even qualitatively. Candel [18] has given transformations by which the effect of the <u>same</u> uniform axial flow everywhere (inside and outside the duct) can be assessed. The case of real interest, however, involves different flow inside and outside the duct, with a shear layer shed from the lip. A vortex sheet model of the shear layer, with uniform flow inside the duct and no flow outside, is relevant if one accepts that diffraction and refraction effects are determined by the early thin part of the shear layer. Leaving until §4 the question of shear layer instabilities, the problem of sound propagation out of a duct and across the vortex sheet can be solved formally, but sets heavy computational problems at realistic frequencies and Mach numbers. The approximate method is unfortunately of no use here. It now has no physical basis, and in any case completely fails to predict any effect of uniform flow on a given transverse mode, $\cos \frac{n\pi}{2R} (y - R)$ for example. No doubt <u>one</u> aspect of mean flow and the shear layer is to produce a refractive effect, shifting the whole directivity pattern to higher angles, and creating a zone of silence around the exhaust. But how large the refractive effect is remains undetermined, so that we do not know if it is sufficient to shift the principal static lobe round to angles of 50 - 70° at which intense fields (including turbine tones) are often observed.

4. PARAMETRIC AMPLIFICATION OF INTERNAL NOISE.

The diffraction and refraction of sound generated inside a duct, as it passes across the exit plane and through the shear layer, are energy-conserving processes. Energy is not necessarily conserved in the interaction between a sound wave and a shear layer. A shear layer may develop unstable oscillations in response to a sound wave, and some of the energy in the unstable mode will be radiated away as sound. This radiated energy can only come from the mean flow, and thus the unstable shear layer can act as a parametric amplifier of an incident sound field. In the case when the shear layer is shed from a duct, a triple interaction occurs; the sound wave excites instabilities on the shear layer, and the unstable modes radiate a primary field (as if no duct were present) plus a scattered field arising from coupling of the unsteady flow to the duct. The primary fields have a directivity concentrated in the rear arc, around the region of peak jet mixing noise, while the scattered fields have the forward or sideline directivity associated with most flow-surface interaction fields (see §2). Parametric amplification of internally generated noise has thus the possibility of producing fields with either rearward or forward directivity - even though that internal noise could only be heard appreciable in the rear arc in the absence of flow.

Before going further, we must acknowledge that many workers feel that calculations of the unstable response of laminar shear layers have no relevance at all to the behaviour of a fully turbulent shear layer at very high Reynolds numbers. They argue that the flow is already under a broad spectrum of excitation, and that external stimulation of a jet by even a relatively intense sound wave cannot possibly override the excitation already present. That is not our point of view here, however. Most of the energy of jet turbulence resides in intense fine-scale modes, with which no external sound field of comparable scale can hope to compete. Spasmodically, however, the energy organises a fraction of itself in a coherent large-scale fashion. Coherence is the attribute which enables the large-scale mode (even if not particularly intense) to overcome the background fluctuations, and to compel the whole jet column to respond unstably just as a laminar flow might. An external excitation, suitably coherent and suitably tuned to the intrinsic jet structure, would trigger off similar instabilities. The experimental work of Crow & Champagne |19| and Crow |3| has confirmed such ideas, at any rate for fully turbulent jets at Reynolds numbers around 10^5 |19| and 10^6 |3|. These show that the most easily excited instability is an axisymmetric one at a Strouhal number of 0.3. Michalke |20| has shown that this Strouhal number is predictable from the linear theory of spatial instability, that it depends on the ratio of momentum thickness to jet radius, and that it usually lies between 0.3 and 0.6, close to the Strouhal number for peak jet mixing noise. It is all too easy to dismiss these ideas on the ground that they have only been shown to be relevant at Reynolds numbers a little below those of importance in jet engines. Refusal to accept them seems merely likely to prolong the sterility into which jet noise theory must fall in the absence of any other satisfactory model of jet structure.

Detailed calculation relevant to any realistic situation is still some way off. The simplest case, involving uniform unbounded flows and vortex sheet shear layers, has only recently been worked out |21, 22|, together with extensions |23| to describe the triple interaction between an acoustic source, a vortex sheet and the plate from which the sheet is shed. A further extension of this work to the excitation of the circular vortex sheet shed from a round duct by a source within the duct (and including coupling between the shear layer and duct) is shortly to be completed.

The vortex sheet models of the shear layer permit unbounded exponential growth of unstable disturbances, and preclude realistic estimates of the sound field. There are three obvious mechanisms which can terminate the growth of instabilities in jet flow - (i) nonlinear saturation occurs, (ii) spreading of the mean flow cuts off the growth of a disturbance as it travels into more stable regions. (iii) fine-scale background turbulence attenuates the disturbance in the manner of an eddy viscosity. Mechanism (i) is proposed by Crow & Champagne as the dominant feature, though calculations carried out so far by the author indicate, on the contrary, that (ii) controls the growth and decay of jet instabilities much more effectively.

Crow |3| has fitted a convenient analytical expression to experimental results on the development of axisymmetric disturbances on a jet. An expression for the sound field is then obtained from Lighthill's integral. The formula shows that the far field of a source in a duct in the presence of flow can greatly exceed the far field of the same source in the absence of flow - i.e., that the unstable jet oscillations act as an amplifier of internally generated noise. Experiments |3| on a tone at 850 Hz in a 6" tailpipe and exhaust speed between 800 and 1400 ft/sec confirm the general idea, and also confirm Crow's prediction of an amplification of 34 dB under the right conditions (although there are points of possible contention in the experimental set-up and the interpretation of the measurements).

Just what the position of this mechanism is in the broad-band excess noise context is not yet clear. Many engine spectra show odd large spikes under some unpredictable conditions, and these spikes are not usually regarded as due to any systematic phenomenon. Perhaps Crow's mechanism is the cause of the spikes, and perhaps, more importantly, it is the mechanism behind much of the more widely occurring broad-band noise.

5. CONCLUSIONS.

Three distinct mechanisms of broad-band excess noise have been identified in theoretical work. These comprise unsteady flow interaction with the tailpipe, propagation of internal noise out of the tailpipe, and the amplifying effect on internal noise of unstable jet oscillations. They are distinguished principally by directivity properties, by the effects which sound or turbulence suppressors in the tailpipe have upon them, by forward motion effects, and by velocity dependence. Of course, different mechanisms share some properties in common, but there is enough theoretical evidence to enable circumstantial evidence to be built up, from which source location and data correlation methods may be developed. The experiments of Gordon |1| set a good example of the appropriate use of pieces of

qualitative theory as an aid to definition of an excess noise source and to the development of simple correlation laws with some logical basis. Hopefully, similar use of more recently discovered features, such as those associated with directivity and forward motion effects, will provide a basis for the clearer interpretation of experimental data taken in more complex situations.

REFERENCES

|1| C.G. Gordon. NASA SP-189 (1969), 319-334.

|2| J.F. Brausch. NASA CR-120961 (1972),

R.A. Burley & R.J. Karabinus NASA TM X-68161 (1973).

|3| S.C. Crow. "Acoustic Gain of a Turbulent Jet" Paper IE.6 American Physical Society Meeting, Univ. Colorado Nov. 1972.

|4| M.J. Lighthill. Proc. Roy. Soc. A.211,1952, 564-587.

|5| N. Curle. Proc. Roy. Soc. A.231, 1955, 505-514.

|6| J.E. Ffowcs Williams & C.G. Gordon. AIAA J 3, 1965, 791-793.

|7| J.E. Ffowcs Williams. Proc. AFOSR/UTIAS Symposium on Aerodynamic Noise (ed. H.S. Ribner). Univ. Toronto 1969.

|8| J.E. Ffowcs Williams & L.H. Hall. J. Fluid Mech. 40, 1970, 657-670.

|9| D.G. Crighton & F.G. Leppington. J. Fluid Mech. 43, 1970, 721-736.

|10| D.G. Crighton & F.G. Leppington. J. Fluid Mech. 46, 1971, 577-597.

|11| D.G. Crighton. J. Fluid Mech. 51, 1972, 357-362.

|12| . G. Crighton. Proc. Roy. Soc. A.330, 1972, 185-198.

|13| . G. Leppington. ARC C.P.1195, 1972, Ch.5.

|14| D.G. Crighton. J. Fluid Mech. 56, 1972, 683-694.

|15| P.C. Cannell & J.E. Ffowcs Williams. J. Fluid Mech. 58, 1973, 65-80.

|16| M.E. Goldstein & B.M. Rosenbaum. NASA TN D-7118, 1973.

|17| J.J. Bowman, T.B.A. Senior & P.L.E. Uslenghi "Electromagnetic and acoustic scattering by simple shapes" Amsterdam, North Holland Publ. Co. 1969.

|18| S.M. Candel "Analytical studies of some acoustic problems of jet engines" Ph.D. Thesis CalTech 1972.

|19| S.C. Crow & F.H. Champagne, J. Fluid Mech. 48, 1971, 547-591.

|20| A. Michalke. Z. Flugwiss. 18, 8/9, 1971, 319-328.

|21| M.S. Howe. J. Fluid Mech. 43, 1970, 353-367.

|22| D.S. Jones & J.D. Morgan. Proc. Camb. Phil. Soc. 72, 1972, 465-488.

|23| D.G. Crighton & F.G. Leppington. Two papers to appear in J. Fluid Mech. 1973.

ACKNOWLEDGMENT

This work was supported by a contract from the Ministry of Defence (Procurement Executive), administered by the National Gas Turbine Establishment, Pyestock, Hampshire.

EXPERIMENTS CONCERNING THE FLOW DEPENDENT ACOUSTIC PROPERTIES OF PERFORATED PLATES

by

Jürgen Kompenhans,
Dirk Ronneberger
III. Physikalisches Institut der Universität Göttingen
D 34 Göttingen
Bürgerstraße 42-44
Germany

SUMMARY

The sound propagation in a flow duct is influenced by the acoustical impedance of the walls. In many cases perforated plates are used as acoustic lining. Therefore investigations of the influence of grazing flow on the impedance of a single orifice serving as a simplified model of a perforated plate were started. At small flow velocities the impedance curve plotted in the complex plane passes through a spiral. For higher flow velocities the resistive part of the impedance increases linearly with the flow velocity whereas the reactive part decreases. A relation between the impedance and the static flow resistance can be established. Possible nonlinear properties of the orifice are discussed.

NOTATION

a = radius of the orifice, A = slope of the real part of W_N, c = sound velocity, C = compliance of the measuring cavity, Im(z) = imaginary part of a complex number, $i = \sqrt{-1}$, l = length of the orifice, p = sound pressure, Re = Reynolds number $\rho U a/\mu$, Re(z) = real part of a complex number, S = Strouhal number $a\omega/U$, U = flow velocity, v = particle velocity, W_T = total impedance of the orifice, W_R = radiation impedance of the orifice, W_N = normalized impedance W, δ = boundary layer thickness, μ = viscosity, ν = frequency, ρ = density of the medium, ω = angular frequency.

1. INTRODUCTION

The propagation of sound in ducts is influenced by the acoustic properties of the walls. To achieve noise damping very often linings of perforated plates are therefore mounted some distance from the rigid wall. The interspace is subdivided into seperate cavities and in some cases filled with sound absorbing material (rock wool) to prevent sound propagation in this area. In this case the attenuation of sound is caused by the loss of kinetic energy by frictional forces in the neck of the resonators formed by the perforated plates and the cavities, or by the losses in the absorbing material. To get the desired sound absorbing properties of the duct the resonators have to be designed carefully (that means a suitable resonance frequency has to be installed by choosing the correct dimensions of the resonator's neck and cavity). Such problems have been treated e.g. by U. Ingard /1/ . Thus it is possible to calculate the properties of resonators with adequate accuracy for applications.

In the presence of a mean flow through the duct (e.g. in wind tunnels, fans etc.) the situation changes. From experiments made by Meyer, Mechel and Kurtze /2/ , it is known that the sound attenuation in absorbing ducts is influenced by flow. One can imagine that interactions between the fluid oscillating in the orifice of a resonator and the shear layer of the mean flow above the orifice may take place. Therefore, to calculate the sound attenuation in a duct in the presence of a mean flow the acoustical impedance of the walls (in this case: perforated walls or Helmholtz-resonators) must be known as a function of the grazing flow. As a first approach to the understanding of those interactions investigations of the influence of grazing flow on the impedance of a single orifice were carried out. This influence being explained one may hope to be able to give instructions for the design of sound absorbing linings even in the presence of a mean flow.

2. EQUIPMENT FOR THE MEASURING OF THE ACOUSTICAL IMPEDANCE OF AN ORIFICE WITH LAMINAR GRAZING FLOW

The orifice under investigation is located in the wall of a flow duct (see fig. 1). The end of the orifice averted from the wind tunnel leads into a cavity terminated by a loudspeaker the membrane of which is very stiff. In the neck of the orifice a hot wire probe is fixed with the aid of which the particle velocity through the orifice can be measured. At the wall of the cavity a condenser microphone picks up the sound pressure within the measuring chamber. As the dimensions of the cavity are small compared to the sound wavelength the pressure may be considered constant all over the cavity. Therefore the sound pressure measured by the microphone equals that near the inner end of the orifice. Downstream of this arrangement a second loudspeaker generating the sound in the duct is located. Fig. 1 also shows the according electroacoustical equivalent-circuit diagram of the equipment. The impedance W_T of the total orifice is given by the difference of the sound pressures at both the sides of the orifice divided by the particle velocity through it:

$$W_T = \frac{p_1 - p_2}{v}$$

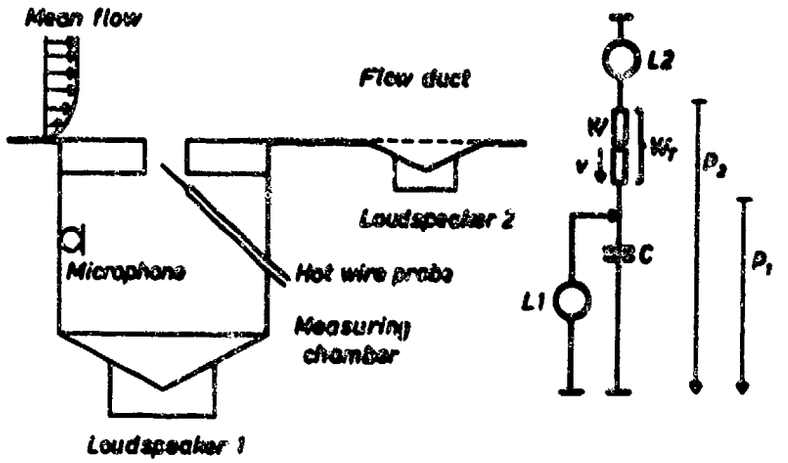

Fig. 1: Sketch of the measuring equipment

As the particle velocity v inside the cavity equals

$$v = j\omega C p_1$$

where C is the spring-like impedance of the cavity. It follows

$$W_f = \frac{1}{j\omega C}\left(\frac{p_2}{p_1} - 1\right)$$

Thus the measuring of the impedance can be reduced to the measuring of sound pressures. To get p_2 the phase and amplitude of an additional sound pressure generated within the cavity is matched to zero the particle velocity through the orifice. (This process is controlled by the hot wire probe.) Then the sound pressure at both the sides of the orifice must be equal. p_2 can be measured with the same microphone as p_1. Additional calibrations of instruments are not necessary.

3. THE ACOUSTICAL IMPEDANCE OF AN ORIFICE FOR AIR AT REST

For air at rest the impedance of an orifice mainly consists of a reactive part which is represented by the mass of the plug of air oscillating in the neck of the orifice and its vicinity (endcorrection). Additionally there is a small resistive part due to viscous losses in the orifice. Measurements of the impedance with air at rest were carried out to check the accuracy of the whole arrangement. After introducing all necessary corrections (e.g. for the influence of the rigid walls of the cavity on the impedance) good agreement was found between experimental and theoretical values of the impedance. The range of the frequencies investigated was 200 - 600 Hz. The diameter of the orifices varied between 2 and 7 mm, the length between 4 and 12 mm. Thus the dimensions of the orifices were slightly greater than the thickness of the boundary layer of the laminar grazing flow in the duct.

4. THE ACOUSTICAL IMPEDANCE OF AN ORIFICE WITH LAMINAR GRAZING FLOW

4.1 General

With laminar grazing flow the impedance changes in dependence on parameters of the flow above the orifice (flow velocity, boundary layer thickness). As already pointed out in /3/ there exists a typical shape of the impedance curve in the complex plane as a function of the flow velocity (fig. 2). At small flow velocities (high Strouhal numbers $S = a\omega/U$, formed with the radius a of the orifice) the impedance passes through a spiral. This spiral can be smaller or larger depending on parameters like the diameter of the orifice or the frequency. In the second so-called 'quasistatic' region (low Strouhal numbers) where the transit time of particles across the orifice is small compared with the period of oscillation the resistive part of the impedance increases linearly with the flow velocity whereas the reactive part decreases (fig. 3 and 4). These statements are valid for all impedance curves measured up to now.

The essential experimental results can be described qualitatively by a model of the flow above the orifice which is presented in /2/. This model is based on the assumption that waves are excited in the shear layer above the orifice by the sound pressure difference between both the sides of the orifice; these waves influence the particle velocity through the orifice.

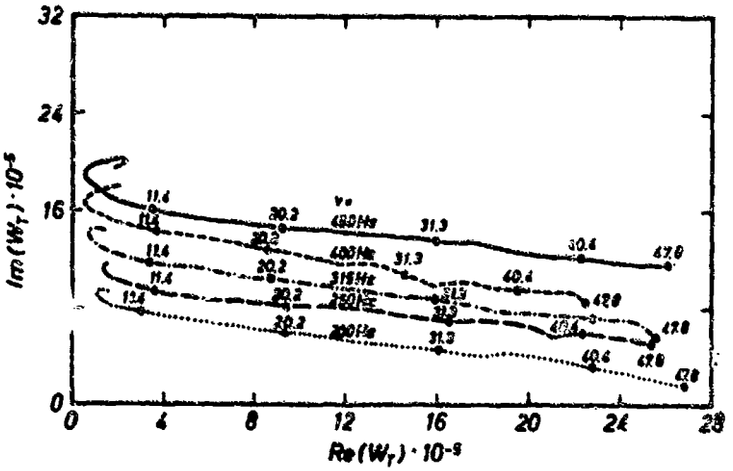

Fig. 2: Impedance W_T (Ns/m^5) of an orifice with grazing flow at various frequencies. The flow velocity U (m/s) is written at the measured points. (Radius a = 2 mm, length l = 4 mm)

4.2 Normalization of the impedance

The flow dependance of the impedance is found to be nearly independent of the length of the orifice, at least if the length is greater than the diameter of the orifice. Therefore, we assume that all changes of the impedance W_T are due to changes of the impedance W of the endcorrection exposed to the grazing flow. This means that we subtract from the impedance of the orifice the parts due to the neck and the inner endcorrection.

With air at rest Re(W) is very small and it is due to viscous losses in the vicinity of the orifice and to the radiation of acoustic energy. Im(W) (ω=0) corresponds to the mass of the endcorrection. In the following it is used to normalize the impedance W_T thus obtaining W_N. The flow velocity is normalized by the factor $a\omega$ obtaining the reciprocal Strouhal number $S^{-1} = U/a\omega$.

As an example W_N of an orifice of a diameter of 4 mm at a frequency of 315 Hz can be seen in fig. 5. At very small flow velocities an increase of the mass part is accompanied by a decrease of the resistance. At $S^{-1} \approx 1$ the situation changes, the imaginary part increases as a function of the flow velocity. One should realize that in the presence of flow the increase of Re(W) does not correspond to an increase of sound radiation but to the dissipation of acoustic energy by viscosity or turbulence production. At a flow velocity of about 13 m/s the imaginary part becomes negative indicating that the mass of

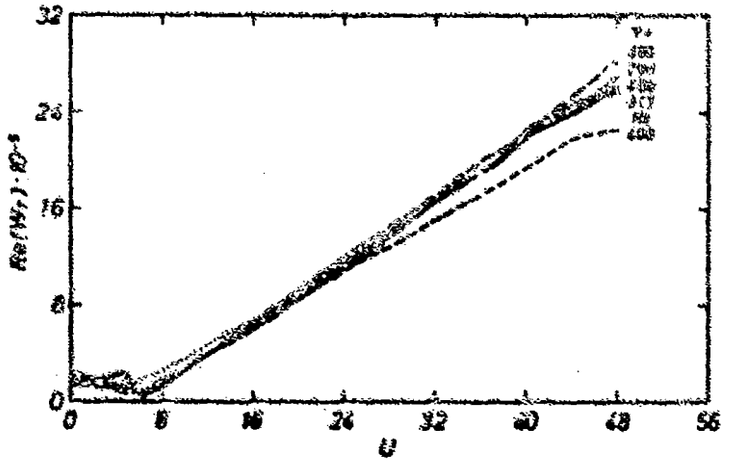

Fig. 3: Real part of the impedance W_T (Ns/m^5) at various frequencies as a function of the flow velocity U (m/s). (Same orifice as in fig.2)

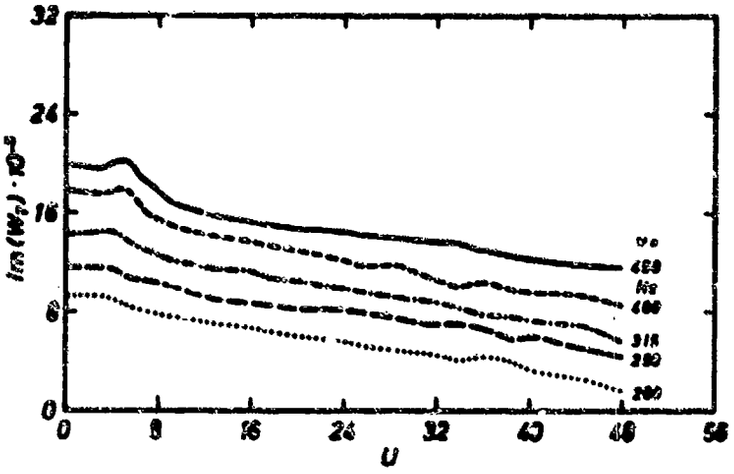

Fig. 4: Imaginary part of the impedance W_T (Ns/m^5) at various frequencies as a function of the flow velocity U(m/s). (Same orifice as in fig. 2)

the endcorrection is 'blown' away. Then, in the 'quasistatic' region the impedance curve changes into a straight line. At flow velocities greater than 40 m/s measurements made with the described measuring equipment no longer led to reproducible results. Therefore it is not yet possible to decide whether the decrease of mass continues with increasing flow velocity resulting in a spring-like behaviour of the orifice.

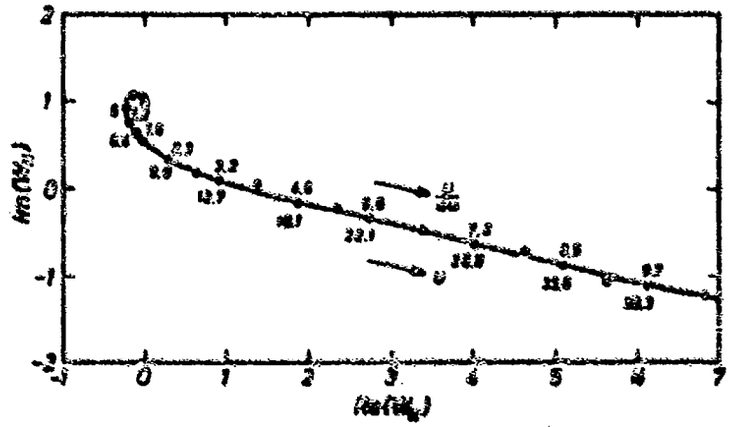

. 5: Normalised impedance W_N of an orifice as a function of the reciprocal Strouhal number. (Frequency ν = 415 Hz, radius a = 2 mm). The flow velocity U (m/s) is written below the measured points.

4.3 The impedance as a function of various parameters

The impedance W_N may depend on the following parameters: flow velocity U, angular frequency ω, radius a, boundary layer thickness δ and the kinematic viscosity μ/ρ. From these parameters the following non-dimensional numbers can be calculated: Strouhal-numbers $S = a\omega/U$, $S_\mu = \rho\omega a^2/\mu$, the Reynolds-number $Re = \rho U a/\mu$ and the ratio δ/a. From our measurements we obtained a linear relation for $Re(W_N)$ in the 'quasistatic' region:

$$Re(W_N) = A\frac{U}{a\omega} + B$$

A and B may be functions of S_μ, Re and δ/a. The coefficient A seems to be independent of the Reynolds number, whereas it depends on δ/a. Up to now further relations could not be established because only too few data are available.

In reference /4/ a linear relation between A and $(\delta/a)^2$ was found for small values of δ/a.

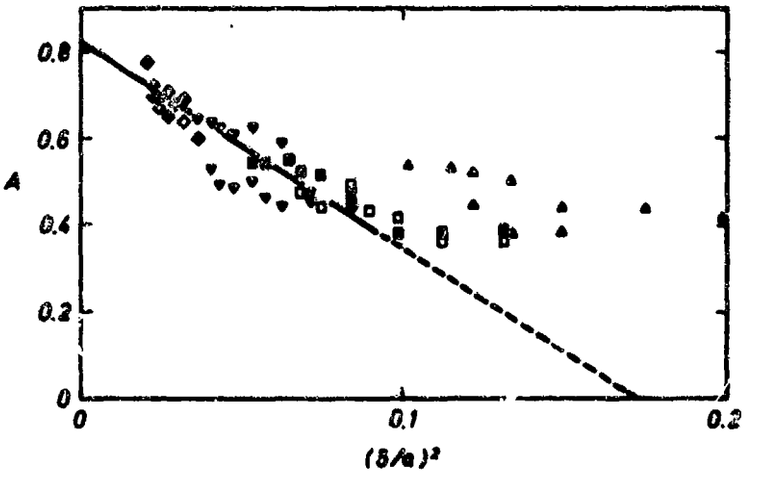

Fig. 6: Coefficient A as function of $(\delta/a)^2$. Acoustic: o , 2a = 1.9 mm; Δ , 2a = 3 mm; □ , 2a = 4 mm; ▽ , 2a = 5 mm; ◇ , 2a = 7 mm. Static: ● , 2a = 1.9 mm; ▲ , 2a = 3 mm; ■ , 2a = 4 mm; ▼ , 2a = 5 mm; ◆ , 2a = 7 mm.

For comparison, A as obtained from the recent measurements is plotted in the same manner (fig. 6, open points). The boundary layer at these measurements was thicker than that at the measurements of /3/ where δ had not been measured directly but was assumed to be proportional to $(U)^{-1/2}$. For small $(\delta/a)^2$ the data plotted in fig. 6 show a linear dependence as in/3/ .

$$A = 0.82 - 4.8(\delta/a)^2$$

(straight line in fig. 6) For higher values of δ/a the measured points lie above this straight line. This is reasonable since otherwise the real part of the impedance would get negative for $(\delta/a)^2$ greater than 0.17.

Another kind of normalization of the impedance could be achieved dividing by the factor ρc . A brief calculation shows that

$$\frac{Re(W)}{\rho c} = 0.85\, A \frac{U}{c}\left(1 + \frac{B}{A}\frac{\omega l}{U}\right)$$

is valid. The extrapolation of ω down to zero yields:

$$\frac{Re(W)}{\rho c} \xrightarrow{\omega \to 0} 0.85\, A \frac{U}{c} .$$

The coefficient A can be regarded as a coefficient of proportionality which is given by the static flow resistance $(\omega=0)$. This static flow resistance of the orifice was measured by a small steady flow through the orifice; it increases linearly with the flow velocity. In fig. 6 the coefficient A as calculated from the static measurements (solid points) is compared with the acoustically measured points. There are some discrepancies which probably arise from the limited accuracy in extrapolating the coefficient A from the acoustical measurements.

In case δ/a gets large compared to unity one should obtain a linear relation

$$A = A' \frac{a}{\delta}$$

(according to /3/). Therefore the measured data for A are plotted as a function of a/δ in fig. 7. There is some evidence that A goes to zero if a/δ does. The scattering of the measuring points is too great to verify the linear relation given above. Especially it is not possible to determine the value of A'.

6. NONLINEAR PROPERTIES OF THE ORIFICE

Another interesting fact is that the flow dependence of the impedance very strongly changes if a narrow-meshed gauze screen is stretched across the orifice at various distances from its top edge /4/ . It is remarkable that an influence of the gauze screen on the change of the impedance in the presence of flow occurs even if the screen is located at the bottom edge of the orifice. Additionally, recent measurements showed that the flow dependent changes of the impedance vary with the volume of the cavity. A provisional explanation can be given as follows.

For air at rest the orifice is driven in the linear region. But in the presence of flow the properties of the orifice become nonlinear though the particle velocity still remains small. In spite of the laminar flow above the orifice turbulent fluctuations of the particle velocity through the orifice were measured by the hot wire probe. These fluctuations might originate from the instabilities of the free shear layer above the orifice and might lead to nonlinear interactions with the sinusoidal measuring signal. There could be some dependence of the instability or the nonlinear interaction on the acoustical impedance of the orifice together with the cavity and eventually the gauze

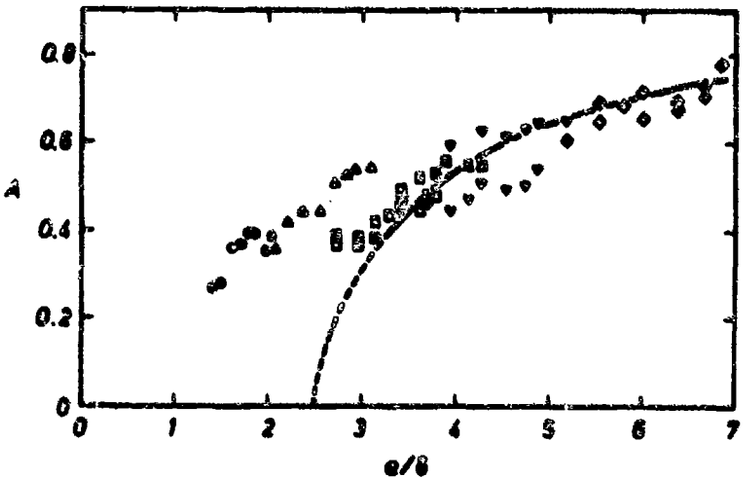

Fig. 7: Coefficient A as function of a/δ . The symbols have the same meaning as in figure 6.

screen. This, indeed, would cause such changes of the impedance as mentioned above. From this point of view it is interesting to investigate the change of the impedance by grazing turbulent flow because there would be a stronger evidence of such postulated nonlinear effects. Therefore an improved measuring equipment has been built up by which it is possible to measure even in the case of turbulent flow.

REFERENCES

/1/ U. Ingard (1953), JASA 25, 1037-1061 On the theory and design of acoustic resonators

/2/ E. Meyer, F. Mechel, G. Kurtze (1958), JASA 30, 165-174 Experiments on the influence of flow on sound attenuation in absorbing ducts

/3/ D. Ronneberger (1972), J. Sound Vib. 24, 133-150 The acoustical impedance of holes in the wall of flow ducts

/4/ D. Ronneberger, B. Ackeleit (1973), Acustica 28, 188-191 Akustische Impedanz überströmter und mit Gaze überspannter Öffnungen

A DETERMINISTIC MODEL OF SONIC BOOM PROPAGATION THROUGH A TURBULENT ATMOSPHERE

by

B.H.K. Lee
National Aeronautical Establishment
National Research Council of Canada
Ottawa, Canada

H.S. Ribner
Institute for Aerospace Studies
University of Toronto
Toronto, Canada

SUMMARY

The propagation of a weak normal shock wave through a turbulent atmosphere is studied in terms of an idealized model. The turbulent field is assumed to be weak and represented by the superposition of two inclined shear waves of opposite inclination to the mean flow. The resulting flow is of a cellular nature. The cells are rectangular in shape and the sense of rotation of the flow alternates from cell to cell. If the angles made by the normal of the incident shear waves with the direction of the mean flow are greater than some critical value an exponentially decaying pressure wave is generated behind the shock. 'Spiked' or 'rounded' waveforms are obtained by adding or subtracting this pressure wave from the steady state pressure field. An illustrative example for a mean flow Mach number of 1.0005 is considered. This gives a steady state overpressure of 2.45 lb. ft.$^{-2}$ across the shock which is typical of the overpressure in a sonic boom.

LIST OF SYMBOLS

Symbol	Definition
A'	amplitude of perturbed u' velocity component
B'	amplitude of perturbed v' velocity component
C_v	specific heat at constant volume
c	speed of sound
F	defined in Equation (22)
f	perturbed shock position
M	Mach number
P	defined in Equation (8)
p	pressure
p'	perturbed pressure
S'	amplitude of the entropy perturbation
s'	perturbed entropy
t	time
U	velocity
u', v'	perturbed velocities in the x and y-directions respectively
W	amplitude of shear wave
x, y	cartesian coordinate
$\bar{x}_s$	non-dimensional shock displacement
α =	cos θ
β =	sin θ
γ	specific heats ratio
θ	angle made by the normal of the disturbance wave with the x-axis
$\theta_{1_{cr}}$	critical angle
λ	wavelength
ν	damping coefficient
ρ	density
σ	defined in Equations (6) and (7)
τ	period
ϕ_p	phase angle of perturbed pressure
ϕ_f	phase angle of perturbed shock position
ω	circular frequency
Subscripts	
1	denotes conditions in front of shock wave
2	denotes conditions behind shock wave

1.0 INTRODUCTION

The effects of atmospheric turbulence on sonic boom propagation have received widespread interest in recent years. Ground measurements of the pressure traces generated by bomber and fighter aircraft show that precise N-waves are rarely encountered, but instead, 'spiked', 'rounded' or approximately N-shaped signatures are observed. These various waveforms are generally attributed to turbulence in the planetary boundary layer[1]. Other interesting features of the sonic boom are the anomalous rise times large differences in overpressures over short distances, and large temporal variations in maximum overpressures at a fixed location.

Complementing these experimental observations a number of theoretical attempts have been made to establish a model of sonic boom distortion. Crow[2] proposed a first order scattering theory incorporating both inertial and thermal interactions and was successful in predicting some of the statistics of random perturbations in the boom signature. An improvement of this model taking into consideration the thickened shock structure has been given by George and Plotkin[3] who argued that the rounding and thickening of the shock structure are due to the strong turbulent scattering of high frequency wave components.

The narrow 'spike' widths have been explained by Pierce[4] as being due to loss by diffraction of the lower frequency portion of the boom. However, the theory is primarily qualitative and gives relatively few predictions which can be quantitatively compared with existing sonic boom data. Pierce[5] also gives an explanation of the anomalous rise times caused by atmospheric turbulence based on an extension of the concept of geometrical acoustics. He suggested a wavefront-folding mechanism such that the shock is made up of a large number of microshocks, and the long rise time is due to the gradual build up of pressure across these very weak shocks. However, most of these theories are based on a number of approximations and assumptions which lack rigorous justification, and experimental verification is non-existent.

In this paper a different approach is used to investigate the distortion of the sonic boom waveform. Instead of the usual statistical approach as used in the above mentioned studies, a regularized model of turbulence (an array of rectangular cells) is proposed and the interaction with a normal shock wave is analysed. The ideas originate from the earlier work of Ribner[6], who considered the convection of a certain pattern of vorticity through a shock wave (Fig. 1).

The specified pattern of vorticity consisted of a single Fourier component of an arbitrary velocity field (which might be a turbulent field) and can be represented by a planar shear wave which is being carried along by the mean flow. The shear wave has vorticity by virtue of a sinusoidal variation in velocity with distance perpendicular to the wavefront. If we superimpose two such shear waves which are inclined to the shock front but in opposite inclination, the resulting flow is of a cellular nature (Fig. 2). The cells are rectangular in shape and the sense of rotation of the flow alternates from cell to cell. In a coordinate system where the mean shock position is stationary these cells are convected by the main flow, and the two velocity components in the cells have sinusoidal variations in the directions along and perpendicular to the flow.

Figure 3 shows the undulations of the shock front to be expected as it propagates through the cellular flow 'turbulence'. Associated with the undulations will be distortions of the shock profile. The analysis herein will be directed toward calculating these distortions.

In Ribner's solution the unsteady flow problem was treated as an equivalent steady flow problem by a coordinate transformation. When considering two shear waves inclined to the shock in the opposite sense it is necessary, however, to choose a stationary coordinate system and consider the flow to be time dependent. It is assumed that the amplitudes of the shear waves are equal but small compared to the mean flow so that they can be combined linearly. The undisturbed shock wave is taken to be stationary and perturbations of the shock front are generated by the rotating flow in each cell.

Similar to Ribner's results for a single shear wave, if the inclination of the shear wave to the shock is greater than some critical value the individual shock disturbances can combine to radiate sound waves. However, if the angle is less than the critical an exponentially decaying pressure field will be generated. Now if the cells are made up by shear waves inclined at angles to the shock front less than the critical value, then 'spiked' or 'rounded' waveforms can be obtained by adding or subtracting the decaying pressure wave from the steady state pressure field.

In extending the results to sonic boom studies, it should be noted that the analysis considers the pressure behind the unperturbed shock jump to be uniform. However, following the leading shock of a sonic boom N-wave, the pressure decreases linearly owing to the expansion waves trailing behind the shock front. The situation is, however, correctly modelled for the rear shock of the N-wave, downstream of which the pressure is uniform. Experimentally, both front and rear shocks appear to suffer virtually identical incremental distortions on passage through atmospheric turbulence; thus the linear pressure decay behind the undisturbed front shock does not appear to have a significant influence.

2.0 THEORETICAL FORMULATION

2.1 Governing Equations

Consider the uniform flow of a nonviscous, nonconducting perfect gas. With reference to a stationary rectangular frame of coordinates with the x-axis in the direction of the main flow, the equations of the propagation of weak plane disturbances can be written as:

$$\frac{1}{c^2}\left(\frac{\partial p'}{\partial t} + U\frac{\partial p'}{\partial x}\right) + \rho\left(\frac{\partial u'}{\partial x} + \frac{\partial v'}{\partial y}\right) = 0 \tag{1}$$

$$\frac{\partial u'}{\partial t} + U\frac{\partial u'}{\partial x} = -\frac{1}{\rho}\frac{\partial p'}{\partial x} \tag{2}$$

$$\frac{\partial v'}{\partial t} + U\frac{\partial v'}{\partial x} = -\frac{1}{\rho}\frac{\partial p'}{\partial y} \tag{3}$$

$$\frac{\partial s'}{\partial t} + U\frac{\partial s'}{\partial x} = 0 \tag{4}$$

where U, ρ and c are the velocity of the mean flow, unperturbed density and speed of sound respectively. The primed quantities, that is, p', u', v', and s', denote the perturbed pressure, velocity components in the x and y directions, and the entropy respectively.

Following an approach similar to that given by Johnson[7] in the study of the interaction of a sound wave with a shock, we let θ be the angle made by the normal of the disturbance wave with the x-axis. Furthermore, we define $\alpha = \cos\theta$ and $\beta = \sin\theta$ and assume the perturbations of the mean flow to be of the form:

$$\begin{aligned} p' &= C'e^{i\sigma(\alpha x+\beta y) - i\omega t} \\ u' &= A'e^{i\sigma(\alpha x+\beta y) - i\omega t} \\ v' &= B'e^{i\sigma(\alpha x+\beta y) - i\omega t} \\ s' &= S'e^{i\sigma(\alpha x+\beta y) - i\omega t} \end{aligned} \tag{5}$$

where C', A', B', and S' are the amplitudes of the perturbed quantities and ω is the circular frequency. Substituting Eq. (5) into Eqs. (1) to (4) we obtain (Fig. ?),

$$\sigma = \pm\frac{\frac{\omega}{c}}{1 \pm M\alpha} \quad \text{(sound wave)} \tag{6}$$

or

$$\sigma = \frac{\frac{\omega}{c}}{M\alpha} \quad \text{(shear-entropy wave)} \tag{7}$$

where M is the Mach number of the mean flow. The negative sign in Eq. (6) corresponds to a sound wave propagating in the direction against the flow and this is discarded in the present study. Since the flow is irrotational in a sound wave, the coefficient in Eq. (5) can be chosen accordingly to give:

$$\left.\begin{aligned} p' &= \rho c P e^{i\frac{\omega}{c}\frac{(\alpha x+\beta y)}{1+M\alpha} - i\omega t} \\ u' &= \alpha P e^{i\frac{\omega}{c}\frac{(\alpha x+\beta y)}{1+M\alpha} - i\omega t} \\ v' &= \beta P e^{i\frac{\omega}{c}\frac{(\alpha x+\beta y)}{1+M\alpha} - i\omega t} \end{aligned}\right\} \text{(sound wave)} \tag{8}$$

and for the shear-entropy wave we specify a flow of zero pressure perturbation (the sound wave accounts for the entire amount) and zero divergence. Thus, the two terms of Eq. (1) vanish separately and Eq. (5) takes the form:

$$\left.\begin{aligned} u' &= -\beta W e^{i\frac{\omega}{c}\frac{(\alpha x+\beta y)}{M\alpha} - i\omega t} \\ v' &= \alpha W e^{i\frac{\omega}{c}\frac{(\alpha x+\beta y)}{M\alpha} - i\omega t} \\ s' &= S' e^{i\frac{\omega}{c}\frac{(\alpha x+\beta y)}{M\alpha} - i\omega t} \end{aligned}\right\} \text{(shear-entropy wave)} \qquad (9)$$

where W is the amplitude of the shear wave.

2.2 Boundary Conditions

Let $x = f(y,t)$ be the perturbed shock front displacement from its steady state value. Using the oblique shock relations and making the assumption that $\partial f/\partial y$ and $\partial f/\partial t$ are small, the linearized Rankine-Hugoniot relations for the perturbations behind the shock wave are:

$$p_2' = \frac{p_2}{p_1} p_1' + \frac{4\gamma}{\gamma+1}\frac{M_1}{c_1} p_1 (u_1'-f_t)$$

$$u_2' = f_t + \left\{\frac{(\gamma-1)M_1^2 - 2}{(\gamma+1)M_1^2}\right\}(u_1'-f_t)$$

$$v_2' = v_1' + \frac{2M_1 c_1 (M_1^2-1)}{(\gamma+1)M_1^2} f_y \qquad (10)$$

$$s_2' = s_1' + \frac{4\gamma}{c_1} c_v \left\{\frac{M_1}{2\gamma M_1^2 - (\gamma-1)} - \frac{1}{M_1[(\gamma-1)M_1^2+2]}\right\}(u_1'-f_t)$$

The subscripts '1' and '2' refer to conditions in front and behind the shock respectively, and M_1 is the mean flow Mach number.

2.3 Angle Relations for Refracted Shear Wave and Sound Wave

Consider a single shear wave convected by the main flow at a velocity U. Let θ_1, θ_2 and θ_3 represent the angles made by the normals of the incident shear wave, refracted shear wave and sound wave respectively with the horizontal (see Fig. 1) and α and β to be the cosine and sine of θ with the appropriate subscripts for each of the three different sets of waves. Immediately behind the shock ($x = 0$), the refracted shear wave and sound wave must combine to be in phase with the input shear wave. From Eqs. (8) and (9), the exponential factors must be equal and we obtain the following equation for $x = 0$:

$$\frac{\omega}{c_1}\frac{\beta_1}{M_1\alpha_1} = \frac{\omega}{c_2}\frac{\beta_2}{M_2\alpha_2} = \frac{\omega}{c_2}\frac{\beta_3}{1+M_2\alpha_3} \qquad (11)$$

After some simplifications, we have:

$$\cos\theta_2 = \frac{(\gamma+1)M_1^2}{\sqrt{(\gamma+1)^2 M_1^4 + [(\gamma-1)M_1^2+2]^2 \tan^2\theta_1}}$$

and

$$\cos\theta_3 = \left\{-\frac{\tan^2\theta_1}{(\gamma+1)^2 M_1^4}\sqrt{[2\gamma M_1^2 - (\gamma-1)][(\gamma-1)M_1^2+2]} + \sqrt{1 - \frac{1}{M_1^4}\frac{(M_1^2-1)}{(\gamma+1)}[(\gamma-1)M_1^2+2]\tan^2\theta_1}\right\} \Big/ \left\{1 + \frac{[(\gamma-1)M_1^2+2]^2}{(\gamma+1)^2 M_1^4}\tan^2\theta_1\right\} \qquad (13)$$

In order that $\cos\theta_3$ be real, we require

$$\tan \theta_1 \leq M_1^2 \sqrt{\frac{(\gamma+1)}{(M_1^2-1)[(\gamma-1)M_1^2 + 2]}} \tag{14}$$

The critical angle $\theta_{1_{cr}}$ is determined as arc-tan of the R.H.S. of Eq. (14) and is a function of the mean flow Mach number only. For $\theta_1 < \theta_{1_{cr}}$, the individual sound disturbances behind the shock can combine to radiate plane sound waves. If $\theta_1 > \theta_{1_{cr}}$ an exponentially decaying pressure field will be generated instead. Since the latter is the case of interest in studying the distortion of the waveform behind the shock, the analysis will only be carried out for $\theta_1 > \theta_{1_{cr}}$.

2.4 Decaying Pressure Wave

For $\theta_1 > \theta_{1_{cr}}$, let us assume the exponential factor in Eq. (5) to be of the form $i[(\sigma\alpha+i\nu)x + \sigma\beta y - \omega t]$. If $\nu > 0$, the pressure wave decays exponentially in the x-direction but not in the y-direction since it must be in phase with the input shear wave. Using this exponential factor for the perturbation quantitatives in Eq. (5), we obtain the following expressions for σ and ν after substituting Eq. (5) into Eqs. (1) to (4):

$$\sigma = \frac{\frac{\omega}{c}}{M\alpha} \text{ and } \nu = 0 \text{ (shear-entropy wave)} \tag{15}$$

$$\left.\begin{aligned} &\text{or} \quad \sigma = -\frac{\omega}{ac}\frac{M}{1-M^2} \\ &\text{and} \quad \nu^2 = \frac{\sigma^2(1-M^2\alpha^2) + 2\frac{\omega}{c}\alpha M - \frac{\omega^2}{c^2}}{1-M^2} \end{aligned}\right\} \text{(decaying sound wave)} \tag{16}$$

Equation (15) is the same as the results obtained from Eq. (7), and unlike the sound wave, the refracted shear wave does not decay along the x-axis. Behind the shock wave we have:

$$\frac{\omega}{c_1}\frac{\beta_1}{M_1 a_1} = \sigma\beta,$$

by equating the exponential factor of the incident shear wave to the sound wave. Using this expression and the fact that $\alpha_1^2 + \beta_1^2 = 1$, Eq. (16) can be simplified to give:

$$\sigma = \frac{\frac{\omega}{c_2}}{M_1^2 a_1(\gamma+1)(M_1^2-1)} \sqrt{[(\gamma-1)M_1^2 + 2]\{(M_1^2-1)^2 + (2M_1^2-1)a_1^2\}\{2\gamma M_1^2 - (\gamma-1)\}} \tag{17}$$

$$\nu = \frac{2\gamma M_1^2 - (\gamma-1)}{M_1^2 a_1(\gamma+1)(M_1^2-1)} \frac{\omega}{c_2} \sqrt{\frac{\{2\gamma M_1^2 - (\gamma-1)\}\{(\gamma-1)M_1^2+2\}(-a_1^2) - (\gamma+1)M_1^2 a_1^2}{(\gamma+1)}} \tag{18}$$

and

$$\alpha_1 = \frac{-M_1^2 a_1}{\sqrt{(M_1^2-1)^2 + (2M_1^2-1)a_1^2}} \tag{19}$$

$$\beta_1 = \frac{\beta_1(M_1^2-1)}{\sqrt{(M_1^2-1)^2 + (2M_1^2-1)a_1^2}} \tag{20}$$

To determine the disturbance field we superimpose the solutions for two shear waves inclined at θ_1 and $-\theta_1$ to the main flow. The perturbed shock front is assumed to consist of two components f_1 and f_2 proportional to

$$e^{i\frac{\omega}{c_1}\frac{\beta_1}{M_1 a_1}y - i\omega t} \quad \text{and} \quad e^{-i\frac{\omega}{c_1}\frac{\beta_1}{M_1 a_1}y - i\omega t}$$

respectively. Making use of the boundary conditions given in Eq. (10), we obtain the following expressions for the decaying pressure field downstream of the shock wave and the shape of the perturbed shock:

$$\frac{p_2'}{p_2} = -i2\gamma \frac{W_1}{c_1}\frac{c}{c_2} P \sin\left(\frac{\omega}{c_1}\frac{\beta_1}{M_1\alpha_1} y\right) e^{-\nu x - i\left(\frac{M_2}{1-M_2^2}\frac{\omega}{c_2} x + \omega t - \phi_P\right)} \tag{21}$$

$$\frac{f}{\lambda} = -\frac{W_1}{\pi c_1}\frac{1}{M_1} F \sin\left(\frac{\omega}{c_1}\frac{\beta_1}{M_1\alpha_1} y\right) e^{i(\phi_F - \omega t)} \tag{22}$$

where P, ϕ_P, F and ϕ_F are given in the Appendix. W_1 and λ are the amplitude and wavelength of the incident shear wave respectively. Since the shear waves are convected by the mean flow, ω is related to the mean flow Mach number by the following relation:

$$\omega = \frac{2\pi}{\lambda}\frac{M_1}{c_1}\alpha_1 \tag{23}$$

Finally, the velocity disturbance field upstream of the shock - the cellular flow 'turbulence' - is given by:

$$u_1' = -i2W_1\beta_1 \sin\left(\frac{\omega}{c_1}\frac{\beta_1}{M_1\alpha_1} y\right) e^{i\frac{\omega}{c_1}\frac{x}{M_1} - i\omega t}$$

$$v_1' = 2W\alpha_1 \cos\left(\frac{\omega}{c_1}\frac{\beta_1}{M_1\alpha_1} y\right) e^{i\frac{\omega}{c_1}\frac{x}{M_1} - i\omega t} \tag{24}$$

3.0 AN ILLUSTRATIVE EXAMPLE

A numerical example of the propagation of a weak shock through our cellular flow 'turbulence' will illustrate the formation of 'spiked' or 'rounded' waveforms. The mean flow Mach number is taken to be 1.0005 giving a steady state overpressure of 2.45 lb. ft.$^{-2}$ across the shock which is typical of the overpressure in a sonic boom*. In order to obtain an exponentially decaying pressure wave behind the shock the angle θ_1 made by the normal of the incident shear wave with the x-axis must be greater than the critical value $\theta_{1_{cr}}$. In this example θ_1 is taken to be equal to $\theta_{1_{cr}}$ and the results for $\theta_1 > \theta_{1_{cr}}$ are quantitatively the same since the pressure amplitudes change only very slightly with θ_1 for this Mach number.

In Figure 4 the non-dimensional pressure disturbance field $\frac{p_2'}{p_2}\left(\frac{c_1}{W_1}\right)$ and perturbed shock shape $\bar{x}_s = \frac{f}{\lambda}\frac{\pi M_1 c_1}{W_1}$ are plotted using the real part of Eqs. (21) and (22) for $M_1 = 1.0005$. The x and y coordinates are non-dimensionalized with respect to the wavelength λ of the incident shear wave, while the time t is normalized with respect to the period of one oscillation $\tau = \frac{2\pi}{\omega}$. For $\theta_1 = \theta_{1_{cr}}$ the computations show that p_2' lags f by 90 degrees; this can be seen in the figure for times $\frac{t}{\tau} = \frac{1}{4}$ and $\frac{3}{4}$, when the pressure reaches a maximum while the deviation of the perturbed shock shape from the mean is zero. At times $\frac{t}{\tau} = 0, \frac{1}{2}$ the perturbed pressure behind the shock is negligibly small.

The sinusoidal variations of the perturbed pressure and shock front with y are clearly indicated in Eqs. (21) and (22). Since ν is very large ($\nu = 3100\,\frac{\pi}{\lambda}$) for $M_1 = 1.0005$, the pressure profile decays very rapidly and the wave is damped out completely before any oscillations in the x direction can be detected. If the amplitude W_1 and the wavelength λ of the incident shear wave are given, then p_2' can be determined, and the shape of the 'spiked' or 'rounded' waveform can be obtained by adding or subtracting p_2' from p_2.

To obtain an idea of the magnitude of the 'spike' for a realistic level of 'turbulence', we assume a value of $\frac{W_1}{c_1} = 0.1$ and find that the peak pressure fluctuation is approximately 50% of the steady state pressure p_2. In the planetary boundary layer a value of $\frac{W_1}{c_1} = 0.1$ corresponds to gusts of approximately 70 m.p.h., which are not infrequent.

---

*More specifically, it is of the order of the peak overpressure produced at the ground by an SST in cruising flight; this includes a reflective pressure doubling. Thus somewhat away from the ground our example has about twice the strength of an SST pressure signature and is more typical of a strong boom from a fighter airplane at lower altitude.

However, with this choice of 'turbulence' level $\frac{W_1}{c_1}$ we have violated a basic assumption implicit in the analysis. For a given value of the mean flow velocity there is a corresponding maximum shear wave velocity W_1 (analogous to turbulent 'wind' velocity) which must not be exceeded; this results from the requirement in the theory that the velocity normal to the shock wave be everywhere greater than the speed of sound. This limiting value of W_1 scales downward with decreasing shock strength and is very small indeed for sonic boom shocks. For realistic value of atmospheric turbulence velocities the limit must be exceeded manyfold, and thus the theory is applied well outside its valid region.

4.0 CONCLUDING REMARKS

The interaction of a weak shock with a regularized model of a turbulent field - a cellular flow - has been studied. 'Spiked' or 'rounded' waveforms are obtained as a superposition of a decaying pressure wave perturbation on the steady state pressure field. For weak shocks typical of those in sonic booms and moderate turbulence wind velocities (peak velocities of the order of 70 m.p.h.) the equations of the analysis predict pressure fluctuations of the order of plus or minus 50%, according to whether the waves are 'spiked' or 'rounded'.

If two of the planar cellular flows of our model are superimposed with their flow planes at right angles, the result is a three-dimensional cellular flow in long, narrow boxes. This somewhat more realistic simulation of turbulence will double the predicted pressure fluctuations, for the same peak 'turbulence' velocity.

Although the heights of the 'spikes' appear to be simulated reasonably well, the widths are not. According to Figure 4, the spikes decay so fast as to be much too narrow compared with those typically observed in sonic boom signatures; the factor appears to be 10- to 50-fold.

The theoretical model is, moreover, limited to very weak 'turbulence' velocities when the shocks are very weak: the permissible 'turbulence' level and shock strength are tied together. This is dictated by the basic assumption that the flow be everywhere supersonic upstream of the shock. Thus for the cited results the equations were applied well outside their legitimate range of validity. The example should, nevertheless, be adequate to demonstrate qualitative behavior; it may be expected to show least error for the 'spiked' waveform prediction, upstream of which the flow is always locally supersonic. In particular the height of the largest spikes along the sinuous shock should be correct, as it depends solely on the Rankine-Hugoniot relations applied to a normal shock.

Some more serious difficulties with our model are as follows. The 'turbulence' is simulated - even in the more realistic three-dimensional version - as a cellular flow in long, narrow boxes. For the specified Mach number M = 1.0005 only slightly above unity, theoretical considerations constrain these boxes to have a length/width ratio of the order of 30. Such boxes are indeed Fourier components (in a sense) of the turbulence, but are hardly 'typical' components. The analysis suggests that these are the components that dominate the 'sonic boom' pressure signature distortion, but this is not really proven.

To carry the thought further, the several shear waves constituting our cellular flow model are properly regarded as Fourier components of an arbitrary flow. The results developed herein for the individual shear wave-shock interactions can be put into statistical relations to yield the interaction of a turbulent flow with a shock wave (the general procedure is developed in Ref. 8). In this case, however, only statistical quantities, e.g. r.m.s. height of the spike, can be computed for given circumstances, and the shape of individual spiked signatures is not predicted. The deterministic model has then been exchanged for a stochastic one.

5.0 REFERENCES

1. Herbert, G.A., Hass, W.A. and Angell, J.K. A Preliminary Study of Atmospheric Effects on Sonic Boom. Journal Appl. Meteorology, Vol. 8, 1969, pp. 618-626.
2. Crow, S.C. Distortion of Sonic Bangs by Atmospheric Turbulence. J. Fluid Mech., Vol. 37, pt. 3, 1969, pp. 529-563.
3. George, A.R. and Plotkin, K.J. Propagation of Sonic Booms and other Weak Nonlinear Waves through Turbulence. Phys. Fluids, Vol. 14, No. 3, 1971, pp. 548-554.
4. Pierce, A.D. Spikes on Sonic Boom Pressure Waveform. J. Acoust. Soc. Amer., Vol. 44, 1968, pp. 1052-1061.
5. Pierce, A.D. Statistical Theory of Atmospheric Turbulence Effects on Sonic-Boom Rise Times. J. Acoust. Soc. Amer., Vol. 49, 1971, pp. 906-924.
6. Ribner, H.S. Convection of a Pattern of Vorticity through a Shockwave. NACA Rept. 1164, 1954.
7. Johnson, W.R. and Laporte, O. (Project Supervisor). The Interaction of Plane and Cylindrical Sound Waves with a Stationary Shock Wave. Univ. of Michigan Tech. Rep. 253 9-8-T (Project 2539, Dept. of Navy, ONR Contract No. Nonr-1224(8)), June 1957.
8. Ribner, H.S. Shock-Turbulence Interaction and the Generation of Noise. NACA Rept. 1233, 1955.

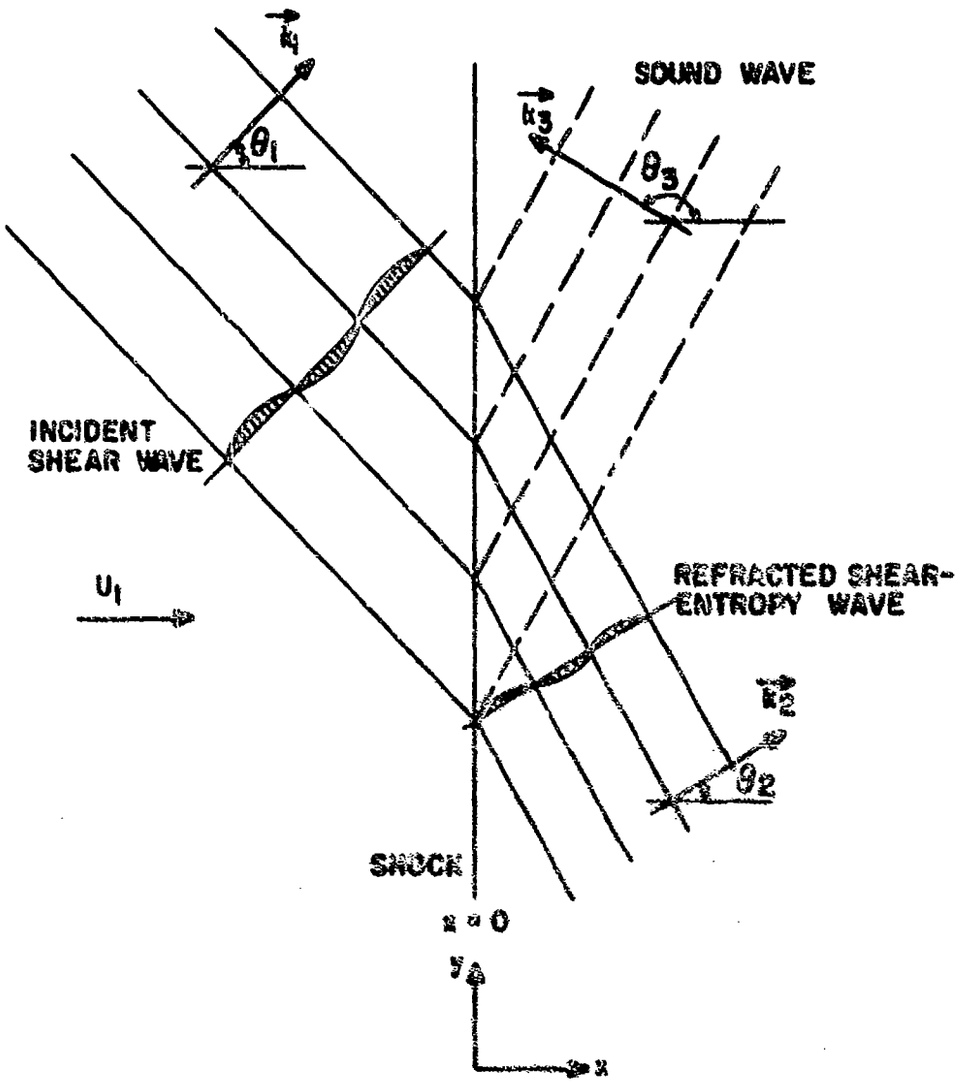

FIG. 1 - INTERACTION OF AN OBLIQUE SHEAR WAVE WITH A SHOCK
(SHOCK DISTORTION NOT SHOWN)

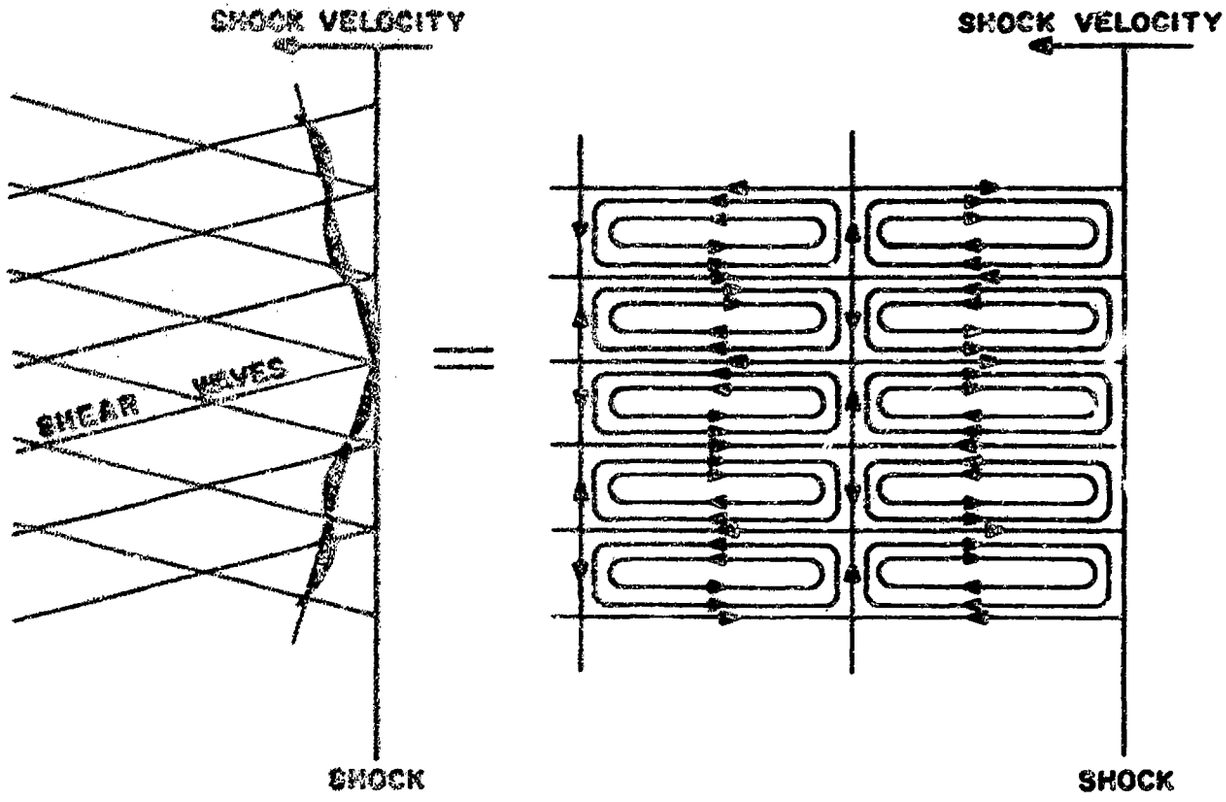

FIG. 2: OBLIQUE SHEAR WAVES COMBINE TO A CELLULAR FLOW SHOCK INTERACTION WITH CELLULAR FLOW MODELS PASSAGE OF SONIC BOOM THROUGH ATMOSPHERIC 'TURBULENCE' (SHOCK DISTORTION NOT SHOWN)

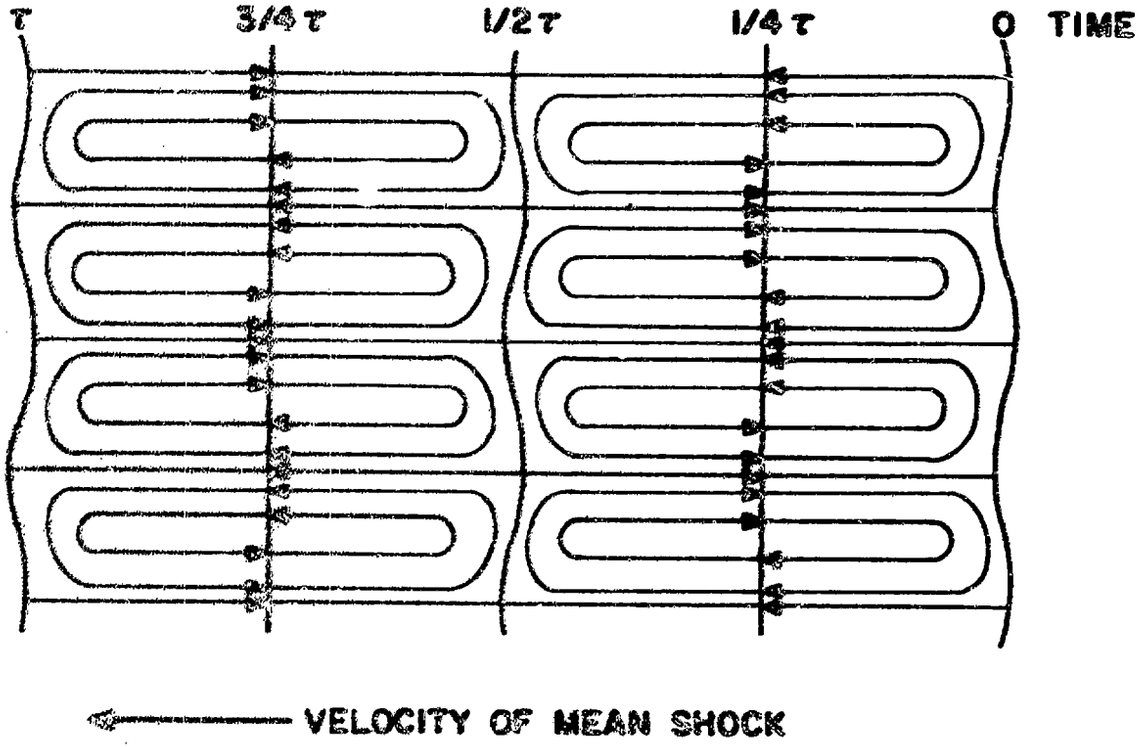

FIG. 3: SUCCESSIVE CONFIGURATIONS OF SHOCK PROPAGATING THROUGH CELLULAR FLOW ('TURBULENCE')

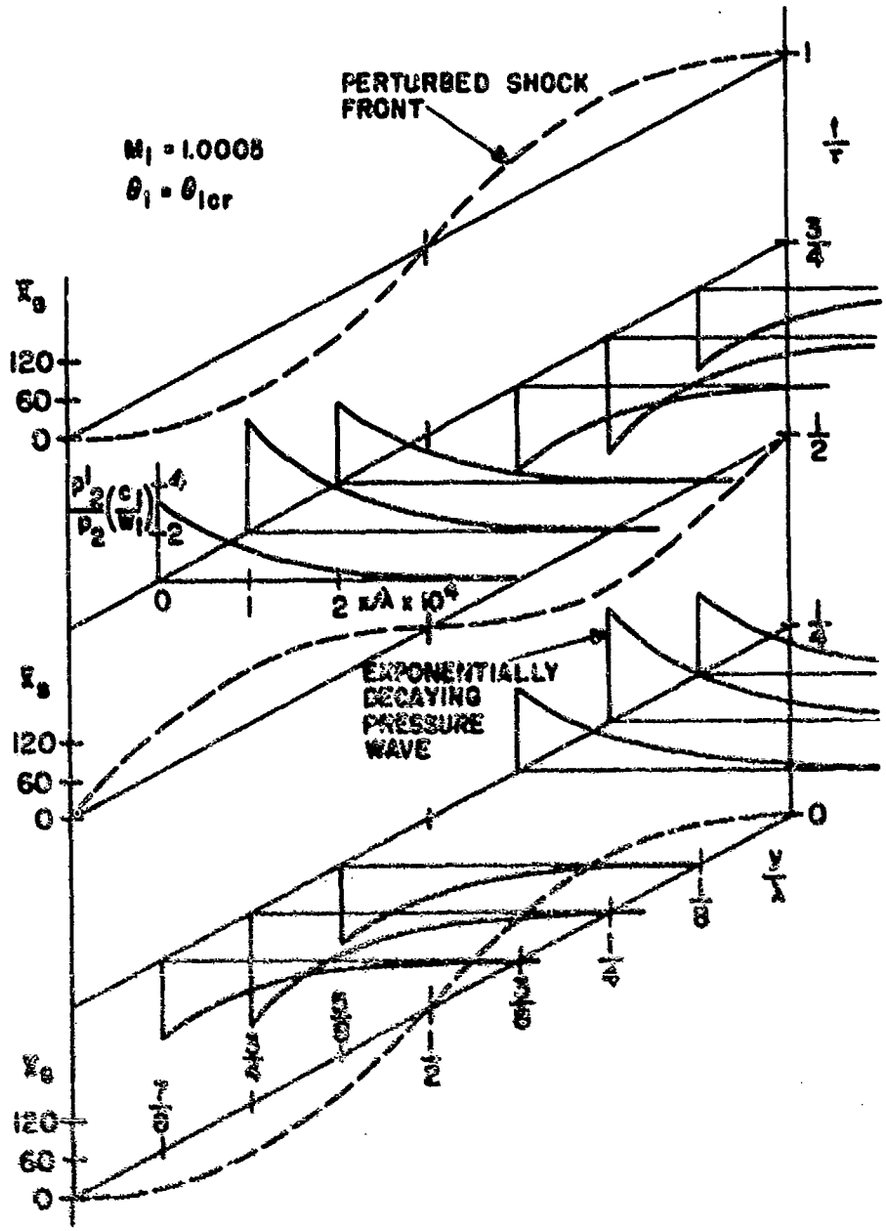

FIG. 4: PERTURBED SHOCK FRONT AND PROFILES OF THE EXPONENTIALLY DECAYING PRESSURE WAVE FOR A MEAN FLOW MACH NUMBER M_1=1.0008

APPENDIX

In Eqs. (21) and (22), the values of P, ϕ_p, F and ϕ_p for the pressure field and shock shape are given as

$$P = \frac{g}{\sqrt{a^2+b^2}} \tag{A1}$$

$$\phi_p = \arctan - \frac{b}{a} \tag{A2}$$

$$F = \sqrt{\frac{c^2+d^2}{a^2+b^2}} \tag{A3}$$

$$\phi_p = \arctan - \left[\frac{ad+bc}{ac-bd}\right] \tag{A4}$$

where

$$g = \frac{4}{\gamma+1} M_1 \left\{ \frac{2\beta_1}{(\gamma+1)M_1^2} \left[(M_1^2+1)\,\alpha_1\alpha_2 - (M_1^2-1)\,\beta_1\beta_2\right] + \left[\frac{(\gamma-1)M_1^2 - 2}{(\gamma+1)M_1^2}\right] \alpha_1\beta_1\alpha_2 - \alpha_1^2\beta_2 \right\}$$

$$a = \frac{p_2}{p_1}\frac{c_1}{c_2}\frac{2}{(\gamma+1)M_1^2}\left[(M_1^2+1)\,\alpha_1\alpha_2 - (M_1^2-1)\,\beta_1\beta_2\right] + \frac{4M_1}{\gamma+1}(\alpha_1\alpha_2\delta_1 + \alpha_1\beta_2\delta_2)$$

$$b = \frac{4M_1}{\gamma+1}\alpha_1(\alpha_2\delta_3 + \beta_2\delta_4)$$

$$c = \frac{p_2}{p_1}\frac{c_1}{c_2}\left[\frac{(\gamma-1)M_1^2 - 2}{(\gamma+1)M_1^2}\beta_1\alpha_2 - \alpha_1\beta_2\right] - \frac{4}{\gamma+1}M_1\beta_1(\alpha_2\delta_1+\beta_2\delta_2)$$

$$d = \frac{4}{\gamma+1}M_1\beta_1(\alpha_2\delta_3+\beta_2\delta_4)$$

and

$$\delta_1 = -\frac{B^2C}{\alpha_1^2 + \beta_1^2 B}$$

$$\delta_2 = \frac{\alpha_1\beta_1 C}{\alpha_1^2 + \beta_1^2 B}$$

$$\delta_3 = \frac{\alpha_1}{\alpha_1^2 + \beta_1^2 B}\sqrt{A\beta_1^2 - \alpha_1^2}$$

$$\delta_4 = \frac{\delta_1 B}{\alpha_1^2 + \beta_1^2 B}\sqrt{A\beta_1^2 - \alpha_1^2}$$

where

$$A = \frac{1}{M_1^4}\frac{M_1^2 - 1}{\gamma+1}\left[(\gamma-1)M_1^2 + 2\right]$$

$$B = \frac{\left[(\gamma-1)M_1^2 + 2\right]^2}{(\gamma+1)^2 M_1^4}$$

$$C = \frac{(\gamma-1)M_1^2 + 2}{(\gamma+1)^2 M_1^4} \sqrt{[2\gamma M_1^2 - (\gamma-1)][(\gamma-1)M_1^2 + 2]}$$

$$D = \frac{(\gamma+1)M_1^2}{(\gamma-1)M_1^2 + 2} C$$

$$E = \frac{1}{(\gamma+1)M_1^2} [(\gamma-1)M_1^2 + 2]$$

SONIC BOOM BEHAVIOR NEAR A CAUSTIC

by

Frank Obermeier +)
MAX-PLANCK-INSTITUT FÜR STRÖMUNGSFORSCHUNG
34 Göttingen, Böttingerstr. 6/8
Germany

SUMMARY

This paper is concerned with the pressure signature of an ideal N-shaped sonic boom caused by an accelerated projectile; especially its signature in the surroundings of the so-called caustic and behind the caustic is discussed by the equations of linear wave acoustics. The calculations are performed for a special case, analytically easily handled, where the acceleration phase is chosen in such a way that the corresponding Mach-cone, modified by the acceleration, is composed of a truncated cone, the lower part of which has a circle like curved surface and the upper part is an ordinary straight cone.

The proposed theory yields results which are in good agreement with measurements.

SOMMAIRE

Dans ce travail, on traite de la signature de la pression d'un bang supersonique idéal, en forme de N causé par un avion. On en détermine notamment le comportement dans le voisinage immédiat d'une caustique et à une distance suffisamment grande derrière la caustique à l'aide des équations de l'acoustique linéaire des ondes. Les calculs sont effectués pour un cas type facile à traiter analytiquement. En effet, la phase d'accélération de l'avion est interprétée de telle façon que le cosoïde de Mach qui en fait partie et qui est modifié par l'accélération se compose d'un tronc de cône avec génératrice circulaire et pointe de tronc droite.

La théorie proposée conduit à des résultats qui correspondent bien aux résultats expérimentaux.

+) Dr. rer.nat, wissenschaftlicher Mitarbeiter

1. INTRODUCTION

The basic mechanisms of sonic boom development caused by an unaccelerated, supersonically moving projectile and its propagation through a layered, homogeneous atmosphere are now sufficiently well understood. This subject can be handled with linear techniques, if one is interested only in local characteristics of the sonic boom. One such case is the behavior of the flow in the near field of the moving projectile (apart from the immediate vicinity). Consideration of non-linear effects becomes necessary when the propagation distance of the sonic boom must be taken into account. This is the case during the development of the sonic boom, i.e. the steepening phase of the shock wave system as it propagates from the near field to the far field.

In general, ray tube theories, i.e. modified geometric wave theories, constitute the starting point for the latter discussion. These theories take non-linear effects into account only in the direction of the ray tubes; the position and the differential cross section of the ray tubes, on the contrary, are evaluated by using methods of geometric acoustics.

In contrast to the problems mentioned above, the behavior of a sonic boom caused by an accelerated projectile has been less satisfactorily solved in the literature, especially its behavior near a caustic. Here, within the framework of a ray tube theory, one understands a caustic to be the envelope of converging ray tubes. Physically, this implies a zero differential cross-section of the ray tubes at the caustic and thereby leads to infinitely large pressure values. This means a failure of the concept of ray tube theories near a caustic.

The aim of the present paper, therefore, is to discuss an approach to overcome these difficulties connected with the singular results of ray tube theories. We shall proceed from the assumption that sonic boom focusing is a local phenomenon which can be discussed in terms of linear wave acoustics, taking into account diffraction effects. For this case, non-linear terms in the corresponding equations of motion discribing cumulative effects due to wave propagation over long distances have no meaning.

By means of a special case, in which the acceleration phase of the flying projectile is chosen in such a way that the corresponding Mach-cone, modified by the acceleration, is composed of a truncated cone with a circlelike curved surface and a straight cone apex, we shall show that the theory we suggest leads to results which agree well with the experimental results.

2. TRANSONIC THEORIES

Before we discuss our theory in detail, we shall give a short survey of previous attempts to overcome the difficulties related to the infinite peak overpressure obtained by ray tube theories at a caustic by other investigators.

Such investigations are similar to those of boundary layer theories (M.J. Lighthill [1]; R.N. Buchal, J.B. Keller [2]), where the flow field is divided into two regions; the first is the region outside the vicinity of the caustic, in which geometric wave theories can be applied, and the second is the region near the caustic itself - the so-called boundary layer region - in which the equations of motion are reduced to modified transonic differential equations. The asymptotically valid equations of motion for these "outer" and "inner" regions can then be solved, at least in principle, by using methods such as the "Matched Asymptotic Expansions".

For this purpose, W.D. Hayes [3] and A.R. Seebass [4] proceed from the following conception in their "transonic" theories. They introduce a special coordinate system moving with the velocity $a_0 \cdot \underline{n}$ (where a_0 is the velocity of sound, $\underline{n}$ is a normal vector pointing in the direction of the propagation of the shock system at this caustic) and having its origin always on the caustic (see Fig. 1). In this coordinate system the caustic turns out to be, with restrictions, stationary and the flow field itself is transonic. The original focusing of the shock wave system appears as a "reflection" of the shock waves at the sonic line, whereby in the literature a simplified shock represented by a Heavyside-function is discussed, but not a N-shaped shock wave system.

The first attempt to describe the reflection of a weak discontinuity (i.e. a discontinuity in the derivations of the flow variables and not in the flow variables themselves) at the sonic line with the help of a transonic theory was made, as far as we are aware, by L.D. Landau and E.M. Lifschis in 1934 (see [5]). They proceed from the non-linear transonic differential equation for the flow potential, $\Phi(x,y)$:

$$\Phi_x \Phi_{xx} - \Phi_{yy} = 0 \qquad (1.1)$$

whereby x and y are space coordinates strained in the usual way (see, for example, K.G. Guderley [6]).

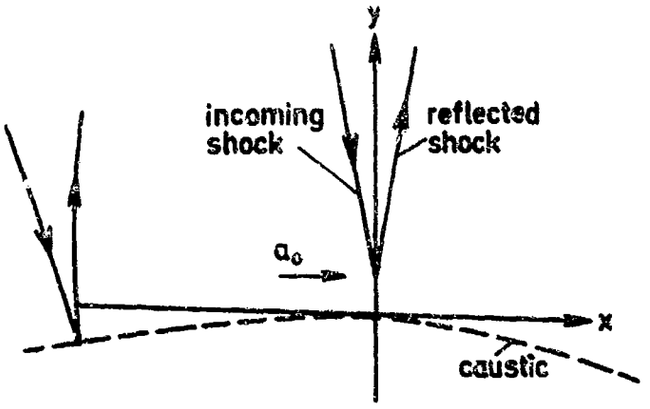

Fig. 1: Coordinate system used in transonic theories

By virtue of a Legendre-transformation

$$\varphi(u,v) = xu + yv - \phi(x,y)$$

this equation can be brought into the form of a Tricomi-equation

$$\varphi_{uu} - u\varphi_{vv} = 0 \tag{1.2}$$

whereby $\varphi(u,v)$ describes the potential in the hodograph plane, and u and v represent the components of the velocity field.

The solution given in [5] is expressed in terms of hypergeometric functions

$$\varphi = -Auv - B\xi^2 v^{1/6} F\left(\tfrac{13}{12}, \tfrac{19}{12}, 3, \xi\right) \tag{1.3}$$

where A and B are arbitrary constants, and ξ is given by

$$\xi = 1 - \frac{4}{9}\frac{u^3}{v^2}$$

Further details can be found in [5]. Since that time, however, it has been shown that this solution leads to inconsistencies and does not describe satisfactorily the effects in question [7].

W.D. Hayes [3] likewise suggests a Tricomi-equation of the form (1.2.) as an approximate equation of motion, but with the space coordinates x and y as independent variables. The solution for the immediate vicinity of the caustic is again expressed by hypergeometric functions, but it is not discussed in depth. Thus it is not shown how the flow field described by this solution looks in the entire vicinity of the coordinate origin, nor is it shown what the shock conditions are or what shape the shocks themselves have.

Similarly, A.R. Seebass [4] reduces a more general problem to the Tricomi-equation as well, whereby in his work, the independent variables are expressed by suitable functions dependent not only on the space variables but also on the hodograph variables. The solution of this Tricomi-equation given finally by A.R. Seebass has, however, certain disadvantages. In the physical plane it does not cover the entire vicinity of the reflection point of the shock wave at the sonic line, but rather leaves a "gap" for which an additional solution must be determined.

To summarize, it seems to us that the difficulties connected with the application of the transonic theories, mentioned in brief above, lie primarily in the fact that diffraction phenomena, which have considerable meaning for this problem, remain, for the most part, neglected in the transonic theories.

In the present report then, we shall not further pursue the question of the extent to which the transonic theories are nevertheless suitable for describing the flow field of a shock wave system in the vicinity of a caustic; rather, we shall discuss an alternative theory.

3. LINEAR WAVE ACOUSTICS

In this section, we shall discuss the flow field of a focused sonic boom in the vicinity of a caustic, using equations of linear wave acoustics.

Our attention was drawn to this method by its analogy to optics. Namely, if one discusses the behavior of a plane light wave focused by a lens, then this problem can be handled sufficiently exactly outside of the focal point region by linear geometrical optics. Near the focal point itself - a special case of a caustic which has degenerate to one point - this geometric theory, however, yields vanishing ray tube cross sections and, therefore, infinitely large intensities. But it is known (see, for example, P. Debey [8]) that these difficulties can be easily overcome by considering only linear optics and by disregarding the condition $\lambda/D \ll 1$ which characterizes geometric optics (λ is the wavelength of light and D is a characteristic geometric length of the problem in question). The success of this procedure is based on the fact that a linear wave theory which takes diffraction phenomena, among others, into consideration is considerably less limiting than a geometric wave theory.

This fact, in our opinion, has received too little attention in the literature on sonic boom focusing, perhaps because ray tube theories are primarily used in treating ordinary sonic booms in a real atmosphere. This is even mirrored in the terms used, e.g. the "caustic".

In addition, keeping in mind the analogy to optics mentioned above, it seems to us that non-linear effects in the near field of the caustic itself are not meaningful. In the first place, as was already mentioned, sonic focusing is a local phenomenon so that non-linearities caused by cumulation can be neglected. In the second place, the peak pressure amplitudes measured near a caustic do not justify taking non-linear terms into account. Finally, the execution of the method suggested will show that it yields results which correspond quite well to the experimental results of J. Vallee [9].

For clariffication of the problem to be discussed, first a qualitative representation of the development of a caustic is given in Fig. 2a in the framework of geometric wave theory. This representation satisfies the geometry of the problem in question completely, but it does not allow quantitative statements about the pressure distributions near and behind the caustic which could be compared with the experimental results of J. Vallee shown in Fig. 2b.

Hence, our goal is to determine the pressure distribution of a focused sonic boom theoretically, with the aid of linear wave acoustics methods.

Such a linear treatment has a basic advantage in that, using Fourier-transforms, we can reduce the problem in question to the description of cylindrical, harmonic waves in the vicinity of a caustic. In order to be able to execute the necessary Fourier-transforms and the inverse transforms without difficulty, we shall use an incoming N-shaped shock wave system with a very short, yet finite, rise time, τ, (see, Fig. 3), whose value is adjusted to real values.

The Fourier-transform

$$\hat{p}(\underline{x},\omega) = \int p(\underline{x},t)\, e^{-i\omega t}\, dt$$

for the pressure distribution, $p(t)$, of an N-wave then yields

$$\hat{p}(\underline{x},\omega) = \frac{2i\hat{p}_{MAX}(\underline{x})}{a(b-a)\omega^2}\left(a\sin b\omega - b\sin a\omega\right) \qquad (2)$$

where $\hat{p}_{MAX}(\underline{x})$ is the maximum value of $p(\underline{x},t)$ at a fixed point $\underline{x}$. T is the duration of the sonic boom, τ is the rise time of the front shock, $a = 1/2(T - \tau)$ and $b = 1/2(T + \tau)$.

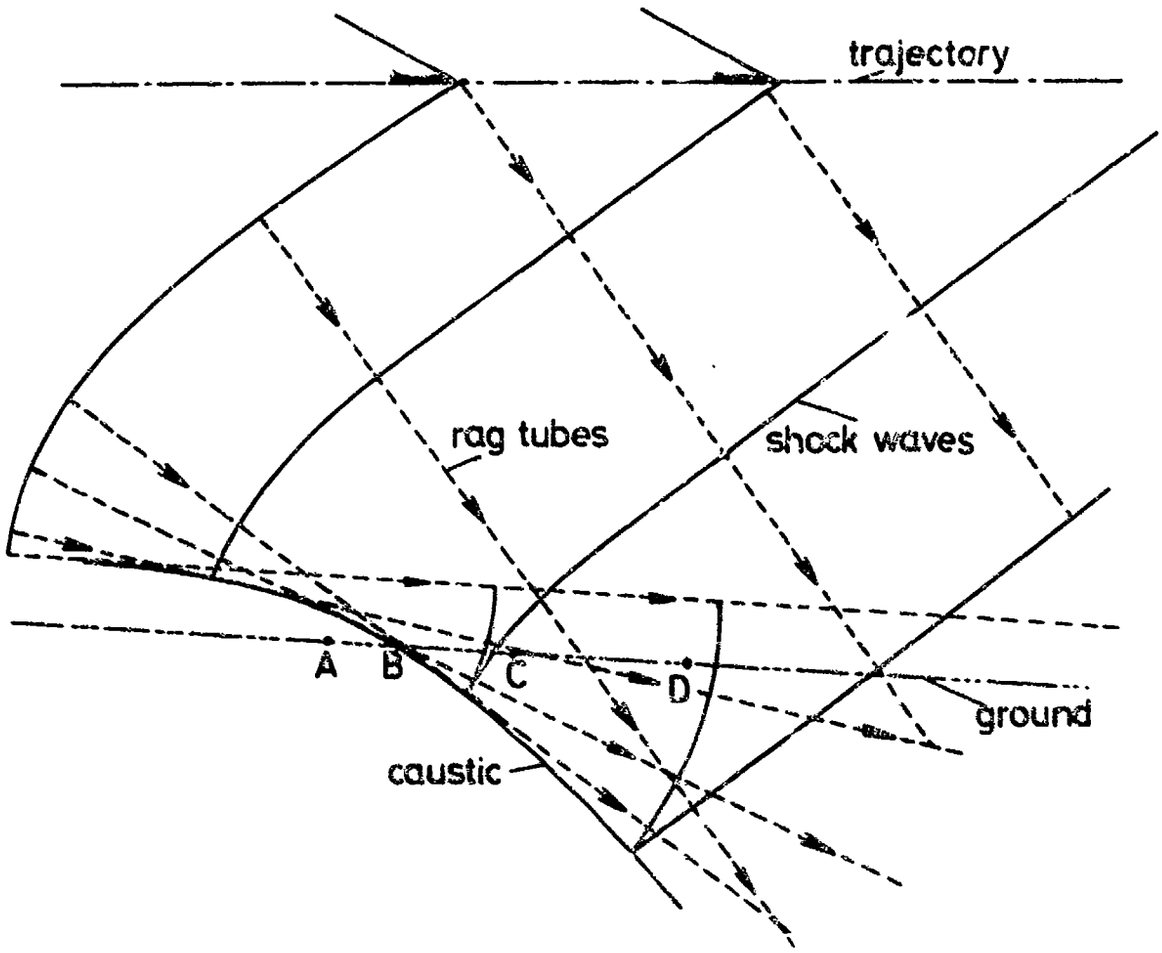

Fig. 2 a: Geometry of the development of a caustic due to converging ray tubes. A, B, C, D observation points on the ground.

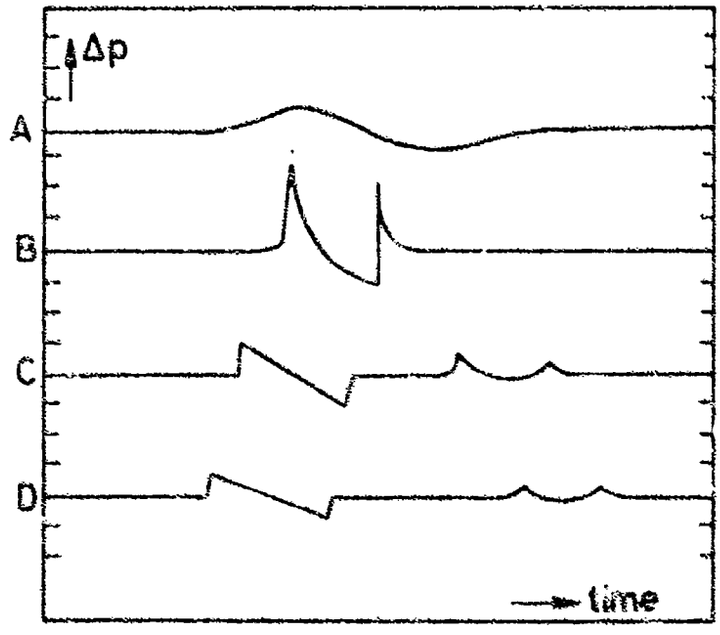

Fig. 2 b: Qualitative plot of the pressure signature in the vicinity of a caustic. A, B, C, D observation points specified in Fig. 2 a.

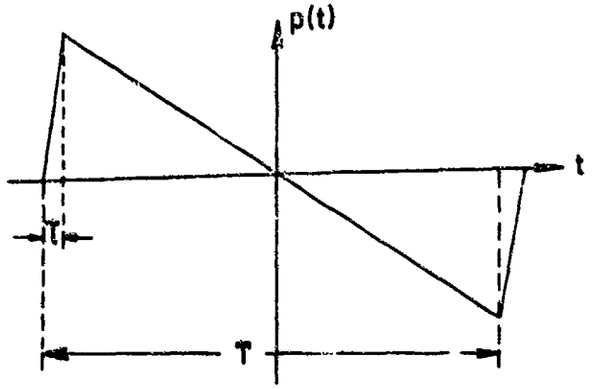

Fig. 3: Pressure signature of a N-wave

In order to simplify the following calculations even further, we shall assume, in addition, a two-dimensional flow field. This is certainly justified for the present discussion, since the radius of the Mach-cone is large compared with the radius of curvature of the conical surface in the focusing region.

We have now reduced the solution of the present problem to the evaluation of a pressure field caused by converging acoustic waves of arbitrary frequencies in two dimensions.

This pressure field is analytically determined in that it must satisfy the reduced wave equation

$$\left(\frac{\partial^2}{\partial x^2}+\frac{\partial^2}{\partial y^2}+\frac{\omega^2}{a_0^2}\right)\hat{p}=0 \tag{3}$$

and in that the incident wave must exhibit a prescribed behavior on the given surface F (Fig. 4).

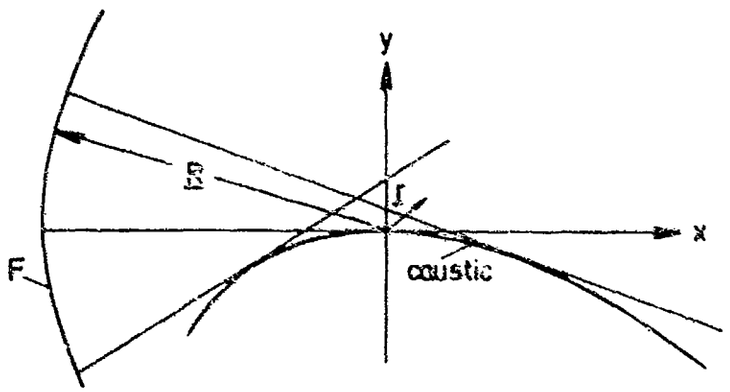

Fig. 4: Coordinate system

This latter is the boundary condition

$$\hat{p}(r,\omega)=\frac{-i}{4}\int_F \frac{\partial \hat{p}}{\partial n}\cdot H_0^{(2)}\left(\frac{\omega}{a_0}\cdot|\underline{r}-\underline{R}|\right)-\hat{p}\,\frac{\partial}{\partial n}H_0^{(2)}\left(\frac{\omega}{a_0}\cdot|\underline{r}-\underline{R}|\right)\,dF \tag{4.1}$$

In the limiting case of very large distances this boundary condition can be replaced by (see [2])

$$\lim_{R\to\infty}\ \frac{a_0}{2i\omega}\,e^{-i\frac{\omega}{a_0}R}\,R^{1/2}\left(i\frac{\omega}{a_0}\hat{p}+\frac{\partial\hat{p}}{\partial R}\right)=I(\Theta)\,e^{i\frac{\omega}{a_0}a(\Theta)} \tag{4.2}$$

Here, R and Θ are polar coordinates and the functions $I(\Theta)$ and $a(\Theta)$ describe the amplitude and phase of the wave, respectively, which propagates in Θ-direction from the surface F which is displaced to infinity.

The complete boundary conditions are thereby: in the region of the surface F, an irradiation condition in form of a cylindrical wave is prescribed, while for the remaining region, the Sommerfeld's radiation condition must be fulfilled.

It then turns out that the solution of equations (3) and (4.2) at the caustic yields a finite maximum of the pressure amplitude, while the singularity due to geometric acoustics does not exist, as we shall discuss in detail.

As is well known, the solution of the wave equation, eq. (3), and the boundary condition, eq. (4.2.), can be described by the following integral representation

$$\hat{p}(r,\Theta,\omega) = \frac{e^{-\frac{3}{4}i\pi}}{\sqrt{\frac{2\pi a_0}{\omega}}} \int_F I(\Theta') e^{i\frac{\omega}{a_0}\left[a(\Theta') - r\cos(\Theta-\Theta')\right]} d\Theta' \qquad (5)$$

Here one must integrate for arbitrary frequencies ω across the entire angle sector, Θ, i.e. across the entire surface, F. Unfortunately, the analytical evaluation of this integral with the functions $I(\Theta)$ and $a(\Theta)$ seems to be possible only in special cases. In general one would have to apply numerical methods, which are quite time-consuming on account of the alternating behavior of the integrand.

4. MODEL CAUSTIC

We can simplify the problem in question, eq. (5), considerably if we confine ourselves to special geometries of the curve F. In the following we will discuss the case in which the acceleration phase of the projectile is chosen in such a way that the shock wave system is composed of a circlelike part F_1 and a straight part F_2. Physically this means that the caustic degenerates to one single point, O (see Fig. 5).

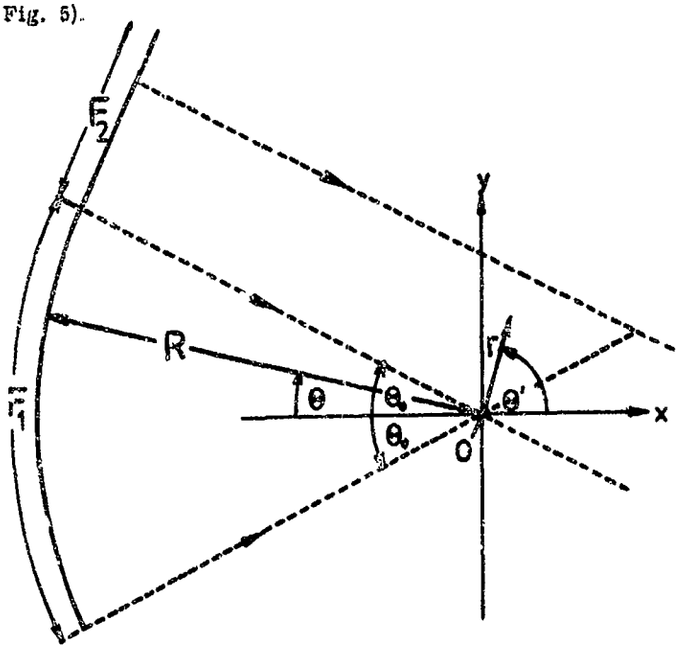

Fig. 5: Degenerated caustic

In determining the total pressure field in the vicinity of the focusing point, O, we discuss the contributions from F_1 and F_2 separately, and we finally superimpose them. This is justified on the basic of the linearity of our basic differential equation, eq. (3).

4.1. Contribution from F_1

Let $\hat{p}_F(\Theta,\omega)$ be the required amplitude of the pressure field on the surface F_1. Then, for sufficiently large R-values, $I(\Theta)$ is

$$I(\Theta) = \hat{p}_F(\Theta)\, R^{1/2}$$

with R independent of Θ.

As additional conditions, we postulate that the amplitude, $p_F(\Theta)$, be independent of Θ and that the angle, Θ_0, under which the surface F_1 is seen from the focal point, be small in comparison to 1, in the sense that we can replace $\cos\Theta_0$ by $1-1/2\Theta_0^2$ and $\sin\Theta_0$ by $\Theta_0-1/6\Theta_0^3$. These assumptions do not, however, basically limit the generality, since in the case of a real caustic which does not

degenerate to one focal point, the flow field at each point on the caustic is also determined, respectively, by a small segment of the total shock wave system, F, on which the pressure amplitude can be considered a constant.

Keeping in mind that, on accout of the geometry of F_1 ($a(\Theta) = R$ is valid) the contribution from F_1 is represented by

$$\hat{p}(r,\Theta,\omega) = \frac{e^{-\frac{3}{4}i\pi}}{\sqrt{\frac{2\pi a_0}{\omega}}} \int_{-\Theta_0}^{\Theta_0} \hat{p}_F(\omega) \sqrt{R}\, e^{i\frac{\omega}{a_0}\left[R - r\cos(\Theta-\Theta')\right]} d\Theta' \tag{6}$$

Now we would like to show that the singularity of the pressure amplitude at the focal point resulting from geometric acoustics can be avoided. The use of wave acoustics yields a completely regular behavior of this pressure field.

For this purpose, we evaluate the integral, eq. (6), for small r-values and any given angle Θ, taking into account the relationship

$$e^{i\frac{\omega}{a_0} r\cos(\Theta-\Theta')} = J_0\left(\frac{\omega r}{a_0}\right) + 2\sum_{n=1}^{\infty} (-i)^n J_n\left(\frac{\omega r}{a_0}\right)\cos n(\Theta-\Theta')$$

We obtain approximately

$$\hat{p}(x,y,\omega) = \sqrt{\frac{R\omega}{2\pi a_0}}\, e^{-\frac{3}{4}\pi i + \frac{\omega}{a_0} Ri}\, \hat{p}_F(\omega)\, 2\Theta_0 \left\{1 - i\frac{\omega}{a_0}\left(1 - \frac{\Theta_0^2}{6}\right)x - \left(\frac{\omega}{a_0}\right)^2\left[\left(\frac{1}{2} + \frac{1}{6}\Theta_0^2\right)x^2 - \frac{\Theta_0^2}{6}y^2\right] + O(x^3, y^3)\right\} \tag{7.1}$$

where $x = r\cos\Theta$ and $y = r\sin\Theta$.

In the same approximation, one can acquire from this for the amplitude of $\hat{p}$

$$|\hat{p}|^2 = \frac{2\Theta_0^2 R\omega}{\pi a_0} |\hat{p}_F(\omega)|^2 \left\{1 - \left(\Theta_0 \frac{\omega}{a_0}\right)^2\left(\frac{2}{3}x^2 + \frac{1}{3}y^2\right)\right\} \tag{7.2}$$

Physically this implies an elliptic intensity distribution in the vicinity of the focal point with a finite maximum value at the focal point itself. Further, it can be gathered from this result that the intensity distribution becomes flatter and wider with smaller the angles Θ_0.

The phase distribution $\tilde{\varphi}$ of the pressure function $\hat{p}$ near the focal point can likewise be easily stated; it is

$$\tilde{\varphi} = \arctan \frac{\left(1 - \frac{\Theta_0^2}{6}\right)\frac{\omega x}{a_0}}{1 - \left(\frac{1}{2} + \frac{\Theta_0^2}{6}\right)\left(\frac{\omega x}{a_0}\right)^2 - \frac{\Theta_0^2}{6}\left(\frac{\omega y}{a_0}\right)^2} \tag{7.3}$$

and in a lowest approximation in terms of x and y

$$\tilde{\varphi} \approx 1 - \frac{\Theta_0^2}{6}\frac{\omega}{a_0} x$$

This result indicates that in the immediate vicinity of the focal point, the original incoming cylindrical waves are converted into plane waves.

Let us now consider the further vicinity of the focal point. In order to point out the basic aspects of the behavior of the pressure field as clearly as possible, we shall confine ourselves in the following to discussing the integral, eq. (6), only for the special Θ-values: a) $\Theta = 0$ and $\Theta = \pi$ and b) $\Theta = \pi/2$ and $\Theta = 3/2\pi$.

In the case of a), observing that $\Theta_0 \ll 1$, the integral (6), is reduced to a representation by Fresnel integrals

$$\hat{p}(x,y=0,\omega) = 2\sqrt{\frac{\omega R}{2\pi a_0}}\, e^{i\left[\frac{\omega}{a_0}(R-x)-\frac{3}{4}\pi\right]} \hat{p}_F \sqrt{\frac{\pi a_0}{\omega|x|}} \int_0^{\xi_0} \left[\cos\left(\frac{\pi}{2}\xi^2\right) \mp i\sin\left(\frac{\pi}{2}\xi^2\right)\right] d\xi \qquad (8.1)$$

with $\xi_0 = \sqrt{\omega x / \pi a_0}\,\Theta_0$, (+) for $x>0$ and (-) for $x<0$.

From these the dependence on the distance from the focal point of the amplitude variations and the phase of the function p can be directly stated as

$$\hat{p}(x,y=0,\omega) = \hat{p}_0 \Theta_0 \sqrt{\frac{2\omega R}{\pi a_0}}\, e^{i\left[\frac{\omega}{a_0}(R-x)-\frac{3}{4}\pi\right]} A(\xi_0)\, e^{\mp i\tilde{\phi}(\xi_0)} \qquad (8.2)$$

$$A(\xi_0) = \frac{1}{\xi_0}\left[\left(\int_0^{\xi_0}\cos\left(\frac{\pi}{2}\xi^2\right)d\xi\right)^2 + \left(\int_0^{\xi_0}\sin\left(\frac{\pi}{2}\xi^2\right)d\xi\right)^2\right]^{1/2}$$

$$\tilde{\phi}(\xi_0) = \arctan \pm \frac{\int_0^{\xi_0}\sin\left(\frac{\pi}{2}\xi^2\right)d\xi}{\int_0^{\xi_0}\cos\left(\frac{\pi}{2}\xi^2\right)d\xi}$$

The values of the Fresnel integrals are tabulated as functions of ξ_0 (see, for example, M. Abramowitz, J.A. Stegun [10]). The functions $A(\xi_0)$ and $\tilde{\phi}(\xi_0)$ are shown graphically in Fig. 6.

Particularly, for the limiting case $\frac{\omega x}{a_0} \to \pm\infty$ not yet discussed, we obtain

$$\lim_{\frac{\omega x}{a_0}\to\pm\infty} \hat{p}(x,y=0,\omega) = \begin{cases} \sqrt{\frac{R}{2x}}\,\hat{p}_F(1+i)\, e^{i\left[\frac{\omega}{a_0}(R-x)-\frac{3}{4}\pi\right]} & x>0 \\ \sqrt{\frac{R}{2x}}\,\hat{p}_F(1-i)\, e^{i\left[\frac{\omega}{a_0}(R-x)-\frac{3}{4}\pi\right]} & x<0 \end{cases} \qquad (9)$$

i.e., an amplitude independent of the frequency and a total phase shift for the transition from $\omega x/a_0 = -\infty$ to $\omega x/a_0 = +\infty$ of $\pi/2$, in agreement with results obtained by geometric acoustics. Obviously this result means that the odd functions describing the N-shaped pressure signature at $\lim x \to -\infty$ must be changed into even functions describing the modified signature after the sonic boom passed through the caustic region and propagates to $x \to \infty$. This intuitive explanation is verified by the explicit calculations in chapter 5.

To conclude the discussion of the integral, eq. (6), we shall consider case b), $\Theta = \pi/2$ and $\Theta = 3/2\pi$, which leads to

$$\hat{p}(x=0,y,\omega) = \sqrt{\frac{\omega R}{\pi a_0}}\,\hat{p}_F\, e^{i\left[\frac{\omega}{a_0}R-\frac{3}{4}\pi\right]} \int_{-\Theta_0}^{\Theta_0} e^{-i\frac{\omega}{a_0}y\left(\Theta-\frac{1}{6}\Theta^3\right)} d\Theta \qquad (10)$$

In this case, the analytical treatment corresponding to case a) seems to be possible only for $y\omega/a_0 \gg 1$ and $\ll 1$, whereby the latter is already included as a special case ($x = 0$) in the discussion on page 16- . Therefore, we confine the discussion to the first case, in which the above integral is transformed into an integral representation of the Airy-function:

$$\hat{p}(0,y,\omega) = \sqrt{\frac{2\omega R}{\pi a_0}}\,\hat{p}_F\,\left(\frac{a_0}{\omega y}\right)^{1/3} e^{\,i\left[\frac{\omega}{a_0}R - \frac{3}{4}\pi\right]} \int_0^{\xi_0} \cos\left[t\xi - \frac{1}{3}\xi^3\right]\,d\xi \qquad (11.1)$$

with $t = \left(\frac{\omega |y|}{a_0}\right)^{2/3}$ and $\xi_0 = t \cdot \Theta_0$

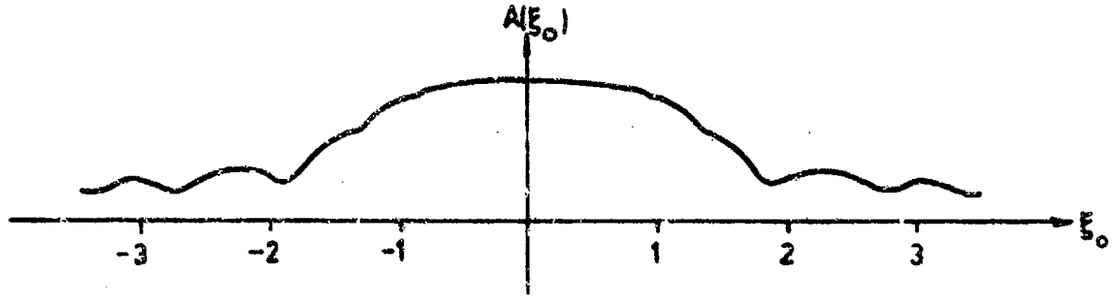

Fig. 6 a: The amplitude variation $A(\xi_0)$ of the pressure field

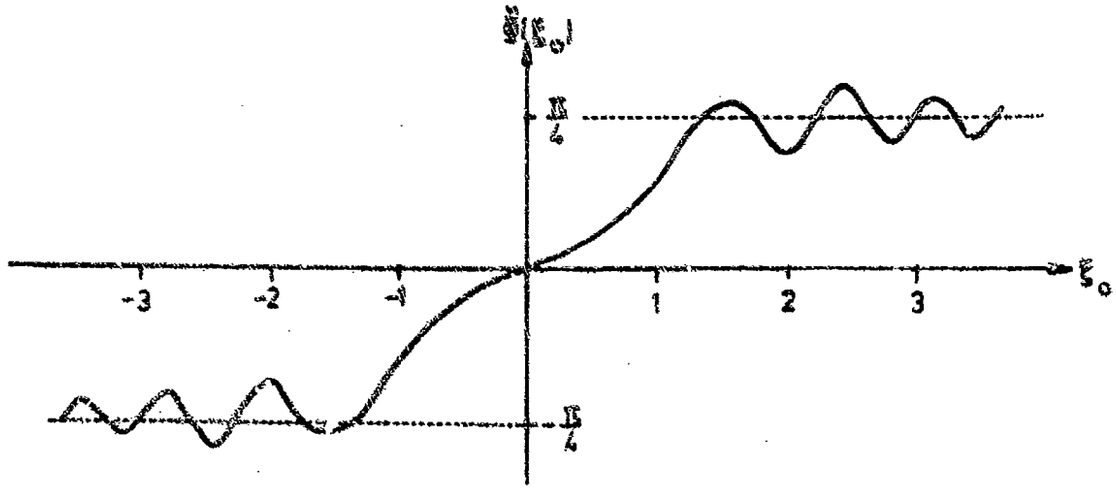

Fig. 6 b: The phase variation $\ddot{\varphi}(\xi_0)$ of the pressure field

From that we finally obtain

$$\lim_{\frac{\omega y}{a_0} \gg 1} \hat{p}(0,y,\omega) = \sqrt{\frac{2R}{y}}\,\hat{p}_F\,e^{\,i\left[\frac{\omega}{a_0}R - \frac{3}{4}\pi\right]} \sin\left(\frac{2}{3}\frac{\omega}{a_0}y + \frac{\pi}{4}\right) \qquad (11.2)$$

We shall not discuss this result here, but only mention that the physical interpretation proceeds similarly to the case of $\Theta = 0$ and $\Theta = \pi$.

4.2. Contribution from F_2

In order to determine the contribution from F_2 to the flow field in the vicinity of the focal point O the following problem must be solved. A plane wave of arbitrary wave length propagating in the ξ-direction strikes a half-infinitely extended, rigid plane (see Fig. 7). We are especially interested in the pressure distribution near the "shadow"-line $\xi > 0$, $\eta = 0$ for distances characterized by $\frac{\omega \xi}{a_0} \gg 1$; this case corresponds well to the situation caused by real Mach-cone data.

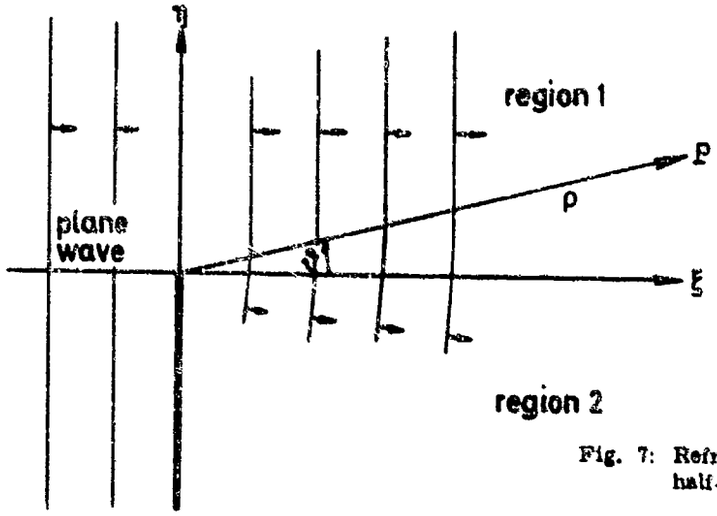

Fig. 7: Refraction of a plane wave by a half-infinitely extended solid wall

It is not necessary to go into details on determining this solution here, since it can be found in textbooks (see, for example, P.M. Morse and K.U. Ingard [11]). We obtain

$$\hat{p} = \hat{p}_F \left[e^{i \frac{\omega}{a_0} \rho \cos \vartheta} E\left[(2\rho \tfrac{\omega}{a_0})^{1/2} \cos \tfrac{\vartheta}{2} \right] + e^{i \frac{\omega}{a_0} \rho \cos \vartheta} E\left[(2\rho \tfrac{\omega}{a_0})^{1/2} \cos(\tfrac{3\pi}{2} - \tfrac{\vartheta}{2}) \right] \right] \quad (12)$$

$$E(t) = \frac{1}{\sqrt{i\pi}} \int_{-\infty}^{t} e^{it'^2} dt'$$

For the limiting case $\lim \frac{\omega \rho}{a_0} \to \infty$ and $\vartheta = 0$, the above solution is simplified to

$$\hat{p}(\xi, 0, \omega) = \frac{1}{2} \hat{p}_F$$

for all frequencies.

This means that on the "shadow"-line between region 1 and region 2, we again obtain an N-shaped shock wave system. This system has only half the amplitude of the incoming shock wave system, however. For r, ϑ-values which lie in region 1, yet are removed sufficiently far from the shadow line, one obtains easily in a first approximation the unchanged plane wave propagating in the ξ-direction. For any given ϑ-values, however, the solution to equation (12) will have to be calculated numerically.

4.3. Complete solution

In order to determine the total pressure of the shock wave system at the focal point O and at sufficiently great distances behind the caustic, the two partial solutions in chapters 4.1. and 4.2. are superimposed. The results are discussed in the next paragraph.

5. NUMERICAL EVALUATION

The pressure distribution of the shock wave system to be investigated, as it is obtained from the solutions in chapters 4.1. and 4.2., after applying the inverse Fourier-transform

$$p^{(i)}(t) = \frac{1}{2\pi} \int \hat{p}^{(i)}(\underline{x}, \omega)\, e^{i\omega t}\, d\omega$$

(i = 1, 2 corresponds to the contributions from F_1 and F_2) was determined numerically at and far behind focal point for the following representative case: Let us assume a pressure distribution on the surfaces F_1 and F_2 located at a distance of 3000 m from the focal point O. Let the circular curved part F_1 of the surface F appear at the point O under the angle of 2°. The numerical evaluation of the results of the above paragraph then yields the pressure distributions at and far behind the focal point, shown in figures 8 and 9.

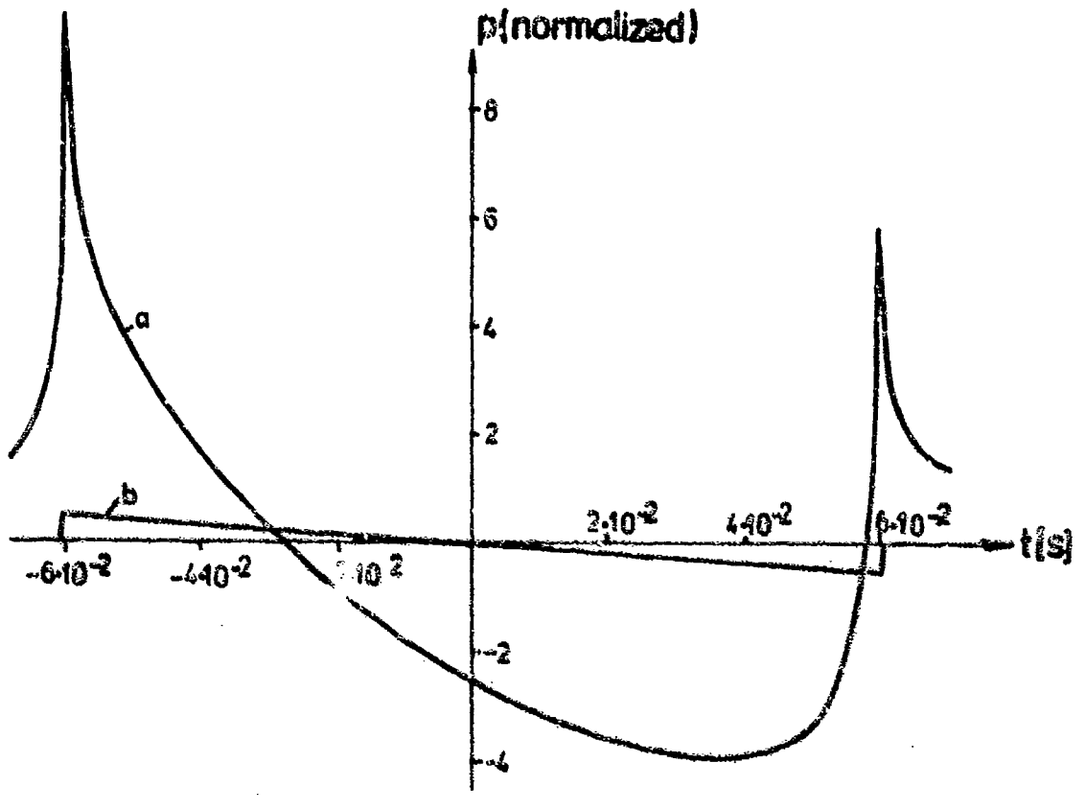

Fig. 8: Pressure signature of the shock wave system at the focal point. Contribution from F_1 (curve a), from F_2 (curve b); incoming wave: $\hat{p}_{MAX} = 1$, $T = 1{,}2075 \cdot 10^{-1}$ s, $\tau = 7{,}5 \cdot 10^{-3}$ s.

The forms of these curves agree very well with the pressure distributions measured by J. Vallee [9].

The amplitudes of our curves on the contrary cannot be directly compared with those of [9]. While they are of the same magnitude, they are so dependent upon the radius R of the surface F and the angle Θ_0 so that a quantitative agreement can only be expected when the calculations are carried out with real surfaces F.

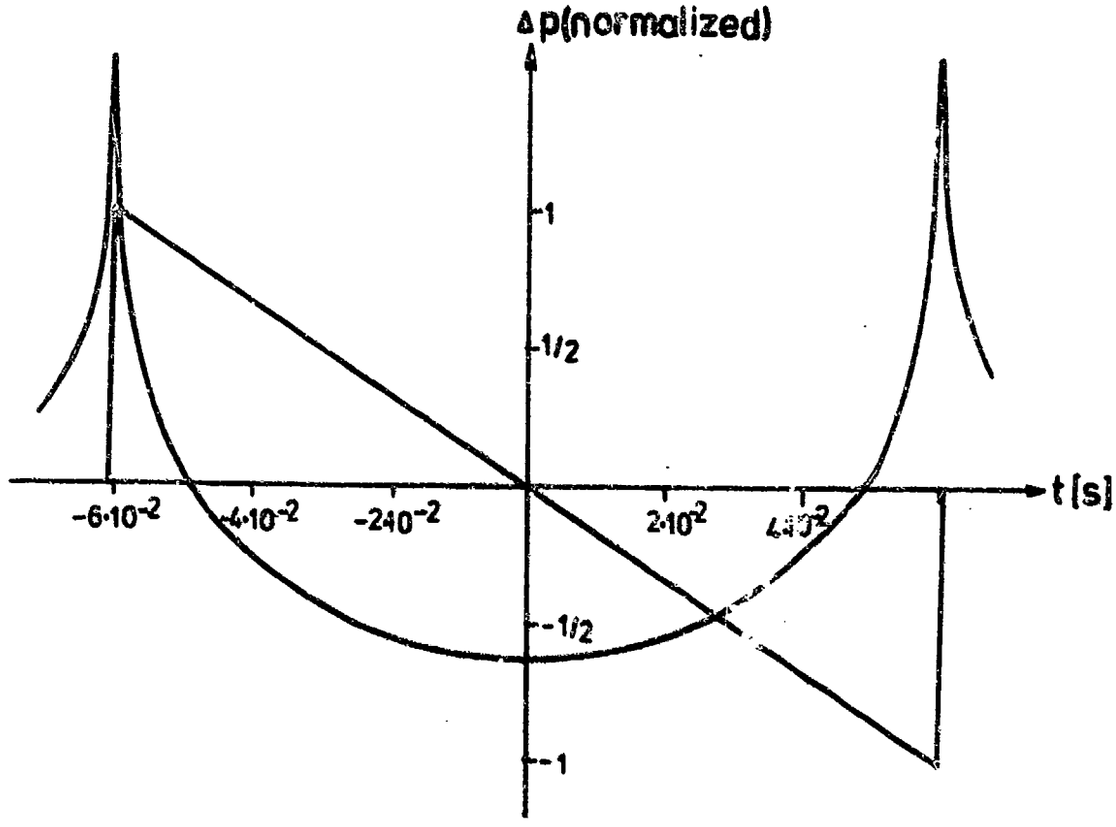

Fig. 9: Pressure signature of the shock waves far behind the caustic compared with the original N-shaped signature; incoming wave: $\hat{p}_{MAX} = 1$, $T = 1{,}2075 \cdot 10^{-1}$ s, $\tau = 7{,}5 \cdot 10^{-4}$ s.

6. CONCLUSIONS

Based upon the fact that the focusing of a sonic boom is a local phenomenon, the equations of linear wave acoustics were applied to determine the pressure distribution of such a sonic boom near and behind the caustic.

Explicit results were obtained for an analytically easy-to-handle case. In this case the acceleration phase of the supersonically flying projectile causing this sonic boom is chosen so that the corresponding Mach-cone consists of a truncated cone to which the lower part has a circle like curved surface, and the upper part is an ordinary straight cone apex. That means the caustic degenerates to a focal line.

The main results of these discussions were:

(i) The proposed theory yields finite pressure amplitudes at the caustic and avoids the singular behavior obtained by geometric acoustics.

(ii) The pressure signature of a N-shaped sonic boom changes behind the caustic to a pressure distribution with two positive peak values, consistent with the experimental results.

Finally, one can expect that our theory will give results which agree quantitatively with experimental data, if the calculations are performed for a real shock wave system and a real Mach-cone, which do not imply that the caustic degenerates to a focal line.

7. REFERENCES

[1] M.J. Lighthill: Reflection at a Laminar Boundary Layer of a Weak Steady Disturbance to a Supersonic Stream, Neglecting Viscosity and Heat Conduction. Quart. J. Mech. Appl. Math. 3 (1950), 303-325.

[2] R.N. Buchal, J.B. Keller: Boundary Problems in Diffraction Theory. Comm. Pure Appl. Math. 13 (1960), 85-114.

[3] W.D. Hayes: Similarity Rules for Nonlinear Acoustic Propagation Through a Caustic. Second Conference on Sonic Boom Research, NASA SP 180 (1968), 165-171.

[4] A.R. Seebass: Nonlinear Acoustic Behaviour at a Caustic. Third Conference on Sonic Boom Research, NASA SP 255 (1971), 87-119.

[5] L.D. Landau, E.M. Lifschiz: Lehrbuch der theoretischen Physik, Bd. VI: Hydrodynamik § 113. Akademie Verlag Berlin (1966).

[6] K.G. Guderley: Theorie schallnaher Strömungen. Springer Verlag (1957).

[7] F. Obermeier: Ähnlichkeitslösungen der Gleichungen für die transsonische Strömung idealer Gase und die hyperkritische Strömung elektrisch leitender Medien. Diplomarbeit, Göttingen (1965).

[8] P. Debey: Das Verhalten von Lichtwellen in der Nähe eines Brennpunktes oder einer Brennlinie. Ann. d. Phys. 30 (1909), 755

[9] J. Vallee: Operation Jericho-Vague. AGARD CP-No 42, St. Louis, Mai 1969.

[10] M. Abramowitz, J.A. Stegun: Handbook of Mathematical Function, published by the National Bureau of Standards, 1969.

[11] P.M. Morse, K.U. Ingard: Theoretical Acoustics. McGraw Hill Book Company (1968).

INFLUENCE DES CONDITIONS METEOROLOGIQUES SUR LA POSITION AU SOL DU TAPIS DE BANG

M.Schaffar - C.Théry
Institut Franco-Allemand de Recherches de Saint-Louis
12, rue de l'Industrie
68300 Saint-Louis
France

RESUME

On étudie numériquement les déplacements du tapis de bang liés aux conditions météorologiques (2 années de sondage) pour différents cas de vol. On constate que les longueurs permettant de positionner le tapis de bang par rapport à la trajectoire de l'avion peuvent varier de manière considérable : les distances d'extinction longitudinale (extrémité arrière du tapis) et latérale peuvent être triple de la valeur standard, suivant que le vent présente une composante élevée longitudinalement ou transversalement. La position du point de focalisation sous trace (extrémité avant du tapis) pour un vol rectiligne accéléré (1 m/s^2) s'écarte de ± 10 km par rapport à la valeur standard.

L'analyse de la dispersion, liée à la précision des données météorologiques, montre que l'incertitude n'est pas négligeable au niveau de l'extinction longitudinale (3 à 7 km), et la comparaison des résultats fournis par des sondages décalés de six heures fait apparaître des incertitudes comparables.

NOTATIONS

M	nombre de Mach
M_e	nombre de Mach d'extinction
z	altitude de vol de l'avion
γ	angle de montée de l'avion
w	projection dans le plan horizontal du trajet parcouru par un rayon caractéristique entre le point d'émission et le point d'arrivée au sol
w_e	distance w pour l'extinction longitudinale
$\overline{w_e}$	moyenne de plusieurs distances d'extinction
w_{stand}	distance w en atmosphère standard
w_f	distance w à la focalisation sous trace, mais comptée à partir de l'origine M = 1,0
V_L, V_T	composantes longitudinale et transversale de la vitesse V du vent par rapport à l'axe de vol à l'altitude de l'avion
η	direction du vent
σ	écart type
θ	angle du rayon caractéristique sous l'horizontale
$a(z)$	vitesse du son en fonction de l'altitude
$u_\eta(z)$	composante du vent suivant la normale au front d'onde en fonction de l'altitude

1. INTRODUCTION

Le bang produit par un avion en vol supersonique est un phénomène physique dont la plupart des aspects commencent à être bien connus, tant au point de vue de sa propagation en atmosphère standard qu'au point de vue de ses effets. L'Institut Franco-Allemand de Recherches de Saint-Louis a déjà apporté une certaine contribution à l'ensemble des connaissances du bang (focalisation - réflexion au sol - pénétration dans l'eau) et a mis en oeuvre un générateur de bang qui, par ses dimensions et ses performances, a permis la réalisation d'une série de recherches tant structurelles que physiologiques.

L'imminence de l'entrée en service d'avions supersoniques commerciaux (TSS) a mis cependant en évidence l'importance de la position du tapis de bang pour la préparation des vols. En effet, il importe de connaître, avec une bonne précision, l'influence des conditions météorologiques sur les différentes grandeurs caractérisant le tapis de bang, ainsi que l'intensité des bangs sur les limites extérieures du tapis.

Le présent travail rend compte des études en cours (réf. [1] et [2]) sur ce sujet et menées en coopération avec le Royal Aircraft Establishment (RAE). D'un point de vue pratique, on a adopté le principe de séparer l'étude géométrique de celle de l'intensité, l'étude géométrique du bang devant permettre la détermination des paramètres atmosphériques influents et une analyse statistique des positions du tapis de bang, tandis que l'étude de l'intensité du bang devrait apporter des compléments utiles dans des cas particuliers. Par ailleurs, on a admis une schématisation des cas de vol pour permettre une étude géométrique plus simple ; les différents paramètres d'un cas de vol gardent cependant des valeurs réalistes. Les conditions météorologiques utilisées correspondent à une série de sondages réels qui seront décrits dans la suite de cet article.

Après la description du tapis de bang et des méthodes numériques utilisées, on exposera les principaux résultats concernant l'influence des données météorologiques sur la dispersion du tapis de bang.

2. METHODES ET PRINCIPES DU TRAVAIL

2.1. Le tapis de bang et les cas de vol schématisés

Le tapis de bang peut être simplifié (fig.1) ; il comporte trois parties principales, dans le sens du vol :

- la portion du tapis qui contient la zone de focalisation, qui correspond à la phase accélérée du vol ;
- la portion du tapis, limitée par deux segments de droite, qui contient l'extinction latérale ; cette partie correspond à la phase du vol en croisière ;
- la partie terminale du tapis de bang, où les derniers bangs émis lors de la phase décélérée arrivent au sol.

En fait, toute la zone terrestre couverte par le tapis est touchée par des bangs, mais en pratique, seules les limites extérieures du tapis ont une importance pour la préparation des plans de vol. Enfin, l'ISL et le RAE ont étudié chacun une partie du tapis : le RAE a traité le cas du vol en croisière (extinction latérale) et l'ISL a déterminé la propagation des bangs émis sous trace pour les phases accélérée et décélérée du vol.

Les cas de vol ont été schématisés suivant les quatre paramètres : M, z, cap, γ. Pour le vol de croisière, le RAE a choisi : M = 1,3 - 1,6 - 2,0 ; z = 12 000 - 15 000 - 18 000 m ; γ = 0°. Les cas de vol traités à l'ISL correspondent à M = 1,0 à 1,7, z = 9000 - 11 000 - 13 000 m, γ = -3°, 0°, +3°. Les valeurs numériques ont été choisies dans le but d'encadrer au mieux les valeurs réelles pour une loi de montée d'un transporteur supersonique et de permettre d'éventuelles interpolations (ou extrapolations) à partir des abaques déterminées pour les valeurs choisies. Les caps correspondent à des vols transatlantiques Amérique - Europe et retour (70° et 250°) et à des vols dans le sens Nord-Sud et Sud-Nord (160° et 340°).

La figure 2 montre une méthode d'utilisation des courbes M = f(w), - liant le nombre de Mach et la distance horizontale franchie par le bang pour un certain nombre de sondages météorologiques -, dans le cas où l'on veut déterminer le point de départ de l'accélération transsonique (quelles que soient les conditions météorologiques). Dans une première étape, le tracé des courbes M = f(w) par cas de vol permet, pour z,γ variable, de déterminer l'enveloppe limite inférieure donnant la distance minimale d'arrivée au sol du bang et d'en déduire ensuite les abaques M, z, γ. A partir du profil d'accélération M,z, on détermine par interpolation la courbe M,w correspondant au cas de vol. Dans la deuxième étape, on suppose que l'avion se dirige vers une frontière séparant deux zones : la zone II où les bangs ne sont pas admis, et la zone I où les bangs sont permis. Le profil d'accélération peut être traduit en une courbe M,x où x représente la distance séparant l'avion de la frontière des deux zones. Dans la dernière étape, il suffit de déterminer par translation le point de tangence des deux courbes reproduites sur un même graphique ; le point x_0 ainsi trouvé donne le point de départ de l'accélération transsonique. De ce fait, le premier bang qui arrive au sol et qui correspond à la focalisation sous trace touche le sol sur la frontière des deux zones. Cette méthode peut aussi être utilisée pour déterminer le départ de l'accélération pour des conditions météorologiques particulières. On étudiera cependant, dans la suite, la position du point de focalisation sous trace pour un cas de vol accéléré, rectiligne (z = 11 000 m et accélération de 1 m/s^2), afin de déterminer l'influence du vent sur la focalisation.

2.2. Méthodes numériques et bases théoriques

Pour une étude géométrique, l'approche acoustique de la propagation du bang est justifiée. Dans cette théorie, on détermine la propagation des rayons sonores - ou rayons caractéristiques - qui sont, à chaque instant, normaux à la nappe de choc qui constitue le bang. La loi de réfraction des rayons caractéristiques devient, en atmosphère réelle :

$$\cos\varphi = \frac{a(z)}{C_0 + u_n(z)}$$

avec $$C_0 = \frac{*_0}{\cos\varphi_0} - u_{n_0} ,$$

l'indice 0 indiquant les conditions initiales à l'altitude de vol.

Les méthodes numériques utilisées intègrent l'équation (1) pas à pas, en tenant compte des paramètres de vol et des conditions météorologiques dans des tranches horizontales.

Le programme ARAP de W.D. HAYES (réf.[5]) a été simplifié par la suppression de ce qui concerne le calcul de l'intensité du bang. Ce programme a été employé dans deux versions : ARAP1 simple précision (6 chiffres significatifs), et ARAP2 double précision (15 chiffres significatifs).

Un deuxième programme a été fourni par le Service Technique Aéronautique (STAé) et modifié pour traiter l'ensemble des cas de vol.

Des vérifications en atmosphère standard, où les distances de propagation peuvent être calculées exactement, montrent que la précision des programmes est inégale et qu'en particulier les distances d'extinction longitudinale sont sous-estimées. Le tableau suivant donne les différents écarts enregistrés par rapport aux valeurs exactes et fournit une estimation des écarts en atmosphère réelle où le contrôle n'est possible qu'avec des méthodes spéciales, comme p.ex. la méthode des caractéristiques.

		STAé	ARAP1	ARAP2
Atmosphère standard	à Mach donné	-1 km et moins	< 100 m	< 50 m
	à l'extinction	- 4 à 5 km	- 1 km	- 100 à 200 m
Atmosphère réelle	à Mach donné	± 1 à 2 km	100 m	50 m
	à l'extinction	(- 20 à 30 km)	(- 5 à 10 km)	(- 1 km)

Ce tableau appelle quelques commentaires :

- Dans certains cas atmosphériques particuliers, des rayons d'extinction peuvent aller à l'infini en théorie et la précision devient illusoire, d'autant plus que l'intensité de ces bangs finira par tendre vers zéro.

- Malgré son imprécision au voisinage de l'extinction, le programme STAé permet d'obtenir correctement, pour un ensemble de données atmosphériques, des valeurs telles que les écarts et les écarts type.

- Le programme STAé est 8 à 16 fois plus rapide du point de vue temps machine que la méthode de HAYES, si bien qu'on a utilisé ce programme pour une étude statistique en vérifiant certaines valeurs avec les méthodes ARAP1 ou ARAP2, suivant les cas.

2.3. Données météorologiques

Les sondages météorologiques servant au calcul sont de provenance diverse : de la station de Camborne, Cornwall (GB) d'une part, et de la station de Nancy-St-Dizier (Fr) d'autre part. Les valeurs fournies par la station anglaise ont été utilisées conjointement par l'ISL et le RAE ; elles se présentent sous forme de 104 sondages hebdomadaires, alternativement à 12h et à 0h, réalisés pendant les années 1963 et 1967. La position géographique de la station - latitude 53°13' Nord et longitude 05°19' Ouest - garantit aux sondages une certaine représentativité des conditions météorologiques au point de départ de la trajectoire supersonique de CONCORDE pour les vols Europe - USA. Une analyse de la vitesse longitudinale du vent, dans la tranche d'altitude 7000 - 13 000 m pour un vol USA - Europe (cap 70°), montre que les vents dominants sont des vents d'Ouest et que la composante longitudinale dépasse souvent 30 m/s (108 km/h) et atteint parfois 60 m/s (voir fig.3).

Les données météorologiques de Nancy s'étendent seulement sur une quinzaine de jours (1-15 avril 1972) et comprennent : deux sondages (6h-12h) par jour pour le vent en vitesse et en direction, un sondage en température à 12h par jour ainsi que l'évolution de la température au sol, de 3h en 3h. Ces conditions météorologiques permettent de juger les écarts qu'on peut enregistrer dans les distances de propagation du bang entre deux sondages décalés de 6h. En effet, à partir des données initiales, il est possible de construire des couples de sondages, le premier à 6h et le deuxième à 12h, en admettant que les deux sondages en température se raccordent pour $z = 1500$ m.

Dans les données de Nancy, les vents dominants sont aussi des vents d'Ouest, avec des vitesses maximales voisines de 60 m/s.

Un aspect, dépendant des données météorologiques et d'une importance non négligeable pour les calculs de propagation, est la précision même des différentes valeurs d'un sondage. Pour déterminer la dispersion des distances de propagation, liée à la dispersion des variables météorologiques, on admet la méthode suivante :

- A partir d'un sondage donné, indice 0, on crée 20 sondages légèrement différents, déterminés par :

$$\begin{cases} z_i = (z_i)_0 + \alpha_i \Delta z \\ V_i = (V_i)_0 + \beta_i \Delta V \\ T_i = (T_i)_0 + \gamma_i \Delta T \\ n_i = (n_i)_0 + \delta_i \Delta n \end{cases}$$

où α_i, β_i, γ_i, δ_i sont des suites aléatoires des nombres 0, +1, -1, et Δz, ΔV, ΔT, Δn des écarts possibles pour les quatre paramètres du sondage suivant leur présentation originale.

- Après les calculs de propagation, on détermine, soit pour l'extinction, soit pour $M > M_0$, la distance moyenne de propagation et son écart type qui définit alors la dispersion cherchée.

3. RESULTATS NUMERIQUES

L'étude systématique de 36 cas de vol pour l'ensemble des conditions météorologiques décrites en 2.3. a fourni un grand nombre de résultats dont les plus importants seulement vont être discutés dans ce paragraphe. Les figures 4 et 5 montrent quelques courbes $M = f(w)$ obtenues par le programme STAé avec les données météorologiques de Camborne pour l'année 1963 d'une part, et pour le cas de vol $z = 11\,000$ m, $\gamma = 0°$, cap = 70° d'autre part. La figure 6 présente les origines pour $M = M_e$ des courbes $M = f(w)$ pour le cas de vol précédent (valeurs calculées avec le programme ARAP1). On peut déjà juger de l'importante dispersion due aux conditions météorologiques, aussi bien au niveau de l'extinction longitudinale que pour $M > M_e$.

3.1. Extinctions longitudinale et latérale

Extinction longitudinale :

Pour les deux années de sondages 1963 et 1967 et pour tous les cas de vol, le Mach d'extinction M_e peut varier de 1,001 à 1,355 et la distance d'extinction longitudinale w_e de 30 à 120 km, soit de la moitié au triple environ de la valeur standard pour $z = 13\,000$ m. Bien que pénalisante pour un vol supersonique, cette dispersion dépend fortement de la direction du vent, donc du cap de l'avion, comme le montre l'analyse statistique.

En admettant comme paramètre de classification la direction du vent à l'altitude de vol, on peut définir quatre groupes symétriques, deux à deux - vent arrière et vent de face, vent travers gauche et vent travers droit -, et les conclusions suivantes s'imposent :

- Le vent arrière augmente la distance d'extinction : la probabilité pour que w_e dépasse le double de la valeur standard est de 12%.

- Le vent de face diminue la distance d'extinction avec une probabilité de 89% pour que $w_e < w_{stand}$.

- L'importance de l'augmentation ou de la diminution de w_e semble liée, comme le montre la figure 7, à la grandeur de la composante longitudinale V_L du vent ; la corrélation entre V_L et w_e est de 0,6.

- Les deux groupes où la vitesse du vent est transversale donnent des résultats voisins et les écarts par rapport à la valeur standard sont négligeables.

- D'une manière générale enfin, la distance d'extinction diminue en moyenne avec l'altitude ($\overline{w_e} = 45$ km, $\sigma = 13$ km pour $z = 9000$ m contre $\overline{w_e} = 55$ km, $\sigma = 16$ km pour $z = 13\,000$ m) et, de même, la distance d'extinction croît si l'angle de montée passe de -3° à +3°.

Dans ces résultats, il faut aussi introduire la dispersion liée à la précision des données météorologiques. Cette dispersion, de 5 à 7 km sur l'extinction longitudinale, n'est pas négligeable et semble aussi fonction de la composante V_L du vent, car les dispersions maximales se trouvent pour des sondages où le vent dépasse 40 m/s.

L'étude des sondages décalés de 6h montre, au niveau de l'extinction, une tendance à la diminution entre w_e, trouvée pour le sondage de 12h par rapport à w_e liée au sondage de 6h. L'écart moyen est de l'ordre de 5 km et subsiste malgré la dispersion due à la précision des données. Cette tendance demanderait à être confirmée par une statistique sur un plus grand nombre de couples de sondages décalés (11 seulement pour cette étude), mais elle indique l'importance de sondages météorologiques récents pour la préparation d'un plan de vol supersonique.

Extinction latérale :

Ce travail réalisé par le RAE (réf.[5]) montre que, dans ce cas, il faut distinguer deux extinctions latérales, l'une à droite, l'autre à gauche par rapport à la trace au sol de la trajectoire, car suivant la direction du vent, une isoémission est plus ou moins déformée par rapport à la forme symétrique déterminée en atmosphère standard sans vent. Pour les cas M,z étudiés, la dominante des vents d'Ouest est sensible, et pour chaque extinction latérale la même séquence se reproduit :

- Pour l'extinction babord, les distances de l'extrémité du tapis à la trace de l'avion sont croissantes dans l'ordre suivant des caps : 340° - 250° - 70° - 160°.

- Pour l'extinction tribord, ces mêmes distances croissent dans l'ordre des caps : 250° - 160° - 340° - 70°.

Exprimées en fonction de la demi-largeur nominale correspondante - en atmosphère standard sans vent -, les distances d'extinction latérale dépendent moins des conditions météorologiques si z ou M augmente.

Il faut remarquer enfin que pour les cas limites - qui ont une probabilité de 1% -, l'extinction latérale peut être doublée et même triplée par rapport à la demi-largeur nominale.

3.2. Distances de propagation sous trace pour $M > M_e$

D'une manière générale, les distances de propagation sous trace deviennent de moins en moins dépendantes des conditions météorologiques dès que le nombre de Mach est supérieur au Mach d'extinction.

Pour l'année 1963 (fig.4), l'écart entre la plus grande et la plus faible distance passe de 20,5 km (M = 1,375) à 8,3 km (M = 1,7).

Les distances de propagation anormalement longues par rapport à la valeur standard correspondante n'existent plus, les dépassements maximaux enregistrés étant de l'ordre de 42% (M = 1,2) et de 24% (M = 1,6), cependant en moyenne, on retrouve les valeurs standards correspondantes. La dispersion due à la précision des données météorologiques suit la même logique et le tableau suivant montre l'évolution de celles-ci en fonction de M.

M	Dispersion moyenne	Valeur maximale
1,2	320 m	850 m
1,4	110 m	410 m
1,7	60 m	300 m

Enfin, dans le cas de sondages décalés de 6h, la tendance à la diminution entre la distance liée au deuxième sondage par rapport à celle liée au premier, remarquée à l'extinction, disparaît et fait place à une dispersion moyenne qui décroît si M augmente : 1 à 2 km pour M = 1,2 et 350 m pour M = 1,7.

3.3. Cas particuliers et remarques sur l'influence dans la dispersion de la précision des paramètres du sondage

L'étude des rayons caractéristiques, au voisinage de l'extinction longitudinale, montre que, dans le cas de trajets très longs doubles ou triples de la valeur standard correspondante, ces rayons n'arrivent pas tangents au sol, comme c'est le cas en atmosphère standard, mais qu'ils sont voisins de l'horizontale dans une tranche d'altitude où, en général, la vitesse du vent est relativement forte. De tels trajets sont représentés sur la figure 8, où l'on peut aussi remarquer le nombre réduit de points de sondage dans les zones où les rayons sont voisins de l'horizontale. Cette remarque peut réduire l'importance des trajets d'extinction anormalement longs, car pour un rayon voisin de l'horizontale, une petite variation de vent ou de température peut soit le faire remonter, soit le faire descendre plus rapidement. Un phénomène de ce genre a été noté pour l'un des sondages de la station de Nancy. Des variations aléatoires dans les paramètres du sondage (± 0,1°C sur T, ± 1 m/s sur la vitesse du vent et ± 5° sur sa direction) ont fait varier la distance d'extinction longitudinale de 80 à 124 km, soit un écart de 44 km.

De telles structures atmosphériques sont cependant relativement rares (< 5% des cas) et sont caractérisées par des couches de "courbure nulle", déjà remarquées par NICHOLLS et JAMES (réf.[4]), où la somme de la vitesse du son et de la projection du vent sur la normale au front d'onde, a + Vn, est constante.

L'analyse de la dispersion, liée à la précision des variables météorologiques, bien que manquant de confirmation statistique à cause du nombre réduit des sondages testés, montre que, si la dispersion normale est de 3 à 7 km sur la distance d'extinction longitudinale, elle peut être notablement réduite si une plus grande précision est apportée à la mesure de la température (à 0,1°C près). Cette remarque est d'ordre mathématique, car du point de vue des météorologistes il semble illusoire de mesurer T à moins de 0,5°C. De plus, une meilleure précision sur le vent ne semble pas diminuer la dispersion, sauf peut-être dans le cas où le vent est fort.

3.4. Influence de la direction du vent sur la focalisation sous trace

Le cas de vol choisi (z = 11 000 m, angle de montée nul, accélération de 1 m/s²) correspond d'un point de vue accélération à un avion militaire, mais il permet de mettre en évidence les effets de la direction du vent sur la position de la focalisation sous trace. Plusieurs cas de vent ont été traités : vent de face et arrière très fort, moyen et faible, et les résultats sont à comparer avec la valeur obtenue en atmosphère standard sans vent. Les figures 9 et 10 regroupent les résultats numériques en prenant comme origine la position où l'avion passe par M = 1,0.

Par rapport à la valeur x_f en atmosphère standard, on remarque que :

- le vent arrière rapproche x_f de l'origine, tandis que le vent de face l'en éloigne ; les écarts maximaux sont de l'ordre de ± 10 km ;
- la composante longitudinale de la vitesse du vent intervient dans l'importance de l'écart : plus V_L est faible, plus on se rapproche de la valeur standard de x_f.

Ces résultats, bien que fragmentaires, précisent déjà l'influence du vent sur la focalisation sous trace. Ils seront complétés par l'étude de la focalisation pour des lois de montée correspondant à celles d'un transporteur supersonique.

3.5. Remarques et critiques

La principale critique inhérente à ce travail réside finalement dans la méthode adoptée, à savoir la séparation du calcul géométrique et du calcul d'intensité. En effet, l'étude géométrique de la propagation des bangs a mis l'accent sur des distances d'extinction longitudinales et latérales anormalement longues, et ce phénomène peut être préjudiciable pour des transporteurs supersoniques commerciaux. Bien qu'on puisse prévoir que de tels bangs seront faibles et distordus, leur estimation reste à faire, par le calcul d'une part afin de déterminer une borne supérieure de leur intensité, et par l'expérimentation d'autre part afin de connaître leur signature et leur affaiblissement dû à l'hygrométrie ou à la turbulence atmosphérique. Il existe vraisemblablement un seuil d'intensité (surpression et forme) au-dessous duquel le bang sera jugé comme tolérable et cessera d'être perçu comme un bang véritable.

Des expériences, réalisées en France (réf.[6]) avec 40 Contrôleurs Automatiques de Niveau de Bang Local (CANIBAL) répartis dans trois départements relativement fréquentés par des avions militaires en vol supersonique, ont permis de tirer quelques conclusions intéressantes quant à la largeur du tapis de bang :

- La largeur du tapis observé est sensiblement la largeur nominale, et la probabilité d'entendre des bangs décroît rapidement à partir de 0,5 fois la largeur nominale.

- Les appareils CANIBAL ayant un seuil de déclenchement compris entre 0,2 et 0,34 mbar (le bang moyen sous trace est de 0,5 mbar), aucun bang supérieur à ces seuils n'a été mesuré à une distance de la trace égale à 1,2 fois la demi-largeur nominale. De plus, pendant toute la période des essais, aucun bang n'a été perçu à cette même distance par le personnel servant les CANIBAL. On peut donc en conclure que la probabilité "d'entendre" des bangs (supérieurs à 0,2 - 0,34 mbar) est nulle (ou à peu près nulle) à une distance égale à 1,2 fois la demi-largeur nominale.

Ce résultat semble donc en désaccord avec les calculs de J.B.W. EDWARDS (réf. [5]), qui donne, pour une distance de 1,2 fois la demi-largeur nominale (M = 1,6 ; z = 15 000 m), une probabilité d'entendre le bang de 0,7 à 0,1 selon que le vent est défavorable ou favorable. Il devient donc nécessaire d'obtenir, par d'autres essais en vol, des informations supplémentaires sur l'intensité des bangs sur la périphérie du tapis, du point de vue calcul et surtout d'un point de vue expérimental.

4. CONCLUSION

L'étude géométrique de la propagation du bang en atmosphère réelle met en évidence, dans certains cas, la déformation importante du tapis de bang par rapport à sa forme normale en atmosphère standard : extinctions longitudinale et latérale doubles ou triples de la valeur standard, variations importantes de la focalisation sous trace, suivant que le vent présente une composante élevée longitudinalement ou transversalement (fig.11). De plus, une dispersion non négligeable, 3 à 7 km, au niveau de l'extinction est liée à la précision des sondages météorologiques.

Les cas anormaux sont relativement rares, mais leur existence reste pénalisante pour les vols supersoniques et des compléments d'informations sont nécessaires, tant du point de vue calcul que du point de vue expérimental, pour déterminer l'intensité de tels bangs qui, d'après les rares résultats déjà connus et contrôlés, paraissent être faibles et pratiquement inaudibles.

REFERENCES BIBLIOGRAPHIQUES

[1] M.SCHAFFAR, C.THERY, F.SCHLOSSER
Calcul de la propagation géométrique du bang sous trace dans le cas d'atmosphères réelles avec vent.
Rapport ISL 57/72.

[2] M.SCHAFFAR, F.SCHLOSSER
Influence des conditions météorologiques et de leur précision sur la position au sol du tapis de bang (extinction - focalisation sous trace).
Rapport ISL (en cours d'impression).

[3] W.D.HAYES, R.C.HAEFELI, H.E.KULSRUD
Propagation des bangs soniques dans une atmosphère stratifiée avec programme de calcul.
NASA C.R. 1299.

[4] J.M.NICHOLLS, B.F.JAMES
The location of the ground focus line produced by a transonically accelerating aircraft.
Journal of Sound and Vibration (1972) 20(2), 145-167.

[5] J.B.W.EDWARDS
Lateral extents of sonic boom carpets in real atmospheres.
R.A.E. Tech.Memo. Aero 1465.

[6] Société d'études, de construction de souffleries, simulateurs et instrumentation aérodynamique.
Opération CANIBAL - 2ème campagne de mesure - février 1973.

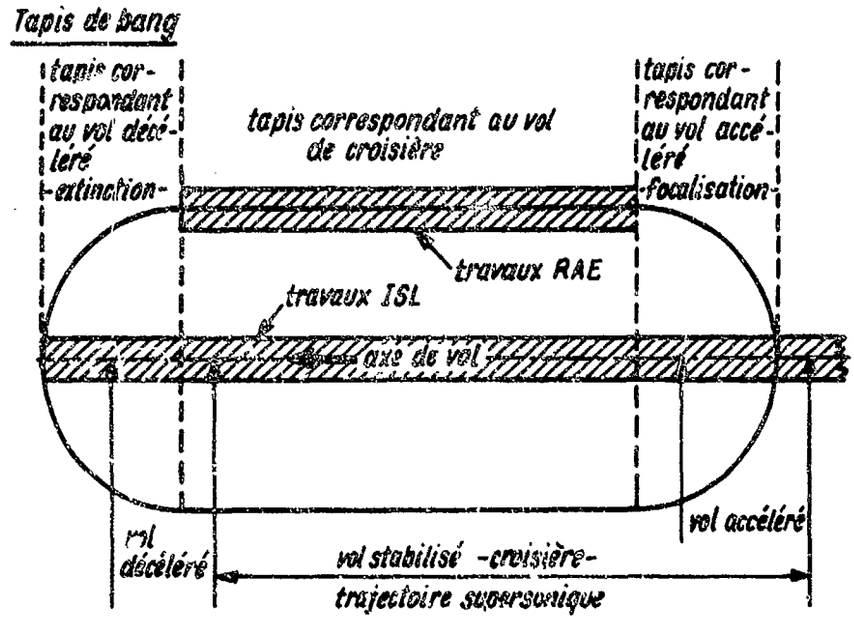

Fig.. - Propagation du bang en atmosphère réelle : zone de bang et schématisation du problème.

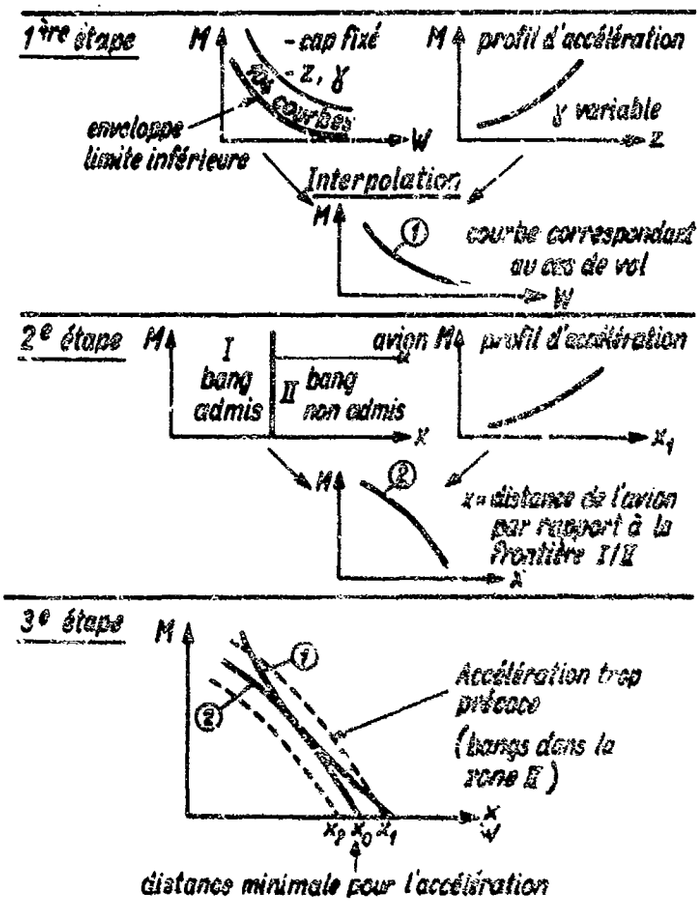

Fig.2 - Utilisation des courbes M = f(w) pour déterminer le départ de l'accélération transsonique.

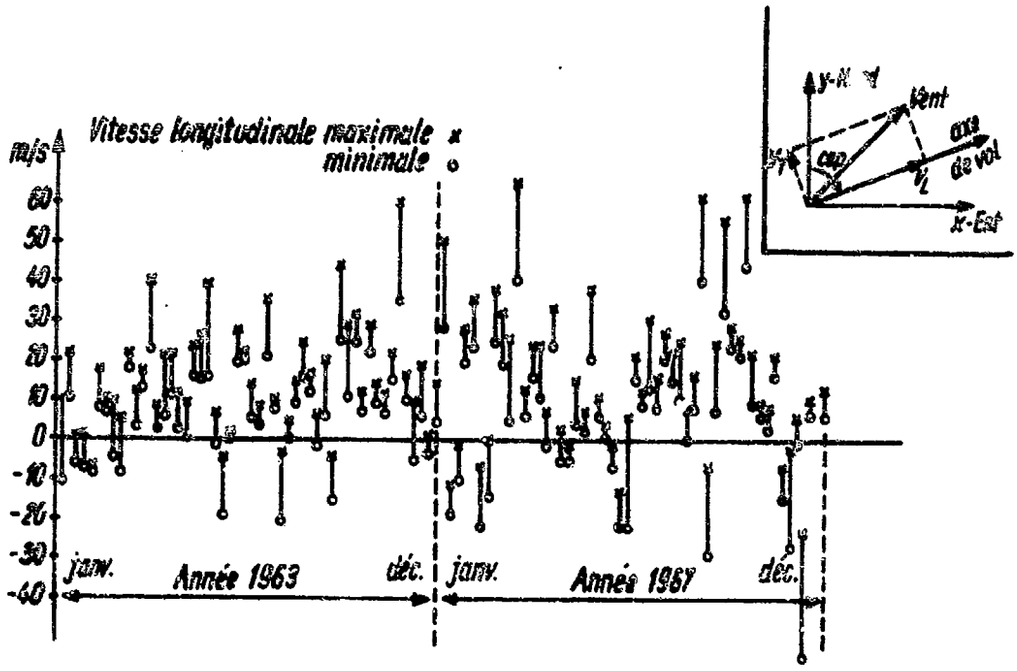

Fig.3 - Analyse de la vitesse longitudinale du vent (max. et min.) dans la tranche d'altitude 7000 - 13 000 m pour le cap 70° et pour les années de sondage 1963 et 1967.

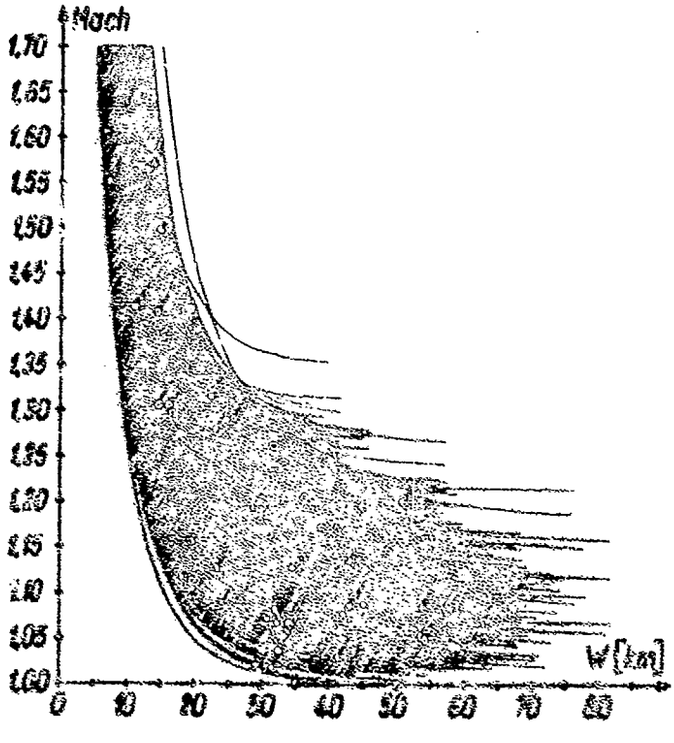

Fig.4 - Distances de propagation du bang égale sous trace, en fonction du Mach et des conditions météorologiques de l'année 1963, pour tous les cas de vol traités (52 × 36 = 1872 courbes).

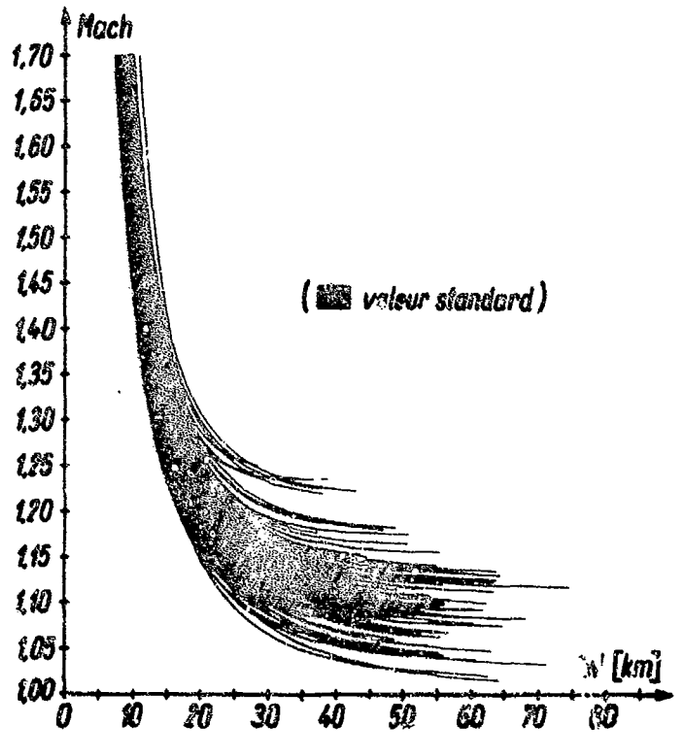

Fig.5 - Distances de propagation du bang émis sous trace, en fonction du Mach et des conditions météorologiques (104 sondages), pour le cas de vol : altitude = 11 000 m, angle de montée = 0°, cap = 70°.

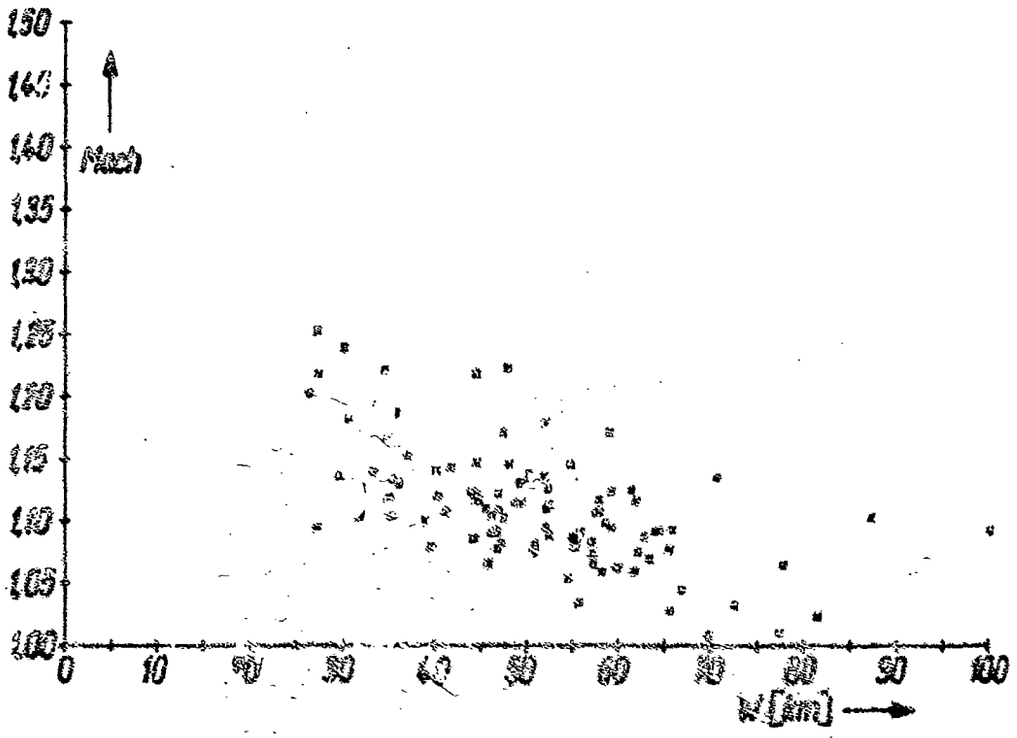

Fig.6 - Distances de propagation à l'extinction du bang émis sous trace en fonction du Mach et des conditions météorologiques (104 sondages), pour le cas de vol : altitude = 11 000 m, angle de montée = 0°, cap = 70°.

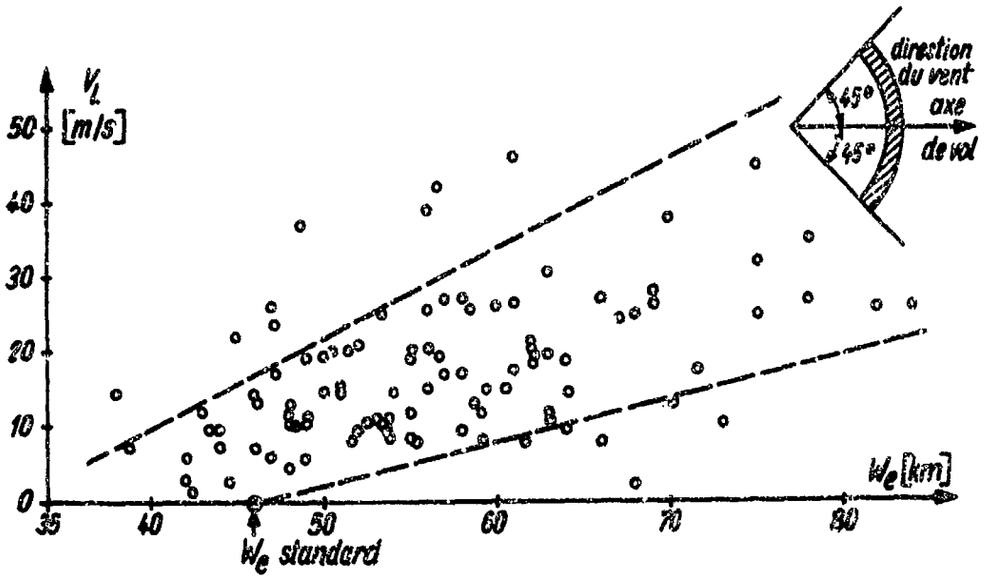

Fig.7 - Distances w_e à l'extinction en fonction des vitesses longitudinales à l'altitude de vol (13 000 m, $\gamma = 0°$, résultats STA6) pour les cas où la direction du vent et l'axe de vol sont voisins (vent arrière).

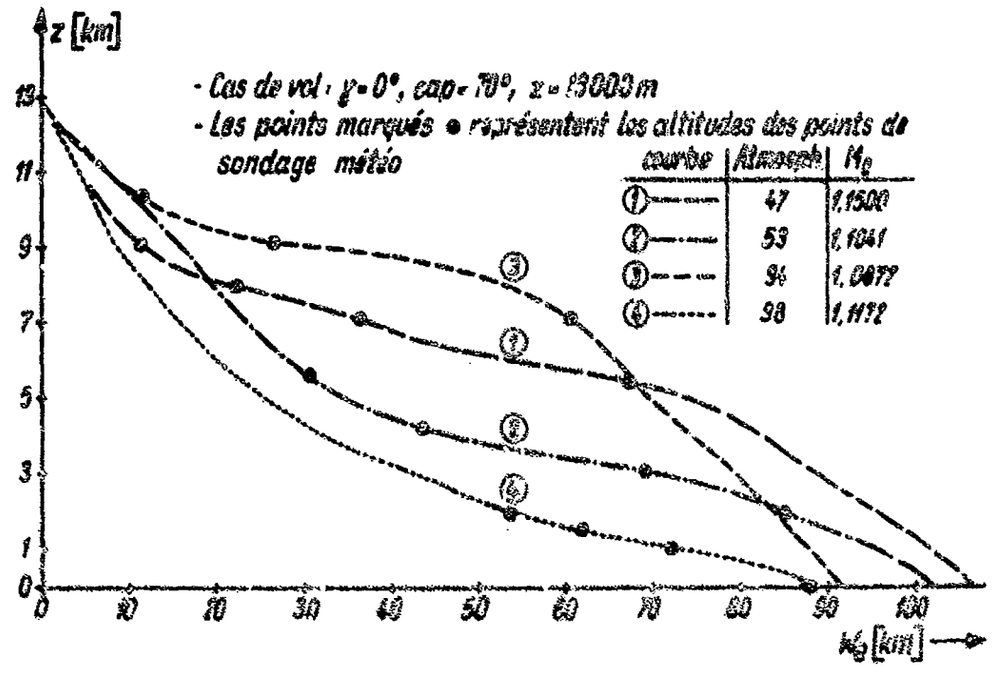

Fig.8 - Tracé des rayons caractéristiques au voisinage du Mach d'extinction pour quelques atmosphères à vent fort (programme ARAP1).

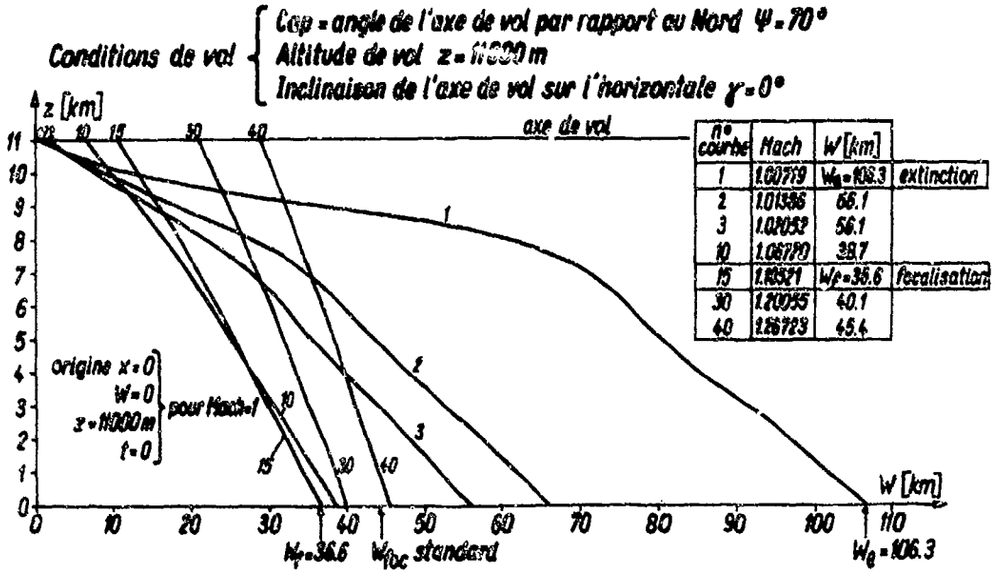

Fig.9 - Tracé de la projection (dans le plan vertical de la trajectoire) de rayons émis "sous trace".
Atmosphère 88 Vol rectiligne uniformément accéléré : Accélération = 1 m/s².

Origine des axes : M = 1.0
Résultats du programme ARAP 1

	Atmosphère	M_f	W_f	Remarques sur le vent
⊕	standard	1,2443	44,4 km	Vent nul
×	n°83 du 3.9.67 cap = 70°	1,1052	36,6 km	Vent arrière très fort (114 Nds)
⊛	n°83 du 3.9.67 cap = 250°	1,3858	54,2 km	Vent de face très fort (114 Nds)
·	n°59 du 1.1.67 cap = 70°	1,1183	35,7 km	Vent arrière fort (100 Nds)
⊛	n°53 du 1.1.67 cap = 250°	1,3987	54,2 km	Vent de face, fort (100 Nds)
⊡	n°65 du 26.3.67 cap = 70°	1,1514	39,8 km	Vent arrière moyenne intensité (65 Nds)
△	n°64 du 23.3.67 cap = 70°	1,1962	41,4 km	Vent arrière moyenne intensité (inaccoutumé)
▽	n°39 du 27.2.67 cap = 70°	1,1634	40,7 km	Vent arrière de faible intensité (40 Nds)
•	n°73 du 4.6.67 cap = 70°	1,1373	45,6 km	Vent de face de faible intensité

Arrivée au sol à la focalisation des rayons émis sous trace, par rapport à l'axe de vol

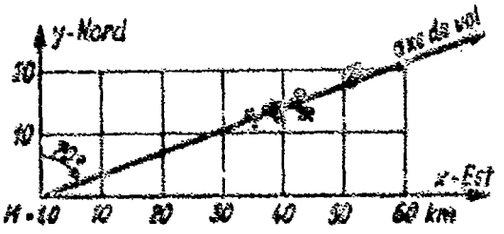

Fig.10 - Distances de focalisation, déterminées à partir des rayons émis sous trace, pour un vol rectiligne, uniformément accéléré (accélérations = 1 m/s²) pour z = 11 000 m, γ = 0° et pour plusieurs sondages atmosphériques.

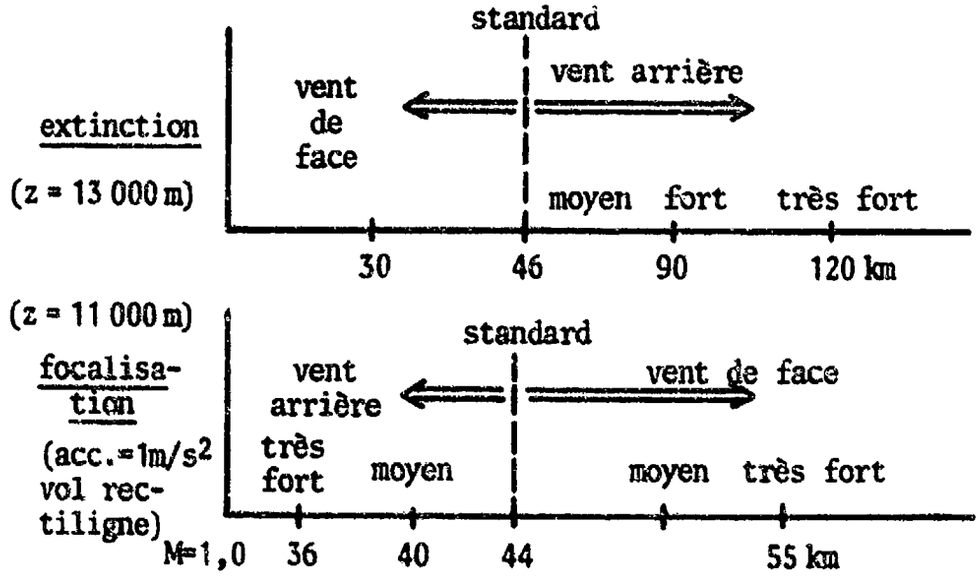

Fig.11 - Schéma des influences des données météo sur l'arrivée au sol à l'extinction et à la focalisation du bang émis sous trace.

RECENT STUDIES INTO CONCORDE NOISE REDUCTION

by

R. Hoch
SNECMA
150 Boulevard Haussmann,
75 Paris 8e,
France.

R. Hawkins
Rolls-Royce (1971) Limited,
Bristol Engine Division,
P.O. Box 3,
Filton, Bristol, England.

SUMMARY

This report summarises recent research which has been conducted over the past two years by SNECMA and Rolls-Royce, as part of a continuing noise reduction programme on the Concorde powerplant. The studies were aimed at (a) improving knowledge of certain noise sources of the Olympus 593 turbojet engine and (b) evaluating potential means for noise reduction either at source by alteration to the various engine components, or by addition of attenuating devices. Some of the results of these studies have been applied to the powerplant design standard intended for entry into service, others are mentioned only for their technical or didactic interest, and others after engineering evaluation, may lead to acoustic improvements to the Concorde powerplant after entry into service.

1. INTRODUCTION

Until such time as considerable technological progress has been made, for instance, in the field of variable cycle turbojet engines, the manufacturers of supersonic transport aircraft will be obliged to use turbojets or turbofan engines of low bypass ratio to power such aircraft. Compared with high bypass ratio engines, which have become a feature of modern subsonic transport aircraft and which are particularly well suited to a high degree of silencing treatment, these engines are, by their very design, noisy, particularly at take-off, due to the high velocity of the exhaust gases.

The manufacturers of the Concorde have, from the outset of the project, recognised the necessity to make the aircraft acceptable to the public from the noise point of view and the Engine Companies of SNECMA and Rolls-Royce have carried out intensive research in order to achieve, to the greatest possible extent

- the reduction of the noise of the high velocity jet of the Olympus 593 turbojet engine at the supercritical expansion ratios in the take-off and flyover phases and

- the reduction of engine internal noise which dominates the overall noise in the approach phase.

This paper summarises some of the results obtained during the comprehensive and integrated research programmes which have been carried out by the two Companies in collaboration with universities and the national research establishments in France and Britain.

2. CHOICE OF POWERPLANT FOR CONCORDE

The effective control of operational noise levels has been a key objective of the Concorde manufacturers from the inception of the programme. However, in selecting and developing the propulsion system and various silencing means for Concorde, account has had to be taken of the peculiar characteristics of the SST and the impact of any performance losses or weight increases on the viability of long range supersonic operation. The most important of these special factors and their influence on the choice of powerplant and the consequent aircraft noise levels are examined in this paragraph.

There are fundamental differences between the aircraft configuration required for efficient operation at supersonic speeds and that necessary for efficient subsonic cruising. The reduced span and high slenderness ratios which are needed to give good supersonic performance, result in less efficient low speed operations. Consequently, a supersonic aircraft requires higher take-off and approach thrust at a given operational weight than does its subsonic counterpart, and so will be noisier in these phases of flight. In principle, the adverse consequence on aircraft noise could be alleviated by the use of variable sweep wings. However, the state of the art is such that the complexity, increased structure weight and loss of usable volume incurred by their use would be unacceptable in a long range supersonic transport aircraft.

The payload which can be carried by supersonic aircraft is proportionately smaller than that of an equivalent subsonic aircraft. With Concorde it amounts to less than 7% of the maximum take-off weight. It follows that any installed weight increase or any increase in fuel weight resulting from thrust losses or specific fuel consumption

increases, will have a large impact on the payload which can be carried. This has important consequences on the choice of powerplant and silencing systems for Concorde. For subsonic aircraft the evolution of the high bypass ratio turbofan for improving performance and economics, made possible significant reductions in take-off and approach noise levels. Such an engine with its low specific thrust (high mass flow and low jet velocity) is incompatible with supersonic operation. Even an engine with a moderate bypass ratio would represent a serious loss in overall mission performance through increased installation drag and increased powerplant weight.

In a Mach 2 supersonic transport such as Concorde, a substantial compression occurs in the intake at high speeds and this component plays an important role in the achievement of high propulsive efficiency. Therefore the optimum pressure ratio required from the basic engine is lower than for a subsonic engine. To ensure that its efficiency is high and that the flow demands of the engine can be met at all flight speeds, the intake must have variable geometry. The exhaust nozzle system must also be variable to make the most efficient use of the available turbo-machinery at both take-off and supersonic speeds. Consequently the weight of the air intake and exhaust system in a supersonic aircraft represents a much larger proportion of the powerplant weight than for a subsonic nacelle. Since this weight increases faster than the design mass flow it is important to choose an engine of high specific thrust (high jet velocity) for supersonic transports.

From specific fuel consumption considerations alone, the optimum bypass ratio for a Mach 2 transport would be around 0.6 to 0.8 depending upon turbine entry temperature (see figure 1). The specific thrust would be only about 30% lower than that of a turbojet yet this increase in engine mass flow with the attendant increase in powerplant weight and drag would more than offset the potential improvement in engine specific fuel consumption. The situation is not improved by using a low bypass ratio turbofan with reheat to give the same specific thrust in cruise as that of the Olympus 593 - see figure 2.

Thus, although a turbofan would be desirable to reduce noise levels at take-off and landing, the supersonic transport requires engines of high specific thrust for cruise. One possible method of meeting these conflicting requirements would be to use an engine of variable bypass ratio. Such engine concepts are being examined and may form the basis of future powerplants for second generation supersonic transport aircraft.

The type of engine chosen to power the BAC/SNIAS Concorde is the RR/SNECMA Olympus 593 turbojet, a section of which is shown in figure 3. It is a twin spool engine of modest pressure ratio which incorporates a reheat system delivering a thrust boost of about 20% for take-off and transonic acceleration.

The Type 28 exhaust system with which the first production engines will be equipped incorporates three major components in a single integrated design:

a) a variable primary nozzle, in order to optimise the engine performance over a wide range of operating conditions, and to allow for reheat operation. The variable nozzle has been used effectively to reduce jet noise during climb and on approach, since by opening the nozzle with the twin spool engine its mass flow can be increased (and hence jet velocity reduced) whilst maintaining the same thrust.

b) a secondary nozzle, closely integrated to the wing structure incorporates two buckets which can be rotated in order to achieve optimum matching of the secondary nozzle exit area to the pressure ratio imposed by the flight speed and the engine power. In addition, at large deflection angles of the buckets, attenuations of sideline noise can be achieved at take-off. When fully closed at landing, the buckets act as a thrust reverser.

c) a jet silencer, incorporating eight "spades" which is used to reduce the jet noise in flyover at cut-back power, and which can be retracted into the secondary nozzle structure to avoid internal losses during climb and cruise.

The configurations of the Type 28 exhaust system in the main flight phases are illustrated in figure 4.

3. NOISE CHARACTERISTICS OF THE UNSILENCED OLYMPUS 593

Having outlined the aerodynamic, propulsive and economical considerations which led to the choice of the Olympus 593, a short description of the noise characteristics of this engine when fitted with a convergent primary nozzle follows. Figure 5 presents a summary of the normalised linear peak noise levels for this engine compared with those obtained with "pure" jets at the same velocity. At take-off conditions, because of the high specific thrust of the engine (the exhaust velocity is nearly 850 m/s), the jet is the predominant noise source. The noise originates from the classical mixing of the jet with the ambient air and, in directions normal to the jet axis and in the forward arc, from the interaction of eddies with the shocks of the underexpanded jet. A large number of model and full scale tests have shown that in the peak noise direction, the reheat has no peculiar effects. The relatively small noise increments resulting from the reheat boost (figure 6) are predictably associated

with the velocity, density and nozzle area variations.

Concorde, in common with most aircraft, will use a noise abatement procedure during take-off and it is well known that the effectiveness of such a procedure increases as the engine bypass ratio decreases. During climb at reduced thrust jet mixing noise is still the predominant noise source in the rearward arc. Nevertheless, a progressive increase of the noise level at high angles to the jet axis can be observed. This increase is attributed to "internal noise", which is examined in detail in paragraph 4.3. Since this contribution of internal noise is most noticeable in the high frequency part of the noise spectra, it will lead to greater increases over pure jet noise when expressed in PNdB than the divergences in figure 5 would suggest. Under approach conditions, the internal noise is largely predominant over the other noise sources of the Olympus 593, including the compressor noise radiating from the inlet.

Also shown in figure 5 are the peak noise levels obtained in flight presented as a function of relative instead of absolute jet velocity. It will be noted that there is good correlation between static and flight levels at the highest jet velocities, although as jet velocity is reduced, progressive divergence of the data from the static levels occurs as the contribution of the internal noise to the overall noise increases. Furthermore, this divergence suggests that the internal noise component is more dependent on the internal flow conditions of the engine than on the relative jet velocity. These flight effects will be discussed more fully in paragraph 5.

The divergences between the overall engine noise and the threshold formed by the pure jet noise (deduced from model tests in an anechoic chamber) are illustrated in detail in figure 7 which shows the differences in the rearward arc between the engine noise level and the corresponding pure jet noise level as a function of the exhaust velocity. The differences can be seen to be maximum at low velocities and at angles between 70° and 80°, being progressively reduced as the exhaust velocity is increased. When the pressure ratio becomes supercritical, it can also be seen that the differences are small in the rearward arc, but increase significantly towards the forward arc. This trend results probably from the greater level of shock associated noise which is present in the engine compared with that of models for which the jet turbulence level is much lower.

An examination of sound pressure spectra at low engine thrust provides a better assessment of the contribution of internal noise to the overall engine noise. As an example, the spectra shown in figure 8 highlight a medium and high frequency content much greater than that expected from turbulent mixing of the exhaust jet with the surrounding air. Possible origin of this noise will be discussed in paragraph 4.3. The corresponding perceived noisiness spectrum emphasises the weighting this noise component puts on perceived noise levels expressed in PNdB.

These characteristics of engine exhaust noise are not specific to the Olympus 593 but with minor differences appear to be common to most engines.

4. IDENTIFICATION AND SUPPRESSION OF THE MAIN NOISE SOURCES

Before describing a number of investigations carried out by the manufacturers, we will outline the solutions adopted and developed for the entry into service of Concorde.

4.1 Acoustic properties of the exhaust system designed for entry into service

Although the overall design of the Olympus 593 was frozen as early as 1965, the engine manufacturers have progressively applied all possibilities offered by available noise reduction techniques compatible with the technological, economical and operational constraints of the supersonic aircraft (1) (2).

Once the engine cycle most appropriate to the Concorde mission had been defined, suppression techniques for reducing noise at source were limited. Nevertheless, the Olympus 593 engine offered some potential for source noise reduction other than at full power because of its twin spool layout. Opening the primary nozzle to the maximum possible area compatible with a safe surge margin, while maintaining the thrust constant by increasing the low pressure compressor speed, will reduce considerably the jet velocity and, as a consequence, the jet mixing noise. Considerable progress in this direction has been achieved since the prototype engine tests, without affecting the engine handling characteristics. Prototype and preproduction aircraft flight tests have demonstrated the validity of this technique and the noise reductions already demonstrated in flight are shown in figure 9 at Concorde approach and cut-back conditions respectively.

Other jet noise reduction techniques are built into the general design of the exhaust system being developed for entry into service, and which is designated the Type 28 Nozzle. The sideline noise reduction at take-off is achieved by fishtailing of the jet by rotating the buckets at an angle of about 30° as soon as the aircraft is airborne (3). The performance of this device is summarized in figure 10. At cut-back, which provides a noise reduction of the order of 10 PNdB, the spade silencer is introduced into the jet and the bucket angle is reduced to about 10°. The performance

of this silencer, which is completely retractable, is shown on figure 11.

It is worth recalling that the take-off and climb trajectory for a given weight is dependant on the installed thrust. Figure 12 shows for a given silencer attenuation, the changes in flyover noise level for Concorde at maximum weight due to changes in thrust (2). An increase in take-off thrust leads to an increased throttling altitude, a greater height over the measuring point, and a lower flyover noise level, although the optimum throttling distance from start of roll is reduced. The figure also indicates the importance of reducing losses in take-off thrust by, for example, avoiding the premature deployment of silencers.

Although actions and devices described are intended to ensure that, at the time of entry into service, Concorde will not be noisier than most long-range aircraft in service today the manufacturers are fully aware that this initial target, which corresponds to a total reduction of the order of 20 EPNdB at the three measuring points relative to the prototype Concorde noise levels, cannot be considered as satisfactory in the longer term. Because of this, close cooperation between SNECMA and Rolls-Royce has resulted in many investigations being carried out aimed at achieving a better understanding of the noise generating processes, and at exploring new silencing devices to attenuate these noise sources. To ensure that no aspect of the problem is overlooked, the manufacturers are using the assistance of several University and Research organisations in the fields of acoustics with the main objective of improving the systems designed for the entry into service, and evolving new attenuation devices.

4.2 Jet noise reduction

Two ranges of jet velocities are of major importance as related to the Concorde noise problem : the low velocity range, corresponding to the approach power of the Olympus 593, and the high velocity range (including the case of underexpanded jets) corresponding to the take-off conditions.

Until recently, there were some inconsistencies in the jet noise prediction methods at low exhaust velocities. This situation, which has lasted for a long time, has made it difficult both to identify and to quantify the internal noise sources on jet engines running at intermediate power. In order to solve this problem, SNECMA and NGTE conducted, a few years ago, a systematic research programme on the effect of the temperature of a jet on its noise emission (4), showing mainly that at low velocities a hot jet is noisier than a cold one, the reverse being confirmed at high exhaust velocities. From this work experimental values of a variable jet density exponent were determined which, when introduced into the usual jet noise normalising function, enabled a single prediction curve for jet noise to be obtained, applicable to a wide range of exhaust conditions. Figure 13 shows the jet density index which has been introduced in the acoustic power normalising function of a jet, the results of which is to produce the jet noise correlation curve shown in figure 14. This concept of a variable density index has been incorporated in the recently proposed revision of the S.A.E. jet noise prediction method A.R.P. 866.

In the high jet velocity range, research has been conducted chiefly on noise generated by shock waves in underexpanded jets. The best known phenomenon is a discrete tone emission, often termed "screech", but considering that it generally appears only on cold model jets, it is essentially of academic interest. Of greater importance when considering engines and particularly the reheated Olympus 593, is the high frequency broadband noise which appears at angles around 90° to the jet and in the forward arc and which is generated when eddies from the jet mixing layer interact with the shock waves of the underexpanded jet. This interaction mechanism and the laws governing this noise emission were described by Fisher (5) who showed in particular that the emitted sound intensity varies like the square of the pressure jump across the shock-wave. By using an adapted con-di nozzle it is possible to suppress this interaction noise as shown on figure 15, but the mixing noise in the peak noise direction is only marginally modified. Attempts to use an ideal con-di nozzle on an engine however, raises several design problems in connection with weight, overall dimensions, and the difficulty of achieving a variable throat area whilst maintaining a smooth internal nozzle profile. Research on con-di nozzles was therefore oriented towards the possible use of shorter nozzles with a conical profile. As can be seen on figure 15, the noise characteristics of the nozzle deteriorate as the length of the divergent part of the nozzle is reduced. Other devices such as perforated ejectors, or slotted nozzles (6) have been investigated in an attempt to obtain a shock free expansion of the jet.

In the field of jet noise attenuation, in addition to evaluating many different silencing concepts, a major effort has been directed naturally towards improving acoustic properties of the Type 28 exhaust system defined for entry into service. Several different approaches have been explored and they are described fully in reference (7). Some of these studies are mentioned below and basically consist of the following:

a) Using internal and external side plates to reproduce in the flyover plane, noise reductions comparable to those achieved in the lateral plane by rotating the Type 28 nozzle buckets. The side plates which are devices hinged in a vertical plane, fishtail the jet and give directional silencing under the aircraft.

b) Determining possible ways of improving the Type 28 nozzle noise attenuations in the lateral plane by reducing the secondary flow, and therefore the secondary pressure ratio within the nozzle.

c) Optimising the geometry of the thrust reverser buckets and deflectors. The study of the Type 28 nozzle acoustic characteristics has shown that the thrust reverser deflectors play a modest part in the sideline noise attenuation achieved by fishtailing the jet with the buckets. The likely action of these deflectors is to produce an additional squeezing at the side of the jet which magnifies the effect produced by the buckets. Several shapes and sizes of deflectors have therefore been tested and the performance obtained with the widest deflectors is given in figure 16. The problems raised by the use of such enlarged deflectors in the Type 28 nozzle (losses in cruise, mechanical integrity, performance in reverse thrust etc.) are presently undergoing technological evaluation.

In view of the directional acoustic properties of the Type 28 nozzle with buckets deflected, a great amount of research work (6) has also been devoted to the study of various types of nozzle designs capable of producing fishtailed jets. One of the simplest and most efficient designs is a notched nozzle, obtained by cutting two triangular notches in the sides of a convergent nozzle (figure 17). With such nozzles it is possible to achieve a wide spreading of the jet in the plane of the notches, as shown by the shadowgraphs presented in figure 18. Noise fields measured in the principle planes of the nozzle are compared with that of a convergent nozzle in the same figure, and a close analogy between the acoustic behaviour of these nozzles and that of Type 28 nozzle can be seen. It is possible that the high noise reduction observed in the plane where the jet spreads most rapidly, results from the high eddy diffusivity in this plane. However, in a recent private communication, Dr. Fisher suggests that the noise reduction, noticed in the "silent plane" of such jets, could result from a progressive decrease in the role of convective amplification with increase of jet spreading angle.

Because of possible adverse interaction between two fishtailed jets when placed in close proximity, as in the twin Concorde nacelles, this problem has been investigated closely. One series of studies covered the interaction of two asymmetric jets, viz jets from a pair of notched nozzles each incorporating one and two notches respectively. The nozzle centre-lines were parallel and separated from each other by 1.5 nozzle diameters. Noise was measured along the two main axes of the nozzle group by symmetrically varying the angle φ of the notch plane relative to the plane of both nozzle centre-lines. Attenuations relative to a group of two convergent reference nozzles, are shown by figure 19. It can be seen, in particular, that, at right angles to the twin nozzle ($\delta = 90^{\circ}$), the optimum attenuation is not achieved when $\varphi = 90^{\circ}$, but when the two fishtailed jets interact with each other at $\varphi = 120^{\circ}$. Also an attenuation is observed in the direction normal to the plane of the notches ($\varphi = 0^{\circ}$ and $\varphi = 180^{\circ}$), which is not the case with a single notched nozzle (refer to figure 17). The optimum attenuation from this twin nozzle arrangement is the same as that obtained in the plane $\delta = 0^{\circ}$, when the notches are coplanar ($\varphi = 0^{\circ}$).

Another group of experiments was related to the study of acoustic masking effects. A model of the twin Type 28 nozzle arrangement in Concorde was used for these tests, and measurements were taken in the horizontal plane containing both nozzle centre-lines. The upper curves in figure 20 show noise fields obtained at low bucket angles ($\gamma = 5^{\circ}$ and 20°) with the Type 28 nozzles both fitted with standard deflectors. The experiment was then repeated but with the buckets of the nozzle located nearest the microphone set at an angle of 30° and fitted with wide thrust reverser deflectors - a configuration corresponding to the maximum possible attenuation, (refer to figure 16). The buckets of the standard nozzle on the far side of the microphone were successively set at 5, 20 and 30°. It can be seen that the noise fields and spectra are virtually unchanged, which suggests the existence of a nearly perfect masking by the "quiet" jet of the adjacent noisier one. Other twin nozzle configurations (Type 28 nozzle, notched nozzles etc.) have been observed to give identical effects which, although not yet fully understood, open the way to promising possibilities in the field of jet noise reduction.

In parallel with studies on novel silencer designs, the manufacturers are proceeding with the evaluation of a number of known silencer concepts, with stress being placed upon silencers capable of being fully retracted in order to avoid the very severe penalty which would result from thrust losses in cruise. They include studies on multitube silencers similar to those studied by Boeing and General Electric as part of the American SST programme (8). Studies are being made also in cooperation with Société Bertin on nozzle concepts as illustrated in figure 21. Attempts to apply such nozzles to the current Concorde powerplant pose extremely difficult technological problems due to the very severe environment existing at the engine exhaust. The need to incorporate variable geometry to adapt the nozzle to the various phases of flight and to retract silencing elements wherever possible, raises weight and drag penalties which, being much more critical in a supersonic than in a subsonic aircraft, could prevent the use of such silencing systems.

To conclude this section, figure 22 shows the potential performance of some silencer systems investigated as part of this research work, but the actual application of such systems often presents severe problems to the design engineers.

4.3 Internal noise

When describing the acoustic characteristics of the Olympus 593 (in paragraph 3) the presence of internal noise was postulated and this component, which radiates at high angles to the jet axis, becomes the dominant engine noise source at low thrust levels. Conventionally, "internal noise" includes any noise component emitted by an engine exhaust and which is not pure jet noise. In this context, pure jet noise is taken as the data obtained from exhaust nozzle rigs of high internal flow quality mounted in an anechoic chamber. Such data is given in reference 4. This definition of internal noise does not include compressor noise (or fan noise in the case of a bypass engine).

Extensive theoretical and experimental investigations have been made to define and characterise the sources of internal noise in turbojet engines, which first becomes apparent as an increasing divergence of the total noise from pure jet noise as exhaust velocity decreases - see figure 5. At very low jet velocities (about 200 m/s) the total noise follows a law like $(Vj)^4$ rather than the $(Vj)^8$ law which is appropriate to pure jet noise. Examination of engine noise spectra shows medium and high frequency contents which are considerably greater than those resulting from the pure jet. Peak noise spectra for the Olympus 593 at jet velocities around 350 m/s are shown in figure 8. The high frequency region of the spectra appears to be characterised by broadband turbine tones associated with blade interaction phenomena in the H.P. and L.P. turbine assemblies. The corresponding perceived noisiness spectra emphasise the serious weighting of this noise component when deriving the PNdB levels.

The changes in spectra at 90^o to the engine as jet velocity is reduced are shown in constant band width format in figure 23. At jet velocities around 500 m/s (condition D) where the exhaust nozzle is just choked, the low frequency part of the spectrum is almost entirely accounted for by jet noise. At high frequencies the broadband noise level is greater than that expected from a pure jet. As jet velocity is reduced the fine character of the spectrum becomes apparent as the broadband component of internal noise falls. At low jet velocities (condition A) the tonal components from the turbine can be clearly seen, being dominated by the low pressure turbine tone which appears to have suffered considerable spectral broadening. The high pressure turbine fundamental tone which appears at about 9 KHz is even more broadened. Tones are present also at frequencies which are related to the differences between the high and low pressure turbine tones.

Thus with jet velocities around 400 m/s internal noise in turbojet engines is essentially of a broadband high frequency character peaking around $70-80^o$ to the jet axis. At low jet velocities where internal noise is the dominant exhaust noise source in a turbojet, the spectra at high angle to the jet are much more tonal in character although the tones are broadened considerably.

These general internal noise characteristics are not peculiar to the Olympus 593.

Clearly the turbine assembly has a significant influence on the source characteristics of internal noise at low jet velocities. Figure 24 shows the internal noise component at 70^o to the jet axis for two standards of Olympus 593, plotted as a function of H.P. turbine tip speed. The correlation, which covers the range of jet velocities from 250 to 500 m/s, is reasonably good, and does not suggest any change in source mechanism as thrust is reduced. If the H.P. turbine with its essentially subsonic blading were the main source of internal noise (tone and broadband components) then the velocity exponent given by the correlation (viz Vr^{13}) is different from that obtained from correlating subsonic compressor and fan noise, suggesting that different generation mechanisms may be involved. It is relevant to note that the nozzle control characteristics of the twin spool Olympus 593 are such that over the thrust range indicated by figure 23, thrust and hence jet velocity are almost proportional to H.P. turbine speed, so that alternative interpretations of this figure are possible. However the best correlation of data from different standards of Olympus 593 was obtained when internal noise was plotted as a function of H.P. turbine speed rather than jet velocity or other aero-thermodynamic parameters.

Many diagnostic studies have been made, some at full scale using the Olympus 593 and other turbojet engines, in an attempt to determine the influence of other parameters on internal noise. They include the effects of major changes to the design of combustor, turbine, turbine diffuser and tailpipe. Although in many cases measurable changes to the internal noise component were obtained and beneficial changes to the engine have resulted (for example see figure 25) in none of them has any convincing evidence been found of any major change to the source of broadband internal noise.

Since there is evidence that at least part of the internal noise of a turbojet has its origin in the turbine assembly it is relevant to examine possible propagation paths and expected far field acoustic characteristics. For noise sources located in the tailpipe, there would be a propagation path through the nozzle exit and thence by refraction and scattering through the jet shear layer to the surrounding atmosphere. Such radiation would peak in the rear arc. Theoretical studies by Ffowcs-Williams et al (9) (10) (11) suggest that sound radiated in this manner would be expected to vary with a typical velocity like V^6 or V^6. The same exponents should apply to noise generated by turbulence contained in a pipe with various end constraints. There are

several aspects of the experimental results which are not explained by this modelling of internal noise. Also the observed directivities, and changes with forward speed which are discussed in the next section, indicate a much higher level of internal noise at high angles to the jet and in the forward arc than appears possible solely by considering noise refracted and scattered by the jet shear layer.

There is a second family of internal noise generation processes which involves interaction of unsteady internal flow with the nozzle exit region. Interactions of this type have been studied theoretically with several different mechanisms and lip boundary conditions being postulated (11) (12). Several such interaction mechanisms could give acoustic efficiencies comparable with that of the jet, and with jet velocity dependence and pronounced high angle and forward arc directivities which are in accord with experimental results both static and in-flight.

The unsteady exhaust flow, which may be regarded as fluctuations in engine mass flow combined with fluctuations in axial and transverse momentum, has its origin essentially in the unsteady expansion process through the turbine assembly with modulations due to fluctuations in turbine entry conditions and the flow about components in the tailpipe, i.e. turbine exhaust diffuser vanes, etc. Experiments have been carried out to study nozzle lip interaction phenomena and to attempt to modify the lip/turbulence interaction process by changes both to the character and intensity of the unsteady flow approaching the nozzle, and to the acoustical impedance of the lip and initial jet shear layer.

Figure 26 shows the changes in linear field shape produced by fitting an acoustical lining to the Olympus tailpipe whilst the corresponding spectral changes at 90° to the jet are shown in figure 27. The lining, which was designed to be most effective in the frequency range 800 to 3000 Hz, reduced both the tone and broadband noise. The maximum attenuation was in the rear arc centred at about 80°. Very similar results were obtained by use of a relatively small screen placed just downstream of the nozzle exit and to the side of the jet, as shown in figure 28.

These and other diagnostic exhaust screening tests on the Olympus 593 which indicate the presence of important noise sources other than those related to jet mixing processes, are discussed in more detail in reference 6.

Attempts to modify lip sources by changes to the character of the unsteady flow at the nozzle of the engine included tests in which a honeycomb flow straightener was installed in the tailpipe just downstream of the turbine exhaust diffuser. The honeycomb, which had a rectangular cell structure of 3 x 3 x 15 cms, produced significant reductions in the high frequency broadband noise in the forward arc - see figure 29. These results suggest that unsteady flow interaction with the nozzle exit is an important mechanism in the generation of internal noise - certainly of the forward radiated component. The investigation of this phenomenon involves the application of advanced analysis techniques; in flow measurements, narrow band analysis, auto and cross correlation etc., and major research programmes are being carried out by the Concorde engine manufacturers and their collaborators in order to understand and to silence the various sources of internal noise. Several improvements have already been effected and others, involving the lining of the engine tailpipe and secondary nozzle system are being actively studied.

5. THE EFFECTS OF FORWARD SPEED ON ENGINE EXHAUST NOISE

The Olympus, having significantly higher jet velocities than turbofan engines representative of today's subsonic transport aircraft has been shown to pose peculiar silencing problems. One important aspect of these problems is the changes in noise generation and propagation mechanisms which occur between static and flight situations. Such changes might be expected to be different from those which are experienced by engines whose acoustical characteristics are dominated by turbo-machinery noise. Several fundamental investigations of the influence of forward speed on jet and exhaust noise characteristics have been conducted in support of the Concorde programme, and although these studies are not yet complete, sufficient work has been done to highlight the most important changes which occur. These changes are presented and discussed in this section.

In order to study such changes systematically it is desirable to make direct comparison between the static and flight acoustical characteristics of a given engine. Unfortunately acoustical data from an aircraft flight programme, although appropriate for establishing the noise levels of the aircraft, cannot be compared directly with that from static calibrations of the corresponding engine. The aircraft itself tends to mask fundamental effects associated simply with forward motion. Attempts to correct for differences in environmental effects including ground reflection, and specific aircraft/engine installation features - particularly with a multi-engined aircraft, frequently introduce sound level corrections which are bigger than the static to flight changes being studied. Consequently, flying test beds and flight simulation facilities have played and will continue to play an important role in providing fundamental data on the effects of motion on engine noise.

Two major flight simulation facilities which have been used to support the Concorde programme are the Rolls-Royce spinning rig and the Vulcan/Olympus 593 flying test bed - see figure 30. The Rolls-Royce spinning rig is a simulated flight facility

for the study of jet and exhaust noise at forward speeds up to 150 m/sec. The facility is designed to spin modal nozzles of approximately 1/10th Concorde scale at the end of a rotor of 10 metre radius, and is capable of reproducing jet stagnation conditions up to a pressure of 4 atmospheres and a temperature of 1300°K. By tethering the rotor, the static acoustical characteristics of a given exhaust system can be determined, and these data can then be compared directly with the acoustic characteristics determined when the system is in motion. The Vulcan flying test bed which has now been withdrawn from the programme, was powered by four Olympus 101 engines and was fitted with an Olympus 593-4 engine and a type 10 (prototype) exhaust system in a complete Concorde nacelle installed beneath the aircraft fuselage. The position of the secondary nozzle system relative to the trailing edge of the Vulcan wing was different from that of the Concorde installation. Although this difference had a measurable effect upon the acoustical field shape compared with that of Concorde, it is considered that meaningful studies of the changes in engine acoustical characteristics with forward speed were possible. Using the Vulcan F.T.B. and the variable primary nozzle of the twin spool Olympus 593 it was possible to study the effect of increasing forward speed at constant exhaust velocity and at constant relative jet velocity. The results from these tests are summarised below.

The linear OASPL field shapes at 305 metres altitude at forward speeds of 90 and 180 m/s are shown in figures 31 and 32 respectively. These field shapes, which are presented as functions of noise emission angle, have been corrected for differences in aircraft attitude and for aircraft self-noise at the two forward speeds, and the noise levels have been normalised to standard atmospheric conditions. In general, increasing the flight speed leads to a reduction in rear arc noise and an increase in forward arc noise. The changes at a given jet (exhaust) velocity are shown in figure 33. Although the trends in directivity changes with forward speeds at these jet velocities are broadly in line with predictions of the effect of motion on jet mixing noise (13), the extent of the changes at right angles to the jet and particularly in the forward arc, are greater than predicted. At about 40° - 50° to the jet axis (i.e. the angular range in which jet mixing noise would be expected to dominate) the reduction in OASPL with increase in forward speed at the higher jet velocities (greater than 600 m/s) is approximately that which would be expected from jet relative velocity considerations. At jet velocities below about 550 m/s the reduction in rear arc noise level with increasing forward speed is markedly less than expected. This suggests that "internal" noise sources are present and influential at higher jet velocities than would be suggested by static jet studies - see figure 5. Such a postulation is supported by the observed changes in field shape with forward speed at high angles to the jet where a reduction in jet relative velocity does not lead to a reduction in noise level, even when the jet velocity is high. This result suggests that the source strength for the high angle radiation actually increases with forward speed.

In the forward arc there appears to be an increase in noise level with forward speed although with critical and subcritical pressure ratios this increase is small. The increase in forward arc noise at high jet velocities (600 m/s) could be related to the presence of shock associated noise from the supercritical jet since examination of spectra suggests that shock noise dominates in the forward arc under these conditions. The increase in OASPL in the forward arc with flight speed at high jet velocities is well predicted by the fourth power of the Doppler factor ($1-M\cos\theta$) except in the extreme forward arc where shock associated noise is probably effectively shielded by the aircraft itself.

At the lower jet velocities where the changes in the forward arc are small, the lack of any significant attenuation at high angles to the jet suggests the presence of important non-convected disturbances which would also be expected to suffer amplification in the forward arc with increase in forward speed. From the Vulcan flight test with the Olympus 593 shut down, an increase in forward arc noise level relative to that at 90° to the jet was observed, being 3 dB at 150° to the jet axis. This is almost the value expected from Doppler amplification of monopole and dipole sources moving with the aircraft. These experimental results suggest there is a range of jet velocities around the critical value in which non-convected phenomena have a weaker influence on forward arc field shape changes. This range is bordered at the higher velocities by the presence of shock associated noise and at the lower velocities by the dominance of nozzle based internal noise sources.

Comparison of the linear acoustic field shapes and of the spectra in directions approximately normal to the jet axis shows no significant changes with flight speed for the jet velocity range studied ($350 \leq V_J \leq 650$ m/s). This observation apparently applies also to static-to-flight comparisons with other engines and to results obtained from the spinning rig. Whether this phenomenon is to some extent fortuitous, being the result of the general reduction with flight speed of jet mixing (convected) noise in the rear arc and of the increase with flight speed of aircraft and powerplant based (non convected) noise in the forward arc, is not certain. However it seems likely that as exhaust velocity is reduced the noise levels at high angles to the jet in-flight become increasingly dominated by nozzle based and tailpipe noise sources which appear to be non-convected phenomena. With exhaust velocities below about 350 m/s these become the main noise sources and the in-flight acoustical changes are then associated more with noise sources attached to the aircraft than with sources convected in the rearward direction by the jet. As a result of the above transition, the peak noise in flight is observed to move progressively away from the jet axis to angles where there are essentially no changes with flight speed - see figure 34. It is relevant to note that

the Vulcan flights with the Olympus shut down showed a general increase in overall sound pressure level at all angles to the aircraft when the flight speed was increased. The increase at 90° to the jet axis was 9.5 dB which corresponded to a variation in noise level with aircraft speed of $V^{3.4}$. The increase in the forward arc was somewhat greater with the peak noise occuring at 110° to the jet axis.

With engines other than turbojets turbo-machinery noise sources would make an increasingly important contribution to the non-convected noise sources as jet velocity is reduced. In the present flight studies however such sources were found by narrow band analysis to be relatively unimportant, (compressor noise on the Vulcan FTB is effectively attenuated by the intake), and are avoided entirely in the case of the spinning rig. Thus, in considering the effects of forward motion on jet and exhaust noise alone, three regimes can be identified. They are illustrated diagrammatically in figure 35, and may be described as follows:

a) At high (supercritical) jet velocities ($>$ 550 m/s) where jet mixing noise dominates, peak noise occurs well in the rear arc at about 40° to the jet axis. The peak level in flight follows the trends expected from jet relative velocity considerations. At high angles to the jet axis non-convected noise sources appear to be important, whilst in the forward arc noise levels increase with forward speed due to the dominance of shock associated noise.

b) As jet velocity is reduced below 500 m/s sources other than of jet mixing noise become increasingly important in the rear arc until, at intermediate jet velocities (around 350 m/s), the peak noise characteristics are dominated by non-convected internal noise. In this regime peak noise occurs in flight at about 80° to the jet axis and the peak noise level appears to be only weakly dependant on flight speed. The field shape changes in the rear and forward arcs follow trends expected from consideration of Doppler effects although the magnitude of the changes in the forward arc are somewhat less than predicted.

c) Ultimately at very low jet velocities ($<$ 200 m/s), in the absence of turbo-machinery noise, the aircraft self-noise becomes the dominant source. In this regime the peak noise angle moves into the forward arc and the noise level increases with aircraft forward speed like $(V)^{3.4}$.

6. REFERENCES

1. Calmon J. / Hoch R. — Performance and Noise Aspects of Supersonic Transports. Inter-Noise 73, Copenhagen August 1973.

2. Hawkins R. / Hoch R. — Studies into Concorde's Engine Noise Emission and Reduction. 10th Int. Aero. Congress Paris June 1971.

3. Devriese J. / Young P.H. — L'Olympus sur le Concorde. Aeronautique et Astronautique No. 37, 1972-5.

4. Hoch R. / Duponchel J.P. / Cocking B.J. / Bryce W.D. — Etude de l'influence de la masse volumique d'un jet sur son emission acoustique. 1er Symposium Int. sur les Progres des Reacteurs d'Aviation - Marseille, Juin 1972

5. Fisher M.J. / Bourne M.H. / Lush P.A. — Shock Associated Noise. Paper No. 73 ANA 1. B.A.S. Spring Meeting - London April 1973.

6. Voce J.D. / Simson J. — Some Recent Developments in the Understanding of Jet Noise. 8th ICAS Congress - Amsterdam September 1972.

7. Hoch R.G. / Julliand M. / Lacombe H. — Dispositifs directionnels de reduction du bruit des jets a grande vitesse. 1er Symposium Int. sur les Progres des Reacteurs d'Aviation - Marseille, Juin 1972.

8. Swan W.C. / Simcox C.D. — A Status Report on Jet Noise Suppression as seen by an Aircraft Manufacturer. 1st International Symposium on Air Breathing Engines - Marseille, June 1972.

9. Davies N.G. / Ffowcs-Williams J.E. — Aerodynamic Sound Generation in a Pipe. Journal Fluid Mechanics Vol. 32 Pt. 5 (1968).

10. Ffowcs-Williams J.E. — Transmission of Low-Frequency Jet Pipe Sound through a Nozzle Flow. Lecture to von Karman Institute of Fluid Dynamics. Series 36. Turbulent Jet Flows (1971).

11. Ffowcs-Williams J.E. (Chairman) et al — Report of the ARC Working Party on Novel Aerodynamic Noise Source Mechanisms at Low Jet Speeds. Aeronautical Research Council, Noise Research Committee Report ARC 32925 May 1971.

12. Crighton D.G. Leppington F.G. — On the Scattering of Aerodynamic Noise. Journal of Fluid Mechanics Vol. 46 Pt. 3 (1971).

13. Ffowcs-Williams J.E. — Jet Noise from Moving Aircraft. AGARD Conference Proceedings No. 42 (1969).

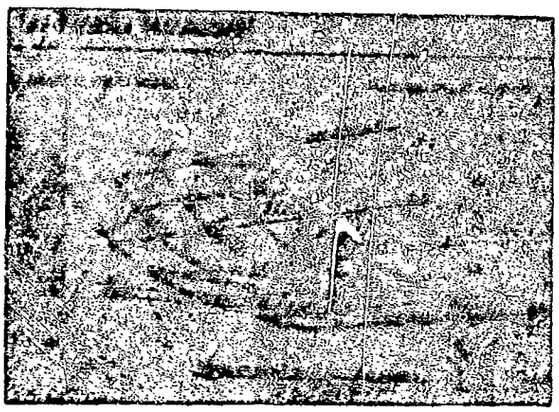

Figure 1

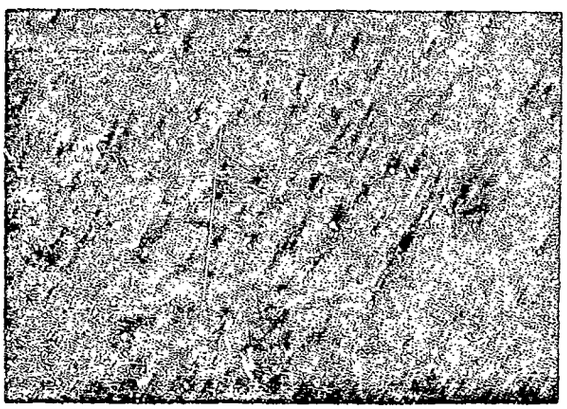

Figure 2

Figure 3

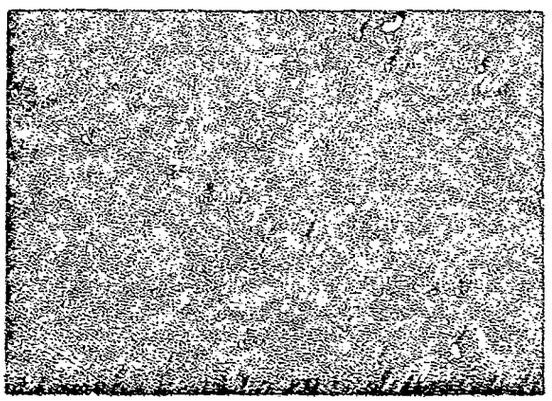

Figure 4

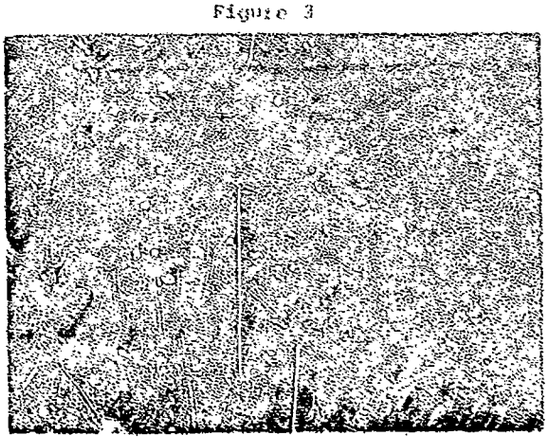

Figure 5

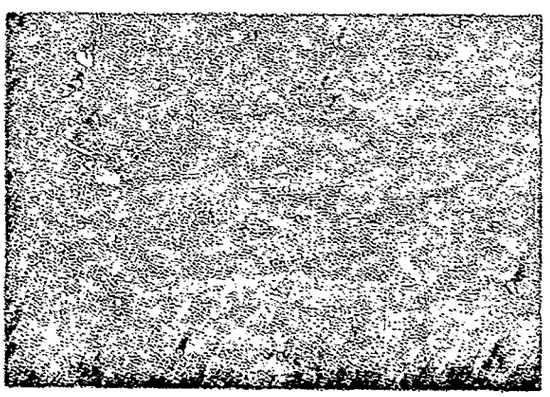

Figure 6

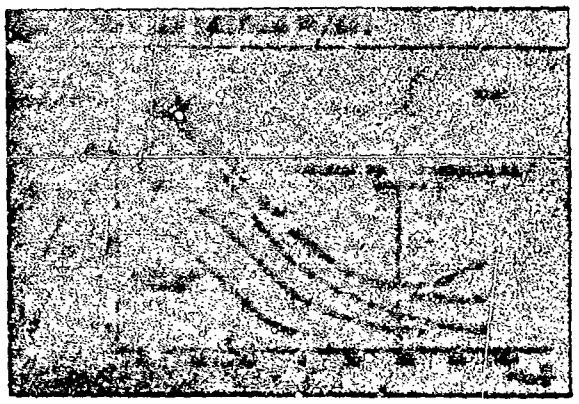

Figure 7

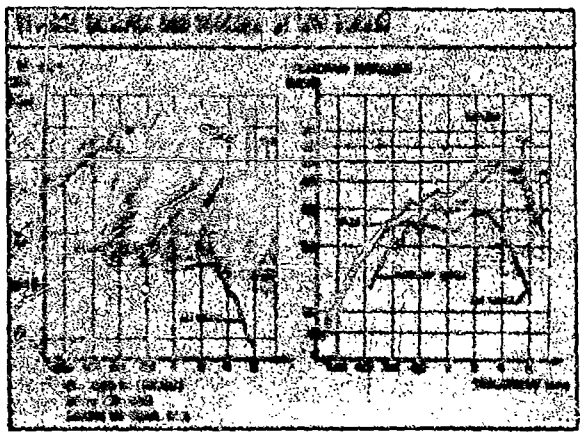

Figure 8

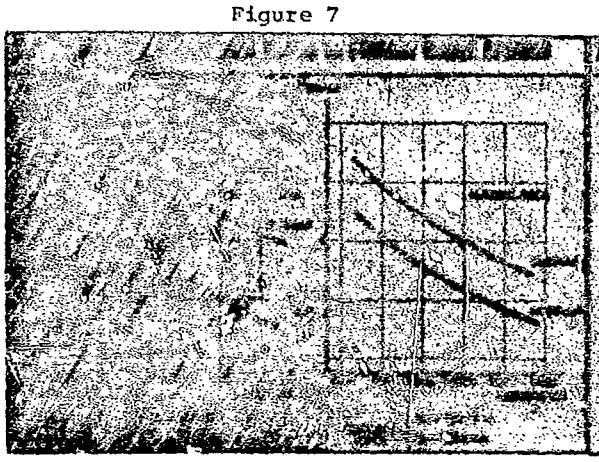

Figure 9

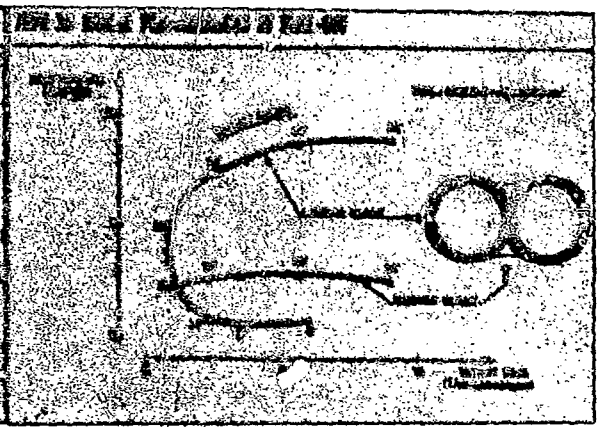

Figure 10

Figure 11

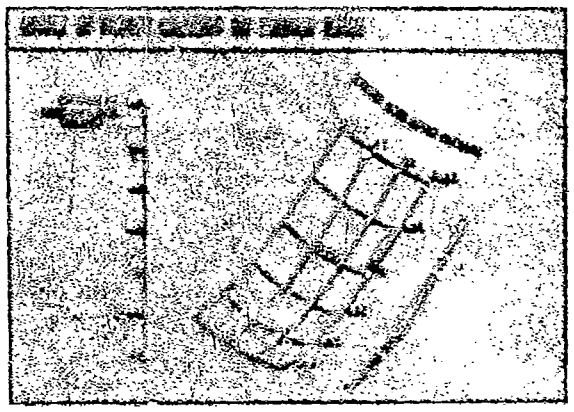

Figure 12

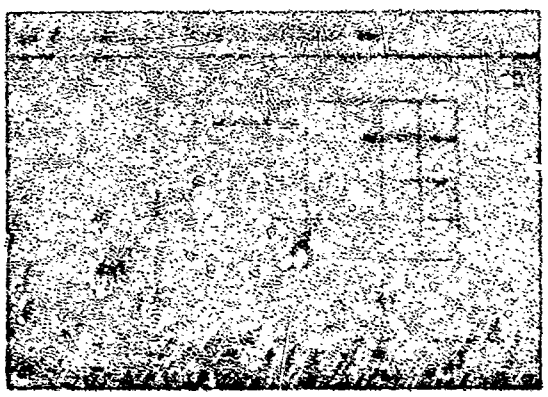

Figure 13

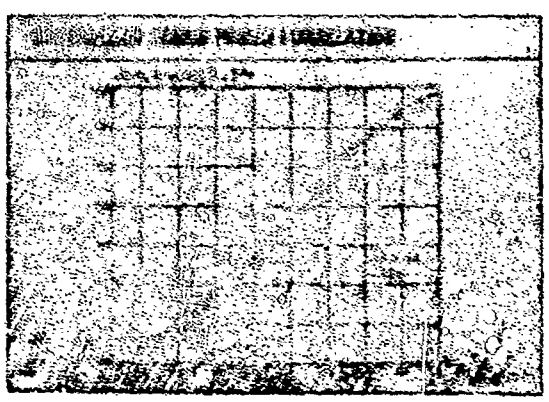

Figure 14

Figure 15

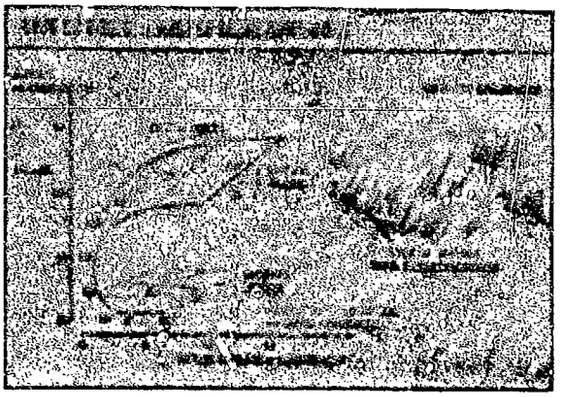

Figure 16

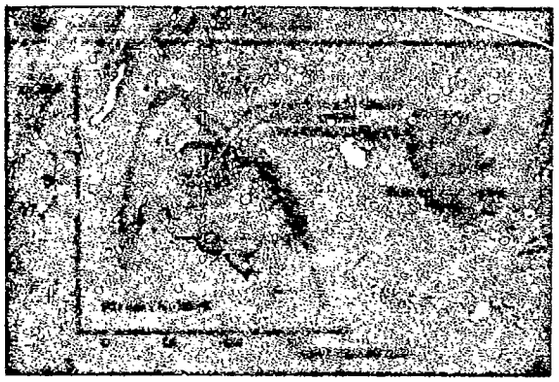

Figure 17

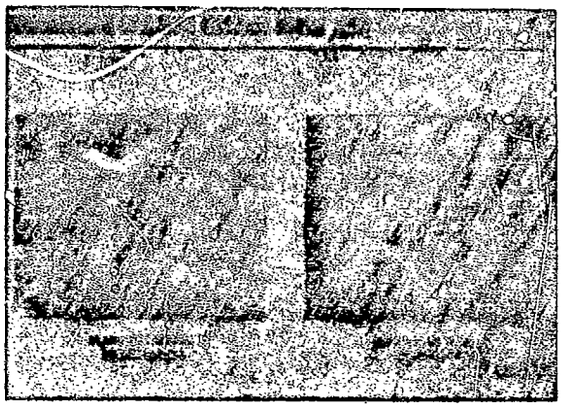

Figure 18

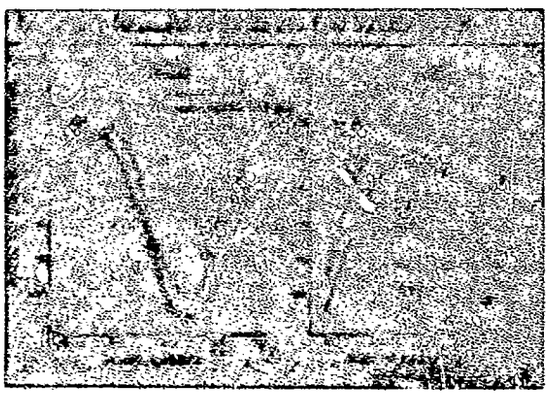

Figure 19

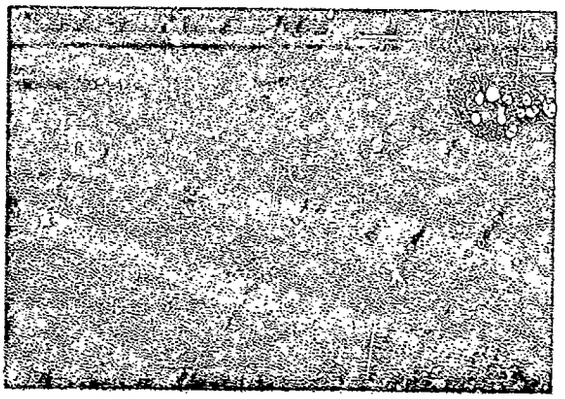

Figure 20

Figure 21

Figure 22

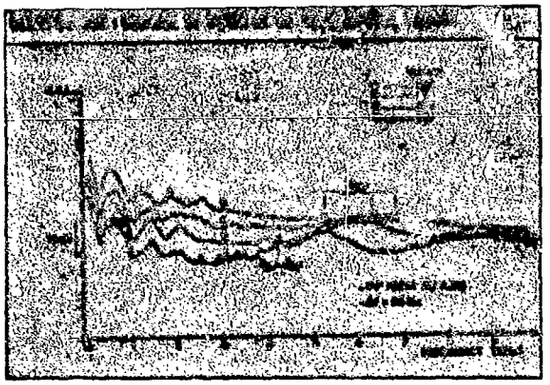

Figure 23

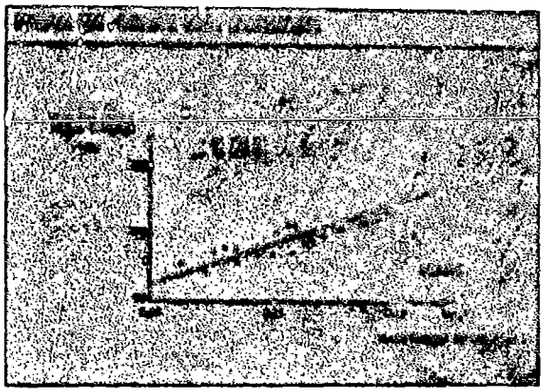

Figure 24

Figure 25

Figure 26

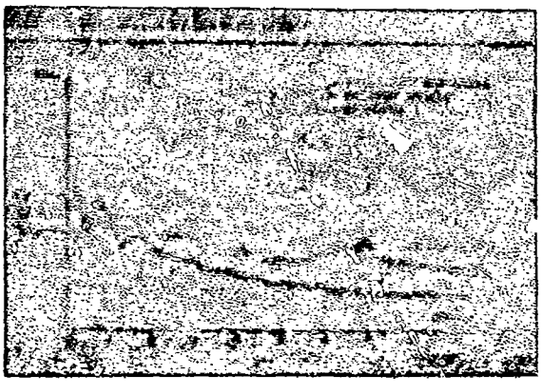

Figure 27

Figure 28

Figure 29

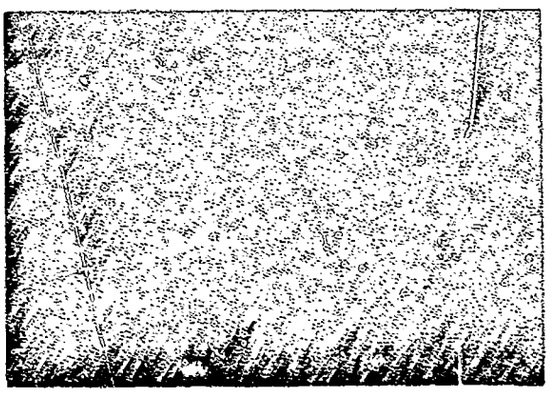

Figure 30

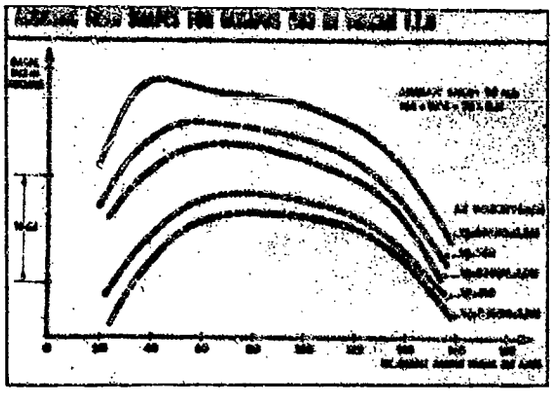

Figure 31

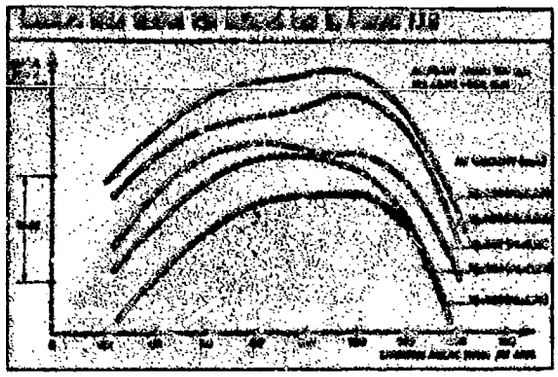

Figure 32

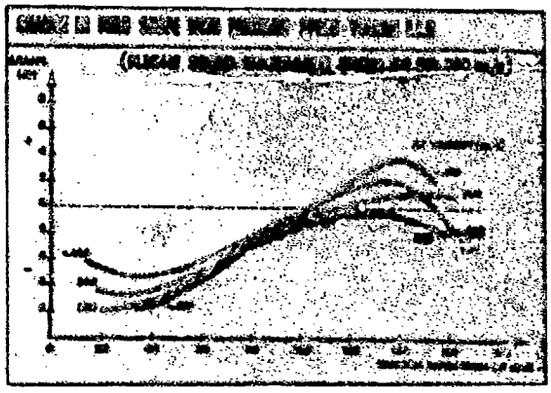

Figure 33

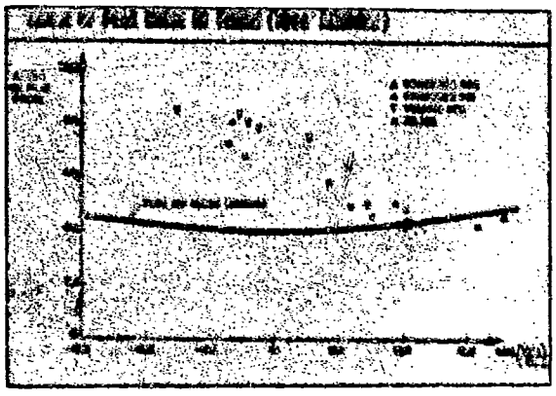

Figure 34

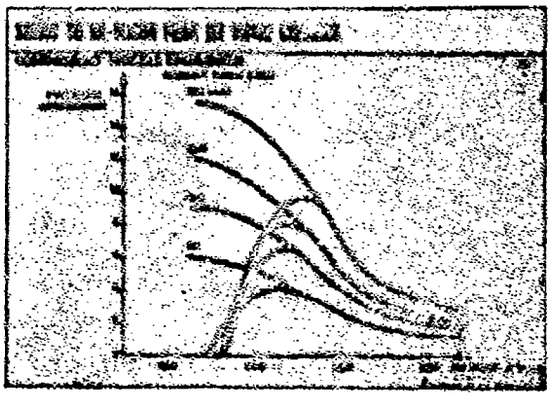

Figure 35

AEROSONIC GAMES WITH THE AID OF CONTROL ELEMENTS AND EXTERNALLY GENERATED PULSES

L.J.Poldervaart, A.P.J.Wijnands and L.Bronkhorst
Fluid Mechanics Laboratory, Physics Department
Eindhoven University of Technology
The Netherlands

1. SUMMARY

With the aid of control elements one can generate the following modes of vibration of a 2-dimensional sonic jet:

- zero mode
- oscillatory mode, natural and forced
- pulsatory mode
- coupled pulsatory-oscillatory mode.

We have found strong evidence for the fact that the eddy does not play the role in the feed back loop given in the Powell model.

With the aid of externally generated pulses one can show for example how the information – near the nozzle tip – is transferred from the pulse into the jet. The nozzle tip as a discontinuity proves to be a dominant factor in the interaction process of the pulse with the boundary layer and with the jet.

The three items will be illustrated with a film and a video recording.

2. INTRODUCTION

One of our interests in the study of the self-maintained vibrations of two-dimensional underexpanded sonic jets was to know the possible modes of vibration for such a jet, and in particular to find the fundamental mode – the natural vibration.

We were able to produce a satisfactory approach to this basic mode. Starting with this mode we could produce, by changing only the acoustic part of the feedback loop, the above mentioned modes of vibration.

That means that the natural vibration thus produced is a reasonable starting point in the study for instance of the feedback mechanisms for this type of vibrations as well.

Using different types of control elements we found that:

- feedback on only one side of the jet is sufficient. The loop can be interrupted on the other side.
- the vortex formed in the boundary layer as a result of the acoustic pulse-boundary layer interaction is only one result of this interaction that must be taken into account in the study of feedback mechanisms.
- without a vortex there is still pulse production.
- the Powell feedback loop model has to be redesigned, from our experiments; some suggestions for a new model can be given.

The study of feedback mechanisms on vibrating jets is hampered by the very complex nature of both the flow field and the acoustic field and moreover in the case of self-maintained vibrations one is not free to vary for instance the amplitude, rise time of the front, the angle of incidence, etc. of the pulses independent of (a) the parameters of the jet, and (b) the acoustic conditions of the outer part of the feedback loop.

So we tried to find a more suitable arrangement for fundamental studies. We chose the single pulse technique.

That means one uses a non-vibrating jet, which as a matter of fact does not produce discrete pulses, and introduces externally generated pulses in order to study the pulse-boundary layer interaction including the results of this interaction on the jet.

2.1 Experimental rig

The nozzle, the air supply and the conditions necessary for a well defined stable oscillation and the requirements for the fotonic registration are described in Reference 2. The pulses were produced as described in Reference 3. As a pulse generator we used a Fischer Nanolite plus a parabolic reflector. The pulses were sufficiently flat and have a diameter of about 10 cm. The rise time of the front of the pulse is in the order of a few m secs. The amplitude can be varied between 0.003 atm – 0.1 atm. The pulse form is that of a N wave (Fig.13).

The angle of incidence can be varied from $-60°$ to $+90°$.

2.2 Observation and registration techniques

We used the shadow technique for the visualisation of the flow field and the discrete part of the sound field.

As a light source a Fischer Nanolite (Fr.Früngel Hamburg) is used.

For observation and registration we used the synchro-strobe film technique in the study of the modes of vibration.

Strobe TV is used in connection with the single pulse technique.

3. EXPERIMENTS

3.1 Modes of vibration

Starting with the natural vibration – oscillatory mode (Fig.2) the non-vibrating or zero mode (Fig.1) is obtained if one fully intersects the feedback loop at both sides.

The forced vibration – oscillatory mode is obtained by introducing two reflectors at the same distance from the nozzle (phase shift left – right is zero) (Fig.3). The coupled oscillatory – pulsatory mode is obtained by using two reflectors with a phase shift left-right of 90° (Fig.4).

The phase shift between successive pulses generated at the right and the left side of the jet respectively is equal to 180°. The phase shift of these pulses after reflection against the reflectors is equal to zero, which means that these pulses introduce the pulsatory mode when they arrive at the nozzle tip.

The pulsatory mode is produced if the feedback loop is partially interrupted (Fig.5).

The modes mentioned here are shown in the film. Moreover the coupled oscillatory-pulsatory mode is shown in an animated film as well due to the fact that a stroboscopic registration does not offer a smooth image of the process.

3.2 Feedback loop model

The configurations of Figures 6, 7, 8 and 9 give a contribution to the answer on the question whether the vortex that is formed in the boundary layer due to the interaction of an acoustic pulse with the boundary layer plays a rôle in the feedback loop as indicated by Powell[1] (Fig.10).

Our answer is "no", based on these experiments and moreover confirmed by the single external pulse technique.

In Figure 9 the feedback loop on the right side is fully interrupted. Still there is pulse production on both sides of the jet although there is no pulse-boundary layer interaction at the right side.

If (Fig.7) one skims off the vortex there is still pulse production on both sides. Similar results are obtained with the configurations of Figures 8 and 9.

Figure 11 (Ref.2) shows the feedback loops in the natural and the forced case.

Our conclusion was then that, concerning the phase throughout the loop, the Powell model is a possible solution.

Figure 12 shows our point of view in 1972 (Göttingen). Then we knew that feedback at one side is sufficient for a steady oscillation. Only the outer part (acoustical part) of the feedback loop is in agreement with the Powell model. For the mechanisms at the nozzle tip and in the source of the pulse new solutions have to be formulated. The same holds for the inner part of the feedback loop between lip and source and the necessary amplification.

3.3 Single pulse technique

The configuration for subsonic (and supersonic) jets is shown in Figure 14, and that for sonic jets in Figure 15. In Figure 16 is indicated the way the angle of incidence α of the pulse is varied between $-60°$ and $+90°$. The configurations of Figures 17 and 18 are used to decide whether the region near the nozzle tip is important in the interaction process or whether the interaction is smeared out over the whole length of the boundary layer.

From the configuration of Figure 17 where the interdistance between the nozzle tip and the pulse reflector is about 0.2 mm it proved that the interaction takes place directly near the lip. There is negligible effect observed downstream of this region. Moreover in the case of no flow one sees that the lip acts as an acoustic line source.

The merits of the external pulse technique combined with strobe TV (strobe film) as an observation and registration technique are obvious from the film. One can quickly obtain a survey of the results of the interaction pulse-boundary layer over a range of pressure ratios, pulse amplitudes, angles of incidence and obtain an insight into the history of the transmitted pulse, the multiple reflections of the pulse inside the jet against the two boundary layers, the outgoing pulse on the other side of the jet, the deformation of the cells, etc.

One can also use pulses at both sides of the jet, the phase shift can be chosen. The amplitude, the rise time of the front of the pulse, the angle of incidence, phase-shift left-right, etc. can be varied independently of the parameters of the jet.

3.4 Results obtained

With the aid of control elements plus the natural vibration configuration one is able to produce the different modes of vibration of a 2-dimensional jet. These modes are shown in the film (16 mm, 7 min. duration).

Moreover some insight is obtained in feedback processes.

The configuration in 6 is also shown in the film.

From our experiments we get the impression that oscillation is a necessary condition for the generation of pulses. Feedback is necessary for the steady oscillations of the jet. The onset of oscillation is initiated by the pulse-boundary layer interaction at the nozzle lip.

One pulse is sufficient to start a complete oscillation with pulse production on both sides.

The area near the tip of the nozzle is dominant in the interaction process. It seems that the acoustical lip effect is responsible for the fact that the interaction is not confined to the boundary layer.

The processes as given by configurations 14, 15, 16, 17 and 18 are shown by means of a video recording (16 minutes).

4. REFERENCES

1. Powell: 4th International Congress on Acoustics. 1962.
2. Poldervaart, et al: 6th International Congress on Acoustics. 1968.
3. NASA technical note TN D-5306.

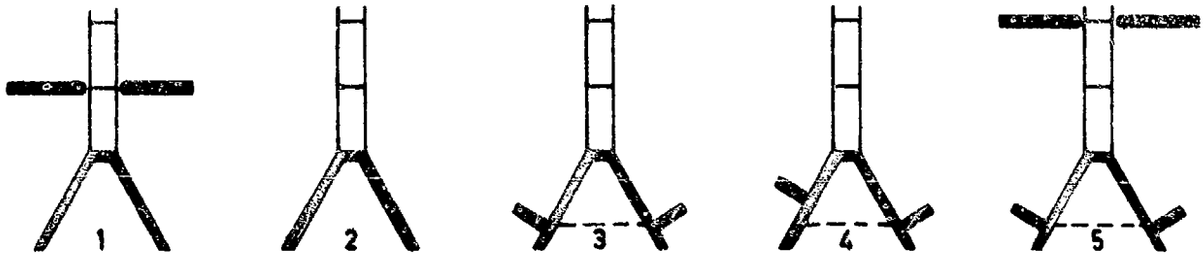

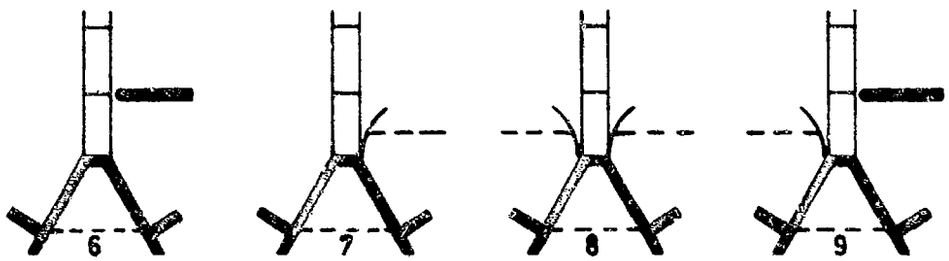

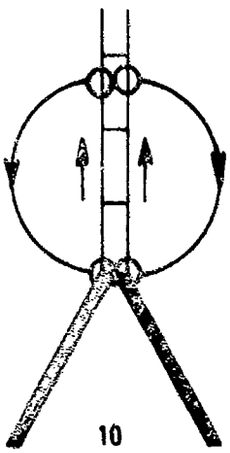

POWELL. 1962

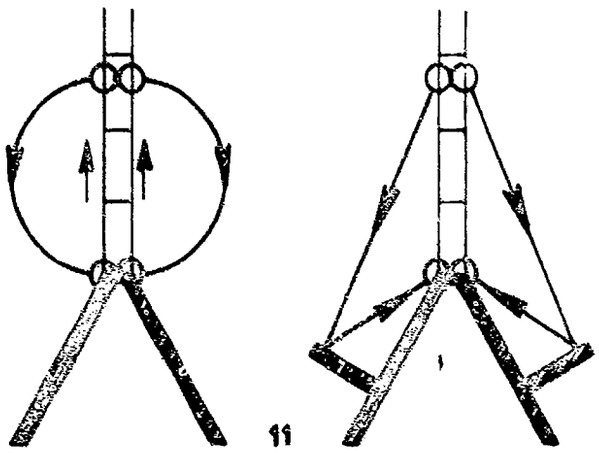

POLDERVAART. C.S. 1969

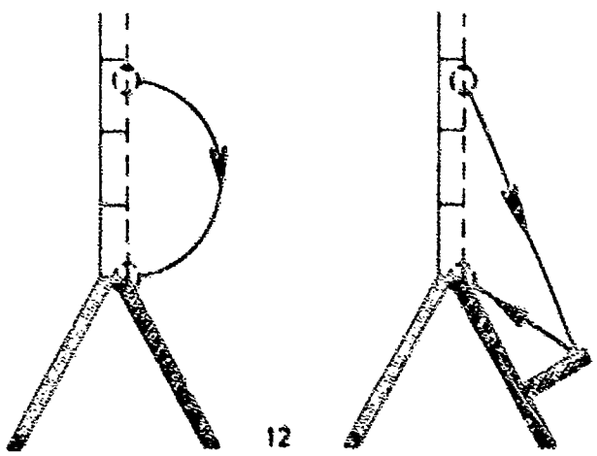

POLDERVAART. C.S. 1972

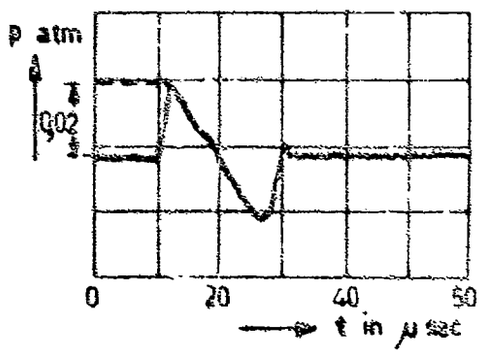

N-WAVE
13

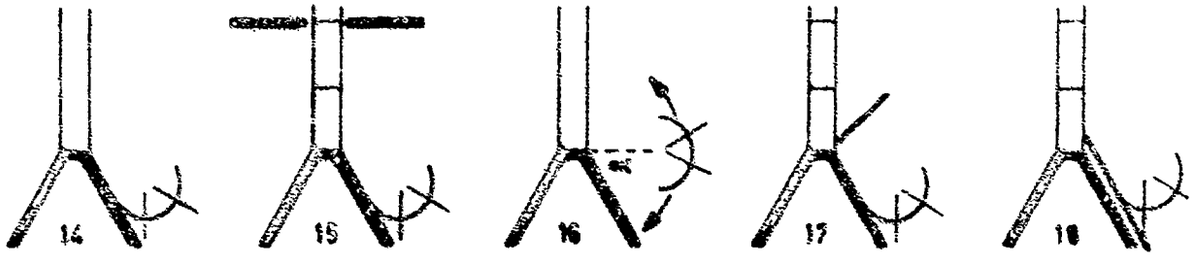

ON THE GENERATION OF JET NOISE

by

J. Laufer*, R. E. Kaplan** and W. T. Chu***
Department of Aerospace Engineering
University of Southern California
Los Angeles, California 90007 U.S.A.

SUMMARY

The present paper proposes that the rate of subharmonic production, that is, the rate at which large scale vortex-ring like structures interact with each other, is the primary mechanism responsible for most of the noise generation of a subsonic jet. The interaction consists of simultaneous acceleration and deceleration of vorticity containing coherently moving regions followed by a pairing process. This picture is consistent with Lighthill's quadrupole like sources, as well as with the formulation of Powell's "vortex sound" theory. It is suggested that more direct experiments are necessary to examine the validity of the above proposition.

1. INTRODUCTION

Search for a better understanding of the nature of the acoustic sources generated by turbulent shear layers has been one of the principal goals of aerodynamic noise research for the past twenty years. The main stumbling block of major progress can be attributed to an insufficient knowledge concerning the turbulent flow itself. In recent years, on the basis of experimental observations, a new point of view is emerging in treating the turbulence problem. The present paper attempts to exploit this view in examining its relevance to the noise producing aspects of a turbulent flow. First, however, a brief review of some of the more important proposals concerning the sources pertinent to this paper will be given.

After mathematically formulating the noise problem, Lighthill (Ref. 1) has spent considerable effort in speculating about the nature of the noise sources. He argued that regions of turbulence that move more or less in a coherent fashion should be considered as a measure of the source size. He logically chose the integral length scale of turbulence as the quantity characteristic to the size of these regions. This turned out to be a very judicious choice: on the basis of it he obtained the famous U^8 law, a result well substantiated by experiments. The fact that the integral scale rather than a smaller one (micro scale or Kolmogoroff scale) is a more appropriate choice will be further discussed in the following sections.

In addition to the scaling, Lighthill provided further insight concerning the sources. His mathematical formulation of the problem led him to conclude that they must behave as acoustic quadrupoles. Conceptionally, at least on the basis of our knowledge of turbulence at the time, this was most difficult to comprehend. It meant that within a correlation distance very specific phase relations must exist in the velocity field, relationships that have not been observed. Hopefully, the proposal advanced in this paper will clarify somewhat this difficulty.

Following Lighthill's work several other speculations have been advanced concerning the nature of the sources. In particular, some ten years later Powell suggested (Ref. 2) that aerodynamic noise generation may be explained as a result of moving vortices or vorticity in the flow field and showed that this point of view is consistent with Lighthill's theory. It will be shown that Powell's theory of vortex sound adopts itself quite readily to recent observations and - at least in the view of the authors - gives a conceptionally clearer physical picture of the sound generation process.

The idea of orderly structures existing in turbulent shear layers was suggested by a number of experimental workers (Refs. 3 and 4) and on the basis of their work a detailed experimental investigation was undertaken by Lau, Fisher and Fuchs (Ref. 5). As a result of their measurement, they postulated a model of the flow field consisting of "an array of evenly spaced discrete vortices disposed in the mixing region, sweeping downstream at a speed equal to about 0.6 of the jet efflux velocity". As will be seen, this model predicts one important feature: the existence of a more or less coherent vortex motion in the mixing region. Otherwise it is an oversimplified model since it does not contain another most essential feature: the average spacing of these vortices in the mixing layer must increase linearly with x, or equivalently, the frequency of fluctuations associated with them must decrease as $1/x$. In fact, their proposed model cannot generate sound in a subsonic jet.

Finally, the work of Crow and Champagne should be mentioned (Ref. 6). They have very convincingly demonstrated the existence of quasi-orderly structures in a turbulent jet by artificially introducing disturbances of specified frequency, which interact strongly with these structures influencing the early development of the jet. While their interpretation differs somewhat from the one described subsequently in this paper, the consequence of their findings related to the noise generation mechanism is considered most essential.

In Section 2, very general arguments are reiterated that underline the important role the large scale structures play in the development of free turbulent shear layers. In Section 3, observations are

---

* Professor and Chairman
** Associate Professor
*** Assistant Professor

described indicating that these large scale structures are, in fact, randomly occurring quasi-orderly motions. In the last section, conjectures are made concerning the far field pressure field produced by these structures.

2. THE ROLE OF THE LARGE SCALE STRUCTURES

In the study of free turbulent shear flows the principle of the Reynolds similarity proved to be a useful concept. It states that at sufficiently high Reynolds numbers the direct action of viscosity is negligible in free shear layers and as a consequence, the mean flow development is independent of the Reynolds number. Indeed, experimental evidence indicates that subsonic circular jets issuing into an ambient volume are geometrically similar: the whole flow field scales with the diameter only. (An exception might be the region near the nozzle exit where viscous effects could change the effective origin of the flow field.) This simple, but powerful, argument together with the notion of the existence of a double structure* in turbulence, leads to another important conclusion. Since the size of the large scale structures scales with the flow geometry (independently of the Reynolds number), the flow development is governed by the dynamics of the large scale structures. There is growing experimental evidence to support this contention, as described in the next section.

3. THE GENERATION AND MOTION OF THE LARGE SCALE STRUCTURES

3.1 Flow Observations

A number of visual observations (Refs. 7-9) have been made in the past describing the large structures in a free turbulent shear layer. With one exception (Ref. 8) they were made at relatively low Reynolds numbers, primarily because few visual techniques exist that can be applied to high speed flows. Hot wires on the other hand are difficult to use since simultaneous observations at many points are necessary. On the basis of the Reynolds similarity principle, discussed previously, one may expect that the behaviour of the large structures as observed at low Reynolds number will not be significantly different at high speeds. The most remarkable, and perhaps surprising, aspect of these observations is the relatively high degree of coherence the structures exhibit so that their generation and development in time can be described in a quasi-deterministic fashion. It should be emphasized, however, that their occurrence at a given point in the flow is probabilistic.

The most complete observations have been made recently by Browand and Winant (Ref. 9) in a two-dimensional mixing layer. On the basis of other supportive evidence one may apply their results qualitatively to the mixing layer of a round jet. Accordingly, the following four flow regimes can be distinguished during the development of the large scale structures (Fig. 1 shows schematically these four regimes; for simplicity a two-dimensional rather than an axisymmetric view is indicated):

1. instability: the shear layer produced by the lip wake and the nozzle boundary layer is intrinsically unstable (whether turbulent or not) and develops periodic oscillations (Fig. 1a);

2. vorticity concentration: as the amplitude of the oscillations increases the vorticity tends to be concentrated in separated regions (Fig. 1b);

3. formation of vortex-ring-like structures: the concentrated regions of vorticity clearly display their ring-like structure as their scales approach the jet diameter (Fig. 1c);

4. vortex interaction: neighboring vortex-rings interact with each other in the following manner; one decelerates and the other accelerates, until the two pair with each other, doubling the size of the vorticity concentration region and doubling the spacing between adjacent vorticity concentration. The rate of pairing determines the spreading rate of the layer and, thus, the length of the potential core. Incidentally, there is some evidence that the pairing process continues to occur considerably beyond the potential core, but its detection is increasingly difficult. The pairing process is believed to be the key to the understanding of the turbulent mixing process and (as will be argued subsequently) to the noise generation as well.

3.2 The Pairing Process

The experimental study of the large scale structures in general, and of the pairing process in particular, is a difficult task especially within the shear layer. This is mainly due to the fact that the energy in the small scale motion at high Reynolds numbers is larger than that in the large scales, consequently the transducer signal is dominated by the small scale fluctuations. Conventional filtering is considered inadequate; only some modern techniques, such as the conditional sampling or VITA (variable interval time averaging) method has a possibility of providing the required information. This technique is presently being adopted for our jet studies.

However, some indirect measurements are available from which certain information can be obtained. It is known that the flow field just outside of the turbulent shear layer is induced by the large scale motion within the shear layer. Therefore, examination of this near field should shed some light on the problem.

Three pressure transducers were placed just outside of the shear layer of a 1" jet at stations $x = 3.10$, 4n, and 4.50.** The jet velocity was approximately 100m/sec. A sample of the instantaneous signals are

---

* By double structure one refers here to Townsend's suggestion that at sufficiently large Reynolds number the flow field consists of a large scale motion, its scale being of the order of the shear layer thickness and a fine scale motion the "graininess" of which is governed by the dissipation rate and is strongly Reynolds number dependent.

** This experiment was carried out by Mr. R. Petersen, a graduate student at USC.

shown in Fig. 2. The slope of the dashed lines connecting corresponding peaks is a measure of the convection velocity (analogous to the phase speed of amplitude crests). The most interesting aspect of these traces is the fact that the number of peaks exhibited by the upper trace (upstream gage) is higher than that of the bottom trace. If one interprets the signals as the pressure field induced by a convected row of ring vortex-like structures, the disappearing peaks, as indicated by the arrows, are attributed to the pairing process. It is also to be noted that from the position of the corresponding arrows one estimates a convection velocity that decreases with x; this suggests that the structure decelerates before pairing (disappearing peak) takes place. The average distance between neighboring structures, s, can be estimated roughly from the average period between peaks and from the convection velocity.

Actually a more quantitative value of s can be obtained from two-point space-time or spatial correlation measurements. In Fig. 3 values of s/D versus x/D are plotted. The values of s were estimated from a number of experiments (Refs. 5, 10 and 11) and are plotted in Fig. 3, together with Petersen's data. As expected, s varies linearly with x independently of the jet Reynolds number. It should be pointed out that s is not to be interpreted as the size of the large scale structures or a measure of "the compactness of the sources" as concluded by Fuchs (Ref. 11). The size is more likely of the order of the shear layer thickness and is, therefore, at least 2.5 times smaller than s.

The visual observations of Becker and Massaro (Ref. 7) give further evidence of the pairing process in a jet. They artificially disturbed a low Reynolds number jet by a sound field of known frequency. Shear layer oscillations, vortex ring formation and pairing are clearly evident in their photographs.

It should be noted at this point that the fundamentally non-linear process is incapable of being represented by a dispersive wave system. Although space-time correlations (both filtered and unfiltered) permit the assignment of local frequencies and wave numbers to this phenomenon, this form of description is not at all useful, for the following reasons. A fundamental precept in the theory of dispersive waves is the principle of "conservation of crests" (Ref. 14). It is clear from Figure 2 that "crests" are lost, causing the change in apparent "wave length". Hence, the new "wave length" some distance downstream is not due to the change of wave number and frequency slowly in space and time, but to an actual merging of two local maxima. From this we conclude that the concept of "phase speed" is not helpful since phase reference is lost.

3.3 Artificial Excitation

A most effective and productive means of studying the motion of the large scale structures was made by Crow and Champagne (Ref. 6). They found that by introducing sound disturbances of certain frequency, they interact with the naturally present large structures. Specifically, they observed that the disturbance amplitudes increase with x and reach a maximum at a certain x depending on the frequency. For instance, the frequency that was amplified over the largest distance corresponded to a Strouhal number of approximately .3 and a wave length of 2.4D and the amplitude of the disturbance peaked at $x = 3.8D$. Using a higher frequency, the peak occurred closer to the jet exit. Plotting the measured wave lengths of these disturbances against the x position where the peak was measured one finds that λ exhibits the same x dependance as s (Fig. 3). This most interesting result may be interpreted as follows: as the jet is being disturbed by a perturbation, a "resonance" occurs at that x station where the disturbance wave length and the average separation distance between the naturally present vortex-like structures happen to coincide. The reason that Crow and Champagne finds no resonance for frequencies less than $.30j/D$ is because, according to our picture, the resonance would have to occur beyond the potential cone where the large structures lack the coherence necessary for the artificial and natural disturbances to "lock in".

It is quite clear that considerably more work is necessary to clarify the motion of the large structures, nevertheless, it is felt that sufficient supporting evidence is available pointing to their existence, to warrant additional work and to speculate about their effect in the far field.

4. ON THE FAR FIELD NOISE GENERATION

Following the previous discussion, it is quite natural to inquire to what extent, if any, are the generation and interaction of the vortex ring like structures responsible for the far field noise. A direct experimental examination of this question presents a most difficult problem. The difficulty lies in the fact that the noise at a given point in the far field is the result of an integrated effect occurring within a certain volume. It would, therefore, be desirable to measure a judiciously chosen quantity spatially averaged over a volume or over a surface and relate it to the far field noise. Point measurements, such as a two-point space-time correlation of the near and far field pressure, and/or velocity fluctuations are not likely to be helpful, although they have been tried in the past (Ref. 12).

Lacking direct experimental support one is obliged at this stage to present only indirect evidence and qualitative arguments to support our suggestion, namely, that the dynamics of the large scale structures plays an essential role in the generation of subsonic jet noise.

First of all, recent measurements (Ref. 13) of the noise generated by the various regions of the jet situated along its axis clearly show that the most intense noise production occurs in the early stages of the jet development, exactly in the regions where the large scale structures exhibit strong coherence.

Secondly, there is evidence that the normalized overall noise power spectrum scales with the jet diameter. This result can be attributed to the fact that the volume containing the "equivalent acoustic sources" is generated by the large scale structure, and this volume scales with a single length parameter, the diameter. Incidentally, this result is quite remarkable in contrast to the well known fact that no single characteristic length can scale the energy spectrum within the shear layer.

As indicated earlier these arguments are qualitative and indirect. There is, however, another inference that one might draw from the observed interaction of the large scale motion that is most interesting, although still speculative at this stage. In the previous section the pairing process was described as the result of a simultaneous deceleration and acceleration of two neighboring vortex-ring like structures.

Their motion produces a zero net change of momentum; they each behave as a dipole with a combined instantaneous strength equal to zero. However, in the far field they degenerate into a quadrupole. Thus, according to this picture, the rate of subharmonic production, that is, the rate of the pairing process is capable of producing a quadrupole type of sound field.

This description fits very well into the framework of Powell's "vortex sound" theory (Ref. 2). He has approximated Lighthill's source expression and has written it in terms of the vorticity. According to Powell the source term in the shear layer has the form: $\partial[(\omega x\vec{u})x\vec{u}]/\partial t$; it is the vorticity interaction term arising from the acceleration and deceleration of vorticity. The far field noise at a given point will depend on the rate of change of the component of this vector directed toward the point of observation.

Whether or not this formulation is more helpful for an experimental verification of the proposed picture remains to be seen. Nevertheless, it is an interesting, new point of view that is worthwhile to examine.

5. REFERENCES

1. Lighthill, M. J., Proc. Roy. Soc. A, 222, 1954, 1-32.
2. Powell, Alan, J. Acoust. Soc. Am., 36, No. 1, 1964, 177-195.
3. Bradshaw, P., Ferris, D. H. and Johnson, R. F., J. Fluid Mech., 19, 1964, 591-624.
4. Mollo-Christensen, E., J. Appl. Mech., 89, 1967, 1.
5. Lau, J. C., Fisher, M. J. and Fuchs, H. V., J. Sound Vibr., 22, 4, 1972, 379-406.
6. Crow, S. C. and Champagne, F. H., J. Fluid Mech., 48, 3, 1971, 547-591.
7. Becker, H. A. and Massaro, T. A., J. Fluid Mech., 31, 3, 1968, 435-448.
8. Brown, G. and Roshko, A., AGARD CP 93, 1971, 23.1-23.12.
9. Browand, F. K. and Winant, C. D., XIIIth International Congr. Appl. Mech., Moscow, 1972.
10. Ko, N. W. M. and Davies, P. O. A. L., J. Fluid Mech., 50, 1, 1971, 49-78.
11. Fuchs, H., Deutsche Luft-und Raumfahrt FB-72-07, 1972.
12. Lee, H. K. and Ribner, H. S., J. Acoust. Soc. Am., 52, 5, Pt. 1, 1972, 1280-1290.
13. Laufer, J., Kaplan, R. and Chu, W. T., Proc. Symp. on University Research in Transportation Noise, Stanford U., 1973.
14. Wiltham, G. B., J. Fluid Mech., 9, 3, 1960, 347-352.

6. ACKNOWLEDGEMENT

This research was supported by the Department of Transportation under Grant DOT-05-00002.

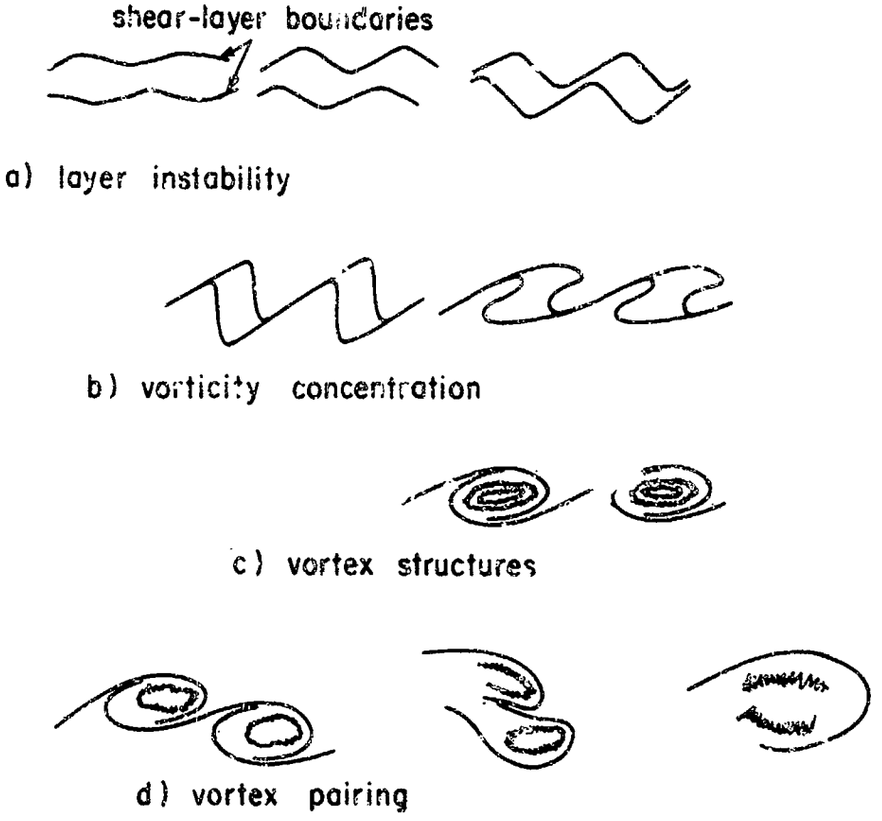

Figure 1 Schematic Diagram Showing Vortex Development and Pairing.

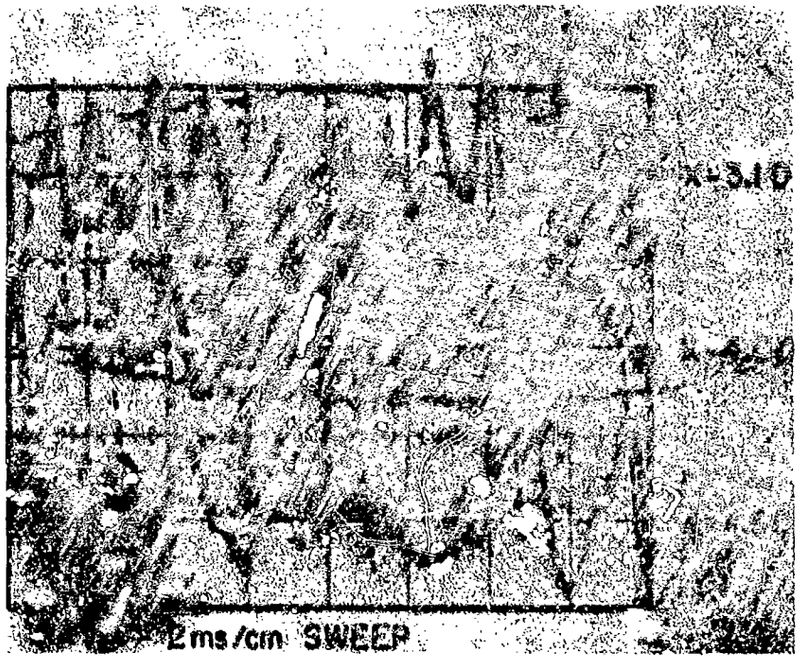

Figure 2 Instaneous Pressure Signals at Three Stations Just Outside of the Jet. U_j = 100m/sec D = 1"

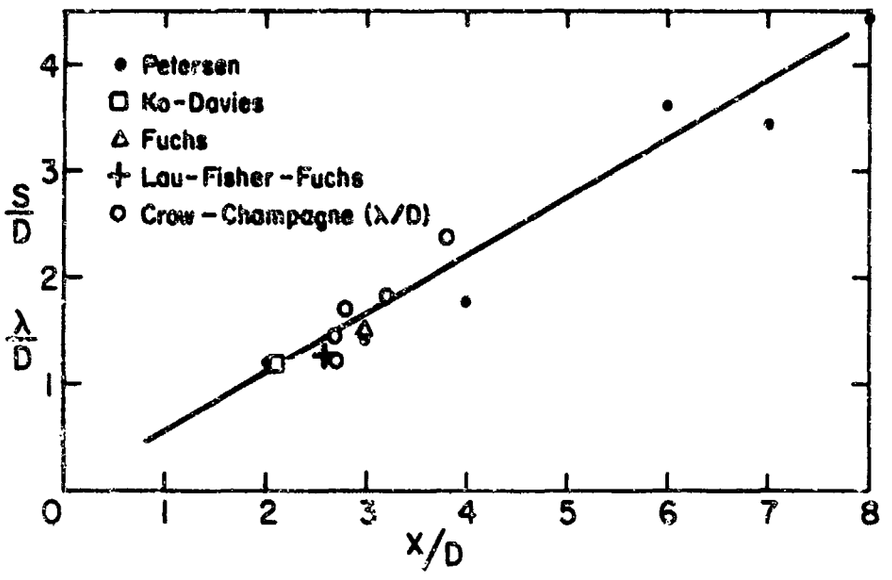

Figure 3 Mean Separation Distance Between Neighboring Structures.

DISCUSSION

Professor Michalke: On pages 21–3 it is stated that the non-linear process of vortex pairing is incapable of being represented by a dispersive wave system. This statement seems to be misleading, since it has been shown theoretically by R.E.Kelly (1967) that the appearance of a subharmonic fluctuation component can be explained by means of the non-linear interaction of waves. Therefore I think that, at least as an ensemble average, the pairing process of the vortices can be analyzed by waves. However, during the pairing process the content of the fundamental frequency component should decrease in downstream direction, while the content of the subharmonic component should increase, as it is suggested from your Figure 2. Do you agree that this phenomenon can be measured using narrow-band filters? The measurements of Crow and Champagne (1971) (cf. Figure 14) have at least shown a strong decay of the fundamental frequency component downstream of its peak within one wave length.

Kelly, R.E. J.Fluid Mech. 27, 657–89, (1967).

Crow, S.C. J.Fluid Mech. 48, pp.547–91, (1971).
Champagne, F.H.

Professor Laufer:

1. R.E.Kelly (1967) analyzed the problem of growth of subharmonic fluctuations due to non-linear wave interaction by assuming the presence of a first order perturbation in the time domain and identifying that it supports a secular growth of subharmonic fluctuations (by appealing to the Mathieu equation) for a sufficiently large amplitude of the fundamental. Kelly did not discuss the disappearance of the fundamental, for that is clearly inconsistent with the notion of a weakly non-linear stability theory. In addition, Kelly's problem involved a purely temporal amplification phenomena, and it has not been demonstrated (for non-linear waves) that the relationship between temporal and spatial amplification is as straight-forward as shown by Gaster (1962).

2. We agree that the phenomenon can be measured with narrow band filters, but that measurement would yield limited information. There is a relatively strong phase coherence of the generated paired vortices (subharmonic in wave terminology) following a Lagrangian path. Since these passages dominate the fluctuation amplitudes, they would cause a filter to ring for a time inversely proportional to its bandwidth, and, hence, be phase related to the subsequent passage of the vortex at a downstream station. If two stations are separated by Δx, this characteristic passage time is $\Delta x/U_c$. Hence, wide band filters of bandwidth $B \gg U_c/\Delta x$ would be appropriate, i.e., $B\Delta x/U_c \gg 1$, as has been required by years in turbulence research.

3. It is obvious that we interpret the measurements of Crow and Champagne (1971) in an entirely different manner. What they observed was not the decay of the fundamental but the probability density of the time between vortex passages at a fixed x station.

Dr Fuchs: Overall and narrowband space correlations in References 5 and 11 seem to have described certain aspects of the quasi-deterministic turbulence model proposed in this paper. The energy of the large-scale ring vortex structure and not that of small-scale fluctuations was found to dominate pressure transducer signals. Would the authors, please, elaborate on their statement on pp.21–2 that conventional filtering is inadequate and that only conditional sampling has a possibility of providing the required information on the formation of mutual interaction of the vortex structures?

Professor Laufer: Part of our response is covered in (2) of my reply to Prof. Michalke. To elaborate further, let us first emphasize that we view a spatially compact structure as the predominant feature of the turbulence. (This is in essential agreement with Lighthill's original postulate of the structure of the acoustic sources, and with the experience of the past 20 years of jet noise.) This "spatially compact" structure, hence, generates a broad spectrum (either in space or space-time) with phase coherence among various components in the transform domain. By ignoring these phase relationships between bands, one would infer from measurements of a fixed band, that the structures are not compact, as Fuchs has in 1972. In particular, the measurements we have made at USC with the directional microphone system (1973) and at D.V.L. Grosche (1973) both strongly suggest that by summing the *intensity* of radiation from different "slices" of the jet, one can recover the total radiated sound field at a point in the far field, which is not the case if the structures are not compact.

ERRATA TO PAPER 22

p. 22-2, Section 1.2, i, 3rd line: Tollmien instead of Tollmein

p. 22-3, 3rd line: Tollmiem instead of Tollmein
Section 1.3, 2nd paragraph, line 5: Tollmien instead of Tollmein

p. 22-4, Section 2.2, 10th line from bottom: Tollmien instead of Tollmein

p. 22-7, Section 3.3, lines 3, 18 and 22: Tollmien instead of Tollmein

p. 22-8, 6th line from bottom: identifiable instead of identificable

p. 22-9, Eq. 10: $(x_m - x_o) = \frac{U_c}{U_G}\left(\frac{U_t}{U_e}\right) U_e(\tau_B)_{max}$ instead of

$$(x_m - x_o) = \frac{1}{2}\frac{U_c}{U_G}\left(\frac{U_t}{U_e}\right) U_e\,(\tau_B)_{max}$$

p. 22-11, Section 5, line 13: Tollmien instead of Tollmein
Section 5, 3rd line from bottom: increases instead of increase

p. 22-12, Reference 30: November 1973 instead of May 1973

p. 22-17, Figure 31: Block No. 5 instead of Block No. 2; Data points for Run No. 272 are plotted incorrectly (see Table III, cont. p.22-12).

AN EXPERIMENTAL STUDY OF THE INTERMITTENT WALL PRESSURE BURSTS DURING NATURAL TRANSITION OF A LAMINAR BOUNDARY LAYER

by

Fred C. DeMetz*
and
Mario J. Casarella+
Naval Ship Research and Development Center, Code 1942,
Bethesda, Maryland 20034, USA, and Catholic University of America,
School of Engineering and Architecture, Washington, D.C. 20017, USA

SUMMARY

The properties of the intermittent wall pressure field have been measured in the transition boundary layer on a large flat plate in an anechoic wind tunnel. Natural transition was achieved with a mild favorable pressure gradient at Reynolds numbers, based on downstream distance from the plate's leading edge, in excess of 7×10^6. The development of the laminar boundary layer prior to transition was in agreement with numerical solutions to the laminar boundary layer equations and with stability criteria for pressure gradient effects.

The temporal, spatial, and spectral properties of the transition wall pressure field associated with the natural transition process occurring on the plate are obtained as a function of the intermittency factor, γ, and compared with those of the fully turbulent pressure field. Specifically, the mean-square pressure, spectral densities, convection velocities, distributions of burst periods and burst rates of the intermittent pressure field are computed from the data.

NOTATIONS

C_p - pressure coefficient = $\frac{p-p_B}{\frac{1}{2}\rho U_B^2}$

d - plate thickness length parameter

dB - decibel

f - frequency in Hertz

f_B - number of bursts per second

H^B - Shape factor = $\frac{\delta^*}{\theta}$

m - velocity gradient parameter $\frac{x}{U_e}\frac{dU_e}{dx}$

n - number of bursts of period τ_B

N - total number bursts occurring in sample time T

p - static pressure on plate surface

p(t) - instantaneous value of the pressure field

p_B - static reference pressure at x = 8 ft

$\overline{p^2}$ - mean square pressure = $2\int_0^\infty \Phi(f)\, df$

$\sqrt{\overline{p^2}}$ - root-mean square pressure

R_e, R_x - Reynolds number = $\frac{U_e x}{\nu}$

T - Sample time in seconds

t - time

t_i - increment of averaging time, T, during which point in boundary layer is turbulent

U(y), U, u - mean velocity at normal distance, y, from plate surface

u', v', w' - fluctuating velocity components in x,y,z directions

U_B - freestream reference velocity at x = 8 ft

$U_e(x)$ - potential flow velocity at the edge of the boundary layer at distance x from plate's leading edge

U_L - streamwise velocity of leading edge of burst

U_t - streamwise velocity of trailing edge of burst

U_∞ - freestream flow velocity upstream of plate

v - volts

x - streamwise distance from the plate's leading edge

y - normal distance from plate surface

z - coordinate on plate surface transverse to flow

β - streamwise Reynolds number variation in intermittent boundary layer region = $\frac{R_{\gamma=.99} - R_{\gamma=.01}}{6}$

γ - intermittency factor = $\frac{\sum_{i=1}^{N} t_i}{T}$

Δ - maximum variation of power spectral density results in dB

δ - boundary layer thickness = y at which $U(y)=0.99U_e$

Δt - transit times of burst between pressure transducers

Δx - streamwise separation distances between transducers

Δz - transverse separation distance between transducers

$\Delta\tau_B$ - time interval used for tabulating burst periods

δ^* - boundary layer displacement thickness = $\int_0^\infty [1 - \frac{U(y)}{U_e}]\, dy$

η - dimensionless length parameter = $y\sqrt{\frac{U_e}{\nu x}}$

θ - boundary layer momentum thickness = $\int_0^\infty \frac{U(y)}{U_e} \cdot (1 - \frac{U(y)}{U_e})\, dy$, also used as angle denoting burst shape (see Fig. 20)

α - maximum growth angle of burst (see Fig. 20)

μ - air viscosity

μPa - micro-pascal = $10^{-6}\ \frac{\text{newton}}{\text{meter}^2}$

ν - kinematic viscosity of air = $\frac{\mu}{\rho}$

ξ - normalized Reynolds number = $\frac{R_\gamma - R_{\gamma=.5}}{\beta}$

ρ - air density

τ_B - burst period in seconds

$\overline{\tau_B}$ - average burst period

$2\Phi(f)$ - measured power spectral density of the wall pressure field

P - point on plate surface in transition region

P_o - point of burst origin

L' - longitudinal length of burst

$\overline{L'}$ - average burst length

g - burst source density function

---

*Physicist
+Professor

SUBSCRIPTS

turb - fully developed turbulent boundary layer
lam - laminar boundary layer
c - critical value
t - transition value or value at trailing edge of bursts
L - value at leading edge of burst
e.t. - end of transition
e - edge of boundary layer
B - streamwise reference position at x = 8 ft, also denotes burst properties
exp - experimental
cal - calculated by computer
∞ - undisturbed stream upstream of plate
x - based on streamwise distance x
δ^* - based on boundary layer displacement thickness
θ - based on boundary layer momentum thickness
γ - value of parameter at measured or designated value of γ
i - summation index over N bursts
o - spatial origin
m - measurement position
max - maximum value

1. INTRODUCTION

This paper presents the results of an experimental study of the features of the intermittent wall pressure field associated with a natural transition boundary layer on a large flat plate in a mild accelerated flow. Since the properties of the intermittent wall pressure field are inherently associated with the transition flow field, a brief review of some of the known features of the transition process along with the objectives of the present investigation will first be presented.

1.1 Background on the Problem

The process of natural transition from laminar to turbulent flow on a flat plate has been the subject of intense research for many years, the most comprehensive being the systematic investigations performed at the National Bureau of Standards [1,2,3]. Recent studies have been pursued to include the effects of a large number of factors such as pressure gradient, surface roughness, freestream turbulence level and acoustic noise [4-7]. These studies have indicated that the various factors exhibit interdependences between each other. Consequently, a complete study of the transition process, as it would occur in an operational environment, would be very difficult. Indeed, progress has been achieved only by isolating these controlling factors and investigating their effects, both theoretically and experimentally, for the most elementary laminar boundary layers under controlled environmental conditions. In this manner, a fairly clear conceptual model of the transition process has begun to evolve from the investigations.

1.2 Conceptual Model of Transition Process

The laminar flow under investigation is that developed along a smooth, thin flat plate which is parallel to a low turbulence upstream flow. For the case of a zero pressure gradient external to the boundary layer region, a "Blasius" laminar boundary layer develops downstream from the plate's leading edge. With increasing downstream distance from the leading edge, the transition region is reached where the mean boundary layer flow features (characterized by the boundary layer properties of δ, δ^*, and θ) undergo progressive modification from those of the theoretical laminar flow results, eventually representing those features for a fully developed turbulent flow [8,9,10]. Typical ratios of the fully developed turbulent and laminar mean flow properties are

$$\frac{\delta_{turb}}{\delta_{lam}} \approx 3.9, \quad \frac{\delta^*_{turb}}{\delta^*_{lam}} \approx 1.41, \text{ and } \frac{\theta_{turb}}{\theta_{lam}} \approx 2.84.$$

If, on the other hand, the instantaneous flow features of the boundary layer velocity field are monitored with a hot wire anemometer (or Laser Doppler Velocimeter), then as the monitor is moved downstream, three stages of a "natural transition" process can be observed:

i) A critical Reynolds number, $R_c = \left(\frac{U_\infty x}{\nu}\right)_c$, is reached where amplification of small disturbances, naturally present in the stream, generates detectable two-dimensional oscillations characterized by the periodic Tollmein-Schlichting (T-S) waves which are predicted by the linearized theory of laminar instability [1,11]. With further increase of Reynolds number these oscillations grow in amplitude into a three-dimensional non-linear regime.

ii) The termination of the non-linear development is indicated by the formation of intermittent "bursts" or "spots" of local turbulence which propagate downstream with the flow. This portion of the boundary layer consists of an irregular sequence of laminar and turbulent regions. The Reynolds number at which this breakdown occurs is commonly termed the transition Reynolds number, R_t.

iii) The bursts grow in size and spread into the neighboring laminar flow until the boundary layer is fully turbulent. The Reynolds number at which the boundary layer becomes fully turbulent is known as the end of transition Reynolds number, $R_{e.t.}$.

The three stages of the transition process are shown schematically in Figure 1.

Schubauer and Skramstad [1] established that in a zero pressure gradient environment, the bounds of the transition stages are, for a turbulence intensity <0.1%, given by

$$R_c \approx .595 \times 10^5$$
$$R_t \approx 2.8 \times 10^6$$
$$R_{e.t.} \approx 3.9 \times 10^6.$$

Furthermore, they were able to characterize many of the spatial and temporal features of the turbulent bursts in the transition stage utilizing an electric spark technique.

If a pressure gradient exists along the plate, it is found to have a strong effect on the onset of the above three stages of the transition process. The effects of a strong favorable pressure gradient have been found to stabilize or delay the growth of the Tollmein-Schlichting waves and therefore increase the values of R_c, whereas an unfavorable or adverse pressure gradient have been found to amplify the laminar boundary layer oscillations, thereby decreasing the values of R_c, causing transition to occur earlier.

Several reviews of the above outlined mean and instantaneous physical features of transition theory and of stability theory can be found in the literature [11,12].

1.3 Hydroacoustic Aspects of Transition Process

Whereas past studies of the transition process have concentrated primarily on understanding the mean and fluctuating velocity fields in the light of theoretical considerations, recently the hydroacoustic aspect of the transition phenomenon has been of interest. The unsteady flow in the boundary layer region near the surface of a structure causes pressure fluctuations [13] which, when coupled dynamically to the structure, can result in high structural and fluid borne noise levels, such as those experienced inside aircraft or in sonar systems of naval vessels [14-16]. Heretofore, the hydroacoustic aspects of boundary layers have been modelled solely from experiments with fully developed turbulent boundary layers [17] which were conducted in wind tunnels and other flow facilities. Now, however, due to design and manufacturing improvements of modern aerodynamic and hydrodynamic vehicles, the flow noise associated with the laminar-turbulent transition region is of particular importance since this region on the nose of the structure can be a significant portion of the surface.

The experimental study of the pressure field in the transition region has been restricted in the past by the high levels of incident turbulence intensity associated with experimental flow facilities. The high noise levels tend to mask out the fluctuating pressures associated with the transition and prevent the boundary layer from developing on the model surface in a "natural manner" [18]. "Natural transition" is defined as the transition resulting from Tollmein-Schlichting oscillations naturally present in the laminar boundary layer and not resulting from the presence of extraneous controlling factors such as, for example, protuberances, excessive surface roughness, or freestream turbulence level.

The first known attempts to measure the quantitative features of the transition wall pressure field were made by Blackman [19] at the University of Southampton who conducted measurements of the transition wall pressure field on a small flat plate in an open jet wind tunnel. In this study, he was unable to obtain "natural transition" due to limitations imposed by the capabilities of the wind tunnel and the small physical size of the plate. The origin of the burst generation mechanism for his experiment appeared to be the leading edge of his plate. However, Blackman's enlightening experimental data, along with the interpretation of the results, are valuable in understanding those transition burst features which are independent of the burst generation mechanism. Furthermore, his experimental techniques reflected a great deal of originality and contributed significantly to our experimental effort.

1.4 Objectives of the Present Investigation

The direction of the present investigation was to determine the properties of the intermittent pressure field for a natural transition boundary layer which includes the three distinct stages illustrated in Figure 1. With the construction of the new Anechoic Flow Facility (AFF) at the Naval Ship Research and Development Center (NSRDC), suitably low levels of background acoustic noise and freestream turbulence intensity have made it possible to conduct a study of the flow noise features of a transition boundary layer on a large flat plate whose qualitative flow features are included in Figure 1. The spatial, temporal, and spectral properties of the transition wall pressure field are obtained as a function of the intermittency and compared with those of the fully turbulent pressure field. The convective velocities, distribution of burst periods, burst frequency, burst growth rate, mean-square pressures, and spectral densities of the intermittent pressure field are computed from the data.

2. APPARATUS AND PROCEDURE FOR THE EXPERIMENT

2.1 Anechoic Flow Facility

The Anechoic Flow Facility in which the measurements were conducted was designed specifically for flow-related acoustic experiments. The general design features of the flow facility are shown in Figure 2 and are described in detail by Brownell [20]. The tunnel is a reinforced concrete, horizontal circuit of rectangular cross sections with corner fillets. The air in the tunnel is moved by a fan around a closed loop, passing through the closed-jet test section into the anechoic chamber which provides an open-jet test section. The facility has a maximum design air speed of 200 ft/sec in the test sections at atmospheric pressure. To minimize acoustic background noise, acoustic mufflers are located upstream and downstream of the fan to attenuate fan noise and the tunnel walls are lined with acoustic absorption material. To minimize structureborne noise, the tunnel circuit and drive machinery are built over a solid rock foundation and isolation joints are provided throughout the circuit. Turbulence reducing screens are used in the stilling chamber to reduce the turbulence level in the test sections.

An evaluation of the aerodynamic [21] and acoustic performance of the wind tunnel was conducted. The freestream turbulence level was measured in the "clean" closed jet test section with a hot wire anemometer and was found to be approximately $\frac{\sqrt{u'^2}}{U_\infty} \times 100 = 0.09\%$ or less over the range of flow velocities. (It was assumed that the presence of the flat plate in the tunnel would not alter this level significantly although this assumption was not checked by repeating the turbulence intensity measurements). According to the results of Schubauer and Skramstad [1], this value of the turbulence level should allow the transition process on a smooth flat plate to develop in a "natural" manner provided that the background tunnel noise is not excessive [4].

The background acoustic noise levels were measured in the closed jet test section with the wind tunnel in the "clean condition and also with the Flat Plate Fixture installed in the test section. The clean tunnel evaluation of the background acoustic noise levels was made over the range of tunnel flow speeds as part of the Acoustic Performance Evaluation† following completion of the construction

†Report in preparation by Mr. R.W. Brown of NSRDC.

of the facility. Figure 3 shows the measured levels of the pressure spectral densities over the range of flow speeds. The figure includes, for comparison, the wind tunnel's acoustic noise design specifications at each flow velocity. Generally, it can be seen that above a frequency of 100 Hz the measured noise values are below the design values. For these measurements a 1/2-inch Bruel and Kjaer (B & K) Condenser Microphone, Type 4134, was mounted on a strut on the centerline of the closed jet test section, approximately 6 feet upstream of the anechoic chamber. The microphone diaphram was covered with a Nose Cone, Type UA 0052, which provided a streamlined covering to reduce the wind noise generated by the air flow over the microphone and produce a relatively flat frequency response for a sound field of random incidence direction.

Measurements were also made of the free-field sound pressure spectral densities outside of the plate's boundary layer, 2 feet from the plate surface. Comparison of these results with the clean tunnel levels indicates that the presence of the plate increased the background noise levels by approximately 10 dB. Below 1 kHz a peak was detected in the free-field noise spectra whose frequency depended on flow velocity. This peak was found to be attributable to sound generated by plate vibration due to vortex shedding from the plate's blunt trailing edge. These peak levels were as much as 15 dB above the free-field spectral levels.

2.2 Flat Plate Fixture

The large flat plate test fixture was designed to provide laminar, transition, and turbulent boundary layer flows over a smooth, rigid surface. The plate is mounted in the wind tunnel's closed-jet test section in a vertical plane intersecting the centerline of the test section. The upstream, leading edge of the plate is mounted adjacent to the upstream edge of the instrument trench. At this point the flow has stabilized following passage through the flow facility's settling screens and contraction section. A view of the plate is shown in Figure 4.

As shown schematically in Figure 5, the fixture is constructed in various sections which are machined from 1-inch thick aluminum stock and bolted together to provide a maximum waviness of .020 inches per foot. The sectional construction permits the variation of the streamwise distance from the leading edge to the four rotatable test disks on which instruments are mounted. By inserting or removing the 18 inch spacer section and rotating the test disks the streamwise location of any transducer can be varied continuously from 1.2 to 13.8 feet. Although the joints between plate sections were machined only within easily achievable tolerances, the roughnesses which remained after assembly of the fixture were filled with epoxy and smoothed.

The structural and aerodynamic performance of the plate fixture was evaluated to determine the effectiveness of the design pertaining to the fixture's response to vibration excitation by the flow and the boundary layer development, respectively.

The plate was designed to be of sufficient mass and rigidity to minimize its response to vibration excitation by the transition and turbulent boundary layers. This structural requirement was necessary to maximize the signal to noise ratio of the pressure transducers which are used to study the boundary layer pressure fields and which invariably have some response to the plate acceleration. The possible effects of surface motion on the boundary layer transition process are not yet fully understood and therefore, it was desired to eliminate, or at least minimize, this factor from the study.

Figure 6 shows the measured values of the acceleration spectral density utilizing a B & K Accelerometer, Type 4344, mounted on the back of Disk 3, near the location of the flush mounted microphones used to make the pressure field measurements. The acceleration levels are shown for two flow velocities, that at which transition occurs on Disk 3, and at a fully turbulent velocity. In both spectra, speed dependent peaks in the acceleration levels are apparent.

The peak at 400 Hz for the lower speed spectrum, and the peak at 520 Hz for the higher speed case, both satisfy the common vortex shedding Strouhal number relation of $\frac{fd}{U_\infty} = 0.2$, where d is taken as the plate thickness. This, together with the free-field acoustic noise measurements mentioned above, indicates that shedding from the blunt trailing edge of the plate fixture was a mechanism of plate excitation.

By covering the plate mounted microphones so that they could not sense the boundary layer pressure field, it was found that the plate's vibration field influenced the plate's boundary layer pressure field measurements at frequencies below 1 kHz. Above 1 kHz, the signal to noise ratio which is represented by the differences in the levels of the uncovered and covered microphones, is generally in excess of 10 dB for the intermittent and fully turbulent boundary layer pressure fields. Hence, from the standpoint of structural vibration, it is assumed that above 1 kHz, the flat plate fixture serves as a useful model for studying the transition and turbulent boundary layer pressure field. The extent to which the plate's vibrations may possibly affect the actual transition process of the laminar boundary layer to turbulent flow could be investigated in future tests by artifically shaking the plate.

Studies of the pressure fields associated with laminar boundary layers, such as attempting measurements of the fluctuating pressures associated with Tollmein-Schlichting waves, will require further reduction in the plate's vibration levels through trailing edge streamlining and structural damping.

The essential aerodynamic requirement of the plate fixture was that a prescribed, controllable, laminar, transition, and turbulent boundary layer could be achieved over the surface of the test disks. To accomplish this, the fluid adjacent to the leading edge of the plate must not encounter a sufficiently large positive pressure gradient to cause the streamlines to separate from the plate surface, in which case, the flow could immediately become turbulent at the leading edge [22]. It was found that a leading edge with a sharp asymmetric taper of 5 degrees (see Figure 5) did not trip the boundary layer over the range of flow velocities when the plate was oriented at a -1.5 degree attack angle to the flow. With the plate fixture at this orientation, a naturally developing transition boundary layer was obtained.

2.3 Instrumentation and Measurement Procedure

The instrumentation for the experimental measurements fall essentially into the three basic categories of aerodynamic, vibration, and acoustic, depending on the parameters to be measured. The vibration and free-field acoustic instrumentation were previously discussed. This section gives a brief summary of the instrumentation used for the boundary layer measurements and discusses the measurement and data analysis procedures.

Aerodynamic Instrumentation

The flat plate mean velocity distributions across the boundary layer were measured with a modified version of a United Sensor Total Head Probe, Model BA-20-12-C-11-650, mounted on a test disk utilizing a Nash Control, Inc., Linear Actuator, Model DL 1326M22. The electromechanical linear actuator functions as a remote positioning device and permits the positioning of the velocity probe (or hot wire anemometer) at varying distances normal to the plate's surface. The linear actuator contains a DC motor which positions an extending tube within an accuracy of .001 inch by monitoring a position indicating potentiometer which is directly coupled to the actuator. The position of the probe on the plate surface is changed by rotating the disk and re-alining the probe with the flow direction. The static reference pressure is measured through a 1/32-inch diameter hole which is flush with the plate's working surface, adjacent to the probe tip.

The differential pressures between the total head probe and the static wall hole are monitored by a CGS Electronic Manometer, Type 1018-B, which utilizes a capacitive type Barrel Pressure Sensor, Type 538-3, with a $\pm$ 1 psi range. This instrument provides digital differential pressure readings accurate to within $\pm$ .001 psi. The time constant of the system was generally less than 30 seconds, with approximately 10 feet of tubing between the probe and the pressure sensor.

A dual channel Flow Corp. Constant Temperature Anemometer, Model 900-1, was utilized for measuring mean and fluctuating velocity components near the plate surface and for measuring the freestream turbulence level.

The static pressure gradient was measured along the plate surface utilizing a series of 12 -1/32 inch diameter holes drilled along the plate in the streamwise direction. Plastic tubing connected each hole in the plate to a large alcohol manometer and the static pressures along the plate relative to atmospheric pressure were recorded visually over the range of tunnel flow velocities.

Acoustic Instrumentation

The fluctuating pressures on the plate surface were measured with B & K 1/4-inch Condensor Microphones, Type 4136, and B & K 1/8-inch Condensor Microphones, Type 4138. Both size microphones, through use of an appropriate adapter, were used with B & K Cathode Follower Preamplifiers, Type 2615 or 2619, and with B & K Measuring Amplifiers, Type 2606. To facilitate the measurement of the pressure on the plate surface over as small an area as possible, the microphones were used with solid protective caps mounted flush with the plate surface in a test disk and in each of which was drilled a single 1/32-inch diameter hole. The fluctuating pressure on the plate surface was sensed through the 1/32-inch diameter hole which led to a small cavity enclosed by the protective cap and the microphone diaphram. This microphone system has a resonance frequency in the response curve due to the fact that the combined hole and cavity behave like a simple Helmholtz resonator.

The sensitivity levels of the microphones for the flat portion of their pressure response curves were determined at 250 Hz using a B & K Pistonphone Type 4220. The frequencies of resonance of the 1/4 and 1/8 inch microphone systems were determined from the resonant peaks in the power spectral density curves of the fully developed turbulent pressure fields which occurred on the plate surface at the higher wind velocities. Frequency response curves near the Helmholtz resonance frequencies for the 1/4 inch and 1/8 inch microphone systems, which were determined employing free-field calibration methods in the anechoic chamber of the wind tunnel, are given in Figure 7. The low frequency roll-off was controlled by the preamplifier and was determined from the manufacturer's response data.

Two 1/4-inch pinhole microphones are flush mounted in a test disk utilizing a positioning device which allows the separation distance between the transducers to be varied from 0.531 to 4.552 inches. Larger separation distances of up to approximately 10.75 feet in the streamwise direction can be achieved by mounting microphones in two separate 25 inch test disks.

The analysis of the root-mean-square (RMS) properties of the pressure field was done employing a Ballantine, Model 320, True RMS Electronic Voltmeter. A number of external capacitors were employed in the meter circuit to increase the meter response time and decrease meter fluctuations during voltage measurements of the intermittent pressure field at low values of the intermittency factor.

The power spectral densities of the fluctuating pressure fields on the flat plate were determined by use of a Time Data Real-Time Analyser System, Type 1923/A.

The intermittency factors, average burst period, and burst convection velocities of the transition pressure field were determined either visually from oscillograph records or by employing an electronic device which automated the process [30].

Response Characteristics of Circuitry

A schematic of the electronic circuitry used in the tape recording (and during reproduction for analysis) of the data of the fluctuating pressure and velocity fields in the flat plate boundary layer is shown in Figure 8.

The frequency and phase response of the system and the effects of extraneous noise sources on the signal to noise ratios of the signals were evaluated. As shown in Figure 8, a sine wave oscillator or a white noise source of known RMS level can be connected to the direct input stage of the microphone amplifiers simultaneously, and passed through the complete electronic circuit and recorded on the multichannel magnetic tape recorder. When these recorded signals are reproduced through the data analysis systems, a calibration of system performance can be obtained.

Figure 9 shows an x-y plot of the frequency response (power spectral density) of the circuit for a pair of data channels, through which white noise was passed simultaneously. This represents the approximate features of the circuit response at the input of the oscillograph, or the intermittency measuring devices, used to calculate γ and the other space-time properties of the turbulent bursts. The low-frequency roll-off is due to the characteristics of the hi-pass filter in the circuit, while the decrease in response at high frequency is due to the decreasing tape recorder response above 10 kHz. In addition to the electronic circuit response shown in Figure 9, the frequency response of the pinhole microphones must also be taken into account in measurements of the properties of plate pressure fields.

The frequency response of the galvanometers used in the Honeywell Visicorder Oscillograph Model 1108 was flat within + 1/2 dB between 0 and 3000 Hz. The 3 dB down point of the upper frequency galvanometer's response occurred at 5500 Hz. The bursts displayed on the

oscillographs consisted, therefore, of frequency components within an approximate 3 dB down bandwidth between 2800 and 5500 Hz, which resulted through use of the Krohn-Hite Filters and the fluid damped galvanometers. It was found that burst frequency components, within this bandwidth, accurately defined the temporal features of the burst envelopes on the oscillographs. The inherent phase angle between the two electronic data channels was found to be negligible.

Generally, the procedure for the measurements of the boundary layer pressure field was to locate the microphones at the desired streamwise distances along the plate and then record the microphone signals on magnetic tape for a series of different wind velocities. Two or three microphones were generally used simultaneously to permit simultaneous recording on the multi-channel tape recorder for later determination of the convective and growth properties of the intermittent boundary layer pressure bursts.

3. EXPERIMENTAL RESULTS OF THE BOUNDARY LAYER FLOW

This section evaluates the measured mean flow boundary layer profiles in terms of their consistency with respect to well known analytical predictions based on viscous flow theories. As previously discussed, it was necessary to orient the plate's working surface at a -1.5 degree attack angle to the flow to prevent leading edge tripping. This orientation resulted in a mild acceleration of the external velocity above the boundary layer along the plate and therefore, a laminar flow which slightly differs from the Blasius velocity profile. The measured features of the boundary layer under the conditions of a mildly accelerating external velocity along the plate will be presented. First a discussion of the measured external velocity gradient along the plate will be given.

3.1 Pressure Distribution Along the Plate

Figure 10 shows the pressure distribution along the plate's streamwise dimension as measured by static pressure holes in the wall of the plate. The non-dimensional pressure coefficient, $C_p = \frac{p-p_B}{(1/2)\rho U_B^2}$, is shown in Figure 11. The reference pressure, p_B, and velocity, U_B, are measured by a pitot-static tube located outside the boundary layer 8 feet downstream of the plate's leading edge. The fact that C_p collapses at different freestream velocities allows one to establish a single semi-empirical relationship for the potential flow velocity $U_e(x)$ at the edge of the boundary layer.

If the fluid is considered incompressible and the density ρ = constant, then the momentum equation can be integrated along a streamline in the x-direction, to give

$$p + 1/2\ (\rho U_e^2) = \text{constant} \tag{1}$$

This is valid along any streamline of the flow sufficiently removed from the body surface to be unaffected by the thin region near the surface dominated by large viscous forces. The constant of integration in Equation (1) is taken as $p_B + (1/2)\ \rho U_B^2$, where p_B and U_B are the static pressure and flow velocity, respectively, measured on a streamline which is assumed to run along the outer edge of the plate's boundary layer. Equation (1) then becomes

$$p(x) + 1/2\rho U_e^2(x) = p_B + 1/2\rho U_B^2 \tag{2}$$

or

$$\frac{U_e(x)}{U_B} = \sqrt{1-C_p(x)} \tag{3}$$

Also note that the upstream reference velocity U_∞ can be computed from Equation (3), or by extrapolation of the U_e/U_B data to the x = 0 position.

Figure 12 shows the ratio of the velocity at the edge of the boundary layer, to the velocity of the freestream just upstream of the leading edge U_e/U_∞, as a function of downstream distance x. A velocity gradient parameter, $m = \frac{\nu}{U_e}\frac{dU_e}{dx}$, versus x is shown in Figure 13. The dimensionless parameter, m, is useful as a measure of the effect of the pressure gradient on the laminar boundary layer [23]. Exact solutions, referred to as similar solutions, exist for flows in which m = constant along the streamline of the flow.

A semi-empirical equation was used to model the accelerated flow data as given below:

$$\frac{U_e}{U_\infty} = 1.10457 + 0.07740 \tan [0.130\ (x-7.2033)] \tag{4}$$

$$m = \frac{0.01006\ \sec^2 [0.130\ (x-7.2033)]}{1.10457 + 0.07740 \tan [0.130\ (x-7.2033)]} \tag{5}$$

The comparisons of Equations (4) and (5) with the experimental data are shown in Figures 12 and 13. Equations (4) and (5) are seen to be in good agreement with the experimental data and were chosen for use in the numerical computational scheme used to predict the laminar boundary layer properties along the flat plate.

3.2 Laminar Boundary Layer Velocity Distributions

Comparison with Blasius Solutions

Downstream of the leading edge of the plate, the boundary layer which develops on the surface is initially that for laminar flow. Since the plate's measured pressure gradient was small, it is instructive to compare the experimental properties of the laminar boundary layer region with the classical results derived by Blasius for the zero pressure gradient flow along a flat plate. Figures 14 through 17 give the experimental laminar boundary layer velocity profiles measured at four streamwise locations on the plate surface compared to the Blasius profiles. The ratio of the velocity U(y) to the freestream velocity, U_e, plotted versus the dimensionless length parameter, $\eta = y\sqrt{\frac{U_e}{\nu x}}$, is shown in each of these figures.

Once the velocity distribution in the boundary is known, the boundary layer thickness, δ, is determined as the distance from the wall at which $U(y) = 0.99\ U_e$.

Figure 18 shows the growth of the laminar boundary layer thickness as calculated by the Blasius solution compared with those measured along the plate in the streamwise direction. It is seen that the experimental values of δ, measured on the plate in the mild favorable pressure gradient, deviate from the values predicted by the Blasius solution which is based on the zero pressure gradient condition.

Comparison with Pressure-Gradient Solution

It is desirable to ascertain the effects of pressure gradient on the laminar boundary layer. This was done by numerically computing an exact solution of the laminar boundary layer equations with a semi-empirical equation for the exterior accelerating flow. A finite-difference numerical procedure proposed by Fannelop [24] was used for the computation. The semi-empirical equation for the external flow, $U_e(x)$, given by Equation (4), was used in the computations for the velocity profiles at discrete locations along the plate's streamwise direction. A computer program developed by Smith [25] was used for these computations. The values of δ which were calculated by this procedure are shown in Figure 18. The effect of the accelerated flow can be seen to have retarded the laminar boundary layer growth along the plate relative to the growth predicted by the Blasius solution. The calculated profiles are shown in Figures 14-17.

To facilitate this comparison between the analytical and experimental values of δ, the experimental data was put in dimensionless form and corrected to the proper external velocity $U_e(x)$ in order to provide the results at the specific set of speeds and locations shown in Figure 18.

The boundary layer displacement thickness, δ^*, is generally accepted as a more accurately determinable boundary layer length parameter than the boundary layer thickness, δ. The experimental values of δ^* are compared in Table I with the values calculated employing the computer program.

It is concluded that the qualitative features of the experimental data for the laminar boundary layer are in reasonably good agreement with analytical results which take into account the favorable pressure gradient which existed on the plate.

3.3 Instability and Natural Transition to Turbulence

As previously discussed, the transition process can be influenced by a large number of factors. In the absence of a strong predominance of one or more of these factors, the transition boundary layer which developes along the plate is said to occur in a "natural" manner and be characterized by the Tollmein-Schlichting waves observed by the classical experiments performed at the National Bureau of Standards.

In the introduction, it was explained that the natural transition process had three distinct stages. In this particular study, the primary objective was to experimentally determine the characteristics of the fluctuating pressure field associated with these three stages of an incompressible transition boundary layer on a flat plate. Attempts were made to achieve "natural" transition in the absence of aforementioned extraneous effects. This plan was generally successful with the exception that it was necessary to orient the plate obtaining a mild accelerated flow (favorable pressure gradient) condition over the plate to prevent leading edge tripping. This favorable pressure gradient has a significant effect on delaying the initial stage of the transition process. For example, the transition Reynolds number for the Blasius transition obtained by Schubauer and Skramstad was $R_t = \left(\frac{U_\infty x}{\nu}\right) = 2.8 \times 10^6$. In this study, laminar flow was found to occur at Reynolds number as high as 8.7×10^6.

Although the favorable pressure gradient obviously delayed the onset of the transition process, it did not, it is felt, significantly alter the basic mechanism associated with the bursting stage of the transition process, though it can alter the width of the transition region.

Tollmein-Schlichting Waves

T-S waves were not experimentally observed due to plate vibrations and high associated acoustic noise levels in the frequency range where T-S oscillations were expected. However, it is shown by the authors in Reference 30, that comparisons of the laminar flow data of δ, δ^*, and θ, with various stability criteria tend to support the belief that the Tollmein-Schlichting wave stage of the transition process was present between the laminar and intermittent bursting stages on the plate. The results indicated that the laminar profiles at the 3, 6, and 9 foot positions, shown in Figure 18, are in the unstable region of the neutral stability curves at a flow speed of 100 ft/sec. At the 12 foot location from the leading edge, however, the more pronounced favorable pressure gradient causes the profile to fall in the stable region. Stability theory implies, that once R_c is reached, the T-S waves should be growing in the unstable region and, if the oscillation amplitudes are sufficiently large, the experimentally obtained boundary layer properties should exceed the computed values for the laminar solution. In the stable region, the T-S waves could be damped out and the flow restabilized to the laminar flow solution again [1]. Therefore a study of Figure 18 suggests that for that prescribed speed, the T-S waves are initially disturbed, grow to finite amplitude, and then are damped out as the effects of the favorable pressure gradient become more pronounced downstream.

Hopefully, in the future, the plate's vibration levels will be improved in the low frequency region where T-S waves are expected and the T-S pressure oscillations can be measured and confirmed by hot wire detection of the laminar oscillation phenomena. For the present, the assumption of the existence of the T-S waves prior to the onset of bursting, although still in question, allows the data in this study to be considered as representing that for a natural transition process.

Onset of Bursting

At flow velocities in excess of 150 ft/sec, the laminar boundary layer eventually underwent transition at the 9 foot measuring station on the plate. The onset of bursting, which identified R_t, was determined by Schubauer and Skramstad with the use of hot wire anemometers positioned in the boundary layer. In the present experiment, bursting onset was observed with the flush mounted microphones. An approximate value of R_t determined by the onset of bursting in the pressure field was between 7.4 to 8.7×10^6.

Detailed measurements of the velocity profiles in the transition region on the large plate were not obtained. Consequently, the onset of bursting was determined solely through use of the microphones and could not be compared with that predicted by the abrupt decrease of the shape factor H.

Beginning of Turbulent Flow Region

The value of the Reynolds number at the end of the transition process, $R_{e.t.}$, was also determined from the microphone signals. This Reynolds number was taken as that for which the bursting process became continuous, indicating fully developed turbulent flow. The measured values of $R_{e.t.}$ fell within the range of results $8.6 \times 10^6 < R_{e.t.} < 11.0 \times 10^6$.

4. EXPERIMENTAL RESULTS OF INTERMITTENT FLOW FEATURES

4.1 Comparison of Velocity and Wall Pressure Bursts

In the present study of the intermittent wall pressure field during the transition process, the level of intermittency was varied by changing the wind tunnel flow speed. The locations of the flush-mounted pressure transducers were held in a fixed position along the plate and could not be varied remotely during the operation of the wind tunnel. In order to evaluate whether the burst generating mechanism of the natural transition process has been noticeably altered by the varying speeds, the intermittency factors, γ, was plotted versus a normalized transition Reynolds number and compared with the known experimental data of Schubauer and Klebanoff (26) on the intermittent velocity field bursts. Specifically, the question is whether the secondary effects on transition, such as the turbulence intensity, plate vibrations, etc., are significantly affected by the slight change in the stream velocity.

The intermittency factor γ is defined as the fraction of the total sample time T_{total} that the flow is turbulent at any point P in the transition region and can be expressed as

$$\gamma(P) = \frac{\sum_{i=1}^{N} \tau_{B_i}}{T_{total}} \qquad (6)$$

where τ_{B_i} denotes a bursts period and N denotes the number of bursts during the total sample time, T_{total}. Figure (19) shows the intermittency factors, γ, of the pressure bursts measured at both different downstream positions and flow velocities in terms of a normalized Reynolds number $\xi=(R_\gamma-R_{\gamma=.5})/\beta$. R_γ is the Reynolds number (based on x) at which the value of γ is measured, $R_{\gamma=.5}$ is the Reynolds number at which the pressure field was turbulent half the time, and $\beta=(R_{\gamma=.99}-R_{\gamma=.01})/6$. The quantity β is a measure of the width of transition for a constant flow velocity and was obtained by extrapolating the data when plotted versus Reynolds number. The figure includes a Gaussian integral curve which has been fitted to the normalized quantity ξ and shows good agreement with the data. With this limited data, it can be inferred that the general characteristics of the distribution of γ for a wall pressure field in a mild, favorable pressure gradient appear to be similar to that for the velocity field in a zero pressure gradient when normalized with respect to the width of the transition region.

To provide a more direct comparison and verification that the bursts detected in the intermittent boundary layer region are directly related and have the same geometrical and convective features as bursts detected by an adjacent pressure transducer mounted of the wall, simultaneous measurements of the instantaneous velocity and wall pressure fields are required. Some data which showed excellent agreement between the bursts were obtained but for a smaller prototype flat plate. Future tests on the large plate will include hot wire anemometer measurements.

4.2 Spatial and Temporal Features of Transition Bursts

Figure 20 illustrates the shape and growth of a velocity field burst generated by an electric spark by Schubauer and Klebanoff [26]. Results will be presented on the features of these bursts as measured by one or more microphones positioned on the plate which sample these propagating bursts at different levels of intermittency.

Oscillograph Records of Propagating Bursts

Oscillographs of the intermittent pressure field are shown in Figure 21 for low and high values of intermittency. The oscillographs show simultaneous outputs of three pinhole microphones mounted flush with the plate surface at increasing streamwise distances from the plate's leading edge. These oscillographs clearly indicate the transition process, whereby intermittent bursts of local turbulence are formed and propagate downstream, growing in length as they go, until they merge forming a fully developed turbulent boundary layer. Adjacent to each transducer is shown the Reynolds number based on downstream distance from the plate's leading edge, the separation distance between transducers, and the intermittency factor.

Each of the above oscillographs was recorded after passing the microphone signals at the amplifier output through a 2500 Hertz (6 dB down) high-pass filter. This filtering removed low frequency vibration signals which were picked up by the pressure transducers as previously discussed. The upper frequency components of the oscillograph records were limited by the galvanometer response which was 3 dB down at 5500 Hz. Comparisons of the filtered and unfiltered microphone signal are shown in Figure 22. It can be seen that the temporal properties of the pressure bursts are more clearly illustrated by filtering out the low-frequency noise components. Further verification that the low frequency components in the microphone signal are due to vibration of the microphone mounting disk is given by Figure 23 which compares the power-spectral densities of the microphone signals without the high pass filtering with those of the covered microphone for the same flow conditions. The close agreement in the spectral levels at the peak frequencies below 2500 Hz indicate that the vibration sensitivity of the pressure transducers is sufficient to detect the plate's vibration modes at low frequencies.

Figure 24 gives oscillographs of the signals from two microphones, with a streamwise separation of 1.62 feet, for a range of pressure field intermittencies from $\gamma=0$ to $\gamma=1$. It is noted that bursts which pass the upstream microphone are generally still identifiable at the downstream transducer. The growth in length of the bursts during the transition between the transducers is readily apparent.

Convective and Spatial Features of Bursts

As illustrated in Figure 24 the oscillographs can be used to calculate the velocities of the leading (downstream)and trailing (upstream) edges of the bursts. The travel time between the two streamwise transducers can be determined from the timing lines on the oscillographs. The streamwise velocities

of the leading and trailing edges of the bursts are given by $U_L = \Delta x/\Delta t_L$ and $U_t = \Delta x/\Delta t_t$ respectively, where Δx is the streamwise separation distance between the transducers and Δt_L and Δt_t are the respective transit times of the leading and trailing edges of the burst between the microphones.

It was found that the propagation velocity of the leading edge of the burst is $U_L \approx .97U_e$ while the propagation velocity of the trailing edge of the pressure bursts is $U_t \approx .31U_e$. A number of these calculations are tabulated in Table II. These values differ from the values measured near the surface with a hot wire probe by Schubauer and Klebanoff [26] who obtained $0.88U_e$ for the leading edge velocity and $0.5U_e$ for the trailing edge velocity for the case of a zero pressure gradient along the plate. This discrepancy is related to a difference in burst growth rates which is reflected in the fact that widths of the transition regions for both sets of experiments were not comparable.

The burst growth rate, U_G, defined as the rate of growth of the length of the burst, and the convective velocity of the burst, U_c, defined as the average propagation speed of the bursts, are expressed as

$$U_G = \frac{dL'}{dt} = U_L - U_t \text{ and } U_c = 1/2\ (U_L + U_t) \tag{7}$$

respectively. L' represents the longitudinal length of the bursts. The experimental results obtained in this study give $U_G \approx .66U_e(x)$ and $U_c \approx .64U_e(x)$ as compared to $U_G \approx .38U_e$ and $U_c \approx .69U_e$ from the Schubauer and Klebanoff data.

Figure 20 illustrates the reported geometrical shape of a burst along with the downstream growth envelope. From the figure, one can easily derive a relation between the half-angle of the growth envelope, α, and the interior wedge angle of the bursts, θ, given as

$$\tan \alpha = \left(\frac{U_L - U_t}{U_c}\right) \tan \theta \tag{8}$$

Again for comparison, the test data gives $\tan \alpha \approx 2.13 \tan \theta$, while the Schubauer and Klebanoff data gives $\tan \alpha \approx .76 \tan \theta$.

To examine more carefully the burst geometry along with the growth features, some measurements were made with two microphones mounted at the same downstream distance from the leading edge but with a spatial separation transverse to the flow. This was done in order to observe the width of a burst as well as to compute the interior wedge angle θ. Figure 25 shows oscillographs for a range of intermittencies for two pressure transducers separated in the transverse direction to the flow by 17/32 inch. It is seen that most bursts pass simultaneously over both flush mounted pressure transducers separated by this distance. A few fairly short bursts are noticed to have passed over only one transducer. Figure 26 shows oscillographs for a range of intermittencies for two transducers with 1-1/8 inch transverse separation distance. For this transverse separation slightly more variation is detectable between the burst signatures at the two transducers. Some differences are detectable between the arrival and departure times of the bursts at the two transducers and several bursts are noted which pass over only one transducer. Figure 27 shows oscillographs of the signals of transducers with 2-1/4 inch transverse separation distance. Now a large degree of independence is seen between the two signatures.

By measuring the time difference, Δt_L, between the detections of the leading edge of a burst as observed by two microphones with Δz transverse separation distance and at identical downstream distances, the interior wedge angle can be computed. The equation is

$$\tan \theta = \frac{1}{U_L} \frac{\Delta z}{\Delta t_L} \tag{9}$$

From data taken from selected burst, clearly identified as coincidental to both microphones, the angle θ was computed as $10^\circ \leq \theta \leq 15^\circ$ and in reasonable agreement with Schubauer and Klebanoff which observed $\theta \approx 15^\circ$.

By examining Equation (8) for the angle α, the maximum growth angle is computed as $\alpha \approx 30^\circ$ compared to $\alpha \approx 11^\circ$ from the earlier study. This clearly indicates a smaller width of transition than was found in the Schubauer and Klebanoff experiments. This is in disagreement with the empirical relation established by Dhawan and Narasimha [8] which predicts increasing width with increasing Reynolds number.

Probability Distributions of the Burst Period

When observing the distribution of burst periods in an oscillograph record from a microphone at position P, some insight can be gained on the spatial origin of the burst formation at points P_o since the convective and growth velocities are constants along the downstream path. For an isolated burst, a relationship can be derived for the upstream origin x_o which is

$$(x_m - x_o) = 1/2 \frac{U_c}{U_G} \left(\frac{U_t}{U_c}\right) U_e\ (\tau_B)_{max} \tag{10}$$

where x_m is the microphone position. By neglecting the slight variation in $U_e(x)$, the burst period at the centerline of the burst $(\tau_B)_{max}$ is proportional to the propagation distance that the burst has travelled. However, it should be noted that a burst with period τ_B detected at point P can be either,

a. An isolated burst originating exclusively at point P_o,
b. the merging and interacting of two or more bursts originating at different spatial positions, or
c. the superposition of two or more bursts with non-detectable separation times.

Furthermore, by observing an oscillograph record of the intermittent pressure field one cannot distinguish between τ_B, the burst period along an arbitrary section of the wedge shaped burst, and $(\tau_B)_{max}$, the centerline period.

Figures 28 and 29 show the distributions of the frequency of occurrence ratios for bursts of different periods. The frequency ratio, $\frac{n}{N}$, is defined as the ratio of the number of bursts, n, of a given period, τ_B, with that of the total number of bursts, N, observed during a finite time sample T. In each figure, the values of n were tabulated for a range of $\Delta\tau_B$, i.e., n values were determined for $\tau_B - \frac{\Delta\tau_B}{2} < \tau_B < \tau_B + \frac{\Delta\tau_B}{2}$, where $\Delta\tau_B = .0025$ seconds. The distribution shown in Figure 28 was determined from a set of 455 bursts over a continuous 33.7 second oscillograph record of the intermittent pressure field which had an intermittency factor of $\gamma = .227$. It was found that subsets of N=150 bursts provided reasonably good approximations to these distributions. Figure 29 shows that when the intermittency value has more than doubled to a value of $\gamma = .468$, the general features of the distributions do not change significantly. At the higher intermittency levels a noticable increase in some large burst periods is observed possibly indicated more frequent occurrence of merging of bursts. In both cases shown, the distributions of τ_B are not symmetric about the mean burst period, $\bar{\tau}_B$. In Figure 28 equations of the general form of a Poisson and Rayleigh distribution function are shown which approximately fit the experimental results.

Figure 30 shows the variation of average burst period, $\overline{\tau_B}$, with intermittency factor, γ. It is noted that if one neglects some data points, τ_B is approximately constant at low levels of intermittency. (However, closer inspection of the data in Table 3 indicates that for those data runs with pairs of microphones with a streamwise separation, τ_B always increases slightly with increasing intermittency.) As γ increases above a value of $\gamma \approx .7$, τ_B increases rapidly towards the limiting value which equals the record period since the boundary layer becomes fully turbulent at $\gamma=1$.

It should be noted that the length of the burst, L', is related to the burst period, τ_B, by the expression $L'=U_c\tau_B$. Therefore, the data also represents the variation in the average burst length $\overline{L'}$ at fixed position P.

The measured values of the burst rate f_B are shown in Figure 31 for the range of γ values. Again, neglecting some data points, the number of bursts per second, f_B, is seen to increase linearly with increasing γ, reach a maximum of about 30 bursts/second at $\gamma \approx 0.7$, and then decrease to zero as the bursts merge into fully developed turbulent flow at $\gamma=1$. Table III summarizes some of the results plotted in Figures 30 and 31.

Using the definition of intermittency, one can show that at some point P

$$\gamma(P) = \frac{\sum_{i=1}^{N} \tau_{B_i}}{T_{total}} = \frac{\overline{\tau_B}\, N}{T_{total}} = \overline{\tau_B}\, f_B \qquad (11)$$

hence

$$\overline{\tau_B} = \gamma(P)/f_B(P). \qquad (12)$$

This equation leads to the interesting observation that, when the burst rate varies linearly with the intermittency, the average burst period τ_B remains constant. At low levels of intermittency, the weak dependence of τ_B on γ displayed in Figure 30 and the approximate linear variation of f_B with γ in Figure 31 is consistent with this observation.

These results seem to give some support to the argument that during the initial stage of the burst growth, prior to the merging of the bursts, new bursts are being generated at a uniform rate with increasing downstream distance. However, until more refined data is obtained, one cannot rule out the possibility that bursts are being generated at fixed locations on the plate, e.g., where slight protuberances exist and that the burst rate increases with increasing speed.

Measurements of Mean-Square Pressure of Bursts Signals

Figure 32 shows the ratios of the mean-square values of the intermittent pressure field to the reference level at which the boundary layer just becomes fully turbulent ($\gamma=1$). The signals were passed through a 1500 Hz (6 dB down) high pass filter before the RMS values were measured, to remove vibration induced noise components. However, the RMS ratios shown in Figure 32 did not change significantly when the measurements were repeated without the high pass filters. This data can be seen to satisfy, reasonably well, the relation [19],

$$\overline{p^2}\,(\gamma) = \gamma\, \overline{p^2}\,(\gamma=1) \qquad (13)$$

4.3 Probabilistic Model of Transition Bursts

Emmons [27] has developed a statistical theory related to the prediction of the intermittency $\gamma(P)$ measured at a point P due to velocity burst formation at points P_o upstream of P. Assuming the existence of a source density function $g(x_o,z_o,t_o)$, Emmons [27] and Steketee [28] derived the relation

$$\gamma(P) = 1 - \exp\left[-\int_R g(P_o)\, dV_o\right] \qquad (14)$$

where $dV_o = dx_o\, dz_o\, dt_o$ and the integration is performed for all points lying in the cone which defines the domain of dependence or volume R of point P. Emmons considered the case when g=Constant. Narashimha [29] assumed that burst can be generated in a restricted region along a line perpendicular to the flow and assumed $g(x_o)$ can be approximated by Dirac's delta function. Emmons' statistical analysis allows one to predict the numbers of bursts per second and average burst period along with other burst features.

Inherent in Emmons' analysis is the requirement for experimental data on the propagation and geometrical features of the bursts. The data presented in this paper partially fulfills this requirement. The authors are currently attempting to use the Emmons' model, along with experimental data to resolve the question of the nature of the spatial distribution of the burst formation, or more explicitely, to derive or confirm an expression for the source density function g.

4.4 Spectral Features of Transition Bursts

For a stationary random process the mean square of the wall pressure $\overline{p^2}$, (shown versus γ in Figure 32) is related to the pressure spectral density $2\Phi(f)$, by the relation $\overline{p^2} = 2\int_0^\infty \Phi(f)\, df$, where we integrate over positive values of frequency f.

Measurements were performed of the physically realizable power spectral density denoted by $2\Phi(f)$, employing a digital spectrum analyzer.

Spectra of Intermittent Pressure Field

Figure 33 shows the power spectral densities of the wall pressure field, measured with the flush mounted 1/8 inch pinhole microphone for some of the data runs of Table III, over the range of intermittency factors from zero (no turbulence) to 1 (fully turbulent flow). These power spectral densities were determined for an averaging time which included many alternations of the calm and turbulent burst regions in the intermittent flow which passed over the measuring point on the plate surface. These results indicate that once turbulent bursts occur, even though comprising a small fraction of the total averaging time of the data sample, the power spectral density of the pressure field jumps some 30 dB, or more, above that of the laminar boundary layer. As the intermittency factor increases, the spectral densities increase systematically to the maximum value at the fully turbulent condition.

To obtain a measure of the stationarity of the process associated with the intermittent pressure field, the spectral density computations were repeated for four or more different, non-overlapping, 3.2

second time periods for each value of the intermittency factor shown in Figure 33. At each value of γ, the maximum spread, Δ, in the values of the spectral density determined for the different data samples is shown in Figure 33.

Spectra of Turbulent Burst Region of Intermittent Pressure Field

Figure 34 indicates the range of the spectral densities measured for the turbulent portion of the intermittent pressure field over the range of intermittencies from 0 to 1. These spectra were determined by the digital analyzer which triggered its sampling process on each of 64 consecutive bursts of the intermittent pressure field and graphically displayed the average of the 64 individual power spectra. Each of the 64 spectra was determined by the analyzer for an averaging time of .0125 seconds. Since this averaging time is significantly less than the average burst length (see Table III, Chan 6-data) the spectra in Figure 34 represent the frequency distribution of the energy in only the turbulent regions of the intermittent pressure field. As can be seen from the figure, the spread in the spectra was less than 2 dB over the range of intermittency factors. This result, together with those of Figure 32, indicates that the average fluctuation amplitudes in the intermittent wall pressure bursts remain essentially constant after burst generation and equal to those in the fully turbulent boundary layer. In addition, although the pressure bursts have been found to grow in streamwise length as they convect with the flow, there is no apparent change in the frequency distribution of the energy with changing intermittency factor. Future improvements in the plate's low frequency vibration levels below 1 kHz and in the equipment high frequency response should permit detection of any subtle changes in shape of pressure burst spectra as well as any low frequency periodic oscillations in the calm regions between bursts.

The fully turbulent wall pressure spectral densities compared well with those of other investigators when non-dimensionalized in terms of ρ, δ^*, and U_∞, and displayed as a function of a Strouhal number $\frac{f\delta^*}{U_\infty}$.

5. SUMMARY AND CONCLUSIONS

A flat plate test fixture was carefully designed to provide laminar-turbulent flow under a controlled environment in a newly completed Anechoic Flow Facility. Unique measurements were made on the wall pressure fluctuations to give insight on the natural transition process and extend the pioneering work performed at the National Bureau of Standards. The primary effort of this investigation was directed in obtaining the spatial, temporal and spectral features of the bursts erupting during the natural transition process.

The laminar flow along the flat plate, prior to the transition process, was measured and found to be in agreement with that predicted by the boundary layer equations for the case of a mild favorable pressure gradient. The pressure gradient significantly delayed the onset of transition and resulted in the transition Reynolds number three times larger than those in a zero pressure gradient environment. Furthermore, it appeared that the first stage of the transition process was noticably affected by the pressure gradient. For this stage, at low flow speeds ($U_\infty \approx 100$ fps) the boundary layer computations, supported by some stability considerations, indicates that the Tollmein-Schlichting waves are initially disturbed, grow to finite amplitude, and then damped out further downstream. At higher flow speeds ($U_\infty \approx 160$ fps), the T-S waves grow to finite amplitude and subsequently cause the burst generating mechanism, characteristic of the second stage of transition, to occur causing the complete natural transition process.

The detailed features of the propagating bursts erupting in the boundary layer were obtained by measurements of the wall pressure signatures. Oscillograph records of the microphones, after filtering the plate's vibration below the 2500 Hz range, clearly displayed the intermittent nature of the bursts. Simultaneous records are included for microphones positioned both in the longitudinal and transverse positions. The computations of the spatial features include the convective velocity, U_c, burst growth rate, U_g, growth angle, α, and interior wedge angle, θ. These are in qualitative agreement with the data obtained at NSS for the bursts in the velocity field allowing for differences which exist since the pressure gradient environment for both experiments are not identical.

The probability distributions of burst periods were obtained from the records and computations of the intermittency, γ, average burst period, T_p, and burst frequency f_p were performed. Some insight has been gained on the spatial origin of the burst formation but further analytical and experimental work is required.

The measurements of the mean-square pressure of burst signals were made indicating a linear relation with the intermittency factor of the form, $\overline{p^2}(\gamma) = \gamma \overline{p^2}(\gamma=1)$. Power spectral densities of the wall pressure measurements were made for both the total intermittent signals and for the individual bursts. The results indicate that once the slightest indication of turbulent bursts occur, the power spectral density jumped some 30 dB above that of the laminar flow with essentially little change in the frequency distribution as the intermittency increases. Furthermore, the spectra of the individual bursts show that the average features of both the amplitudes and frequency distributions essentially remain constant over the full range of intermittency.

6. REFERENCES

1. C.B. Schubauer and H.K. Skramstad, "Laminar Boundary Layer Stability and Transition on a Flat Plate," NACA Tech Report No. 909, 1948
2. P.S. Klebanoff and K.D. Tidstrom, "Evaluation of Amplified Waves Leading to Transition in a Boundary Layer with Zero Pressure Gradient," NASA Tech Note D 195, 1959
3. P.S. Klebanoff, K.D. Tidstrom, and L.M. Sargent, "The Three-Dimensional Nature of Boundary Layer Instability," J. Fluid Mech., Vol. 12, 1962
4. J.G. Spangler and C.S. Wells, Jr., "Effect of Freestream Disturbances on Boundary Layer Transition," AIAA, Vol. 6, No. 3, p. 543, Mar 1968
5. F.W. Boltz, G.C. Kenyon, and C.Q. Allen, "The Boundary Layer Transition Characteristics of Two Bodies of Revolution, A Flat Plate, and an Unswept Wing in a Low Turbulence Wind Tunnel," NASA TN D-309, Apr 1960
6. E.R. Van Driest and C.B. Blumer, "Boundary-Layer Transition: Freestream Turbulence and Pressure Gradient Effects," AIAA, p. 1303, 1963
7. H.L. Dryden, "Transition from Laminar to Turbulent Flow," Turbulent Flows and Heat Transfer, Vol. V, High Speed Aerodynamics and Jet Propulsion, Editor, C.C. Lin, Princeton University Press, 1959

8. S. Dhawan and R. Narasimha, "Some Properties of Boundary Layer Flow During Transition from Laminar to Turbulent Motion," J. Fluid Mech., Vol. 3, pp. 418-436, 1958
9. L. Rosenhead, Laminar Boundary Layers, Oxford at the Clarendon Press, 1963
10. H. Schlichting, Boundary Layer Theory, 6th Edition, McGraw Hill, 1968
11. I. Tani, "Boundary-Layer Transition," Annual Review of Fluid Mechanics , 1, 169 (1969) Annual Reviews, Inc.
12. M.V. Morkovin, "On the Many Faces of Transition," pp. 1-31, Viscous Drag Reduction, C.S. Wells, Editor, Plenum Press (1969)
13. J.E. Ffowcs Williams, "Hydrodynamic Noise," Annual Review of Fluid Mechanics, Editor, W.R. Sears, Annual Rev., Inc., Vol. 1, 1969
14. E.J. Skudrzyk and G.P. Haddle, "The Physical Picture of Flow-Noise," AGARD Report No. 462, Apr 1963
15. P. Leehey, "A Review of Flow Noise Research Related to the Sonar Self Noise Problem," Department of Navy, Bureau of Ships Report No. 4110366, Mar 1966
16. G. Maidanik, "Domed Sonar Systems," Vol. 44, No. 1, JASA, pp. 113-124, Jul 1968
17. W.A. Strawderman and R.A. Christman, "Turbulence Induced Plate Vibrations: Some Effects of Fluid Loading on Finite and Infinite Plates," JASA, Vol. 52, No. 5 (Part 2), Nov 1972
18. F.H. Barnes, J.G. Burns, et al., "Natural Transition of a Boundary Layer on a Flat Plate," Aeronautical Research Council Natural Philosophy Dept., Edinburgh Univ., Nov 1965, DDC 477999
19. D.R. Blackman, Wall Pressure Fluctuations in the Laminar-Turbulent Transition Region of a Boundary Layer, Ph.D. Dissertation, Faculty of Engineering, University of Southampton, Apr 1964
20. W.P. Brownell, "A Anechoic Flow Facility Design for Naval Ship Research and Development Center, Carderock," NSRDC Report 2924, Sep 1968
21. B.E. Bowers, "The Anechoic Flow Facility - Aerodynamic Calibration and Evaluation," Naval Ship Research and Development Center Evaluation Report SAD-488-1942, May 1973
22. P.K. Chang, Separation of Flow, Pergamon Press, 1970
23. H.L. Evans, Laminar Boundary-Layer Theory, Addison-Wesley Pub. Co., Inc., p. 20, 1968
24. T.K. Fannelop, "Rapid Calculations of Boundary-Layers with Coupled Heat and Mass Transfer," AIAA, p. 1433, Aug 1966
25. R.A. Smith, Unpublished Notes, School of Engineering and Architecture, Catholic University, Washington, D.C.
26. G.B. Schubauer and P.S. Klebanoff, "Contributions on the Mechanics of Boundary Layer Transition," NACA Report No. 1289, 1956
27. H.W. Emmons, "The Laminar-Turbulent Transition in a Boundary-Layer - Part I," J. Aero Sci, 18, 490, 1951
28. J.A. Steketee, "A Note on a Formula of H.W. Emmons. Readers' Forum, Journal of Aeronautical Sciencies, Vol. 22, No. 8, p. 578, Aug 1953
29. R. Narasimha, "On the Distribution of Intermittency in the Transition Region of a Boundary Layer," J. Aeron. Sci., 24, 711-12, 1957
30. F.C. DeMetz and M.J. Casarella, "An Experimental Study of the Intermittent Properties of the Boundary Layer Pressure Field During Transition on a Flat Plate," NSRDC Report 4140, May 1973

7. ACKNOWLEDGMENT

This work was supported by the Ship Silencing Division of the Naval Ship Systems Command and performed within the Hydroacoustic Branch of the Ship Acoustics Department of NSRDC.

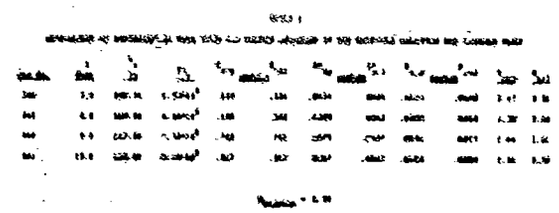

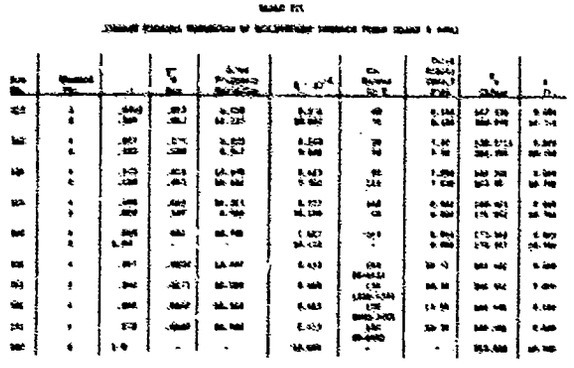

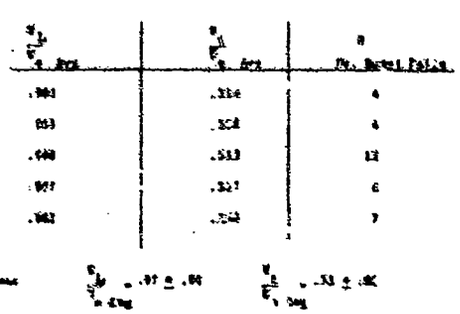

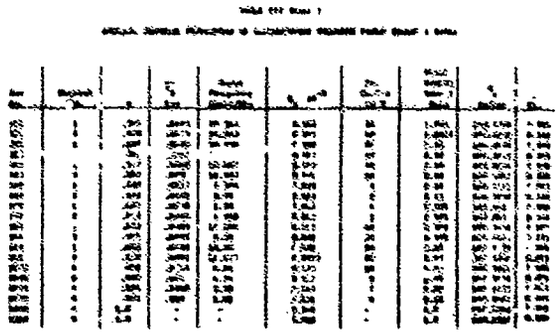

FIG. 1. BOUNDARY — LAYER DEVELOPMENT

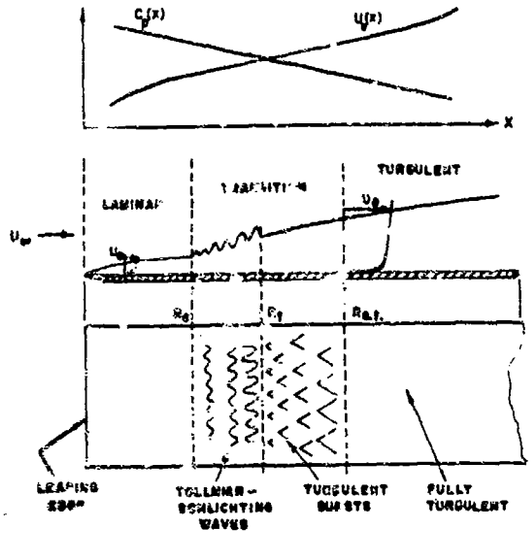

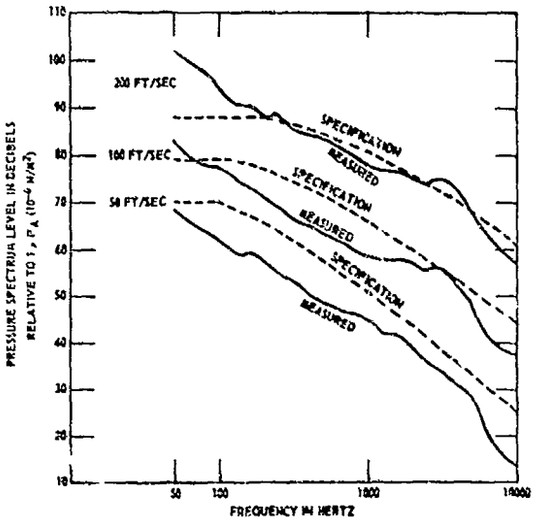

FIG. 3. ANECHOIC FLOW FACILITY CENTERLINE BACKGROUND NOISE

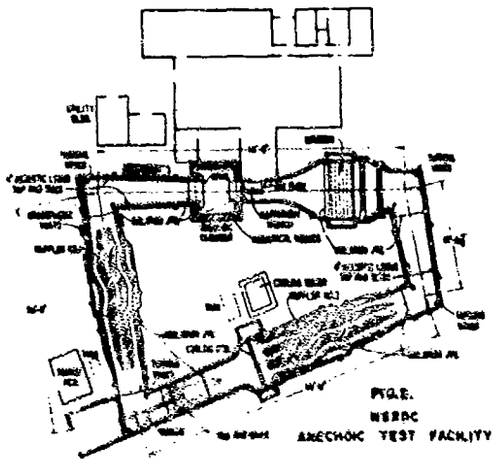

FIG. 4. PLATE VIEW FROM UPSTREAM

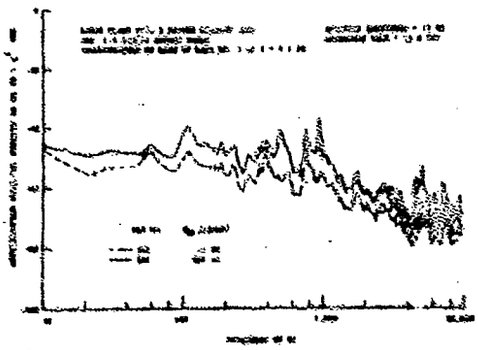

FIG. 6.

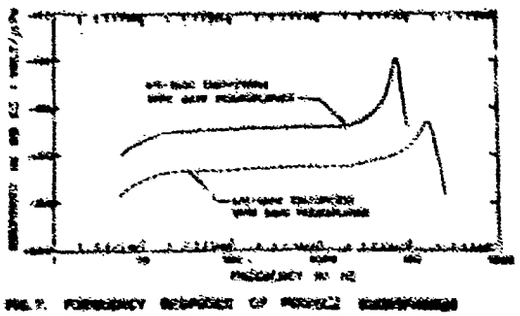

FIG. 7.

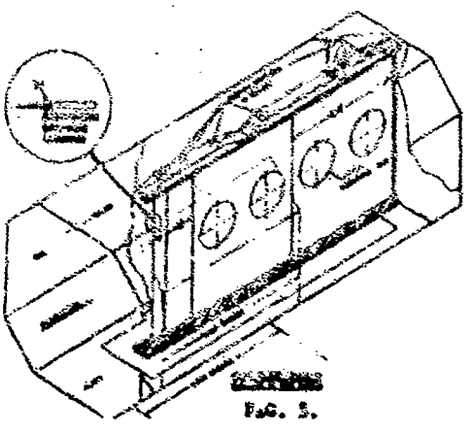

FIG. 5.

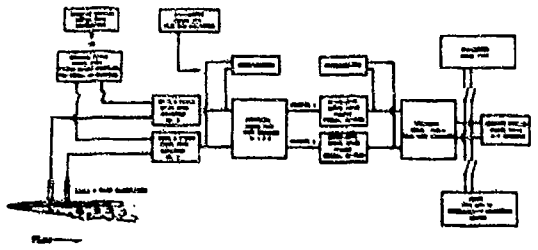

FIG. 8. SCHEMATIC OF ELECTRONIC CIRCUITRY

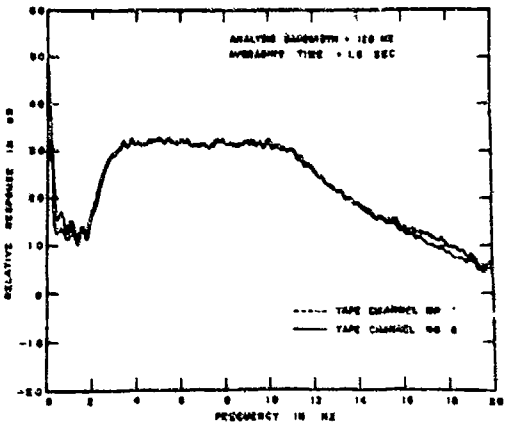

FIG. 9. FREQUENCY RESPONSE OF CIRCUITRY

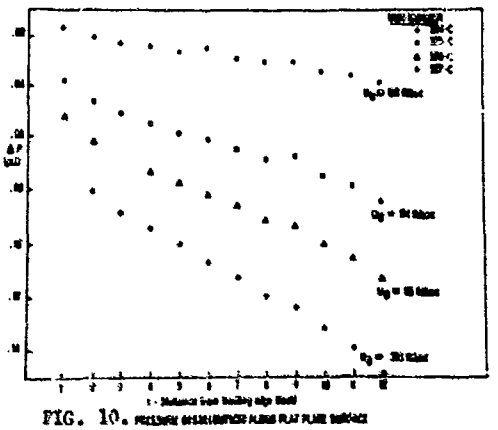

FIG. 10.

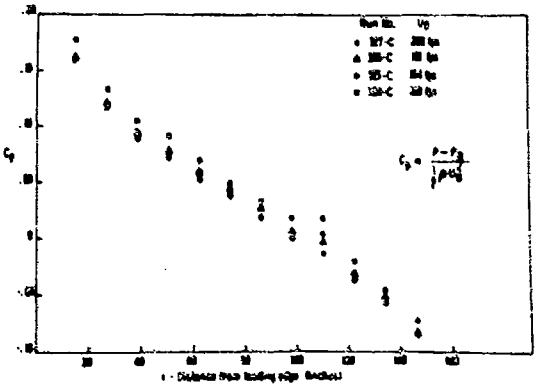

FIG. 11. PRESSURE COEFFICIENT C_p ALONG FLAT PLATE SURFACE

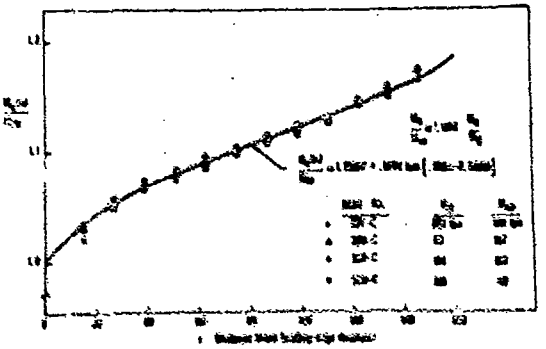

FIG. 12.

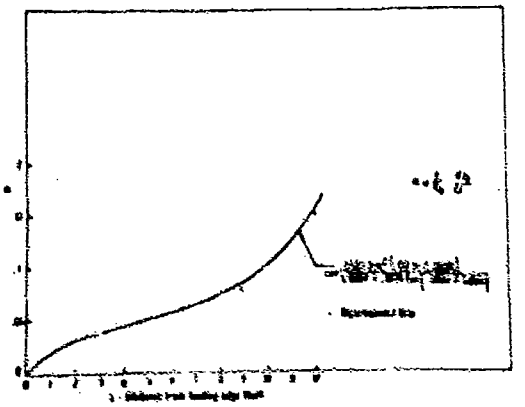

FIG. 13.

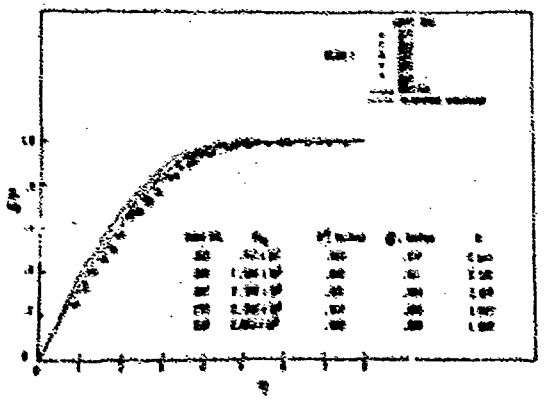

FIG. 14.

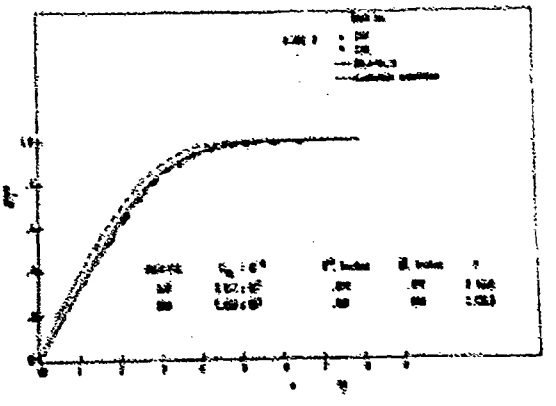

FIG. 15.

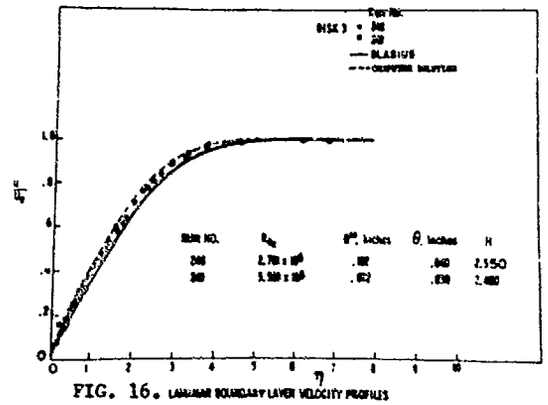

FIG. 16. LAMINAR BOUNDARY LAYER VELOCITY PROFILES

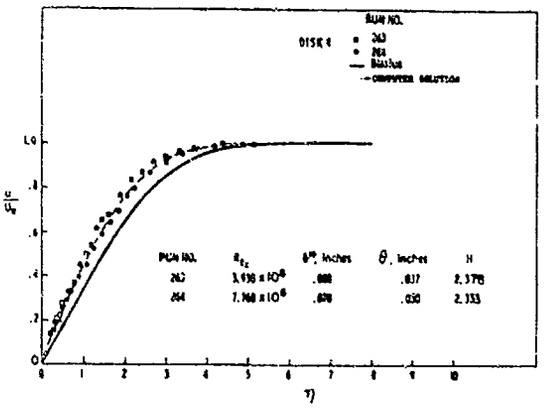

FIG. 17. LAMINAR BOUNDARY LAYER VELOCITY PROFILES

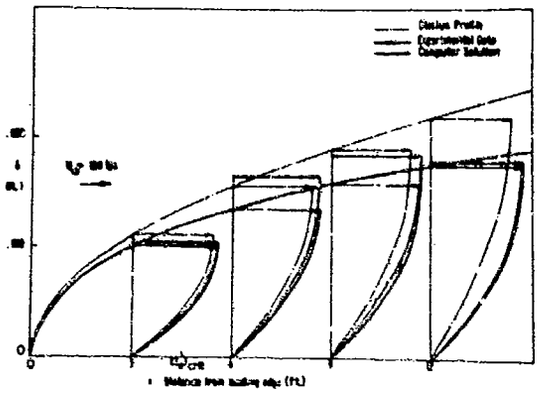

FIG. 18. BOUNDARY LAYER GROWTH AND VELOCITY PROFILES ALONG THE FLAT PLATE SURFACE

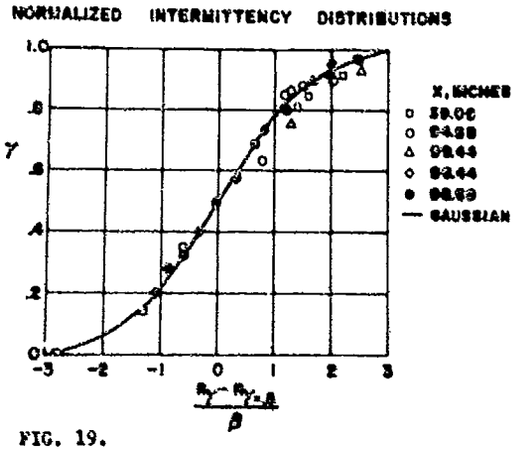

FIG. 19.

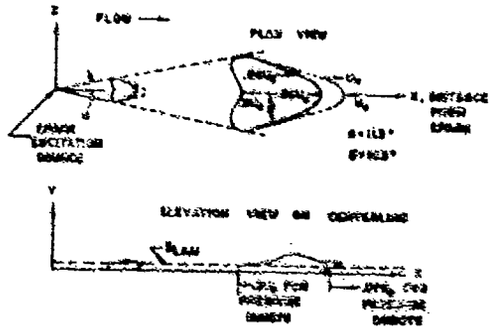

FIG. 20.

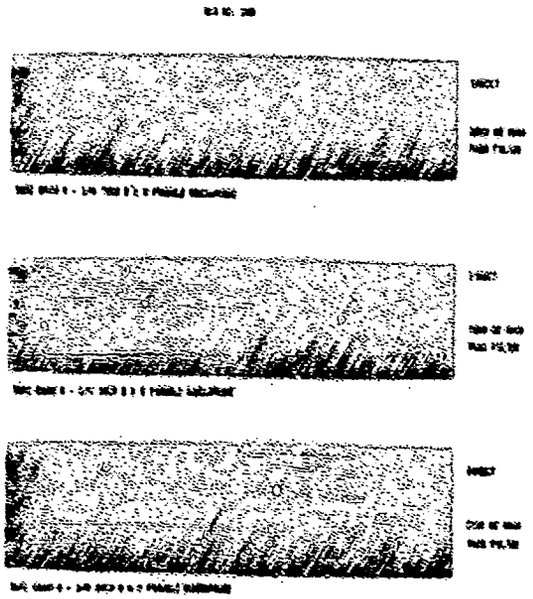

FIG. 22.

OSCILLOGRAPHS OF DIRECT AND FILTERED INTERMITTENT SIGNALS FROM MICROPHONES MOUNTED ON LARGE PLATE

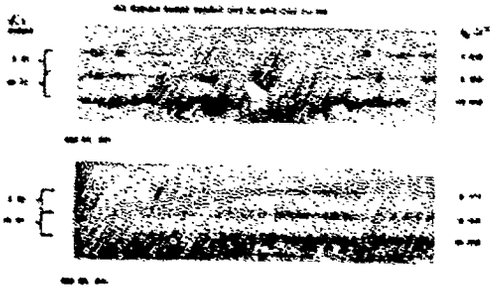

FIG. 21.

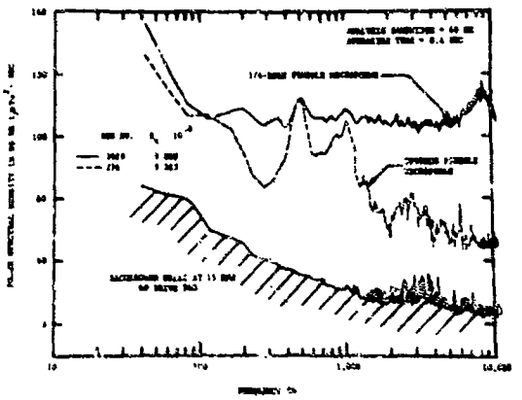

FIG. 23.

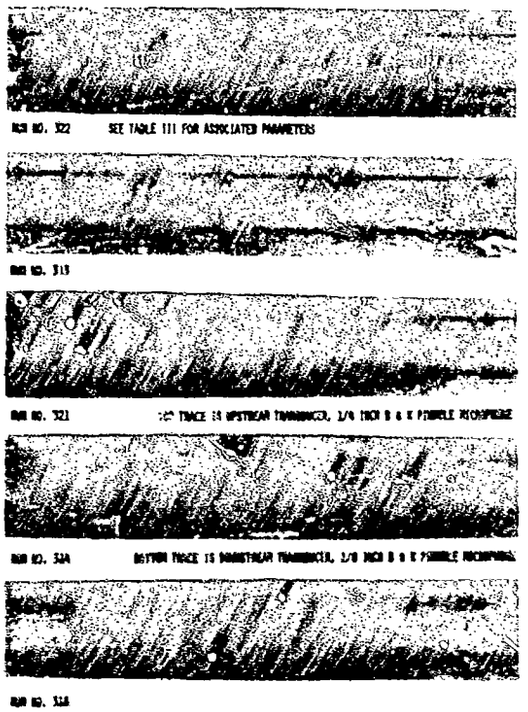

FIG. 24.

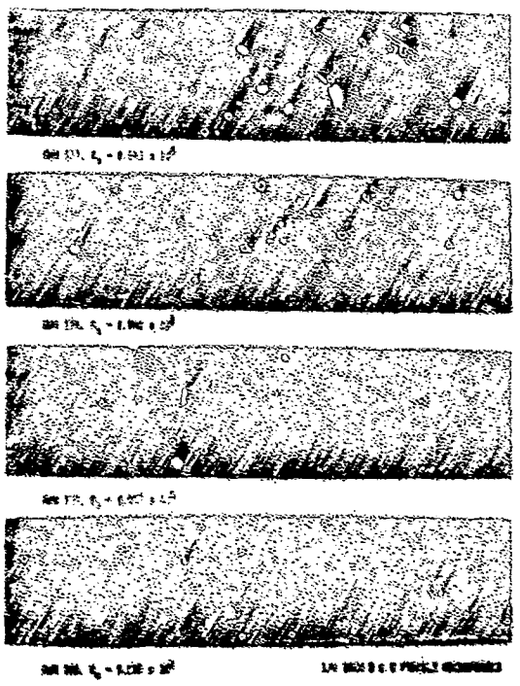

FIG. 25.

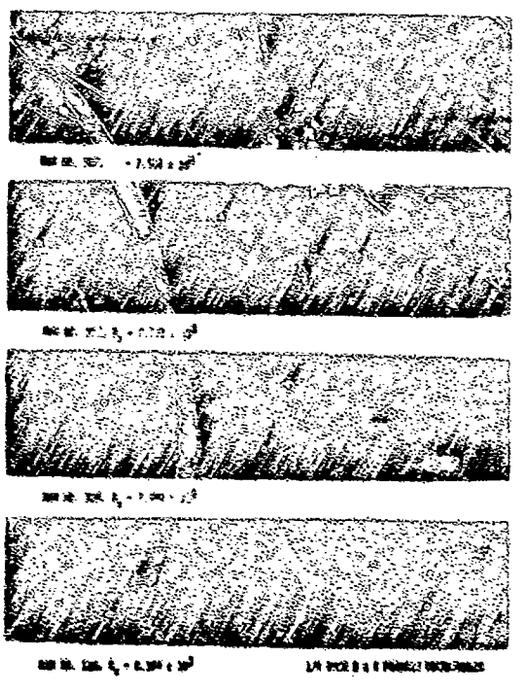

FIG. 26.

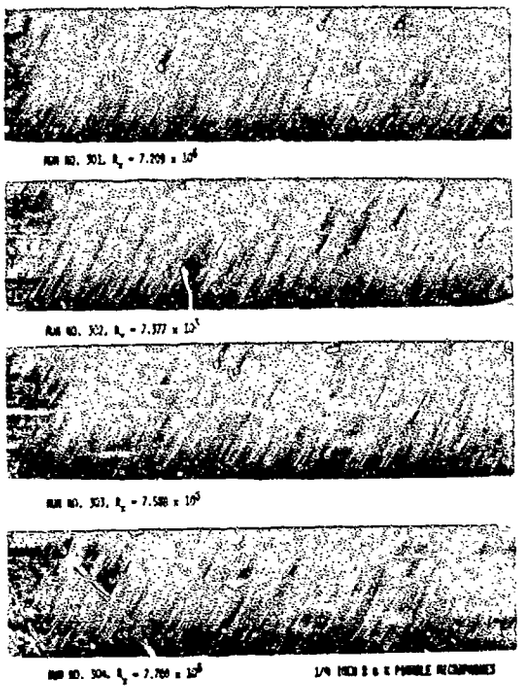

FIG. 27. OSCILLOGRAMS OF INTERMITTENT SIGNALS FROM PRESSURE TRANSDUCER WITH TRANSVERSE SEPARATION OF 7-1/4 INCHES ON LARGE FLAT PLATE

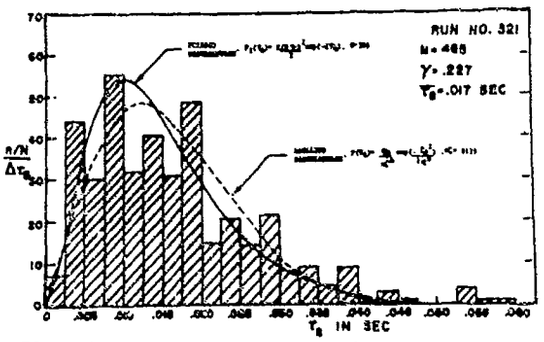

FIG. 28. BURST PERIOD DISTRIBUTIONS

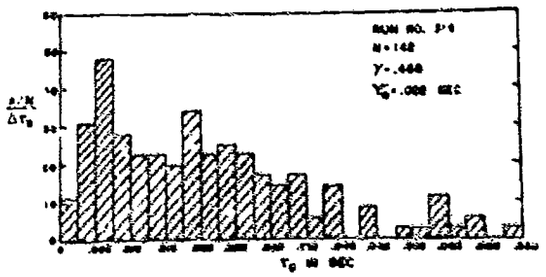

FIG. 29. BURST PERIOD DISTRIBUTIONS

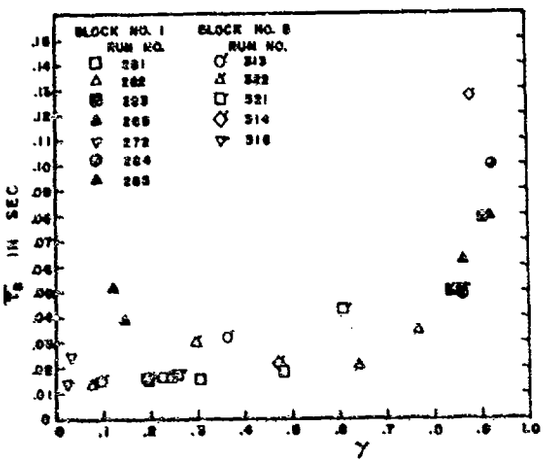

FIG. 30. AVERAGE BURST LENGTH VERSUS γ

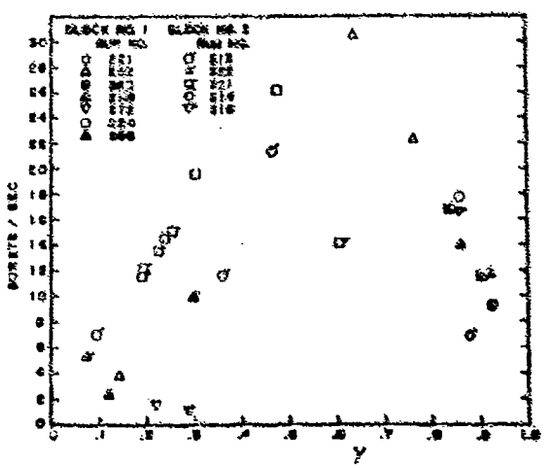

FIG. 31. BURST FREQUENCY VERSUS γ

FILTERED
EXPERIMENTAL MEAN SQUARE PRESSURE
RATIOS VERSUS INTERMITTENCY FACTOR

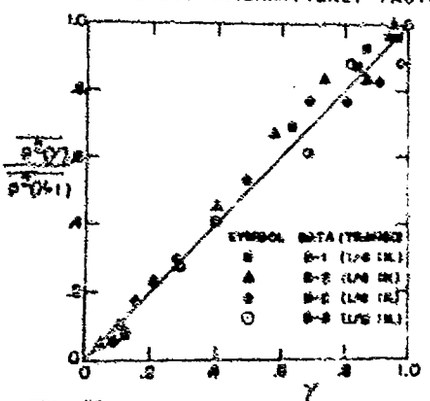

FIG. 32.

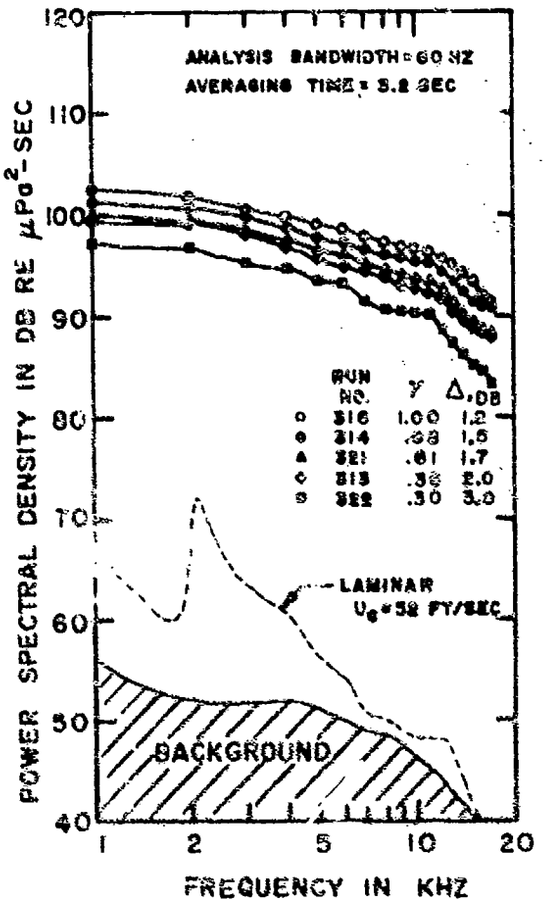

FIG. 33. POWER SPECTRAL DENSITY FOR INTERMITTENT WALL PRESSURE FIELD

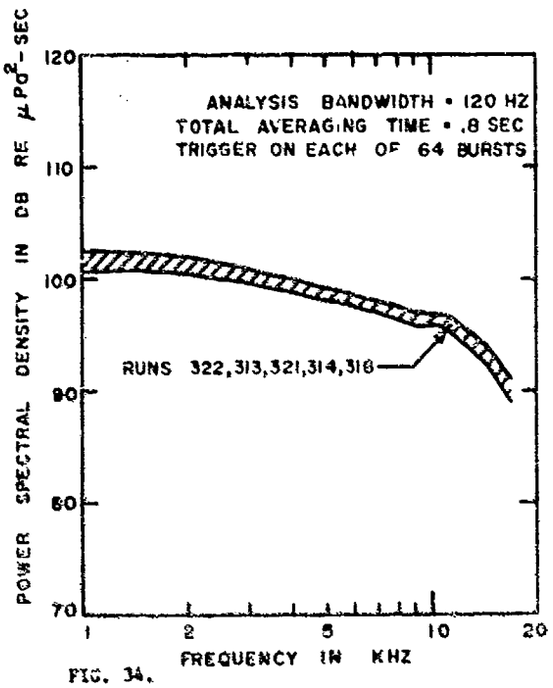

FIG. 34.

POWER SPECTRAL DENSITY OF WALL PRESSURE BURSTS

ON THE INTERACTION BETWEEN A SHOCK WAVE AND A VORTEX FIELD

A. NAUMANN [+], E. HERMANNS [++]

Aerodynamisches Institut der Techn. Hochschule Aachen

SUMMARY

In a double side shock tube the flow pattern produced by the interaction of a weak shock wave with a vortex field is observed by means of Mach-Zehnder interferograms; the vortex circulation and the pressure ratio of the shock are varied. The evaluation of the interferograms give the time dependent density fields. The deformation of the interacting shock leads to a discontinuity in slope of its front and to the formation of a secondary wave from the sharp bending point. With the assumption of linear superposition the flow pattern can be explained in a very good agreement between the theoretical and experimental results.

Introduction

Since Lighthill [1], Ribner [2,3] and Kovásznay [5] have published the first systematic investigations on the noise generated by flows, many interesting work has been done by several authors trying to explain the physical features of the noise generation. Inside of a turbulent mixing zone incoherent density disturbances are interacting with each other or with waves produced by the disturbances themselves. Such fields of pressure disturbances can be generated by velocity or temperature inhomogeneities too. Ribner [4] showed that the interaction produces secondary pressure waves, th. m. sound waves. In total these emitted pressure waves or density waves resp. represent the noise.

The process as a whole is a very complicated one; so it seems to be useful to study systematically the details. This paper reports about one example, namely the time dependent interaction between a vortex field and a pressure wave of weak intensity [11]. We feel this may be one element in the manyfold noise generation phenomena.

Without going into details we remember to the analogous experimental and theoretical investigations of Ribner [3,3,5], Hollingworth and Richards [6,7], Dosanjh and Weeks [8,9,10] a.o.

Experimental methods

The experimental equipment is a double side shock tube (fig. 1). In the left-hand high pressure part HD II a weak shock wave is excited by the bursting of the diaphragm MD II; the wave produces a kind of starting vortex at the trailing edge of a profile in the test chamber. Then in the adapted moment the interacting shock wave, which is excited in the right-hand high pressure part HD I, is running from right to left into this vortex field.

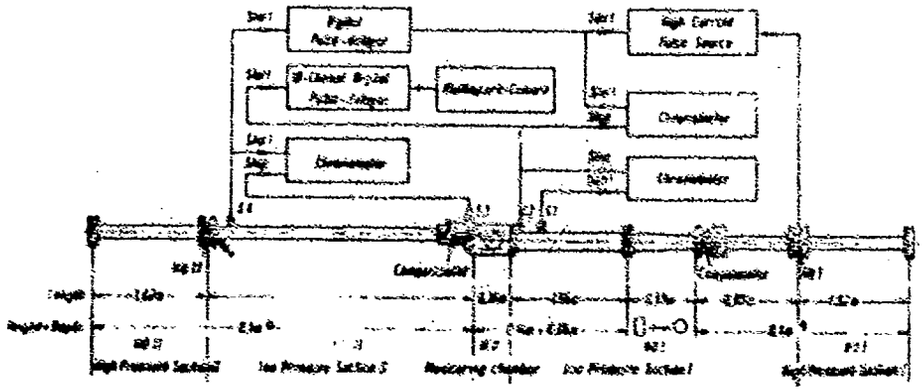

Fig. 1 Sketch of the shock tube and switching diagram of the electronic equipment

---

[+] Professor Dr., Director of the Inst.

[++] Dr.-Ing.

Fig. 2 shows the vortex and its drift from the trailing edge; on the left the trailing edge of the profile can be seen.

In order to observe the flow field and to evaluate the density field we used a Mach-Zehnder interferometer. The interferograms were taken by a high speed camera constructed in our institute. The camera is a multiple spark camera similar to the well known Cranz-Schardin system; it gives series of eight pictures with a frequency of 1 MHz; the pictures have a diameter of 5 cm each. The development and the optical and electronic calibration have been carried out by my former coworkers Dr. Hermanns and Dr. Schultz [11, 12, 13, 14, 15]. A small parallaxis of the light beams crossing the test chamber and the disposition of a high voltage circuit with an electrical energy of 200 wattseconds [14] are very important preconditions for the use of the camera. It is clear that the electronic control is one of the deciding features for the success of the testing procedure. This control concerns the exact triggering of the bursting of the diaphragms as well as the triggering of the spark camera.

Experimental results

From the great number of our interferograms a first example is shown in fig. 3. The pressure ratio of the interacting shock is 1,20. Again on the left one sees the trailing edge from which the vortex has been started. The shock wave has produced the vortex and is run out of the picture on the right side. Coming from the right the interacting shock wave reached the testing region; it is nearly plan yet. About 100 μsecs later (c) the wave becomes curved immediately before it reaches the vortex center; this happens in fig. 3 d. This moment is chosen as t = 0. Then only a few microseconds later a discontinuity in slope of the shock front occurs and from here a secondary wave is formed. This wave is considered to be a sound wave. Then this secondary wave becomes stronger; the region into which it radiates, defined by the (not exactly determinable) spreading angle φ_s, enlarges. The fig. 3f has been taken 42 μsecs and the fig. 3g 72 μsecs after the shock had reached the vortex center. The intensity of the secondary wave has its highest value at the discontinuity point, decreases gradually and disappears finally at the spreading angle φ_s dependent on the interacting shock intensity and on the vortex strength.

The characteristic experimental parameters are the strengthes of the vortex and of the interacting shock wave. The first one can be varied by the producing wave; but till now it was not possible to find a good method to measure exactly the vortex circulation (see [16]). The intensity of the interacting shock can be represented by its pressure ratio or by the shock Mach number.

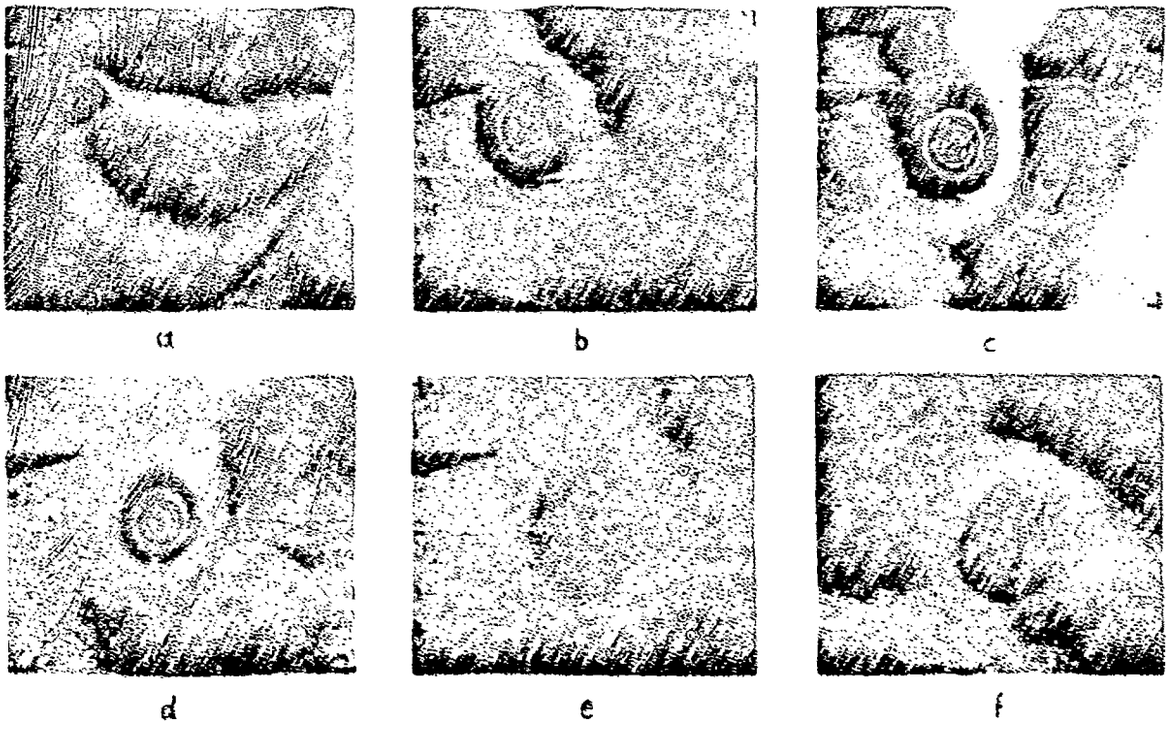

Fig. 3 Drift of the vortex, interferogram.

a	b	c	d	e	f
210	610	1110	1610	2010	2310 μs

The spreading angle φ_s seems to be mainly depending on the maximum speed in the vortex field. The amplitude of the secondary (sound) wave depends mainly on the strength of the interacting shock wave. So it was necessary to combine various vortex strengthes with various shock wave strengthes.

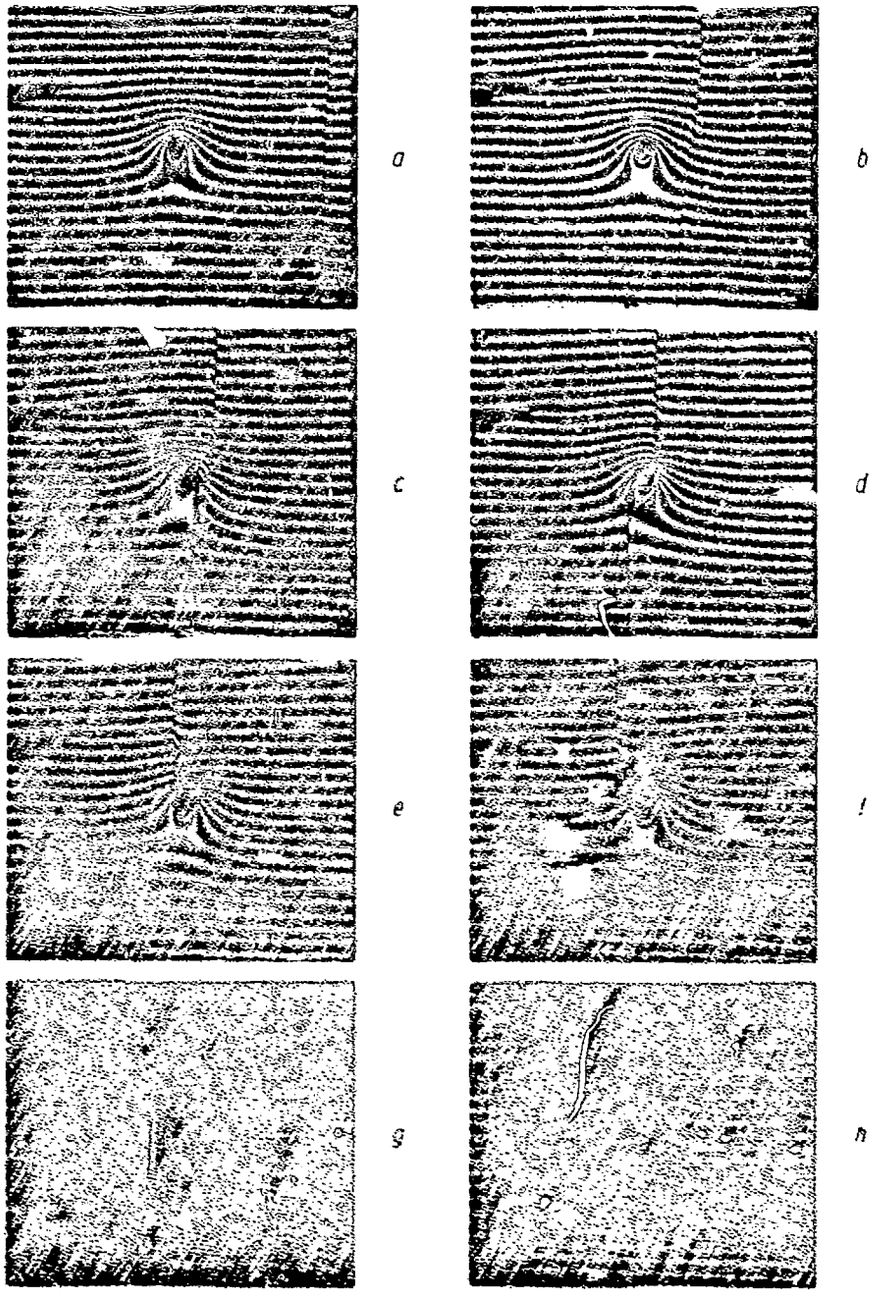

Fig. 3 Interferograms of the interaction shock-vortex.

weak vortex; $p_2/p_1 = 1,20$

a	b	c	d	e	f	g	h
-118	-38	-18	2	22	42	72	102 µs

Fig. 4 shows another example gained with an higher vortex strength and a somewhat higher shock intensity. Here the pressure ratio of the shock wave is $p_2/p_1 = 1,27$; we have the case of a weak wave in the interaction with a strong vortex. In fig. 4b the shock has reached the vortex center; in the following pictures the same history of the development of the secondary wave can be seen as in fig. 3. Without going into details it may be pointed to the much greater spreading angle of the sound wave; e.g. fig. 4e and g compared with fig. 3f and h.

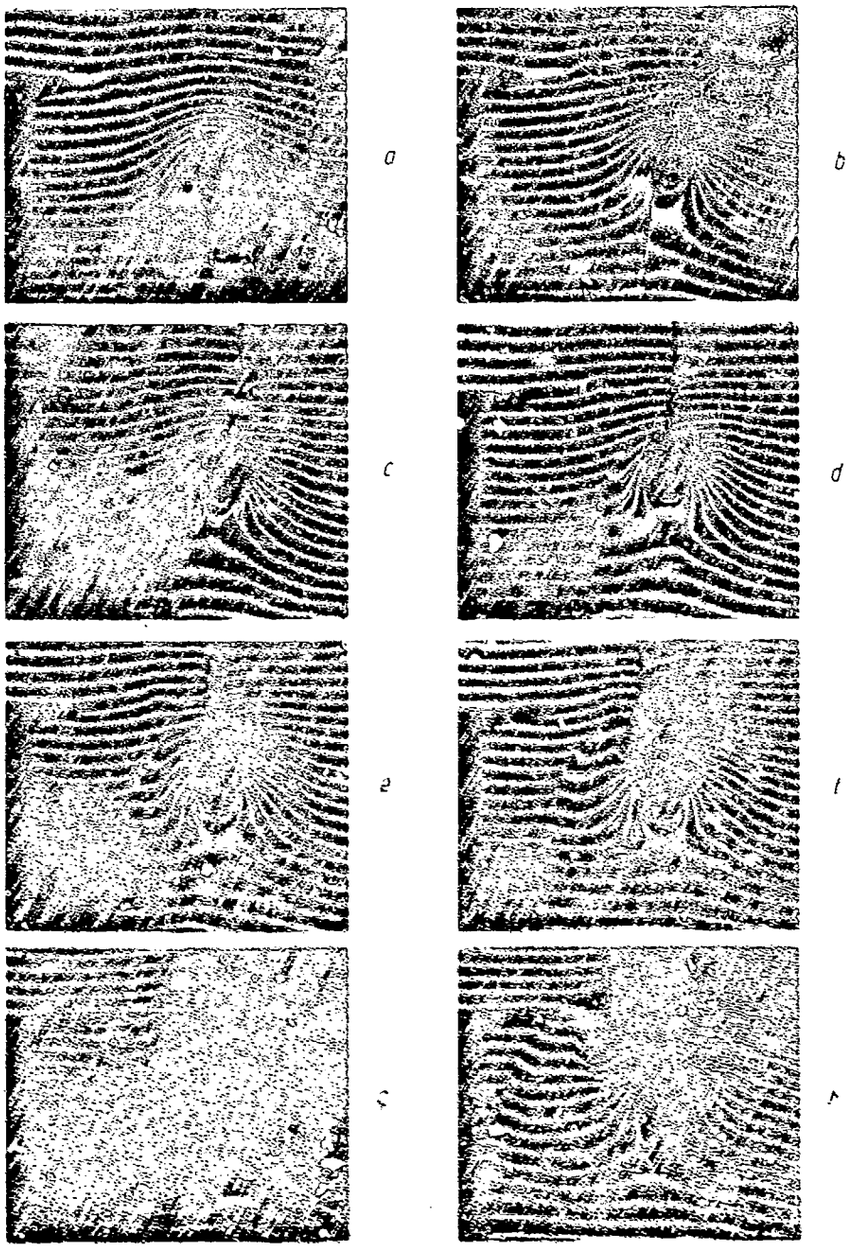

Fig. 4 Interferograms of the interaction of a strong vortex with a strong shock ($p_2/p_1 = 1,27$)

a	b	c	d	e	f	g	h	
-72	-2	18	38	58	78	98	118	µs

The quantitative evaluation of the interferograms is a hard work, because no proper device like an optical equipment combined with a digital computer was available till now. The density distribution is gained along the direction of the radii r for different azimuth angles φ (fig. 5).

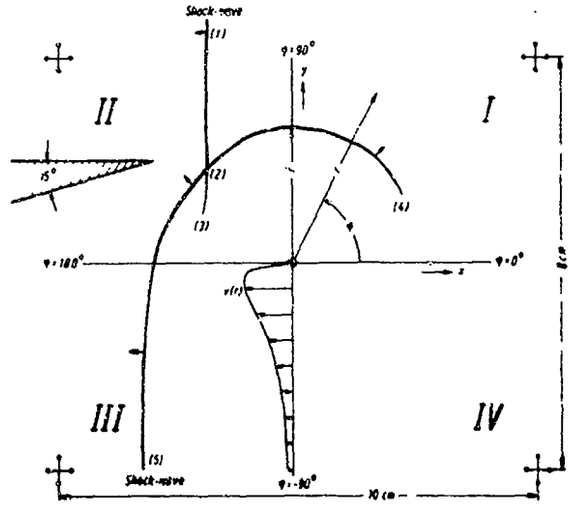

Fig. 5 Notations

The shock wave is running from the right to the left; only the half of the vortex field is drawn in; the crosses mark the field of the observation. One example for the density distribution may be shown in fig. 6; it corresponds to the fig. 4g for t = 98 µsec.

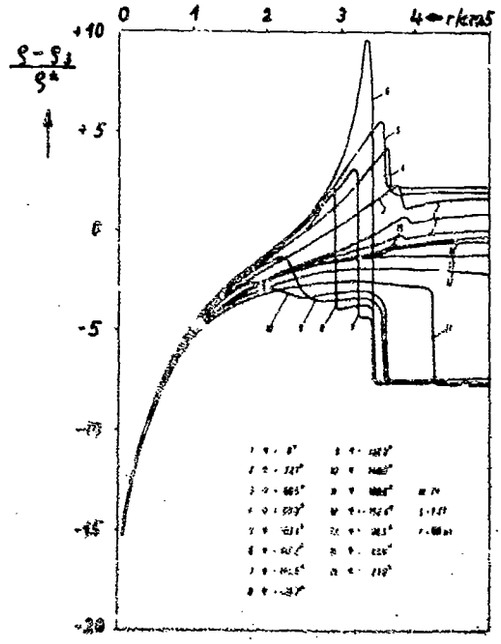

Fig. 6 Density distribution along the radius r

Because the imagination of such a complicated field is somewhat difficult, the density profiles of one serie, namely of the last shown one, have been modelled in a system; two selected cases are shown in the fig. 7 and 8. In the center one sees the depression in the vortex. Fig. 7 is taken at t = 18 µsec, th.m. immediately after the shock has passed over the vortex center. The lines represent density contour lines. The shock wave came from the direction $\varphi = 0^{\circ}$; therefore the initial

plan was parallel to the axis $-90^{\circ} \leftrightarrow 90^{\circ}$ (fig. 5). On the bending point (2) zones with different density levels come together, produced by the strong front (1), which runs against the velocity of the gas particles, and by the weaker wave (5) which runs in the direction of the flow of the vortex field. The maximum of the density discontinuity occurs at the bending point (2).

Fig. 8, corresponding to the picture fig. 4g, shows the state 80 µsecs later than fig. 7. Now the maximum of the density discontinuity takes place as a distinct peak, from which the sound wave has its origin. Between the vortex center and the wave (5) a saddle is formed in the density relief. Finally the ratio of the density jumps of the fronts (1) and (5) at the crossing point (2) is nearly three.

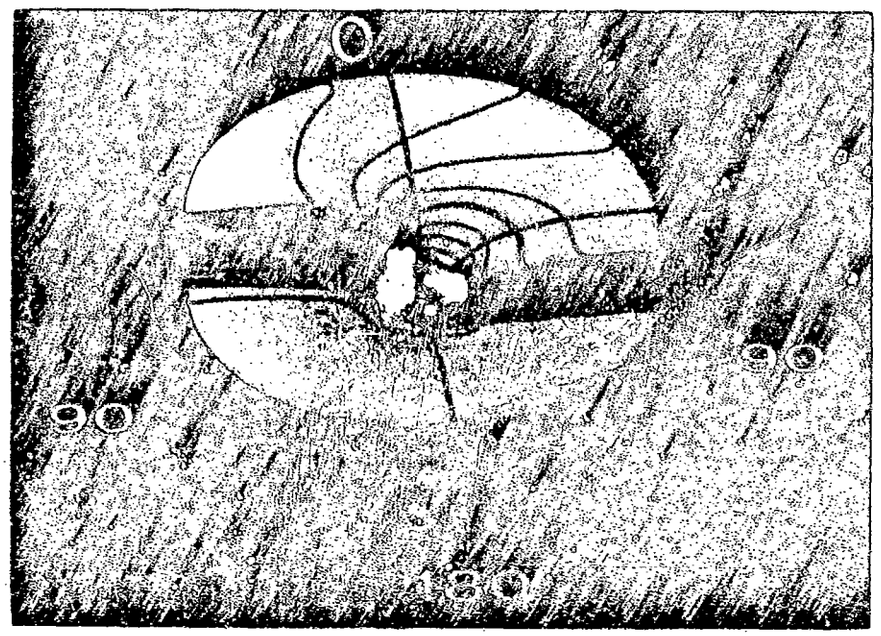

Fig. 7 Density relief $p_2/p_1 = 1,27$ $t = 18\ \mu s$

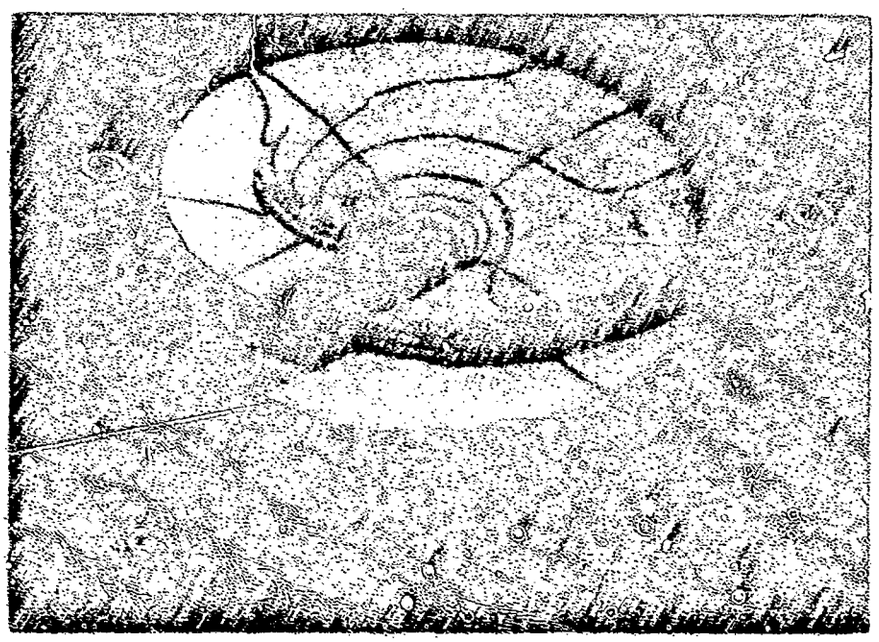

Fig. 8 Density relief $p_2/p_1 = 1,27$ $t = 98\ \mu s$

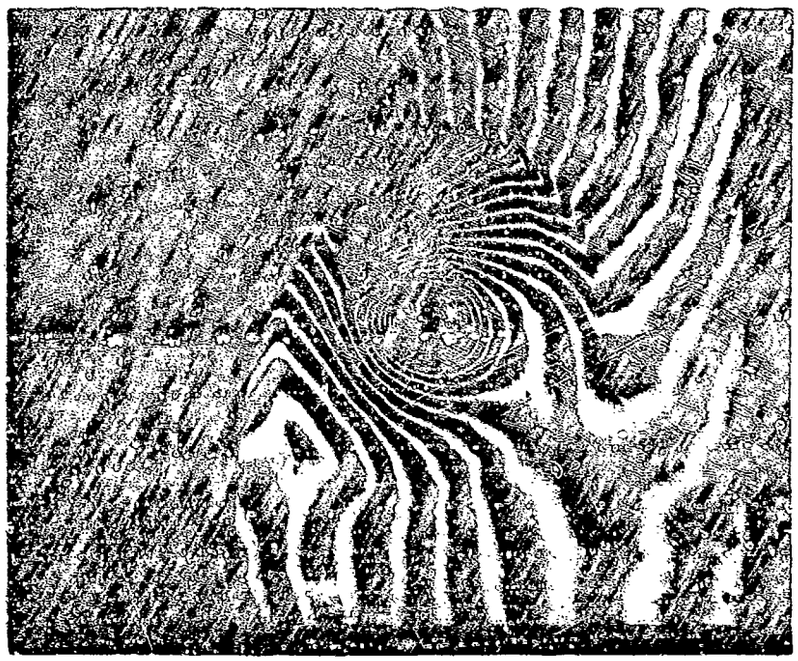

Fig. 9 Mach-Zehnder interferogram
strong vortex; strong shock wave t = 63 μsec

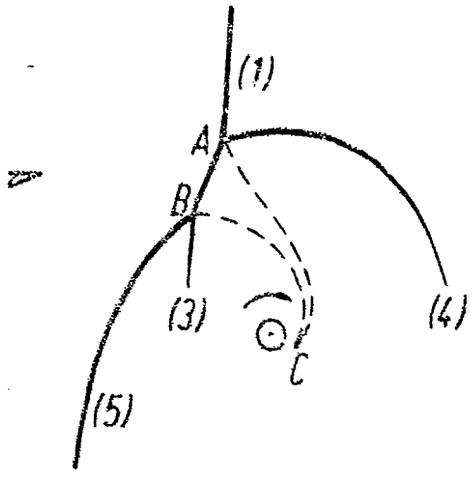

Fig. 10

With increasing shock intensity the propagation conditions of the shock and noise fronts are influenced by the convection and the temperature increase behind the shock. In the fig. 9 additional contact zones th. m. entropy discontinuities occur; they form a kind of curved funnel. This is schematically sketched in fig. 10. The interacting point A between the shock front (1) and noise wave front (4) as well as the contact point B between the fronts(5) and (3) do not coincide; but there is a front section AB which enlarges with time. The reason for this may be seen in the higher speeds downstream of the fronts (1) and (5). In the region behind AB a density decrease occurs; and the limits AC and BC have the character of entropy discontinuities, the pressure is the same on both sides, but the temperatures are different. In the zone ABC the temperature is higher and the density is lower than in the regions neighbouring with AC and BC. In this case a linearized description of the flow behaviour is inadmissible.

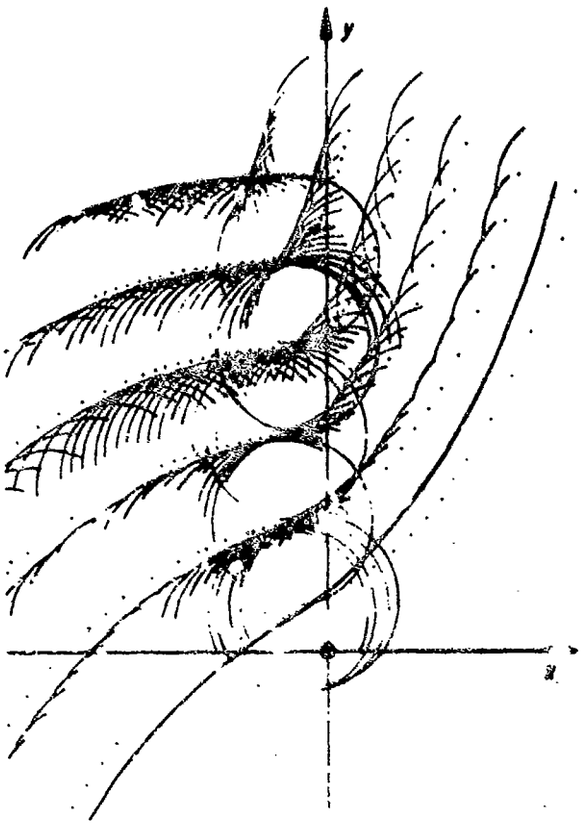

Fig. 11 Designing of the wave fronts after Huygens principle

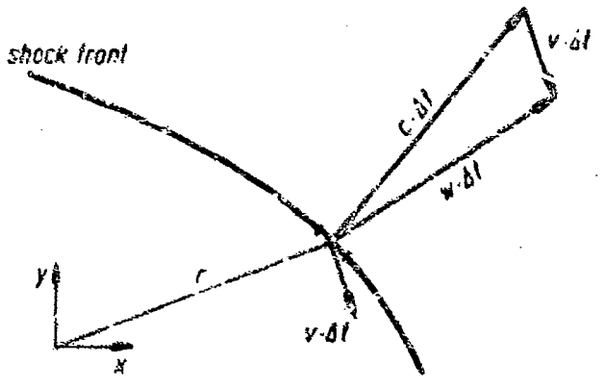

Fig. 12
c = wave speed
v = particle speed
w = propagation speed of the shock front

Physical explanation

In order to give a physical interpretation of the observations a graphic-numerical treatment was used. As the first step this was a purely graphic method based on Huygens principle; this gives no quantitative determination of the distribution of the wave insensity; but the position and the form of the shock front can be well seen as the envelop of the cylindrical elementary waves (fig. 11). Starting from an observed initial shock taken from the photos the fronts can be designed step by step. The small circle x = y = 0 is the position of the vortex center.

A more quantitative treatment becomes possible, when the propagation of a wave element and by this the time dependent deformation of the wave form is gained as the vectorial sum w of the wave speed c and the local speed v of the gas particles (see fig. 12), if one assumes incompressible behaviour of the air and a low (th. m. acoustic) wave speed, so that the linear superposition is admissible. When the end points of the pathes of the adjacent wave front elements are designed using the corresponding speeds, the position of the wave front due to the time element t + Δt is found.

An enormous number of vectorial additions is necessary; in order to obtain a sufficient accuracy this could be done by use of a computer with a high storage capacity and a high calculation velocity only.

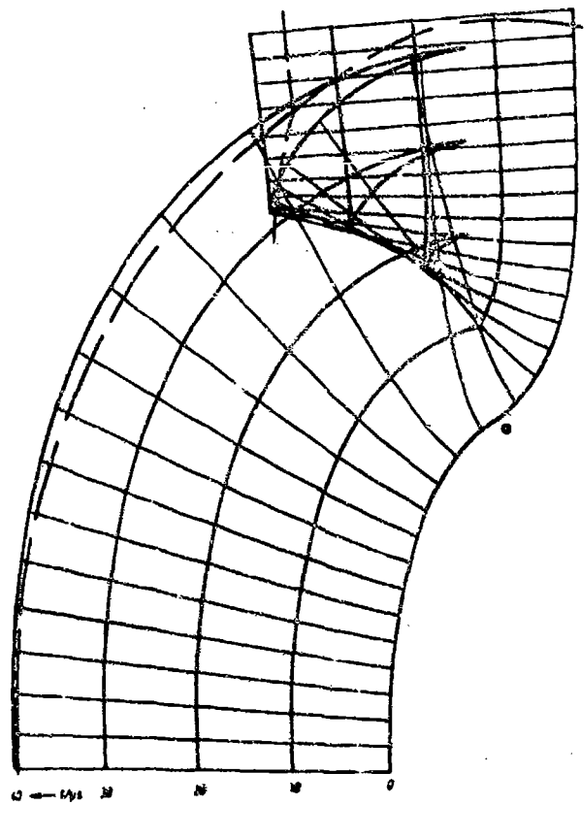

Fig. 13 Propagation of the wave front in a vortex field (corresp. fig. 3)

v_{max} = 70 m/s c = 335 m/s

Fig. 13 gives an example, calculated for the case of fig. 3; the initial values for the wave form were taken from fig. 3d, the vortex field from a measurement [16]. So we have the same initial situation as in fig. 11. The time steps are 0,25 μsec; in the diagram only each fortieth wave front and each forth path are plotted. Already after 10 μsecs the shock front shows a discontinuity in slope and two reversing points. The region between the two front sections is growing with increasing time; the divergence of the streamlines is equivalent to a decrease and the convergence to an increase of the pressure amplitude of the wave front element.

For comparison the observed shock front form after t = 40 μsecs has been drawed in; the differences are relatively small and may be caused by the simplifications mentioned above, namely the assumption of constant entropy and constant temperature in the whole field.

References

1. M.J. Lighthill — On the Energy Scattered from the Interaction of Turbulence with Sound or Shock Waves. Proc. Cambr. Phil. Soc. 49 (1953) p. 531
2. H.S. Ribner — Convection of a Pattern of Vorticity through a Shock Wave. NACA Rep. 1164 (1954)
3. H.S. Ribner — Shock Turbulence Interaction and the Generation of Noise. NACA Rep. 1233 (1955)
4. H.S. Ribner — The Sound Generated by Interaction of a Single Vortex with a Shock Wave. Univ. Toronto Inst. Aerophys. Rep. 81 (1959)
5. L.S.G. Kovásznay — Turbulence in Supersonic Flow. Journ. Aeron. Sci 20 (1953)
6. M.A. Hollingworth, E.J. Richards — A Schlieren Study of the Interaction Between a Vortex and a Shock Wave in a Shock Tube. ARC 17 (1955), 983
7. M.A. Hollingworth, E.J. Richards — On the Sound Generated by the Interaction of a Vortex and a Shock Wave. ARC 18 (1956) 267

8. D.S. Dosanjh, T.M. Weeks — Interaction of a Columnar Starting Vortex with a Propagating Shock Wave. Syracuse Univ. Rep. [illegible] 931-6411 (1964)

9. D.S. Dosanjh, T.M. Weeks — Interaction of a Starting Vortex as well as Vortex Street with a Travelling Shock Wave. AIAA Journ. 3 (1965) p. 216

10. D.S. Dosanjh, T.M. Weeks — Sound Generation by Shock-Vortex Interaction. AIAA Journ. 5 (1967) p. 660

11. E. Hermanns — Die Ausbreitung von ebenen Stoßwellen im Strömungsfeld eines einzelnen Wirbels. Thesis T.H. Aachen 1972

12. S. Schultz — Theoretische und experimentelle Untersuchungen zur Beugung von Stoßwellen. Thesis T.H. Aachen 1970

13. S. Schultz — Über die Beugung von Stoßwellen an scharfen Kanten. Abh. Aerodyn. Inst. Aachen 20 (1970) p. 31

14. E. Hermanns — Funkenentladungskreise mit Eigenfrequenzen von 2,5 und 1 MHz, elektrischen Energien zwischen 5 und 200 Wattsec und rasch abklingendem Strom. Proc. VII Int. Congr. High Speed Photogr. Zürich (1965)

15. E. Hermanns, C. Kramer, M. Maszerik, S. Schultz — Entwicklung einer Mehrfunkenkamera für Strömungsuntersuchungen. Abh. Aerodyn. Inst. Aachen 20 (1970) p. 15

16. E. Hermanns — Methoden zur Bestimmung der Zustandsgrößen in realen Wirbeln. Abh. Aerodyn. Inst. Aachen 20 (1970) p. 20

Acknowledgement

The work was carried out within the scope of a research program of the "Sonderforschungsbereich 83" sponsored by the "Deutsche Forschungsgemeinschaft".

INVESTIGATION OF THE INSTANTANEOUS STRUCTURE OF THE WALL PRESSURE UNDER A TURBULENT BOUNDARY LAYER FLOW

by

R. Emmerling, G. E. A. Meier, A. Dinkelacker
Max-Planck-Institut für Strömungsforschung
34 Göttingen, Böttingerstr. 6-8, Germany

SUMMARY

An optical method was used to investigate the instantaneous structure of the wall pressure under a turbulent boundary layer flow in air. The optical apparatus consisted basically of a Michelson-interferometer. One mirror of the interferometer was replaced by a reflecting flexible wall, which was also part of the wall bounding the flow being investigated. The turbulent wall pressure fluctuations cause the flexible wall to be displaced by several light wave-lengths. The instantaneously occurring fringe patterns were recorded with a high-speed film camera. The wall area observed was 48 mm x 29 mm (10.5 δ^* x 6.5 δ^*), and the flow velocity outside the boundary layer was U_∞ = 8.5 m/sec. The optical method used made it possible to determine the instantaneous values of the wall pressure distribution, the convection velocity and the wall pressure gradient.

LIST OF SYMBOLS

a	radius of a circular membrane
d	pressure-sensitive diameter of pressure transducer
e	distance between the circular membranes
f	frequency
f_E	resonance frequency
l	distance between the rows
p	instantaneous value of the wall pressure fluctuation
$\sqrt{\overline{p^2}}$	r. m. s. value of the wall pressure fluctuations
p_{crit}	critical pressure
$q_\infty = \frac{\rho}{2} U_\infty^2$	dynamic pressure of the free stream
u	instantaneous value of the velocity fluctuation
x	coordinate in the direction of the flow
y	coordinate normal to the wall, extending into the flow (y = 0 corresponds to the center of the flexible wall)
$y^+ = \frac{y \cdot U_\tau}{\nu}$	non-dimensional distance from the wall
z	coordinate perpendicular to the direction of flow (x, y, z form a right-hand coordinate system)
D	diameter of the flexible wall
H	characteristic measure of the flexible wall (see Fig. 6)
Re_Θ	Reynolds number, referred to the momentum thickness
$Tu = \frac{\sqrt{\overline{u^2}}}{U}$	turbulence intensity
U_∞	free stream velocity
U_τ	shear stress velocity
U_c	convection velocity
U	local mean flow velocity
Δp_{st}	static pressure difference
Δx	distance between the pressure transducers
δ	boundary layer thickness
δ^*	displacement thickness of the boundary layer
λ	wave length
ν	kinematic viscosity
ρ	density
τ_0	mean shear stress at the wall
Ω	phase angle between the driving wall pressure and the membrane displacement
ω	angular frequency
$\omega^+ = \frac{\omega \nu}{U_\tau^2}$	non-dimensional angular frequency

1. INTRODUCTION

Boundary layer pressure fluctuations are direct or indirect sources of noise in many technical applications. For instance, the noise heard inside the fuselage of an aircraft is often caused by wall pressure fluctuations outside the fuselage.

In recent investigations boundary layer pressure fluctuations were measured with the help of electromechanical transducers flush mounted in the wall adjacent to the flow. For the evaluation of these mea-

surements mean values were formed, in particular the r. m. s. value of the pressure fluctuations, frequency-spectra and - where several transducers were used - correlation functions. Table 1 gives a survey of these investigations.

Investigator	Flow medium	U_∞ [m/sec]	free stream $\sqrt{u^2}/U_\infty$ (%)	d [mm]	δ^* [mm]	$\frac{d}{\delta^*}$	$\frac{U_\tau}{U_\infty}$	U_τ [m/sec]	$\frac{d \cdot U_\tau}{\nu}$	Re_Θ	$\frac{\sqrt{p^2}}{q_\infty}$	$\frac{\sqrt{p^2}}{\tau_0}$	$\frac{U_c}{U_\infty}$ at $\frac{\Delta x}{\delta^*}$	
Harrison (1958) [1]	Air	30		2.1	2.8	1.2	0.04	1.2	248	$2.8 \cdot 10^3$	$8.5 \cdot 10^{-3}$	3.0		
Willmarth (1956) [2]	Air					1.1	0.035			$13 \cdot 10^3$	$5.5 \cdot 10^{-3}$	2.32		
Skudrzyk u. Haddle (1960) [3]	Water	6		12.5	3.8	3.3	0.034	0.22	2750	$17 \cdot 10^3$	$1.8 \cdot 10^{-3}$	0.77		
Bull u. Willis (1963) [4]	Water	6.7 5.8		4.2	2.1 0.85	2.0 4.9	0.035 0.037	0.23 0.22	965 924	$11 \cdot 10^3$ $4.3 \cdot 10^3$	$5.8 \cdot 10^{-3}$ $5 \cdot 10^{-3}$	2.4 1.8	0.7 -0.85	2-20
Willmarth u. Woolridge (1963) [5]	Air	62.2	0.08	4.1	12.5	0.33	0.0336	2.09	562	$36 \cdot 10^3$	$8.6 \cdot 10^{-3}$	2.64	0.59-0.83	0-20
Serafini (1963) [6]	Air	200	2	1.6	8 3.2	0.2 0.5	0.03 0.035	6.0 7.0	646 746	$80 \cdot 10^3$ $32 \cdot 10^3$	$7 \cdot 10^{-3}$	3.8 2.9		
Willmarth u. Roos (1965) [7]	Air	62.2	0.08	1.53 5.9	12.5	0.122 0.441	0.0335	2.03	186 713	$28 \cdot 10^3$	$5.4 \cdot 10^{-3}$ $4.7 \cdot 10^{-3}$	2.84 2.25		
Schloemer (1967) [8]	Air	34 33	0.3	1.6	3.66 3.84	0.41	0.0304 0.0367	0.95 1.24	101 131	$4.5 \cdot 10^3$ $5.5 \cdot 10^3$	$4.6 \cdot 10^{-3}$	1.46		
Bull (1967) [9]	Air	100	0.25	0.74	3.8 2.1	0.13 0.36	0.0337 0.033	3.37 3.33	158 173	$19 \cdot 10^3$ $19 \cdot 10^3$	$8 \cdot 10^{-3}$ $6.8 \cdot 10^{-3}$	2.45 2.2	0.53-0.825	0-20
Blake (1970) [10]	Air	22 50	0.75	0.79	7.85 7.1	0.101 0.113	0.0383 0.033	0.85 1.68	45 87	$6.2 \cdot 10^3$ $17 \cdot 10^3$	$10.6 \cdot 10^{-3}$ $7.6 \cdot 10^{-3}$	3.6 3.6	0.53-0.8	0-20
Willis (1970) [11]	Air	38			3.3								0.53-0.88	
Hammerling (1972) [12]	Air	6.5	<2	*0.8 3.1 9.1	4.6	0.17 0.46 1.56	0.04	0.34	16 47 203	$2 \cdot 10^3$	$10.8 \cdot 10^{-3}$ $8.3 \cdot 10^{-3}$ $8.3 \cdot 10^{-3}$	3.4 2.8 1.24	0.59-0.83	

* from Bull (1967, Fig. 7)

• measured with pinhole

Table 1. *Various measurements of turbulent wall pressure fluctuations on smooth flat walls with very small pressure gradients*

In the work reported here, a new method is described which made possible the visualization and measurement of the instantaneous structure of the wall pressure field using a mechanical-optical flush mounted transducer plate consisting of several hundred small membranes, the displacement of which is measured with the help of a Michelson-interferometer.

The objectives of this investigation were:

(a) To obtain insight into the mechanisms of the generation of boundary layer wall pressure fluctuations.
(b) To use this insight for a better understanding of the structure of boundary layer turbulence.

2. EXPERIMENTAL ARRANGEMENT AND PROCEDURE

2.1. The method

For the investigation described here an optical technique was used for the measurement of wall pressure fluctuations under a turbulent boundary layer flow. The arrangement can be seen in Figure 1. Boundary layer flow occurs in a wind tunnel which is driven by suction. The optical apparatus consists basically of a Michelson-interferometer, one mirror of which is replaced by a light-reflecting flexible wall flush mounted in a wall of the flow duct. In the investigation reported here this flexible wall consisted of an arrangement of 650 small, silver-plated rubber membranes each of 2, 5 mm diameter. The displacement of these membranes is, for a wide range of conditions, proportional to the local, instantaneous wall pressure. This displacement produces in the interferometer a fringe pattern which can be photographed with a high speed camera at about 7000 frames per second. The evaluation of the films has been done to date by hand and is very time consuming. Improvement of the evaluation technique is planned by digitising the fringe pattern and evaluating with a digital computer.

2.2. The flow arrangement

The test section of the wind tunnel has a cross section of 300 mm x 100 mm and a length of 2.4 m. In the inlet of the tunnel two sets of drinking straws were arranged as a honeycomb. The flow is driven by suction and controlled by a sonic nozzle. Great care was taken to reduce noise and vibrations in the whole arrangement (for details see Section 2.5.). Flow parameters were measured with the help of static pressure holes in the tunnel walls, with a Pitot tube and with a hot-wire probe. The measurement of the

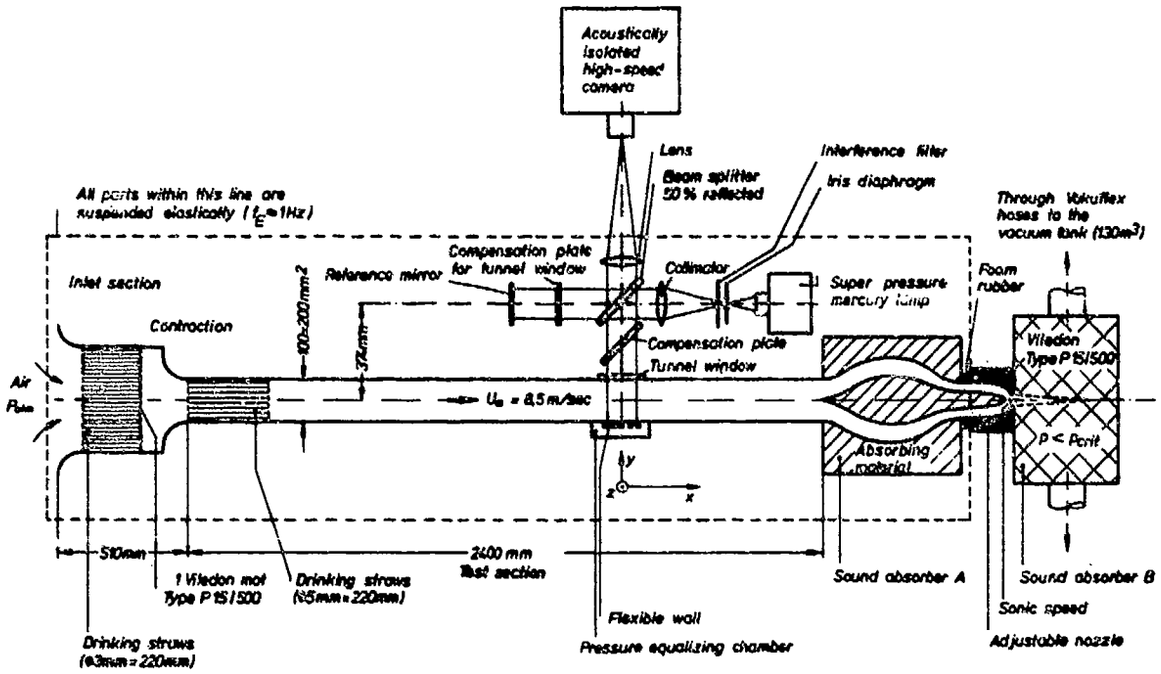

Figure 1. Schematic diagramm of the experimental facility

instantaneous wall pressure fluctuations was done with the flexible wall and occasionally also using microphones mounted flush into one of the 200 mm wide tunnel walls. The air flow investigated had a flow velocity of about U_∞ = 8.5 m/sec, where U_∞ is the velocity outside of the boundary layer. Because of the growth of the boundary layer, U_∞ increased slightly with x, causing a small negative pressure gradient (at the position of the pressure sensitive wall dp/dx = -53 µbar/m). More of the flow parameters are shown in Figures 2 to 5.

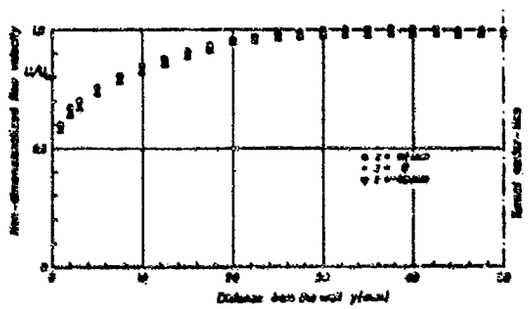

Figure 2. Velocity profiles in the test section (at x = -150 mm, measured with total pressure probe)

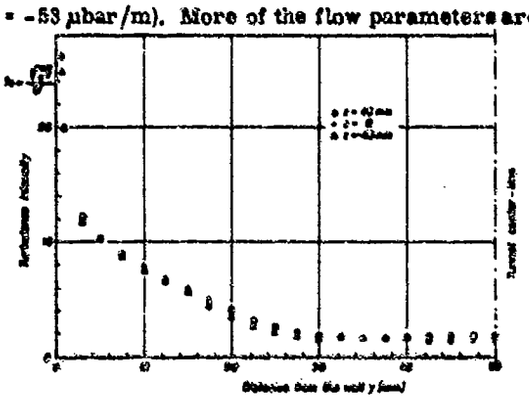

Figure 3. Turbulence intensity profiles in the test section (at x = -150 mm, measured with a hot-wire)

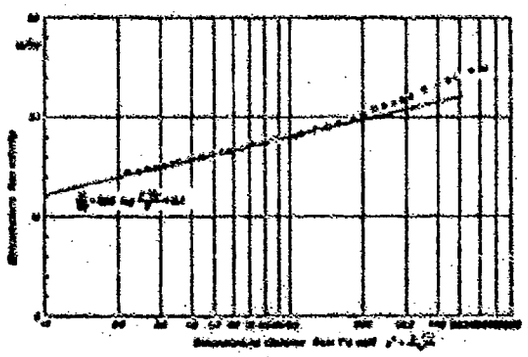

Figure 4. Velocity distribution in the logarithmic law region (x = -150 mm, z = 0)

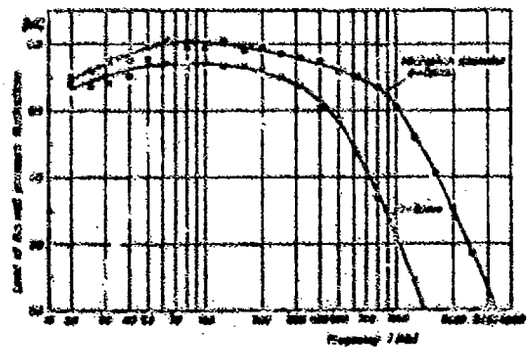

Figure 5. Frequency spectra of the wall pressure fluctuations (per 1 Hertz bandwidth, U_∞ = 8.5 m/sec, δ^{**} = 4.0 mm, 0 dB ≙ 2 · 10^{-4} µbar)

The coordinate system used here is taken so that its origin lies in the middle of the flexible wall. The positive x-axis points in the streamwise direction; the positive y-axis extends away from and normal to the flexible wall. The z-axis is perpendicular to the x-y plane, forming with them a right-hand system.

2. 3. The optical apparatus

The arrangement of the optical apparatus is shown in Figure 1. The individual parts of the interferometer are mounted on a stable steel frame. The face of the beam splitter facing the light source reflects approximately 50 % of the incident light in the direction of the pressure sensitive flexible wall section. The unreflected part of the beam passes through the finite glass thickness of the beam splitter on its way to the reference mirror where it is reflected back toward the beam splitter. Because of the small coherence length of the light used (approximately 100 μm), the reflected part of the beam must pass through a compensation plate with the same thickness and refractive index as the beam splitter in order to yield high-contrast interference fringes. For the same reason, a compensation plate is also required for the tunnel window. A 100-Watt super pressure mercury lamp served as the light source. Passing through an iris, an interference filter (λ = 0.547 μm) and a collimator (100 mm ϕ), the light reaches the beam splitter. The object to be reproduced, i. e. the pressure sensitive flexible wall, was positioned between one and two focal lengths of the objective lens.

As can be seen in Figure 1, one part of the interferometer beam passes through the turbulent flow twice. Since the refractive index of air is dependent upon density, sufficiently large pressure fluctuations can change the optical path of the beam indicating a pseudo displacement of the membrane. It can be shown [12] that at a flow velocity of 8. 5 m/sec, this disturbance is completely negligible.

Photographs of the interference patterns were taken with a high-speed camera (Fastax WF-4 m). Using 120 m film, the maximum possible frame frequency of the camera was about 9000 frames per second. The frame rate at any point on the film can be determined with the aid of timing marks (1 msec) on the edge of the film. For all experimental runs in this investigation 30 m long 16 mm films (XT-negative film, Type 7220, Kodak) were used. With this film length, a maximum frequency of 7000 frames per second was achieved which corresponds to a run time of about 1 sec.

2. 4. The pressure sensitive flexible wall

2. 4. 1. Manufacture

A schematic view of the flexible wall is shown in Figure 6. A thin silicon rubber foil (approximately 35 μm thick) is stretched across a rigid base constructed of brass which has about 550 small holes of 2. 5 mm inner diameter. The surface of the base was lapped so that the deviation from flatness across the entire surface was reduced to the order of only 1 μm.

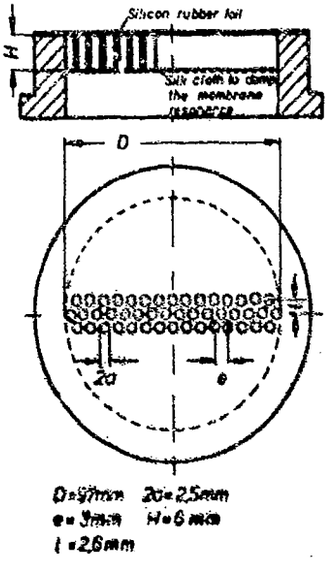

The main problem in producing these plates is obtaining a thin foil with a smooth surface and uniform thickness, accurate to within a fraction of a light wave-length. This extreme accuracy is necessary because, even without flow, a dense interference fringe picture would otherwise appear which would make determining the displacement of the membrane practically impossible. The foils used here were produced with silicon rubber (for details see [12]). To make the rubber foils light reflecting they were silvered with the help of a vacuum coating device. The thickness of the silver layer was smaller than 0. 3 μm, the light reflection factor about 70 %. The reflecting layer was also not damaged when the membrane was strained by 20 %. The pressure sensitive section was fixed in a metal ring and together with it mounted flush in the wall of the tunnel. In the symmetry axis of this ring and normal to the direction of flow, small holes were drilled (0. 4 mm ϕ) to allow for pressure equalization between the wind tunnel and the chamber behind the membranes.

Figure 6. Sketch of the flexible wall

2. 4. 2. Calibration

Static calibration of the flexible wall was done by applying a static pressure difference to the membranes. Figure 7 shows that the number of interference fringes (usually concentric rings) occurring on a membrane is proportional to the static pressure and, for the membranes used for the experiments reported here, is equal to 3. 5 μbar per fringe ring. The equality of the individual membranes can be checked in the same way. In fact the membranes of the plate used had astonishingly low inequalities.

Dynamic calibration was accomplished with a loudspeaker and two calibrated microphones. Figure 8 shows the frequency response and Figure 9 shows the phase angle Δ between the excitation force and the membrane displacement. It should be noted that the relatively flat frequency response in Figure 8 was only

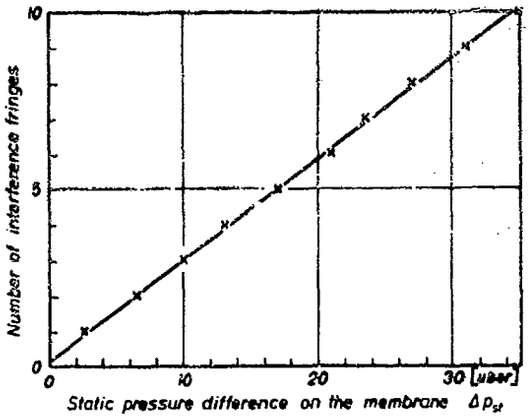

Figure 7. Relationship between the static pressure difference and the displacement of the circular membranes

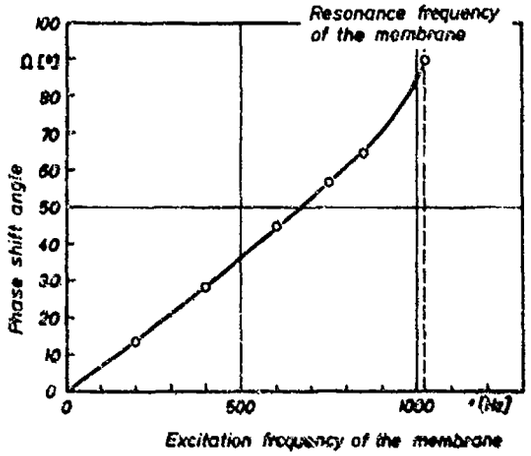

Figure 9. Frequency response of the phase angle for the flexible wall with the additional damping of a silk cloth (calculated using data from Figure 8).

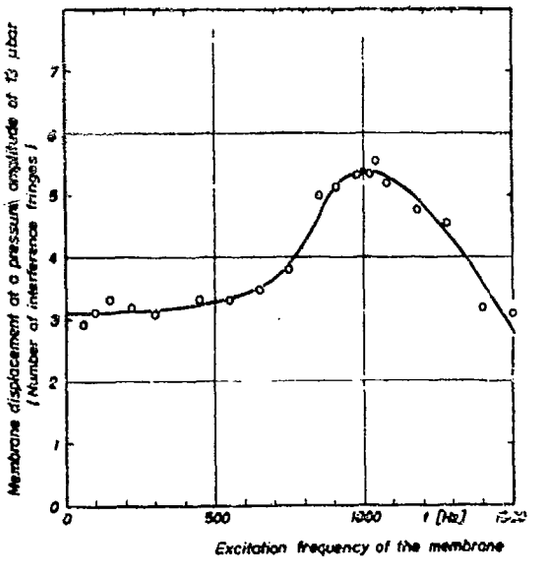

Figure 8. Frequency response of the membrane displacement for the flexible wall with the additional damping of a silk cloth

achieved after placing a damping layer (silk cloth) at the rear side of the base plate (compare Fig. 6). Without this damping the membranes showed very sharp resonance peaks.

An additional problem encountered was that the thin rubber foils loose their tension after periods of a month or so. For this reason, before each run the static calibration of the membranes had to be repeated.

2. 4. 3. Evaluation of fringe patterns

With the method as described above it was not possible to determine whether fringe rings are produced by local overpressure or underpressure. To establish this a base fringe pattern was produced by turning the reference mirror of the interferometer slightly. It was adjusted so that with no pressure difference on the membrane approximately two interference fringes, extending lengthwise in the x-direction, appear on each circular membrane. Figure 10b shows this base fringe pattern (produced without flow), and in Figure 10a a typical fringe pattern with flow is shown. In evaluating the patterns, the difference between the two has to be taken.

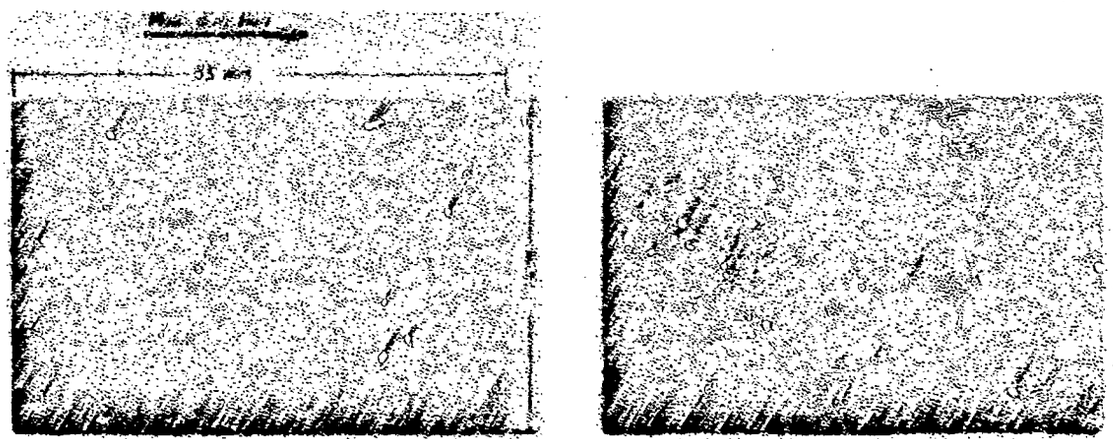

a. With flow in the tunnel (U_{∞} = 6.5 m/sec, δ^{**} = 4.6 mm, frame frequency 7000 sec^{-1})

b. Without flow in the tunnel (base fringe pattern)

Figure 10. Determination of the instantaneous displacement of the circular membranes (16 mm film, membrane diameter 2.5 mm, distance between the circular membranes 3 mm)

It can also be seen in Figure 10a that some of the fringes have an S-shape. This results from an overpressure and an underpressure occurring simultaneously over different areas of the same membrane.

Important in the film evaluation is whether the phase shift between the excitation force (pressure) and the membrane displacement is of importance. As can be seen Figure 9 the phase angle, Ω , increases nearly linear with the excitation frequency up to about 900 Hz. Thus it follows that, up to 900 Hz, the displacement follows the wall pressure with a constant time lag of about 0.2 msec. For the investigation reported here this lag is unimportant, but if the instantaneous velocity field is studied in connection with the wall pressure field, it will be necessary to take this fact into account.

Another important question for the evaluation is whether the observed pressure pattern on the "flexible wall" is the same as it would be on a rigid wall. It can be assumed that this is so, because the displacement of the small membranes is orders of magnitude smaller than the thickness of the viscous sublayer, defined with $y^+ = 5$.

2.5. Insulation of noise and vibrations

The whole flow arrangement is extremely sensitive to noise and vibrations and therefore several precautions were necessary:

(a) The tunnel is of heavy construction with walls of cast aluminium about 20 mm thick. All the parts lying within the dotted lines shown in Figure 1 are rigidly connected and elastically suspended on springs. The fundamental frequency of this system is less than 1 Hz.

(b) The sonic nozzle was specially designed in order to produce low noise levels. The outside casing of the nozzle is constructed with inner and outer walls, and the space between is filled with sand to reduce sound radiation. A sound absorber is mounted downstream of the nozzle (absorber B in Figure 1). The static pressure in the sound absorber is always less than critical so that the flow downstream of the nozzle is supersonic.

(c) In principle a sonic nozzle does not radiate sound upstream, but in practice it still produces some noise in that direction (flow noise in the convergent area and possibly transmission in the flow boundary layer and in the walls of the nozzle). To eliminate these influences the sonic nozzle is connected to the test section only with a soft rubber gasket and a specially designed sound absorber is fitted at the end of the test section (absorber A in Figure 1).

(d) The high speed film camera, which is rather noisy, was put into a double walled sound insulation housing.

Using all these precautions, it was possible to reduce outside disturbances at the pressure sensitive flexible wall to a level lower than $\pm$ 0.2 fringe widths.

3. EXPERIMENTAL RESULTS

3.1. Measurements with the pressure sensitive flexible wall

With turbulent boundary layer flow and the pressure sensitive flexible wall described in the previous section several films of interference patterns were taken. In Figures 11, 12 and 13 some of the results from one film are presented.

Figure 11 shows 6 two dimensional pictures (x-z plane) of a wall pressure distribution as it develops in time. The pictures were obtained by evaluating 6 frames in a film where each frame contains information about the displacement of 12 x 17 membranes covering a wall area of 29 mm x 48 mm or 6.5 δ^* x 10.5 δ^*. The regions indicated by solid lines are areas of local overpressure; the regions indicated by dashed lines are areas of local underpressure. The type of cross-hatching denotes the magnitude of the deviation from the mean pressure. Figure 11 seems to indicate that the spanwise extension of the pressure patterns is somewhat larger than the streamwise extension.

Figure 12 shows the temporal development of the pressure field. This figure was obtained by determining the displacement of 17 membranes (row no. 5 of Figure 11) for 149 consecutive frames of the film (the time interval between two consecutive frames was 0.14 msec. The zero times in Figure 11, 12, 13 are identical). Frame numbers 0-50 show how a higher amplitude wall pressure structure travels across the circular membranes in the streamwise direction. After that, follows a time interval (frames numbers 51-105) in which practically only low-amplitude wall pressure fluctuations occur over the membranes. In this phase too, however, there are wall pressure extrema, which move in the streamwise direction. In frames numbers 106-148, a high-amplitude wall pressure structure again travels across the membranes. The 149 frames shown in Figure 12 represent only a very short section of a 30 m film (4000 frames). It turns out, however, that the sequence described above is characteristic of all the films evaluated, whereby the sequence is repeated at random time intervals.

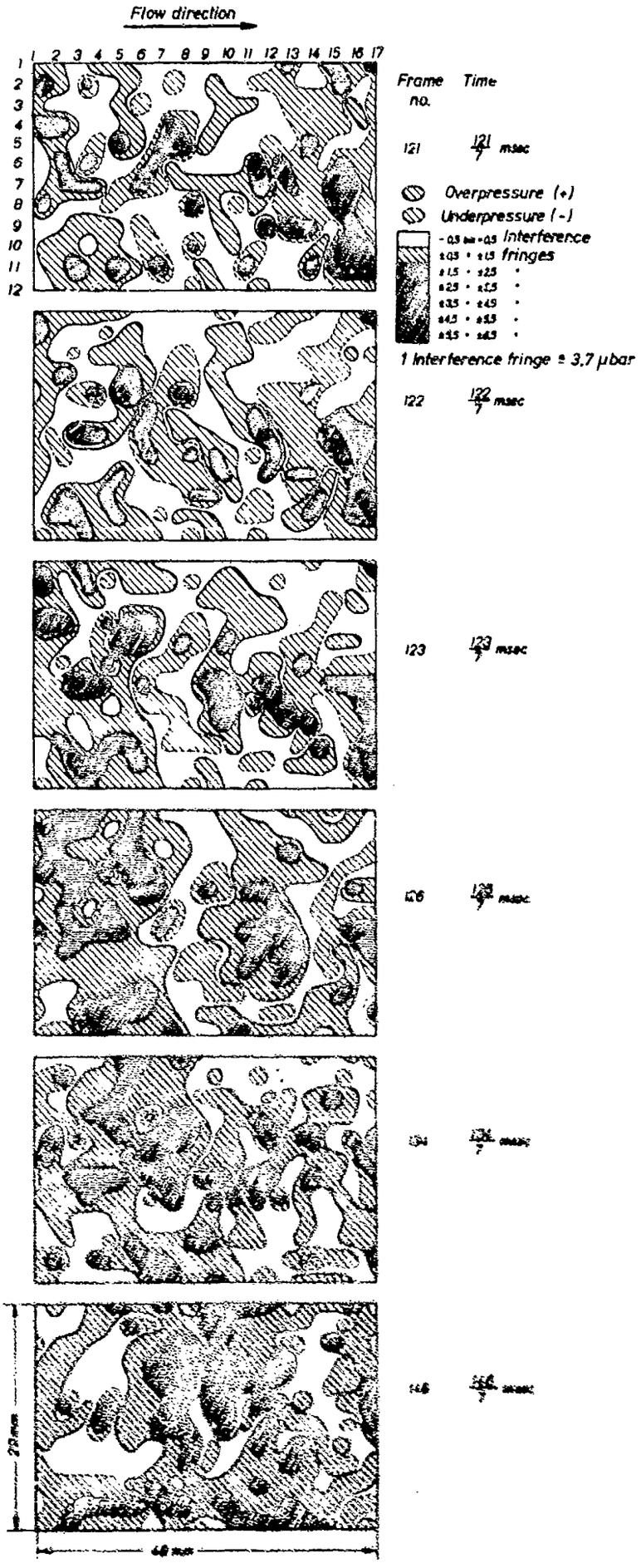

Figure 11.

Temporal change of the wall pressure distribution of a turbulent boundary layer flow measured by means of 12 membrane rows each consisting of 17 circular membranes lying one behind the other in the streamwise direction
(membrane diameter = 2, 5 mm, distance between the membranes = 3 mm, free stream velocity U_∞ = 8. 5 m/sec, displacement thickness δ^* = 4. 6 mm, row 5 is presented in consecutive frames in Figure 12, time zero points are identically in Figure 11 and Figure 12).

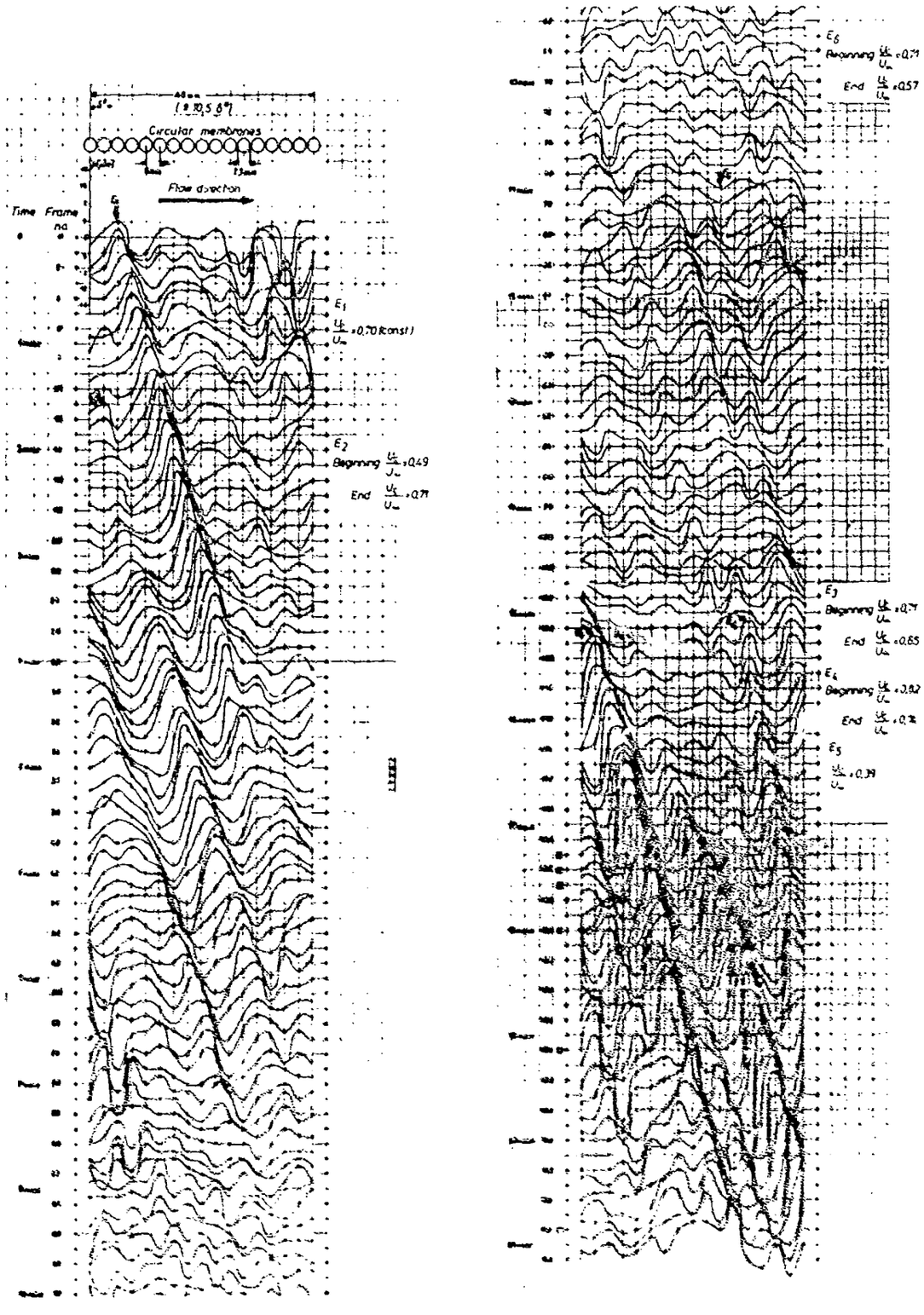

Figure 12. Temporal change of the wall pressure of a turbulent boundary layer flow measured by means of 17 circular membranes lying one behind the other in the streamwise direction (membrane diameter = 2.5 mm, distance between the membranes = 3 mm, free stream velocity U_∞ = 8.5 m/sec, displacement thickness δ^* = 4.6 mm, frame frequency 7000 sec^{-1}, + corresponds to overpressure, - corresponds to underpressure, E_i = local wall pressure extremum, □ = two-dimensional wall pressure distribution for this frame - see Figure 11)

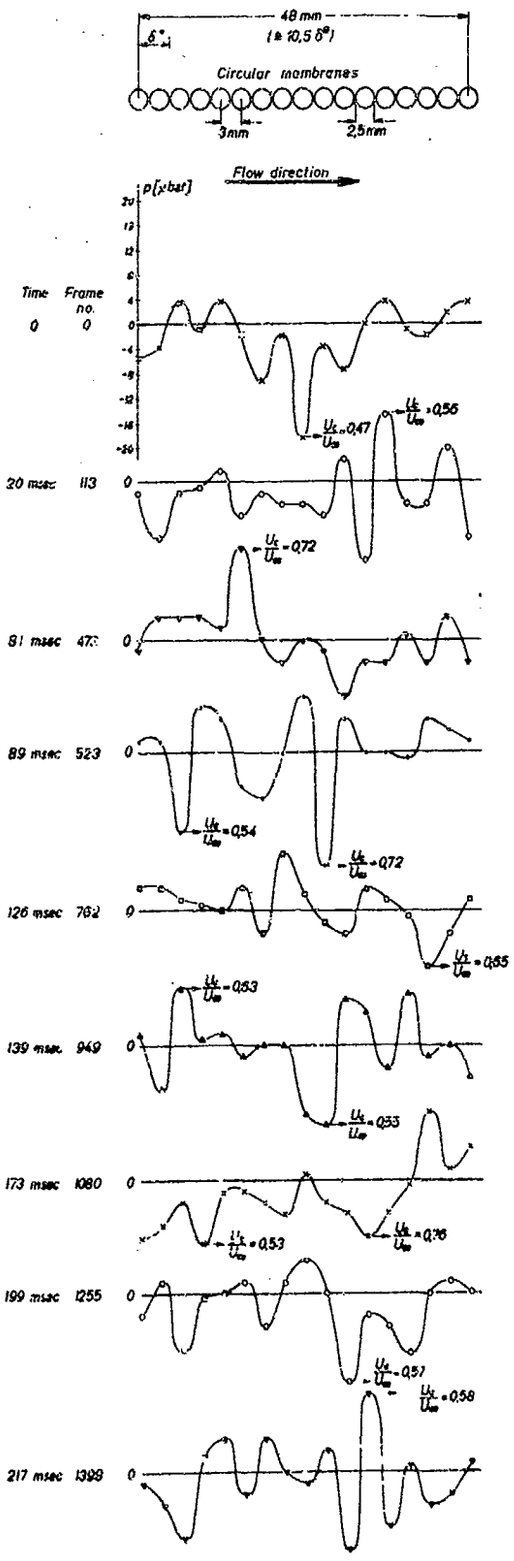

Figure 13. Several time points, taken from a 30 m film, for the occurrence of high-amplitude wall pressure fluctuations over 17 circular membranes lying one behind the other in the streamwise direction (data as in Figure 11)

Figure 13 shows some selected points in time for the occurrence of zones of high-amplitude wall pressure fluctuations over a row of 17 circular membranes lying behind each other in the streamwise direction. No clear connection between convection velocity and the structure of the pressure field has been detected.

Figures 12 and 13 show that the pressure extrema have a lengthwise extension of the order of 0.5 δ^* ($50 \frac{\nu}{U_\tau}$) and that these extrema can be followed downstream over distances of about 9 δ^* ($900 \frac{\nu}{U_\tau}$). Both values should be understood as limits only. 0.5 δ^* is about the resolution length of a circular membrane of our flexible wall so that the pressure extrema could possibly be even smaller, and distances of observation (9 δ^*) are partly limited by the borders of our flexible wall section, so that it might well be, that some extrema can be followed over larger distances.

From Figure 12 one can calculate the convection velocity, U_c, of the pressure extrema. For the ratio U_c/U_∞, values between 0.39 and 0.82 were found. The convection velocities of the pressure extrema changed along the path - some were increasing and some decreasing. No clear connection between convection velocity and the structure of the pressure field has been detected so far (see Figure 13).

Pressure extrema with peak values up to 24 μbar (corresponding to 0.055 q_∞) have been observed. The wall pressure extrema within the zones of high-amplitude pressure fluctuations often have rather steep flanks. Values up to $\frac{dp}{dx} = 0.09 \cdot q_\infty / \delta^*$ have been observed. Because of the limited resolution of the circular membranes it might well be that the really occurring gradients are sometimes larger.

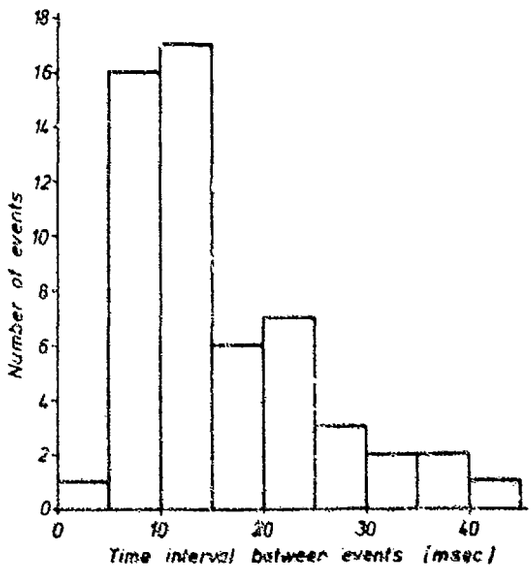

Figure 14. Histogram of time interval between the occurrence of zones of high-amplitude wall pressure fluctuations (U_∞ = 8.5 m/sec, δ^* = 4.6 mm)

The time which elapses between the occurrence of two zones of high-amplitude wall pressure fluctuations was determined for 55 consecutive such zones. The results are given in Figure 14. This determination was done by evaluation of several thousand consecutive frames. The definition of a "zone of high-amplitude wall pressure fluctuations" has here been made for practical reasons so that in a certain surrounding at least one pressure amplitude with modulus larger 9 µbar occurs. The mean frequency so obtained for the occurrence of such zones was 67 Hz.

3. 2. Measurements with wall microphones

For purposes of comparison the wall pressure fluctuations have also been measured with microphones mounted flush in the wall. Figure 15 shows our results for three effective microphone diameter (0. 1 mm, 2. 1 mm and 0. 8 mm) compared with the results of other authors. Our measurements were made using condenser microphones (Bruel and Kjaer Type 4136 and 4134). The smallest diameter measurements were made by arranging a metalshield with a pinhole in front of the microphone diaphragm. Some of power spectra measured with a 1/3-octave band filter (Bruel and Kjaer Type 2112) are shown in Figure 5. For the plot in Figure 5 the 1/3 octave bandwidths have been transformed to constant bandwidths using the assumption that the filtered fluctuating signals in each band is random.

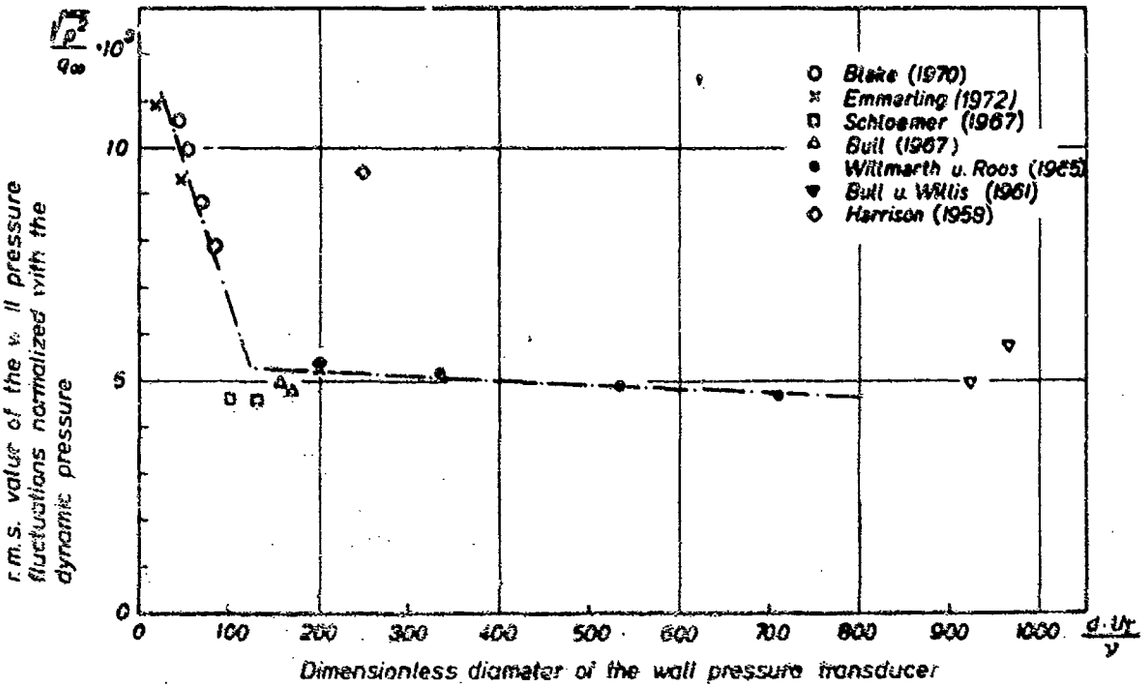

Figure 15. Dependence of the measured r. m. s. value of the wall pressure fluctuations upon the dimensionless pressure transducer diameter

4. DISCUSSION OF RESULTS AND CONCLUSIONS

(a) The convection velocities of the wall pressure extrema were found to be U_c/U_∞ = 0. 59 to 0. 82. Only limited comparison of these values with measurements reported in the literature can be made, since the latter results are mean values. As can be seen in Table 1 normalised values for mean convection velocities reported by other investigators are between 0. 59 and 0. 66.

(b) Assuming that the sources of wall pressure fluctuations move, on the average, at the local mean flow velocity, it can be estimated that 90 % of all the pressure extrema observed here originate in the wall region of $y^+ \approx 110$. As the characteristic length of the wall region is ν/U_c, it is to be expected that the dimensions of the wall pressure extrema should vary proportionally with ν/U_c.

(c) The suggested scaling with ν/U_c is strongly supported by Figure 15. Nearly all r. m. s. values of normalised pressure fluctuations reported by several investigators fall together onto one curve if the microphone diameter is normalised with ν/U_c. If δ^* is used instead of ν/U_c the values do not fall onto one curve.

(d) The fact that the r. m. s. values increase as soon as $d\,U_c/\nu$ becomes smaller than 100 (compare Figure 15) can be explained by the observation that the lengthwise extension of the pressure extrema is about 50 ν/U_c. Transducers which measure the real r. m. s. value of the pressure fluctuations should be considerably smaller than this length. With the smallest transducer ($d\,U_c/\nu$ = 18) used in this investiga-

tion, $\frac{\sqrt{\overline{p^2}}}{q_\infty} = 10.3 \cdot 10^{-3}$ was measured. This value is higher than most values given in literature (compare Table 1).

(e) Figure 5 shows that with a large transducer not only the high frequency components of the spectra are lower than with a small transducer but also the low frequency components. This can be explained with the help of Figures 12 and 13. According to these Figures especially the zones of high-amplitude wall pressure fluctuations supply the pressure amplitudes for the large wave numbers but simultaneously the cyclical occurrence of these fluctuations gives contributions to small wave numbers. So transducers, which do not fully pick up the high wave number extrema because of limited spatial resolution, will also produce too small low frequency components. Similar results as in Figure 5 were reported by Geib ([13], Figure 2).

(f) For the occurrence of the zones of high-amplitude pressure fluctuations a mean frequency of 67 Hz has been found (compare Section 3.2.). This frequency is in good agreement with results of other boundary layer investigations.

Black [14, 15] found that boundary layer turbulence should have a fundamental frequency $\omega = 0.056\, U_\infty^2/\nu$. With the values of our investigation this formula yields a value of 67 Hz. With another point of Black's theory our experimental results do not agree: According to Black two basic pressure phases occur. There occurs a weak negative pressure over a larger region and then a high positive peak occurs locally (caused by an eruptive jet in the vicinity of the wall). Figures 11-13 show, however, that positive as well as negative pressure peaks occur.

Visual observations of the flow near the wall by Kline et al. [16], Kim et al. [17], Corino and Brodkey [18] and Nychas [19] show that events, which have been described as "burst periods", actually do occur in the wall region. Further, during such occurrences it has been shown that the instantaneous velocity profile deviates considerably from the mean, and that, instantaneously, very large shear stresses arise. In addition transverse and longitudinal vortices are formed in the wall region. The question arises, which process in the flow produces the zones of high-amplitude wall pressure fluctuations. Kline et al. ([16], p. 764) and Kim et al. ([20], p. 122) found the non-dimensional frequency of the burst periods, $\omega^+ = \omega \cdot \nu / U_\infty^2$, to be about 0.06 (with $Re_\Theta \approx 10^3$). When this value of ω^+ is used for the flow studied in our investigation, a burst frequency of 72 Hz is obtained, which is in remarkably good agreement with the observed value of 67 Hz. This indicates strongly that these events are related to one another.

According to Rao et al. [21] and also Laufer and Narayanan [22], the mean occurrence frequency of the "burst periods" scales with the flow velocity outside the boundary layer, U_∞, and the displacement thickness.

Rao determined a burst frequency $f \approx U_\infty / 32\,\delta^*$. With the values of the flow investigated here this formula leads to $f = 58$ Hz which again is not far from the observed frequency. These considerations essentially support the model of interaction between events in the inner and outer layer of a turbulent boundary layer suggested by Laufer ([23], Figure 10). According to this model a pressure gradient in the direction of flow is induced as a result of the interaction between large-scale turbulent motion and non-turbulent flow. This pressure gradient causes periods of instability in the layer near the wall and, as a result, the occurrence of small-scale "bursts". Nychas [19] also concludes from his visual observations that the large scale transverse vortices he observed induce conditions in the wall region which lead to the occurrence of "ejections" (bursts).

5. REFERENCES

[1] Harrison, M.: David Taylor Model Basin Rep. no. 1260 (1958).

[2] Willmarth, W. W.: NASA Mem. 3-17-59 W (1959).

[3] Skudrzyk, E. F., Haddle, C. P.: Noise production in a turbulent boundary layer by smooth and rough surfaces. J. Acoust. Soc. Am. 32 (1960), 19-34.

[4] Bull, M. K., Willis, J. L.: Some results of experimental investigations of the surface pressure field due to a turbulent boundary layer. Dept. Aero. Astro., Univ. of Southampton, Rep. no. 199 (1961).

[5] Willmarth, W. W., Wooldridge, C. E.: Measurements of the fluctuating pressure at the wall beneath a thick turbulent boundary layer. J. Fluid Mech., vol. 14, part 2 (1962), pp. 187-210.

[6] Serafini, J. S.: Wall pressure fluctuations and pressure velocity correlations in turbulent boundary layers. AGARD Rep. no. 453 (1963).

[7] Willmarth, W. W., Roos, F. W.: Resolution and structure of the wall pressure field beneath a turbulent boundary layer. J. Fluid Mech., vol. 22, part 1 (1965), pp. 81-94.

[8] Schloemer, H.: Effects of pressure gradients on turbulent boundary layer wall pressure fluctuations. J. Acoust. Soc. Am. 42 (1967), 93-113.

[9] Bull, M. K.: Wall pressure fluctuations associated with subsonic turbulent boundary layer flow. J. Fluid Mech., vol. 28, part 4 (1967), pp. 719-754.

[10] Blake W. K.: Turbulent boundary layer wall pressure fluctuations on smooth and rough walls. J. Fluid Mech., vol. 44, part 4 (1970), pp. 637-660.

[11] Wills, J. A. B.: Measurements of the wave-number/phase velocity spectrum of wall pressure beneath a turbulent boundary layer. J. Fluid Mech., vol. 45, part 1 (1970), pp. 65-90

[12] Emmerling, R.: Die momentane Struktur des Wanddruckes einer turbulenten Grenzschichtströmung. Mitt. MPI Strömungsforsch. u. Aerodyn. Versuchsanst., Göttingen, Nr. 56 (1973).

[13] Geib, F. E.: Measurements on the effect of transducer size on the resolution of boundary layer pressure fluctuations. J. Acoust. Soc. Am. 46 (1969), 253-261.

[14] Black, T. J.: Some practical applications of a new theory of wall turbulence. Proceedings of the 1966 Heat Transfer and Fl. Mech. Institute, Stanford Univ. Press (1966).

[15] Black, T. J.: An analytical study of the measured wall pressure field under supersonic turbulent boundary layers. NASA Contractor Report - 868, April 1968.

[16] Kline, S. J., Reynolds, W. C., Schraub, F. A., Runstadler, P. W.: The structure of turbulent boundary layers. J. Fluid Mech. vol. 30, part 4 (1967), pp. 741-773.

[17] Kim, H. T., Kline, S. J., Reynolds, W. C.: The production of turbulence near a smooth wall in a turbulent boundary layer. J. Fluid Mech., vol. 50, part 1 (1971), pp. 133-160.

[18] Corino, E. R., Brodkey, R. S.: A visual investigation of the wall region in turbulent flow. J. Fluid Mech., vol. 37, part 1 (1969), pp. 1-30.

[19] Nychas, S. G.: A visual study of turbulent shear flow. Ph. D. Thesis, Ohio State University (1972).

[20] Kim, H. T., Line S. J., Reynolds, W. C.: An experimental study of turbulence production near a smooth wall in a turbulent boundary layer with zero pressure gradient. Report MD-20, Department of Mechanical Engineering, Stanford University (1968).

[21] Rao, K. N., Narasimha, R., Badri Narayanan, M. A.: The bursting phenomenon in a turbulent boundary layer. J. Fluid Mech., vol. 48, part 2 (1971), pp. 339-352.

[22] Laufer, J., Badri Narayanan, M. A.: Mean period of the turbulent production mechanism in a boundary layer. Phys. Fluids, vol. 14, no. 1 (1971), pp. 182-183.

[23] Laufer, J.: Recent developments in turbulent boundary layer research. Instituto Nazionale di Alta Matematica, Symposia Mathematica, Vol. IX, (1972), pp. 299-313.

6. ACKNOWLEDGEMENTS

The authors thank Prof. Dr. E.-A. Müller for enabling us to carry out this investigation at the Max-Planck-Institut für Strömungsforschung and for his continuing interest in the project. For many helpful discussions we would also like to thank the staff of the institute, especially Dr. H. Eckelmann, Dr. F. Obermeier, Dr. J. M. Wallace and Dr. G. Zimmermann.

SOME AEROMEDICAL ASPECTS OF NOISE

by

GROUP CAPTAIN P F KING
Royal Air Force
Central Medical Establishment
Kelvin House
Cleveland Street
London W1P 6AU
England

Noise is a produce of propulsion systems and the use of weapons, and although its effect on the human ear has been known for many years it is only in the past 35 years that interest has been directed increasingly to investigating the effects of noise on man, and in attempting to prevent them.

Sound is vibration which is detectable by the organ of Corti in the inner ear; noise is loosely, but conveniently, defined as unwanted sound.

Noise may be unwanted.

1. Because it is loud and harsh and physically or mentally distressing.
2. Because it interferes with communication by speech or other auditory signals; interference with intermittent communication occurs at 72dB, and with minimal communication at 82dB.
3. It may reduce working efficiency.
4. It may be harmful to the ear to the extent of causing deafness.

All these factors may operate together when one considers noise in aviation. In human terms one is concerned with the effects of noise on aircrew, on ground support staff, and on those who work or live in close proximity to noisy airfields. While for all these groups the source of the noise, namely the aircraft engines, is the same - and while the principles of investigation and protection will remain the same, the solutions will vary according to the group under review.

THE EFFECT OF NOISE ON HEARING

Good hearing is essential for members of aircrew. Instructions must be heard clearly while under training and later during flight. Accurate reception of speech signals is essential; and this may be required under poor listening conditions, in high ambient cockpit noise, and when general and auditory fatigue are also exercising an adverse effect on the hearing.

Intense noise may damage any or all of the peripheral parts of the hearing mechanism - and the extent of the damage will depend on the character, intensity and duration of the noise. Damage to the eardrum and ossicular system will result from explosive noise and blast. The hair cells of the organ of Corti in the inner ear are damaged by sudden impulsive noise, or by prolonged exposure to intensive noise. It is this latter which commonly effects the hearing of aircrews although blast or explosive damage to the hearing may be seen.

Originally this sort of damage was described as "acoustic trauma" but it is now called noise-induced hearing loss. The effects of such exposure may be temporary, and recoverable (Temporary threshold shift, TTS) or permanent and non-recoverable (Permanent threshold shift, PTS).

Temporary Threshold Shift is a short term effect following exposure to noise. There is a change in the hearing with respect to a previously ascertained level; it may be accompanied by tinnitus but recovery of hearing to the original level occurs.

The extent of TTS and consequent degree of recovery will depend on several factors, eg

a) the individual susceptibility of the subject
b) the subject's age
c) the nature and intensity of the noise
d) duration and character of exposure
e) presence of previous damage to the cochlea
f) the nature and noise attenuating property of any aural protective device worn

Occasionally recovery of the hearing may be delayed, when the condition is termed persistent threshold shift, but in general full recovery can be expected in 10 days. (1)

Where there is a failure of the hearing to recover, the new level of hearing is called the permanent threshold shift. As the hearing loss is now established it is referred to as noise induced hearing loss.

Such a hearing loss will have developed slowly over months or years - and the rate of deterioration will be controlled by the level of the exposures and the frequency of their occurrence. Generally, it is difficult to determine the time of onset. At the start the hearing will be dulled by noise, with recovery. As the acoustic insult is repeated, recovery times lengthen while the degree of recovery shortens until a hearing loss is seen to be established. Tinnitus is relatively common. An audiogram will show a characteristic pattern of loss, the greatest appearing at 4kHz, with losses of varying severity at 6 and 8 kHz. As the loss worsens 3kHz and then 1kHz become involved; when the speech frequencies become involved so difficulty is experienced in interpreting speech, particularly in ambient noise.

In general, once started the hearing loss has a relatively rapid initial growth, the rate of change diminishing over a period of years - and latterly the physiological effects of presbycusis are added, increasing the overall hearing loss.

Susceptibility to noise varies from person to person, but repeated work has failed to find a predictive test of susceptibility which is reliable for individuals.

Pain will occur after noise exposure but the level at which this appears varies from person to person, though the onset of pain is a symptom which should not be ignored. In some, discomfort can occur with exposure to noise of 110dB, and this would indicate undue susceptibility to noise damage. On average, pain will be experienced at 130dB.

For those working in noise, the need to protect and preserve the hearing is obvious, and hearing conservation calls for three straightforward requirements:-

1) a knowledge of the noise exposure and its control

2) the measurement of each person's hearing before employment, and at regular intervals during employment

3) the provision of any necessary protective devices

Such principles call for the co-operation and co-ordination of effort of workers in several fields, but with the close medical supervision exercised over aircrew this presents no organisational problem with regard to this group. Opinions vary as to what constitutes hazardous noise and at what levels conservation should be undertaken. As yet there is no complete agreement. However, all ideas are based on the concept of an eight hour working day, over 5 days per week, spread over a working lifetime. The British "Code of Practice" (2) considers 90dB(A) to be the level at which protection should be given, while 90dB(A) quoted in Stanag No 3437, (3) relating to exposure to hazardous noise, has been generally agreed for military aviation. The adoption of noise control and noise limits to protect the hearing or to maintain voice communication will also take care of the problem of noise-induced performance decrement.

THE ESTIMATION OF HAZARD TO THE HEARING

The first step is to measure and analyse the noise under the conditions in which the worker is exposed to it. In general, full octave band analysis will be required.

The possibility of a hazard to the hearing from a given noise is determined by comparing the spectral analysis of the noise against a chosen damage result criterion (DCR), which has been defined (4) as the maximum sound pressure level of a noise usually a function of frequency to which persons may be exposed if the risk of a significant hearing loss is to be avoided.

Several damage risk criteria are in favour, and each differs only in detail from the others. That employed in the Royal Air Force and the Royal Navy is one modified from Burns and Littler. (5)

A comparison of the spectral analysis of the noise and the chosen DCR will determine if noise levels are in excess of the safety limits. If this is the case subtraction of the attenuation values of any chosen ear protector from the spectral analysis will indicate whether safe limits can be achieved.

SOURCES OF NOISE IN FLIGHT

The engines of the aircraft are the primary source of noise, and this should include the transmission system, propellers and jets. Secondly, interaction between the aircraft and the air through which it is flying - especially aerodynamic or boundary layer noise caused by the rush of turbulent air over the surfaces, edges and projections of the aircraft; and thirdly, subsidiary sources of noise such as internal power generators, hydraulic systems etc. (6)

Different types of aircraft present different problems and patterns of noise, and these are considered briefly.

FIXED WING AIRCRAFT

a) Piston-engined aeroplanes The principal sources of noise in the reciprocating engine are the engines and their exhausts and the propellers. At high indicated air speed the boundary layer turbulence is also a factor. Internally, and particularly in light aircraft, the engine will make a large contribution to the noise and vibration, but externally the noise from the exhausts and propellers is dominant.

b) Turbine-engined aircraft The external noise from jet aircraft is one of the largest problems in this field. Although there are marginal alleviations from improvements in design and acoustical treatment of the turbine engine, the problem is likely to worsen as aircraft get bigger, with more powerful engines, and with proliferation in the number of aircraft employed. However, the internal sound pressure levels in the jet aircraft during flight are lower and much less hazardous to the hearing of the aircrew than in the propeller-driven aircraft. The greatest amount of noise is heard on start up and take-off.

The characteristic broad band noise results from the collision and collapse of vortices generated where the out-rushing gases of the jet mix with the stationary ambient air. Whine from the compressor may also be obtrusive.

In flight, boundary layer noise is the principal noise heard inside the cabin. In some military aircraft, flying at high speed and low altitude, this component of the noise can interfere with communication as well as being a hazard to the unprotected hearing.

c) Turbo-propeller Aircraft Here the principal source of noise is the propeller, and the noise problems arising resemble those from piston-engined aircraft of comparable power, but there are differences. For example, the combination of propeller noise with the turbine engine and its exhaust produces a characteristic howling quality.

V-STOL AIRCRAFT

A variety of fixed wing aircraft have been designed to take off or land vertically, or in a very short space, or to hover or manoeuvre slowly at low altitude. They can operate without airfields or prepared runways and so have a great military potential.

Their principal disadvantage is the noise created inside and outside the aircraft. For the aviator, his situation acoustically is that of the crew man in a conventional aircraft at take-off, except that in the V-Stol aircraft the noise is more intense and the moment more prolonged. The engines are working at full power, and by reflection from the ground the noise is re-inforced. There is serious threat to the hearing as sound pressure levels in the cockpit may exceed 125 dB.

ROTATING WING AIRCRAFT

In the helicopter, the transmission system conveying power to the main and the tail rotors is the important source of internal noise, and produces peaks in the range 300 - 2,000 Hz, and this has a bearing on speech interference and hazard to the hearing. Piston engined helicopters and their exhausts emit noise comparable to that of similar engines in fixed wing aircraft. The main rotor of the helicopter, although it does not work under the same power or at the same tip-speeds as an aeroplane propellor, emits appreciable noise - and "blade-slap", a chopping noise resulting from the passage of the main rotor blades through vortices left by earlier passages, can be prominent. This can resemble machine-gun fire and in a tactical situation can mask the sound of this weapon. The internal sound in a helicopter arises from the transmission system and this is augmented by rotor noise which will change with the power setting and the angle of attack of the blades of the rotor. Although many helicopter flights are brief the noise hazard can, nevertheless, be serious.

AIR CUSHION VEHICLES (ACV)

The noise of an ACV internally or externally is generated by the engines, the transmission system and the propellers - and so resembles that of a propeller driven aircraft. The engines are powerful and the structure relatively light so that internal noise levels are high; this makes speech communication difficult, and can be a hazard to the hearing.

Having considered the source of the noise - we now pass to the question of conservation of the hearing.

AUDIOMETRY

The measurement of each person's hearing before employment, and at regular intervals during employment, is the second principle involved in hearing conservation. The routine use of pure tone audiometry presents no practical problems in the management of aircrew as national regulations for military personnel, and international regulations for civil personnel, require the use of audiometry as part of the initial medical examination. Regular audiometric checking, perhaps on the occasion of an annual medical examination, is well recognised.

Those with unusual or unacceptable patterns of hearing, generally combined with a history of hearing loss, will be weeded out on entry - or accepted and followed closely.

Difficulty may be experienced when at some time in the individual's career a hearing loss is discovered. For the purpose of this paper we will assume that all other possible causes of hearing loss have been excluded, and that one is dealing with a noise induced hearing loss. It may be that the hearing falls below the accepted standard, and the aviator's fitness to continue flying is questioned.

It is useful to bear in mind the following facts when making a decision.

In practice, an aviator is unlikely to make use of a range of speech frequencies greater than from ½ to 3 kHz. He may need to hear audio signals, which have not exceeded 3 kHz to date. In addition, normal ear telephones in use have little significant response above 3 kHz.

While it is attractive to ignore losses at 4 kHz and above, the diagnostic and prognostic value of such losses should be borne in mind.

The function of speech discrimination in a background of noise may be tested and measured. A variety of techniques have been devised to do this, but provided functional efficiency in ambient noise remains, it is safe to permit unrestricted flying. When speech discrimination remains in ambient noise it is likely that recruitment of hearing is occurring. This is a characteristic of deafness in which the cochlear end - organ is involved, and is manifest by a diminution of hearing loss with increasing signal loudness.

In some aircrew the hearing may deteriorate progressively, either from repeated exposure to high noise levels, or from premature ageing, or both. While the higher frequencies are involved initially, eventually losses will spread down to the speech range. If the progress is rapid, unrelieved by rest and aggravated by further exposure to noise - the best policy may be to advocate withdrawal from flying, both in the interests of the individual and of air safety.

It is a point of practical importance that it is the hearing of middle aged aircrew which gives the greatest cause for concern. In military aviation the opportunity for active, operational flying diminishes after the age of 40 with the expectation of Command and Staff posts. In civil aviation the expectancy of an active flying career is longer - perhaps to age 55, though the man may have to contend with medical disabilities associated with increasing age - and which in themselves may be of more serious import than hearing loss.

In modern flight the aviator must place increasing reliance on auditory information; it follows that the quality of hearing of flying personnel is important. Each case should be assessed in relation to his task, and the existence of a hearing defect is not in itself a reasonable cause for arbitrarily ending a flying career.

PROTECTION OF THE HEARING

Protection of the hearing is the third principle invoked. This is achieved by

1) attempting to reduce the noise at source

2) by enclosing the individual to reduce the ambient noise from outside sources

3) by fitting and wearing individual ear protection

4) by reducing the duration of exposure

The reduction in noise at source in aircraft engines is a continuing, but marginal, benefit from improved design - but in this context the benefit is largely the bounty of those outside the aircraft. Improved design will also reduce aerodynamic noise.

Pressure cabins are themselves efficient excluders of noise and additional reduction in ambient noise can be achieved by suitable cladding in the cockpit and the crew spaces. However, secondary power systems in the aircraft can be troublesome, particularly cockpit conditioning and oxygen systems which may augment aerodynamic noise which enters the cockpit.

Personal protection of the ears is provided for aircrew - almost universally - by some form of fluid seal ear muff. There are many patterns of these, all of commercial manufacture.

The basic pattern is a pair of ear cups (7) generally of plastic material, which fit over the ears and are held in position by a tensile headband. The rim of the cup is fitted with a fluid seal of plastic or rubber, with suitable tension in the head band. This provides a close fit to the side of the head. The inside of the cup is filled with sponge rubber, which in the case of the design supplied to aircrew, supports a telephone receiver.

The attenuation provided by a fluid seal muff is better than any other single ear protector, being of the order of 17 dB at 63 and 125 Hz and 40 dB or more at 2000 and 4000 Hz.

For civil aircrew and for military aircrew employed in transport aircraft such a muff, fitted with a boom michrophone provides good protection.

For other military aircrew the same protective device is incorporated into a crash helmet - the "Bone-dome". The padding and the fibreglass shell of the "Bone-dome", as well as the snugness of fit, provide overall protection against noise, and so protect the hearing from sound transmitted to the cochlea via the cranial bones. The attenuation of such a helmet when worn with an oxygen mask is an average of 41 dB and this, coupled with the sealing effect of the pressure cabin, will provide adequate protection for aircrew in most instances.

It is interesting to recall that the "Bone-dome" is the lineal descendant of the original cloth or leather flying helmet - which, as noise levels become louder, developed larger and thicker circumaural padding to protect the hearing.

ADDITIONAL PROBLEMS

There remain additional facets worthy of mention. The first is the problem of noise encountered in communication systems when high ambient noise can be picked up by the crew member's microphone while he is transmitting - and so mask the message. This is particularly the case in military aircraft flying at high speed and low altitude, when boundary layer noise may enter the cockpit. In helicopters engine and transmission noise can be a similar problem in this respect. To some extent this may be alleviated by the use of a "noise-cancelling" microphone; automatic volume control may also be helpful.

Secondly, both military and civil aircrew may be exposed to other sources of hazardous noise, particularly that from weapons. It is not unknown for civil pilots to indulge in game, clay pigeon, or target shooting as a hobby, and for military aircrew personnel training in the use of personal weapons is universal. Care should be taken that aircrew know the risks of such exposure, and that they are protected by suitable plugs or muffs when exposed to weapon noise.

Similarly, the effect of noise from aircraft operations falling on crew rooms and crews' sleeping quarters should be remembered. Disturbed sleep and rest will potentiate the fatiguing effects of noise and further decrease working efficiency. Where such a problem exists it may be eased by the use of double glazing in brick constructed buildings.

REFERENCES

(1) Burns, W. Noise and Man
London: John Murray p 135. 1968

(2) Department of Employment: Code of Practice for Reducing the Exposure of Employed Persons to Noise
London: HMSO 1972

(3) Military Agency for Standardisation: Hearing Conservation
Stanag 3473 NATO Military Agency for Standardisation
London 1969

(4) Harris, C (Ed) Handbook of Noise Control
New York: McGraw-Hill 1957

(5) Burns, W and Littler, T S Modern Trends in Occupational Health
Ed. E N T Gelling
London: Butterworth 1960

(6) Guignard, J C and King, P F — Aeromedical Aspects of Vibration and Noise
Agardograph M 151
Advisory Group for Aerospace Research and Development. NATO London 1972

(7) Shaw, E A G and Thiessen, G J — Improved Cushions for Ear Defenders
J. Acoust. Soc. Amer 30.24 1958

CURRENT STRUCTURAL VIBRATION PROBLEMS ASSOCIATED WITH NOISE

John S.Mixson
National Aeronautics and Space Administration
Langley Research Center
Hampton, Virginia 23665
USA

1. INTRODUCTION

As the performance of aerospace vehicles has increased, the noise generated by the propulsion system and by the passage of the vehicle through the air has also increased, so that now it is possible for this noise to damage the aircraft/spacecraft structures, and to penetrate the structure causing discomfort to passengers or malfunction of expensive payloads and guidance equipment. Further increases in performance are now underway for space vehicles such as the space shuttle vehicle (Fig.1(a)) and for short distance takeoff and landing (STOL) aircraft (Fig.1(c)), and are being planned for supersonic aircraft (Fig.1(b)). In this paper the flight profiles and design features of these high-performance vehicles will be reviewed and an estimate made of selected noise-induced structural vibration problems. As appropriate, considerations for the prevention of acoustic fatigue, noise transmission, and electronic instrument malfunction will be discussed.

2. STOL AIRCRAFT

The class of aircraft under consideration is suggested by the following table of performance features:

Weight class:	200,000 lbs	(890,000 N)
Cruise speed:	500 mph	(224 m/s)
Landing speed:	85 knots	(44 m/s)
Payload:	150 passengers	
Range:	1,000 mi.	(1610 km)

These aircraft are also required to approach and takeoff at steeper angles than current conventional aircraft in order to reduce the noise exposure on the surrounding community, and are required to use short runways, perhaps less than 800 meters (2667 ft). The key to this performance with an aircraft of this size is the use of propulsive lift augmentation concepts such as shown in Figure 2.

2.1 Propulsive lift concepts

For all three concepts shown in Figure 2, the objective is to provide interaction between the engine exhaust stream and the wing-flap surfaces so that the exhaust stream will be directed downward, additional aerodynamic circulation will be induced, and the additional lift needed for steep angle approaches and takeoff will be obtained. The concepts illustrated in Figure 2 include:

(1) externally blown flaps, which deflect the engine exhaust stream by the direct insertion of flaps into the stream;

(2) upper surface blown flaps, which deflect the stream by aerodynamic pressures induced by flow over a curved surface (Coanda effect); and

(3) the augmentor wing, which carries the engine exhaust flow through ducts to the trailing edge of the wing where it is ejected downward through a channel in the trailing edge flaps.

In each concept a high velocity turbulent (perhaps hot) air stream is directed near to aerodynamic structural surfaces. It can be expected that these turbulent air streams will induce dynamic response stresses into the structure; such stresses then must be taken into account in structural design to avoid failure.

2.2 Sources of fluctuating pressures

As shown in Figure 3, there are several distinct sources of fluctuating pressures for both the externally blown flap and the over-wing blown flap. The turbulence scale and intensity and the associated dynamic loading acting on

the structure are different in each of these flow regions. The type of loading action to which any part of the wing-flap system is exposed depends on the geometric arrangement of the configuration (such as the engine location and number of flaps) and upon operating conditions (such as angle of attack, forward speed, and engine power setting). Thus, a great diversity of loading conditions is likely to be encountered during the operation of blown flaps. Clearly the prediction of the dynamic loads for structural design requires a knowledge not only of the jet turbulence/noise mechanism, but also of the effects of interaction of the jet with the structure. Research in this area has been stimulated recently by proposals to use blown flaps, but recent reviews have indicated that additional research is needed before design loads can be predicted confidently.

Some experimental data is available, and sample results will be discussed in the next few paragraphs.

2.3 Experimental studies of jet impingement

Three recent experimental studies of jet-flap interaction have been carried out in an effort to obtain data on realistic aircraft configurations. Photos of the models and test setups are shown in Figure 4. These tests covered ranges of the parameters jet diameter (model size), jet Mach number, jet temperature, forward speed, aircraft angle of attack, and flap angle settings. Fluctuating surface pressures were measured with flush-mounted transducers located along the jet centerline of all three models and at several spanwise locations on the small scale cold-jet model. Results from these tests confirmed the complexity of the jet-flap interaction phenomena by showing complicated relations between the measured pressures and the parameters that were varied (such as jet Mach number, angle of attack, and geometric location). Consistent results were obtained for several gross features of the surface pressures from these series of tests, however. For example, Strouhal number (jet diameter x frequency/jet velocity) was found to be an appropriate non-dimensional parameter for relating spectra of the fluctuating pressures from the various tests. Another example is related to the overall pressures, as described in the next figure.

2.4 Dynamic pressure coefficients

In Figure 5, dynamic pressure coefficients are shown for the three models shown in Figure 4, for a wall jet and for a free jet. Dynamic pressure coefficient is defined as root-mean-square of the fluctuating component of the surface pressure, Prms, divided by the dynamic pressure of the jet exhaust stream at the jet exit, q_j . The hatched areas indicate the range of values obtained for the various tests, the two circles are two individual data points obtained from the hot-jet model. With the exception of the two circle data points, the maximum values of dynamic pressure coefficient obtained for the various tests fall in the range from 0.10 to 0.15. Thus, for preliminary design one might use an upper bound value of 0.15 for Mach numbers up to about one. This value is about the same as the maximum measured in a wall jet, and is about three times the maximum values for a free jet.

Additional understanding of the jet-flap interaction behavior is needed as indicated by the differences in the maximum coefficients obtained for large and small jets, for hot and cold jets, and for different Mach numbers. No such data is available as yet on dynamic loadings of upper surface blown flaps or on the augmentor wing concept.

2.5 Sound pressure loads on aircraft

It is desirable to express these STOL flap loads in dB in order to place them in context with other types of dynamic loads and point out possible implications of the loading levels observed with regard to the design of externally blown flaps. Figure 6 presents a comparison of representative sound pressure levels of several sources of acoustic loading on aircraft structures. Based on past experience, it is known that sonic fatigue becomes a consideration in aircraft structural design when the levels begin to exceed about 130 dB. This lower limit is not absolute as indicated by the vertical shading between the horizontal bars. Sonic fatigue becomes a major design consideration as the levels approach 160 dB. The top four loading actions have been associated with sonic fatigue in the past on aircraft structures. Since flap loads are seen to be of a comparable order of magnitude (and have a broad band spectrum capable of exciting many structural modes as shown in the references) it may be concluded that blown flaps may also be subject to sonic fatigue which must be considered in the design of the wing flap systems.

2.6 STOL engine location

Public acceptance has been described as a key item to the success of commercial STOL aircraft operations. Noise in the passenger cabin is expected to have a significant effect on passenger comfort, and therefore passenger acceptance. As a starting point in evaluating the STOL interior noise situation, the engine location design considerations may be considered. Comparing STOL aircraft to conventional aircraft, as shown in the sketches in Figure 7, it appears that the engines of the STOL aircraft are located farther forward and closer inboard than the engines of conventional aircraft. There are reasons for this that are associated with the STOL mission profile and lift augmentation configuration. First, the engines must be located well forward of the wing to obtain optimum lift-generating interaction between the engine exhaust stream and the wing-flap surfaces. Second, the engines must be located as far inboard as possible so that any rolling moment resulting from an unanticipated engine failure during the propulsion-lift mode of operation can be safely controlled.

The forward-and-in-board engine location, however, brings the noise-generating exhaust jet closer to the passengers (along with other noise generators such as those described in Figure 3). Therefore, for a given engine and structural design concept, the interior noise problem could be expected to be more severe for a STOL design aircraft than for an equivalent conventional design. Of course, many other complicating factors such as engine type and thrust, reverse thrust mechanism, characteristic spectrum, and wing shielding effects (suggested by the front views in Figure 7) enter the interior noise level problem.

An attempt to account roughly for engine thrust level effects and to measure numerically the engine location ideas suggested by Figure 7 has been made and the results are shown in Figure 8.

2.7 Normalized engine location

In Figure 8, the geometric location of the engine exhaust is plotted in plan view relative to the location of the passengers. The fore-and-aft location is plotted relative to aircraft length, i.e. the distance from aircraft nose to engine exhaust has been divided by aircraft length, while the spanwise distance has been divided by engine thrust in an attempt to account for differences in engine thrust. Considering first the data for four engine aircraft, indicated by the circular symbols, it is seen that the STOL engines are indeed farther forward and closer inboard than the engines of conventional aircraft. The same is true for two engine versions of STOL aircraft. These considerations suggest that considerable effort may be required to obtain noise levels low enough to be satisfactory to STOL aircraft passengers.

2.8 Summary of aero-acoustics for STOL

The current situation regarding fluctuating surface pressure loads and the resulting structural effects for STOL aircraft are indicated in Figure 9. The thoughts expressed in Figure 9 are derived from the experiments described in the references and summarized in Figures 4 to 6, from a review of relevant literature, and from discussions with some of those having a practical knowledge of the acoustic/structural design situation. The main thought that comes through is that design of STOL aircraft to have acceptable sonic fatigue life and interior noise levels requires improved ability to predict fluctuating pressure levels for STOL configurations and to modify configurations to obtain lower levels or to withstand the high levels that preliminary estimates indicate. Research programs to develop such prediction techniques and to develop noise resistant structures are underway in the United States.

From the fluid mechanics point of view the STOL situation is somewhat different than past for two reasons. First, the interaction between the engine jet and the wing/flap surfaces changes the jet flow field, and results in a complex flow field whose steady components are not yet fully predictable. Knowledge of the steady components would seem to be required before the turbulent, and resulting fluctuating surface pressure and acoustic components could be understood. Second, the region of interest in the flow field is within the turbulent region where pseudo-sound or hydrodynamic flows may predominate rather than in the acoustic far field or near field. Turbulent regions of flow seem to have yielded slowest to understanding of their behavior.

Direct interaction of an engine exhaust jet with adjacent structural surfaces is of interest not only for the STOL speed range but also for supersonic speeds as discussed in the following paragraphs.

3. ADVANCED SUPERSONIC TRANSPORTS

The outstanding acoustic feature affecting the development of a supersonic transport has been the sonic boom. In the US this feature has eclipsed all other considerations. Nevertheless, there are other important problems associated with the acoustics of supersonic aircraft, some of the sources are indicated in Figure 10.

3.1 Acoustic sources for supersonic aircraft

The fluctuating surface pressures associated with the acoustic sources indicated in Figure 10 must be considered in designing empennage structure to withstand acoustic fatigue and in designing fuselage structure to keep out noise. Current indications are that the considerable efforts that went into the structural design of currently operational supersonic transports have been successful. The noise sources indicated in Figure 10 must also be considered in design of the advanced supersonic transports now under consideration for flight at speeds in the 2.7 Mach number range. In addition, however, current design considerations suggest that engine exhaust impingement loads may be important as indicated in Figure 11.

3.2 Possible engine locations for advanced supersonic transports

The sketches in Figure 11 show two of the engine location configurations under consideration for second-generation supersonic transports. The benefits of these engine locations are suggested at the lower left of Figure 11. Community noise reduction could occur by the shielding effect of the wing, which would reflect engine noise upward and thus away from the community on the ground. Lift augmentation could occur due to the aerodynamic circulation induced by the flow of engine exhaust over the top surface of the wing, at the same time however the

turbulent engine exhaust would be imposing large fluctuating pressures over very large areas of wing and fuselage structure, increasing the difficulty of designing fatigue resistant structure and quiet interiors. It would be valuable if it were now possible to predict the fluctuating surface pressures for these engine-impingement areas so that the penalty, if any, associated with these designs could be balanced against the advantages listed, but to this writer's knowledge this engine loading situation has not been investigated for the engines, exhaust velocities, and forward speeds associated with supersonic flight.

Again from the fluid mechanics point of view the change of jet flow field due to the interaction with the wing, and the central interest in the turbulent region of the flow are features which have not been studied extensively in the past.

4. SPACE SHUTTLE

4.1 Aero-acoustic load sources

The major sources of fluctuating pressure loads on the space shuttle vehicle are indicated in Figure 12. At launch the sound pressures originating in the engine exhaust radiate, and are reflected from the ground, upward along the complete vehicle. These loads subside as the vehicle picks up speed, and the loads associated with ascent increase and reach a maximum near the time of maximum dynamic pressure and Mach 1. During supersonic flight fluctuating pressures associated with shock waves are important. Later the solid rocket motors and the liquid propellant tank are released and the orbiter vehicle proceeds into orbit. At the time of re-entry from orbit separated flows and boundary layer noise may occur, perhaps near the time of maximum heating. In the next few figures the magnitudes and distributions of the fluctuating pressure loads will be discussed for each of these times of flight.

4.2 Shuttle engine launch noise

The magnitudes and spectra of the engine-induced noise loads at lift-off of shuttle are indicated in Figure 13. The overall SPL is shown to be 168 dB at the base of the vehicle, decreasing to 160 dB at the nose of the orbiter and 158 dB at the nose of the liquid propellant tank. The spectra indicate that the maximum energy in the sound occurs at frequencies from about 30 to 125 Hz. Thus, these noise levels are high enough that experience suggests they will constitute a significant design consideration, and the spectra show large energy at frequencies where structures can be expected to have resonances. In particular, the high noise levels surround the entire orbiter which has a unique thermal-protection structure that will be described later. The exterior of the payload bay is covered with intense low frequency noise that may be difficult to keep from damaging delicate scientific payloads.

4.3 Shuttle ascent loads

Fluctuating pressure loads during ascent are shown in Figure 14. The sketch at the upper right indicates that intense pressures exist on the external wall of the payload bay, as they did at launch. Thus, high payload noise levels may exist for long times during launch and ascent. Data from the three locations shown in the sketch at the lower right are graphed at the left of the figure. These data indicated that the noise energy is concentrated at low, structural-resonant, frequencies, and that the noise levels remain at fairly high values over a large range of Mach number.

4.4 Shuttle re-entry fluctuating pressures

Fluctuating pressures estimated for an early version of the shuttle orbiter are shown in Figure 15 for the re-entry phase of flight. While the spectra still indicate energy at (or below) frequencies where structural resonances can be expected, the overall fluctuating pressure levels (OASPL) are somewhat less than for the other phases of flight. These loads may therefore be less critical than launch or ascent loads, as long as they don't interact strongly with effects caused by the high temperatures of re-entry (shown in Figure 16).

4.5 Re-entry temperatures on shuttle orbiter

The distribution of temperature over the surface of the shuttle orbiter during re-entry is shown in Figure 16. These temperatures are typical of re-entry of the atmosphere from orbit, and are high enough that changes of material properties with temperature must be taken into account. In particular, changes of the fatigue failure behavior of shuttle materials and structures under these temperatures, in combination with orbital sub-zero temperatures, must be known in order to assess the effects of the cyclic stresses due to the fluctuating pressure loads. The structural system that has been proposed is shown in Figure 17.

4.6 Shuttle thermal protection system (TPS)

The shuttle thermal protection system (Fig.17) consists of high temperature, thermal insulation materials that enclose the low temperature aluminum load bearing sub-structure. These types of materials are used for different

temperature ranges. The materials are designed to be re-used for as many as 100 missions. The surface areas of the orbiter are covered with rectangular tiles that rest upon a high modulus strain arrestor layer and upon a low modulus strain isolator layer. These layers are intended to prevent strains from occurring in the tile material when the sub-structure flexes due to loads or changes dimension due to temperature. The acoustic loads may thus be the only loads imposed on the tiles. The tile material is a fibre reinforced silica ceramic material for which little basic design information is presently available. Preliminary indications are that the material is of low density (less than 0.24 specific gravity), low modulus (0.006 that of aluminum), and low strain to failure (less than 0.1 percent). The design process intended to prevent acoustic load failures of the TPS is indicated in Figure 18.

4.7 Structural acoustics of TPS

Five major activities indicated in Figure 18 are needed to assure a satisfactory thermal protection system. Early definitions of the loads (due to acoustic sources) and structure serve to support design life predictions that lead to approximately the correct structure. Early definitions of loads and structures have been presented here; damping tests are underway (Ref.13) and analyses are being prepared (Fig.19). Figure 19 indicates that advanced and detailed structural analysis methods are being utilized to obtain detailed stress and strain distributions. Once candidate designs have been obtained mission lifetime tests are carried out to help choose between candidates and to demonstrate the capabilities of the best design. A facility at NASA Langley Research Center used for such tests is shown in Figure 20. Finally, for both the test phase and for routine inspection between missions, methods must be developed for detecting failures using non-destructive tests (NDT) and for solving dynamic problems as they arise either by re-design or by temporary "fixes". As indicated by the word "noise" in the left-hand margin of Figure 18, three of these activities require, or could benefit from, effort and developments in the field of noise mechanisms. Data already presented has shown that aero-acoustic technology has provided estimates of fluctuating pressure loads. Mission lifetime tests depend for their validity on accurate simulation of flight fluctuating pressures; therefore continued efforts by aero-acoustic specialists are required to assure accurate simulation and to develop new simulation techniques. Finally, developments such as acoustic emission techniques for NDT can be valuable contributions, while developments that would reduce the applied loadings either by frequency shifts, re-direction of the noise, or by reduction at the sources (as is being attempted in the community noise area and in the aerodynamic drag area) could greatly ease the structural design problem.

4.8 Summary of aero-acoustics for shuttle

A summary of the aero-acoustic considerations described in this discussion for shuttle is presented in Figure 21. The main points are:

(1) that a substantial effort is required to assure that the thermal protection system does its job without failure due to acoustic-type loads and without weight penalties to the shuttle vehicle, and

(2) that substantial opportunities exist for advances in aero-acoustic technology to contribute to the shuttle development in the areas indicated in the figure.

5. REFERENCES

1. Lansing, D.L. et al. — *Dynamic loading of aircraft surfaces due to jet exhaust impingement.* In AGARD Conference Preprint No.113. Symposium on Acoustic Fatigue. September 1972.
2. Lansing, D.L. et al. — *Externally blown flap dynamic loads.* L-8630, STOL Technology Conference. NASA SP 320.
3. Hubbard, H.H. Chestnutt, D. Mayes, W.H. Magliori, D.J. — *Noise control technology for jet-powered STOL vehicles.* ICAS Paper 72-59 (Int. Coun. of Aero. Sci. 8th Cong.).
4. Janes — *All the world's aircraft.*
5. Fink, D.G. — *McDonnel Douglas AMST in final design.* Av. Week and Space Tech., May 7, 1973.
6. Brown, D.A. — *Public acceptance key to STOL.* Av. Week and Space Tech., March 6, 1972.
7. Brown, D.A. — *Advanced SST concepts studies.* Av. Week and Space Tech., January 17, 1972.
8. May, I.A. — *Acoustic testing, aircraft structures.* TL 950, A58, 1970.
9. Eaton, D.C.G. — *Development and testing of Concorde structure from noise aspects.* Environmental Engineering, September 1969.

10. Love, E.S. — *Advanced technology and the space shuttle.* 10th Von Kármán Lecture. Presented at the AIAA 9th Annual Meeting, Washington, DC. January 1973.

11. K..ker, C.E. Grandle, R.E. — *Thermoacoustic fatigue testing facility for space shuttle thermal protection system panels.* Presented at the 1972 Symposium on Fatigue at Elevated Temperatures, Storrs, Conn. June 1972.

12. – — NASA Space Shuttle Technology Conference: NASA TMX-2570, July 1972.

13. Grandle, R.E. Leadbetter, S.A. — *Vibration tests of candidate re-usable surface insulation tiles for space shuttle.* Presented at the Soc. for Experimental Stress Analysis Fall Meeting, Indianapolis, IN. October 1973.

14. – — NASA Space Shuttle Technology Conference: NASA TMX-2274, April 1971.

DISCUSSION

Prof.F.E.Siddon inquired about the status of some rece work on the use of porous structural surfaces to reduce radiated noise. **Dr Mixson** replied that the Langley sponsored work with BBN was completed, and that significant noise reductions had been observed, but that the effects of the porous surfaces on the lift and drag of the aerodynamic surfaces had not been completely evaluated. Dr Mixson went on to point out that the porous-surface work was one example of studies in the area of interaction of turbulent flows with non-rigid structural surfaces, and that this area holds the opportunity for fluids and structural specialists to cooperate on solutions of such important problems as the reduction of turbulence drag by appropriate fluids/dynamics design of the structural surface.

Dr A.Dinkelacker then observed that he and his colleagues had been working for about ten years on such methods of turbulence drag reduction but had not been able to progress to the solution. The paper co-authored by Dr Dinkelacker was mentioned as his latest effort in this area.

Ing.Gen.R.Legendre pointed out that the acoustic fatigue problem mentioned in the paper was not a new problem, but had occurred and had been solved during the development of the Caravelle Aircraft.

a) SPACE SHUTTLE

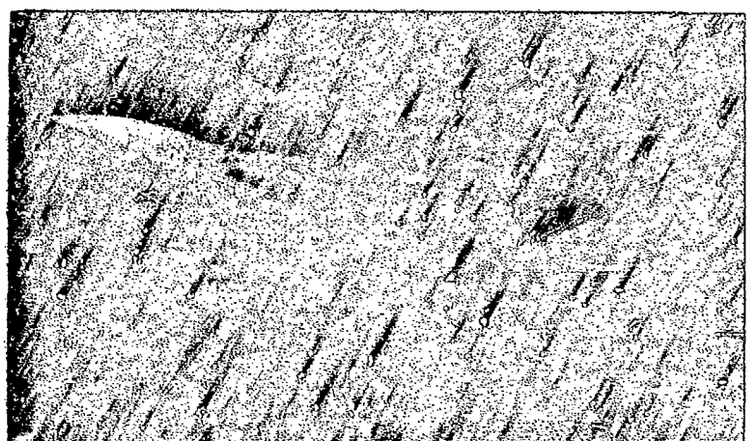

b) ADVANCED SUPERSONIC TRANSPORT

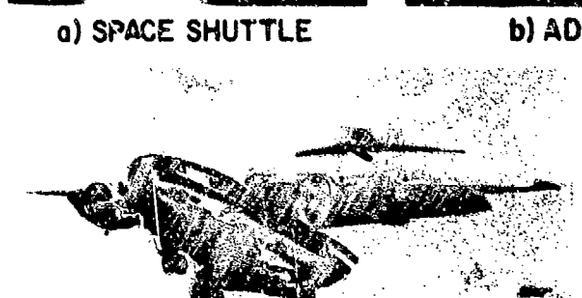

c) STOL TRANSPORT

- ACOUSTIC FATIGUE
- NOISE TRANSMISSION
  - PASSENGERS
  - SPACE PAYLOADS
- ELECTRONICS MALFUNCTION

d) NOISE EFFECTS ON STRUCTURES

Fig.1 Current aerospace vehicles and noise effects

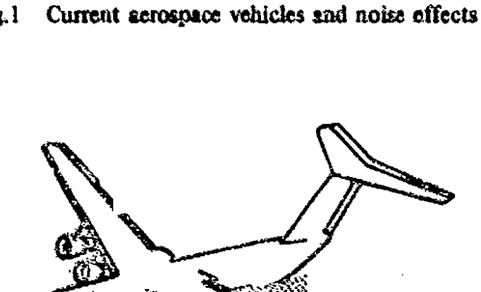

EXTERNALLY BLOWN UPPER SURFACE BLOWN AUGMENTOR WING

Fig.2 Integrated propulsion concepts for jet-powered STOL vehicles

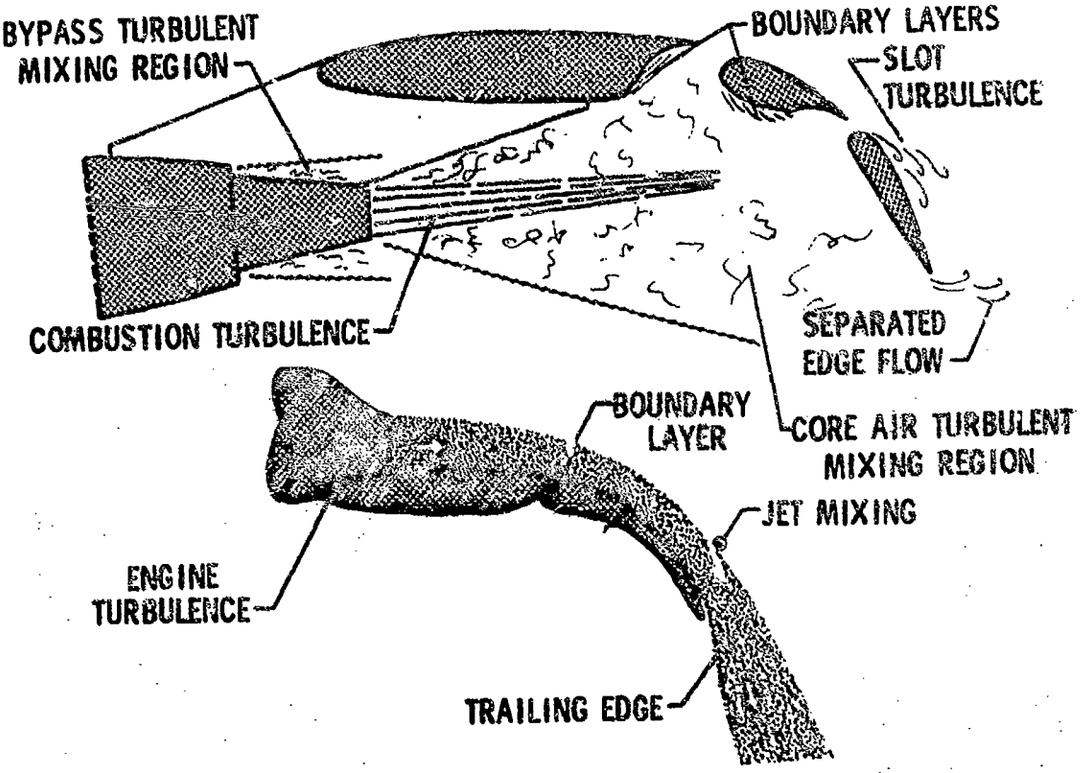

Fig.3 Sources of turbulent pressure fluctuations on blown flaps

Fig.4 Experimental studies of jet impingement surface pressure fluctuations

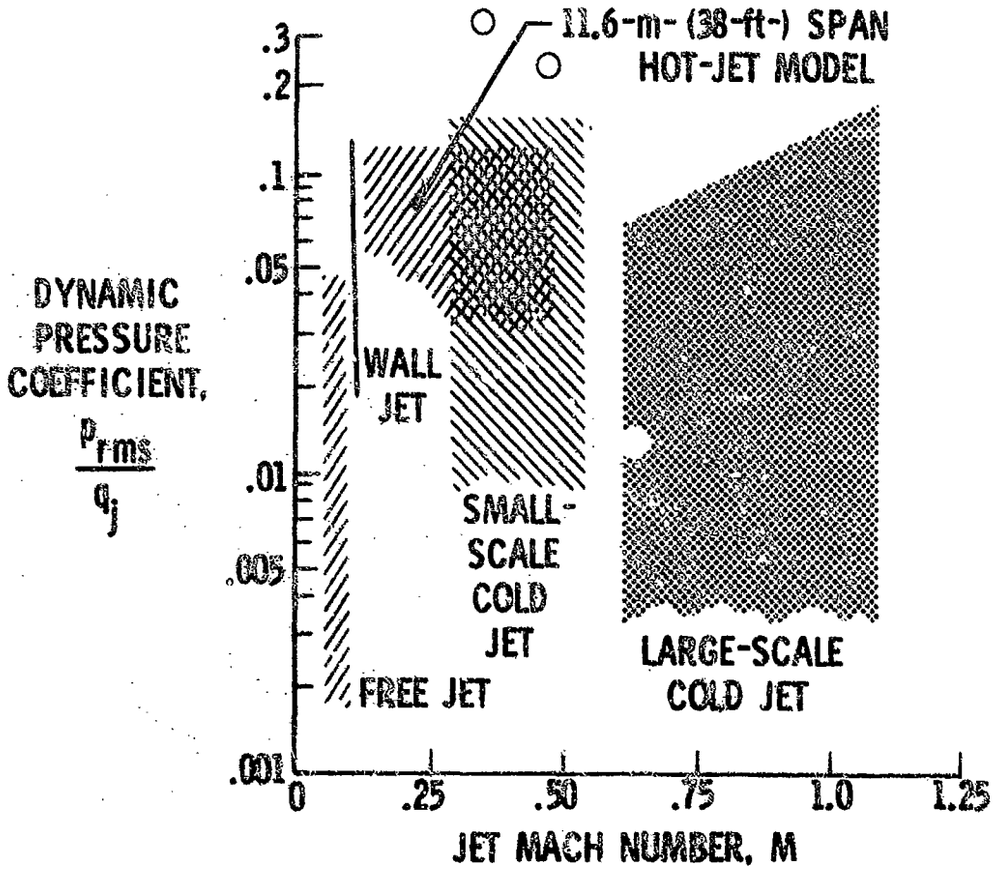

Fig.5 Comparison of dynamic pressure coefficients

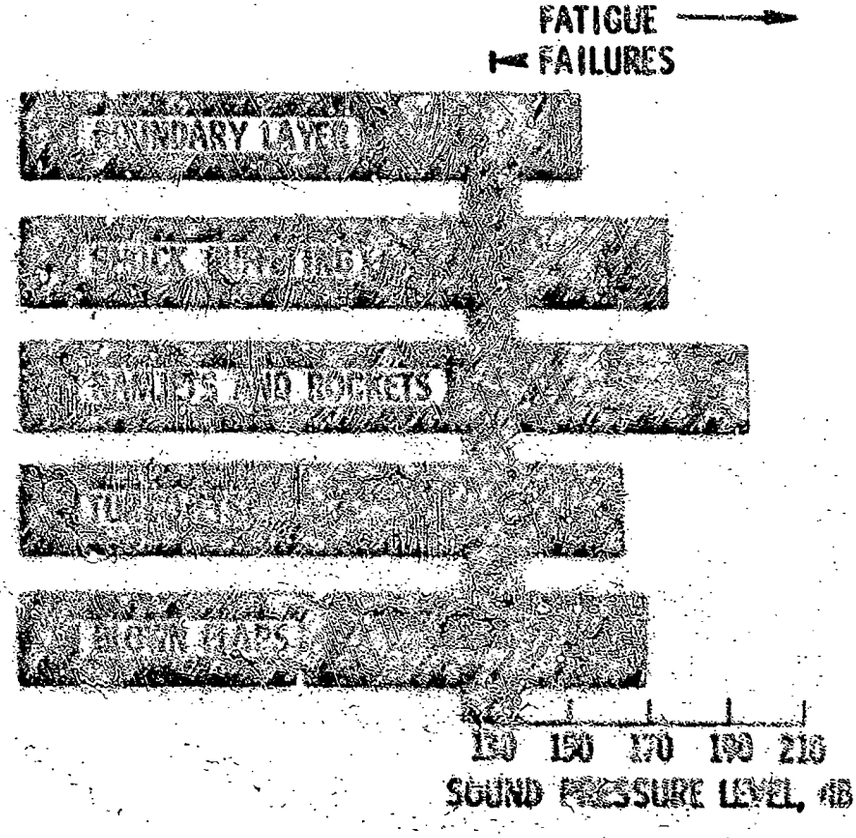

Fig.6 Sound pressure levels of acoustic loading on aircraft structures

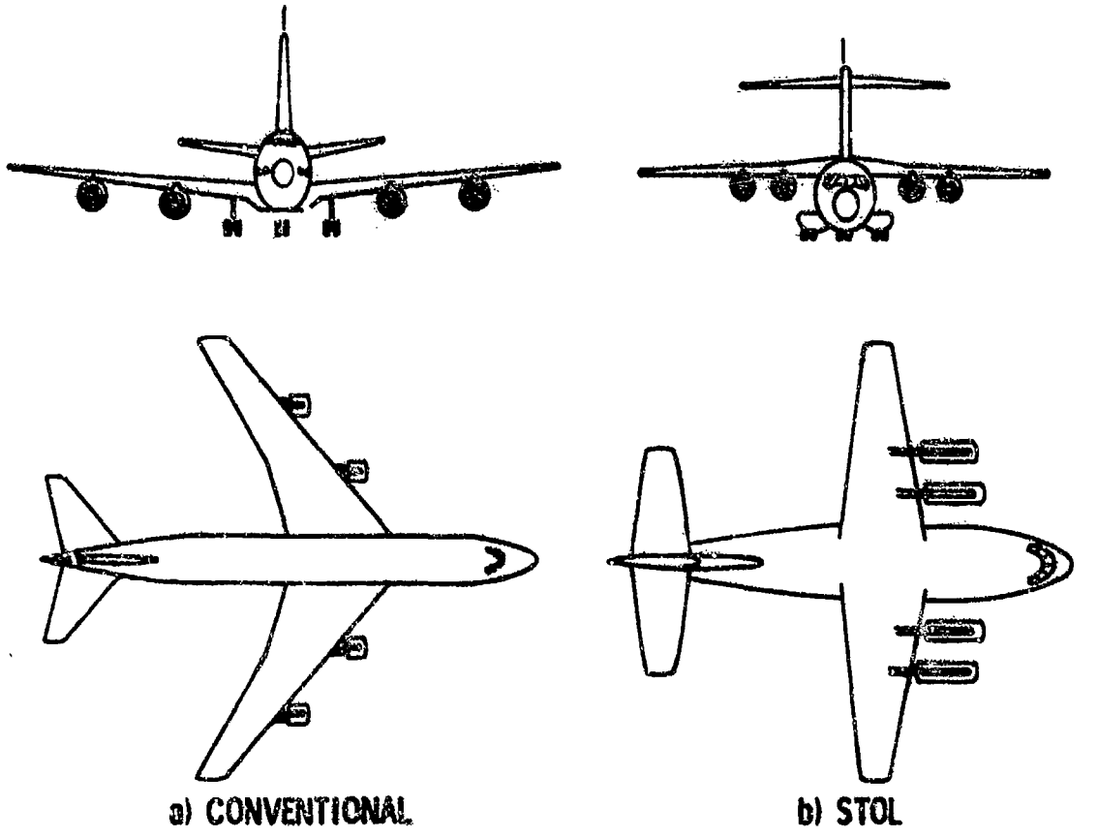

Fig.7 Comparison of engine-fuselage geometry for STOL and conventional aircraft

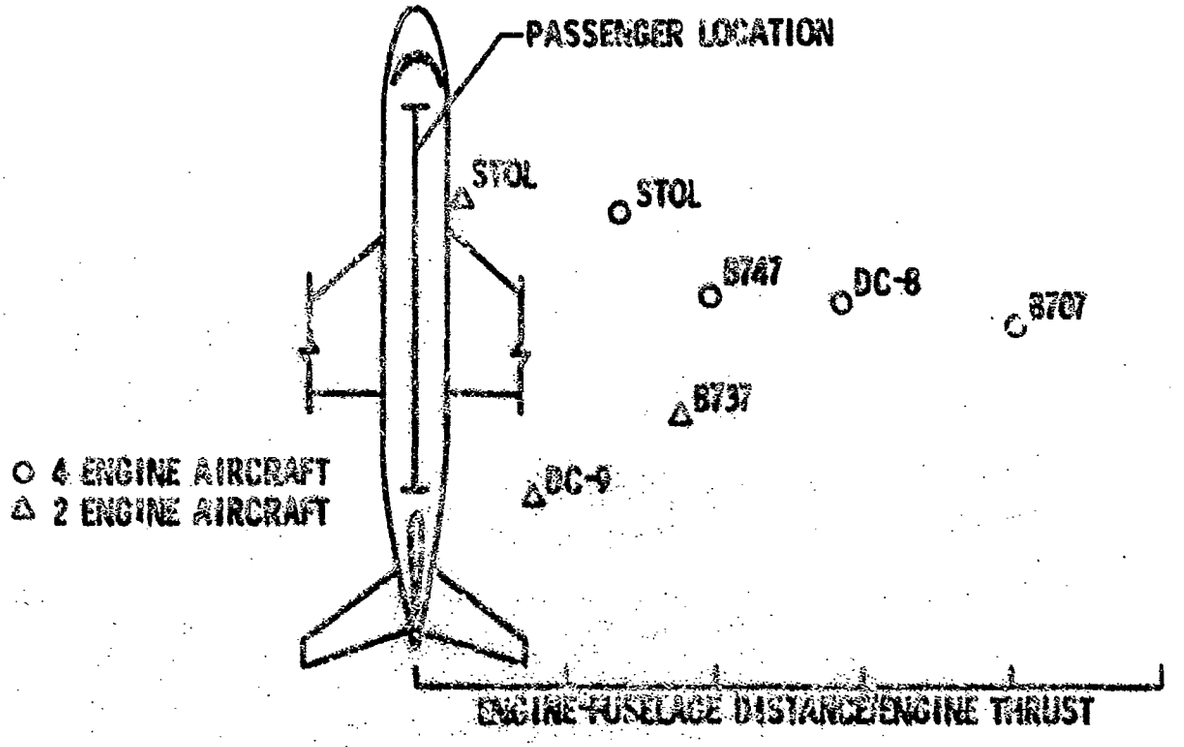

Fig.8 Normalized engine location for STOL and conventional aircraft

- MAJOR FLUCTUATING PRESSURE LOADS ARISE FROM

  ENGINE - JET IMPINGEMENT ON WING-FLAP SURFACES
  LOCATION OF ENGINES FORWARD AND NEAR FUSELAGE

- FLUCTUATING PRESSURES ARE LARGE, MAY COMBINE WITH HEAT
- SOURCES, FLOW/STRUCTURE INTERACTION EFFECTS ARE NOT ADEQUATELY UNDERSTOOD
- PREDICTION AND CONTROL TECHNOLOGY NEEDS DEVELOPMENT

Fig.9 Aero-acoustic considerations for propulsive lift STOL aircraft

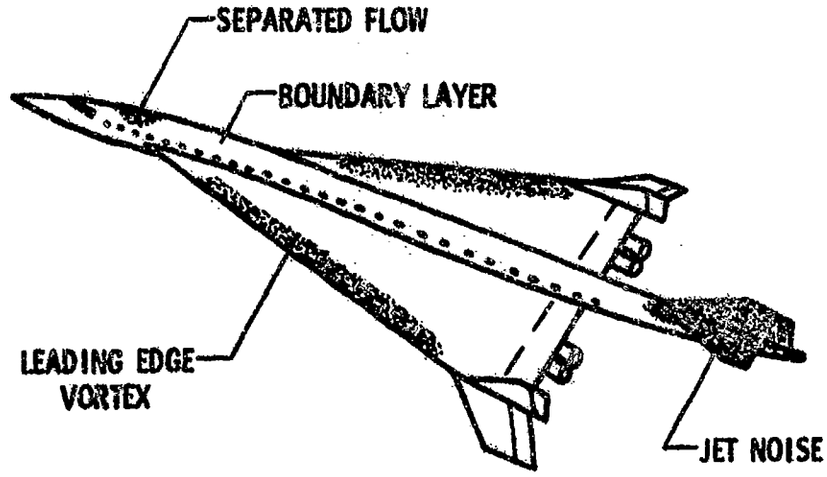

Fig.10 Sources of fluctuating pressures for supersonic aircraft

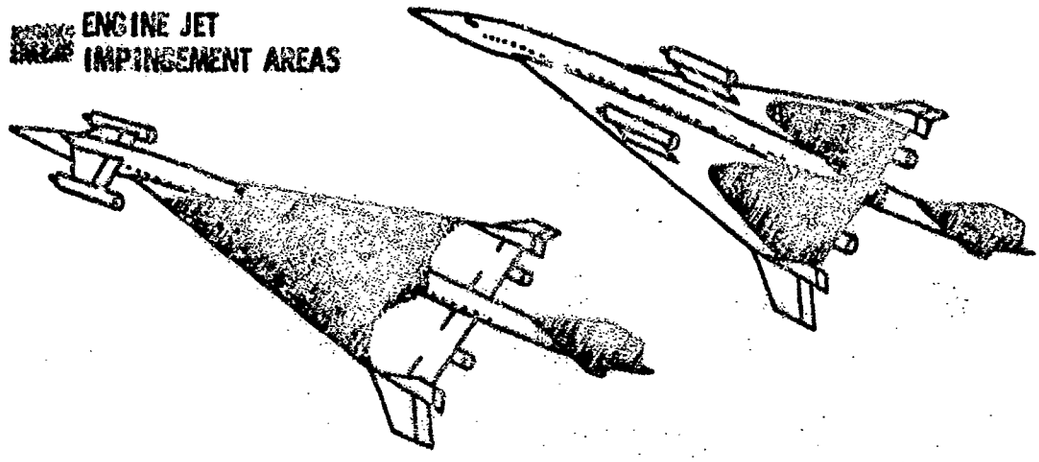

- ADVANTAGES
  - BETTER FLUTTER BEHAVIOR
  - IMPROVED c.g. LOCATION
  - COMMUNITY NOISE REDUCTION
  - LIFT AUGMENTATION
- PROBLEMS
  - HIGH INTERIOR NOISE
  - ACOUSTIC FATIGUE OF WING
  - LARGE AREAS COVERED
  - PREDICTION METHODS NEEDED

Fig.11 Engine noise considerations for advanced supersonic transports

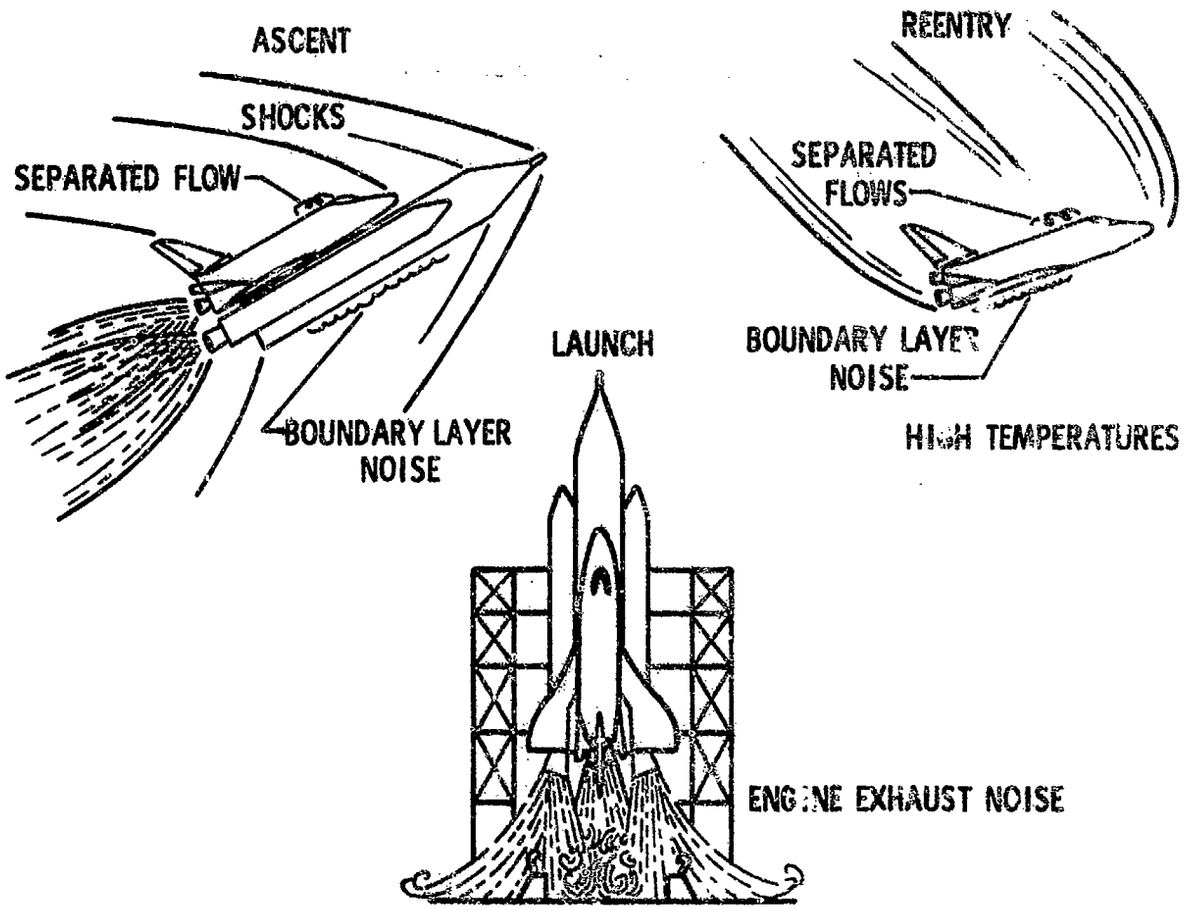

Fig.12 Aero-acoustic load sources for space shuttle

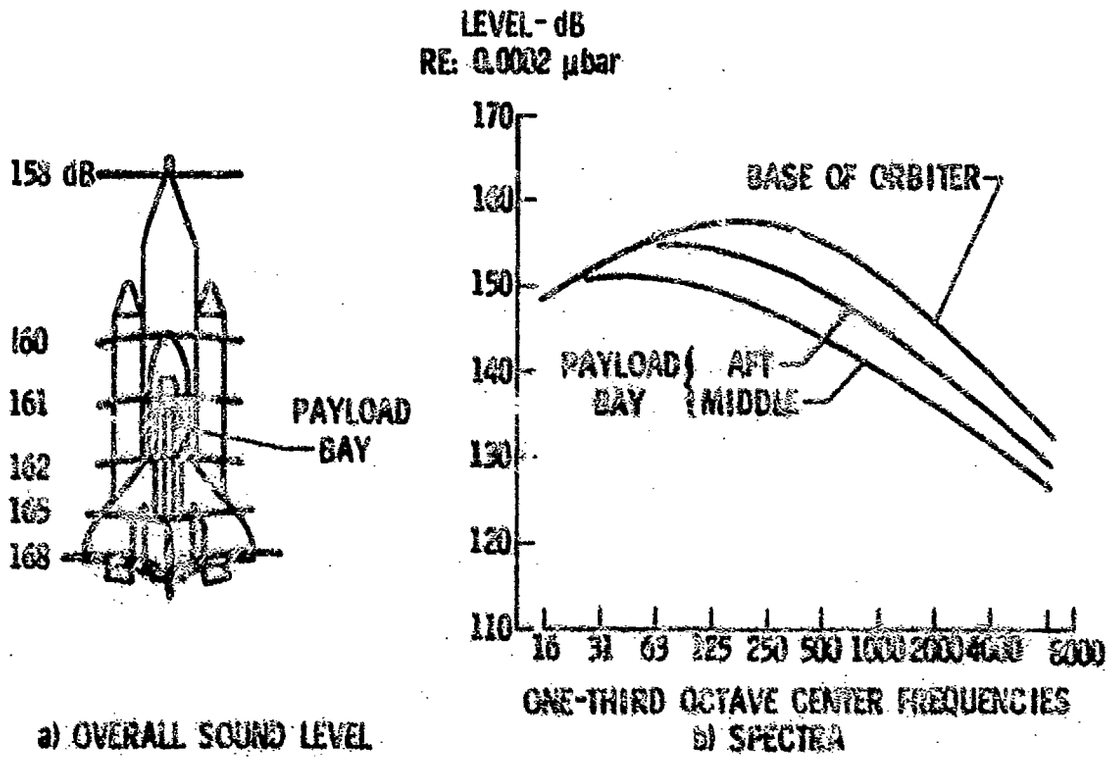

Fig.13 Engine induced acoustic loads at lift-off

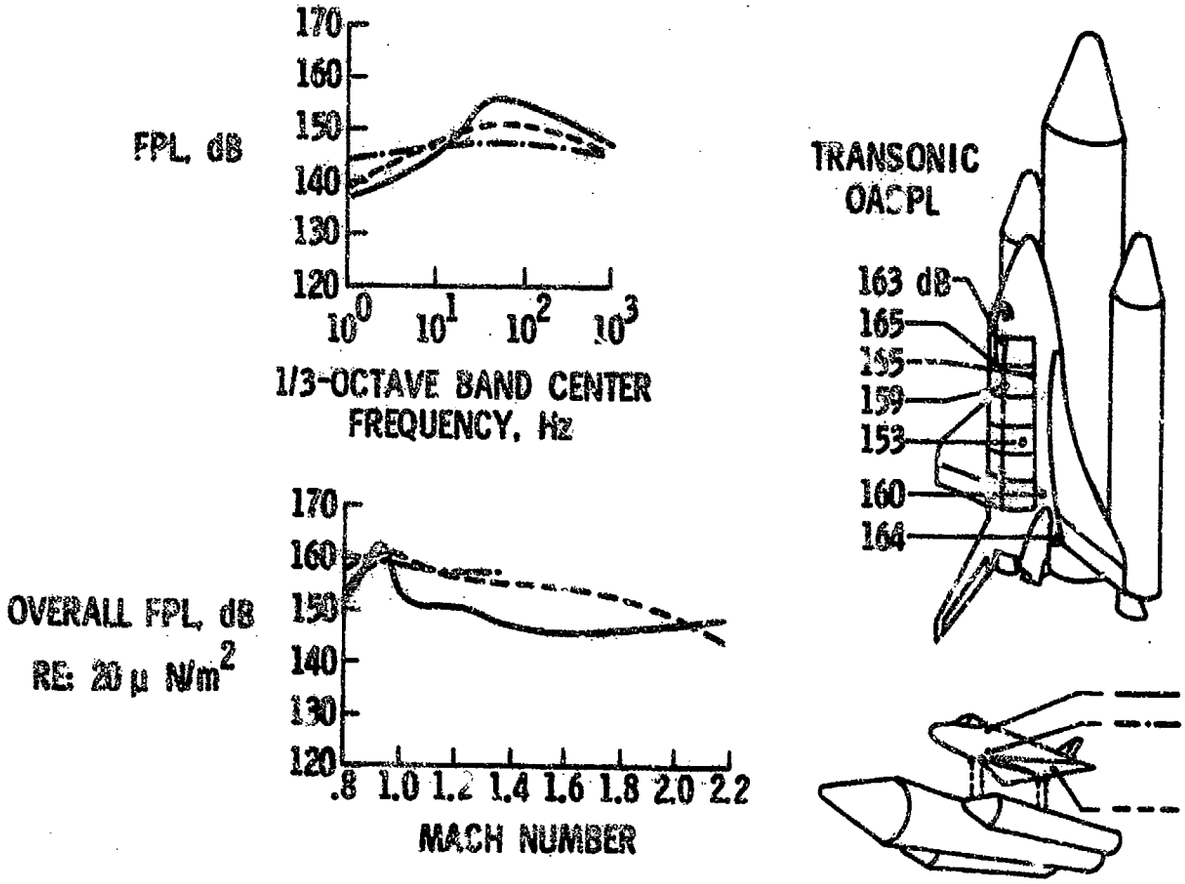

Fig.14 Estimated pressure fluctuations during ascent. $\alpha = \beta = 0°$

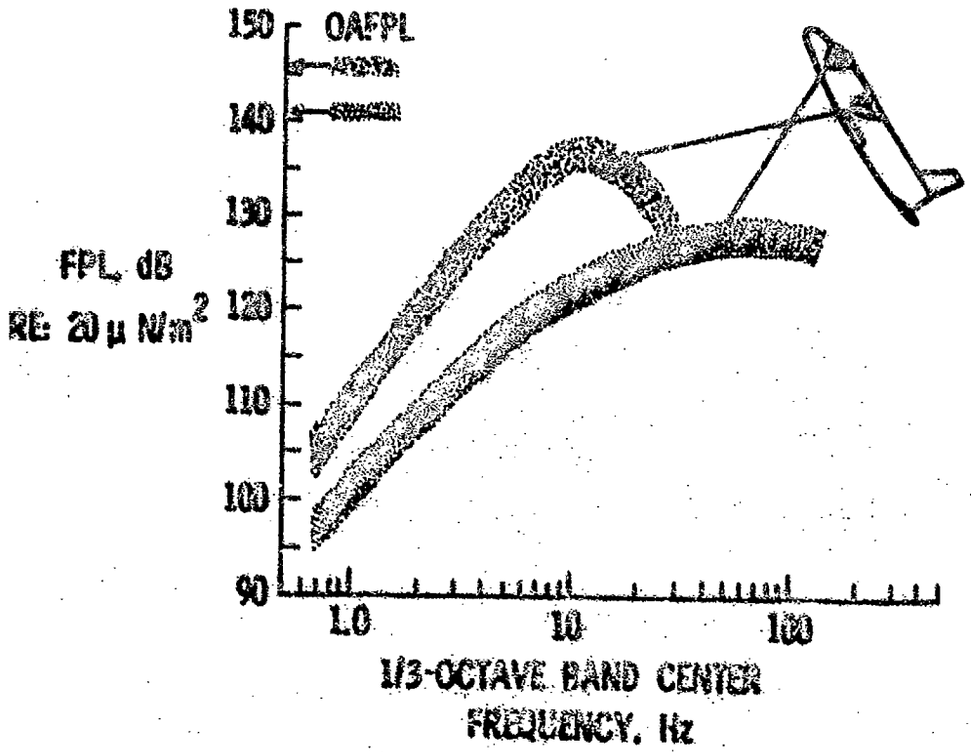

Fig.15 Estimated pressure fluctuations during re-entry. $\alpha = 60°$, $M = 4$

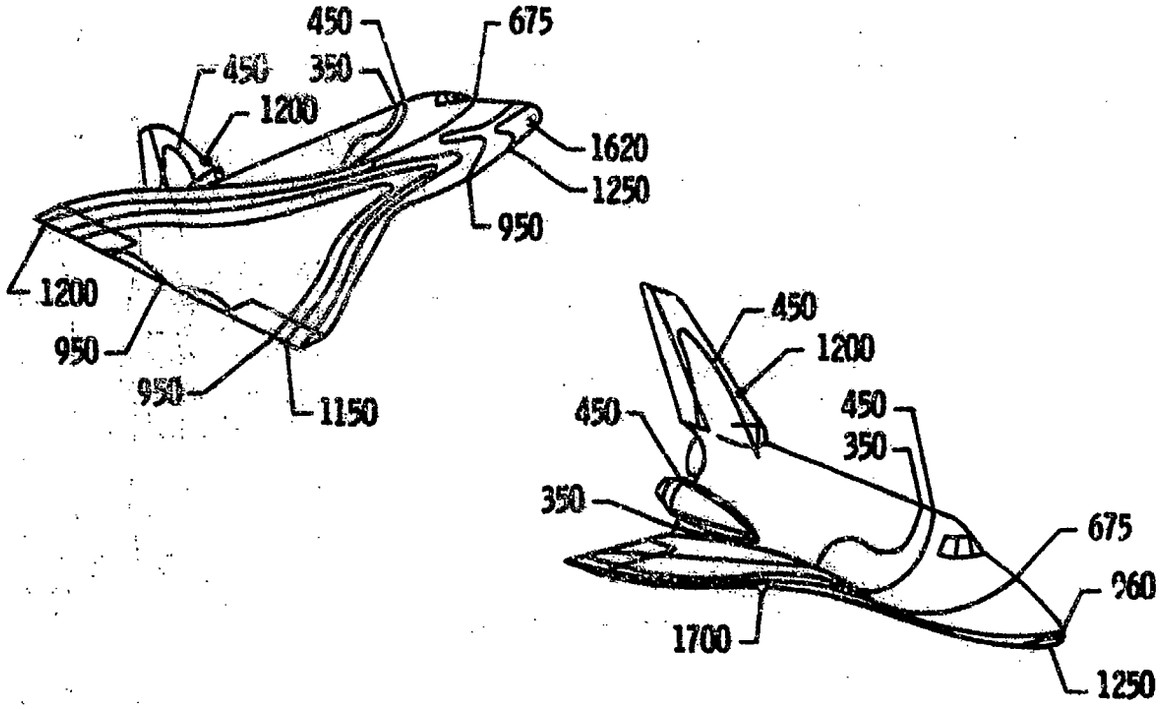

Fig.16 Predicted re-entry temperatures on space shuttle, degrees centigrade

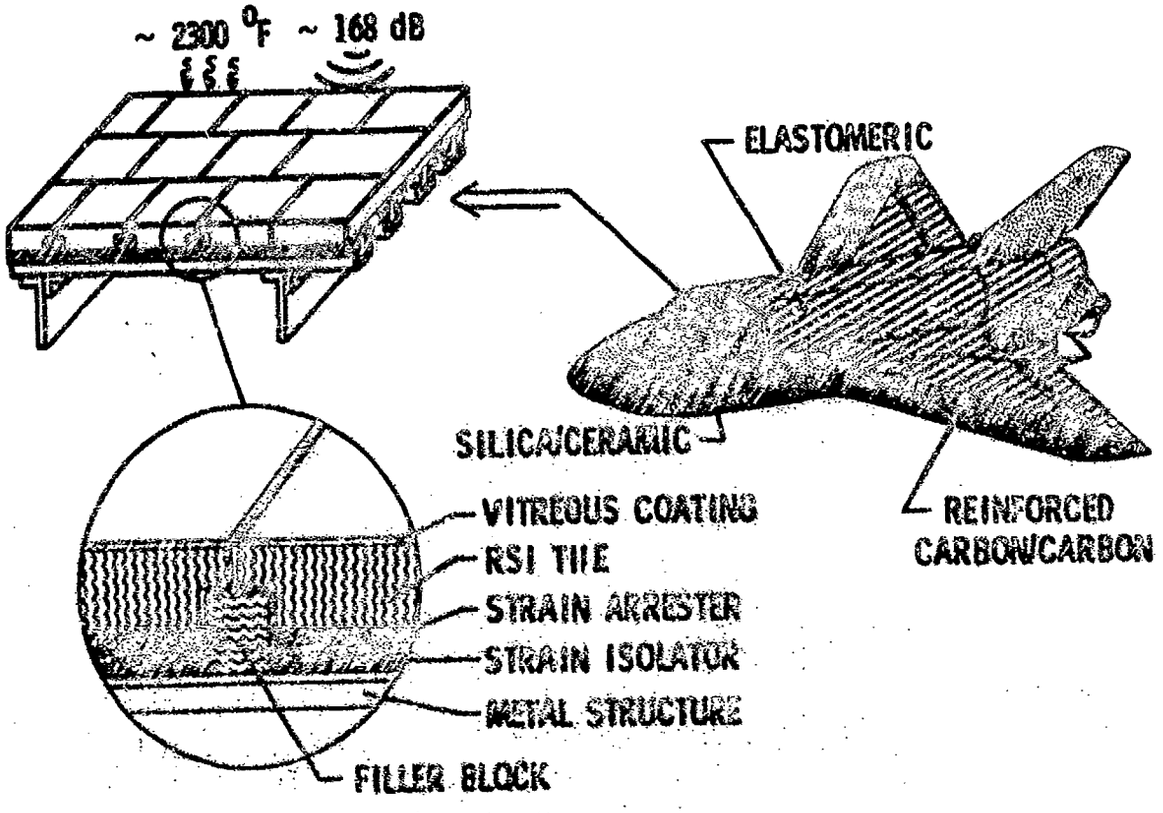

Fig.17 Space shuttle thermal protection system

"NOISE" ● DEFINE AERO-ACOUSTIC LOADS
LEVELS, DISTRIBUTIONS, DURATIONS, CORRELATIONS

● CHARACTERISTIC STRUCTURE AND MATERIAL
BASIC DESIGN FROM THERMAL AND STATIC LOADS
DYNAMIC PROPERTIES VS TEMPERATURE

● PREDICT USEFUL LIFE OF STRUCTURE
DYNAMIC ANALYSIS
TEST FOR DAMPING

"NOISE" ● MISSION LIFETIME TESTS UNDER SIMULATED FLIGHT ACOUSTIC LOADS

"NOISE" ● DEVELOP FAILURE INSPECTION (NDT), REDESIGN TECHNIQUES, PROBLEM FIXES

Fig.18 Structural acoustic development of thermal protection system

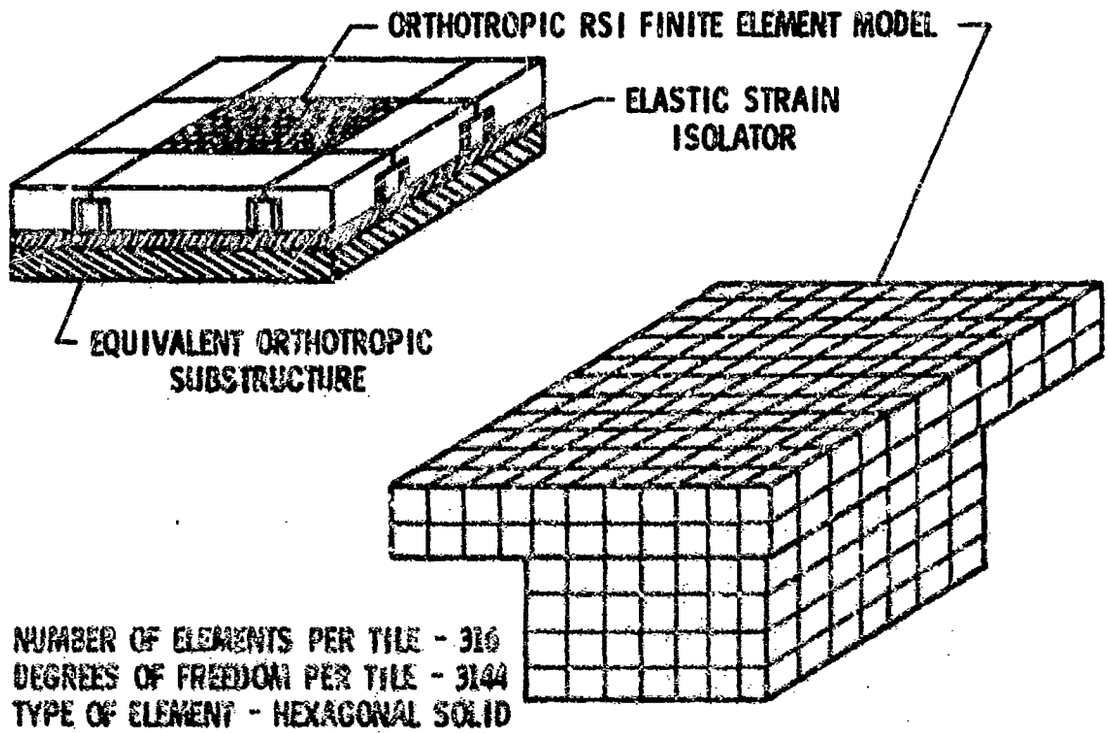

Fig.19 Dynamic analysis of shuttle TPS

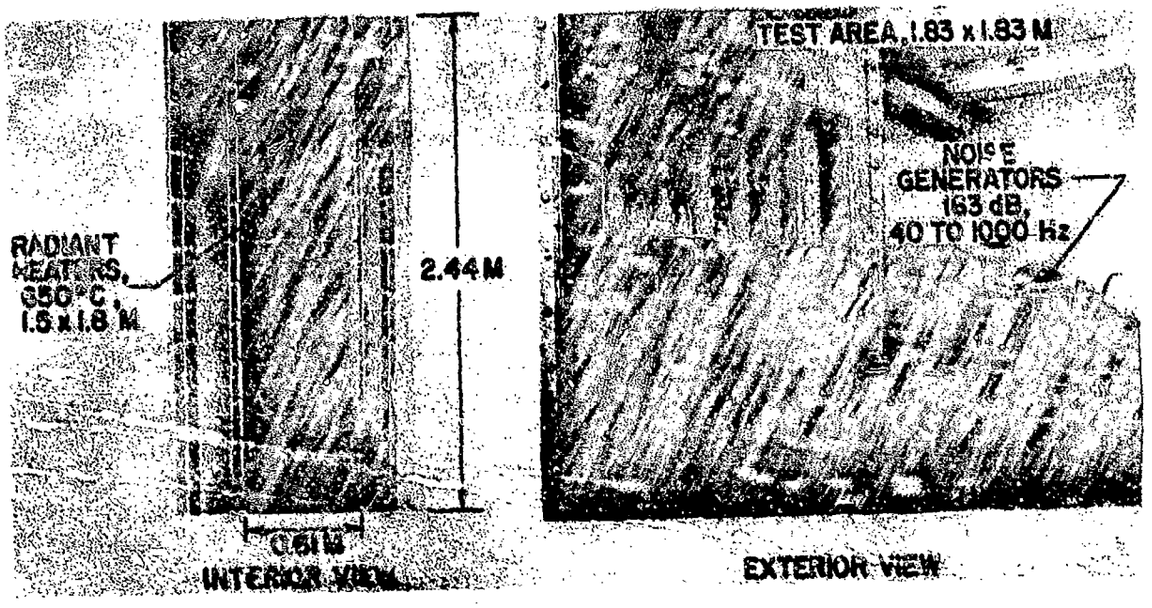

Fig.20 Thermoacoustic mission cycling facility for shuttle

- TECHNOLOGY IS AVAILABLE FOR PRELIMINARY ESTIMATES OF LOADS
- PREDICTED LOADS ARE HIGH, COVER LARGE AREAS OF STRUCTURE
- ACOUSTIC FATIGUE, NOISE TRANSMISSION DESIGN REQUIRES SUBSTANTIAL EFFORT
- ADDITIONAL AERO-ACOUSTIC WORK IS REQUIRED FOR

  FINAL LOADS DEFINITION
  ADEQUATE GROUND TEST SIMULATION
  CONTROL AND REDUCTION OF LOADS

Fig.21 Aero-acoustic considerations for space shuttle

RESOLUTION OF TURBULENT JET PRESSURE INTO AZIMUTHAL COMPONENTS

by

H.V.Fuchs
DFVLR-Institut für Turbulenzforschung, Berlin

(presented during Session I)

1. INTRODUCTION

Ten years have gone by since the first AGARD Specialists' Meeting on Noise Mechanisms was held. The meeting was documented in AGARD Reports 448–469. Many of the problems and ideas first discussed at the 1963 meeting have stimulated research in various fields. Among these problems were the following:

(a) Is there any chance of measuring fluctuating pressure accurately in the stream itself by inserting a probe? (References 1 and 2 pp.8–11)

(b) How do we interpret narrowband time- and space-correlations? (References 3 and 4)

(c) Is turbulence in a jet more coherent than was believed previously; and, if so, would a coherent emitter not be much more efficient than random emitters? (Reference 5)

These questions could be seen to originate from an uncertainty present in aerodynamic noise research, namely, how to find the most appropriate turbulence model to be introduced into the theory. Sears[6] described this continously unsatisfactory situation in his evaluation report on the second AGARD Specialists' Meeting in 1969:

"For the turbulent jet, indeed, fundamental understanding is meager . . . Clearly, we are suffering from our incomplete understanding of turbulence itself and it is commonplace to recommend once again that fundamental studies in that area be encouraged."

To question (a) it was argued by Ffowcs-Williams in 1963 in the discussion of paper[1] and also in the round table discussion[2]:

"I think it is possible, even in principle, to get at the pressure by simple probe measurements... By inserting the probe one changes the flow at the probe position by eliminating the term $\frac{1}{2}\rho u^2$. This, by all accounts, is large, so I doubt whether it will ever be possible to measure static pressure in this way."

Large efforts have nevertheless been expended and considerable progress has been made since 1963 in measuring fluctuating pressures within turbulent flows.

Fuchs[7] and Siddon[8] have shown independently that there are flow configurations where the error mentioned by Ffowcs-Williams does not impair the pressure measurements. In the core region of a subsonic jet, for instance, the ratio $\overline{p}/\rho\overline{u}^2$ (where $\overline{p}$ and $\overline{u}$ represent r.m.s. pressure and velocity) exceeds the critical value one by orders of magnitude as may be seen in Figure 1 which was taken from Reference 9. Static pressure probes are now successfully used in jets by research groups affiliated with Scharton and Meecham (BBN Inc. and University of California), at the General Electric Co. (Nagamatsu and others), and at Pennsylvania State University (Arndt and co-workers). Furthermore a group connected with Nakamaru (Osaka University) uses the pressure-probe technique for measurements in turbulent duct flows.

The measurement of turbulent jet pressure appears to have also stimulated the discussion of the structure of jet turbulence when cross correlations between the signals of an inserted microphone and a hot wire probe were first reported by Lau, Fisher and Fuchs[10]. After this project was completed, Lau[11] developed a new kind of conditional sampling technique in order to get a better understanding of how turbulence behaves in a circular jet. The present author[12], on the other hand, favoured narrowband space correlations as a means of investigating the space-time structure of the turbulent pressure field in more detail.

Question (b) concerning the interpretation of filtered time- and space-correlations was already discussed in 1963 by Skudrzyk and Haddle[4]:

"The time correlation of the received signal is a function of the filter only, and is entirely independent of the turbulence. The transition to the power spectrum has eliminated the phases; the limitation to a narrowband has eliminated all the remaining properties of the turbulence. All statistical phenomena whose spectrum does not vary over the received bandwidth will therefore have the same time-correlation function. . . If the turbulence were frozen, space and time would be interchangeable. Time delay τ would then be equivalent to the coordinate change $U\tau$ in the direction of the flow, which is equal to the distance traveled by the turbulence during the time interval τ; and the space- and time-correlation functions would be the same. But the turbulence is not frozen; the eddies deform, decay, and build up again; and, as a consequence, space- time-correlation functions are different. The two functions have a similar shape, but the oscillations of the space-correlation functions usually decrease at a much higher rate than those of the time-correlation function . . . Thus, the space-correlation function is a measure of the deformation and of the reshaping of the turbulent patches."

It is noted that this interpretation of filtered space correlations agrees with that given in the discussion of equations (A.6) and (A.7) of Reference 12. A strong statistical coherence was found in Reference 12 for certain frequency bands of the pressure in planes normal to the jet axis for lateral as well as for circumferential probe displacements. The corresponding narrowband, longitudinal space correlations indicated that these coherent frequency components travel downstream in an almost wave-like manner. Other frequency bands of the pressure field were found less coherent in the longitudinal as well as in the lateral and circumferential directions.

If the fluctuating pressure in the jet is understood as being induced by the same mechanisms which are responsible for the sound generation process, one arrives at the above mentioned question (c) which was raised in 1963 by Mollo-Christensen[5] (in connection with his strongly coherent, low frequency, near-field pressure patterns):

"Of course, correlation measures only the coherent part, which may be a small fraction of the total energy in the fluctuating field. On the other hand, a coherent emitter is much more efficient than a random emitter. Even if it is weak, it may emit more sound than a much more intense random emitter."

This question (c) could well modify Lighthill's "independent-eddy-concept" which still prevails among aero-acousticians in their picture of how noise is generated aerodynamically.

The importance of coherent structures for jet noise has, on the basis of some new experimental pressure data, become more than pure speculation since Michalke[13] has developed his expansion scheme for noise from circular jets. This scheme not only considers natural symmetry conditions which are typical for circular jets, but is also most capable of taking into account large-scale coherent phenomena of jet turbulence where these are found. The theory readily predicts the relative acoustic efficiency of axisymmetric and other azimuthal source components under varying conditions. The obvious dominance of the lower-order azimuthal components of the turbulent sources brings us to the main topic of this discussion contribution.

2. EXPERIMENTAL ANALYSIS OF THE TURBULENT JET PRESSURE FIELD

The hitherto obtained results from overall and narrowband correlations[10,12] provided an only qualitative idea of the coherent nature of the fluctuating pressure in a jet. The mere existence of statistical interdependence over distances spanning the whole noise-producing region was indeed unexpected and startling. The question about its relevance to the noise problem, nevertheless, requires more quantitative data of how strong (in fluctuating energy, for instance) the large-scale coherent part is relative to the rest of a locally measured turbulent quantity.

- Is the coherent structure perhaps an almost negligible quantity which could only be detected by sophisticated and obscure correlation techniques?
- Is it sensible to normalize correlation functions by local intensities when these vary by a factor of ten and more within "correlation volumes"?
- How can we envisage considerable sound emission from wave-like disturbances which grow and decay while travelling downstream subsonically?

With these and other possible objections in mind a very simple model is proposed here which is based on and adjusted to Michalke's expansion scheme[13].

2.1 The Model

In this set of experiments we will, for simplicity, restrict ourselves to the turbulent pressure field in a fixed plane normal to the jet axis (Fig.2).

For any given instant of time the pressure on a radius r from the jet axis varies with φ in such a way that it repeats itself after 360° no matter how random the distribution may be on such a circle. It is then, of course, trivial to analyse this instantaneous pressure distribution in a Fourier series of m azimuthal components. The

phase character of the lower order components ($m = 0, 1, 2$) is indicated in Figure 2. The $m = 0$ component may be called axisymmetric since both magnitude and phase of this component are constant on r, i.e. independent of φ. At some instant later the magnitude and phase will have changed in an unpredictable manner; but again there will be no variation circumferentially. For the $m = 1$ component the sign of the pressure may be positive on one half-circle and negative on the other simultaneously. The $m = 2$ component changes sign four times, and so on.

It is noted that magnitude and phase of all the individual azimuthal components may vary with r and x. Certain specific features of a circular jet, in particular, enable the following assumptions to be made:

(i) For symmetry reasons the magnitude and phase of the various azimuthal components fluctuate with no statistical coupling between different components. The axisymmetric component in particular, is uncorrelated with the remaining azimuthal components (cf Reference 13).

(ii) The pressure on the axis of a strictly symmetric circular jet consists of only the axisymmetric component with all the others vanishing there.

(iii) The axisymmetric pressure component at a given radius r is assumed to be ideally correlated with that on the jet axis except for a constant phase shift in the time development of both fluctuations.

(iv) The correlation function of two circumferentially displaced probes (Fig.3(c)) is independent of the direction of the displacement ($\Delta\varphi > 0$ or $\Delta\varphi < 0$).

Some of the above assumptions may still require further consideration, but here they are taken for granted and may help to quantify circumferentially coherent turbulence components from three different correlation techniques.

2.2 Experimental Techniques and Results

(a) In the first set of experiments three probes were arranged as in Figure 3(a) with the pressure p_0 detected on the jet axis and the other pressure signals p_1 and p_2 taken at $r = 0.5\,D$ (diametrically opposite locations in the central mixing region). Three different correlations were evaluated, namely $\overline{p_0 p_1}$, $\overline{p_0(p_1 + p_2)}$ and $\overline{p_0(p_1 - p_2)}$, the coefficients of which are given in Table 1. The first one is particularly high when the signals are both passed through narrowband filters at a Strouhal number of about 0.45. An even higher coherence, namely 0.83, results when the sum of p_1 and p_2 is statistically compared to p_0. These values indicate a strong axisymmetric pressure component, which was artificially increased by adding p_1 and p_2 in the mixing region.

When, on the other hand, the axisymmetric and all even azimuthal components are artificially eliminated from the mixing region signals by subtracting p_2 from p_1, a very low coherence is found. This last result proves that the $m = 0$ component on the axis is, to some degree of accuracy, uncorrelated with all odd azimuthal components in the difference signal $p_1 - p_2$ (compared with assumption (i)).

TABLE 1

Normalized Correlation Functions with Pressure Probes Arranged as Shown in Figure 3(a) (corresponding velocity correlations in brackets)

	Signals unfiltered	*Signals filtered at* St = 0.45
$\dfrac{\overline{p_0 p_1}}{\sqrt{\overline{p_0^2}}\sqrt{\overline{p_1^2}}}$	+ 0.35 (+ 0.03)	0.66 (0.13)
$\dfrac{\overline{p_0(p_1 + p_2)}}{\sqrt{\overline{p_0^2}}\sqrt{\overline{(p_1 + p_2)^2}}}$	+ 0.57 (+ 0.07)	0.83 (0.19)
$\dfrac{\overline{p_0(p_1 - p_2)}}{\sqrt{\overline{p_0^2}}\sqrt{\overline{(p_1 - p_2)^2}}}$	− 0.07 (+ 0.04)	0.06 (0.01)

The numbers in brackets in Table 1 give the corresponding correlation results for the case when all three pressures p_0, p_1, p_2 are replaced by the corresponding axial velocity fluctuations u_0, u_1, u_2 from hot-wire probes. Although the coefficients are considerably lower (indicating that the circumferentially coherent part in the velocity is relatively small), the doubling and the eliminating of the axisymmetric ($m = 0$) component has essentially the same effects as in the pressure results.

(b) The second correlation technique used only two microphone probes which were radially displaced by a variable r as shown in Figure 3(b). From these lateral space correlations one can calculate the axisymmetric component contained in the signal at the displaced point using the assumptions (i) to (iii). The details of this procedure are given in Reference 14. A typical result is depicted in Figure 4. Apart from the directly measured spectra at $r = 0.5\,D$ and $r = 0$ the coherence $S_{pp,\omega}$ between the filtered pressures at the displaced points is also plotted as a function of the filter frequency. From these experimental data the spectrum of the axisymmetric pressure component at the displaced point was calculated from

$$\tilde{p}_{\omega,0}(r) = \tilde{p}_{\omega}(r)\, S_{pp,\omega}(r) \tag{1}$$

and plotted as curve (d).

It is possible by this method to map the spectra of the axisymmetric pressure and velocity components throughout the jet by varying r and subsequently changing the plane $x = \text{const}$ in the measurements. One set of these results is shown in Figure 5 for the plane $x = 3\,D$.

So far, we were only able to separate the $m = 0$ component from the other azimuthal components. The distribution of the fluctuating energy is probably best seen in a plot like that in Figure 6. A comparison of the curves (a) and (b) shows that for Strouhal numbers from 0.4 to 0.5 about half of the energy is concentrated in the axisymmetric component, whereas both sides of the spectral peak much more energy is contained in non-symmetric components.

(c) To further analyse the non-symmetric components of turbulence (curve (b) in Figure 6) still another correlation technique was employed which more rigorously breaks down the turbulence into a series of azimuthal components.

The third method is based on circumferential space correlations with r and x held constant for one set of correlations. (Compare Figure 3(c).) A curve like that in Figure 7 for which pressures in the mixing region were correlated, for example, at $St = 0.45$ is Fourier-analysed with respect to $\Delta\varphi$, and the corresponding Fourier coefficients $R_{\omega,m}$ for $m = 0 \ldots 16$ are depicted as vertical columns in the same figure. For $\Delta\varphi = 0$ the Fourier series

$$R_{\omega}(\Delta\varphi) = \frac{\overline{p_{\omega 1}\, p_{\omega 2}}}{\sqrt{\overline{p_{\omega 1}^2}}\,\sqrt{\overline{p_{\omega 2}^2}}} = \sum_{m=0}^{15} R_{\omega,m} \cos(m\,\Delta\varphi) \tag{2}$$

reduces to the sum of the fluctuating energies contained in the various azimuthal pressure components:

$$R_{\omega}(0) = 1 = \sum_{m=0}^{16} R_{\omega,m} = \sum_{m=0}^{16} \frac{\overline{p_{\omega,m}^2}}{\overline{p_{\omega}^2}}\,. \tag{3}$$

A number of 16 Fourier coefficients was deemed sufficiently large, since most of the energy is stored in the lower order azimuthal components from 0 to 3 or so, at least for the pressure at Strouhal numbers about 0.45.

From the corresponding narrowband circumferential correlations at other frequencies one may find the power spectral distributions of any single azimuthal component of the pressure according to

$$\overline{p_{\omega,m}^2(x, r)} = R_{\omega,m}(x, r)\, \overline{p_{\omega}^2(x, r)}. \tag{4}$$

Figure 8 shows a superposition of the $m = 0$ to 3 power spectral densities (PSD) suitably normalized as

$$\text{PSD} = \frac{\overline{p_{\omega}^2}/(\rho_0 U_0^2)^2}{\Delta f D/U_0} \tag{5}$$

where U_0 is the jet exit velocity, D the nozzle exit diameter, ρ_0 the density and Δf the bandwidth of the filter.

The upper solid curve is the PSD measured directly at $x = 3\,D$, $r = 0.5\,D$ and the lower solid curve represents the PSD of the axisymmetric turbulent fluctuations obtained from circumferential correlations. The latter may be compared with corresponding results from the lateral correlation method; the open circles at curves (a) in Figure 6 indicate reasonable agreement between the two independent sets of results.

In Figure 9, where the PDSs are plotted without superposition, the dominance of the $m = 0$ component is again apparent, and the other components are seen to peak in roughly the same range of Strouhal numbers although their energy is spread more evenly with increasing m.

3. CONCLUDING REMARKS

The results presented so far are only the first stage of a continuing effort to fully analyse the turbulent pressure field with respect to the jet noise problem. Much more information is required involving the more general cross-correlation functions (cross-spectral density distributions in the frequency domain) with all three displacements: longitudinal, lateral and circumferential.

The analysing techniques employed have already proven useful. The preliminary results have contributed to the question of exactly how strong the coherent part of the pressure field is in a plane $x = 3D$ normal to the jet axis. Future research will also have to compare the structure of the tubulent pressure field with that of the turbulent velocity field.

It is hoped that investigations along these lines will finally enable us to introduce a realistic turbulence model into a theory like that proposed by Michalke[13]. Three points will be summarized at the end, which are felt to support our belief that this is a promising approach to the jet noise problem too:

(i) Michalke's expansion scheme predicts that, for small Strouhal numbers, the lower-order azimuthal turbulence components play a dominant role in the noise generating mechanisms provided such components are present in the source region at all.

(ii) The experimental analysis of the turbulent pressure field at low Mach numbers seems, in fact, to indicate that considerable turbulent energy is stored in lower order azimuthal components and, in particular, in the large-scale coherent axisymmetric type of fluctuation. This confirms earlier experimental results by Crow and Champagne[14], who showed how orderly structures develop in the turbulent region of an externally excited jet.

(iii) It would still be feasible that all the coherent phenomena (ii) together with their being efficient sound emitters (i) occur in a range of frequencies or Strouhal numbers which is entirely unimportant with respect to radiated noise. In this context it may be worth mentioning that it is very roughly the same range of Strouhal numbers between 0.1 and 1.0 where a strong radiated farfield coincides with dominating orderly structures in the turbulent near-field.

Some of the suggestions put forward in this paper are far from being conclusive. There is still the question of how close we are to the real turbulent sound sources even when analysing the pressure in the mixing region. Some clarifying information may probably be obtained from so-called causality correlations which were initiated in several research groups by Siddon[15]. Results from correlating the acoustic pressure with the pressure in the jet by Scharton, Meecham and others[15,17] indicated a relatively high maximum correlation coefficient (up to 0.5) when both fluctuations are filtered in the relevant range of Strouhal numbers.

ACKNOWLEDGEMENT

This work was performed in close cooperation with Prof. Michalke of the Technische Universität Berlin and was partially supported by the Deutsche Forschungsgemeinschaft. Part of the correlation measurements were done by cand. ing. F.Bischoping as a Diplomarbeit. The author wishes to thank colleagues for many stimulating discussions.

REFERENCES

1. Strasberg, M. — Measurements of fluctuating 'static' and totalhead pressure in turbulent wake. AGARD Report 464 (1963).

2. Ginoux, J.J. — Future research on noise. (A round table discussion.) AGARD Report 469 (1963).

3. Wills, J.A.B. — On convection velocities in turbulent shear flows. AGARD Report 457 (1963).

4. Skudrzyj, E.J. Haddle, G.P. — The physical picture of flow noise. AGARD Report 462 (1963).

5. Mollo-Christensen, E. — Measurements of near-field pressure of subsonic jets. AGARD Report 449 (1963).

6. Sears, W.R. — Technical evaluation report on AGARD Specialists' Meeting on *Aircraft Engine Noise and Sonic Boom*. AGARD Advisory Report 22 (1970).

7. Fuchs, H.V. — *Survey of Pressure Fluctuations Associated with Turbulence*. University of Southampton, ISVR Mem. 282 (1969).

8. Siddon, T.E. — *On the Response of Pressure Measuring Instrumentation in Unsteady Flow*. University of Toronto, UTIAS Report 136 (1969).

9. Fuchs, H.V. — *Measurements of Pressure Fluctuations within Subsonic Turbulent Jets.* J. Sound and Vibr. Vol.22, pp.361-378, (1972).

10. Lau, J.C. et al. — *A Study of Pressure and Velocity Fluctuations Associated with Jet Flows.* University of Southamptoc, ISVR Report 28 (1970).

11. Lau, J.C. — *The Coherent Structure of Jets.* University of Southampton, Ph.D.Thesis (1971).

12. Fuchs, H.V. — *Space Correlations of the Fluctuating Pressure in Subsonic Turbulent Jets.* J. Sound and Vibr. Vol.23, pp.77-99, (1972).

13. Michalke, A. — *An Expansion Scheme for the Noise from Circular Jets.* Z.Flugwiss, Vol.20, pp.229-237, (1972).

14. Crow, S.C. Champagne, F.H. — *Orderly Structure in Jet Turbulence.* J. Fluid Mech., Vol.48, pp.547-591, (1971).

15. Siddon, T.E. — *New Correlation Method for Study of Flow Noise.* 7th Int. Congr. Acoust., Paper 25N12, Budapest 1971.

16. Scharton, T.D. White, P.H. — *Simple Pressure Source Model of Jet Noise.* J. Acoust. Soc. America, Vol.52, pp.399-412, (1972).

17. Hurdle, P.M. et al. — *Correlation Investigation of the Noise Generating Region of a Jet Engine by Means of the Simple Source/Fluid Dilatation Model.* Symp. Transp. Noise, pp.64-85, Stanford (1973).

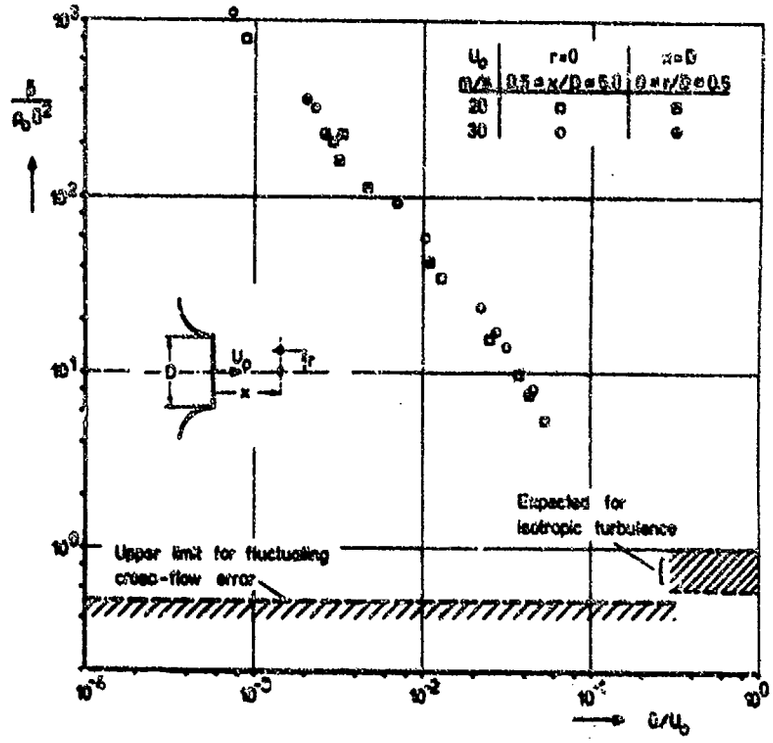

Fig. 1 Approximate signal-to-noise-ratio for fluctuating pressure measurements in the core of a jet

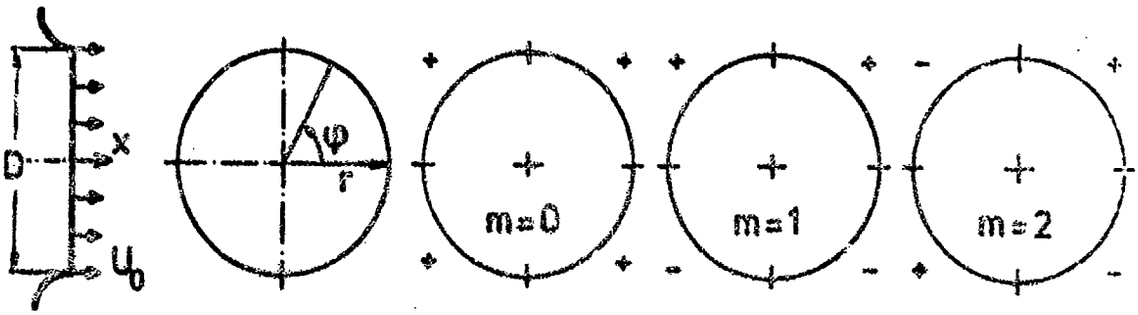

Fig. 2 Illustration of azimuthal components of the turbulence in a plane normal to jet (x = const)

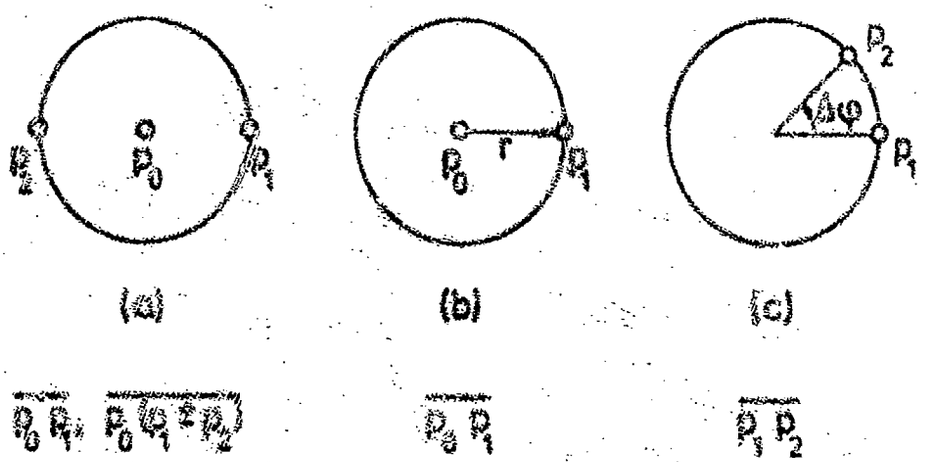

Fig. 3 Probe arrangement for correlation measurements in a plane normal to jet

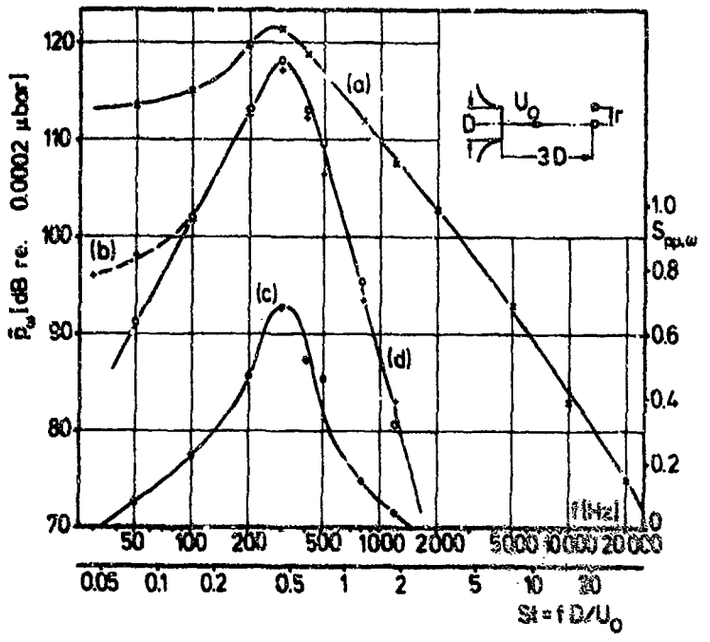

Fig. 4 (a) Power spectral density $\tilde{p}_\omega$ as measured at r = 0.5 D,
(b) Power spectral density $\tilde{p}_\omega$ as measured at r = 0
(c) Lateral coherence $S_{pp,\omega}$ of turbulent pressure field,
(d) Spectral distribution $\tilde{p}_{\omega 0}$ of axially symmetric pressure disturbance at r = 0.5 D
x = 3 D, D = 100 mm, U_0 = 65 m/s, Δf = 10 Hz

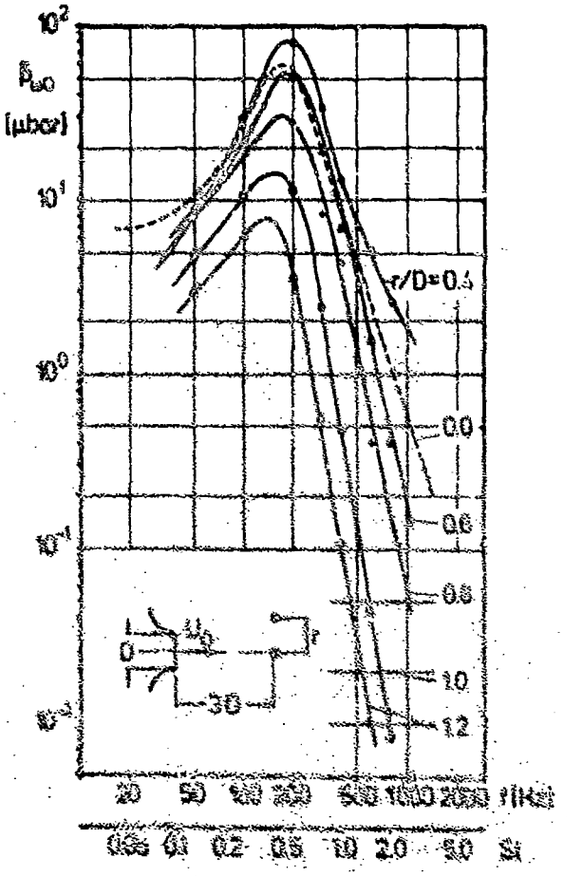

Fig. 5 Power spectral density $\tilde{p}_{\omega 0}$ of axially symmetric pressure disturbance for varying radial position r
x = 3 D, D = 100 mm, U_0 = 40 m/s, Δf = 10 Hz

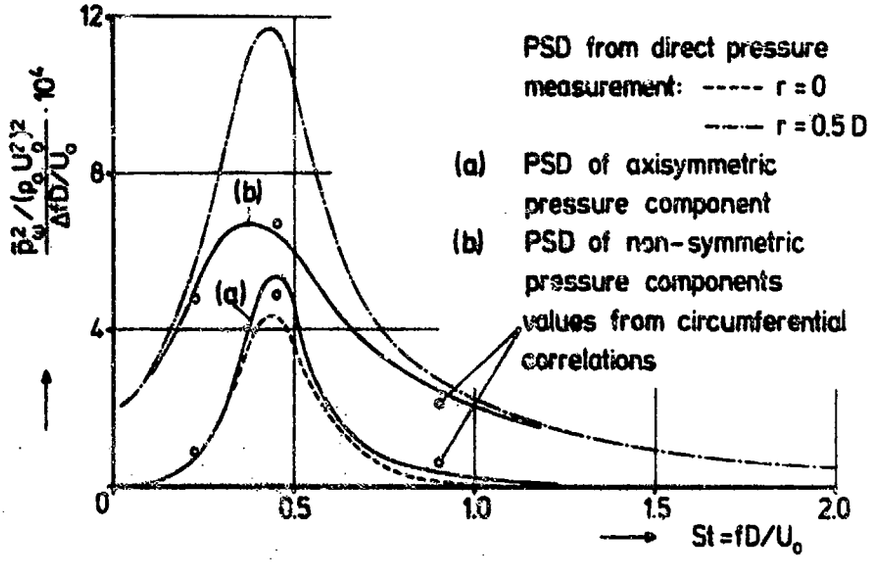

Fig. 6 Synthesis of normalized PSD of jet pressure from axisymmetric and non-symmetric components (from lateral correlations)
D = 10 cm U_0 = 60 m/s Δf = 10 Hz x = 3 D r = 0.5 D

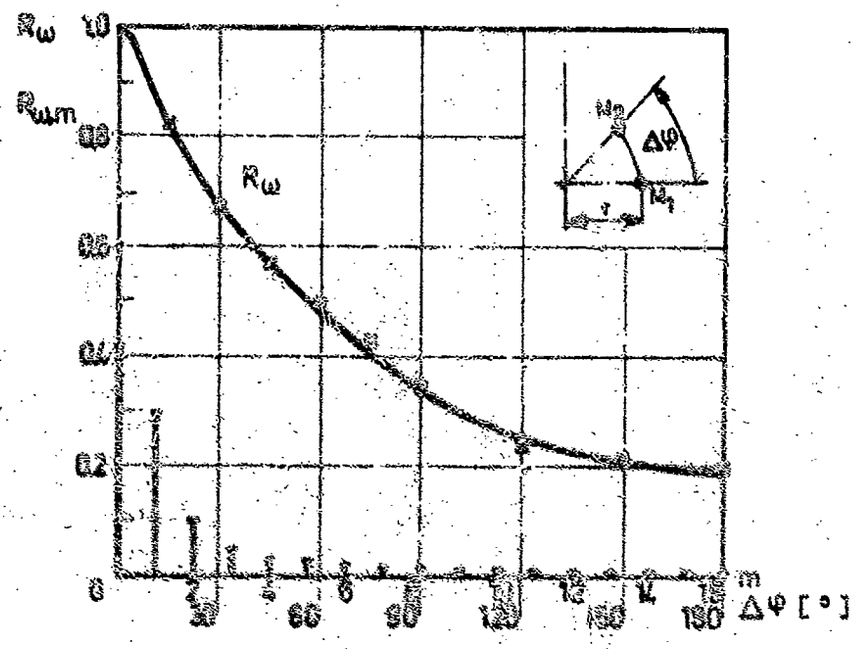

Fig. 7 Circumferential correlation of filtered pressure R_ω and corresponding Fourier coefficients $R_{\omega,m}$ (m = 0 ... 16)
x = 3 D r = 0,5 D U_0 = 60 m/s St = 0.45

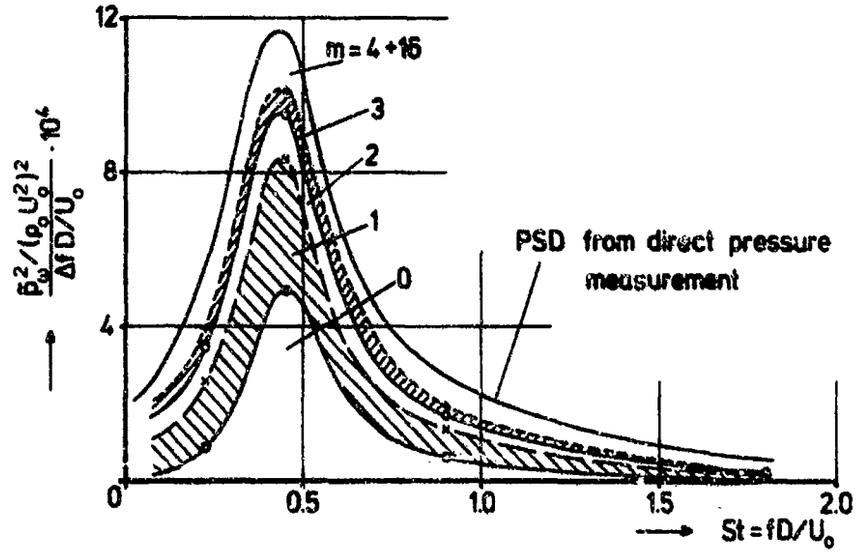

Fig. 8 Synthesis of normalized PSD of jet pressure from m = 16 azimuthal components (from circumferential correlations)
D = 10 cm U_0 = 60 m/s Δf = 10 Hz x = 3 D r = 0.5 D

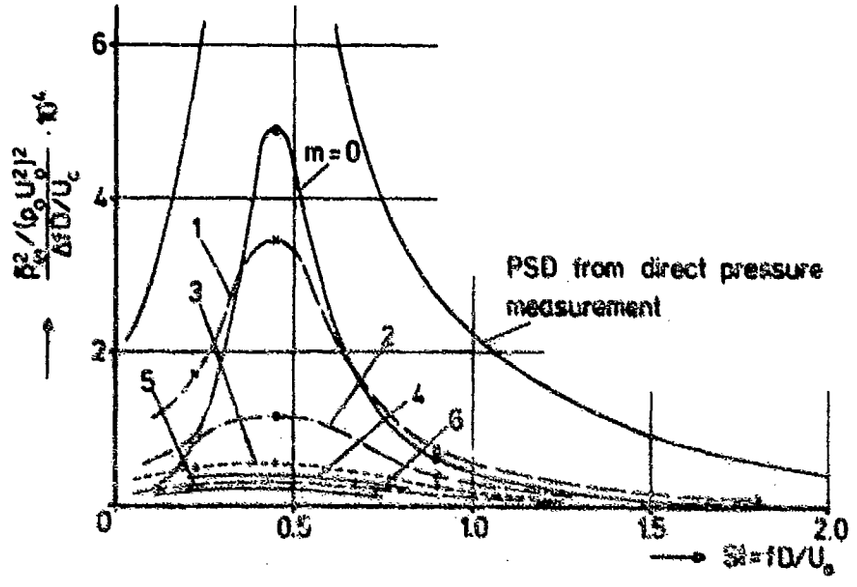

Fig. 9 Normalized PSD of different azimuthal components of jet pressure (from circumferential correlations)
D = 10 cm U_0 = 60 m/s Δf = 10 Hz x = 3 D r = 0.5 D

SOME EXPERIMENTAL RESULTS ON EXCESS NOISE

by

A.D.Young
Department of Aeronautical Engineering
Queen Mary College
(University of London)

(presented during Session I)

It will be of interest to particips. at this stage of the Meeting to hear a brief summary about some experimental results on excess noise obtained by a student of mine, Mr K.K.Ahuja[1], using a test installation at the National Gas Turbine establishment.

EXPERIMENTS

Compressed air was ducted from a 12 in diameter pipe through a diffuser into a plenum chamber 24 in in diameter and 4 ft long followed by a contraction leading to a nozzle from which the air emerged into the atmosphere in an anechoic chamber as a jet. The plenum chamber contained a honeycomb and gauze to help reduce the flow turbulence and the exit nozzles had diameters of 1.52 in, 2.4 in and 2.84 in so that the contraction ratios correspondingly ranged from 130:1 to 250:1. The resulting jets were therefore very steady and with low turbulence levels. Noise measurements were made at a distance of 6 feet from the nozzle exit.

In addition to the measurements on the basic jets, various modifications were introduced upstream of the nozzle exit to produce various intensities and scales of turbulence or overall disturbances there and the consequent effects on the noise characteristics were measured. These modifications included:

(a) Insertion of 1 ft, 2 ft and 3 ft lengths of pipe of same diameter as nozzle.

(b) Cylindrical obstructions of circular (1 in diameter) and rectangular section (0.4 in × 1.0 in) inserted 4 in upstream of the nozzle exit (see Figure 1(a)).

(c) Eight radial jets of air from $\frac{1}{4}$ in diameter pipes impinging on the main flow in the nozzle (see Figure 1(b)).

(d) Four tangential jets from $\frac{1}{4}$ in diameter pipes impinging on the main flow in the nozzle (see Figure 1(c)). These introduced a swirl as well as turbulence.

(e) A guide vane in the form of a plate spanning the plenum chamber and twisted through 180° along its length to produce a swirl without a major increase of turbulence.

The turbulence introduced by (a) was typically boundary layer turbulence of relatively small scale but with an intensity reaching a maximum near the wall of the order of 10%. The obstructions (b) introduced eddies of size comparable to their dimensions and with fairly well defined frequencies. The radial jets (c) introduced large scale turbulence with an intensity that varied between 15% and 25%. The turbulence introduced by the tangential jets (d) had also major large scale components and the intensity was believed to be even larger than with the radial jets, reliable measurements were not possible because the hot wires repeatedly broke. The swirl angles produced by the tangential jets depended on their velocity relative to that of the main jet but angles as high as 25° were obtained. The twisted plate (e) produced angles of swirl of the order of 10°.

The main jet speed was varied between 200 and 1000 ft/s. The auxiliary radial and tangential jets derived from the same source as the main jet and their speed therefore depended to some extent on the main jet speed, at the highest main jet speeds auxiliary jet speeds of about 300 ft/s were possible, whilst at the lowest main jet speeds the auxiliary jet speeds could be as high as 700 ft/s.

MAIN RESULTS

The main results for the normalised peak overall sound pressure levels measured are illustrated in Figure 2.

The curve for the clean jet follows a power law varying between V^8 and V^9 down to about 300 ft/s; at $\theta = 90°$ the law is very closely V^8 but the index tends to increase from 8 to 9 as the angle θ is reduced to the peak OASPL value ($\theta = 20°$)*. However, it is found that the acoustic power watt levels follow a V^8 law for the same speed range. Below 300 ft/s the index decreases to a value between 6 and 7. Detailed examination of the spectra shows good agreement with the predictions of Lighthill's theory[2] for low frequencies, but for the higher frequencies the predicted convective amplification close to the jet axis was not in evidence possibly due to scattering and refraction effects by the jet turbulence at these frequencies. Similar results were obtained by Lush[5].

It is clear from these results that if adequate care is taken to eliminate upstream sources of turbulence the dominant noise sources associated with a jet remain the clasical quadripoles and the V^8 law is closely followed down to jet speeds as low as 300 ft/s. Figure 2 shows for comparison the spread of results (shaded area) obtained for various engines and it will be seen that marked departure from the V^8 law has occurred for them at jet speeds of upwards of 800 ft/s. This illustrates the marked amount of excess noise to be found in practice on current engines.

If we now consider the circular and rectangular cylindrical obstructions we see from Figure 2 that the former shows a noise increase of about 30 dB, over the speed range tested, of which 4 dB can be associated with the discrete tones characteristic of the obstruction, whilst for the latter the increase is about 5–6 dB down to about 600 ft/s and at 300 ft/s the increase is about 20 dB. The discrete tones for the rectangular obstruction account for about 2–4 dB. It is, however, surprising to note that the curve for the circular obstruction runs more or less parallel to the 'clean jet' curve down to 300 ft/s whilst that for the rectangular obstruction is similarly parallel down to about 500 ft/s. One would expect that the pressure fluctuations associated with the separated flow past such obstacles to result in a strong dipole content in the resulting noise generators and a consequent V^6 law. A possible explanation is that the variation with Reynolds number in the fluctuating lift forces on the obstructions is such as to raise the effective index from 6 to 8 or more. Evidence in support of this can be derived from experiments of Gerrard[3]. The angle relative to the jet axis of peak overall sound pressure load with the obstructions present was between 45° and 60°, as compared with about 20° for the clean jet.

The pipe insertions of up to 3 ft in length upstream of the nozzle exit produced no significant change in the noise characteristics and intensity as compared with the clean jet. However, it will be seen that the large scale eddies engendered by the radial and tangential tubes were associated with both a marked increase in noise intensity particularly at the lower jet speeds and also a marked reduction in the index of the velocity law for the peak overall sound pressure level ($\theta = 60°$). In more detail, it was found that at values of θ between 60°and 90° the velocity law index was between 5 and 8 for low frequencies but it progressively reduced with increase of frequency, whilst at angles less than about 30° the high frequency noise was sharply reduced, again possibly because of scattering and refraction effects by the jet turbulence.

The swirl produced by the twisted plate in the plenum chamber produced no significant increase of turbulence in the jet and it resulted in a small reduction of about 2½ dB, in noise intensity at the single jet speed tested (260 ft/s†).

CONCLUDING REMARKS

Inferences that can be drawn from these results:

(1) Excess jet noise does not arise from small scale turbulence but is largely associated with the development of eddies of a scale comparable with the nozzle diameter. Thus the pipe extensions produced no effect but the large scale eddies associated with the obstructions or the auxiliary radial and tangential jets produced very marked increase of noise.

(2) Swirl by itself, in the absence of large scale turbulence, may in fact reduce the noise intensity rather than increase it.

These inferences need more data to confirm them than were obtained in the present set of experiments, but in the light of current theories they seem plausible. Thus, we may well expect that large scale eddies would be associated with both the variations in overall mass flow rate that Ffowcs Williams[6] suggested would give rise to monopole sources and the variations in pressure developed over the nozzle exit end lip that he argued would give rise to dipole sources. On the other hand small scale turbulence of the boundary layer type would not be expected to contribute significantly to either of these possible modes of contribution to excess noise.

The effect of swirl may well be to stabilize the flow and so reduce the turbulence and hence the noise if the associated transverse velocity gradients are of the right sign.

---

* Here θ is the angle between jet axis and the line joining the nozzle exit and the microphone.

† The twisted plate required a special drive to be fitted to the plenum chamber and it was not found possible to secure this in such a way as to permit higher jet speeds.

These arguments suggest that excess noise may be minimised by suppressing as far as possible all sources of large scale turbulence, whilst by the use of a suitable swirl significant overall reductions of jet noise may be obtained.

REFERENCES

1. Ahuja, K.K. — *An Experimental Study of Subsonic Jet Noise with Particular Reference to the Effects of Upstream Disturbances.* Thesis submitted for M.Phil degree of University of London, 1972.

2. Lighthill, M.J. — *On Sound Generated Aerodynamically.* I General theory. Proc. Roy. Soc. A211, 564–578 (1952). II Turbulence as a source of sound. Proc. Roy. Soc. A222, 1–21 (1954).

3. Gerrard, J.W. — *An Experimental Investigation of the Oscillating Lift and Drag of a Circular Cylinder Shedding Turbulent Vortices.* J.F.M., 11, 244–256 (1961).

4. Ffowcs Williams, J.E. — *Jet Noise at Very Low and Very High Speeds.* AFSOR-UTIAS Symposium on Aerodynamic Noise, Toronto (1968).

5. Lush, P.A. — *Measurements of Subsonic Jet Noise and Comparisons with Theory.* J.F.M. 46 Pt. 3, 477–500 (1971).

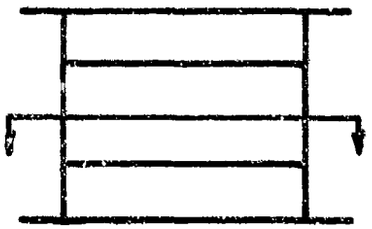

CIRCULAR OBSTRUCTION

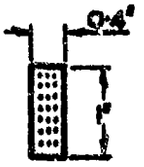

RECTANGULAR OBSTRUCTION

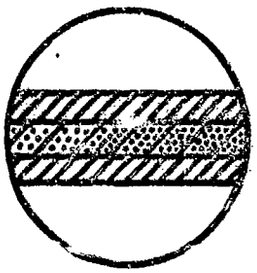

a) THE OBSTRUCTIONS AND THE DUCT THAT TAKES EITHER OF THE TWO OBSTRUCTIONS

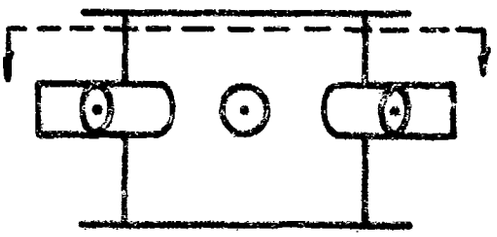

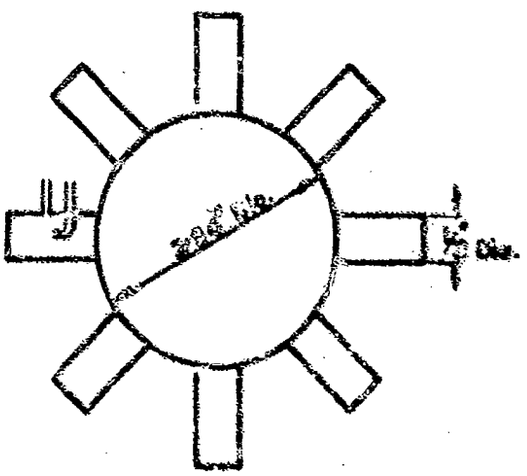

b) THE RADIAL FLOW DUCT

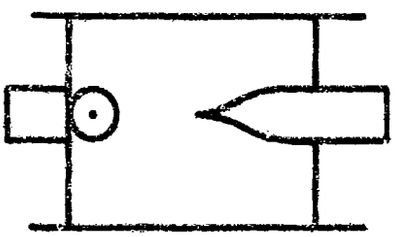

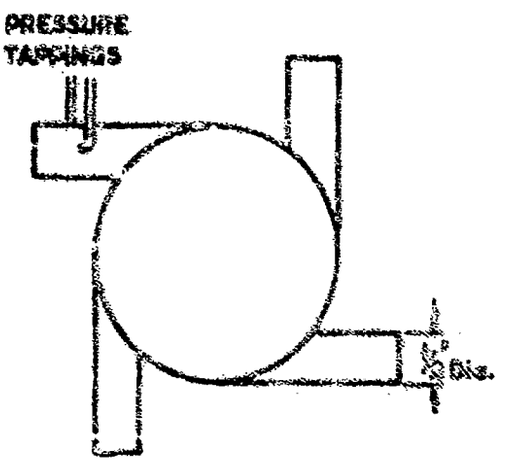

c) THE SWIRL DUCT

Fig.1 The obstructions, the radial flow duct and the swirl duct

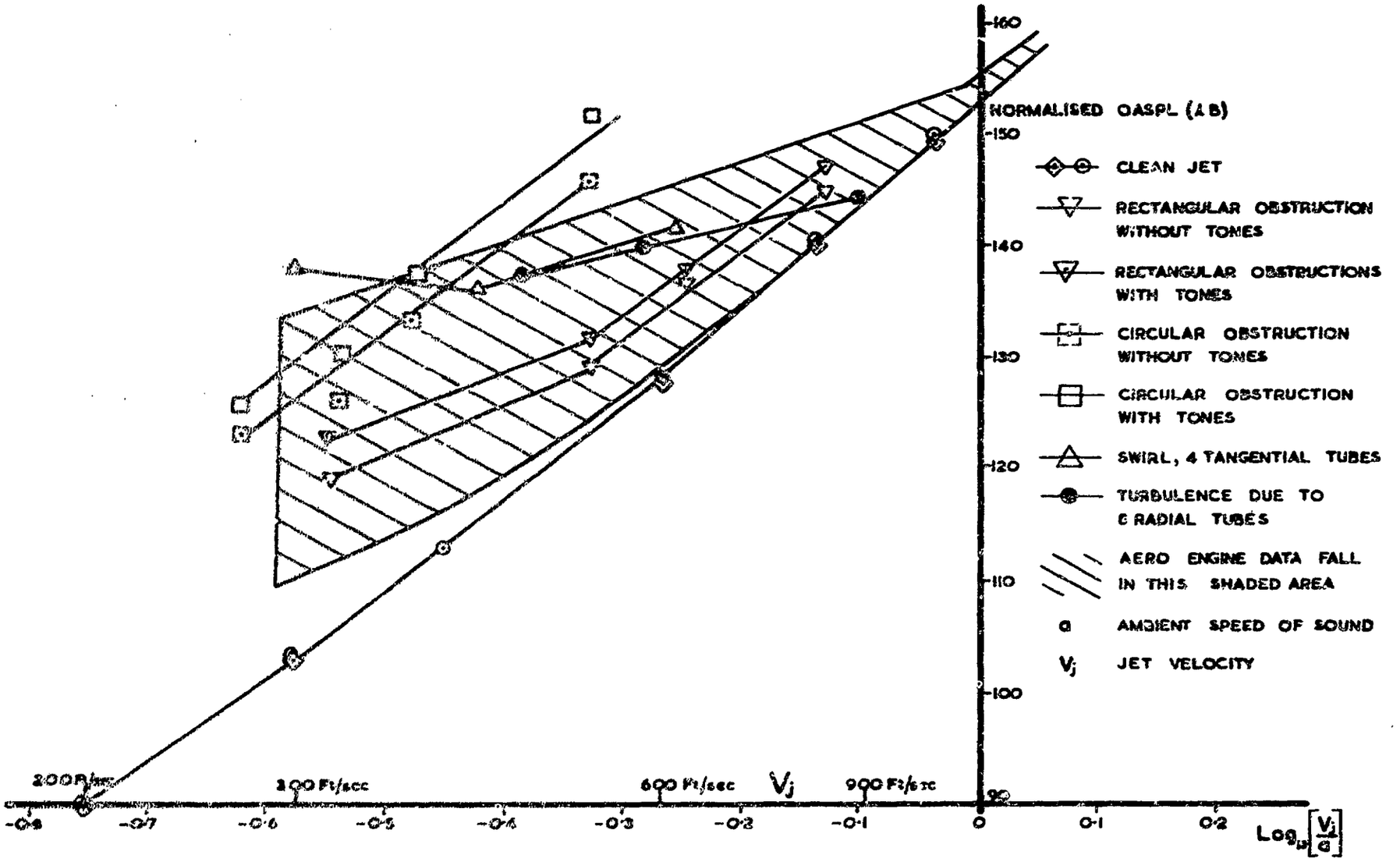

Fig.2 Peak noise – jet velocity relations

APPENDIX A

ROUND TABLE DISCUSSION HELD AFTER THE PRESENTATION OF PAPERS

Chairman: Professor J.E.Ffowcs Williams
University Engineering Department
Cambridge

ROUND TABLE DISCUSSION

Chairman, Prof. Ffowcs Williams: I have decided not to have a round table, but to hold a discussion without the establishment put up in front, because the last thing we want at this stage in the development of the subject, I think, is to declare who the establishment is!

There has been a clear change in the way of thinking about the noise problem since the last AGARD meeting, and I would like to be an impartial chairman, putting some provocative observations to you experts for discussion. Perhaps I could start by observing that during the last 10 years we have talked much more about how to measure the location of sources. Now, I would like to take the blackboard and make some comments on what we mean by a source. The people that were brought up on theory are accustomed to reading Lighthill's paper, and there he says that the pressure squared can be given as a volume integral of something, and that something we call the source strength per unit volume. But many different things can integrate to a common result as long as the pointwise differences balance out. In particular, Lighthill encourages us to regard the contribution to $\overline{p^2}$ from unit source volume as being the simple integrand; the noise source Q.

$$\overline{p^2} = \int_V Q\,dV .$$

However, the integral is completely unchanged if we add to it "plus the gradient of anything", because that gradient will disappear if S is zero at infinity, i.e.

$$\overline{p^2} = \int_V (Q + \nabla S)dV .$$

Are we then to regard this different integrand as the noise source? Clearly it would be stupid to do so. Yet this ambiguity is inherent in the formal definition of one of the source location procedures that we have heard about during the meeting. I am clearly being provocative, and I hope you will respond.

Correlations have been established between measures in the flow and the sound outside. Amongst those correlations is the pressure inside the turbulence. Now, at the 1963 meeting here, there was one splendid article by Strasberg from the David Taylor Model Basin, as it then was, who proposed to measure the pressure in a turbulent water flow, by observing the sound radiated by a bubble driven by the turbulence to radiate sound. However, that came to a full stop because in the discussions that involved the experts then assembled, it was said that it was rather difficult to work out what the pressure would be when the bubble had perturbed the flow. We were reminded of two papers, one by Goldstein, who considered one limit and Toomre who considered the other where the presence of the probe disturbed the pressure by $-\frac{1}{2}\rho u^2$ and $+\frac{1}{2}\rho u^2$ respectively. I think that it is just not clear what the pressure is on a probe when it is put into the stream to bring the flow locally to rest. What is the meaning, therefore, of correlating the signal measured by the probe in the turbulence with the sound outside?

Let me be even more provocative. The fact that the correlation is high seems to me, in itself, to be no great point in favour. For example, if you were to measure the sound produced by my voice at the lips of Prof. Küchemann and at the ears of somebody beyond him you would find that the correlation between the pressures was perfect. Yet is Prof. Küchemann talking or am I? The film shown by Dr Poldervaart today shows how beautiful the subject can be when we concentrate on the individual event rather than on the statistics of the process. Is it time to de-emphasise that statistical approaches in favour of a more deterministic view?

Let me throw that as a debating point to you.

Mr Harper-Bourne: It may be true that a significant proportion of the source fluctuation that we measure at a fixed point in the turbulence is of the type which contributes relatively little to the far-field sound. However it is equally true that fluctuations of this type will not contribute to the cross-correlation of far-field microphone and inflow probe signals and therefore do not contaminate measurements of local source strength. They can, however, significantly reduce the level of correlation *coefficient* that might otherwise have been obtained and therefore make a reliable estimate of source strength difficult to obtain.

A more fundamental difficulty is that that portion of the source fluctuation which does contribute to the sound field may itself be contaminated by the sound radiated from other *uncorrelated* parts of the turbulence. Clearly, if the relative contamination is large, which might be the case when the pressure is chosen to represent the source fluctuations, it then becomes meaningless to think in terms of local source strength.

Chairman: I am not proposing actually to carry on a debate with individuals in the audience: I am hoping to provoke a debate amongst members of the meeting, but let me take up your point. We do have a theory that says

that the source of aerodynamic sound is quadrupole. That means that for every positive source element there is guaranteed to be a negative element opposing it, and every such dipole combination is adjacent to an opposite combination somewhere else. Therefore it would be absolutely the height of folly to concentrate too much on any one particle, i.e., on one region of flow. In isolation that region would generate very much more sound than it does in its natural environment, where it is surrounded by all the other elements that destroy the sound.

Mr Harper-Bourne: Yes, this is very true, but in practice we believe that we avoid the first difficulty by measuring the quadrupole stress rather than a quantity which is related to its constituent monopole elements.

I feel that measurement of local statistical information should not be entirely dismissed even if the results are sometimes of uncertain value. For example, if we integrate the necessary space-time statistics for the stress fluctuations about a fixed point in the shear-layer, making due allowance for differences in retarded times and phase due to convection, the result we obtain is the contribution to the far-field sound intensity from unit volume of turbulence at the point under consideration. This is a finite and positive quantity. Furthermore, it is exactly this quantity which the correlation scheme can, in principle, measure.

Chairman: Obviously, I agree with you, but it is bad for me to agree when I am trying to provoke a discussion.

Prof. Sidden: Professor Ffowcs Williams has opened the discussion by raising, in a rather provocative manner, three criticisms which reflect on the efforts of several groups of researchers who are trying to develop *practical experimental methods* for noise source localization and strength estimation. These efforts employ the so-called pressure-source model (or alternatively the Lighthill-Proudman model) coupled with a quantitative real time means of *correlating* local source disturbances and the overall far-field sound. In order that the implications of the chairman's remarks are not mis-understood by others present, I should like to lend my point of view on each of the three questions:

(i) *On the matter of measuring static pressure fluctuations in turbulent flows*. Professor Ffowcs Williams has today repeated his opinion, first stated at the 1963 Brussels Round Table Discussion[1], that it is "impossible, even in principle to get at the pressure" (because of the inevitable pressure error arising from interaction between the probe and flow). He will recall that others at that meeting expressed the optimistic counter-view that "it should be, in principle, possible to determine the pressure that would have been there (at a point in the turbulence) in terms of the reading that the probe gives when you put it there". Ribner likened this to the well known method of measuring static pressure in a supersonic flow; even though the probe produces a bow wave which substantially modifies the flow field around it, the effect can be calibrated out.

Indeed in the intervening period since 1963, the present speaker and others have shown that in certain cases the probe/flow interaction error can be suppressed using specially shaped probes which minimize sensitivity to incidence changes in the approaching flow, or probes which actively compensate for the interaction error in real time.[2,3,4] This research has extended our knowledge of the origins and magnitude of turbulence interaction errors. While it is true that the errors, of order $1/4\rho(v^2 + w^2)$ or less, may be as large as the inherent pressure fluctuations in isotropic turbulence ($p \sim 1/2\rho u^2$), the pressure fluctuations characterizing the shear layers of turbulent jets are much larger, of order $\rho u\bar{U}$ (References 2, 5 and 6). Thus in many circumstances a relatively uncontaminated measurement of static pressure fluctuation can be made with a simple uncompensated pressure probe.[3,6,7]

(ii) *On the validity of various source models* all aerodynamic noise generators, the chairman has rightfully pointed out that one can arbitrarily add in the divergence of any contrived source distribution function to the integrand on the right hand side of the Kirchoff solution, or one of its derivative forms, without modifying the answer for $\overline{p^2}$ on the left hand side. However the intent of his comment is somewhat obscure. No one, to my knowledge, is pulling invented source terms out of the sky and tacking them onto the solution integral. Indeed if Mr Chairman is questioning the credibility of the Ribner/Meecham-Ford dilation formalism as an *alternative* to the Lighthill turbulent stress tensor model for low speed flows, then I wish to remind him of the demonstrated equivalence of these source models,[8] as acknowledged by Sir M.J.Lighthill himself.[9] In fact the work of Batchelor[10] shows us that the Ribner assumption $\nabla^2 p^{(0)} \propto -\dfrac{\partial^2 \rho u_i u_j}{\partial x_i \partial x_j}$ becomes exact in the incompressible limit.

It has been suggested that the distribution of statistical quadrupole strength might look somewhat different than that for pressure sources, even though they both integrate out to the same answer for $\overline{p^2}$. Personally however, I expect a unique source distribution on time average, irrespective of the experimental method used.

The dilatation method separates the pressure fluctuation into two parts $p = p^{(0)} + p^{(1)}$. In the source region the pseudosound $p^{(0)}$ (inertial in origin) is said to dominate over the acoustic fraction $p^{(1)}$; the

converse is true in the acoustic far-field. That the first assumption holds for low speed jets can be confirmed by a simple experiment. If one plots the radial distribution of fluctuating pressure from the jet centerline outwards to large distance, one gets a picture as shown in the figure on page A-4. If we assume for the moment that all of the acoustic power of the jet is radiated by one equivalent point source, than by extrapolation of the free field line into the source region (dashed) we must conclude that the net acoustic pressure level of that one source will fall well below the overall jet pressure level, by 20 decibels or more, for most points within the turbulent region. Indeed if the total jet acoustic power is viewed as coming from a large number of uncorrelated sources, their individual acoustic fields will be even less significant with respect to the total jet pressure fluctuations. Thus the inertially induced pseudosound pressures may be viewed as a causative mechanism for a major portion of the far-field sound.

(iii) *The Chairman has questioned an apparent ambiguity in the causality correlation methods* presented by myself elsewhere in these proceedings. (Paper 7.) Using a simile in which he and Prof. Lilley are imagined to be carrying on a conversation in this hall, he intimates that if a microphone were to be placed near each speaker and cross-correlated, the resulting correlation functions could not distinguish the cause from the effect. This is not the case; in fact the time delay feature of causality correlations works to advantage. The cross-correlation functions will maximize at either positive or negative time delay appropriate to the separation distance, depending on which person was source and which was receiver. Furthermore, if both talked simultaneously, the relative magnitudes of the correlation "bumps" at appropriate positive and negative time delays would tell us who was doing the *the most talking*.

It is important to point out that the causality correlations, if normalized by the individual root mean square values of the partner variables, will give an erroneous impression of the source distribution. For example, two microphones both in the far-field of, but on a radial line from a complex source will give a maximum correlation coefficient of unity, when normalized in the foregoing manner. In contradistinction, the un-normalized causality functions (Equations 8 and 9 of Paper 7) yield legitimate distribution functions, which quickly drop to zero outside the source region, as depicted in Figures 7.1 and 7.2. These functions are integrable; validation by integral closure has been obtained in several instances.

Chairman: I think Prof. Siddon that you are making your point very well but it really won't be a discussion if I don't stop you here to allow time for other contributions.

Prof. Siddon: Thank you for allowing me a lengthy response.

REFERENCES

1. Ginoux, J.J. (Editor) — *Future Research on Noise*, (A Round Table Discussion), AGARD Report 469, Brussels, April 1963.

2. Siddon, T.E. — *On the Response of Pressure Measuring Instrumentation in Unsteady Flow*, University of Toronto, UTIAS Report 136 (January 1969), also abridged as *Investigation of Pressure Probe Response in Unsteady Flow*, Proc. of NASA Basic Noise Research Conference, Washington D.C., (NASA SP-207), July 1969.

3. Siddon, T.E.
Rackl, R. — *Cross Correlation Analysis of Flow Noise with Fluid Dilatations as Source Fluctuation*, 82nd Mtg Acoust. Soc. of America, Denver, October 1971, Abstract in JASA, January 1972.

4. Willmarth, W.W. — *Unsteady Force and Pressure Measurements*, Annual Review of Fluid Mechanics, pp.147-170 Annual Reviews Inc., Palo Alto, California, (1971).

5. Kraichnan, R.H. — *Pressure Field within Homogeneous Anisotropic Turbulence*, Journal of Acoust. Soc. of America, Vol.28, No.1, January 1956.

6. Fuchs, H.V. — *Measurements of Pressure Fluctuations within Subsonic Turbulent Jets*, J. Sound and Vibration Vol.22, pp.361-378, (1972).

7. Scharton, T.D.
White, P.H. — *Simple Pressure Source Model of Jet Noise*, J. Acoust. Soc. of America, 52, pp.399-411 (1972).

8. Ribner, H.S. — *Aerodynamic Sound from Fluid Dilatations*, University of Toronto, Institute of Aerophysics Report 86, July 1962.

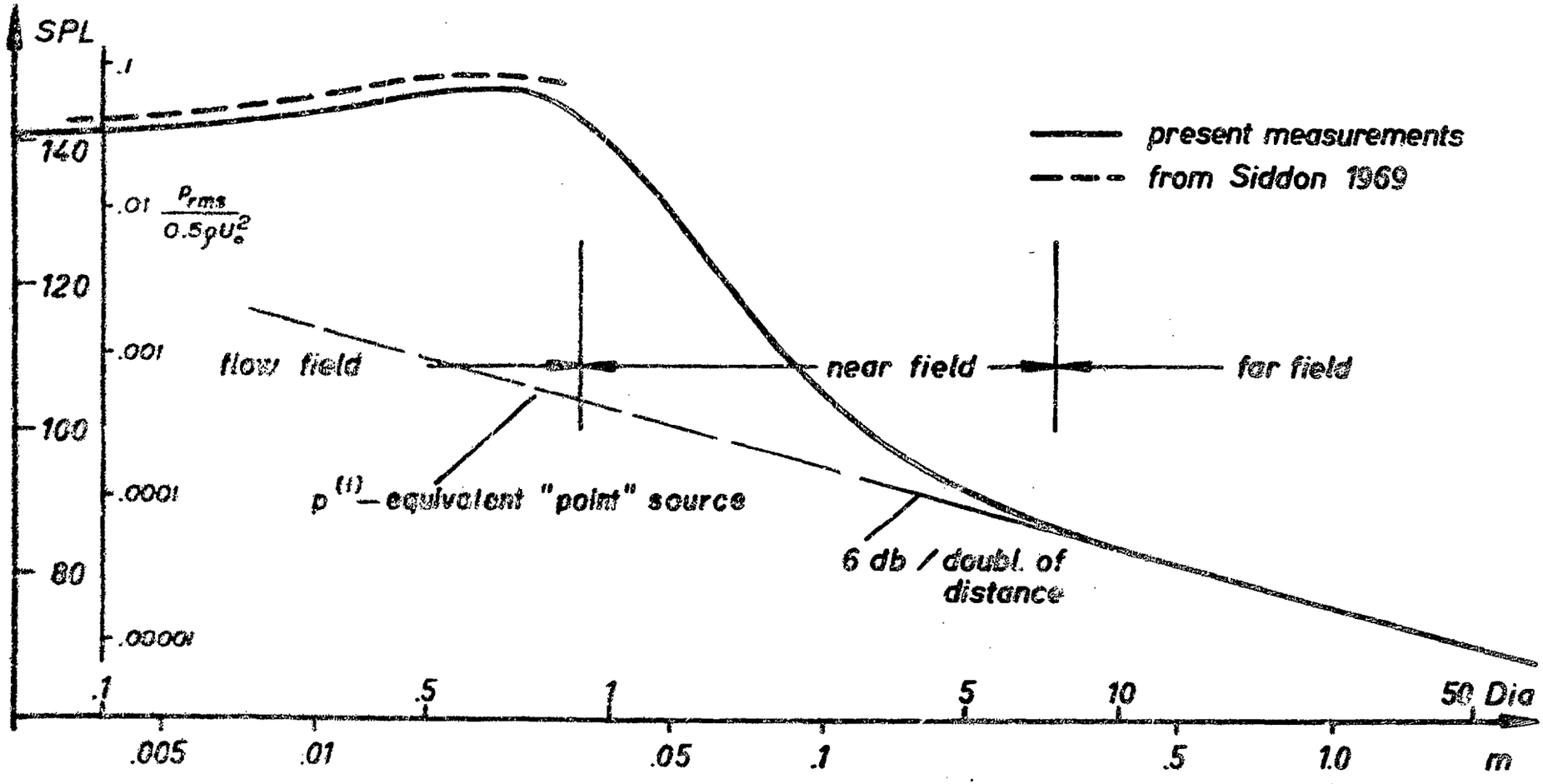

Variation of pressure fluctuation with distance from a 38 mm jet, starting at 4 diameters downstream in the jet and proceeding at right angles to the jet axis

9. Lighthill, M.J. *Jet Noise*, AIAA Journal 1(7), pp.1507-1517, (Wright Brothers Lecture), July 1963.

10. Batchelor, G.K. *Pressure Fluctuations in Isotropic Trubulence*, Proc. Cambridge Phil. Soc. 47, 359 (1951).

Chairman: Does anybody else have anything pertinent to say regarding the question of how we can produce positive identifications of the sources, or whether or not we can in principle do so?

If not, perhaps we have worn that subject out already, and I can go on to provoke somebody else! One of the items which impressed me greatly during the meeting, and I will now choose my words with great care, was the paper given by Mani, who discussed the exact influence that the flow would have on the linearized acoustic equations. He showed that the effect of the jets surrounding a source was to completely destroy the convective amplification, which is the principal effect of high speed eddy motion on the sound generation. It accounts for the forward radiation and the increased power about u^8 and this sort of thing. Mani showed that if you take into account a simple model of the flow, then you destroy the convective amplification, and this is consistent indeed with the experimental evidence that Lush has put forward in the past. How should we go about trying to incorporate the effect of mean flow in a more general way? Mani's slug flow clearly exhibits instabilities, and if the instabilities are driven, then there is a very difficult problem to cope with in that set of equations. Do we think that the real problem should be described by a small perturbation, an acoustic perturbation about a mean flow? Or, do we think now that there are likely to be essential non-linear aspects of the problem which make the linear modelling of the source of the sound generation aspect rather trivial. Does anyone want to take up that aspect?

Mr Bowe: May I ask another question which is closely related to yours? It would seem that there are two influences that have received little discussion here: the effects of aircraft motion in reducing the relative velocity of the jet, and the point that Roy Hawkins raised – the shielding of noise from one jet by another jet nearby. If in fact a turbulent layer can absorb or shield noise from another layer then to what extent can one shield a jet by a jet of intermediate velocity round it or partly surrounding it? These practical sorts of effect could be extremely important from an engineer's point of view, and also from the theoretical view point of transmission of noise from "noise sources" deeply immersed inside jet turbulence.

Mr Bore contributed: Since the conference, an extensive report on co-axial jets (but still exhausting into a stationary atmosphere) has come to hand, by Eldred et al: FAA-RD-71-101. This appears to support a simple mechanism of relative-velocity noise generation in the various shear layers, without significant shielding effect of the outer jet in the sense of opacity to noise. Does this imply that shielding only occurs with a completely separate jet?

Dr Lush: I would like to make a comment on the shielding effects of jets. There seem to be two distinct mechanisms involved here. There is the mechanism in which the spread rate of the shear layer is artificially increased, thereby reducing the convective amplification and increasing refraction so that the peak noise level is reduced. For instance this mechanism presumably occurs in the fish-tail nozzle which increases its jet spread rate in one plane. It is found that the peak noise can be reduced by as much as 10 dB in this plane but not the other.

The second mechanism is the reduction in the actual source strength which can be detected by measurements at 90° to the jet where convection and refraction are absent. This mechanism has been observed in measurements of the noise from co-axial jets, where for a constant core velocity the noise level actually reduces when the annulus flow is present. An annulus flow of width equal to about $\frac{1}{4}$ the core diameter, with a velocity of about 40% of the core velocity will give a reduction in OASPL of about 5 dB, and somewhat more at high frequencies.

Chairman: Well, let me develop this line a little further. When we think of attacking the problem on the basis of linearized equations about the steady mean state, in the way that Prof. Lilley described during his lecture, do we consider that as being a description of what the flow actually looks like, or is it intended to be only right in some statistical sense? If it is intended to be a description of the flow, can it ever be made to match the pictures that we saw this morning, where vortices grow on shear layers and become non-linear very, very rapidly? Are the small perturbation theories about a mean state compatible with the clear observation that there are large structures present in the jet which represent anything but small perturbation about the mean?

Prof. Laufer: I think it would be too much to hope that a linear approach could help us completely solve the problem. On the other hand, I think an approach of that type can be extremely helpful. A very good example is the boundary layer transition problem. Certainly the solution of Orr-Sommerfeld equation does not explain boundary layer transition, but it helps us at least with the initial phase, as to how the flow becomes unstable. After that, we have to use some modelling or make some good engineering guesses, to estimate the location of the transition point itself. As you know, certain guesses seem to be working very well. To talk about our special

problem of the jet flow, the linear stability calculations help us in telling us what mode of disturbances are most likely to occur. In addition to that, they can also give us an idea about the most unstable frequencies present. However, any predictions based on linear theory concerning the rate at which the initial vortex rings actually appear must be taken with great suspicion.

Chairman: By that you mean predictions of the flow state? It may be that the linear theory is not intended to predict the flow state, but rather some pertinent information about how sound is generated in the mean or some statistical sense. I would like some opinions on that.

Prof. Laufer: I was mainly referring to amplification rates and such quantities. I do not know what you mean by a statistical sense.

Chairman: I was merely making the observation that clearly any linear perturbation would not describe the vortices that we saw rolling up in your film and in Dr Poldervaart's film. But, on the other hand, there is a very impressive agreement of the predicted correlation structure through linear stability analysis in the diverging shear layer. I would be very loth to suggest that it is irrelevant, but I don't quite know what the relevance is.

Prof. Laufer: I think it is accidental.

Chairman: That is fighting talk.

M. Legendre: I wish to have the opinion of the assembly on what I said in my introductory speech on the relative displacement of vortex rows. The mechanism I suppose is not very far from Prof. Laufer's but more adequate for well established turbulence. If the velocity in the jet is V_1 and the velocity outside is V_2, I imagine, to start with, two vortex rows with velocities $\frac{3V_1 + V_2}{4}$ and $\frac{V_1 + 3V_2}{4}$. I made a rough calculation giving the order of magnitude of such a sound source which is not a noise source, since it would be necessary to put in the scheme some randomness and certainly more than two vortex rows, I found an energy much greater than what is known, because I did not take into account the oscillations of the vortices around their mean trajectories but it seems to me that a deeper investigation would give a physical support for the calculation of Lighthill's quadrupole intensities.

Chairman: I am reminded of calculations that I think were done by Prof. Heckl of the sound radiated by vortices moving in defined paths. If my memory serves me correctly, one has to be extremely careful to be sure that the path that the vortices are said to be following actually satisfies the equations of motion, because if it doesn't, one is implying that one has a force actually driving the vortex in that path and the force makes sound.

Prof. Kibchenko: Following on what M. Legendre said, I think at this point we should just remind ourselves again of what Brown and Roshko found, because I think that it is still the most impressive demonstration of regularity in these flows (see CP-93). Miss Demuns did a very straightforward analysis of the film they have taken. She plotted an x–t diagram and went through the film frame by frame and made a point where the centre of a vortex core happened to be at any given time. It was very easy to identify where the cores were, and the outcome of it was a number of lines, all parallel; that is, the cores were all moving at about the same speed (see figure opposite). But not all of these lines continued. Some did go further than others. At any given time, there were a number of cores which were equidistant, and then suddenly one was missing and the distances were larger. One could even get the impression that they were exponentially spaced. That was just brought about by the disappearance of cores. That is what Prof. Laufer was talking about this morning. I am now almost optimistic enough to assume that this is not just random, that we can calculate it. The point I want to make, if one looks at these data, and they are really very good data, is that one finds that there is a remarkable order in it. It is a most regular flow pattern, I hope we can make use of that and get somewhere. It really comes down to what you said, Mr Chairman, i.e., let us look at the events or what Prof. Laufer called the actual process. I would like to know what the fluid motion element really is and what brings it about.

Prof. Kovasznay: Referring to your question with regard to the validity of linear theory I think I did present this morning that linear perturbation theory for the diverging shear flow does indicate many of the features that we observe. That package is good enough proof. It is true that when the amplitudes do become large, then we might have to apply some non-linear analysis. It is not clear to me whether we stand to benefit in getting a physical picture by starting with a non-linear theory, disregarding the diverging shear flow. You can produce the same result

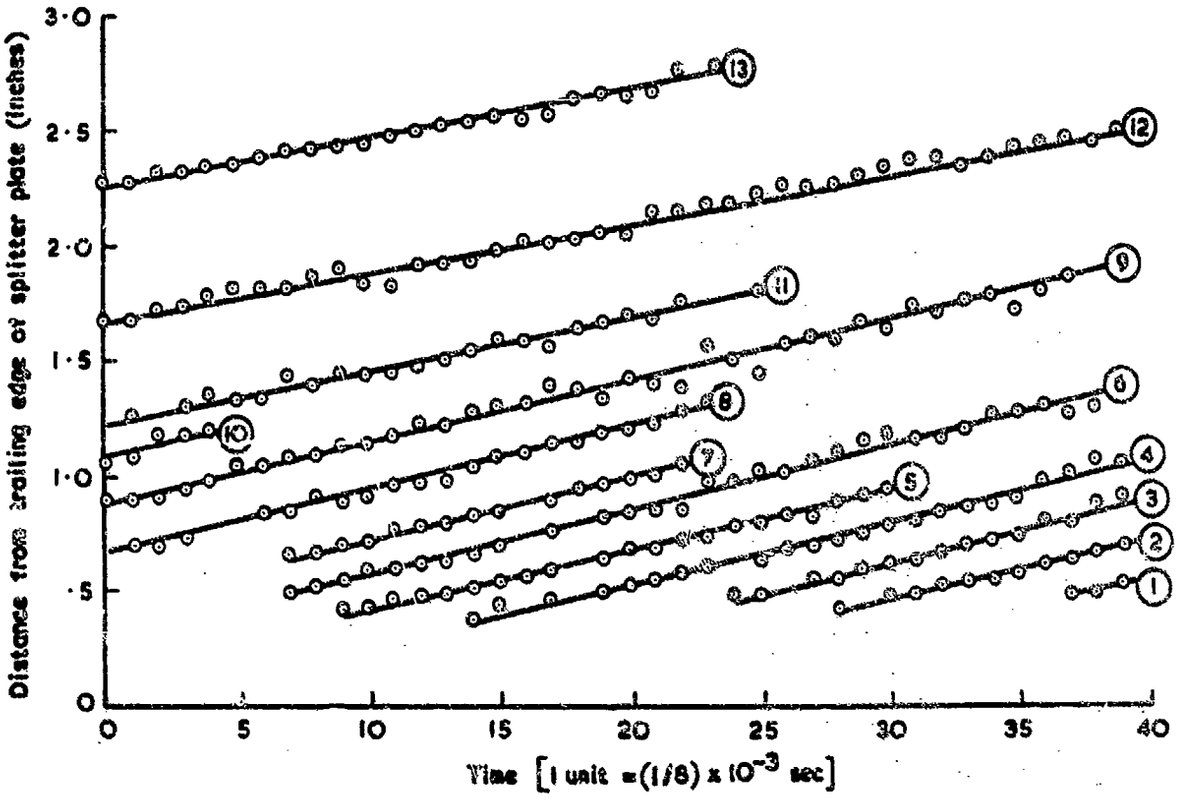

Experimental spacing of cores. From experiments by Brown and Roshko

by either means if you so wish. It appears to me that first thing to account for is really the non-parallel nature of the shear flow. That does limit the amplitude also. Another question naturally is, what is the initial amplitude one would put? This we do not know. What are the amplitudes one should put at the exit of a nozzle for the various spectral components?

Chairman: That is not the only question in that respect. If one does an analysis of the type you described this morning, the waves grow because the system is unstable and they move into a region where they are no longer unstable so they are controlled again. The amplitude of the wave is determined by some initial condition. But in fact, the non-linear small-scale turbulence will no doubt be continually exciting the waves, too. Is it clear that the excitation at the initial condition is more pertinent than the continuous excitation of the waves as they travel downstream?

Prof. Karamcheti: It is not clear exactly what the initial conditions should be, and I think that that is where some of the difficulty actually lies. I do not know the answer to that question, but I think in the light of the so-called coherent structure, the regular pattern, that stability analysis has a much better chance of a proper description where we could lead ourselves to coherent structures.

Chairman: Well, it gives different information, doesn't it? It is presumably a good prediction of the measured correlation data in the shear layer. That is the claim that is being made, is it not? While the other more phenomenological approach tries to identify the source in a sufficiently simple form that one can possibly hope to understand the essential mechanics and then bring about change.

Prof. Karamcheti: Perhaps I could ask the following question: granting that we did picture what we observe, how are we going to model the structure of a jet such that we shall be able to compute the far-field noise given the total conditions? What is the mathematical model we make?

Chairman: If I could put that in another way, is it reasonable to expect that we would ever be able to compute the radiation from a shear layer when we cannot even compute the rate of spread?

Prof. Karamcheti: In the light of the experimental observations, the pictures which have been seen, what is the best one can do so that we could get as much of the information as possible?

Chairman: What other views are there here on this point?

Prof. Lilley: All these views and these various approaches must be very helpful. The important thing is that we are all trying to search for the appropriate structure of the turbulent flow. If we go back to some of the measurements that Prof Laufer and others made earlier some 20 years ago, we find that they gave a picture of the turbulent structure in jets which has gradually been improved as more and more experimental data has become available. In his book on Shear Flow Turbulence, Townsend described a deterministic structure for the very large-scale eddy motion which was based on the measurements of the two-point velocity correlations at large separations. Further understanding has awaited the more recent measurements involving the advanced techniques based on conditional sampling methods. However, paralleling these experimental studies theoretical work has displayed a connection between the large eddy structure and that described by stability theory. We have now found that linear stability theory applies to the turbulent flow in a jet mixing region does in fact describe a most unstable wave packet at each downstream station which to some extent can be argued to be representative of some of the deterministic or coherent structures which Prof. Laufer and others have in fact recently measured. Others of us have been trying to see how we can piece together these various pictures of the flow into an appropriate model from which we can estimate the noise generated. Of course, I agree with Prof. Laufer that we cannot expect a completely linear theory to cope entirely with this problem of the large scale structure. Clearly, non-linearity has to be included in the problem and plays an important part in our work in determining the limiting amplitude of the wave packet. However, as Prof. Karamcheti has said, linear theory goes a long way in explaining many interesting features of the large-scale motion. It is therefore essential to see how far linear theory, allowing for flow divergence, predicts the main features of the motion as compared with experiment. David Crighton now has some detailed results for jets allowing for flow divergence and this complements some of the results we have obtained by a different approach. My own feeling is, after working on these theoretical approaches for a number of years, that in aerodynamic noise studies it is essential to get as good a model of the turbulent flow structure as is possible. The pioneering work of Lighthill in which noise generation was described in terms of the stress tensor T_{ij} has indeed been very helpful in giving us a picture of the noise field and the general properties of the sound radiation. However, it is now clear that only a limited picture of sound generation is obtained by the use of a theory based on the concept of an acoustic analogy and a distribution of equivalent acoustic sources. As more and more detailed measurements of the unsteady flow properties in jets become available, including measurements of velocity, pressure and density fluctuations, so we need to include them within a theoretical framework so that the greatest possible opportunity is established for getting closer to the true mechanisms of sound generation. By using a theoretical framework based on the convected wave equation for disturbances within the flow I believe we have a powerful model which governs the generation propagation and transmission of sound within and outside the flow. Even in low speed flows it seems to me essential to include the compressibility of the fluid both inside as well as outside the flow if the complete interaction between the sound and the flow, which generates it, is to be considered. I believe descriptions of the pressure in the near-field of jets as pseudosound and describing the flow as if it were incompressible are unhelpful concepts. The essential difficulty, as specified by Lighthill, is that in any theory of jet noise the noise generated by the turbulence has an energy very small compared with the kinetic energy of the turbulence and hence errors in its estimation can be very great indeed. This is aggravated if as we suppose much of the noise generation comes from the larger eddies which may contain little energy themselves and whose description is not known precisely. The method we are evolving at the present time makes the best use of the current information on jet structure and it is only a matter of convenience that we have used a linear theory, backed up by certain non-linear effects, for the description of what we have judged to be the more important noise generating mechanisms. One important feature of these models was also referred to by Prof. Karamcheti this morning. It is clear that even in very elementary calculations on jet noise, in which some model for the turbulent structure is included, that the far-field noise is very dependent on the characteristic frequencies in the turbulence that are associated with each downstream section of the jet. It appears therefore that in such flows the flow divergence is important in determining these characteristic frequencies and once calculated the remaining detailed description of the turbulent structure is not important in providing an estimate of the far-field noise radiation – its intensity and spectral characteristics. However the amplitude of the convected wave-packet at each station is also required and this can only strictly be obtained from a non-linear theory such as used by Morris or from experiment. The picture described by us said Prof. Karamcheti of the large scale motion in jets does not seem to be too much in disagreement with the turbulent structure Laufer and others have observed and measured and this applies also to the picture of sound generation.

Chairman: One thing that they measured evidently is a rather abrupt event where vortices swallow up one another or pair with one another. Furthermore, it is suggested, I think, that that event is probably violent enought to be a very impressive source of sound. Is it likely that linear stability theory will ever get anywhere near the heart of that problem?

Prof. Lilley: Linear theory alone, of course, cannot. But I believe the roots of that, or the essential elements of the birth process of these structures will come out of a linear study.

Dr Crighton: I think perhaps the best documented evidence on orderly jet structure is the well-known paper of Crow and Champagne. In that paper there are measurements of filtered signals corresponding to the fundamental and first harmonic of what appeared to be the most rapidly amplified disturbances. It was never found that more than the fundamental and one harmonic were needed to almost completely describe the energy balance in the first six diameters of the jet. Despite this, Crow and Champagne seem to be rather obsessed by the non-linear aspects of the mechanism that decides what is the preferred mode. They have a lengthy discussion of the reasons why it is non-linear mechanisms that give you 0.3, essentially, as the preferred Strouhal number, the one that is most rapidly amplified. I think that it is rather odd that they should have fixed on that idea in view of their measurements, which show that non-linearity is not very strong. I do not believe that it is a controlling influence. In fact, on the contrary, I would like to refer people to a paper by Prof. Michalke which shows that, whereas no proof has yet been given to show that non-linearity gives this preferred Strouhal number, linear stability theory for the right (i.e. the *measured*) velocity profile does it, and very nicely, too, to within a few percent.

Chairman: What is it predicting? Could it possibly predict the sort of flow structure that we saw clearly visualized in the films? Is it important that it should?

Dr Crighton: No. But let me ask if there is any other theory besides the one that I have been working on, which obviously agrees very closely with what Prof. Karamcheti was describing this morning, which would predict, in pretty good numerical agreement with the Crow and Champagne experiments, that a 1% forcing of the exit plane could be magnified to 15% in five diameters, and thereafter, decay. This is the sort of thing that can be predicted and agrees very closely with the measurements.

Chairman: Could you predict the streamline pattern that we saw in Prof. Poldervaart's film?

Dr Crighton: No, certainly not. But I believe that there are certain aspects which are predictable by linear theory. You seem to be asking for a non-linear theory to predict something far bigger. There are some things which can be predicted very closely indeed, and not in the dB sense either. I am talking about algebraic terms. I think what's happened so far strongly gives support to the view that linear theory is highly adequate for the moment. I am not saying that it is not a non-linear process. It is a different matter to say that non-linearity is there than to say that non-linearity is the controlling process on eddy growth, for example. What I am saying, is that that is not the dominant process, and that is to a large extent borne out by the Crow-Champagne experiments. I think that you will shortly find a lot of very careful measurements, very well supported by the theories of Prof. Karamcheti and others.

Prof. Laufer: Being an experimentalist, I must strongly disagree with our theoreticians. I doubt very much that a linear stability theory can treat the vortex formation region and the vortex interaction region. While admittedly, a wave like description of the flow field, assignment of local wave numbers is possible in principle, I question its usefulness. It is clear from our observations that wave crests are lost causing a change in apparent "wave length". This new "wave length" is not due to a change of frequency in space and time but to an actual merging of two local crests. Consequently, the concept of "phase speed" is not helpful since phase reference is lost.

Dr Crighton: I would just like to say that the theoreticians obviously agree on what is happening, and I suggest that the experimentalists agree among themselves. The Crow-Champagne paper contains detailed measurements of wave-like processes of an altogether familiar kind. I would just like to ask Dr Laufer how he views that particular piece of experimental work, which has a great overlap with the work of Dr Fuchs, Dr Fisher and a number of other people who do see wave-like structures, who can define phase velocities and wavelengths and whose measurements of these quantities do agree with stability theory.

Prof. Laufer continued: Section 3.3 (pages 21–3) of my paper directly answers this question.

Prof. Karamcheti: I think that I would like to add a little bit to this. When I am with theoreticians I usually say I am an experimentalist, and when I am with experimentalists I say that I am a theoretician. In the same manner, when I am with acousticians, I say I work in rarefied gas dynamics, and vice versa. I think it is a matter of interpretation, for after all, the disturbance field is indeed a vortex field. I think one could make this type of picture represent the flow description. As a matter of fact, Landau has probably solved it a long time ago also. I must say the idea of investigating non-parallel shear flows is motivated by experiment, not by theory. I think that some measurements we are trying to study very carefully may indeed prove what are some of these effects of the diverging shear flow. Still it is not complete, but in fact, we are trying to draw on your experiments to show this effect.

Prof. Michalke: Concerning the controversy whether the pairing process of vortices as shown by Professor Laufer can be described by a linear or non-linear stability theory, I agree with Professor Laufer. I am convinced that the pairing of consecutive vortices and their coalescence to a bigger vortex, which are well-known phenomena in the lamlar-turbulent transition of circular jets (cf References 1 and 2), is a highly non-linear process due to the mutual induction of the vorticity concentrated in the vortices. On the other hand, Professor Laufer argued that in his film sinusoidal wavelike deformations of the shear layer were restricted to a very small flow region and that therefore the flow region amenable to a linear theory is also very restricted. In my opinion this is not strictly true. What we saw in the film were streaklines. A couple of years ago I calculated the streakline pattern of a disturbed free shear layer using the solution of the linearized instability problem[3]. I found that the calculated streaklines showed the rolling-up process of the shear layer which was in good agreement with experimental results. This seems to indicate that even the non-sinusoidal deformation of the streaklines and the formation of vortices can be described by linear theory – at least to a certain degree.

Another question is: How important is the orderly wave or votex structure with respect to the jet noise radiation? In a circular jet, ring vortices may develop due to the instability of the turbulent jet boundary and undergo pairing processes like that observed by Professor Laufer in the plane shear layer. He emphasized that the pairing process may be a strong source of noise and I agree completely. On the other hand, even if no pairing process were present and the ring vortices would only move downstream in the jet with constant speed, yet growing in intensity and decaying again further downstream, why should this type of orderly structure not radiate sound? It is well-known that a frozen pattern moving with constant subsonic convection speed does not radiate any sound, since a moving frame of reference then exists in which the pattern is stationary. But, when we consider the case of a jet emerging from a nozzle, a moving frame of reference in which the vortex motion is stationary doesn't exist because of the vortex growth and decay. Therefore, even if the ring vortices in the jet would move with constant speed and without pairing, they should always radiate sound.

Finally, if we adopt the instability of the turbulent jet boundary layer as the cause of the existing ring vortices and as a source of noise, then we should also consider that a circular jet is also unstable with respect to non-axisymmetric disturbances. These azimuthal disturbances should lead to a type of helical vortices. In fact, the contribution of Dr Fuchs has shown that, apart from the axisymmetric turbulence components, there is among others also a relatively strong first azimuthal component for Strouhal numbers 0.1 . . . 1.0 in a low Mach number jet. It may, however, be interesting to note here that for Mach numbers above 0.7–0.8 the first azimuthal instability mode can be more unstable than the axisymmetric mode as was shown theoretically in Reference 4. This implies that the structure of jet turbulence may possibly change and that the content of higher azimuthal components may become stronger with increasing jet Mach number.

REFERENCES

1. Wille, R. — *Beiträge zur Phänomenologie der Freistrahlen*. Z. Flugwiss, 11, pp.222-233, (1963).

2. Freymuth, P. — *On Transition in a Separated Laminar Boundary Layer*. J. Fluid Mech. 25, pp.683-704, (1966).

3. Michalke, A. Freymuth, P. — *The Instability and the Formation of Vortices in a Free Boundary Layer*. AGARD Conference Proceedings No.4, *Separated Flows*, pt II, pp.575-595, (1966).

4. Michalke, A. — *Instabilität eines kompressiblen runden Freistrahls unter Berücksichtigung des Einflusses der Strahlgrenzschichtdicke*. Z.Flugwiss, 19, pp.319-328, (1971).

Dr Dinkelacker: In the Max-Planck-Institut für Strömungsforschung in Göttingen F.Albers, H.Stiewitt and myself have made some measurements recently on jet structure with the help of an integrating method. I think the results fit well into the picture presented by Dr Laufer this morning. For this reason I would like to report briefly on these experiments.

The method uses the scattering of sound by turbulence as a means of investigating the turbulence. The experimental arrangement can be seen in Figure 1 opposite. A small beam of continuous sound waves (typical beam diameter 3 mm, typical sound frequency 4.3 MHz) is sent through the mixing region of a submerged water jet. The flow causes phase fluctuations in the sound beam. These phase fluctuations, which are of the order of a few angular degrees, are measured. In general the theoretical treatment of scattering of sound by turbulence is rather complicated. In the case of water as a medium, with negligible temperature fluctuations and with frequencies of a few MHz, however, the phase fluctuations $\phi(t)$ can be calculated to a good approximation by a superposition of the local velocity $\underline{v}(\underline{x}, t)$ and the sound velocity c_0. This superposition which was first used by G.I.Taylor in 1916 in a paper on sound propagation in the atmosphere – leads to

$$\phi(t) = \frac{2\pi \cdot f_s}{c_0^2} \cdot \int \underline{v}(\underline{x}, t)\, d\underline{l}.$$

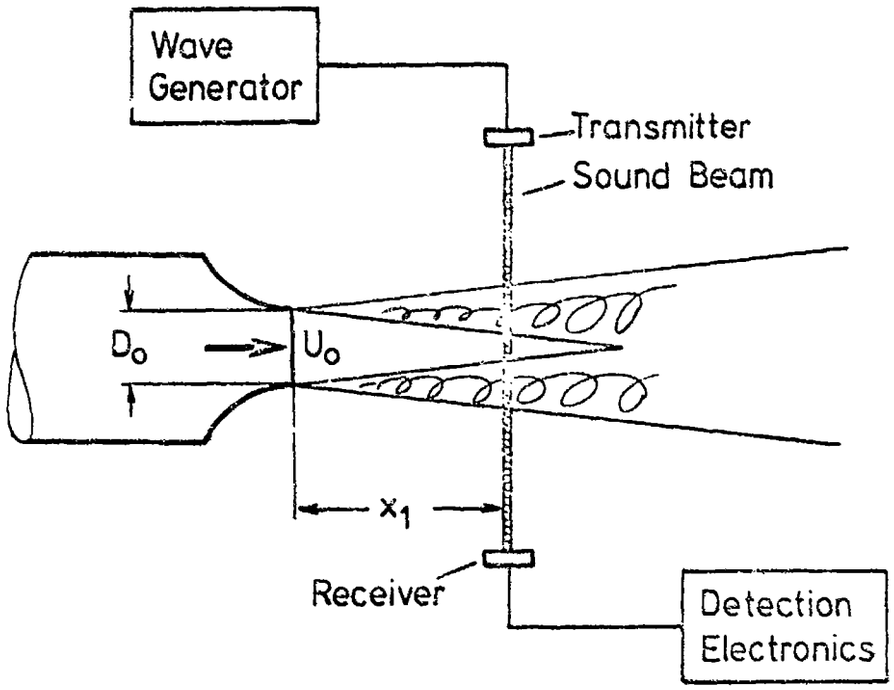

Fig.1 Experimental arrangement for the investigation of turbulence in a submerged water jet with the help of ultrasound

Here f_s is the sound frequency at the transmitter, l is the sound path and underlined symbols represent vectors. According to this formula the measured fluctuations $\phi(t)$ are proportional to the integrated flow velocity along the path of the sound beam. As this method gives a space averaged turbulence signal it seems to be especially useful for the detection of large scale structures in turbulence.

For the measurements reported in Figure 2 (overleaf) the sound beam was directed through the axis of the jet at a right angle. The measured fluctuations $\phi(t)$ are analysed with respect to frequencies. Different curves correspond to different distances x_1 between nozzle and sound beam. As can be seen the frequency spectra of $\phi(f)$ change with increasing distances x_1 so that the phase fluctuations become larger and simultaneously the maxima of the curves shift towards lower frequencies. This could be interpreted as an increase in the size of the eddies combined with a decrease in the recurrency frequency of the eddies. Figure 3 (on page A-13) shows the overall levels of the phase fluctuations ϕ as a function of the distance x_1. In addition to the measurements a calculated curve for the phase fluctuations is plotted in this figure. The calculation was done on the basis of a correlation length $l_y = 0.04x$ taken from the literature. As can be seen the measured values are higher than the calculated ones. This could possibly be explained by the existence of a high correlation of the velocity fluctuations across the jet. Figure 4 (on page A-14) gives cross correlation curves gained with the help of two sound beams sent through the jet perpendicularly to one another (details of the arrangement see Figure 4). This figure shows that the correlation between the phase fluctuations in the two sound beams extends in the x-direction over fairly large distances, indicating again the existence of large scale structures in the jet.

The results given here have still a preliminary character. More details will be published shortly in two reports of the Max-Planck-Institut für Strömungsforschung, Göttingen.

Chairman: Very interesting. Does anyone else have a contribution to make on this item?

Prof. Siddon: There seems to me to be a bit of paradox concerning which region of the jet is emitting frequencies coincident with the Strouhal peak of the far-field noise spectrum ($f \sim .2U_o/D$). If we look at the various experiments employing ray-acoustic types of directional detectors, for example the data of Chu and Laufer of one year ago (Washington Internoise Meeting) and the data which Dr Grosch presented on Wednesday we see that the frequencies coincident with the Strouhal peak seem to be coming from distances of 10 to 15 diameters downstream in the sonic jet. Admittedly the extent of this region is rather broad, but nevertheless the observation is not consistent with the classical notion that most of the sound power should be coming from the first 4–6 diameters of jet length.

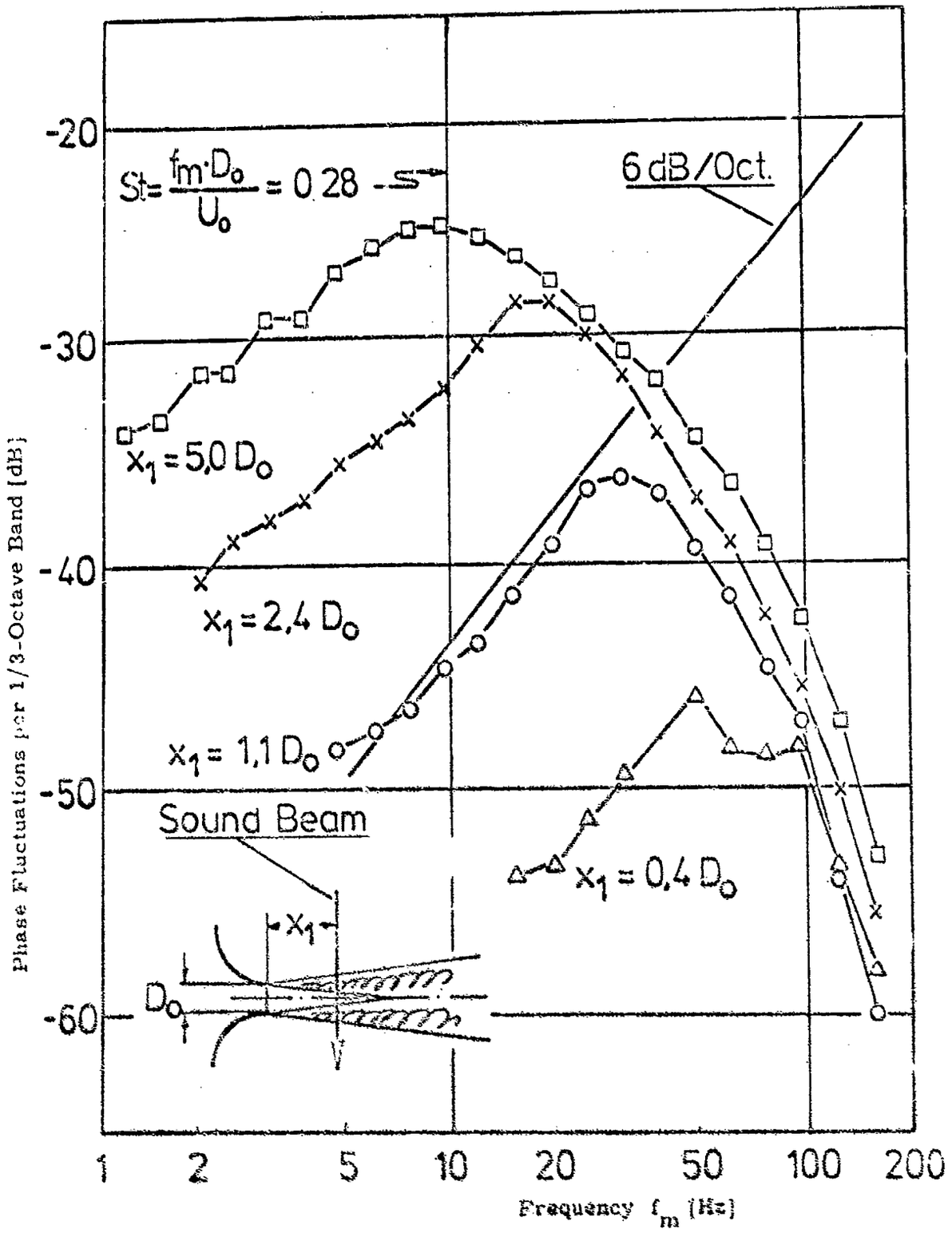

Fig.2 Frequency spectra of phase fluctuations in a sound beam after passing through the turbulent mixing region of a submerged water jet (sound frequency f_s = 4.3 kHz, flow velocity at the nozzle U_0 = 2.2 m/s, nozzle diameter D_0 = 61 mm, diameter of sound beam D_s = 13 mm, distance between nozzle and sound beam x_1, 0 dB corresponds to ϕ_{RMS} = 1)

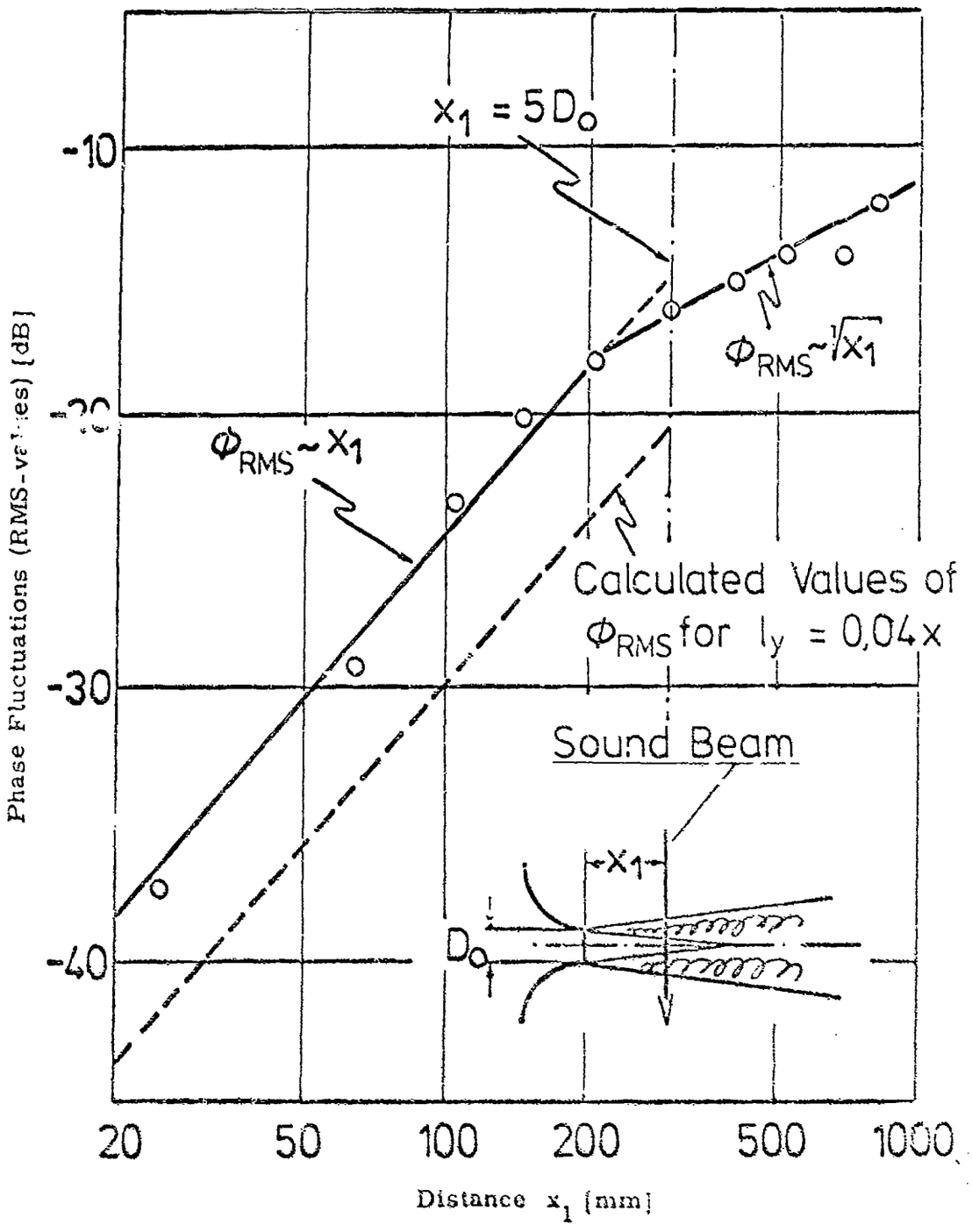

Fig.3 RMS-values of phase fluctuations in a sound beam after passing through the turbulent mixing region of a submerged water jet (same data as in Figure 2)

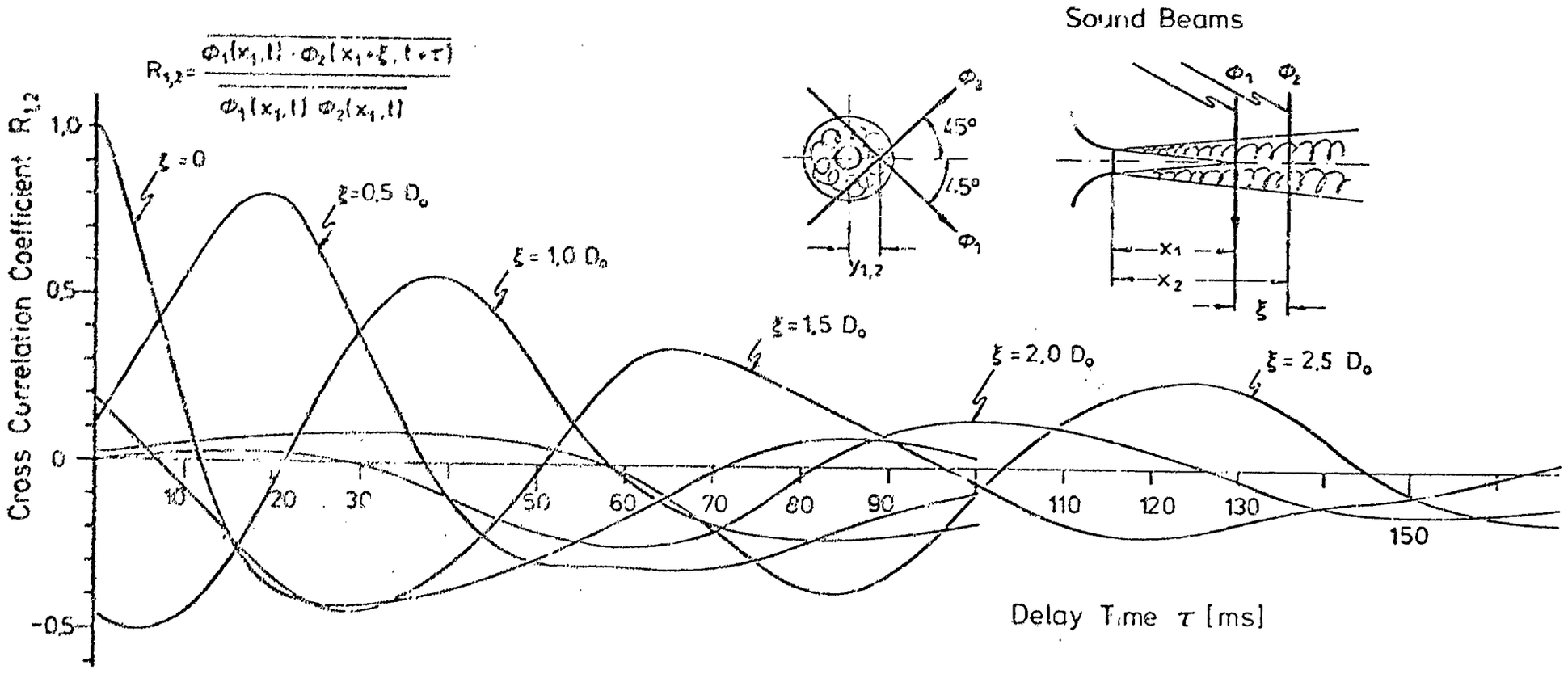

Fig. 4 Experimentally obtained cross correlations of phase fluctuations in two sound beams crossing a submerged water jet
($f_s = 4.3$ MHz, $U_o = 2.0$ m/s, $D_o = 61$ mm, $x_1 = 5\,D_o$, $x_2 = x_1 + \xi$, $y_{1,2} = 0.5\,D_o$,
$Re = \frac{U_o \cdot D_o}{\nu} = 1.2 \cdot 10^5$)

Secondly, in the context of coherent structure models for jet turbulence I seem to detect the suggestion that the coincidence between characteristic frequencies of passage for vortex rings and the corresponding peak frequencies in the jet noise spectrum may be more than accidental. Is there an explanation for this in terms of the phenomenological pictures which Prof. Laufer and others have given us today?

Prof. Laufer: Actually, we find that the peak occurs closer to 8 to 10 diameters, as far as the total energy is concerned. I think some of the curves that you have seen corresponded to just one particular frequency. That might explain one of the questions. As to the other one, I am not sure whether I understand you correctly; that the frequencies that you see in the far-field, at least where the maximum energy occurs, are different from the frequency of passages of these structures, is that your question?

Prof. Siddon: No, in fact the frequencies of vortex passage and of peak noise emission are rather similar. This would suggest that your notion of vortex breakdown, through pairing, might indeed hold the key to the basic noise generation mechanism. It was interesting to note in your film strip earlier this morning that as the vortices paired there was an almost catastrophic "explosion" of ordered vorticity. The smoke filaments suddenly distorted and broke apart, appearing to generate turbulence of all scales in a region beginning at approximately the end of the "potential core". This annihilation of organized vortices may occur quasi-regularly, at the vortex pairing frequency, almost as if they were being slammed against a wall. Noise of all frequencies, but modulated at the Strouhal frequency, could result, much as in the familiar case of waves breaking and crashing at the sea shore.

Chairman: Time is getting on. We ought not to introduce another topic that will take as long again. I will remark a little on the way the meeting has gone. This meeting has concentrated very much on jet noise. That really was rather unexpected judging by the topics discussed at the meeting 10 years ago. We have heard how there has been some progress evidently in the suppression of the high speed jet. We had a hint that the situation was likely to be different when the nozzle was tested in flight, all coming from the presentation yesterday afternoon. Does this mean that we are going to have to put much more effort on simulating flight effects in searching for jet noise suppression in the future? What are we going to do about that? Do we need perhaps an acoustic wind tunnel of the type we heard described this morning from the Naval Ship Research Development Center? It would really be a very useful tool to have in the aeronautical world. I am not aware that there is an acoustic wind tunnel program, but it looks to me as if there ought to be one.

The shielding of a noisy jet by a quiet jet is again something that is very striking indeed. It goes quite against the way one likes to model these things in any form of source analogy, when one looks at the source and presumes that it propagates without change through the flow. This is done in all forms of the acoustic analogy. It is striking that it is possible to shield a very noisy jet by a small quiet jet. Surely, that will be an area which will demand much more attention in the years to come.

Dr Dinkelacker: I would like to second the statement of one of the previous speakers, who suggested doing more work on shielding flow noise. I think that the possibilities of decreasing jet noise by different sorts of shielding have not been explored enough. We have recently done experiments with coaxial jets with different gas temperatures and to some extent also with combustion. These experiments show that small changes in the flows can change the directivity pattern of the noise radiation remarkably. It seems that these effects are partly due to real shielding of the inner jet by the outer one and partly due to flow interactions between the two jets. Clear differentiation between these two mechanisms seems to be important.

Prof. Küchemann: A very quick question, Mr Chairman, you have mentioned yourself that we had concentrated very much on jet noise. If you listen to two contributions from the Medical Panel and the Structures Panel, they want a good deal of information from us of an aerodynamic nature concerning other applications. Was this just chance, or was it the intention, that the program turned out as it did? We have, for instance, not mentioned intake noise at all. Does that mean that it isn't important anymore, or was it just chance that it was left out?

Chairman: I do not think it was chance. I think the net was cast pretty widely, and we have today the selection of the papers that were admitted.

M. Lagenaire: You could not, Professor Küchemann, take part in the final selection of papers. It was considered preferable to leave the subject of intake noise to the Propulsion and Energetics Panel.

Dr Rogers: You asked a direct question, and I think you deserve a direct reply. You said, "would it be necessary to have acoustic wind tunnels and make experiments with a moving stream", and I think the answer can only be yes.

This is the process we are now in. There are obvious problems. Acoustic wind tunnels are expensive, and need to be large. Therefore, there are likely to be only a few tunnels in which definitive experiments can be made. If anyone has some millions of dollars available, I would earnestly ask them to put it towards a good acoustic wind tunnel, preferably in Europe. Having said that, I have been struck at this meeting by the neglect of forward speed effects by the theoretical and experimental acoustic experts. Roy Hawkins trailed his coat earlier with the first reference in the meeting to the effect of forward speed. Cliff Bore attempted to intervene earlier and was brushed aside. We have had a very entertaining and highly sophisticated bout of infighting on the mechanisms of what one is measuring, or indeed whether one is measuring anything. But this does not give me great faith in trying to go from these results, with static surrounding air, into the cases where, (a) the jet exhausts into moving air, and (b) is surrounded by a distorted air field due to the presence of the airframe. If one is being a coarse engineer, which I think is the phrase Cliff Bore used, how is one to interpret and assess existing theories and experiments? Will it be simple to move from our present knowledge towards the real problem, or are we still in the situation which I seem to remember hypersonic aerodynamics was in 20 years ago, where every meeting I ever went to was concerned with the discussion of esoteric points of technique and philosophy, and the real problems were brushed aside. Hence, can anyone assure me that it is but a simple step towards the jet in a moving air stream?

Prof. Lilley: The answer to Rogers' question is clearly "No". There is obviously a complicated picture to be unravelled of what happens in the static jet which will be helpful in our understanding of the jet in a moving stream. However the structure of the jet in the moving stream will be different and work is in progress to establish these differences. It is quite clear that there are certain effects, as Roy Hawkins and M.Hoch have demonstrated in their measurements, that have displayed important differences between static and forward flight noise characteristics; these cannot be simply explained at the present time. It is clear that more and more measurements are urgently needed of the noise field from turbulent sources of sound in motion, and coupled with such measurements it is essential to add the more difficult job of studying the turbulent field itself. A number of facilities for studying the noise generated 'in-flight' need to be developed.

Chairman: I might tell you that many people here have been thoroughly involved in trying to understand forward speed effects and are having great difficulty.

M. Hoch: I want to emphasize the problems of flight effects on jet noise described yesterday by my colleague Roy Hawkins. Every time we, engineers, make in-flight measurements, care is taken in order to get good data. In spite of this, it happens that, even with simple convergent nozzles or with some types of silencers, we find a lot of unexplained differences from one experiment to another, from one test vehicle to another. We do not fully understand the reasons for these differences nor some unexpected phenomena, completely unpredictable from available theories. Therefore, it is obvious that I want to stress his view that an enormous effort is needed to study in-flight effects both in the theoretical and experimental fields. This means that, besides the classical measurements on aircraft with all the difficulties implied, we need some in-flight simulation facilities more suitable for research work, i.e. ground vehicles, spinning rigs, acoustic wind tunnels, etc... Obviously a lot of problems have still to be solved. For wind tunnels for instance, how can the results be interpreted i.e. what correction should be applied to the data to account for the complicated propagation effects through the coaxial outer flow and its shear layer, how can the results be transposed to a real flight situation, etc . . .?

For all these reasons and because of the practical importance of the flight effects on jet noise and other engine noise sources, my colleague and I would like to suggest the idea of having a future specialists meeting on these difficult problems.

Dr Dinkelacker: In his comment Dr Rogers has raised the question whether a large wind tunnel specifically designed for aeroacoustic investigations should be built. In my opinion such a facility could become a very helpful tool for further research in aeroacoustics. I fear, however, that more detailed planning will show that such a facility, if it is to be useful for a wide range of experiments, has to be large and will be very expensive. The crucial point in the planning might well be the "low-frequency limit" of the facility i.e. the frequency down to which acoustical free field conditions can be simulated. The lower this frequency limit has to be, the larger the dimensions and hence the costs will be. I do not think that one should compromise here too early, e.g. by declaring that frequencies under 100 Hz are unimportant. My opinion is – if such a general purpose facility is to be built – it should be large and especially the low-frequency limit should be as low as possible. For this purpose it seems to be reasonable to solicit money from different countries and to do the work in international cooperation.

Chairman: That is a fine note on which we can close this round table discussion. I thank everybody who took part, and I am glad that I was able to promote a discussion. I think that possibly most of the points were resolved in the discussion, but I apologise if I have omitted topics that members might have preferred to discuss.

M. Legendre: I thank you for the excellent way you led the discussion.

APPENDIX B

A SELECTION OF AGARD PUBLICATIONS IN RECENT YEARS – FOR AVAILABILITY SEE BACK COVER

1965

Report 514	**The production of intense shear layers by vortex stretching and convection** By J.T.Stuart, May 1965. (Report prepared for the AGARD Specialists' Meeting on "Recent developments in boundary layer research", May 1965.)
AGARDograph 91	**The theory of high speed guns** By A.E.Seigel, May 1965.
AGARDograph 97 (in four parts)	**Recent developments in boundary layer research** AGARD Specialists' Meeting, Naples, May 1965.
AGARDograph 102	**Supersonic inlets** By Ione D.V.Faro, May 1965.
AGARDograph 103	**Aerodynamics of power plant installation** AGARD Specialists' Meeting, Tullahoma, October 1965.

1966

Report 525	**The pitot probe in low-density hypersonic flow** By S.A.Schaaf, January 1966.
Report 526	**Laminar incompressible leading and trailing edge flows and the near wake rear stagnation point** By Sheldon Weinbaum, May 1966.
Report 539	**Changes in the flow at the base of a bluff body due to a disturbance in its wake** By R.Hawkins and E.G.Trevett, May 1966.
Report 542	**Transonic stability of fin and drag stabilized projectiles** By B.Cheers, May 1966.
Report 548	**Separated flows** (Round Table Discussion), Edited by J.J.Ginoux, May 1966.
Report 550	**A new special solution to the complete problem of the internal ballistics of guns** By C.K.Thornhill, 1966.
Report 551	**A review of some recent progress in understanding catastrophic yaw** by J.D.Nicolaides, 1966.
AGARDograph 109	**Subsonic wind tunnel wall corrections** By Gardner, Acum and Maskell, 1966.
AGARDograph 112	**Molecular beams for rarefied gasdynamic research** By J.B.French, 1966.
AGARDograph 113	**Freeflight testing in high speed wind tunnels** By B.Dayman, Jr, 1966.

Conference Proceedings 4 (two parts and one supplement)	**Separated flows** Specialists' Meeting, Rhode-Saint-Genèse (VKI), May 1966.
Conference Proceedings 10	**The fluid dynamic aspects of ballistics** Specialists' Meeting, Mulhouse, September 1966.
Conference Proceedings 12 (in two parts)	**Recent advances in aerothermochemistry** 7th AGARD Colloquium sponsored by PEP and FDP, Oslo, May 1966.

1967

Report 558	**Experimental methods in wind tunnels and water tunnels, with special emphasis on the hot-wire anemometer** By K.Wieghardt and J.Kux, 1967.
Advisory Report 13	**Aspects of V/STOL aircraft development** (This report consists of three papers presented during the joint session of the AGARD FDP and FMP held in Göttingen, September 1967.)
AGARDograph 98	**Graphical methods in aerothermodynamics** By O.Lutz and G.Stoffers, November 1967.
AGARDograph 117	**Behaviour of supercritical nozzles under three-dimensional oscillatory conditions** By L.Crocco and W.A.Sirignano, 1967.
AGARDograph 119	**Thermo-molecular pressure effects in tubes and at orifices** By M.Kinslow and G.R.Arney, Jr, 1967.
AGARDograph 121	**Techniques for measurement of dynamic stability derivatives in ground test facilities** By C.J.Schueler, L.K.Ward and A.E.Hodapp, Jr, 1967.
AGARDograph 124	**Nonequilibrium effects in supersonic-nozzle flows** By J.Gordon Hall and C.E.Treanor, 1967.
Conference Proceedings 19 (in two parts)	**Fluid physics of hypersonic wakes** Specialists' Meeting, Fort Collins, Colorado, May 1967.
Conference Proceedings 22	**Fluid dynamics of rotor and fan supported aircraft at subsonic speeds** Specialists' Meeting, Göttingen, September 1967.
Conference Proceedings 22 – S 4	As above – with supplement

1968

AGARDograph 132	**The electron beam fluorescence technique** By E.P.Muntz, 1968.
Conference Proceedings 30	**Hypersonic boundary layers and flow fields** Specialists' Meeting, London, May 1968.
Conference Proceedings 30 Suppl.	Supplement to the above.
Conference Proceedings 35	**Transonic aerodynamics** Specialists' Meeting, Paris, September 1968.
Conference Proceedings 35 Suppl.	Supplement to the above.

1969

Advisory Report 17	Technical Evaluation Report on AGARD Specialists' Meeting on Transonic aerodynamics By D.Küchemann, April 1969.

AGARDograph 134	**A portfolio of stability characteristics of incompressible boundary layers** By H.J.Obremski, M.V.Morkovin and M.Landahl, 1969.
AGARDograph 135	**Fluidic controls systems for aerospace propulsion** Edited by R.J.Reilly, September 1969.
AGARDograph 137 (in two parts)	**Tables of inviscid supersonic flow about circular cones at incidence $\gamma = 1.4$** By D.J.Jones, November 1969.
Conference Proceedings 42	**Aircraft engine noise and sonic boom** Joint Meeting of the Fluid Dynamics and Propulsion and Energetics Panels, held in Saint-Louis, France, May 1969.
Conference Proceedings 48	**The aerodynamics of atmospheric shear flow** Specialists' Meeting, Munich, September 1969.

1970

Report 575	**Test cases for numerical methods in transonic flows** By R.C.Lock, 1970.
Advisory Report 22	**Aircraft engine noise and sonic boom*** By W.R.Sears. (Technical Evaluation Report on AGARD FDP and PEP Joint Meeting on "Aircraft engine noise and sonic boom".) January 1970.
Advisory Report 24	**The aerodynamics of atmospheric shear flows** By J.E.Cermak and B.W.Marschner, May 1970. (Technical Evaluation Report on AGARD Specialists' Meeting on "The aerodynamics of atmospheric shear flows".)
Advisory Report 30	**Blood circulation and respiratory flow** By J.F.Gross and K.Gersten, December 1970. (Technical Evaluation Report on AGARD Specialists' Meeting on the above subject.)
AGARDograph 138	**Ballistic range technology** By T.N.Canning, November 1970.
AGARDograph 144	**Engineering analysis of non-Newtonian fluids** By D.C.Bogue and J.L.White, July 1970.
AGARDograph 145	**Wind tunnel pressure measurement techniques** By D.S.Bynum, R.L.Ledford and W.E.Smotherman, December 1970.
AGARDograph 146	**The numerical solution of partial differential equations governing convection** By H.Lomax, P.Kutler and F.B.Fuller, November 1970.
AGARDograph 147	**Non-reacting and chemically reacting viscous flows over a hyperboloid at hypersonic condition** Edited by C.H.Lewis. (M.Van Dyke, J.C.Adams, F.G.Blottner, A.M.O.Smith, R.T.Davis and G.L.Keltner were contributors.) November 1970.
Conference Proceedings 60	**Numerical methods for viscous flows** By R.C.Lock, November 1970. (Abstracts of papers presented at a Seminar held by the FDP of AGARD at the NPL, Teddington, UK, 18–21 September 1967.)
Conference Proceedings 62	**Preliminary design aspects of military aircraft** March 1970, AGARD Flight Mechanics Panel Meeting held in The Hague, The Netherlands, September 1969.
Conference Proceedings 65	**Fluid dynamics of blood circulation and respiratory flow** Specialists' Meeting, Naples, May 1970.
Conference Proceedings 71	**Aerodynamic Interference** Specialists' Meeting, Silver Springs, Maryland, USA, September 1970.

* See also Advisory Report 26 by J.O.Powers and M.Pinsky, June 1970. AR26 has the same title as AR22 but was produced by the Propulsion and Energetics Panel of AGARD and deals primarily with engine noise.

1971

Report 588	**Aerodynamic testing at high Reynolds numbers and transonic speeds** By D.Küchemann, 1971
Advisory Report 34	**Aerodynamic interference** By D.J.Peake, May 1971. (Technical Evaluation Report of the Specialists' Meeting on "Aerodynamic interference", September 1970.)
Advisory Report 35	**Report of the high Reynolds number wind tunnel study group of the Fluid Dynamics Panel** April 1971
Advisory Report 36	**Report of the AGARD Ad Hoc Committee on Engine-airplane interference and wall corrections in transonic wind tunnel tests** Edited by A.Ferri, F.Jaarsma and R.Monti, August 1971.
Advisory Report 37	**Facilities and techniques for aerodynamic testing at transonic speeds and high Reynolds number** By R.C.Pankhurst, October 1971. (Technical Evaluation Report on Specialists' Meeting held in Göttingen, Germany, April 1971.
AGARDograph 137 (third volume)	**Tables of inviscid supersonic flow about circular cones at incidence, $\gamma = 1.4$** Part III, by D.J.Jones, December 1971.
AGARDograph 148	**Heat transfer in rocket engines** By H.Ziebland and R.C.Parkinson, September 1971.
Conference Proceedings 83	**Facilities and techniques for aerodynamic testing at transonic speeds and high Reynolds number** August 1971. Specialists' Meeting held in Göttingen, Germany, April 1971.
Conference Proceedings 91	**Inlets and nozzles for aerospace engines** December 1971. Meeting held in Sandefjord, Norway, September 1971.

1972

Report 598	**Experiments on management of free-stream turbulence** By R.I.Loehrke and N.M.Nagib, September 1972.
Report 603	**Aerodynamic test simulation: Lessons from the past and future prospects** Ed. J.Lukasiewicz, December 1972.
AGARDograph 156	**Planar inviscid transonic airfoil theory** By H.Yoshihara, February 1972.
AGARDograph 161	**Ablation** By H.Hurwicz, K.M.Kratsch and J.E.Rogan, March 1972.
AGARDograph 163	**Supersonic ejectors** Ed. J.J.Ginoux, November 1972.
AGARDograph 164	**Boundary layer effects in turbomachines** Ed. J.Surugue, December 1972.
Conference Proceedings 93	**Turbulent shear flows** January 1972. Specialists' Meeting held in London, England, September 1971.
Conference Proceedings 102	**Fluid dynamics of aircraft stalling** November 1972, Specialists' Meeting held in Lisbon, Portugal, April 1972.
Advisory Report 46	**Turbulent shear flows** By R.Michel, July 1972 (Technical Evaluation Report of the Specialists' Meeting on "Turbulent Shear Flows", September 1971.
Advisory Report 49	**Fluid dynamics of aircraft stalling** By R.C.Pankhurst (Technical Evaluation Report on Fluid Dynamics Panal Specialist's Meeting) November 1972.

Advisory Report 50	**Energetics for aircraft auxiliary power systems** By R.H.Johnson, C.E.Oberly and R.E.Quigley, Jr (Technical Evaluation Report on 39th Propulsion and Energetics Panel Meeting), November 1972.
Advisory Report 60	**The need for large wind tunnels in Europe** Report of the Large Wind Tunnels Working Group, December 1972.
Lecture Series LS42	**Aerodynamic problems of hypersonic vehicles. (Two volumes)** Ed. R.C.Pankhurst, July 1972.
Lecture Series LS48	**Numerical methods in fluid dynamics** Ed. J.J.Smolderen, May 1972.
Lecture Series LS49	**Laser technology in aerodynamic measurements** Ed. R.C.Pankhurst, March 1972.
Lecture Series LS53	**Airframe/engine integration** May 1972.
Lecture Series LS57	**Heat exchangers** Ed. J.J.Ginoux, January 1972.

1973

Report 600	**Problems of wind tunnel design and testing** December 1973.
Report 601	**Problems in wind tunnel testing techniques** April 1973.
Report 602	**Fluid motion problems in wind tunnel design** April 1973.
Advisory Report 58	**Technical Evaluation Report on the Fluid Dynamics Panel Specialists Meeting on Aerodynamic Drag** By S.F.J Butler, September 1973.
Advisory Report 61	**Technical Evaluation Report on the Fluid Dynamics Panel Specialists Meeting on Aerodynamics of Rotary Wings** By N.D.Ham, March 1973.
AGARDograph 165	**Heat-transfer measurements in short-duration hypersonic facilities** By D.L.Schultz and T.V.Jones, February 1973.
AGARDograph 169	**Effects of streamline curvature on turbulent flow** By P.Bradshaw. Edited by A.D.Young, August 1973.
AGARDograph 171	**Magnus characteristics of arbitrary rotating bodies** By I.A.Jacabson. Edited by P.F.Yaggy, November 1973.
AGARDograph 172	**Dynamic stall** By P.Crimi. Edited by P.F.Yaggy, November 1973.
AGARDograph 173	**Aerodynamic interference induced by reaction controls** By F.W.Spaid, L.A.Cassel and R.E.Wilson (Editor), November 1973.
AGARDograph 174	**Digital techniques in turbulence research** By C.H.Gibson. Edited by P.A.Libby, December 1973.
Conference Proceedings 111	**Aerodynamics of rotary wings** February 1973, Specialists' Meeting held in Marseilles, France, September 1972.
Conference Proceedings 124	**Aerodynamic Drag** October 1973.
Lecture Series LS56	**Aircraft performance -- Prediction methods and optimization** Ed. J.Williams, March 1973.

Lecture Series LS64 **Advances in numerical fluid dynamics**
February 1973.